NASA Contractor Report 4611

11-37
P. 420

Vibration Reduction in Helicopter Rotors Using an Actively Controlled Partial Span Trailing Edge Flap Located on the Blade

T. A. Millott and P. P. Friedmann

CONTRACTS NAG2-477, NGT-50444
June 1994

National Aeronautics and
Space Administration

NASA Contractor Report 4611

Vibration Reduction in Helicopter Rotors Using an Actively Controlled Partial Span Trailing Edge Flap Located on the Blade

T. A. Millott and P. P. Friedmann

University of California
Mechanical, Aerospace and Nuclear Engineering Department
Los Angeles, CA 90024

Prepared for
Ames Research Center
CONTRACTS NAG2-477, NGT-50444
June 1994

National Aeronautics and
Space Administration

Ames Research Center
Moffett Field, California 94035-1000

PREFACE

This report describes in detail innovative analytical research aimed at demonstrating the remarkable potential of an actively controlled partial span flap, located on the trailing edge of the blade, for vibration reduction in helicopter rotors in forward flight.

The research described in this report was carried out in the Mechanical, Aerospace and Nuclear Engineering Department at UCLA, and it was funded jointly by NASA Grants NAG 2-477 and NASA NGT-50444 with Dr. S. Jacklin, from the Rotorcraft Aeromechanics Branch at NASA Ames, as the grant monitor. The authors express their appreciation to the grant monitor for his useful comments and suggestions.

The principal investigator for this sponsored research activity was Professor Peretz P. Friedmann. This constitutes essentially the first author's Ph.D. dissertation; however, certain changes were made to the dissertation, so as to improve it, before turning it into this report.

CONTENTS

LIST OF FIGURES

LIST OF TABLES

NOMENCLATURE

$\vec{a}_b$	Absolute acceleration of point on blade cross-section
A_b	Rotor blade cross-sectional area
$\vec{a}_c$	Absolute acceleration of point on control flap cross-section
A_c	Control surface cross-sectional area
a_o	Incompressible airfoil lift curve slope
A_{nm}	Blade aerodynamic lift and moment coefficients
$\vec{a}_p$	Absolute acceleration of point in rotating frame
A_R	Rotor disk area $= \pi R^2$
b	Blade semi chord
ba	Offset between midpoint of chord and axis of twist
bc	Offset between midpoint of chord and flap hinge axis
B_n	Blade drag coefficients
C(k)	Theodorsen's lift deficiency function
c_a	Speed of sound in air
c_b	Blade chord $= 2b$
C_{nm}	Control surface aerodynamic coefficients
c_{cs}	Control surface chord length
C_β, C_ζ, C_ϕ	Blade damping coefficients in flap, lead-lag, and torsion, respectively
C_{do}	Blade drag coefficient
C_{mo}	Blade moment coefficient
C_T	Thrust coefficient $= \dfrac{\text{Thrust}}{\pi R^2 \rho_A R^2 \Omega^2}$
C_W	Weight coefficient $= \dfrac{\text{Weight}}{\pi R^2 \rho_A R^2 \Omega^2}$
[D]	Control matrix during i-th control step
D, D*	Blade drag force
D_f	Fuselage drag force

e	Blade root offset from the hub
E	Modulus of elasticity
$EI_{yy}, EI_{yz}, EI_{zz}$	Bending stiffness of the blade
$EI_{\eta\eta}, EI_{\zeta\zeta}$	Principal bending stiffness of the blade
$\hat{e}_{xi}, \hat{e}_{yi}, \hat{e}_{zi}$	Unit vectors along the axes of the "i" coordinate system
$\vec{f}_b$	Vector of blade equations
$\vec{f}_t$	Vector of trim equations
$\vec{F}_H$	Vector of hub shear components
$\vec{F}_R$	Vector of root force components
fC_{df}	Equivalent fuselage flat plate area
g	Acceleration due to gravity
G	Shear modulus
g_{SF}, g_{SL}, g_{ST}	Structural damping coefficients of the blade in flap, lag and torsion, respectively
GJ_b	Torsional stiffness of the blade
GJ_c	Torsional stiffness of the control surface
$h(t)$	Plunging motion of airfoil-aileron system
I_b	Blade flapping inertia about the blade root
I_c	Control surface flapping inertia about the blade root
I_{MB2}, I_{MB3}	Principal mass moments of inertia of the blade cross-section
$I_{mbr2}, I_{mbr3}, I_{mbr23}$	Integrals of the blade principal mass moments of inertia
I_{MC2}, I_{MC3}	Principal mass moments of inertia of the control surface cross-section
$I_{mcr2}, I_{mcr3}, I_{mcr23}$	Integrals of the control surface principal mass moments of inertia
I_{yb}, I_{zb}	Blade flapping inertias associated with the offset between the blade center of gravity and the elastic axis
I_{yc}, I_{zc}	Control surface flapping inertias associated with the offset between the hinge point and the center of gravity
I_{yh}, I_{zh}	Control surface flapping inertia associated with the offset between the control surface hinge and the elastic axis

J	Quadratic cost functional or performance index
J_b	Blade pitch inertia
J_c	Control surface pitch inertia about hinge
J_h, J_{yh}, J_{zh}, J_{yzh}	Control surface pitch inertias about the elastic axis
J_{hc}, J_{yhc}, J_{zhc}, J_{yzhc}	Cross-products of control surface pitch inertias
k	Reduced flutter frequency
K_β, K_ζ, K_ϕ	Blade spring constants in flap, lead-lag, and torsion, respectively
L_b	Blade length
L_{cs}	Control surface length
L_{NC}, L_C	Noncirculatory and circulatory lift per unit span, respectively
m_b	Mass per unit length of the k-th blade
m_c	Mass per unit length of the control surface
M_b	Total mass of one blade
M_c	Total mass of one control surface
M_δ	Control surface hinge moment
$\vec{M}_H$	Vector of hub moment components
$\vec{M}_R$	Vector of root moment components
M_{tip}	Mach number at blade tip in hover $= \Omega R/c_a$
$M_{x,\psi}$	Mach number at (x, ψ)
M_{yNC}, M_{yC}	Noncirculatory and circulatory aerodynamic moment per unit span, respectively
N_b	Number of blades
N_{max}	Highest input frequency multiple used for control
N_{DOF}	Number of degrees of freedom of each blade
N_H	Number of harmonics used in Fourier expansion
O_H	Location of hub center
P_{cs}	Power required to drive control flap actuators

P_{IBC}	Power required to implement conventional IBC
P_R	Power required to turn the rotor
P_{trim}	Power required to trim the rotor
R	Rotor radius
$\vec{r}_b$	Position vector of an arbitrary point on the blade
$\vec{r}_c$	Position vector of an arbitrary point on the control surface
R_C	Flap-lag elastic coupling parameter
R_D, R_{LM}	Reverse flow parameters
$\vec{R}_{EA}$	Position vector of a point on the elastic axis before deformation
$\vec{r}_{EA}$	Position vector of a point on the elastic axis after deformation
$\vec{R}_p, \vec{r}_p$	Position vector of an arbitrary point in the rotating reference frame
$\vec{R}_0$	Position vector of origin of rotating reference frame relative to the inertial reference frame
$T(x)$	Axial tension in blade
$[T_i]$	Transfer matrix relating control input harmonics to the vibration harmonics during the i-th control step
$T_1, \ldots, T_{14}$	Coefficients used in Theodorsen's theory
u, v, w	Displacement of a point on the elastic axis due to the blade's deformation
$\vec{u}_i$	Control input vector during the i-th control step
U_P, U_T	Perpendicular and tangential velocities seen by blade, respectively
V_F	Forward flight velocity of the helicopter
W	Helicopter weight
W_f	Weight of fuselage $= W - gN_bM_b$
W_F, W_M	Scalar weighting factor on squares of hub shear and moment amplitudes, respectively
$[W_Z], [W_u]$ $[W_\Delta]$	Weighting matrices on the vibrations, control, and rate of change of control, respectively

x	Distance from blade root along undeformed elastic axis
x_i, y_i, z_i	Axes of the "i" coordinate system
X_A	Offset between the aerodynamic center and the elastic axis
x_b, y_b, z_b	Position of the blade center of gravity from the blade root
x_c	Distance to center of gravity of the control surface from the blade root
x_{cs}	Distance to inboard edge of the control surface from the blade root
X_{FA}	Horizontal offset of fuselage aerodynamic from hub
X_{FC}	Horizontal offset of fuselage center of gravity from hub
X_H	Offset between the hinge point of the control flap from the elastic axis (positive aft)
X_{Ib}	Offset between the elastic axis and the blade cross-sectional center of mass
X_{IIb}	Offset between the elastic axis and the blade cross-sectional center of area
X_{Ic}	Offset between the hinge point and the control surface cross-sectional center of mass
X_{IIc}	Offset between the hinge point and the control surface cross-sectional center of area
y_{0b}, z_{0b}	Coordinates of an arbitrary point on blade cross-section relative to the elastic center in the "4" system
$\bar{y}_{0b}, \bar{z}_{0b}$	Coordinates of an arbitrary point on blade cross-section relative to the elastic center in the "5" system
y_{0c}, z_{0c}	Coordinates of an arbitrary point on flap cross-section relative to the hinge point in the "C" system
$\bar{y}_{0c}, \bar{z}_{0c}$	Coordinates of an arbitrary point on flap cross-section relative to the hinge point
y_A, z_A	Coordinates of the area centroid of the blade cross-section relative to the elastic axis
y_c, z_c	Coordinates of the center of gravity of the control surface relative to the hinge point
y_H, z_H	Coordinates of the control flap hinge point on the blade cross-section relative to elastic axis in the "4" system
$\bar{y}_H, \bar{z}_H$	Coordinates of the control flap hinge point on the blade cross-section relative to elastic axis in the "5" system

Z_{FA}	Vertical offset of fuselage aerodynamic center from hub
Z_{FC}	Vertical offset of fuselage center of gravity from hub
$\vec{Z}$	Vector of amplitudes of N_b/rev cosine and sine components of the vibratory hub loads
$\vec{Z}_0$	Baseline value of $\vec{Z}_i$

Greek Symbols

α	Total angle of attack of blade cross-section
α_R	Rotor plane trim pitch angle
β_p	Precone angle of the blade
$\beta,\ \zeta,\ \phi$	The blade flap, lag, and torsional degrees of freedom
$\delta(\psi)$	Control surface deflection angle
$\delta_{Nc},\ \delta_{Ns}$	N/rev cosine and sine amplitudes of the control surface deflection angle
ε	Small dimensionless parameter on the order of typical blade slopes
ϕ	Elastic twist about the elastic axis
ϕ_{in}	Inflow angle
γ	Lock number
θ_G	Geometric pitch angle $= \theta_{pc} + \theta_{pt}$
θ_{Gr}	Geometric pitch angle at the blade root
θ_{pc}	Pilot pitch input $= \theta_0 + \theta_{1c}\cos\psi + \theta_{1s}\sin\psi$
$\theta_0,\ \theta_{1c},\ \theta_{1s}$	Collective, sine and cosine blade pitch inputs
θ_{pt}	Built in twist distribution of the blade
θ_{IBC}	Additional pitch input used in individual blade control
λ	Inflow ratio $= \dfrac{V_F \sin\alpha_R + v}{\Omega R}$
μ	Advance ratio $= \dfrac{V_F \cos\alpha_R}{\Omega R}$
v	Induced inflow velocity
ρ_A	Air density

ρ_b	Blade mass density
ρ_c	Control surface mass density
ψ	Blade azimuth angle (or non-dimensional time)
ω_β, ω_ζ, ω_ϕ	Fundamental nonrotating flap, lead-lag and torsional frequencies, respectively
ω_{F1}, ω_{L1}, ω_{T1}	Fundamental rotating flap, lead-lag and torsional frequencies, respectively
ω_F, ω_L, ω_T	Rotating flap, lead-lag and torsional frequencies
Ω	Rotor angular velocity
η_b, ζ_b	Principal coordinates of a point on the blade cross-section
η_c, ζ_c	Principal coordinates of a point on the control surface cross-section relative to the hinge point

Special Symbols

$(\bullet)_{,x}$	Derivative with respect to spanwise coordinate x
$(\dot{\bullet})$	Derivative with respect to time
$(\vec{\bullet})$, $\{\bullet\}$	Column vector
$[\bullet]$	Matrix quantity
$(\bullet)^T$	Transpose
$(\tilde{\bullet})$	Approximation of $(\bullet)$

SUMMARY

This report describes an analytical study of vibration reduction in a four bladed helicopter rotor using individual blade control (IBC) implemented through an actively controlled, partial span, trailing edge flap located on the blade. Two different blade models are used in the study: (a) an offset-hinged spring restrained blade model with fully coupled flap-lag-torsional dynamics, and (b) a completely flexible elastic blade model using three flap, two lead-lag and two torsional rotating modes. For both blade models the vibration reduction with the actively controlled flap is compared with the vibration reduction produced by conventional IBC, in which the entire blade undergoes cyclic pitch change. For both cases a deterministic controller is implemented to reduce the 4/rev hub loads. For all cases considered it is found that the actively controlled flap produced vibration reduction comparable with that obtained with conventional IBC, however the power requirements are between 10-30% of those needed for conventional IBC. The control studies performed using the flexible blade model and the offset-hinged spring restrained blade model are compared. It is found that despite large increases in vibration levels due to the more realistic blade model, vibration reduction can still be accomplished without excessive power expenditures or control angle inputs. A careful parametric study is conducted in which the blade torsional frequency, spanwise location of the control flap, and hinge moment correction factor are varied. The results clearly demonstrate the feasibility of this new approach to vibration reduction. There is also indication that this approach, in which a conventional swashplate is used in conjunction with the actively controlled flap such that the vibration reduction device is completely decoupled from the primary flight control system used for trim, has potentially significant advantages over conventional IBC. Finally, time domain simulation of the helicopter response to control is performed, validating the frequency domain based control algorithms that have been implemented to reduce vibrations.

Chapter I

INTRODUCTION AND OBJECTIVES OF THIS STUDY

1.1 INTRODUCTION AND BACKGROUND

Vibrations in helicopters, which arise from such sources as the rotor system, the tail rotor, the engine and the transmission, lead to fatigue damage of the structural components, human discomfort, difficulty in reading instruments and the reduced effectiveness of weapon systems. A comprehensive review on the sources of vibration is presented in Refs. 29 and 41. A major goal of current helicopter research is thus to reduce the vibration levels experienced by crew, passengers and equipment during flight.

Current research has been driven by both commercial and military requirements. Commercial passenger acceptance would greatly benefit from the perception of the helicopter as having a "jet smooth ride". Furthermore, reduction of vibration levels would lead to the reduction of high maintenance/replacement costs associated with the fatigue damage of structural components. Decreasing vibration levels and allowing higher cruise speeds would increase the load utilization of helicopters and so decrease relative capital costs. From a military point of view, increased speed leads to benefits in survivability and deployment response times. The same maintenance and comfort benefits as for civil operations apply. Reduction in vibration levels in military helicopters allows more accurate weapons deployment and more effective intelligence gathering.

The traditional approach to vibration reduction in helicopters is based on the use of passive means such as vibration absorbers or isolation devices. A comprehensive review of helicopter vibration control presented in Ref. 41 describes many of these methods.

More recent investigations into passive means offer promise of reducing vibrations to levels below those attainable by vibration absorbers and isolators. One promising approach involves the design of rotor blades which inherently have low levels of vibration. This may be done by applying optimum structural design techniques to the aeroelastic

tailoring of the blade. Geometry, mass and stiffness distributions may be optimized to give minimum vibration levels at the rotor hub or at specified locations in the fuselage. The fuselage itself may also be tailored to reduce vibrations at various points of interest such as the pilot seat, passenger compartment or the tail boom. Surveys of the application of structural optimization to helicopter vibration problems are presented in Refs. 10 and 33. However, the use of structural optimization may lead to higher manufacturing costs, especially in the manufacturing of aeroelasticaly tailored rotor blades.

The desire to achieve better vibration reduction has also lead to the use of active controls in reducing helicopter vibrations. Active controllers can be used to reduce vibrations by eliminating their source, namely the aerodynamic excitation to the rotor. Among the various approaches which utilize active control for vibration reduction in forward flight, the approach commonly denoted higher harmonic control (HHC) has emerged as a potential candidate for possible implementation in production helicopters. This concept relies on the application of higher harmonic pitch changes (i.e. above the 1/rev pitch changes required for directional control and vehicle trim) to modify the blade airloads so as to minimize harmonic blade loading. For a rotor having N_b blades, the predominant vibrations are at N_b/rev. In HHC, these are normally alleviated by applying N_b/rev pitch excitations superimposed on the collective (i.e. average), lateral (i.e. 1/rev sine) and longitudinal (i.e. 1/rev cosine) pitch inputs used to control the helicopter attitude and velocity. This is done by applying N_b/rev harmonics in the fixed system through an actively controlled conventional swashplate through the use of hydraulic servo-actuators. Numerous studies have demonstrated the validity of this approach for producing substantial reduction in vibration levels in forward flight by analytical simulations[5,7,23,34,36,43, 44,51], wind tunnel tests[27.35,49], and flight tests[31,40,56,57].

In an alternative approach, denoted individual blade control (IBC)[26], the time dependent pitch angle of each blade is independently controlled in the rotating reference frame. This approach removes many of the limitations which exist in active control through a conventional swashplate, but a control system more complex than the conventional swashplate may be required[20,21]. Recent wind tunnel and flight tests illustrate the

considerable mechanical complexity associated with the implementation of this approach[22,42]. It is worthwhile mentioning that both HHC and conventional IBC introduce the control for vibration reduction through the primary flight control system of the helicopter and therefore the presence of such an active vibration control device introduces some constraints on the system from an airworthiness point of view.

The desire to decrease mechanical complexity and weight, and minimize maintenance costs, has lead to the development of hingeless and bearingless rotor hubs. In hingeless rotors the mechanical flap and lead-lag hinges present in articulated blades are replaced by a flexible cantilevered blade, where the blade flexibility provides for virtual hinges. In such blades the mechanical pitch bearing is retained. Bearingless rotor blades are similar to hingeless blades except that the pitch bearing is eliminated and the pitch input is introduced through a torsionally flexible structural element. Typical articulated, hingeless and bearingless rotor configurations are shown in Fig. 1. The mechanical simplicity and weight savings in hingeless and bearingless rotors is generally accompanied by increases in vibratory levels; thus vibration reduction in such rotors becomes an even more important issue than for articulated rotor configurations.

Recently, comparative studies of vibration reduction in forward flight using HHC were carried out for equivalent articulated and hingeless rotor configurations[43,44]. For both configurations substantial vibration reduction was achieved with HHC blade pitch angles under three degrees. However, a comparison of power requirements revealed that the power required to implement HHC on hingeless rotor blades is significantly higher than for the equivalent articulated rotor blades. These higher power requirements appear to be associated with the need to drive harmonically the fairly large and coupled structural dynamic system represented by the hingeless blade.

This provided the motivation for exploring an alternative concept where the modification of the aerodynamic loads on the blade, for vibration reduction in forward flight, is accomplished through the active control of an aerodynamic surface located on the blade, similar to the partial span trailing edge flap shown in Figs. 2 and 3. It was postulated that such a device would produce substantial reduction in power requirements when compared with

HHC or conventional IBC, which require the introduction of cyclic pitch changes for the whole blade. Furthermore, *such an actively controlled flap can be conveniently controlled by a control loop which is separate from the primary control system; thus it will have no influence on airworthiness and it will enable one to retain the conventional swashplate for flight control purposes.* It should also be mentioned that this concept is not entirely new; over twenty years ago researchers at Kaman[28] used a servo flap on a controllable twist rotor (CTR) configuration to produce an external pitching moment to alter the elastic twist distribution of the blade. By cyclically varying the blade twist, they were able to achieve a 30% decrease in blade bending amplitudes, and a considerable increase in rotor performance, as represented by decreases in solidity and rotor power, and an increase in range.

The use of an actively controlled flap located on the blade to reduce vibrations in forward flight falls into the category of IBC since each aerodynamic surface is individually controlled in the rotating system. Such a configuration has the potential for reducing vibrations with much less power while retaining the versatility of conventional IBC, but without requiring the replacement of the conventional swashplate by a more complex mechanical system, and without adversely affecting the airworthiness.

The review of the literature clearly indicates that the use of an actively controlled, partial span, trailing edge flap to reduce helicopter vibrations has not been studied previously. Therefore, the first portion of this study represents a feasibility study of the proposed concept, while the second part deals with issues concerning the practical implementation of the new approach to vibration reduction.

It is expected that this research will have a significant influence on the field of vibration reduction in rotorcraft.

1.2 OBJECTIVES OF THE RESEARCH

The first objective of this study is the development of an aeroelastic analysis for the purposes of studying individual blade control (IBC) as implemented through an actively controlled trailing edge flap located on the blade. After the analysis had been developed, the ultimate goals of this research were addressed. These goals are described below.

Initially, a simple offset-hinged spring restrained rigid blade model is used to study the feasibility of this novel approach for reducing vibrations. The objectives of this first stage of the research are:

1. Study of the relative effectiveness of IBC when implemented through an active control surface to achieve vibration reduction in forward flight and its comparison with conventional IBC.
2. Compare the power required to implement the control for these two alternative approaches.
3. Examine several control algorithms and determine their effectiveness for reducing vibrations in steady forward flight.
4. Determine the influence of the blade torsional flexibility on the vibration reduction effectiveness and power requirements of the various control approaches.

Subsequently, after firmly establishing the feasibility and potential of the actively controlled flap, a more detailed study is carried out which focuses on the practical implementation of this new approach to reducing vibrations. The objectives of this second stage of the research are:

1. Implementation of the actively controlled partial span flap with a fully elastic, geometrically nonlinear, blade model in which the dynamics of the blade are represented by two torsional, two chordwise bending and three flapwise bending modes.
2. Examination of the importance of appropriately modeling the dynamic behavior of the blade by comparing results between the two different blade models.
3. Introduction of compressibility effects and hinge moment correction, which accounts approximately for the gap of the trailing edge flap, so that the aerodynamic loads on the blade and control flap are represented in a more realistic manner.

4. Trend studies of the effect on the vibration reduction potential of the actively controlled trailing edge flap when the following parameters are changed: (a) spanwise location and size of the control flap; (b) torsional stiffness of the blade and (c) the aerodynamic hinge moment correction factor.

In the final stage of this study, the results obtained in the frequency domain are validated in the time domain by direct numerical integration of the nonlinear equations of motion. The specific objectives of this last stage are:

1. Validation of the coupled trim and aeroelastic response solution obtained using the harmonic balance technique.
2. Validation of the optimal control solution obtained in the frequency domain.

It should be emphasized that this is the first study which contains a detailed treatment of an actively controlled flap for vibration reduction in helicopter rotors.

Chapter II

MODELING ASSUMPTIONS AND COORDINATE SYSTEMS

The modeling assumptions which serve as the starting point in the development of the aeroelastic analysis are summarized in this chapter. The orders of magnitude which are assigned, based on experience, to the various parameters appearing in the problem formulation are listed. Finally, the various coordinate systems, and related coordinate transformations, used to formulate the equations of motion are defined.

2.1 MODELING ASSUMPTIONS

(1) The hingeless blade is cantilevered at the hub with an offset e from the axis of rotation, as shown in Fig. 7.

(2) The blade feathering axis coincides with the elastic axis of the blade and is preconed by the angle β_p, which is depicted in Fig. 7. The blade has no torque offset, sweep or droop.

(3) The undeformed blade is straight with a general pretwist distribution $\theta_{pt}(x)$ built in about the elastic axis of the blade.

(4) The blade cross-section is assumed to be symmetrical with respect to its major principal axes in the formulation of the inertial loads but the effect of camber is accounted for in an approximate manner when formulating the aerodynamic loads. The blade cross-section has four distinct points: the elastic center, the aerodynamic center, the mass center, and the tension center (area centroid), as shown in Fig. 10.

(5) The blade chord c_b, mass per unit length m_b , and principal cross-sectional inertias I_{MB2} and I_{MB3}, are allowed to vary along the span of the blade.

(6) The blade has an aerodynamic surface, modeled as a partial span trailing edge flap (as shown in Figs. 2 and 3), with its centroid a distance x_c from the blade root. The control flap has a chord length c_{cs} and a span L_{cs}.

(7) The leading edge of the control surface is attached to the trailing edge of the blade by a series of hinges located at a finite number of discrete points along the control surface span. The axis of each hinge constrains the control flap cross-section to rotate only in the plane of the blade cross-section.

(8) At least one hinge is restrained in torsion about its axis by a spring representing the stiffness of the control system. The control flap actuator deflects the flap by the angle δ (positive down) relative to the blade chordline. This angle represents the control input for the purposes of vibration reduction.

(9) The control surface cross-section is assumed to be symmetrical with respect to its major principal axes and to have the same airfoil section as the blade. The control flap is assumed to have the same pretwist distribution as the blade.

(10) The control flap chord c_{cs}, mass per unit length m_c , and principal cross-sectional inertias I_{MC2} and I_{MC3}, are allowed to vary along its span.

(11) The blade is allowed to have fully coupled flap, lead-lag and torsional dynamics, undergoing moderate deflections and finite rotations. The blade is treated as inextensible.

(12) Two-dimensional quasisteady Greenberg theory, modified to include the effects of an aerodynamic surface, is used to obtain the distributed aerodynamic loads. The aerodynamic force and moment due to the control flap are scaled by $C_f \leq 1$, an empirical correction factor accounting for the presence of a control surface gap, which is not modeled in this study.

(13) Reverse flow is accounted for by setting the lift and moment to zero inside the reverse flow region, and by reversing the sign on the drag term.

(14) Compressibility effects are either neglected, or accounted for in an approximate manner using the Prandtl-Glauert correction factor. Dynamic stall and tip loss effects are neglected.

(15) Uniform inflow is assumed for convenience.

(16) The structural damping in the blade is assumed to be of a viscous type.

(17) The rotor shaft is assumed to be rigid and the rotor speed constant.

(18) Four identical blades are combined to represent a four-bladed, hingeless, fixed-hub rotor configuration in steady, level flight.

The various modeling assumptions listed above are used in the various stages of the problem formulation. Additional modeling assumptions, specific to a particular blade model, are discussed in Chapter 4 for the offset-hinged spring restrained blade model, and in Chapter 5 for the fully elastic blade model.

2.2 EXPLICIT FORMULATION USING A SYMBOLIC COMPUTING FACILITY

There are two distinct approaches commonly used to formulate the equations of motion of a helicopter rotor blade. The first approach is usually denoted as the explicit approach because it leads to a set of detailed aeroelastic equations of motion in which all of the terms (i.e. inertial, aerodynamic and structural) appear as explicit functions of the blade degrees of freedom. The second approach is usually denoted as the implicit approach. In this approach detailed expressions for the aeroelastic equations of motion are avoided. Instead the aerodynamic, inertial and structural loads are generated in matrix form inside the computer. When this approach is used the boundaries between the formulation phase and the solution phase become blurred.

Explicit formulations have some advantages over implicit formulations. Explicit formulations enable one to write out the equations of motion in detail. This allows one to inspect the equations and identify the various terms from a physical point of view, which facilitates the understanding of the equations. Furthermore, explicit equations derived by various researches can be compared, and any differences can be identified, clarified and understood. Thus a given formulation can be validated without having to resort to numerical computations of the blade response and stability.

Computationally, the numerical implementation of blade stability and response calculations based on explicit formulations can be more efficient than implicit formulations, requiring less computer time. This is due to the fact that in explicit formulations much of the algebra is carried out prior to any numerical computations. In addition, explicit ex-

pressions for the stability derivatives are available. Conversely, implicit formulations require the numerical approximation of the stability derivatives by the computer. Furthermore, the implicit approach frequently mandates iterative solutions.

Naturally, explicit formulations also have some disadvantages. The task of formulating explicit equations can be algebraically formidable and involve a large number of terms. For this reason explicit formulations generally require employing an ordering scheme to systematically neglect higher order terms in order to keep the equations to a manageable size[11]. Another disadvantage of explicit formulations is that a small change in the aeroelastic model might require the complete rederivation of the explicit equations. In an implicit formulation the loads are left in general form and are combined numerically, so the model may be changed without requiring substantial changes in the problem formulation.

Fortunately, substantial increases in computer power during the last decade, as represented by high computational speeds and the availability of large core memory at low cost, have facilitated the relegation of tedious algebraic tasks to the computer. Many symbolic manipulation programs exist which can be used to derive the equations of motion of the blade in explicit form. These equations can then be converted into FORTRAN code for inclusion into a computer analysis program. Since the algebraic tasks are relegated to a computer, it is fairly easy to retain as many terms as desired. Furthermore, the equations can easily be rederived by the computer to reflect any changes in the aeroelastic model.

In this study, explicit expressions for the distributed loads on the blade are derived using a special purpose symbolic computing facility consisting of a Symbolics 3650 dedicated LISP machine running the commercially available symbolic manipulation software package MACSYMA. The Symbolics machine is networked with a SUN 3/280 server on which the numerical computations are performed. The mathematical expressions generated by MACSYMA are ultimately expressed in a format suitable for their incorporation into the FORTRAN computer program executed on the SUN machine. The Symbolics/Sun combination, first used in Ref. 38 to formulate explicit helicopter rotor/flexible fuselage equations of motion, represents a powerful tool for deriving helicopter equations of motion.

The description of the application of MACSYMA, and its implementation on a Symbolics 3650 machine, to derive the equations of motion used in this study is presented in Appendix B. The symbolic manipulation procedure used in this study is very similar to the methodology used in Ref. 38. All equations and lengthy derivations presented in this study have been derived using the approach described in Appendix B.

At the time the explicit expressions were formulated in this study the Symbolics/Sun combination was required. This represented a limitation because such combinations were not readily or easily available. However, since then, versions of MACSYMA have become commercially available for Sun workstations and IBM PCs, thus allowing the symbolic manipulations and numerical computations to be performed on a single machine. Furthermore, the continuing trend toward faster computers with larger core memories has lead to substantial decreases in execution times of MACSYMA. For example, MACSYMA installed on a Sparcstation 10/41 runs five times faster than the speeds achieved on the special purpose dedicated symbolics machine.

2.3 ORDERING SCHEME

In the derivation of the equations of motion for an isolated blade a large number of higher order nonlinear terms must be considered. These terms arise due to the assumption of moderate blade deflections which introduces many geometric nonlinear terms in the expressions for the aerodynamic, inertial and structural forces and moments on the blade. These nonlinear terms must be retained for an accurate stability analysis. But the number of terms in the equations of motion of the blade can become too large if all of the nonlinear terms are retained.

Previous research[6,11,38] has demonstrated that the equations of motion may be kept to a manageable size while maintaining accuracy if an ordering scheme is used to systematically neglect the higher order terms. An ordering scheme consists of judiciously assigning orders of of magnitude to the various terms encountered in the equations of motion and then neglecting all terms of an order higher than some preselected order of

magnitude. The highest order of magnitude retained in the expressions determines the accuracy of the equations.

In this study the basis of the ordering scheme is a small dimensionless parameter ε which represents typical blade slopes due to elastic deformation. For helicopter blades ε is in the range

$$0.1 < \varepsilon < 0.2$$

The ordering scheme used in this study is based on the assumption that

$$1 + O(\varepsilon^2) \cong 1 \tag{2.1}$$

i.e., terms of the order of $O(\varepsilon^2)$ may be neglected in comparison with unity. This ordering scheme has been demonstrated[38,45,50,53] to yield equations of manageable size with sufficient numerical accuracy for stability and vibratory hub load calculations.

The majority of the parameters appearing in the equations of motion represent dimensional quantities; thus before orders of magnitude can be assigned, the various parameters must first be expressed in nondimensional form. This is accomplished using the following set of dimensional characteristic parameters:

[length] = R - rotor radius

[mass] = M_b - mass of one rotor blade

[time] = $\frac{1}{\Omega}$ - inverse of the rotor speed

The orders of magnitude assigned to the parameters appearing in the equations of motion are given next. The meaning of each of these parameters is defined in the list of symbols.

O(1): $\frac{x}{R}, \frac{L_b}{R}, \frac{m_b}{(M_b/R)}, \frac{\rho_A}{(M_b/R^3)}, \mu, \psi, \cos\psi, \sin\psi, a_o,$

$$R\frac{\partial}{\partial x},\ \frac{1}{\Omega}\frac{\partial}{\partial t},\ \frac{\partial}{\partial \psi}$$

$O(\varepsilon^{1/2})$: $\quad \frac{L_{cs}}{R},\ \theta_G,\ \delta$

$O(\varepsilon)$: $\quad \frac{c_b}{R},\ \frac{e}{R},\ \frac{c_{cs}}{R},\ \frac{m_c}{(M_b/R)},\ \frac{X_H}{R},\ \theta_{pt},\ \lambda,\ \alpha_R,\ \beta_p,$
$\frac{v}{R},\ \frac{w}{R},\ v_{,x},\ w_{,x},\ \phi$

$O(\varepsilon^{3/2})$: $\quad \frac{M_c}{M_b},\ \frac{X_A}{R},\ \frac{X_{Ib}}{R},\ \frac{X_{Ic}}{R},\ \frac{X_{IIb}}{R},\ \frac{X_{IIc}}{R},\ C_{do},\ C_{mo}$

$O(\varepsilon^{2})$: $\quad \frac{u}{R},\ \frac{EI_{\zeta\zeta}}{M_bR^3\Omega^2},\ \frac{EI_{\eta\eta}}{M_bR^3\Omega^2},\ \frac{fC_{df}}{R^2}$

$O(\varepsilon^{5/2})$: $\quad \frac{I_{MB2}}{M_bR},\ \frac{I_{MB3}}{M_bR}$

$O(\varepsilon^{3})$: $\quad \frac{g}{\Omega^2R},\ \frac{GJ_b}{M_bR^3\Omega^2}$

$O(\varepsilon^{7/2})$: $\quad \frac{I_{MC2}}{M_bR},\ \frac{I_{MC3}}{M_bR}$

The orders of magnitude assigned to the various parameters listed above are consistent with Refs. 38, 45, 50 and 53.

The systematic application of this ordering scheme in the derivation procedure yields a set of explicit nonlinear equations of motion of manageable size, and sufficient accuracy. The application of the ordering scheme in formulating the equations of motion using the symbolic manipulation program MACSYMA is described in detail in Appendix B. Note that the above ordering scheme is used with a certain degree of flexibility so as to enable the retention of certain higher order terms which may be important but appear negligible in light of the ordering scheme.

2.4 COORDINATE SYSTEMS

Before deriving the differential equations of motion of the isolated hingeless rotor blade, it is necessary to define the various coordinate systems used to define the position, velocity and acceleration of arbitrary points on the blade and control flap cross-section. All coordinate systems are rectangular, and are referenced by a number or letter. The "i" coordinate system is defined by the set of mutually orthogonal unit vectors denoted by $\hat{e}_{xi}$, $\hat{e}_{yi}$ and $\hat{e}_{zi}$, which lie along the x_i, y_i and z_i axes, respectively.

The following coordinate systems are needed to formulate the equations of motion:

(1) The "0" system is an inertial reference frame with its origin at the hub center O_H. The "0" system is oriented such that the gravitational vector is oriented along the negative z_0 axis (see Fig. 5).

(2) The "1" system is an inertial reference frame also with its origin located at O_H. However, the "1" system is pitched forward from the "0" system by the angle α_R such that the positive z_1 axis points upward along the rotor shaft (see Fig. 5). The angle α_R is the trim rotor angle of attack. The "1" system represents the nonrotating or "fixed" system.

(3) The "2" system also has its origin at the hub center O_H but rotates with the blade with an angular velocity Ω about the z_1 axis, which is coincident with the z_2 axis (see Fig. 6). The "2" system represents the rotating reference.

(4) The "3" system also rotates with the blade but has its origin at the blade root, located a distance e from the hub along the x_2 axis. Furthermore, the "3" system is preconed by the angle β_p clockwise about y_2 axis such that the x_3 axis is oriented along the undeformed elastic axis of the blade (see Fig. 7). The "3" system represents the undeformed reference frame used to define the undeformed position of the blade. The principal axes of the undeformed blade cross-section are rotated by the pitch angle $\theta_G(x)$ counter-clockwise about the x_3 axis, as shown in Fig. 9.

(5) The "S" system also has its origin at the blade root, rotates with the blade, and is oriented such that the x_S axis and the x_3 axis are coincident. However, the "S" system is rotated by the angle $R_C\theta_{Gr}$ about the x_S axis. The "S" system is used to define the orientation of torsional root springs used in the offset-hinged spring restrained blade model (see

Fig. 2). The parameter R_C is an elastic coupling parameter used to vary the coupling between the flap and lead-lag motions. The angle $\theta_{Gr} = \theta_G(x = 0)$ is the geometric pitch angle of the blade at the root.

(6) The "4" system is a blade attached coordinate system. Before deformation the "3" system and "4" system are parallel. The "4" system bends and twists with the blade such that the x_4 axis remains tangent to the deformed elastic axis at each point (see Fig. 8). Furthermore, the principal axes of the deformed blade cross-section are rotated by the pitch angle $\theta_G(x)$ about the x_4 axis, as shown in Fig. 9. The "4" system represents the deformed reference frame used to describe the position of the deformed blade.

(7) The "5" is also a blade attached coordinate system. The "5" system represents the "4" system with the torsional deformation removed (see Fig. 9) such that the principal axes of the deformed blade cross-section are rotated by the angle $\theta_G + \phi$, where ϕ is the elastic twist. This system is particularly convenient for deriving the distributed aerodynamic loads on the blade since the elastic pitching motion of the blade is explicitly represented in the "5" system. This is described in greater detail in the derivation of the aerodynamic loads in Chapter 3.

(8) The "C" system has its origin at the hinge point of the control flap, located a distance X_H behind the elastic axis. The "C" system rotates with control flap deflection δ such that the x_C axis remains parallel to the x_4 axis, and the y_C and z_C axes remain aligned with the principal axes of the control flap cross-section (see Fig. 11).

2.5 COORDINATE TRANSFORMATIONS

The coordinate transformations between the various coordinate systems listed above needed in the formulation of the equations of motion are defined in this section.

"0" system to the "1" system

The transformation matrix from the "0" to the "1" coordinate system is given by:

$$\begin{Bmatrix} \hat{e}_{x1} \\ \hat{e}_{y1} \\ \hat{e}_{z1} \end{Bmatrix} = \begin{bmatrix} \cos\alpha_R & 0 & \sin\alpha_R \\ 0 & 1 & 0 \\ -\sin\alpha_R & 0 & \cos\alpha_R \end{bmatrix} \begin{Bmatrix} \hat{e}_{x0} \\ \hat{e}_{y0} \\ \hat{e}_{z0} \end{Bmatrix} \tag{2.2}$$

where α_R is the trim rotor angle of attack.

The inverse transformation is given by:

$$\begin{Bmatrix} \hat{e}_{x0} \\ \hat{e}_{y0} \\ \hat{e}_{z0} \end{Bmatrix} = \begin{bmatrix} \cos\alpha_R & 0 & -\sin\alpha_R \\ 0 & 1 & 0 \\ \sin\alpha_R & 0 & \cos\alpha_R \end{bmatrix} \begin{Bmatrix} \hat{e}_{x1} \\ \hat{e}_{y1} \\ \hat{e}_{z1} \end{Bmatrix} \tag{2.3}$$

"1" system to the "2" system

The transformation matrix from the "1" to the "2" coordinate system is given by:

$$\begin{Bmatrix} \hat{e}_{x2} \\ \hat{e}_{y2} \\ \hat{e}_{z2} \end{Bmatrix} = \begin{bmatrix} \cos\psi & \sin\psi & 0 \\ -\sin\psi & \cos\psi & 0 \\ 0 & 0 & 1 \end{bmatrix} \begin{Bmatrix} \hat{e}_{x1} \\ \hat{e}_{y1} \\ \hat{e}_{z1} \end{Bmatrix} \tag{2.4}$$

The inverse transformation is given by:

$$\begin{Bmatrix} \hat{e}_{x1} \\ \hat{e}_{y1} \\ \hat{e}_{z1} \end{Bmatrix} = \begin{bmatrix} \cos\psi & -\sin\psi & 0 \\ \sin\psi & \cos\psi & 0 \\ 0 & 0 & 1 \end{bmatrix} \begin{Bmatrix} \hat{e}_{x2} \\ \hat{e}_{y2} \\ \hat{e}_{z2} \end{Bmatrix} \tag{2.5}$$

"2" system to the "3" system

The transformation matrix from the "2" system to the "3" system is given by:

$$\begin{Bmatrix} \hat{e}_{x3} \\ \hat{e}_{y3} \\ \hat{e}_{z3} \end{Bmatrix} = \begin{bmatrix} 1 & 0 & \beta_p \\ 0 & 1 & 0 \\ -\beta_p & 0 & 1 \end{bmatrix} \begin{Bmatrix} \hat{e}_{x2} \\ \hat{e}_{y2} \\ \hat{e}_{z2} \end{Bmatrix} \tag{2.6}$$

It has been assumed that the precone angle β_p is a small angle.

The inverse of the transformation represented by Eq. (2.6) is given by:

$$\begin{Bmatrix} \hat{e}_{x2} \\ \hat{e}_{y2} \\ \hat{e}_{z2} \end{Bmatrix} = \begin{bmatrix} 1 & 0 & -\beta_p \\ 0 & 1 & 0 \\ \beta_p & 0 & 1 \end{bmatrix} \begin{Bmatrix} \hat{e}_{x3} \\ \hat{e}_{y3} \\ \hat{e}_{z3} \end{Bmatrix} \tag{2.7}$$

"3" system to the "S" system

The coordinate transformation from the "3" to the "S" system is given by

$$\begin{Bmatrix} \hat{e}_{xS} \\ \hat{e}_{yS} \\ \hat{e}_{zS} \end{Bmatrix} = \begin{bmatrix} 1 & 0 & 0 \\ 0 & \cos(R_C\theta_{Gr}) & \sin(R_C\theta_{Gr}) \\ 0 & -\sin(R_C\theta_{Gr}) & \cos(R_C\theta_{Gr}) \end{bmatrix} \begin{Bmatrix} \hat{e}_{x3} \\ \hat{e}_{y3} \\ \hat{e}_{z3} \end{Bmatrix} \tag{2.8}$$

The inverse transformation is given by:

$$\begin{Bmatrix} \hat{e}_{x3} \\ \hat{e}_{y3} \\ \hat{e}_{z3} \end{Bmatrix} = \begin{bmatrix} 1 & 0 & 0 \\ 0 & \cos(R_C\theta_{Gr}) & -\sin(R_C\theta_{Gr}) \\ 0 & \sin(R_C\theta_{Gr}) & \cos(R_C\theta_{Gr}) \end{bmatrix} \begin{Bmatrix} \hat{e}_{xS} \\ \hat{e}_{yS} \\ \hat{e}_{zS} \end{Bmatrix} \tag{2.9}$$

"3" system to the "4" system

The "3" system is used to describe the orientation of the cross-section of the undeformed blade located a distance x along the elastic axis, while the "4" system is used to describe the orientation of the same cross-section after the blade's deformation, consisting of blade bending in two mutually perpendicular planes and twisting about the elastic axis. In this study the elastic deformation of the blade is described completely in terms of the lead-lag deflection v(x), the flap deflection w(x), and the elastic twist $\phi(x)$. Thus the transformation from the "3" system to the "4" system due to blade deformation can be described by a unique sequence of angular rotations involving: the elastic twist angle ϕ; the lead-lag blade bending slope $v_{,x}$; and the flap blade bending slope $w_{,x}$. The specific sequence of the rotations is important; the precise meaning of each of the three angles depends on the order in which they occur. Therefore a particular rotational sequence must be adopted and maintained in each stage of the formulation. The deformation sequence used in this study is flap-lag-torsion. The rotation of the blade cross-section due to blade bending and elastic twist is therefore described by: 1) a flap rotation by the angle $w_{,x}$

clockwise about the y_3 axis; 2) a lead-lag rotation by the angle $v_{,x}$ counter-clockwise about the z_3 axis which has undergone a rotation by the angle $w_{,x}$; and lastly 3) a torsional rotation by the twist angle ϕ counter-clockwise about the x_4 axis.

The transformation matrix associated with a rotation by the slope angle $w_{,x}$ counter-clockwise about the y_3 axis can be expressed as[46]

$$[T_{w_{,x}}] = \begin{bmatrix} 1 & 0 & w_{,x} \\ 0 & 1 & 0 \\ -w_{,x} & 0 & 1 \end{bmatrix} \tag{2.10}$$

when higher order terms are neglected.

The transformation matrix associated with a rotation by the slope angle $v_{,x}$ counter-clockwise about the z_3 axis can be expressed as[46]

$$[T_{v_{,x}}] = \begin{bmatrix} 1 & v_{,x} & 0 \\ -v_{,x} & 1 & 0 \\ 0 & 0 & 1 \end{bmatrix} \tag{2.11}$$

when higher order terms are neglected.

It should be noted that the small angle assumption has been used in the definition of the transformations associated with the slopes $v_{,x}$ and $w_{,x}$, i.e.

$$\cos v_{,x} \cong 1 + O(\varepsilon^2) \quad , \quad \cos w_{,x} \cong 1 + O(\varepsilon^2)$$

$$\sin v_{,x} \cong v_{,x} + O(\varepsilon^3) \quad , \quad \sin w_{,x} \cong w_{,x} + O(\varepsilon^3)$$

The above relations are consistent with the ordering scheme represented by Eq. (2.1).

The transformation matrix associated with a rotation by the angle ϕ counter-clockwise about the x_4 axis is given by

$$[T_\phi] = \begin{bmatrix} 1 & 0 & 0 \\ 0 & \cos\phi & \sin\phi \\ 0 & -\sin\phi & \cos\phi \end{bmatrix} \tag{2.12}$$

The small angle assumption is made for ϕ only when convenient.

For the deformation sequence flap-lag-torsion, the coordinate transformation from the "3" system to the "4" system is given by the matrix product

$$\begin{Bmatrix} \hat{e}_{x4} \\ \hat{e}_{y4} \\ \hat{e}_{z4} \end{Bmatrix} = [T_\phi][T_{v,x}][T_{w,x}] \begin{Bmatrix} \hat{e}_{x3} \\ \hat{e}_{y3} \\ \hat{e}_{z3} \end{Bmatrix}$$

where the transformation matrices $[T_\phi]$, $[T_{w,x}]$ and $[T_{v,x}]$ are defined by Eqs. (2.11) – (2.12). Performing the matrix multiplication yields:

$$\begin{Bmatrix} \hat{e}_{x4} \\ \hat{e}_{y4} \\ \hat{e}_{z4} \end{Bmatrix} = \begin{bmatrix} 1 & v_{,x} & w_{,x} \\ -v_{,x}\cos\phi - w_{,x}\sin\phi & \cos\phi & \sin\phi - v_{,x}w_{,x}\cos\phi \\ v_{,x}\sin\phi - w_{,x}\cos\phi & -\sin\phi & \cos\phi + v_{,x}w_{,x}\sin\phi \end{bmatrix} \begin{Bmatrix} \hat{e}_{x3} \\ \hat{e}_{y3} \\ \hat{e}_{z3} \end{Bmatrix} \tag{2.13}$$

The inverse transformation is given by:

$$\begin{Bmatrix} \hat{e}_{x3} \\ \hat{e}_{y3} \\ \hat{e}_{z3} \end{Bmatrix} = \begin{bmatrix} 1 & -v_{,x}\cos\phi - w_{,x}\sin\phi & v_{,x}\sin\phi - w_{,x}\cos\phi \\ v_{,x} & \cos\phi & -\sin\phi \\ w_{,x} & \sin\phi - v_{,x}w_{,x} & \cos\phi + v_{,x}w_{,x}\sin\phi \end{bmatrix} \begin{Bmatrix} \hat{e}_{x4} \\ \hat{e}_{y4} \\ \hat{e}_{z4} \end{Bmatrix} \tag{2.14}$$

"3" system to the "5" system

The "5" system represents the "4" system with the torsional rotation ϕ removed, therefore the transformation matrix from the "3" system to the "5" system is given by:

$$\begin{Bmatrix} \hat{e}_{x5} \\ \hat{e}_{y5} \\ \hat{e}_{z5} \end{Bmatrix} = [T_{v,x}][T_{w,x}] \begin{Bmatrix} \hat{e}_{x3} \\ \hat{e}_{y3} \\ \hat{e}_{z3} \end{Bmatrix}$$

Carrying out the matrix multiplication yields:

$$\begin{Bmatrix} \hat{e}_{x5} \\ \hat{e}_{y5} \\ \hat{e}_{z5} \end{Bmatrix} = \begin{bmatrix} 1 & v_{,x} & w_{,x} \\ -v_{,x} & 1 & -w_{,x}v_{,x} \\ -w_{,x} & 0 & 1 \end{bmatrix} \begin{Bmatrix} \hat{e}_{x3} \\ \hat{e}_{y3} \\ \hat{e}_{z3} \end{Bmatrix} \tag{2.15}$$

The inverse transformation is given by:

$$\begin{Bmatrix} \hat{e}_{x3} \\ \hat{e}_{y3} \\ \hat{e}_{z3} \end{Bmatrix} = \begin{bmatrix} 1 & -v_{,x} & -w_{,x} \\ v_{,x} & 1 & 0 \\ w_{,x} & -w_{,x}v_{,x} & 1 \end{bmatrix} \begin{Bmatrix} \hat{e}_{x5} \\ \hat{e}_{y5} \\ \hat{e}_{z5} \end{Bmatrix} \tag{2.16}$$

"4" system to the "5" system

Since the "5" system represents the "4" system with the torsional angle ϕ removed, the coordinate transformation from the "4" system to the "5" system is given by:

$$\begin{Bmatrix} \hat{e}_{x5} \\ \hat{e}_{y5} \\ \hat{e}_{z5} \end{Bmatrix} = \begin{bmatrix} 1 & 0 & 0 \\ 0 & \cos\phi & -\sin\phi \\ 0 & \sin\phi & \cos\phi \end{bmatrix} \begin{Bmatrix} \hat{e}_{x4} \\ \hat{e}_{y4} \\ \hat{e}_{z4} \end{Bmatrix} \tag{2.17}$$

The inverse transformation is given by:

$$\begin{Bmatrix} \hat{e}_{x4} \\ \hat{e}_{y4} \\ \hat{e}_{z4} \end{Bmatrix} = \begin{bmatrix} 1 & 0 & 0 \\ 0 & \cos\phi & \sin\phi \\ 0 & -\sin\phi & \cos\phi \end{bmatrix} \begin{Bmatrix} \hat{e}_{x5} \\ \hat{e}_{y5} \\ \hat{e}_{z5} \end{Bmatrix} \tag{2.18}$$

"4" system to the "C" system

The transformation from the "4" system to the "C" system is given by:

$$\begin{Bmatrix} \hat{e}_{xc} \\ \hat{e}_{yc} \\ \hat{e}_{zc} \end{Bmatrix} = \begin{bmatrix} 1 & 0 & 0 \\ 0 & \cos\delta & \sin\delta \\ 0 & -\sin\delta & \cos\delta \end{bmatrix} \begin{Bmatrix} \hat{e}_{x4} \\ \hat{e}_{y4} \\ \hat{e}_{z4} \end{Bmatrix} \tag{2.19}$$

The inverse transformation is given by:

$$\begin{Bmatrix} \hat{e}_{x4} \\ \hat{e}_{y4} \\ \hat{e}_{z4} \end{Bmatrix} = \begin{bmatrix} 1 & 0 & 0 \\ 0 & \cos\delta & -\sin\delta \\ 0 & \sin\delta & \cos\delta \end{bmatrix} \begin{Bmatrix} \hat{e}_{xc} \\ \hat{e}_{yc} \\ \hat{e}_{zc} \end{Bmatrix} \tag{2.20}$$

Chapter III

DISTRIBUTED LOADS ACTING ON THE BLADE

The distributed loads acting on the blade needed to formulate the equations of motion of the isolated blade are developed in this chapter. The inertial loads are obtained using D'Alembert's principle, and a modified version of Greenberg's[18] quasisteady aerodynamic theory, including the effects of a trailing edge flap, is used to calculate the aerodynamic loading. Gravitational loading is accounted for, and the structural damping is modeled as being of the viscous type.

To formulate explicit expressions for the distributed loads acting on the blade, the position, velocity and acceleration of an arbitrary point on the blade or control flap must be defined in terms of the blade degrees of freedom. Unfortunately, the modeling of the blade flexibility differs considerably between the two blade models used in this study; the fully elastic blade model is assumed to be flexible along the entire span, while the spring restrained rigid blade model is assumed to have all flexibility concentrated at the blade root. Thus the kinematic assumptions, and associated blade degrees of freedom, are different between the two blade models. The need to independently derive two separate sets of expressions for the blade loads can be avoided, however, by recognizing that the kinematics of the spring restrained blade model can be considered as a special case of the kinematics of the fully flexible blade. Therefore, only the distributed loads acting on the fully elastic blade model are formulated in this chapter. The procedure for obtaining the distributed loads on the spring restrained blade model from these expressions is described in detail in Chapter 4.

3.1 BLADE KINEMATICS

In this study, the Euler-Bernoulli assumption is used, which implies that during bending, plane cross-sections which are normal to the elastic axis before deformation, remain plane after deformation, and will be normal to the deformed axis. Furthermore, it is assumed that strains within the cross-section can be neglected. The Euler-Bernoulli hypothesis is considered to be a reasonable assumption when applied to a slender flexible beam made of a linearly elastic, isotropic material, such as the rotor blade modeled in this study. The assumption is certainly valid in the case of the spring restrained blade model, where the blade is modeled as rigid outboard of the blade root.

The location of an arbitrary point on the blade cross-section before deformation is described by the position vector

$$\vec{R}_p = e\,\hat{e}_{x2} + x\,\hat{e}_{x3} + y_0\,\hat{e}_{y3} + z_0\,\hat{e}_{z3}$$

It should be recalled that it is assumed that the blade is initially straight in its undeformed state. The coordinate pair (y_0, z_0) represent the coordinates of an arbitrary point on the cross-section of the undeformed blade relative to the elastic axis.

The Euler-Bernoulli hypothesis leads to the following expression for the position vector of the same point after deformation:

$$\vec{r}_p = e\,\hat{e}_{x2} + (x + u)\,\hat{e}_{x3} + v\,\hat{e}_{y3} + w\,\hat{e}_{z3} + y_0\,\hat{e}_{y4} + z_0\,\hat{e}_{z4} \tag{3.1}$$

where u, v, and w represent the displacement of a point on the elastic axis of the blade in the $\hat{e}_{x3}$ (axial), $\hat{e}_{y3}$ (lead-lag), and $\hat{e}_{z3}$ (flap) directions, respectively. An expression identical to Eq. (3.1) is used in Refs. 38, 43, and 53 to define the position of an arbitrary point on the deformed blade cross-section.

The coordinate transformation from the undeformed ("3" system) to the deformed ("4" system) reference frame has been defined in Chapter 2 by Eq. (2.13) for the deformation sequence flap-lag-torsion. In the following sections, the position vector defined by Eq. (3.1), together with the coordinate transformation given by Eq. (2.13), are used to formulate explicit expressions for the distributed inertial, gravitational, damping, and aerodynamic

loads on the blade. The evaluation of the distributed loads is separated into two components: (1) the loads which would act on the blade cross-section if there was no control flap; and (2) the loads due to the presence of a trailing edge flap. This decomposition is particularly convenient since the control flap extends over only a portion of the blade span, and facilitates the integration of the distributed loads along the span of the blade.

The expression "blade loads" is used to identify the loads acting on the blade cross-section without a control flap; and are denoted using the subscript "b". Similarly, the expression "control flap loads" is used to refer the contribution of the control flap, which are denoted by a "c" subscript. The two contributions are ultimately combined, and the sum is referred to as the "total loads" acting on the blade. The blade loads and the total loads are evaluated along the elastic axis of the deformed blade. The control flap loads are initially evaluated at the hinge axis, but are subsequently transferred to the elastic axis before combining them with the blade loads. The loads are ultimately expressed in the "3" system in which the equations of motion are formulated.

All of the expressions presented in this chapter, and throughout this study, have been formulated explicitly using the symbolic manipulation program MACSYMA, executed on a Symbolics 3650 dedicated LISP machine. A description of MACSYMA and its application to the formulation of the explicit expressions is presented in Appendix B. The ordering scheme given by Eq. (2.1) is employed to neglect higher order terms in order to keep the expressions from becoming too large. However, the ordering scheme is used with a certain degree of flexibility so as to enable the retention of certain higher order terms which may be important but appear negligible in light of the ordering scheme.

3.2 INERTIAL LOADS

D'Alembert's principle is used to obtain the inertial force and moment per unit volume from the absolute acceleration of an arbitrary point on the blade or control flap cross-section. The loads per unit volume are subsequently integrated over the cross-sectional area to yield the inertial loads per unit span.

From classical dynamics, the absolute acceleration of a point in a reference frame which is both translating and rotating relative to an inertial reference frame is given[19] by

$$\vec{a} = \ddot{\vec{R}}_0 + \ddot{\vec{r}} + 2\vec{\omega} \times \dot{\vec{r}} + \dot{\vec{\omega}} \times \vec{r} + \vec{\omega} \times (\vec{\omega} \times \vec{r}) \tag{3.2}$$

where $\vec{R}_0$ is the position vector of the origin of the moving reference frame relative to the inertial reference frame, $\vec{r}$ is the position vector of an arbitrary point relative to the moving reference frame, and $\vec{\omega}$ is the angular velocity of the moving reference frame relative to the inertial reference frame. The time derivatives of $\vec{R}_0$ are taken in the inertial reference frame and its second time derivative represents the acceleration of the origin of the moving reference frame relative to the inertial reference frame. The time derivatives of $\vec{r}$ are taken in the moving reference frame and its first and second time derivatives represent the velocity and acceleration, respectively, of the point in the moving reference frame.

In the present analysis, the "1" system with its origin at the center of the fixed hub represents the inertial reference frame; and the "2" system which is also centered at the hub, but rotating with the blade about the z_1 axis (as shown in Fig. 6), represents the moving reference frame. Since the origins of the "1" and the "2" systems are coincident, there is no translational motion of the "2" system relative to the "1" system; consequently

$$\vec{R}_0 = \dot{\vec{R}}_0 = \ddot{\vec{R}}_0 = \vec{0} \tag{3.3}$$

The angular velocity in Eq. (3.2) can be identified as the angular velocity of the "2" system about the z_1 axis given by

$$\vec{\omega} = \Omega \hat{e}_{z1} = \Omega \hat{e}_{z2} \tag{3.4}$$

where Ω is the rotational velocity of the rotor shaft. It is assumed that the rotor speed is constant and the rotor shaft is rigid; therefore

$$\dot{\vec{\omega}} = \vec{0} \tag{3.5}$$

Defining $\vec{r}_p$ as the position vector of an arbitrary point in the rotating frame ("2" system), and substituting Eqs. (3.3)-(3.5) into Eq. (3.2), yields the following expression for the absolute acceleration of the point:

$$\vec{a}_p = \ddot{\vec{r}}_p + 2\Omega\hat{e}_{z2} \times \dot{\vec{r}}_p + \Omega\hat{e}_{z2} \times (\Omega\hat{e}_{z2} \times \vec{r}_p) \tag{3.6}$$

Expressing $\vec{r}_p$ in the "2" system as

$$\vec{r}_p = r_{px2}\,\hat{e}_{x2} + r_{py2}\,\hat{e}_{y2} + r_{pz2}\,\hat{e}_{z2}$$

then substituting it into Eq. (3.6), carrying out the cross-products, and collecting the various terms into x, y and z components, yields:

$$\vec{a}_p = a_{px2}\,\hat{e}_{x2} + a_{py2}\,\hat{e}_{y2} + a_{pz2}\,\hat{e}_{z2}$$

where

$$a_{px2} = \ddot{r}_{px2} - 2\Omega\dot{r}_{py2} - \Omega^2 r_{px2} \tag{3.7a}$$

$$a_{py2} = \ddot{r}_{py2} + 2\Omega\dot{r}_{px2} - \Omega^2 r_{py2} \tag{3.7b}$$

$$a_{pz2} = \ddot{r}_{pz2} \tag{3.7c}$$

where the time derivatives of $\vec{r}_p$ are taken in the "2" system.

Equations (3.7) are used in the following two sections to formulate the distributed inertial loads acting on the blade and control surface cross-sections using D'Alembert's principle.

3.2.1 *Inertial Loads on the Blade*

The derivation of the inertial loads acting on the blade presented below is very similar to those of Refs. 38, 45, and 47. The position vector of an arbitrary point on the cross-section of the deformed blade can be defined using Eq. (3.1) as:

$$\vec{r}_b = e\,\hat{e}_{x2} + (x+u)\,\hat{e}_{x3} + v\,\hat{e}_{y3} + w\,\hat{e}_{z3} + y_{0b}\,\hat{e}_{y4} + z_{0b}\,\hat{e}_{z4} \tag{3.8}$$

where the subscript "b" has been used to indicate a point on the blade cross-section. The coordinate pair (y_{0b}, z_{0b}) represents the coordinates of a point on the blade cross-section relative to the elastic axis, and can be expressed in terms of the principal coordinates of the blade cross-section (η_b, ζ_b) as follows (see Fig. 9)

$$y_{0b} = \eta_b \cos\theta_G - \zeta_b \sin\theta_G \tag{3.9a}$$

$$z_{0b} = \zeta_b \cos\theta_G + \eta_b \sin\theta_G \tag{3.9b}$$

where θ_G represents the total geometric pitch angle of the blade.

To obtain the absolute acceleration it is necessary to take the time derivatives of $\vec{r}_b$ in the "2" system. This is facilitated by expressing $\vec{r}_b$ entirely in the "2" system:

$$\vec{r}_b = r_{bx2}\,\hat{e}_{x2} + r_{by2}\,\hat{e}_{y2} + r_{bz2}\,\hat{e}_{z2}$$

Transforming the unit vectors in Eq. (3.8) to the "2" system using the coordinate transformations defined Chapter 2, and collecting the x, y and z components yields:

$$r_{bx2} = (x+u+e) - w\beta_p - \bar{y}_{0b}v_{,x} - \bar{z}_{0b}(w_{,x} + \beta_p) \tag{3.10a}$$

$$r_{by2} = v + \bar{y}_{0b} \tag{3.10b}$$

$$r_{bz2} = w + (x+u)\beta_p - \bar{y}_{0b}(w_{,x} + \beta_p)v_{,x} + \bar{z}_{0b} \tag{3.10c}$$

where, for convenience, the following quantities have been defined:

$$\bar{y}_{0b} = y_{0b}\cos\phi - z_{0b}\sin\phi \tag{3.11a}$$

$$\bar{z}_{0b} = y_{0b}\sin\phi + z_{0b}\cos\phi \tag{3.11b}$$

The pair $(\bar{y}_{0b}, \bar{z}_{0b})$ can be interpreted as the coordinate pair (y_{0b}, z_{0b}) expressed in the "5" coordinate system, i.e.

$$y_{0b}\,\hat{e}_{y4} + z_{0b}\,\hat{e}_{z4} = \bar{y}_{0b}\,\hat{e}_{y5} + \bar{z}_{0b}\,\hat{e}_{z5} \tag{3.12}$$

Using Eqs. (3.9) and (3.11), the pair $(\bar{y}_{0b}, \bar{z}_{0b})$ can be expressed in terms of the principal coordinates of the blade cross-section

$$\bar{y}_{0b} = \eta_b \cos(\theta_G + \phi) - \zeta_b \sin(\theta_G + \phi) \tag{3.13a}$$

$$\bar{z}_{0b} = \zeta_b \cos(\theta_G + \phi) + \eta_b \sin(\theta_G + \phi) \tag{3.13b}$$

The first time derivative of $\vec{r}_b$ in the "2" system can be expressed as:

$$\vec{r}_b = \dot{r}_{bx2}\,\hat{e}_{x2} + \dot{r}_{by2}\,\hat{e}_{y2} + \dot{r}_{bz2}\,\hat{e}_{z2}$$

where

$$\dot{r}_{bx2} = \dot{u} - \dot{w}\beta_p - \bar{y}_{0b}[\dot{v}_{,x} + (\dot{\theta}_G + \dot{\phi})(w_{,x} + \beta_p)]$$

$$+ \bar{z}_{0b}[(\dot{\theta}_G + \dot{\phi})v_{,x} - \dot{w}_{,x}] \tag{3.14a}$$

$$\dot{r}_{by2} = \dot{v} - \bar{z}_{0b}(\dot{\theta}_G + \dot{\phi}) \tag{3.14b}$$

$$\dot{r}_{bz2} = \dot{w} + \dot{u}\beta_p + \bar{y}_{0b}[(\dot{\theta}_G + \dot{\phi}) - (w_{,x} + \beta_p)\dot{v}_{,x} - \dot{w}_{,x}v_{,x}]$$

$$+ \bar{z}_{0b}(\dot{\theta}_G + \dot{\phi})(w_{,x} + \beta_p)v_{,x} \tag{3.14c}$$

which were obtained by taking the time derivative of Eqs. (3.10), and using the following relations:

$$\dot{\bar{y}}_{0b} = -\bar{z}_{0b}(\dot{\theta}_G + \dot{\phi}) \tag{3.15a}$$

$$\dot{\bar{z}}_{0b} = \bar{y}_{0b}(\dot{\theta}_G + \dot{\phi}) \tag{3.15b}$$

The previous expressions follow directly from Eqs. (3.13).

The second time derivative of $\vec{r}_b$ in the "2" system can be expressed as

$$\ddot{\vec{r}}_b = \ddot{r}_{bx2}\hat{e}_{x2} + \ddot{r}_{by2}\hat{e}_{y2} + \ddot{r}_{bz2}\hat{e}_{z2}$$

where

$$\ddot{r}_{bx2} = \ddot{u} - \ddot{w}\beta_p$$

$$+ \bar{y}_{0b}[(\dot{\theta}_G + \dot{\phi})^2 v_{,x} - \ddot{v}_{,x} - 2(\dot{\theta}_G + \dot{\phi})\dot{w}_{,x} - (\ddot{\theta}_G + \ddot{\phi})(w_{,x} + \beta_p)]$$

$$+ \bar{z}_{0b}[(\dot{\theta}_G + \dot{\phi})^2(w_{,x} + \beta_p) - \ddot{w}_{,x} + 2(\dot{\theta}_G + \dot{\phi})\dot{v}_{,x} + (\ddot{\theta}_G + \ddot{\phi})v_{,x}] \qquad (3.16a)$$

$$\ddot{r}_{by2} = \ddot{v} - \bar{y}_{0b}(\dot{\theta}_G + \dot{\phi})^2 - \bar{z}_{0b}(\ddot{\theta}_G + \ddot{\phi}) \qquad (3.16b)$$

$$\ddot{r}_{bz2} = \ddot{w} + \ddot{u}\beta_p$$

$$+ \bar{y}_{0b}[-(w_{,x} + \beta_p)\ddot{v}_{,x} - 2\dot{w}_{,x}\dot{v}_{,x} - \ddot{w}_{,x}v_{,x} + (\dot{\theta}_G + \dot{\phi})^2(w_{,x} + \beta_p)v_{,x}$$

$$+ (\ddot{\theta}_G + \ddot{\phi})]$$

$$+ \bar{z}_{0b}[2(\dot{\theta}_G + \dot{\phi})(w_{,x} + \beta_p)\dot{v}_{,x} + 2(\dot{\theta}_G + \dot{\phi})\dot{w}_{,x}v_{,x} - (\dot{\theta}_G + \dot{\phi})^2$$

$$+ (\ddot{\theta}_G + \ddot{\phi})(w_{,x} + \beta_p)v_{,x}] \qquad (3.16c)$$

which were obtained by taking the time derivative of Eqs. (3.14), and again making use of Eqs. (3.15).

The absolute acceleration of an arbitrary point on the cross-section of the deformed blade can be expressed in the "2" system as

$$\vec{a}_b = a_{bx2}\hat{e}_{x2} + a_{by2}\hat{e}_{y2} + a_{bz2}\hat{e}_{z2}$$

Substituting Eqs. (3.10), (3.14) and (3.16) into Eqs. (3.7) yields:

$$a_{bx2} = \ddot{u} - \ddot{w}\beta_p - 2\Omega\dot{v} - \Omega^2[(x + e + u) - w\beta_p]$$

$$+ \bar{y}_{0b}[-(w_{,x} + \beta_p)\ddot{v}_{,x} - 2\dot{w}_{,x}\dot{v}_{,x} - \ddot{w}_{,x}v_{,x} + (\dot{\theta}_G + \dot{\phi})^2(w_{,x} + \beta_p)v_{,x}$$

$$+ (\ddot{\theta}_G + \ddot{\phi}) + \Omega^2 v_{,x}]$$

$$+ \bar{z}_{0b}[(\dot{\theta}_G + \dot{\phi})^2(w_{,x} + \beta_p) - \ddot{w}_{,x} + 2(\dot{\theta}_G + \dot{\phi})\dot{v}_{,x} + (\ddot{\theta}_G + \ddot{\phi})v_{,x}$$

$$+ 2\Omega(\dot{\theta}_G + \dot{\phi}) + \Omega^2(w_{,x} + \beta_p)] \tag{3.17a}$$

$$a_{by2} = \ddot{v} + 2\Omega(\dot{u} - \dot{w}\beta_p) - \Omega^2 v$$

$$- \bar{y}_{0b}[(\dot{\theta}_G + \dot{\phi})^2 + 2\Omega\dot{v}_{,x} + 2\Omega(\dot{\theta}_G + \dot{\phi})(w_{,x} + \beta_p) + \Omega^2]$$

$$- \bar{z}_{0b}[(\ddot{\theta}_G + \ddot{\phi}) - 2\Omega(\dot{\theta}_G + \dot{\phi})v_{,x} + 2\Omega\dot{w}_{,x}] \tag{3.17b}$$

$$a_{bz2} = \ddot{w} + \ddot{u}\beta_p$$

$$+ \bar{y}_{0b}[-(w_{,x} + \beta_p)\ddot{v}_{,x} - 2\dot{w}_{,x}\dot{v}_{,x} - \ddot{w}_{,x}v_{,x} + (\dot{\theta}_G + \dot{\phi})^2(w_{,x} + \beta_p)v_{,x}$$

$$+ (\ddot{\theta}_G + \ddot{\phi})]$$

$$+ \bar{z}_{0b}[2(\dot{\theta}_G + \dot{\phi})(w_{,x} + \beta_p)\dot{v}_{,x} + 2(\dot{\theta}_G + \dot{\phi})\dot{w}_{,x}v_{,x} - (\dot{\theta}_G + \dot{\phi})^2$$

$$+ (\ddot{\theta}_G + \ddot{\phi})(w_{,x} + \beta_p)v_{,x}] \tag{3.17c}$$

The distributed inertial loads on the blade are formulated using D'Alembert's principle; the inertial force and moment per unit volume acting on the blade cross-section are integrated over the blade cross-section to obtained the inertial force and moment per unit span acting on the blade. However, before proceeding it is convenient to define certain cross-sectional integrals involving the principal coordinates of the blade cross-section. These integrals are defined as follows:

$$\int_{A_b} \rho_b \eta_b \, dA = m_b X_{Ib} \tag{3.18a}$$

$$\int_{A_b} \rho_b \zeta_b \, dA = 0 \tag{3.18b}$$

$$\int_{A_b} \rho_b \eta_b^2 \, dA = I_{MB3} \tag{3.18c}$$

$$\int_{A_b} \rho_b \zeta_b^2 \, dA = I_{MB2} \tag{3.18d}$$

$$\int_{A_b} \rho_b \eta_b \zeta_b \, dA = 0 \tag{3.18.e}$$

where Eqs. (3.18b) and (3.18e) result from the assumption of a symmetric blade cross-section. The quantity X_{lb} represents the offset of the blade cross-sectional center of mass from the elastic axis and the pair I_{MB2} and I_{MB3} represent the principal mass moments of inertia of the blade cross-section.

The distributed inertial force acting on the blade is obtained by integrating the inertial force per unit volume over the blade cross-section:

$$\vec{p}_{lb} = -\int_{A_b} \rho_b \vec{a}_b \, dA \tag{3.19}$$

which can be expressed in the "2" system as

$$\vec{p}_{lb} = p_{lbx2}\,\hat{e}_{x2} + p_{lby2}\,\hat{e}_{y2} + p_{lbz2}\,\hat{e}_{z2}$$

Evaluating each component of Eq. (3.19) using Eqs. (3.17) yields:

$$p_{lbx2} = -\int_{A_b} \rho_b a_{bx2} \, dA$$

$$= m_b\Omega^2(x + e) + 2m_b\Omega\dot{v} + m_b\beta_p(\ddot{w} - w\Omega^2) + m_b(u\Omega^2 - \ddot{u})$$

$$- 2m_b X_{lb} \sin(\theta_G + \phi)\Omega(\dot{\theta}_G + \dot{\phi}) \tag{3.20a}$$

$$p_{lby2} = -\int_{A_b} \rho_b a_{by2} \, dA$$

$$= 2m_b\Omega\dot{w}\beta_p + m_b(v\Omega^2 - \ddot{v}) - 2m_b\Omega\dot{u}$$

$$+ m_b X_{lb}\cos(\theta_G + \phi)[\Omega(\Omega + 2\dot{v}_{,x}) + (\dot{\theta}_G + \dot{\phi})^2 + 2\Omega(\dot{\theta}_G + \dot{\phi})(w_{,x} + \beta_p)]$$

$$+ m_b X_{lb}\sin(\theta_G + \phi)[(\ddot{\theta}_G + \ddot{\phi}) + 2\Omega\dot{w}_{,x} - 2\Omega(\dot{\theta}_G + \dot{\phi})v_{,x}] \qquad (3.20b)$$

$$p_{lbz2} = -\int_{A_b} \rho_b a_{bz2}\, dA$$

$$= -m_b\ddot{u}\beta_p - m_b\ddot{w}$$

$$+ m_b X_{lb}\cos(\theta_G + \phi)[\ddot{v}_{,x}(w_{,x} + \beta_p) + 2\dot{w}_{,x}\dot{v}_{,x} + \ddot{w}_{,x}v_{,x} - (\ddot{\theta}_G + \ddot{\phi})]$$

$$+ m_b X_{lb}\sin(\theta_G + \phi)[(\dot{\theta}_G + \dot{\phi})^2 - (\ddot{\theta}_G + \ddot{\phi})(w_{,x} + \beta_p)v_{,x}] \qquad (3.20c)$$

The following integral definitions have been used in the integrations over the blade cross-section:

$$\int_{A_b} \rho_b\, dA = m_b \qquad (3.21a)$$

$$\int_{A_b} \rho_b \bar{y}_{0b}\, dA = m_b X_{lb}\cos(\theta_G + \phi) \qquad (3.21b)$$

$$\int_{A_b} \rho_b \bar{z}_{0b}\, dA = m_b X_{lb}\sin(\theta_G + \phi) \qquad (3.21c)$$

The first integral represents the mass per unit span of the blade and the last two integrals follow from Eqs. (3.13) and (3.18).

The distributed inertial moment acting on the blade is obtained by integrating the inertial moment per unit volume over the blade cross-section:

$$\vec{q}_{lb} = -\int_{A_b} (\bar{y}_{0b}\hat{e}_{y5} + \bar{z}_{0b}\hat{e}_{z5}) \times \rho_b\vec{a}_b\, dA \qquad (3.22)$$

which can be expressed in the "2" system as:

$$\vec{q}_{Ib} = q_{Ibx2}\,\hat{e}_{x2} + q_{Iby2}\,\hat{e}_{y2} + q_{Ibz2}\,\hat{e}_{z2}$$

Transforming the unit vectors in Eq. (3.22) to the "2" system using the coordinate transformations defined in Chapter 2, carrying out the cross-product and collecting the various x, y and z components yields:

$$q_{Ibx2} = -\int_{A_b} \rho_b\{\bar{y}_{0b}[a_{bz2} + (w_{,x} + \beta_p)v_{,x}a_{by2}] - \bar{z}_{0b}a_{by2}\}\,dA$$

$$q_{Iby2} = -\int_{A_b} \rho_b\{\bar{y}_{0b}[a_{bz2} - (w_{,x} + \beta_p)a_{bx2}]v_{,x}$$

$$+ \bar{z}_{0b}[(w_{,x} + \beta_p)a_{bz2} + a_{bx2}]\}\,dA$$

$$q_{Ibz2} = -\int_{A_b} \rho_b[-\bar{y}_{0b}(v_{,x}a_{by2} + a_{bx2}) - \bar{z}_{0b}(w_{,x} + \beta_p)a_{by2}]\,dA$$

Substituting Eqs. (3.17) into the previous expressions and performing the integrations over the blade cross-section yields:

$$\begin{aligned}
q_{Ibx2} = {} & m_b X_{Ib}\cos(\theta_G + \phi)[(v\Omega^2 - \ddot{v})(w_{,x} + \beta_p)v_{,x} - \ddot{w} - \ddot{u}\beta_p] \\
& + m_b X_{Ib}\sin(\theta_G + \phi)[(\ddot{v} - v\Omega^2) + 2\Omega\dot{u} - 2\Omega\dot{w}\beta_p] \\
& - (I_{MB2} + I_{MB3})(\ddot{\theta}_G + \ddot{\phi}) \\
& + (I_{MB2} - I_{MB3})\cos(\theta_G + \phi)\sin(\theta_G + \phi)\Omega[(\Omega + 2\dot{v}_{,x}) \\
& \quad + 2(\dot{\theta}_G + \dot{\phi})(w_{,x} + \beta_p)] \\
& + 2[I_{MB2}\cos^2(\theta_G + \phi) + I_{MB3}\sin^2(\theta_G + \phi)]\Omega[(\dot{\theta}_G + \dot{\phi})v_{,x} - \dot{w}_{,x}] \\
& + [I_{MB2}\sin^2(\theta_G + \phi) + I_{MB3}\cos^2(\theta_G + \phi)][2\dot{v}_{,x}\dot{w}_{,x} + v_{,x}\ddot{w}_{,x} \\
& \quad + (w_{,x} + \beta_p)(\Omega^2 v_{,x} + \ddot{v}_{,x})]
\end{aligned} \tag{3.23a}$$

$$q_{lby2} = -m_b X_{lb}\cos(\theta_G+\phi)[\Omega^2 x(w_{,x}+\beta_p)+\ddot{w}]v_{,x}$$

$$+ m_b X_{lb}\sin(\theta_G+\phi)[\Omega^2(x+e)-(\Omega^2 w\beta_p+\ddot{w}w_{,x})+2\Omega\dot{v}+(u\Omega^2-\ddot{u})]$$

$$-(I_{MB2}+I_{MB3})(\ddot{\theta}_G+\ddot{\phi})v_{,x}$$

$$+(I_{MB2}-I_{MB3})\cos(\theta_G+\phi)\sin(\theta_G+\phi)[(v_{,x}\Omega^2-\ddot{v}_{,x})-2(\dot{\theta}_G+\dot{\phi})\dot{w}_{,x}]$$

$$+[I_{MB2}\cos^2(\theta_G+\phi)+I_{MB3}\sin^2(\theta_G+\phi)][\ddot{w}_{,x}-\Omega^2(w_{,x}+\beta_p)$$

$$-2(\dot{\theta}_G+\dot{\phi})(\Omega+\dot{v}_{,x})] \tag{3.23b}$$

$$q_{lbz2} = m_b X_{lb}\cos(\theta_G+\phi)[-\Omega^2(x+e)-2\Omega\dot{v}+(\ddot{u}-u\Omega^2)$$

$$+(w\Omega^2-\ddot{w})\beta_p+(\ddot{v}-v\Omega^2)v_{,x}]$$

$$+ m_b X_{lb}\sin(\theta_G+\phi)(\ddot{v}-v\Omega^2)(w_{,x}+\beta_p)$$

$$-(I_{MB2}+I_{MB3})(\ddot{\theta}_G+\ddot{\phi})(w_{,x}+\beta_p)$$

$$+(I_{MB2}-I_{MB3})\cos(\theta_G+\phi)\sin(\theta_G+\phi)[\ddot{w}_{,x}-2(\dot{\theta}_G+\dot{\phi})(\Omega+\dot{v}_{,x})]$$

$$-[I_{MB2}\sin^2(\theta_G+\phi)+I_{MB3}\cos^2(\theta_G+\phi)][\ddot{v}_{,x}+2(\dot{\theta}_G+\dot{\phi})\dot{w}_{,x}] \tag{3.23c}$$

The following integral definitions, in addition to those represented by Eqs. (3.21), have been used in the integrations over the blade cross-section:

$$\int_{A_b}\rho_b\,\bar{y}_{0b}^2\,dA = I_{MB2}\sin^2(\theta_G+\phi)+I_{MB3}\cos^2(\theta_G+\phi) \tag{3.24a}$$

$$\int_{A_b}\rho_b\,\bar{z}_{0b}^2\,dA = I_{MB2}\cos^2(\theta_G+\phi)+I_{MB3}\sin^2(\theta_G+\phi) \tag{3.24b}$$

$$\int_{A_b}\rho_b\,\bar{y}_{0b}\,\bar{z}_{0b}\,dA = (I_{MB3}-I_{MB2})\cos(\theta_G+\phi)\sin(\theta_G+\phi) \tag{3.24c}$$

The above integrals follow from Eqs. (3.13) and (3.18) .

Transforming the distributed inertial force to the "3" system, in which the equations of motion are formulated, using the coordinate transformation defined in Chapter 2 yields

$$\vec{p}_{Ib} = p_{Ibx3}\hat{e}_{x3} + p_{Iby3}\hat{e}_{y3} + p_{Ibz3}\hat{e}_{z3}$$

where

$$p_{Ibx3} = p_{Ibx2} + \beta_p p_{Ibz2} \tag{3.25a}$$

$$p_{Iby3} = p_{Iby2} \tag{3.25b}$$

$$p_{Ibz3} = -\beta_p p_{Ibx2} + p_{Ibz2} \tag{3.25c}$$

Similarly, the distributed inertial moment acting on the blade can be expressed in the "3" system as:

$$\vec{q}_{Ib} = q_{Ibx3}\hat{e}_{x3} + q_{Iby3}\hat{e}_{y3} + q_{Ibz3}\hat{e}_{z3}$$

where

$$q_{Ibx3} = q_{Ibx2} + \beta_p q_{Ibz2} \tag{3.26a}$$

$$q_{Iby3} = q_{Iby2} \tag{3.26b}$$

$$q_{Ibz3} = -\beta_p q_{Ibx2} + q_{Ibz2} \tag{3.26c}$$

3.2.2 *Inertial Loads on the Control Surface*

The distributed inertial force and moment on the control surface is obtained using D'Alembert's principle in a manner similar to that used in calculating the distributed inertial loads on the blade. The coordinates of an arbitrary point on the control flap cross-section, relative to the elastic axis, can be expressed as (see Fig. 9)

$$y_0 = y_H + y_{0c} \tag{3.27a}$$

$$z_0 = z_H + z_{0c} \tag{3.27b}$$

where

$$y_H = -X_H \cos\theta_G \tag{3.28a}$$

$$z_H = -X_H \sin\theta_G \tag{3.28b}$$

represent the coordinates of the hinge point on the blade cross-section relative to the elastic axis. The quantity X_H represents the offset between the control surface hinge point and the elastic axis, and is defined as positive behind the elastic axis. The pair (y_{0c}, z_{0c}) represents the coordinates of an arbitrary point on the control flap cross-section relative to the "C" system, which is parallel to the "4" system but has its origin at the hinge point. The coordinate pair can be expressed in terms of the principal coordinates of the control surface cross-section (η_c, ζ_c) as follows (see Fig. 11)

$$y_{0c} = \eta_c \cos(\theta_G + \delta) - \zeta_c \sin(\theta_G + \delta) \tag{3.29a}$$

$$z_{0c} = \zeta_c \cos(\theta_G + \delta) + \eta_c \sin(\theta_G + \delta) \tag{3.29b}$$

where δ is the deflection angle of the control surface relative to the blade chord. It should be noted that the origin of the principal coordinates of the control surface (η_c, ζ_c) is located at the control surface hinge point.

Substituting Eqs. (3.27) into Eq. (3.1) yields the position vector of an arbitrary point on the control flap cross-section

$$\vec{r}_c = e\,\hat{e}_{x2} + (x+u)\,\hat{e}_{x3} + v\,\hat{e}_{y3} + w\,\hat{e}_{z3}$$

$$+ (y_H + y_{0c})\,\hat{e}_{y4} + (z_H + z_{0c})\,\hat{e}_{z4} \tag{3.30}$$

which can be expressed in the "2" system in the form:

$$\vec{r}_c = r_{cx2}\,\hat{e}_{x2} + r_{cy2}\,\hat{e}_{y2} + r_{cz2}\,\hat{e}_{z2}$$

Transforming the unit vectors in Eq. (3.30) to the "2" system using the coordinate transformations defined in Chapter 2 and collecting the terms into x, y and z components yields:

$$r_{cx2} = (x + e + u) - w\beta_p - (\bar{y}_H + \bar{y}_{0c})v_{,x} - (\bar{z}_H + \bar{z}_{0c})(w_{,x} + \beta_p) \tag{3.31a}$$

$$r_{yc2} = v + \bar{y}_H + \bar{y}_{0c} \tag{3.31b}$$

$$r_{cz2} = (x + u)\beta_p + w - (\bar{y}_H + \bar{y}_{0c})(w_{,x} + \beta_p)v_{,x} + \bar{z}_H + \bar{z}_{0c} \tag{3.31c}$$

where for convenience the following quantities have been defined:

$$\bar{y}_H = y_H \cos\phi - z_H \sin\phi = -X_H \cos(\theta_G + \phi) \tag{3.32a}$$

$$\bar{z}_H = y_H \sin\phi + z_H \cos\phi = -X_H \sin(\theta_G + \phi) \tag{3.32b}$$

$$\bar{y}_{0c} = y_{0c} \cos\phi - z_{0c} \sin\phi \tag{3.33a}$$

$$\bar{z}_{0c} = y_{0c} \sin\phi + z_{0c} \cos\phi \tag{3.33b}$$

The pair $(\bar{y}_{0c}, \bar{z}_{0c})$ can be interpreted as the coordinate pair (y_{0c}, z_{0c}) expressed in the "5" system, i.e.

$$y_{0c}\hat{e}_{y4} + z_{0c}\hat{e}_{z4} = \bar{y}_{0c}\hat{e}_{y5} + \bar{z}_{0c}\hat{e}_{z5} \tag{3.34}$$

Making use of Eqs. (3.29), the coordinate pair $(\bar{y}_{0c}, \bar{z}_{0c})$ can be expressed in terms of the principal coordinates of the control surface cross-section, i.e.

$$\bar{y}_{0c} = \eta_c \cos(\theta_G + \phi + \delta) - \zeta_c \sin(\theta_G + \phi + \delta) \tag{3.35a}$$

$$\bar{z}_{0c} = \zeta_c \cos(\theta_G + \phi + \delta) + \eta_c \sin(\theta_G + \phi + \delta) \tag{3.35b}$$

The time derivatives of $\vec{r}_c$ in the rotating reference frame ("2" system) can be obtained by differentiating Eqs. (3.31) with respect to time. The first time derivative of $\vec{r}_c$ in the "2" system can be expressed as:

$$\dot{\vec{r}}_c = \dot{r}_{cx2}\hat{e}_{x2} + \dot{r}_{cy2}\hat{e}_{y2} + \dot{r}_{cz2}\hat{e}_{z2}$$

where

$$\dot{r}_{cx2} = \dot{u} - \dot{w}\beta_p$$

$$- \dot{\bar{y}}_{0c}[(\dot{\theta}_G + \dot{\phi} + \dot{\delta})(w_{,x} + \beta_p) + \dot{v}_{,x}] + \dot{\bar{z}}_{0c}[(\dot{\theta}_G + \dot{\phi} + \dot{\delta})v_{,x} - \dot{w}_{,x}]$$

$$- \bar{y}_H[(\dot{\theta}_G + \dot{\phi})(w_{,x} + \beta_p) + \dot{v}_{,x}] + \bar{z}_H[(\dot{\theta}_G + \dot{\phi})v_{,x} - \dot{w}_{,x}] \tag{3.36a}$$

$$\dot{r}_{cy2} = \dot{v} - \bar{z}_{0c}(\dot{\theta}_G + \dot{\phi} + \dot{\delta}) - \bar{z}_H(\dot{\theta}_G + \dot{\phi}) \tag{3.36b}$$

$$\dot{r}_{zc2} = \dot{w} + \dot{u}\beta_p$$

$$+ \bar{y}_{0c}[(\dot{\theta}_G + \dot{\phi} + \dot{\delta}) - (w_{,x} + \beta_p)\dot{v}_{,x} - \dot{w}_{,x}v_{,x}]$$

$$+ \bar{z}_{0c}(\dot{\theta}_G + \dot{\phi} + \dot{\delta})(w_{,x} + \beta_p)v_{,x}$$

$$+ \bar{y}_H[(\dot{\theta}_G + \dot{\phi}) - (w_{,x} + \beta_p)\dot{v}_{,x} - \dot{w}_{,x}v_{,x}]$$

$$+ \bar{z}_H(\dot{\theta}_G + \dot{\phi})(w_{,x} + \beta_p)v_{,x} \tag{3.36c}$$

The previous expressions were obtained by taking the time derivative of Eqs. (3.31), and using the relations

$$\dot{\bar{y}}_{0c} = - \bar{z}_{0c}(\dot{\theta}_G + \dot{\phi} + \dot{\delta}) \tag{3.37a}$$

$$\dot{\bar{z}}_{0c} = \bar{y}_{0c}(\dot{\theta}_G + \dot{\phi} + \dot{\delta}) \tag{3.37b}$$

$$\dot{\bar{y}}_H = - \bar{z}_H(\dot{\theta}_G + \dot{\phi}) \tag{3.38a}$$

$$\dot{\bar{z}}_H = \bar{y}_H(\dot{\theta}_G + \dot{\phi}) \tag{3.38b}$$

Equations (3.37) follow from Eq. (3.35), and Eqs. (3.38) follow from Eqs. (3.28).

The second time derivative of $\vec{r}_c$ in the "2" system can be expressed as:

$$\ddot{\vec{r}}_c = \ddot{r}_{cx2}\hat{e}_{x2} + \ddot{r}_{cy2}\hat{e}_{y2} + \ddot{r}_{cz2}\hat{e}_{z2}$$

where

$$\ddot{r}_{cx2} = \ddot{u} - \ddot{w}\beta_p + \ddot{u}$$

$$+ \bar{y}_{0c}[- \ddot{v}_{,x} + (\dot{\theta}_G + \dot{\phi} + \dot{\delta})^2 v_{,x} - 2(\dot{\theta}_G + \dot{\phi} + \dot{\delta})\dot{w}_{,x}$$

$$- (\ddot{\theta}_G + \ddot{\phi} + \ddot{\delta})(w_{,x} + \beta_p)]$$

$$+ \bar{z}_{0c}[2(\dot{\theta}_G + \dot{\phi} + \dot{\delta})\dot{v}_{,x} + (\ddot{\theta}_G + \ddot{\phi} + \ddot{\delta})v_{,x} - \ddot{w}_{,x}$$

$$+ (\dot{\theta}_G + \dot{\phi} + \dot{\delta})^2(w_{,x} + \beta_p)]$$

$$+ \bar{y}_H[- \ddot{v}_{,x} + (\dot{\theta}_G + \dot{\phi})^2 v_{,x} - 2(\dot{\theta}_G + \dot{\phi})\dot{w}_{,x} - (\ddot{\theta}_G + \ddot{\phi})(w_{,x} + \beta_p)]$$

$$+ \bar{z}_H[2(\dot{\theta}_G + \dot{\phi})\dot{v}_{,x} + (\ddot{\theta}_G + \ddot{\phi})v_{,x} - \ddot{w}_{,x} + (\dot{\theta}_G + \dot{\phi})^2(w_{,x} + \beta_p)] \tag{3.39a}$$

$$\ddot{r}_{cy2} = \ddot{v} - \bar{y}_{0c}(\dot{\theta}_G + \dot{\phi} + \dot{\delta})^2 - \bar{z}_{0c}(\ddot{\theta}_G + \ddot{\phi} + \ddot{\delta})$$

$$- \bar{y}_H(\dot{\theta}_G + \dot{\phi})^2 - \bar{z}_H(\ddot{\theta}_G + \ddot{\phi}) \tag{3.39b}$$

$$\ddot{r}_{cz2} = \ddot{w} + \ddot{u}\beta_p$$

$$+ \bar{y}_{0c}[- (w_{,x} + \beta_p)\ddot{v}_{,x} - 2\dot{w}_{,x}\dot{v}_{,x} - \ddot{w}_{,x}v_{,x} + (\dot{\theta}_G + \dot{\phi} + \dot{\delta})^2(w_{,x} + \beta_p)v_{,x}$$

$$+ (\ddot{\theta}_G + \ddot{\phi} + \ddot{\delta})]$$

$$+ \bar{z}_{0c}[2(\dot{\theta}_G + \dot{\phi} + \dot{\delta})(w_{,x} + \beta_p)\dot{v}_{,x} + 2(\dot{\theta}_G + \dot{\phi} + \dot{\delta})\dot{w}_{,x}v_{,x}$$

$$+ (\ddot{\theta}_G + \ddot{\phi} + \ddot{\delta})(w_{,x} + \beta_p)v_{,x} - (\dot{\theta}_G + \dot{\phi} + \dot{\delta})^2]$$

$$+ \bar{y}_H[- (w_{,x} + \beta_p)\ddot{v}_{,x} - 2\dot{w}_{,x}\dot{v}_{,x} - \ddot{w}_{,x}v_{,x} + (\dot{\theta}_G + \dot{\phi})^2(w_{,x} + \beta_p)v_{,x}$$

$$+ (\ddot{\theta}_G + \ddot{\phi})]$$

$$+ \bar{z}_H[2(\dot{\theta}_G + \dot{\phi})(w_{,x} + \beta_p)\dot{v}_{,x} + 2(\dot{\theta}_G + \dot{\phi})\dot{w}_{,x}v_{,x} + (\ddot{\theta}_G + \ddot{\phi})(w_{,x} + \beta_p)v_{,x}$$

$$- (\dot{\theta}_G + \dot{\phi})^2] \tag{3.39c}$$

The previous expressions were obtained by taking the time derivative of Eqs. (3.36), and making use of Eqs. (3.37) and (3.38) once again.

The absolute acceleration of an arbitrary point on the control surface cross-section can be expressed in the "2" system as:

$$\vec{a}_c = a_{cx2}\,\hat{e}_{x2} + a_{cy2}\,\hat{e}_{y2} + a_{cz2}\,\hat{e}_{z2}$$

Substituting Eqs. (3.31), (3.36) and (3.39) into Eqs. (3.7) yields:

$$\begin{aligned}
a_{cx2} &= \ddot{u} - \ddot{w}\beta_p - 2\Omega\dot{v} - \Omega^2[(x + e + u) - w\beta_p] \\
&+ \bar{y}_{0c}[-(w_{,x} + \beta_p)\ddot{v}_{,x} - 2\dot{w}_{,x}\dot{v}_{,x} - \ddot{w}_{,x}v_{,x} + (\dot{\theta}_G + \dot{\phi} + \dot{\delta})^2(w_{,x} + \beta_p)v_{,x} \\
&\quad + (\ddot{\theta}_G + \ddot{\phi} + \ddot{\delta}) + \Omega^2 v_{,x}] \\
&+ \bar{z}_{0c}[(\dot{\theta}_G + \dot{\phi} + \dot{\delta})^2(w_{,x} + \beta_p) - \ddot{w}_{,x} + 2(\dot{\theta}_G + \dot{\phi} + \dot{\delta})\dot{v}_{,x} \\
&\quad + (\ddot{\theta}_G + \ddot{\phi} + \ddot{\delta})v_{,x} + 2\Omega(\dot{\theta}_G + \dot{\phi} + \dot{\delta}) + \Omega^2(w_{,x} + \beta_p)] \\
&+ \bar{y}_H[-(w_{,x} + \beta_p)\ddot{v}_{,x} - 2\dot{w}_{,x}\dot{v}_{,x} - \ddot{w}_{,x}v_{,x} + (\dot{\theta}_G + \dot{\phi})^2(w_{,x} + \beta_p)v_{,x} \\
&\quad + (\ddot{\theta}_G + \ddot{\phi}) + \Omega^2 v_{,x}] \\
&+ \bar{z}_H[(\dot{\theta}_G + \dot{\phi})^2(w_{,x} + \beta_p) - \ddot{w}_{,x} + 2(\dot{\theta}_G + \dot{\phi})\dot{v}_{,x} + (\ddot{\theta}_G + \ddot{\phi})v_{,x} \\
&\quad + 2\Omega(\dot{\theta}_G + \dot{\phi}) + \Omega^2(w_{,x} + \beta_p)] \qquad (3.40a)
\end{aligned}$$

$$\begin{aligned}
a_{cy2} &= \ddot{v} + 2\Omega(\dot{u} - \dot{w}\beta_p) - \Omega^2 v \\
&- \bar{y}_{0c}[(\dot{\theta}_G + \dot{\phi} + \dot{\delta})^2 + 2\Omega\dot{v}_{,x} + 2\Omega(\dot{\theta}_G + \dot{\phi} + \dot{\delta})(w_{,x} + \beta_p) + \Omega^2] \\
&- \bar{z}_{0c}[(\ddot{\theta}_G + \ddot{\phi} + \ddot{\delta}) - 2\Omega(\dot{\theta}_G + \dot{\phi} + \dot{\delta})v_{,x} + 2\Omega\dot{w}_{,x}]
\end{aligned}$$

$$- \bar{y}_H[(\dot{\theta}_G + \dot{\phi})^2 + 2\Omega\dot{v}_{,x} + 2\Omega(\dot{\theta}_G + \dot{\phi})(w_{,x} + \beta_p) + \Omega^2]$$

$$- \bar{z}_H[(\ddot{\theta}_G + \ddot{\phi}) - 2\Omega(\dot{\theta}_G + \dot{\phi})v_{,x} + 2\Omega\dot{w}_{,x}] \tag{3.40b}$$

$$a_{cz2} = \ddot{w} + \ddot{u}\beta_p$$

$$+ \bar{y}_{0c}[- (w_{,x} + \beta_p)\ddot{v}_{,x} - 2\dot{w}_{,x}\dot{v}_{,x} - \ddot{w}_{,x}v_{,x} + (\dot{\theta}_G + \dot{\phi} + \dot{\delta})^2(w_{,x} + \beta_p)v_{,x}$$

$$+ (\ddot{\theta}_G + \ddot{\phi} + \ddot{\delta})]$$

$$+ \bar{z}_{0c}[2(\dot{\theta}_G + \dot{\phi} + \dot{\delta})(w_{,x} + \beta_p)\dot{v}_{,x} + 2(\dot{\theta}_G + \dot{\phi} + \dot{\delta})\dot{w}_{,x}v_{,x}$$

$$+ (\ddot{\theta}_G + \ddot{\phi} + \ddot{\delta})(w_{,x} + \beta_p)v_{,x} - (\dot{\theta}_G + \dot{\phi} + \dot{\delta})^2]$$

$$- \bar{y}_H[- (w_{,x} + \beta_p)\ddot{v}_{,x} - 2\dot{w}_{,x}\dot{v}_{,x} - \ddot{w}_{,x}v_{,x} + (\dot{\theta}_G + \dot{\phi})^2(w_{,x} + \beta_p)v_{,x}$$

$$+ (\ddot{\theta}_G + \ddot{\phi})]$$

$$- \bar{z}_H[2(\dot{\theta}_G + \dot{\phi})\dot{v}_{,x}(w_{,x} + \beta_p) + 2(\dot{\theta}_G + \dot{\phi})\dot{w}_{,x}v_{,x}$$

$$+ (\ddot{\theta}_G + \ddot{\phi})(w_{,x} + \beta_p)v_{,x} - (\dot{\theta}_G + \dot{\phi})^2] \tag{3.40c}$$

The absolute acceleration of an arbitrary point on the control surface cross-section is used to obtain the inertial force and moment per unit volume from D'Alembert's principle. These inertial loads per unit volume are subsequently integrated over the control surface cross-section to obtain the distributed inertial loads acting on the control surface. But before proceeding it is convenient to define certain cross-sectional integrals of the control surface principal coordinates. These integrals are defined as follows:

$$\int_{A_c} \rho_c \eta_c \, dA = - m_c X_{lc} \tag{3.41a}$$

$$\int_{A_c} \rho_c \zeta_c \, dA = 0 \tag{3.41b}$$

$$\int_{A_c} \rho_c \eta_c^2 \, dA = I_{MC3} \tag{3.41c}$$

$$\int_{A_c} \rho_c \zeta_c^2 \, dA = I_{MC2} \tag{3.41d}$$

$$\int_{A_c} \rho_c \eta_c \zeta_c \, dA = 0 \tag{3.41e}$$

where Eqs. (3.41b) and (3.41e) result from the assumption of a symmetric control surface cross-section. The quantity X_{lc} is the offset of the mass center of the control surface cross-section behind the hinge point, and the pair I_{MC2} and I_{MC3} represent the principal mass moments of inertia of the control surface cross-section about the hinge axis.

The distributed inertial force is obtained by integrating the inertial force per unit volume over the control surface cross-section:

$$\vec{p}_{lc} = -\int_{A_c} \rho_c \vec{a}_c \, dA \tag{3.42}$$

which can be expressed in the "2" system in the form

$$\vec{p}_{lc} = p_{lcx2}\,\hat{e}_{x2} + p_{lcy2}\,\hat{e}_{y2} + p_{lcz2}\,\hat{e}_{z2}$$

Carrying out the integration for each component of Eq. (3.42) using Eqs. (3.40) yields:

$$\begin{aligned} p_{lcx2} &= -\int_{A_c} \rho_c a_{cx2} \, dA \\ &= m_c\Omega^2(x + e) + 2m_c\Omega\dot{v} + m_c\beta_p(\ddot{w} - w\Omega^2) + m_c(u\Omega^2 - \ddot{u}) \\ &\quad + 2m_c X_{lc}\Omega \sin(\theta_G + \phi + \delta)(\dot{\theta}_G + \dot{\phi} + \dot{\delta}) \\ &\quad + 2m_c X_H \Omega \sin(\theta_G + \phi)(\dot{\theta}_G + \dot{\phi}) \end{aligned} \tag{3.43a}$$

$$p_{lcy2} = -\int_{A_c} \rho_c a_{cy2}\, dA$$

$$= 2m_c\Omega\dot{w}\beta_p + m_c(v\Omega^2 - \ddot{v}) - 2m_c\Omega\dot{u}$$

$$- m_c X_{lc} \cos(\theta_G + \phi + \delta)[(\dot{\theta}_G + \dot{\phi} + \dot{\delta})^2 + \Omega(\Omega + 2\dot{v}_{,x})$$

$$+ 2\Omega(\dot{\theta}_G + \dot{\phi} + \dot{\delta})(w_{,x} + \beta_p)]$$

$$- m_c X_{lc} \sin(\theta_G + \phi + \delta)[(\ddot{\theta}_G + \ddot{\phi} + \ddot{\delta}) + 2\Omega\dot{w}_{,x}$$

$$- 2\Omega(\dot{\theta}_G + \dot{\phi} + \dot{\delta})v_{,x}]$$

$$- m_c X_H \cos(\theta_G + \phi)[(\dot{\theta}_G + \dot{\phi})^2 + \Omega(\Omega + 2\dot{v}_{,x}) + 2\Omega(\dot{\theta}_G + \dot{\phi})(w_{,x} + \beta_p)]$$

$$- m_c X_H \sin(\theta_G + \phi)[(\ddot{\theta}_G + \ddot{\phi}) + 2\Omega\dot{w}_{,x} - 2\Omega(\dot{\theta}_G + \dot{\phi})v_{,x}] \qquad (3.43b)$$

$$p_{lcz2} = -\int_{A_c} \rho_c a_{cz2}\, dA$$

$$= -m_c\ddot{w} - m_c\ddot{u}\beta_p$$

$$+ m_c X_{lc} \cos(\theta_G + \phi + \delta)[(\ddot{\theta}_G + \ddot{\phi} + \ddot{\delta}) - (w_{,x} + \beta_p)\ddot{v}_{,x} - 2\dot{w}_{,x}\dot{v}_{,x}$$

$$- \ddot{w}_{,x}v_{,x}]$$

$$- m_c X_{lc} \sin(\theta_G + \phi + \delta)[(\dot{\theta}_G + \dot{\phi} + \dot{\delta})^2 - (\ddot{\theta}_G + \ddot{\phi} + \ddot{\delta})(w_{,x} + \beta_p)v_{,x}]$$

$$+ m_c X_H \cos(\theta_G + \phi)[(\ddot{\theta}_G + \ddot{\phi}) - (w_{,x} + \beta_p)\ddot{v}_{,x} - 2\dot{w}_{,x}\dot{v}_{,x} - \ddot{w}_{,x}v_{,x}]$$

$$- m_c X_H \sin(\theta_G + \phi)[(\dot{\theta}_G + \dot{\phi})^2 - (\ddot{\theta}_G + \ddot{\phi})(w_{,x} + \beta_p)v_{,x}] \qquad (3.43c)$$

The following integral definitions have been used in the integrations over the control surface cross-section:

$$\int_{A_c} \rho_c \, dA = m_c \tag{3.44a}$$

$$\int_{A_c} \rho_c \bar{y}_{0c} \, dA = - m_c X_{Ic} \cos(\theta_G + \phi + \delta) \tag{3.44b}$$

$$\int_{A_c} \rho_c \bar{z}_{0c} \, dA = - m_c X_{Ic} \sin(\theta_G + \phi + \delta) \tag{3.44c}$$

The first integral represents the mass per unit span of the control surface and the last two integrals follow from Eqs. (3.35) and (3.41) .

The distributed inertial moment about the control surface hinge point is obtained by integrating the inertial moment per unit volume over the control surface cross-section:

$$\vec{q}_{Ih} = - \int_{A_c} (\bar{y}_{0c} \hat{e}_{y5} + \bar{z}_{0c} \hat{e}_{z5}) \times \rho_c \vec{a}_c \, dA \tag{3.45}$$

Transforming the unit vectors in Eq. (3.45) to the "2" system using the coordinate transformations defined in Chapter 2, carrying out the cross-product, and collecting the x, y and z components yields:

$$\vec{q}_{Ih} = q_{Ihx2} \hat{e}_{x2} + q_{Ihy2} \hat{e}_{y2} + q_{Ihz2} \hat{e}_{z2}$$

where

$$q_{Ihx2} = - \int_{A_c} \rho_c \{\bar{y}_{0c}[a_{cz2} + (w_{,x} + \beta_p) v_{,x} a_{cy2}] - \bar{z}_{0c} a_{cy2}\} \, dA$$

$$q_{Ihy2} = - \int_{A_b} \rho_c \{\bar{y}_{0c}[a_{cz2} - (w_{,x} + \beta_p) a_{cx2}] v_{,x}$$

$$+ \bar{z}_{0c}[(w_{,x} + \beta_p) a_{cz2} + a_{cx2}]\} \, dA$$

$$q_{Ihz2} = - \int_{A_c} \rho_c [- \bar{y}_{0c}(v_{,x} a_{cy2} + a_{cx2}) - \bar{z}_{0c} a_{cy2}] \, dA$$

Substituting Eqs. (3.40) into the previous expressions and performing the integrations over the control surface cross-section yields:

$$
\begin{aligned}
q_{Ihx2} = {} & m_c X_{Ic} \cos(\theta_G + \phi + \delta)[\ddot{w} + \ddot{u}\beta_p - (v\Omega^2 - \ddot{v})(w_{,x} + \beta_p)v_{,x}] \\
& + m_c X_{Ic} \sin(\theta_G + \phi + \delta)[(v\Omega^2 - \ddot{v}) + 2\Omega\dot{w}w_{,xp} - 2\Omega\dot{u}] \\
& - (I_{MC2} + I_{MC3})(\ddot{\theta}_G + \ddot{\phi} + \ddot{\delta}) \\
& + (I_{MC2} - I_{MC3}) \cos(\theta_G + \phi + \delta) \sin(\theta_G + \phi + \delta)\Omega[(\Omega + 2\dot{v}_{,x}) \\
& \quad + 2(\dot{\theta}_G + \dot{\phi} + \dot{\delta})(w_{,x} + \beta_p)] \\
& + 2[I_{MC2} \cos^2(\theta_G + \phi + \delta) + I_{MC3} \sin^2(\theta_G + \phi + \delta)]\Omega[- \dot{w}_{,x} \\
& \quad + (\dot{\theta}_G + \dot{\phi} + \dot{\delta})v_{,x}] \\
& + [I_{MC2} \sin^2(\theta_G + \phi + \delta) + I_{MC3} \cos^2(\theta_G + \phi + \delta)][2\dot{v}_{,x}\dot{w}_{,x} \\
& \quad + v_{,x}\ddot{w}_{,x} + (w_{,x} + \beta_p)(\ddot{v}_{,x} + \Omega^2 v_{,x})] \\
& - m_c X_{Ic} X_H \Omega(\Omega + 2\dot{v}_{,x}) \cos(\theta_G + \phi) \sin(\theta_G + \phi + \delta) \\
& - m_c X_{Ic} X_H(\ddot{\theta}_G + \ddot{\phi}) \cos\delta \\
& - m_c X_{Ic} X_H(\dot{\theta}_G + \dot{\phi})^2 \sin\delta
\end{aligned}
\tag{3.46a}
$$

$$
\begin{aligned}
q_{Ihy2} = {} & m_c X_{Ic} \cos(\theta_G + \phi + \delta)[x\Omega^2(w_{,x} + \beta_p) + \ddot{w}]v_{,x} \\
& + m_c X_{Ic} \sin(\theta_G + \phi + \delta)[- \Omega^2(x + e) + (w_{,x}\ddot{w} + \beta_p w\Omega^2) \\
& \quad + (\ddot{u} - u\Omega^2) - 2\Omega\dot{v}] \\
& - (I_{MC2} + I_{MC3})(\ddot{\theta}_G + \ddot{\phi} + \ddot{\delta})v_{,x}
\end{aligned}
$$

$$+ (I_{MC2} - I_{MC3})\cos(\theta_G + \phi + \delta)\sin(\theta_G + \phi + \delta)[(v_{,x}\Omega^2 - \ddot{v}_{,x})$$

$$- 2(\dot{\theta}_G + \dot{\phi} + \dot{\delta})\dot{w}_{,x}]$$

$$+ [I_{MC2}\cos^2(\theta_G + \phi + \delta) + I_{MC3}\sin^2(\theta_G + \phi + \delta)][\ddot{w}_{,x}$$

$$- \Omega^2(w_{,x} + \beta_p) - 2(\Omega + \dot{v}_{,x})(\dot{\theta}_G + \dot{\phi} + \dot{\delta})]$$

$$- 2m_c X_{lc} X_H \Omega(\dot{\theta}_G + \dot{\phi})\sin(\theta_G + \phi)\sin(\theta_G + \phi + \delta) \tag{3.46b}$$

$$q_{lhz2} = m_c X_{lc}\cos(\theta_G + \phi + \delta)[\Omega^2(x + e) + (u\Omega^2 - \ddot{u})$$

$$+ 2\Omega\dot{v} + (v\Omega^2 - \ddot{v})v_{,x} + (\ddot{w} - w\Omega^2)\beta_p]$$

$$+ m_c X_{lc}\sin(\theta_G + \phi + \delta)(w_{,x} + \beta_p)(v\Omega^2 - \ddot{v})$$

$$- (I_{MC2} + I_{MC3})(\ddot{\theta}_G + \ddot{\phi} + \ddot{\delta})(w_{,x} + \beta_p)$$

$$+ (I_{MC2} - I_{MC3})\cos(\theta_G + \phi + \delta)\sin(\theta_G + \phi + \delta)[\ddot{w}_{,x}$$

$$- 2(\Omega + \dot{v}_{,x})(\dot{\theta}_G + \dot{\phi} + \dot{\delta})]$$

$$- [I_{MC2}\sin^2(\theta_G + \phi + \delta) + I_{MC3}\cos^2(\theta_G + \phi + \delta)][\ddot{v}_{,x}$$

$$+ 2(\dot{\theta}_G + \dot{\phi} + \dot{\delta})\dot{w}_{,x}]$$

$$+ 2m_c X_{lc} X_H \Omega(\dot{\theta}_G + \dot{\phi})\sin(\theta_G + \phi)\cos(\theta_G + \phi + \delta) \tag{3.46c}$$

The following integral definitions, in addition to those represented by Eqs. (3.44), have been used in the integrations over the control surface cross-section:

$$\int_{A_c} \rho_c \bar{y}_{0c}^2 \, dA = I_{MC2}\sin^2(\theta_G + \phi + \delta) + I_{MC3}\cos^2(\theta_G + \phi + \delta) \tag{3.47a}$$

$$\int_{A_c} \rho_c \bar{z}_{0c}^2 \, dA = I_{MC2} \cos^2(\theta_G + \phi + \delta) + I_{MC3} \sin^2(\theta_G + \phi + \delta) \tag{3.47b}$$

$$\int_{A_c} \rho_c \bar{y}_{0c} \bar{z}_{0c} \, dA = (I_{MC3} - I_{MC2}) \cos(\theta_G + \phi + \delta) \sin(\theta_G + \phi + \delta) \tag{3.47c}$$

The above integrals follow from Eqs. (3.35) and (3.41) .

The distributed inertial loads acting on the control surface can be transformed from the "2" system to the "3" system, in which the equations of motion are formulated, using the appropriate coordinate transformation defined in Chapter 2. The distributed inertial force acting on the control surface can be expressed in the "3" system as:

$$\vec{p}_{Ic} = p_{Icx3} \hat{e}_{x3} + p_{Icy3} \hat{e}_{y3} + p_{Icz3} \hat{e}_{z3}$$

where

$$p_{Icx3} = p_{Icx2} + \beta_p \, p_{Icz2} \tag{3.48a}$$

$$p_{Icy3} = p_{Icy2} \tag{3.48b}$$

$$p_{Icz3} = -\beta_p \, p_{Icx2} + p_{Icz2} \tag{3.48c}$$

Similarly, the distributed inertial control surface hinge moment can be expressed in the "3" system as:

$$\vec{q}_{Ih} = q_{Ihx3} \hat{e}_{x3} + q_{Ihy3} \hat{e}_{y3} + q_{Ihz3} \hat{e}_{z3}$$

where

$$q_{Ihx3} = q_{Ihx2} + \beta_p \, q_{Ihz2} \tag{3.49a}$$

$$q_{Ihy3} = q_{Ihy2} \tag{3.49b}$$

$$q_{Ihz3} = -\beta_p \, q_{Ihx2} + q_{Ihz2} \tag{3.49c}$$

The distributed inertial moment about the elastic axis of the blade due to the control surface inertial loads is given by

$$\vec{q}_{Ic} = \vec{q}_{Ih} + (\bar{y}_H \hat{e}_{y5} + \bar{z}_H \hat{e}_{z5}) \times \vec{p}_{Ic} \tag{3.50}$$

Transforming the unit vectors in the above expression to the "3" system using the appropriate coordinate transform defined in Chapter 2, carrying out the cross-product, and collecting the various terms into x, y and z components yields:

$$\vec{q}_{Ic} = q_{Icx3} \hat{e}_{x3} + q_{Icy3} \hat{e}_{y3} + q_{Icz3} \hat{e}_{z3}$$

where

$$q_{Icx3} = (-v_{,x} w_{,x} \bar{y}_H + \bar{z}_H) p_{Icy3} + \bar{y}_H p_{Icz3} \tag{3.51a}$$

$$q_{Icy3} = (-v_{,x} w_{,x} \bar{y}_H + \bar{z}_H) p_{Icx3} + (v_{,x} \bar{y}_H + w_{,x} \bar{z}_H) p_{Icz3} \tag{3.51b}$$

$$q_{Icz3} = -\bar{y}_H p_{Icx3} - (v_{,x} \bar{y}_H + w_{,x} \bar{z}_H) p_{Icy3} \tag{3.51c}$$

3.3 GRAVITATIONAL LOADS

The distributed gravitational loads are obtained by integrating the gravitational force and moment per unit volume over the cross-sectional area. The gravitational vector is oriented along the negative z_0 axis, i.e.

$$\vec{g} = -g \hat{e}_{z0} \tag{3.52}$$

where g is the acceleration due to gravity. Transforming $\hat{e}_{z0}$ to the "2" system using the coordinate transformations defined in Chapter 2 yields:

$$\vec{g} = g_{x2} \hat{e}_{x2} + g_{y2} \hat{e}_{y2} + g_{z2} \hat{e}_{z2}$$

where

$$g_{x2} = -g \sin \alpha_R \cos \psi \tag{3.53a}$$

$$g_{y2} = g \sin \alpha_R \sin \psi \tag{3.53b}$$

$$g_{z2} = -g \cos \alpha_R \tag{3.53c}$$

The gravitational vector defined above is used in the following sections to obtain the distributed gravitational loads on the blade and control surface.

3.3.1 *Gravitational Loads on the Blade*

The gravitational loads per unit span acting on the blade are obtained by integrating the gravitational force and moment per unit volume over the blade cross-section. The derivation presented below is similar to those of Refs. 38 and 50. The distributed gravitational force on the blade is given by:

$$\vec{p}_{Gb} = \int_{A_b} \rho_b \vec{g}\, dA \tag{3.54}$$

which can be expressed in the "2" system as:

$$\vec{p}_{Gb} = p_{Gbx2}\,\hat{e}_{x2} + p_{Gby2}\,\hat{e}_{y2} + p_{Gbz2}\,\hat{e}_{z2}$$

Evaluating each component of Eq. (3.54) and making use of Eqs. (3.53) yields:

$$p_{Gbx2} = \int_{A_b} \rho_b\, g_{x2}\, dA = -m_b g \sin\alpha_R \cos\psi \tag{3.55a}$$

$$p_{Gby2} = \int_{A_b} \rho_b\, g_{y2}\, dA = m_b g \sin\alpha_R \sin\psi \tag{3.55b}$$

$$p_{Gbz2} = \int_{A_b} \rho_b\, g_{z2}\, dA = -m_b g \cos\alpha_R \tag{3.55c}$$

The gravitational moment per unit span about the elastic axis is obtained by integrating the gravitational moment per unit volume over the blade cross-section

$$\vec{q}_{Gb} = \int_{A_b} (\bar{y}_{0b}\,\hat{e}_{y5} + \bar{z}_{0b}\,\hat{e}_{z5}) \times \rho_b \vec{g}\, dA \tag{3.56}$$

Transforming the unit vectors in Eq. (3.56) to the "2" system using the coordinate transformations defined in Chapter 2, performing the cross-product, and collecting the various terms into x, y and z components yields:

$$\vec{q}_{Gb} = q_{Gbx2}\,\hat{e}_{x2} + q_{Gby2}\,\hat{e}_{y2} + q_{Gbz2}\,\hat{e}_{z2}$$

where

$$q_{Gbx2} = \int_{A_b} \rho_b \{\bar{y}_{0b}[g_{z2} + (w_{,x} + \beta_p)v_{,x}\,g_{y2}] - \bar{z}_{0b}\,g_{y2}\}\,dA$$

$$q_{Gby2} = \int_{A_b} \rho_b \{\bar{y}_{0b}[g_{z2} - (w_{,x} + \beta_p)\,g_{x2}]v_{,x} + \bar{z}_{0b}[(w_{,x} + \beta_p)\,g_{z2} + g_{x2}]\}\,dA$$

$$q_{Gbz2} = \int_{A_b} \rho_b [-\bar{y}_{0b}(v_{,x}g_{y2} + g_{x2}) - \bar{z}_{0b}(w_{,x} + \beta_p)\,g_{y2}]\,dA$$

Substituting Eqs. (3.53) into the previous expressions and performing the integrations over the blade cross-section yields:

$$q_{Gbx2} = -m_b g X_{Ib}\cos(\theta_G + \phi)[\cos\alpha_R - (w_{,x} + \beta_p)v_{,x}\sin\alpha_R\sin\psi]$$
$$- m_b g X_{Ib}\sin(\theta_G + \phi)\sin\alpha_R\sin\psi \qquad (3.57a)$$

$$q_{Gby2} = -m_b g X_{Ib}\cos(\theta_G + \phi)[\cos\alpha_R - (w_{,x} + \beta_p)\sin\alpha_R\cos\psi]v_{,x}$$
$$- m_b g X_{Ib}\sin(\theta_G + \phi)[(w_{,x} + \beta_p)\cos\alpha_R + \sin\alpha_R\cos\psi] \qquad (3.57b)$$

$$q_{Gbz2} = -m_b g X_{Ib}\cos(\theta_G + \phi)\sin\alpha_R(v_{,x}\sin\psi - \cos\psi)$$
$$- m_b g X_{Ib}\sin(\theta_G + \phi)\sin\alpha_R\sin\psi \qquad (3.57c)$$

The integral definitions represented by Eqs. (3.21) have been used above.

The distributed gravitational loads acting on the blade can be transformed from the "2" system to the "3" system, in which the equations of motion are formulated, using the coordinate transformation defined in Chapter 2. The distributed gravitational force acting on the blade can be expressed in the "3" system as:

$$\vec{p}_{Gb} = p_{Gbx3}\,\hat{e}_{x3} + p_{Gby3}\,\hat{e}_{y3} + p_{Gbz3}\,\hat{e}_{z3}$$

where

$$p_{Gbx3} = p_{Gbx2} + \beta_p\, p_{Gbz2} \tag{3.58a}$$

$$p_{Gby3} = p_{Gby2} \tag{3.58b}$$

$$p_{Gbz3} = -\beta_p\, p_{Gbx2} + p_{Gbz2} \tag{3.58c}$$

Similarly, the distributed gravitational moment acting on the blade can be expressed in the "3" system as:

$$\vec{q}_{Gb} = q_{Gbx3}\,\hat{e}_{x3} + q_{Gby3}\,\hat{e}_{y3} + q_{Gbz3}\,\hat{e}_{z3}$$

where

$$q_{Gbx3} = q_{Gbx2} + \beta_p\, q_{Gbz2} \tag{3.59a}$$

$$q_{Gby3} = q_{Gby2} \tag{3.59b}$$

$$q_{Gbz3} = -\beta_p\, q_{Gbx2} + q_{Gbz2} \tag{3.59c}$$

3.3.2 *Gravitational Loads on the Control Surface*

The control surface gravitational loads per unit span are derived in a manner similar to that used in calculating the distributed gravitational force and moment on the blade. The gravitational force per unit span of the control surface is obtained by integrating the gravitational force per unit volume of the control surface over its cross-section, i.e.

$$\vec{p}_{Gc} = \int_{A_c} \rho_c\, \vec{g}\, dA \tag{3.60}$$

which can be expressed in the "2" system in the form:

$$\vec{p}_{Gc} = p_{Gcx2}\,\hat{e}_{x2} + p_{Gcy2}\,\hat{e}_{y2} + p_{Gcz2}\,\hat{e}_{z2}$$

Performing the integration for each component of Eq. (3.60) making use of Eqs. (3.53) yields:

$$p_{Gcx2} = \int_{A_c} \rho_c \, g_{x2} \, dA = - m_c g \sin \alpha_R \cos \psi \tag{3.61a}$$

$$p_{Gcy2} = \int_{A_c} \rho_c \, g_{y2} \, dA = m_c g \sin \alpha_R \sin \psi \tag{3.61b}$$

$$p_{Gcz2} = \int_{A_c} \rho_c \, g_{z2} \, dA = - m_c g \cos \alpha_R \tag{3.61c}$$

The gravitational moment per unit span about the hinge point is obtained by integrating the gravitational moment per unit volume about the hinge over the control surface cross-section

$$\vec{q}_{Gh} = \int_{A_c} (\bar{y}_{0c} \, \hat{e}_{y5} + \bar{z}_{0c} \, \hat{e}_{z5}) \times \rho_c \, \vec{g} \, dA \tag{3.62}$$

Transforming the unit vectors in Eq. (3.62) to the "2" system using the coordinate transformations defined in Chapter 2, performing the cross-product and collecting the various terms into x, y and z components yields:

$$\vec{q}_{Gh} = q_{Ghx2} \, \hat{e}_{x2} + q_{Ghy2} \, \hat{e}_{y2} + q_{Ghz2} \, \hat{e}_{z2}$$

where

$$q_{Ghx2} = \int_{A_c} \rho_c \, \{\bar{y}_{0c} \, [g_{z2} + (w_{,x} + \beta_p) v_{,x} \, g_{y2}] - \bar{z}_{0c} \, g_{y2}\} \, dA$$

$$q_{Ghy2} = \int_{A_c} \rho_c \, \{\bar{y}_{0c} \, [g_{z2} - (w_{,x} + \beta_p) \, g_{x2}] v_{,x} + \bar{z}_{0c} \, [(w_{,x} + \beta_p) \, g_{z2} + g_{x2}]\} \, dA$$

$$q_{Ghz2} = \int_{A_c} \rho_c \, [- \bar{y}_{0c} \, (v_{,x} \, g_{y2} + g_{x2}) - \bar{z}_{0c} \, (w_{,x} + \beta_p) \, g_{y2}] \, dA$$

Substituting Eqs. (3.53) into the previous expressions and performing the integrations over the control surface cross-section yields:

$$q_{Ghx2} = m_c g X_{Ic} \cos(\theta_G + \phi + \delta)[\cos\alpha_R - (w_{,x} + \beta_p)v_{,x} \sin\alpha_R \sin\psi]$$

$$+ m_c g X_{Ic} \sin(\theta_G + \phi + \delta) \sin\alpha_R \sin\psi \tag{3.63a}$$

$$q_{Ghy2} = m_c g X_{Ic} \cos(\theta_G + \phi + \delta)[\cos\alpha_R - (w_{,x} + \beta_p) \sin\alpha_R \cos\psi]v_{,x}$$

$$+ m_c g X_{Ic} \sin(\theta_G + \phi + \delta)[(w_{,x} + \beta_p) \cos\alpha_R + \sin\alpha_R \cos\psi] \tag{3.63b}$$

$$q_{Ghz2} = m_c g X_{Ic} \cos(\theta_G + \phi + \delta) \sin\alpha_R(v_{,x} \sin\psi - \cos\psi)$$

$$+ m_c g X_{Ic} \sin(\theta_G + \phi + \delta) \sin\alpha_R \sin\psi \tag{3.63c}$$

where the integral definitions defined by Eqs. (3.44) were used in the integrations over the control surface cross-section.

The distributed gravitational loads acting on the control surface can be transformed from the "2" system to the "3" system, in which the equations of motion are formulated, using the coordinate transformation defined in Chapter 2. The distributed gravitational force acting on the control surface can be expressed in the "3" system as:

$$\vec{p}_{Gc} = p_{Gcx3} \hat{e}_{x3} + p_{Gcy3} \hat{e}_{y3} + p_{Gcz3} \hat{e}_{z3}$$

where

$$p_{Gcx3} = p_{Gcx2} + \beta_p p_{Gcz2} \tag{3.64a}$$

$$p_{Gcy3} = p_{Gcy2} \tag{3.64b}$$

$$p_{Gcz3} = -\beta_p p_{Gcx2} + p_{Gcz2} \tag{3.64c}$$

Similarly, the distributed gravitational control surface hinge moment can be expressed in the "3" system as:

$$\vec{q}_{Gh} = q_{Ghx3} \hat{e}_{x3} + q_{Ghy3} \hat{e}_{y3} + q_{Ghz3} \hat{e}_{z3}$$

where

$$q_{Ghx3} = q_{Ghx2} + \beta_p q_{Ghz2} \tag{3.65a}$$

$$q_{Ghy3} = q_{Ghy2} \tag{3.65b}$$

$$q_{Ghz3} = -\beta_p q_{Ghx2} + q_{Ghz2} \tag{3.65c}$$

The distributed gravitational moment about the elastic axis of the blade due to the control surface gravitational loads is given by

$$\vec{q}_{Gc} = \vec{q}_{Gh} + (\bar{y}_H \hat{e}_{y5} + \bar{z}_H \hat{e}_{z5}) \times \vec{p}_{Gc} \tag{3.66}$$

which can be expressed in the "3" system as

$$\vec{q}_{Gc} = q_{Gcx3} \hat{e}_{x3} + q_{Gcy3} \hat{e}_{y3} + q_{Gcz3} \hat{e}_{z3}$$

where

$$q_{Gcx3} = (-v_{,x} w_{,x} \bar{y}_H + \bar{z}_H) p_{Gcy3} + \bar{y}_H p_{Gcz3} \tag{3.67a}$$

$$q_{Gcy3} = (-v_{,x} w_{,x} \bar{y}_H + \bar{z}_H) p_{Gcx3} + (v_{,x} \bar{y}_H + w_{,x} \bar{z}_H) p_{Gcz3} \tag{3.67b}$$

$$q_{Gcz3} = -\bar{y}_H p_{Gcx3} - (v_{,x} \bar{y}_H + w_{,x} \bar{z}_H) p_{Gcy3} \tag{3.67c}$$

3.4 AERODYNAMIC LOADS

In this study, an appropriately modified version of quasisteady aerodynamic theory, based on Theodorsen's unsteady aerodynamic theory, is used to predict the aerodynamic forces and moments experienced by a rotor blade in forward flight. A detailed description of the modification of Theodorsen's unsteady aerodynamic theory to include the effects of a time-varying free stream velocity and variable inflow is presented in Appendix A. The expressions developed in that appendix, combined with the quasisteady assumption, are used in this section to develop explicit expressions for the aerodynamic forces and moments acting per unit span of the blade and the control surface.

Theodorsen's unsteady aerodynamic theory[52] is a classical two-dimensional strip theory which describes the aerodynamic loads experienced by a thin airfoil-aileron combination performing small simple harmonic oscillations in a uniform stream of

incompressible flow. It is well known[11] that Theodorsen's theory was developed for fixed-wing applications and is not suitable for rotary-wing studies. Therefore, Theodorsen's theory has to be modified to include the effects of a time-varying free stream velocity (due to blade dynamics) and variable inflow, present in rotary-wing applications.

Greenberg's unsteady aerodynamic theory[18], which represents a modification of Theodorsen's unsteady aerodynamic theory to include the effects of a constant component of the angle of attack and a time-varying free stream velocity, has been used frequently as the basis for generating the required approximate aerodynamic loads for rotary-wing aeroelastic studies. However, Greenberg's theory does not account for the effect of a flap. Therefore, Theodorsen's model for a wing-flap combination has been modified in a manner similar to Greenberg for use in this study. The derivation of the modified expressions is presented in Appendix A. It should be noted that the expressions derived, reduce to Greenberg's theory in the absence of the flap, and no inflow.

Theodorsen separates the aerodynamic loads into a noncirculatory and circulatory component. The noncirculatory portion of the flow results from the pattern of sources and sinks along the airfoil chord such that the two dimensional boundary condition that the airfoil chord is a streamline of the flow is satisfied. The circulatory portion of the flow results from the distribution of vortices on the airfoil chord and counter-vortices along the wake to infinity such that Kutta's condition at the trailing edge is satisfied. Theodorsen assumed that both the noncirculatory and circulatory lift act normal to the resultant flow. However, for mathematical convenience, it is assumed in this study that the noncirculatory lift acts normal to the airfoil chord. The reason for this assumption is explained later in this chapter. The effects of parasitic drag, which is assumed to act parallel to the resultant flow, are included.

3.4.1 *Quasisteady Aerodynamic Loads*

The modified expressions for the total noncirculatory and circulatory lift, pitching moment and hinge moment for a blade with a trailing edge flap are given by Eqs. (A.25) – (A.30) of Appendix A. It is believed that these expressions are new and that the present study is their first application. These are two dimensional loads per unit span. These expressions, including the quasisteady assumption (i.e. C(k) = 1), are presented below. In these expressions, the lift is defined positive up and the pitching and hinge moments are defined positive nose up.

The total noncirculatory lift per unit span is given by:

$$L_{NC} = \frac{1}{8}\rho_A a_o (c_b + c_{cs})^2 \{\dot{U}_T(\theta_G + \phi) + U_T(\dot{\theta}_G + \dot{\phi})$$

$$- [X_A - \frac{1}{4}(c_b + 2c_{cs})](\ddot{\theta}_G + \ddot{\phi}) - \dot{U}_P$$

$$- 2(\dot{U}_T\delta + U_T\dot{\delta})\frac{T_4}{a_o} - (c_b + c_{cs})\ddot{\delta}\frac{T_1}{a_o}\} \tag{3.68}$$

The total circulatory lift per unit span is given by:

$$L_C = \frac{1}{2}\rho_A a_o (c_b + c_{cs}) U_T \{U_T(\theta_G + \phi) - U_P$$

$$+ [\frac{1}{2}(c_b + 3c_{cs}) - X_A](\dot{\theta}_G + \dot{\phi})$$

$$+ 2\frac{T_{10}}{a_o}U_T\delta + \frac{1}{4}(2c_b + 3c_{cs})\frac{T_{11}}{a_o}\dot{\delta}\} \tag{3.69}$$

The total noncirculatory pitching moment is given by:

$$M_{yNC} = \frac{1}{8}\rho_A a_o (c_b + c_{cs})^2 \{U_T^2(\theta_G + \phi) - U_T U_P$$

$$- [X_A^2 - \frac{1}{4}(c_b + 2c_{cs})]^2(\ddot{\theta}_G + \ddot{\phi}) - \frac{1}{32}(c_b + c_{cs})^2(\ddot{\theta}_G + \ddot{\phi})$$

$$+ [X_A - \frac{1}{4}(c_b + 2c_{cs})][\dot{U}_T(\theta_G + \phi) - \dot{U}_P]$$

$$- 2\frac{T_4}{a_o}U_T^2\delta - \frac{T_1}{a_o}(c_b + c_{cs})U_T\dot{\delta}$$

$$+ [\frac{T_8}{a_o}(c_b + c_{cs}) + (\frac{3}{2}c_b - 2X_A)\frac{T_4}{a_o}](\dot{U}_T\delta + U_T\dot{\delta})$$

$$+ \frac{1}{2}(c_b + c_{cs})[\frac{T_7}{a_o}(c_b + c_{cs}) + (\frac{3}{2}c_b - 2X_A)\frac{T_1}{a_o}]\ddot{\delta}\} \tag{3.70}$$

The total circulatory pitching moment per unit span is given by:

$$M_{yC} = \frac{1}{2}\rho_A a_o(c_b + c_{cs})U_T\{U_T(\theta_G + \phi) - U_P$$

$$+ [\frac{1}{2}(c_b + 3c_{cs}) - X_A](\dot{\theta}_G + \dot{\phi}) + 2\frac{T_{10}}{a_o}U_T\delta$$

$$+ \frac{1}{4}(2c_b + 3c_{cs})\frac{T_{11}}{a_o}\dot{\delta}\}[X_A - \frac{1}{4}(c_b + 2c_{cs})] \tag{3.71}$$

The total noncirculatory hinge moment per unit span in given by:

$$M_{hNC} = -\frac{1}{4}\rho_A(c_b + c_{cs})^2\{U_T^2T_4(\theta_G + \phi) + \frac{1}{2}T_{13}(c_b + c_{cs})^2(\ddot{\theta}_G + \ddot{\phi})$$

$$- \frac{1}{2}(2T_9 + T_1)(c_b + c_{cs})U_T(\dot{\theta}_G + \dot{\phi})$$

$$+ \frac{1}{2}(c_b + c_{cs})T_1[\dot{U}_P - \dot{U}_T(\theta_G + \phi)] - U_TU_PT_4$$

$$+ 2U_T^2\frac{T_5}{a_o}\delta - \frac{1}{2}(c_b + c_{cs})^2\ddot{\delta}\frac{T_3}{a_o} - (c_b + c_{cs})\frac{T_2}{a_o}\dot{U}_T\delta\} \tag{3.72}$$

The total circulatory hinge moment per unit span is given by:

$$M_{hC} = -\frac{1}{4}\rho_A(c_b + c_{cs})^2U_T\{U_T(\theta_G + \phi) - U_P$$

$$+ [\frac{1}{2}(c_b + 3c_{cs}) - X_A](\dot{\theta}_G + \dot{\phi})$$

$$+ 2\frac{T_{10}}{a_o}U_T\delta + \frac{1}{4}(2c_b + 3c_{cs})\frac{T_{11}}{a_o}\dot{\delta}\}(T_{12} - T_4) \tag{3.73}$$

The parasitic drag per unit span on the airfoil and control flap is given by

$$D = \frac{1}{2}\rho_A a_o(c_b + c_{cs})(U_T^2 + U_P^2)(\frac{C_{do}}{a_o}) \tag{3.74}$$

The velocities U_T and U_P represent the "tangential" and "perpendicular" air velocities, respectively, sensed by the blade cross-section due to forward flight, inflow and blade dynamics. In this study U_T is defined as the velocity component tangent to the blade's plane of rotation, and U_P is is defined as the velocity component perpendicular to U_T, and lying in the plane of the blade cross-section (see Fig. 12). As shown in Fig. 12, the velocity component U_T makes an angle of $\alpha = \theta_G + \phi$ with the blade chord. In Appendix A the angle α was defined as the local angle of attack of the blade cross-section. The is also the angle between the blade chord and the y_5 axis. For this reason the "5" coordinate system, which represents the "4" (deformed) coordinate system with the torsional deformation of the blade ϕ removed, is selected as the most appropriate coordinate system in which to identify U_T and U_P. This interpretation has been used in many rotor blade studies[38,50,45,53] to define the local velocity components.

Therefore the tangential air velocity can be identified as:

$$U_T = -V_{Ay5} \tag{3.75a}$$

and the perpendicular air velocity can be identified as:

$$U_P = -V_{Az5} \tag{3.75b}$$

where V_{Ay5} and V_{Az5} represent the y and z components, respectively, of the total air velocity sensed by the blade in the "5" system due to forward flight, induced inflow and blade dynamics. It should be noted that, due to the pitching motion of the blade, each point on the blade cross-section senses a different total air velocity. Therefore, in this study, the tangential and perpendicular air velocities are defined as the velocity components at the elastic axis of the blade cross-section.

If $\vec{V}_{AF}$ represents the free stream air velocity due to forward flight and induced inflow and $\vec{V}_{EA}$ represents the velocity of a point on the elastic axis of the deformed blade due to its motion, then the total air velocity seen by the deformed blade can be expressed as:

$$\vec{V}_A = \vec{V}_{AF} - \vec{V}_{EA} \tag{3.76}$$

For a rotor blade in forward flight with velocity V_F

$$\vec{V}_{AF} = \Omega R(\mu \hat{e}_{x1} - \lambda \hat{e}_{z1}) \tag{3.77}$$

where

$$\mu = \frac{V_F \cos \alpha_R}{\Omega R} \qquad \lambda = \frac{V_F \sin \alpha_R + v}{\Omega R}$$

are the advance ratio and inflow ratio, respectively. Transforming the free-stream velocity to the rotating ("2" system) reference frame using the coordinate transformations defined in Chapter 2 yields:

$$\vec{V}_{AF} = \Omega R(\mu \cos \psi \, \hat{e}_{x2} - \mu \sin \psi \, \hat{e}_{y2} - \lambda \, \hat{e}_{z2}) \tag{3.78}$$

The velocity of a point on the elastic axis of the blade due due to forward flight and the motion of the blade can by found from classical dynamics. The absolute velocity of a point moving in a reference frame which is translating and rotating relative to an inertial reference frame is given by

$$\vec{v} = \dot{\vec{R}}_0 + \dot{\vec{r}} + \vec{\omega} \times \vec{r} \tag{3.79}$$

where $\vec{R}_0$ represents the position vector of the origin of the moving reference frame relative to the inertial reference frame, $\vec{r}$ represents the position vector of an arbitrary point in the moving reference frame and $\vec{\omega}$ is the angular velocity of the rotating frame relative to the inertial reference frame. The time derivative of $\vec{R}_0$ is taken in the inertial reference frame and represents the velocity of the origin of the moving reference frame relative to the

inertial reference frame; whereas the time derivative of $\vec{r}$ is taken in the rotating reference frame and represents the velocity of an arbitrary point in the moving reference frame.

As stated previously the "1" system represents the inertial, hub-fixed reference frame and the "2" system, which rotates with the blade, represents the rotating reference frame. Making use of Eqs. (3.3) and (3.4) once again, together with Eq. (3.79), the absolute velocity of an arbitrary point in the rotating reference frame ("2" system) can be expressed as:

$$\vec{v}_p = \vec{r}_p + \Omega \hat{e}_{z2} \times \vec{r}_p \tag{3.80}$$

where again $\vec{r}_p$ is used to represent the position vector of an arbitrary point in the "2" system.

Defining $\vec{r}_{EA}$ as the position vector of a point on the elastic axis, then using the above relation, the absolute velocity of this point can be expressed as:

$$\vec{V}_{EA} = \dot{\vec{r}}_{EA} + \Omega \hat{e}_{z2} \times \vec{r}_{EA} \tag{3.81}$$

where the time derivative of $\vec{r}_{EA}$ is taken in the "2" system.

The position vector $\vec{r}_{EA}$ can be obtained by substituting $y_0 = z_0 = 0$ into Eq. (3.1) to yield

$$\vec{r}_{EA} = e\,\hat{e}_{x2} + (x + e)\,\hat{e}_{x3} + v\,\hat{e}_{y3} + w\,\hat{e}_{z3} \tag{3.82}$$

Before substituting the above expression into Eq. (3.81), it is convenient to express $\vec{r}_{EA}$ entirely in the "2" system. Transforming the unit vectors in Eq. (3.82) from the "3" to the "2" system using the coordinate transformation defined in Chapter 2 yields:

$$\vec{r}_{EA} = (x + e + u - w\beta_p)\,\hat{e}_{x2} + v\,\hat{e}_{y2} + [(x + u)\beta_p + w]\,\hat{e}_{z2} \tag{3.83}$$

Therefore the time derivative of $\vec{r}_{EA}$ in the "2" system can be expressed as:

$$\dot{\vec{r}}_{EA} = (\dot{u} - \dot{w}\beta_p)\,\hat{e}_{x2} + \dot{v}\,\hat{e}_{y2} + (\dot{u}\beta_p + \dot{w})\,\hat{e}_{z2} \tag{3.84}$$

Substituting Eqs. (3.83) and (3.84) into Eq. (3.81) and performing the cross product yields:

$$\vec{V}_{EA} = (\dot{u} - \dot{w}\beta_p - \Omega v)\,\hat{e}_{x2}$$

$$+ [\dot{v} + \Omega(e + x + u - w\beta_p)]\,\hat{e}_{y2}$$

$$+ (\dot{u}\beta_p + \dot{w})\,\hat{e}_{z2} \tag{3.85}$$

The total air velocity seen by a point on the elastic axis of the deformed blade in the "2" system is obtained by substituting Eq. (3.78) and (3.85) into Eq. (3.76) to yield:

$$\vec{V}_A = (\mu\Omega R\cos\psi - \dot{u} + \dot{w}\beta_p + \Omega v)\,\hat{e}_{x2}$$

$$+ [-\mu\Omega R\sin\psi - \dot{v} - \Omega(x + e + u - w\beta_p)]\,\hat{e}_{y2}$$

$$- (\lambda\Omega R + \dot{u}\beta_p + \dot{w})\,\hat{e}_{z2} \tag{3.86}$$

To identify the tangential and perpendicular air velocities it is necessary to express the total air velocity $\vec{V}_A$ in the "5" system. Transforming the total air velocity given by Eq. (3.86) to the "5" system using the coordinate transformations defined in Chapter 2 yields:

$$\vec{V}_A = V_{Ax5}\,\hat{e}_{x5} + V_{Ay5}\,\hat{e}_{y5} + V_{Az5}\,\hat{e}_{z5}$$

where

$$V_{Ax5} = -\dot{u} + \Omega v - \dot{v}v_{,x} - \Omega(x + e + u)v_{,x} - \dot{w}w_{,x} - \lambda\Omega R(w_{,x} + \beta_p)$$

$$+ \mu\Omega R\cos\psi - \mu\Omega R v_{,x}\sin\psi \tag{3.87a}$$

$$V_{Ay5} = -\Omega(x + e + u) - \Omega v v_{,x} + \Omega w\beta_p - \dot{v} - \mu\Omega R v_{,x}\cos\psi$$

$$- \mu\Omega R\sin\psi \tag{3.87b}$$

$$V_{Az5} = -\dot{w} - \Omega v(w_{,x} + \beta_p) - \lambda\Omega R - \mu\Omega R(w_{,x} + \beta_p)\cos\psi \tag{3.87c}$$

where the ordering scheme has been employed to neglect the higher order terms.

Therefore, according to Eqs. (3.75), the tangential and perpendicular air velocity, respectively, seen by the blade are given by:

$$U_T = \Omega(x + e + u) + \Omega v v_{,x} - \Omega w\beta_p + \dot{v}$$

$$+ \mu\Omega R v_{,x} \cos\psi + \mu\Omega R \sin\psi \tag{3.88a}$$

$$U_P = \dot{w} + \Omega v(w_{,x} + \beta_p) + \lambda\Omega R + \mu\Omega R(w_{,x} + \beta_p)\cos\psi \tag{3.88b}$$

Equations (3.88) are used to develop explicit expressions for the distributed aerodynamic loads acting on the blade and control surface.

As stated previously the noncirculatory and circulatory lift are assumed to act normal to the total air velocity and the parasitic drag is assumed to act parallel. Since the total air velocity is expressed as components in the "5" system, it is only natural to resolve the aerodynamic forces and moments into components along the axes of the "5" system, as shown in Fig. 12. Defining ϕ_{in} as the angle between the total air velocity and the y_5 axis in the $y_5 - z_5$ plane, then the aerodynamic force per unit span in the "5" system can be expressed as:

$$\vec{p}_A = p_{Ay5}\hat{e}_{y5} + p_{Az5}\hat{e}_{z5}$$

where are given by:

$$p_{Ay5} = -D\cos\phi_{in} - (L_{NC} + L_C)\sin\phi_{in} \tag{3.89a}$$

$$p_{Az5} = -D\sin\phi_{in} + (L_{NC} + L_C)\cos\phi_{in} \tag{3.89b}$$

The angle ϕ_{in}, denoted as the "inflow angle", is so called because it represents the angle between the tangential velocity U_T and the resultant air velocity $\sqrt{U_P^2 + U_P^2}$ which exists because of the perpendicular air velocity U_P, which is due primarily to inflow. The inflow angle is defined by the following:

$$\sin\phi_{in} = \frac{U_P}{\sqrt{U_T^2 + U_P^2}} \tag{3.90a}$$

$$\cos\phi_{in} = \frac{U_T}{\sqrt{U_T^2 + U_P^2}} \tag{3.90b}$$

Examination of the expressions for U_T and U_P given by Eqs. (3.88) reveals that

$$U_T \sim O(1)$$

$$U_P \sim O(\varepsilon)$$

Thus, within the context of the ordering scheme,

$$U_T^2 + U_P^2 \cong U_T^2 \tag{3.91}$$

Therefore, Eqs. (3.90) can be approximated as:

$$\sin \phi_{in} \cong \frac{U_P}{U_T} \tag{3.92a}$$

$$\cos \phi_{in} \cong 1 \tag{3.92b}$$

Equations (3.91) and (3.92) are not valid in the vicinity of the boundary of the reverse flow region, where the tangential velocity U_T approaches zero. However, since the air loads in this region are small compared to those on the outboard sections of the blade, where the effective air velocities are much greater, their use in Eqs. (3.89) should have only a minor impact on the total air loads.

The use of Eq. (3.92a) is convenient, but can lead to mathematical difficulties in the vicinity of the boundary of the reverse flow region when the tangential velocity U_T approaches zero. Such difficulties can be avoided, however, by assuming in Eq. (3.89a) that the noncirculatory lift L_{NC} acts normal to the blade chord, so that the angle ϕ_{in} can be replaced by the angle of attack $\alpha = \theta_G + \phi$. Furthermore, the use of Eq. (3.91) is made in Eq. (3.74) so that the parasitic drag can be replaced by the expression

$$D^* = \frac{1}{2}\rho_A a_o (c_b + c_{cs}) U_T^2 \left(\frac{C_{do}}{a_o}\right) \tag{3.93}$$

Making the aforementioned substitutions, Eqs. (3.89) become:

$$p_{Ay5} = -D - L_{NC}(\theta_G + \phi) - L_C \frac{U_P}{U_T} \tag{3.94a}$$

$$p_{Az5} = -D^* \frac{U_P}{U_T} + L_{NC} + L_C \tag{3.94b}$$

where it has been assumed in the above expressions that $(\theta_G + \phi)$ is a small angle. Though this is not consistent with the ordering scheme used in this study, it is assumed here to be consistent with the aerodynamic formulations of Refs. 38, 50, and 53.

In the derivation of the aerodynamic loads in Appendix A the noncirculatory and circulatory pitching moment are taken to act about the elastic axis of the blade. Therefore the components of the aerodynamic pitching moment per unit span about the elastic axis can be expressed in the "5" system as:

$$\vec{q}_A = q_{Ax5}\hat{e}_{x5}$$

where

$$q_{Ax5} = M_{yNC} + M_{yC} \tag{3.95}$$

The aerodynamic hinge moment per unit span in the "5" system can be expressed as:

$$\vec{q}_{Ah} = q_{Ahx5}\hat{e}_{x5}$$

where

$$q_{Ahx5} = M_{hNC} + M_{hC} \tag{3.96}$$

In addition to the numerical difficulties associated with the existence of the reverse flow region, problems arise when interpretating what happens to the aerodynamic loads inside this region, where the air is flowing over the airfoil in a reversed direction. A reverse flow model, discussed in the next section, is included in this study to account for this flow reversal in a straightforward manner.

3.4.2 *Reverse Flow Model*

In forward flight, a region on the retreating side of the rotor disk experiences reversed flow. This reverse flow region results from the fact that on the retreating side of the rotor disk the component of the total air velocity relative to the blade due to forward flight is directed from the trailing edge to the leading edge of the blade. At certain inboard sections

of the blade (where the velocity of the blade due to its rotation is small) this reversed component of the total air velocity is larger than the component due to the blade's rotation so that the resultant flow sensed by the blade cross-section is from the trailing edge to the leading edge of the blade. All blade stations and azimuth angles for which the total air velocity relative to the blade is reversed comprise the reverse flow region. The boundary of the reverse flow region is described by the locus of points such that the reversed component of the total air velocity due to forward flight is just cancelled by the component due to the rotation of the blade. The equation describing the boundary of the reverse flow region can be found by equating the tangential air velocity U_T to zero. It is impossible to obtain an exact solution for the boundary of the reverse flow region from $U_T = 0$, unless the motion of the blade is known a priori. However, an approximate solution for the boundary of the reverse flow region can be obtained when blade dynamics are neglected. For this case[25] the equation of the boundary of the reverse flow region is given by:

$$r = x + e = -\mu R \sin\psi \tag{3.97}$$

which represents the circular region shown in Fig. 6. Generally Eq. (3.97) is a reasonable approximation for the reverse flow boundary for low to moderate advance ratios. As shown in the cross-hatched region in Fig. 6, the reverse flow region is bounded by a circle of diameter μR centered at $r = \frac{\mu R}{2}$ for the $\psi = 270^\circ$ azimuthal station on the retreating side of the rotor disk. Since the diameter of the reverse flow region is equal to μR, as the forward flight velocity V_F increases, the size of the reverse flow region also increases. The reverse flow region can have a significant impact on the rotor aerodynamic loads, particularly at high advance ratios; and therefore it should be taken into account when computing the aerodynamic loads.

In this study it is assumed that the aerodynamic lift and moment per unit span are zero inside the reverse flow region and that the aerodynamic drag per unit span reverses its direction inside the reverse flow region, remaining parallel to the total air velocity. Thus the reverse flow model employed in this study consists of setting the noncirculatory and circulatory lift to zero and reversing the sign of the parasitic drag for all blade stations in-

side the reverse flow region. This is accomplished by multiplying all of the lift and moment terms by the reverse flow parameter R_{LM}, and by multiplying the parasitic drag terms by the reverse flow parameter R_D, in the expressions for the components of the distributed aerodynamic loads given by Eqs. (3.94) and (3.95)

$$p_{Ay5} = -R_D D - R_{LM} L_{NC}(\theta_G + \phi) - R_{LM} L_C \frac{U_P}{U_T} \tag{3.98a}$$

$$p_{Az5} = -R_D D^* \frac{U_P}{U_T} + R_{LM}(L_{NC} + L_C) \tag{3.98b}$$

$$q_{Ax5} = R_{LM}(M_{yNC} + M_{yC}) \tag{3.99}$$

where the reverse flow parameters are defined as:

$$R_{LM} = \begin{cases} 0 & \text{for} \quad 0 \le x \le x_{rev}(\psi) \\ 1 & \text{for} \quad x > x_{rev}(\psi) \end{cases} \tag{3.100a}$$

$$R_D = \begin{cases} -1 & \text{for} \quad 0 \le x \le x_{rev}(\psi) \\ 1 & \text{for} \quad x > x_{rev}(\psi) \end{cases} \tag{3.100b}$$

The quantity $x_{rev}(\psi)$ represents the location of the boundary of the reverse flow region on blade span, and using Eq. (3.97) it can be defined as:

$$x_{rev}(\psi) = -(e + \mu R \sin\psi) \tag{3.101}$$

Equations (3.98) – (3.100) are used in the next two sections to develop the distributed aerodynamic loads on the blade and on the control surface.

3.4.3 *Aerodynamic Loads on the Blade*

The expressions for the noncirculatory and circulatory lift and pitching moment acting on the blade without the presence of a control surface can be obtained by setting $c_{cs} = 0$ in Eqs. (3.68) – (3.71).

The noncirculatory lift acting on the blade is given by:

$$L_{NCb} = \frac{1}{8}\rho_A a_o c_b^2[\dot{U}_T(\theta_G + \phi) + U_T(\dot{\theta}_G + \dot{\phi})$$

$$- \dot{U}_P - (X_A - \frac{1}{4}c_b)(\ddot{\theta}_G + \ddot{\phi})] \tag{3.102}$$

The circulatory lift acting on the blade is given by:

$$L_{Cb} = \frac{1}{2}\rho_A a_o c_b U_T[U_T(\theta_G + \phi) - U_P$$

$$+ (\frac{1}{2}c_b - X_A)(\dot{\theta}_G + \dot{\phi})] \tag{3.103}$$

The noncirculatory pitching moment acting on the blade is given by:

$$M_{yNCb} = \frac{1}{8}\rho_A a_o c_b^2[U_T^2(\theta_G + \phi) - (X_A - \frac{1}{4}c_b)\dot{U}_P - U_T U_P$$

$$- (X_A^2 - \frac{1}{2}X_A c_b + \frac{3}{32}c_b^2)(\ddot{\theta}_G + \ddot{\phi})$$

$$+ (X_A - \frac{1}{4}c_b)\dot{U}_T(\theta_G + \phi)] \tag{3.104}$$

The circulatory pitching moment acting on the blade is given by:

$$M_{yCb} = \frac{1}{2}\rho_A a_o U_T c_b(X_A - \frac{1}{4}c_b)[U_T(\theta_G + \phi) - U_P$$

$$+ (\frac{1}{2}c_b - X_A)(\dot{\theta}_G + \dot{\phi})] \tag{3.105}$$

The parasitic drag acting on the blade cross-section is obtained by setting $c_{cs} = 0$ in Eq. (3.74), i.e.

$$D_b = \frac{1}{2}\rho_A a_o c_b(U_T^2 + U_P^2)(\frac{C_{do}}{a_o}) \tag{3.106}$$

Similarly, setting $c_{cs} = 0$ in Eq. (3.93) yields

$$D_b^* = \frac{1}{2}\rho_A a_o c_b U_T^2(\frac{C_{do}}{a_o}) \tag{3.107}$$

Since Theodorsen's theory[52] was derived for a symmetric airfoil, the moment per unit span given by:

$$M_{camb} = \frac{1}{2}\rho_A a_o c_b^2 (U_T^2 + U_P^2)(\frac{C_{mo}}{a_o}) \tag{3.108}$$

accounts for, in an approximate manner, the moment about the elastic axis due to any camber in the airfoil. This was also done in Refs. 38 and 50.

Using Eq. (3.98), the components of the aerodynamic force per unit span acting on the blade in the "5" system can be expressed as:

$$p_{Aby5} = -R_D D_b - R_{LM} L_{NCb}(\theta_G + \phi) - R_{LM} L_{Cb} \frac{U_P}{U_T}$$

$$p_{Abz5} = -R_D D_b^* \frac{U_P}{U_T} + R_{LM}(L_{NCb} + L_{Cb})$$

Substituting Eqs. (3.102), (3.103), (3.106) and (3.107) into the previous expressions yield:

$$p_{Aby5} = -\frac{R_D}{2}\rho_A a_o c_b (U_T^2 + U_P^2)(\frac{C_{do}}{a_o})$$

$$-\frac{R_{LM}}{8}\rho_A a_o c_b^2 [\dot{U}_T(\theta_G + \phi) + U_T(\dot{\theta}_G + \dot{\phi}) - \dot{U}_P$$

$$-(X_A - \frac{1}{4}c_b)(\ddot{\theta}_G + \ddot{\phi})](\theta_G + \phi)$$

$$-\frac{R_{LM}}{2}\rho_A a_o c_b U_P [U_T(\theta_G + \phi) - U_P$$

$$+(\frac{1}{2}c_b - X_A)(\dot{\theta}_G + \dot{\phi})]$$

$$p_{Abz5} = -\frac{R_D}{2}\rho_A a_o c_b U_T U_P (\frac{C_{do}}{a_o})$$

$$+\frac{R_{LM}}{8}\rho_A a_o c_b^2 [\dot{U}_T(\theta_G + \phi) + U_T(\dot{\theta}_G + \dot{\phi}) - \dot{U}_P$$

$$-(X_A - \frac{1}{4}c_b)(\ddot{\theta}_G + \ddot{\phi})]$$

$$+\frac{R_{LM}}{2}\rho_A a_o c_b U_T[U_T(\theta_G+\phi)-U_P$$

$$+(\frac{1}{2}c_b-X_A)(\dot{\theta}_G+\dot{\phi})]$$

Substituting the expressions for U_T and U_P given by Eqs. (3.88) into the above expressions yields:

p_{Aby5} =

$$\rho_A a_o c_b R_{LM}\{\frac{1}{2}(X_A-\frac{1}{2}c_b)(\dot{\theta}_G+\dot{\phi})\dot{w}+\frac{1}{2}(X_A-\frac{1}{2}c_b)\Omega v(\dot{\theta}_G+\dot{\phi})(w_{,x}+\beta_p)$$

$$+\frac{1}{2}(X_A-\frac{1}{2}c_b)(\dot{\theta}_G+\dot{\phi})(\lambda\Omega R)+\frac{1}{2}\dot{w}^2+\Omega v\dot{w}(w_{,x}+\beta_p)$$

$$+(\lambda\Omega R)\dot{w}+\frac{1}{2}\Omega^2 v^2(w_{,x}+\beta_p)^2+\Omega v(\lambda\Omega R)(w_{,x}+\beta_p)+\frac{1}{2}(\lambda\Omega R)^2$$

$$+[\frac{1}{2}(X_A-\frac{1}{2}c_b)(\dot{\theta}_G+\dot{\phi})(w_{,x}+\beta_p)+\dot{w}(w_{,x}+\beta_p)+\Omega v(w_{,x}+\beta_p)^2$$

$$+(\lambda\Omega R)(w_{,x}+\beta_p)](\mu\Omega R)\cos\psi$$

$$+\frac{1}{2}(w_{,x}+\beta_p)^2(\mu\Omega R)^2\cos^2\psi\}$$

$$+\rho_A a_o c_b R_{LM}(\theta_G+\phi)\{-\frac{1}{2}\Omega v\dot{w}v_{,x}-\frac{1}{2}\Omega v v_{,x}(\lambda\Omega R)-\frac{1}{8}c_b\Omega v v_{,x}(\dot{\theta}_G+\dot{\phi})$$

$$+\frac{1}{8}(X_A-\frac{1}{4}c_b)c_b(\ddot{\theta}_G+\ddot{\phi})+\frac{1}{8}c_b\ddot{w}+\frac{1}{2}\Omega w\dot{w}\beta_p-\frac{1}{2}\dot{v}\dot{w}$$

$$-\frac{1}{2}\Omega u\dot{w}-\frac{1}{2}e\Omega\dot{w}+\frac{1}{2}\Omega w\beta_p(\lambda\Omega R)+\frac{1}{8}c_b\Omega w\beta_p(\dot{\theta}_G+\dot{\phi})$$

$$-\frac{1}{2}\Omega v\dot{v}(w_{,x}+\beta_p)-\frac{1}{2}(\lambda\Omega R)\dot{v}+\frac{1}{8}c_b\Omega\dot{v}(w_{,x}+\beta_p)$$

$$-\frac{1}{8}c_b\dot{v}(\dot{\theta}_G+\dot{\phi})-\frac{1}{2}e\Omega^2 v(w_{,x}+\beta_p)+\frac{1}{8}c_b\Omega v\dot{w}_{,x}-\frac{1}{2}\Omega u(\lambda\Omega R)$$

$$-\frac{1}{8}c_b\Omega u(\dot{\theta}_G+\dot{\phi})-\frac{1}{2}\Omega e(\lambda\Omega R)-\frac{1}{8}ec_b\Omega(\dot{\theta}_G+\dot{\phi})$$

$$+ [-\frac{1}{2}\dot{w}v_{,x} - \Omega v v_{,x}(w_{,x} + \beta_p) - \frac{1}{2}(\lambda\Omega R)v_{,x} - \frac{1}{8}c_b(\dot{\theta}_G + \dot{\phi})v_{,x}$$

$$+ \frac{1}{2}\Omega w\beta_p(w_{,x} + \beta_p) - \frac{1}{2}\dot{v}(w_{,x} + \beta_p) - \frac{1}{2}\Omega u(w_{,x} + \beta_p)$$

$$- \frac{1}{2}e\Omega(w_{,x} + \beta_p) + \frac{1}{8}c_b\dot{w}_{,x}](\mu\Omega R)\cos\psi$$

$$+ [-\frac{1}{2}\dot{w} - \frac{1}{2}\Omega v(w_{,x} + \beta_p) - \frac{1}{2}(\lambda\Omega R) - \frac{1}{8}c_b\Omega(w_{,x} + \beta_p)$$

$$- \frac{1}{8}c_b(\dot{\theta}_G + \dot{\phi})](\mu\Omega R)\sin\psi$$

$$- \frac{1}{2}(w_{,x} + \beta_p)(\mu\Omega R)^2\cos\psi\sin\psi - \frac{1}{2}(w_{,x} + \beta_p)v_{,x}(\mu\Omega R)^2\cos^2\psi\}$$

$$+ \rho_A a_o c_b R_{LM}(\theta_G + \phi)^2\{ -\frac{1}{8}c_b\Omega v\dot{v}_{,x} - \frac{1}{8}c_b\Omega\dot{v}v_{,x} + \frac{1}{8}c_b\Omega\dot{w}\beta_p - \frac{1}{8}c_b\ddot{v}$$

$$- \frac{1}{8}c_b\Omega\dot{u} - \frac{1}{8}c_b(\Omega + \dot{v}_{,x})(\mu\Omega R)\cos\psi + \frac{1}{8}c_b\Omega v_{,x}(\mu\Omega R)\sin\psi\}$$

$$+ \rho_A a_o c_b R_{LM}x(\theta_G + \phi)[-\frac{1}{2}\Omega\dot{w} - \frac{1}{2}\Omega^2 v(w_{,x} + \beta_p) - \frac{1}{2}\Omega(\lambda\Omega R)$$

$$- \frac{1}{8}c_b\Omega(\dot{\theta}_G + \dot{\phi}) - \frac{1}{2}\Omega(w_{,x} + \beta_p)(\mu\Omega R)\cos\psi]$$

$$+ \rho_A a_o c_b R_D(\frac{C_{do}}{a_o})\{ -\frac{1}{2}\dot{w}^2 - \dot{w}(\lambda\Omega R) - \frac{1}{2}\dot{v}^2 - e\Omega\dot{v} - \frac{1}{2}(\lambda\Omega R)^2 - \frac{1}{2}e^2\Omega^2$$

$$+ [-\dot{v}v_{,x} - e\Omega v_{,x} - \dot{w}(w_{,x} + \beta_p) - (\lambda\Omega R)(w_{,x} + \beta_p)](\mu\Omega R)\cos\psi$$

$$+ [-\Omega v v_{,x} + \Omega w\beta_p - \dot{v} - \Omega u - \Omega e](\mu\Omega R)\sin\psi$$

$$- v_{,x}(\mu\Omega R)^2\cos\psi\sin\psi - \frac{1}{2}[v_{,x}^2 - (w_{,x} + \beta_p)^2](\mu\Omega R)^2\cos^2\psi$$

$$- \frac{1}{2}(\mu\Omega R)^2\sin^2\psi\}$$

$$+ \rho_A a_o c_b R_D(\frac{C_{do}}{a_o})x[-\Omega^2 v v_{,x} + \Omega^2 w\beta_p - \Omega\dot{v} - \Omega^2 u - \Omega^2 e$$

$$- \Omega v_{,x}(\mu\Omega R)\cos\psi - \Omega(\mu\Omega R)\sin\psi\,]$$

$$- \frac{1}{2}\rho_A a_o c_b R_D\left(\frac{C_{do}}{a_o}\right)x^2\Omega^2 \qquad (3.109a)$$

$$p_{Abz5} =$$

$$\rho_A a_o c_b R_{LM}\{ - \frac{1}{2}\Omega v\dot{w}v_{,x} - \frac{1}{2}\Omega v v_{,x}(\lambda\Omega R) - \frac{1}{8}(X_A - \frac{1}{4}c_b)c_b(\ddot{\theta}_G + \ddot{\phi})$$

$$- \frac{1}{2}(X_A - \frac{1}{2}c_b)\dot{v}(\dot{\theta}_G + \dot{\phi}) - \frac{1}{2}(X_A - \frac{1}{2}c_b)\Omega e(\dot{\theta}_G + \dot{\phi}) - \frac{1}{8}c_b\ddot{w}$$

$$+ \frac{1}{2}\Omega w\dot{w}\beta_p - \frac{1}{2}\dot{w}\dot{v} - \frac{1}{2}\Omega u\dot{w} - \frac{1}{2}e\Omega\dot{w} + \frac{1}{2}\Omega w(\lambda\Omega R)\beta_p$$

$$- \frac{1}{2}\Omega v\dot{v}(w_{,x} + \beta_p) - \frac{1}{2}\dot{v}(\lambda\Omega R) - \frac{1}{8}c_b\Omega\dot{v}(w_{,x} + \beta_p) + \frac{1}{8}c_b\dot{v}(\dot{\theta}_G + \dot{\phi})$$

$$- \frac{1}{2}e\Omega^2 v(w_{,x} + \beta_p) - \frac{1}{8}c_b\Omega v\dot{w}_{,x} - \frac{1}{2}\Omega u(\lambda\Omega R)$$

$$- \frac{1}{2}e\Omega(\lambda\Omega R) + \frac{1}{8}c_b e\Omega(\dot{\theta}_G + \dot{\phi})$$

$$+ [- \frac{1}{2}(X_A - \frac{1}{2}c_b)(\dot{\theta}_G + \dot{\phi})v_{,x} - \frac{1}{2}\dot{w}v_{,x} - \Omega v v_{,x}(w_{,x} + \beta_p)$$

$$- \frac{1}{2}(\lambda\Omega R)v_{,x} + \frac{1}{8}c_b(\dot{\theta}_G + \dot{\phi})v_{,x} + \frac{1}{2}\Omega w\beta_p(w_{,x} + \beta_p)$$

$$- \frac{1}{2}\dot{v}(w_{,x} + \beta_p) - \frac{1}{2}\Omega u(w_{,x} + \beta_p) - \frac{1}{2}e\Omega(w_{,x} + \beta_p)$$

$$- \frac{1}{8}c_b\dot{w}_{,x}](\mu\Omega R)\cos\psi$$

$$+ [- \frac{1}{2}(X_A - \frac{1}{2}c_b)(\dot{\theta}_G + \dot{\phi}) - \frac{1}{2}\dot{w} - \frac{1}{2}\Omega v(w_{,x} + \beta_p)$$

$$- \frac{1}{2}(\lambda\Omega R) + \frac{1}{8}c_b\Omega(w_{,x} + \beta_p) + \frac{1}{8}c_b(\dot{\theta}_G + \dot{\phi})](\mu\Omega R)\sin\psi$$

$$- \frac{1}{2}(w_{,x} + \beta_p)(\mu\Omega R)^2\cos\psi\sin\psi - \frac{1}{2}(w_{,x} + \beta_p)v_{,x}(\mu\Omega R)^2\cos^2\psi\}$$

$$+ \rho_A a_o c_b R_{LM}(\theta_G + \phi)\{\frac{1}{8}c_b\Omega v\dot{v}_{,x} + \Omega v\dot{v}v_{,x} + \frac{1}{8}c_b\Omega\dot{v}v_{,x} + e\Omega^2 vv_{,x}$$

$$- \frac{1}{8}c_b\Omega\dot{w}\beta_p - \Omega\dot{v}w\beta_p - e\Omega^2 w\beta_p + \frac{1}{8}c_b\ddot{v} + \frac{1}{2}\dot{v}^2 + \Omega u\dot{v} + e\Omega\dot{v}$$

$$+ \frac{1}{8}c_b\Omega\dot{u} + e\Omega^2 u + \frac{1}{2}e^2\Omega^2$$

$$+ [\frac{1}{8}c_b\dot{v}_{,x} + \Omega vv_{,x}{}^2 - \Omega wv_{,x}\beta_p + \dot{v}v_{,x} + \Omega(e + u)v_{,x}$$

$$+ \frac{1}{8}c_b\Omega](\mu\Omega R)\cos\psi$$

$$+ [\Omega vv_{,x} - \frac{1}{8}c_b\Omega v_{,x} - \Omega w\beta_p + \dot{v} + \Omega u + e\Omega](\mu\Omega R)\sin\psi$$

$$+ v_{,x}(\mu\Omega R)^2\cos\psi\sin\psi + \frac{1}{2}v_{,x}{}^2(\mu\Omega R)^2\cos^2\psi + \frac{1}{2}(\mu\Omega R)^2\sin^2\psi\}$$

$$+ \rho_A a_o c_b R_{LM}x[-\frac{1}{2}(X_A - \frac{1}{2}c_b)\Omega(\dot{\theta}_G + \dot{\phi}) - \frac{1}{2}\Omega\dot{w}\beta_p(w_{,x} + \beta_p) - \frac{1}{2}\Omega\dot{w}$$

$$- \frac{1}{2}\Omega^2 v(w_{,x} + \beta_p) + \frac{1}{2}\Omega\dot{u}w_{,x} - \frac{1}{2}\Omega(\dot{\lambda}\Omega R) + \frac{1}{8}c_b\Omega(\dot{\theta}_G + \dot{\phi})$$

$$- \frac{1}{2}\Omega(w_{,x} + \beta_p)(\mu\Omega R)\cos\psi]$$

$$+ \rho_A a_o c_b R_{LM}x(\theta_G + \phi)[\Omega^2 vv_{,x} - \Omega^2 w\beta_p + \Omega\dot{v} + \Omega^2 u + e\Omega^2$$

$$+ \Omega v_{,x}(\mu\Omega R)\cos\psi + \Omega(\mu\Omega R)\sin\psi]$$

$$+ \frac{1}{2}\rho_A a_o c_b R_{LM}x^2(\theta_G + \phi)\Omega^2$$

$$+ \rho_A a_o c_b R_D(\frac{C_{do}}{a_o})[-\frac{1}{2}(\dot{w} + \dot{\lambda}\Omega R)(\mu\Omega R)\sin\psi$$

$$- \frac{1}{2}(w_{,x} + \beta_p)(\mu\Omega R)^2\cos\psi\sin\psi]$$

$$+ \rho_A a_o c_b R_D(\frac{C_{do}}{a_o})x[-\frac{1}{2}\Omega\dot{w} - \Omega(\dot{\lambda}\Omega R)$$

$$- \frac{1}{2}\Omega(w_{,x} + \beta_p)(\mu\Omega R)\cos\psi] \tag{3.109b}$$

Using Eq. (3.99), together with Eq. (3.108), the aerodynamic pitching moment about the elastic axis of the blade in the "5" system can be expressed as:

$$q_{Abx5} = R_{LM}(M_{yNCb} + M_{yCb} + M_{camb})$$

Substituting Eqs. (3.104), (3.105) and (3.108) into the previous expression yields:

$$q_{Abx5} = \frac{R_{LM}}{8}\rho_A a_o c_b^2\{(X_A - \frac{1}{2}c_b)(\dot{\theta}_G + \dot{\phi}) - (X_A - \frac{1}{4}c_b)\dot{U}_P$$

$$- [(X_A - \frac{1}{4}c_b)^2 + \frac{1}{32}c_b^2](\ddot{\theta}_G + \ddot{\phi}) + (X_A - \frac{1}{4}c_b)\dot{U}_T(\theta_G + \phi)\}$$

$$+ \frac{R_{LM}}{2}\rho_A a_o c_b U_T X_A[U_T(\theta_G + \phi) - U_P + (\frac{1}{2}c_b - X_A)(\dot{\theta}_G + \dot{\phi})]$$

$$+ \frac{R_{LM}}{2}\rho_A a_o c_b^2(U_T^2 + U_P^2)(\frac{C_{mo}}{a_o})$$

Substituting the expressions for U_T and U_P given by Eqs. (3.88) into the above expression yields:

$q_{Abx5} =$

$$\rho_A a_o c_b R_{LM}\{ - \frac{1}{8}[(X_A - \frac{1}{4}c_b)^2 + \frac{1}{32}c_b^2]c_b(\ddot{\theta}_G + \ddot{\phi}) - \frac{1}{8}c_b(X_A - \frac{1}{4}c_b)\ddot{w}$$

$$- \frac{1}{2}X_A\dot{v}\dot{w} - \frac{1}{2}eX_A\Omega\dot{w} - \frac{1}{2}X_A\dot{v}(\lambda\Omega R) - \frac{1}{2}eX_A\Omega(\lambda\Omega R)$$

$$+ [- \frac{1}{2}X_A\dot{w}v_{,x} - \frac{1}{2}X_A v_{,x}(\lambda\Omega R) - \frac{1}{8}c_b(X_A - \frac{1}{4}c_b)\dot{w}_{,x}$$

$$- \frac{1}{2}X_A\dot{v}(w_{,x} + \beta_p) - \frac{1}{2}eX_A\Omega(w_{,x} + \beta_p)](\mu\Omega R)\cos\psi$$

$$+ [- \frac{1}{2}(X_A - \frac{1}{2}c_b)(X_A - \frac{1}{4}c_b)(\dot{\theta}_G + \dot{\phi})$$

$$+ \frac{1}{8}(X_A - \frac{1}{4}c_b)c_b\Omega(w_{,x} + \beta_p) - \frac{1}{2}X_A\dot{w} - \frac{1}{2}X_A\Omega v(w_{,x} + \beta_p)$$

$$- \frac{1}{2}X_A(\lambda\Omega R) + c_b\dot{v}(\frac{C_{mo}}{a_o}) + c_b e\Omega(\frac{C_{mo}}{a_o})](\mu\Omega R)\sin\psi$$

$$+ [c_b v_{,x}(\frac{C_{mo}}{a_o}) - \frac{1}{2}X_A(w_{,x} + \beta_p)](\mu\Omega R)^2\cos\psi\sin\psi$$

$$- \frac{1}{2}X_A v_{,x}(w_{,x} + \beta_p)(\mu\Omega R)^2\cos^2\psi + \frac{1}{2}c_b(\frac{C_{mo}}{a_o})(\mu\Omega R)^2\sin^2\psi\}$$

$$+ \rho_A a_o c_b R_{LM}(\theta_G + \phi)\{\frac{1}{8}c_b(X_A - \frac{1}{4}c_b)\ddot{v} + \frac{1}{2}X_A\dot{v}^2 + eX_A\Omega\dot{v} + \frac{1}{2}e^2X_A\Omega^2$$

$$+ [\frac{1}{8}c_b(X_A - \frac{1}{4}c_b)\dot{v}_{,x} + X_A\dot{v}v_{,x} + eX_A\Omega v_{,x}$$

$$+ \frac{1}{8}(X_A - \frac{1}{4}c_b)c_b\Omega](\mu\Omega R)\cos\psi$$

$$+ [-\frac{1}{8}c_b(X_A - \frac{1}{4}c_b)\Omega v_{,x} + X_A\Omega vv_{,x} - X_A\Omega w\beta_p + X_A\dot{v}$$

$$+ X_A\Omega u + eX_A\Omega](\mu\Omega R)\sin\psi$$

$$+ X_A v_{,x}(\mu\Omega R)^2\cos\psi\sin\psi + \frac{1}{2}X_A v_{,x}{}^2(\mu\Omega R)^2\cos^2\psi$$

$$+ \frac{1}{2}X_A(\mu\Omega R)^2\sin^2\psi\}$$

$$+ \rho_A a_o c_b R_{LM}x\{-\frac{1}{2}(X_A - \frac{1}{2}c_b)(X_A - \frac{1}{4}c_b)\Omega(\dot{\theta}_G + \dot{\phi}) - \frac{1}{2}X_A\Omega\dot{w}$$

$$- \frac{1}{2}X_A\Omega^2 v(w_{,x} + \beta_p) - \frac{1}{2}X_A\Omega(\lambda\Omega R) + c_b\Omega\dot{v}(\frac{C_{mo}}{a_o}) + c_b e\Omega^2(\frac{C_{mo}}{a_o})$$

$$+ [c_b\Omega v_{,x}(\frac{C_{mo}}{a_o}) - \frac{1}{2}X_A\Omega(w_{,x} + \beta_p)](\mu\Omega R)\cos\psi$$

$$+ c_b\Omega(\frac{C_{mo}}{a_o})(\mu\Omega R)\sin\psi\}$$

$$+ \rho_A a_o c_b R_{LM}x(\theta_G + \phi)[X_A\Omega^2 vv_{,x} - X_A\Omega^2 w\beta_p + X_A\Omega\dot{v} + X_A\Omega^2 u + X_A e\Omega^2$$

$$+ X_A\Omega v_{,x}(\mu\Omega R)\cos\psi + X_A\Omega(\mu\Omega R)\sin\psi]$$

$$+\frac{1}{2}\rho_A a_o c_b R_{LM} x^2 c_b \Omega^2 (\frac{C_{mo}}{a_o})$$

$$+\frac{1}{2}\rho_A a_o c_b R_{LM} x^2 (\theta_G + \phi) X_A \Omega^2 \tag{3.110}$$

The distributed aerodynamic loads acting on the blade can be transformed from the "5" system to the "3" system, in which the equations of motion are formulated, using the co-ordinate transformation defined in Chapter 2. The distributed aerodynamic force acting on the blade can be expressed in the "3" system as:

$$\vec{p}_{Ab} = p_{Abx3}\hat{e}_{x3} + p_{Aby3}\hat{e}_{y3} + p_{Abz3}\hat{e}_{z3}$$

where

$$p_{Abx3} = -v_{,x}\, p_{Aby5} - w_{,x}\, p_{Abz5} \tag{3.111a}$$

$$p_{Aby3} = p_{Aby5} \tag{3.111b}$$

$$p_{Abz3} = -v_{,x} w_{,x}\, p_{Aby5} + p_{Abz5} \tag{3.111c}$$

Similarly, the distributed aerodynamic moment acting on the blade can be expressed in the "3" system as:

$$\vec{q}_{Ab} = q_{Abx3}\hat{e}_{x3} + q_{Aby3}\hat{e}_{y3} + q_{Abz3}\hat{e}_{z3}$$

where

$$q_{Abx3} = q_{Abx5} \tag{3.112a}$$

$$q_{Aby3} = v_{,x}\, q_{Abx5} \tag{3.112b}$$

$$q_{Abz3} = w_{,x}\, q_{Abx5} \tag{3.112c}$$

3.4.4 *Aerodynamic Loads on the Control Surface*

The contributions to the total noncirculatory and circulatory lift and moment acting on the blade due to the presence of an aerodynamic surface on the blade cross-section can be determined by subtracting the contribution due to the airfoil alone given by Eqs. (3.102) – (3.105) from the total airloads due to the airfoil and the control surface given by Eqs. (3.68) – (3.71), i.e.

$$\Lambda L_{NC} = L_{NC} - L_{NCb}$$

$$\Lambda L_C = L_C - L_{Cb}$$

$$\Lambda M_{yNC} = M_{yNC} - M_{yNCb}$$

$$\Lambda M_{yC} = M_{yC} - M_{yCb}$$

where the Λ symbol refers to the change in the quantity due to the presence of the control surface. Carrying out these subtractions yield:

$$\Delta L_{NC} = \frac{1}{8}\rho_A a_o (c_b + c_{cs})^2 [\frac{1}{2} c_{cs}(\ddot{\theta}_G + \ddot{\phi}) - 2(\dot{U}_T\delta + U_T\dot{\delta})\frac{T_4}{a_o}$$

$$- (c_b + c_{cs})\ddot{\delta}\frac{T_1}{a_o}]$$

$$+ \frac{1}{8}\rho_A a_o c_{cs}(2c_b + c_{cs})[\dot{U}_T(\theta_G + \phi) + U_T(\dot{\theta}_G + \dot{\phi})$$

$$- (X_A - \frac{1}{4}c_b)(\ddot{\theta}_G + \ddot{\phi}) - \dot{U}_P] \qquad (3.113)$$

$$\Lambda L_C = \frac{1}{2}\rho_A a_o (c_b + c_{cs}) U_T [\frac{3}{2} c_{cs}(\ddot{\theta}_G + \ddot{\phi}) + 2\frac{T_{10}}{a_o} U_T\delta$$

$$+ \frac{1}{4}(2c_b + 3c_{cs})\frac{T_{11}}{a_o}\dot{\delta}]$$

$$+ \frac{1}{2}\rho_A a_o c_{cs} U_T [U_T(\theta_G + \phi) - U_P - (X_A - \frac{1}{2}c_b)(\dot{\theta}_G + \dot{\phi})] \qquad (3.114)$$

$$\Delta M_{yNC} = \frac{1}{8}\rho_A a_o (c_b + c_{cs})^2 \{ -\frac{1}{32} c_{cs}(2c_b + c_{cs})(\ddot{\theta}_G + \ddot{\phi})$$

$$+ c_{cs}[X_A - \frac{1}{4}(c_b + c_{cs})](\ddot{\theta}_G + \ddot{\phi})$$

$$- \frac{1}{2} c_{cs}[\dot{U}_T(\theta_G + \phi) - \dot{U}_P]$$

$$- 2\frac{T_4}{a_o} U_T^2 \delta - \frac{T_1}{a_o}(c_b + c_{cs}) U_T \dot{\delta}$$

$$+ [\frac{T_8}{a_o}(c_b + c_{cs}) + (\frac{3}{2}c_b - 2X_A)\frac{T_4}{a_o}](\dot{U}_T \delta + U_T \dot{\delta})$$

$$+ \frac{1}{2}(c_b + c_{cs})[\frac{T_7}{a_o}(c_b + c_{cs}) + (\frac{3}{2}c_b - 2X_A)\frac{T_1}{a_o}]\ddot{\delta}\}$$

$$+ \frac{1}{8}\rho_A a_o c_{cs}(2c_b + c_{cs})\{U_T^2(\theta_G + \phi) - U_T U_P$$

$$- [(X_A - \frac{1}{4}c_b)^2 + \frac{1}{32}c_b^2](\ddot{\theta}_G + \ddot{\phi})$$

$$+ (X_A - \frac{1}{4}c_b)[\dot{U}_T(\theta_G + \phi) - \dot{U}_P]\} \qquad (3.115)$$

$$\Delta M_{yC} = \frac{1}{2}\rho_A a_o (c_b + c_{cs}) U_T [\frac{3}{2} c_{cs}(\dot{\theta}_G + \dot{\phi}) + 2\frac{T_{10}}{a_o} U_T \delta$$

$$+ \frac{1}{4}(2c_b + 3c_{cs})\frac{T_{11}}{a_o}\dot{\delta}][X_A - \frac{1}{4}(c_b + 2c_{cs})]$$

$$+ \frac{1}{2}\rho_A a_o c_{cs} U_T [U_T(\theta_G + \phi) - U_P$$

$$- (X_A - \frac{1}{2}c_b)(\dot{\theta}_G + \dot{\phi})][X_A - \frac{1}{4}(3c_b + 2c_{cs})] \qquad (3.116)$$

The additional parasitic drag acting on the blade cross-section due to the presence of the control surface can be defined as:

$$D_c = D - D_b = \frac{1}{2}\rho_A a_o c_{cs}(U_T^2 + U_P^2)(\frac{C_{do}}{a_o}) \qquad (3.117)$$

where Eqs. (3.74) and (3.106) have been used. Similarly,

$$D_c^* = D^* - D_b^* = \frac{1}{2}\rho_A a_o c_{cs} U_T^2 (\frac{C_{do}}{a_o}) \tag{3.118}$$

is obtained by subtracting Eq. (3.93) from Eq. (3.107).

Equations (3.113)-(3.116) represent the contribution to the total lift and pitching moment per unit span acting on the blade cross-section due to the presence of a flap as predicted by 2D quasisteady aerodynamics. Comparisons of experimentally and theoretically determined values of the additional lift and moment produced by a flap have demonstrated in the case of fixed-wing aircraft that 2D quasisteady aerodynamics tend to overestimate the airloads by 25-50%[17]. This discrepancy, which increases with increasing Mach number, has been attributed primarily to the presence of a gap between the trailing edge of the airfoil and the leading edge of the flap, which was not accounted for in the theoretical model. The presence of a gap, which is not modeled in the present study, reduces the effectiveness of the flap[55]. Therefore, a multiplicative correction factor denoted as C_f, which is less than one, is used to scale the control flap aerodynamic loads given by Eqs. (3.113)-(3.116).

Using Eqs. (3.98) the components of the additional distributed aerodynamic force in the "5" system acting on the blade cross-section due to the presence of a control surface are given by:

$$p_{Acy5} = -D_c - C_f[\Lambda L_{NC}(\theta_G + \phi) + \Lambda L_C \frac{U_P}{U_T}]$$

$$p_{Acz5} = -D_c^* \frac{U_P}{U_T} + C_f(\Lambda L_{NC} + \Lambda L_C)$$

where the fact that the control surface is located outside the reverse flow region has been used (i.e. $R_D = R_{LM} = 1$). Substituting Eqs. (3.113), (3.114), (3.117) and (3.118) into the previous expressions yield:

$$p_{Acy5} = -\frac{1}{2}\rho_A a_o c_{cs}(U_T^2 + U_P^2)(\frac{C_{do}}{a_o})$$

Q-2

$$- \frac{C_f}{8}\rho_A a_o (c_b + c_{cs})^2 [\frac{1}{2} c_{cs}(\ddot{\theta}_G + \ddot{\phi}) - 2(\dot{U}_T\delta + U_T\dot{\delta})\frac{T_4}{a_o}$$

$$- (c_b + c_{cs})\ddot{\delta}\frac{T_1}{a_o}](\theta_G + \phi)$$

$$- \frac{C_f}{8}\rho_A a_o c_{cs}(2c_b + c_{cs})[\dot{U}_T(\theta_G + \phi) + U_T(\dot{\theta}_G + \dot{\phi})$$

$$- (X_A - \frac{1}{4}c_b)(\ddot{\theta}_G + \ddot{\phi}) - \dot{U}_P](\theta_G + \phi)$$

$$- \frac{C_f}{2}\rho_A a_o (c_b + c_{cs})U_P[\frac{3}{2}c_{cs}(\ddot{\theta}_G + \ddot{\phi}) + 2\frac{T_{10}}{a_o}U_T\delta$$

$$+ \frac{1}{4}(2c_b + 3c_{cs})\frac{T_{11}}{a_o}\dot{\delta}]$$

$$- \frac{C_f}{2}\rho_A a_o c_{cs} U_P[U_T(\theta_G + \phi) - U_P - (X_A - \frac{1}{2}c_b)(\dot{\theta}_G + \dot{\phi})]$$

$$p_{Acz5} = - \frac{1}{2}\rho_A a_o c_{cs} U_T U_P(\frac{C_{do}}{a_o})$$

$$+ \frac{C_f}{8}\rho_A a_o (c_b + c_{cs})^2 [\frac{1}{2} c_{cs}(\ddot{\theta}_G + \ddot{\phi}) - 2(\dot{U}_T\delta + U_T\dot{\delta})\frac{T_4}{a_o}$$

$$- (c_b + c_{cs})\ddot{\delta}\frac{T_1}{a_o}]$$

$$+ \frac{C_f}{8}\rho_A a_o c_{cs}(2c_b + c_{cs})[\dot{U}_T(\theta_G + \phi) + U_T(\dot{\theta}_G + \dot{\phi})$$

$$- (X_A - \frac{1}{4}c_b)(\ddot{\theta}_G + \ddot{\phi}) - \dot{U}_P]$$

$$+ \frac{C_f}{2}\rho_A a_o (c_b + c_{cs})U_T[\frac{3}{2}c_{cs}(\ddot{\theta}_G + \ddot{\phi}) + 2\frac{T_{10}}{a_o}U_T\delta$$

$$+ \frac{1}{4}(2c_b + 3c_{cs})\frac{T_{11}}{a_o}\dot{\delta}]$$

$$+ \frac{C_f}{2}\rho_A a_o c_{cs} U_T[U_T(\theta_G + \phi) - U_P - (X_A - \frac{1}{2}c_b)(\dot{\theta}_G + \dot{\phi})]$$

Substituting the expressions for U_T and U_P given by Eqs. (3.88) into the above expressions yield:

$$p_{Acy5} =$$

$$\rho_A a_o C_f \{\frac{1}{2}c_{cs}\dot{w}^2 - (c_b + c_{cs})\dot{v}\dot{w}\frac{T_{10}}{a_o}\delta - \frac{1}{8}(c_b + c_{cs})(2c_b + 3c_{cs})\dot{w}\frac{T_{11}}{a_o}\dot{\delta}$$

$$- (c_b + c_{cs})e\Omega\dot{w}\frac{T_{10}}{a_o}\delta + c_{cs}\dot{w}(\lambda\Omega R) - \frac{3}{4}(c_b + c_{cs})c_{cs}\dot{w}(\dot{\theta}_G + \dot{\phi})$$

$$- (c_b + c_{cs})\dot{v}(\lambda\Omega R)\frac{T_{10}}{a_o}\delta - \frac{1}{8}(c_b + c_{cs})(2c_b + 3c_{cs})(\lambda\Omega R)\frac{T_{11}}{a_o}\dot{\delta}$$

$$- (c_b + c_{cs})e\Omega(\lambda\Omega R)\frac{T_{10}}{a_o}\delta + \frac{1}{2}c_{cs}(\lambda\Omega R)^2$$

$$- \frac{3}{4}(c_b + c_{cs})c_{cs}(\dot{\theta}_G + \dot{\phi})(\lambda\Omega R)$$

$$+ [- (c_b + c_{cs})\dot{w}v_{,x}\frac{T_{10}}{a_o}\delta - (c_b + c_{cs})v_{,x}(\lambda\Omega R)\frac{T_{10}}{a_o}\delta$$

$$+ c_{cs}\dot{w}(w_{,x} + \beta_p) - (c_b + c_{cs})\dot{v}(w_{,x} + \beta_p)\frac{T_{10}}{a_o}\delta$$

$$- \frac{1}{8}(c_b + c_{cs})(2c_b + 3c_{cs})(w_{,x} + \beta_p)\frac{T_{11}}{a_o}\dot{\delta}$$

$$- (c_b + c_{cs})e\Omega(w_{,x} + \beta_p)\frac{T_{10}}{a_o}\delta + c_{cs}(w_{,x} + \beta_p)(\lambda\Omega R)$$

$$- \frac{3}{4}(c_b + c_{cs})c_{cs}(w_{,x} + \beta_p)(\dot{\theta}_G + \dot{\phi})](\mu\Omega R)\cos\psi$$

$$+ [- (c_b + c_{cs})\dot{w}\frac{T_{10}}{a_o}\delta - (c_b + c_{cs})\Omega v(w_{,x} + \beta_p)\frac{T_{10}}{a_o}\delta$$

$$- (c_b + c_{cs})(\lambda\Omega R)\frac{T_{10}}{a_o}\delta](\mu\Omega R)\sin\psi$$

$$- (c_b + c_{cs})(w_{,x} + \beta_p)\frac{T_{10}}{a_o}\delta(\mu\Omega R)^2\cos\psi\sin\psi$$

$$+ [-(c_b + c_{cs})v_{,x}(w_{,x} + \beta_p)\frac{T_{10}}{a_o}\delta + \frac{1}{2}c_{cs}(w_{,x} + \beta_p)^2](\mu\Omega R)^2 \cos^2\psi\}$$

$$+ \rho_A a_o C_f(\theta_G + \phi)\{\frac{1}{8}(2c_b + c_{cs})c_{cs}(X_A - \frac{1}{4}c_b)(\ddot{\theta}_G + \ddot{\phi}) + \frac{1}{8}(2c_b + c_{cs})c_{cs}\ddot{w}$$

$$- \frac{1}{2}c_{cs}\dot{v}\dot{w} - \frac{1}{2}c_{cs}e\Omega\dot{w} + \frac{1}{4}(c_b + c_{cs})^2\ddot{v}\frac{T_4}{a_o}\delta + \frac{1}{4}(c_b + c_{cs})^2\dot{v}\frac{T_4}{a_o}\dot{\delta}$$

$$- \frac{1}{2}c_{cs}\dot{v}(\lambda\Omega R) - \frac{1}{8}(2c_b + c_{cs})c_{cs}\dot{v}(\dot{\theta}_G + \dot{\phi}) + \frac{1}{4}(c_b + c_{cs})^2 e\Omega\frac{T_4}{a_o}\dot{\delta}$$

$$+ \frac{1}{8}(c_b + c_{cs})^3\frac{T_1}{a_o}\ddot{\delta} - \frac{1}{2}c_{cs}e\Omega(\lambda\Omega R)$$

$$- \frac{1}{8}(2c_b + c_{cs})c_{cs}e\Omega(\dot{\theta}_G + \dot{\phi}) - \frac{1}{16}(c_b + c_{cs})^2 c_{cs}(\ddot{\theta}_G + \ddot{\phi})$$

$$+ [\frac{1}{4}(c_b + c_{cs})^2\dot{v}_{,x}\frac{T_4}{a_o}\delta - \frac{1}{2}c_{cs}\dot{w}v_{,x} + \frac{1}{4}(c_b + c_{cs})^2 v_{,x}\frac{T_4}{a_o}\dot{\delta}$$

$$- \frac{1}{2}c_{cs}v_{,x}(\lambda\Omega R) - \frac{1}{8}(2c_b + c_{cs})c_{cs}v_{,x}(\dot{\theta}_G + \dot{\phi})$$

$$- \frac{1}{2}c_{cs}\dot{v}(w_{,x} + \beta_p) + \frac{1}{4}(c_b + c_{cs})^2\Omega\frac{T_4}{a_o}\delta$$

$$- \frac{1}{2}c_{cs}e\Omega(w_{,x} + \beta_p) + \frac{1}{8}(2c_b + c_{cs})c_{cs}\dot{w}_{,x}](\mu\Omega R)\cos\psi$$

$$+ [-\frac{1}{4}(c_b + c_{cs})^2\Omega v_{,x}\frac{T_4}{a_o}\delta - \frac{1}{2}c_{cs}\dot{w} - \frac{1}{2}c_{cs}\Omega v(w_{,x} + \beta_p)$$

$$+ \frac{1}{4}(c_b + c_{cs})^2\frac{T_4}{a_o}\dot{\delta} - \frac{1}{2}c_{cs}(\lambda\Omega R) - \frac{1}{8}(2c_b + c_{cs})c_{cs}\Omega(w_{,x} + \beta_p)$$

$$- \frac{1}{8}(2c_b + c_{cs})c_{cs}(\dot{\theta}_G + \dot{\phi})](\mu\Omega R)\sin\psi$$

$$- \frac{1}{2}c_{cs}(w_{,x} + \beta_p)(\mu\Omega R)^2 \cos\psi \sin\psi$$

$$- \frac{1}{2}c_{cs}v_{,x}(w_{,x} + \beta_p)(\mu\Omega R)^2 \cos^2\psi\}$$

$$+ \rho_A a_o C_f (\theta_G + \phi)^2 [- \frac{1}{8}(2c_b + c_{cs})c_{cs}\ddot{v}$$

$$- \frac{1}{8}(2c_b + c_{cs})c_{cs}(\Omega + \dot{v}_{,x})(\mu\Omega R)\cos\psi + \frac{1}{8}(2c_b + c_{cs})c_{cs}\Omega v_{,x}(\mu\Omega R)\sin\psi]$$

$$+ \rho_A a_o C_f x[- (c_b + c_{cs})\Omega\dot{w}\frac{T_{10}}{a_o}\delta - (c_b + c_{cs})\Omega^2 v(w_{,x} + \beta_p)\frac{T_{10}}{a_o}\delta$$

$$- (c_b + c_{cs})\Omega(\lambda\Omega R)\frac{T_{10}}{a_o}\delta$$

$$- (c_b + c_{cs})\Omega(w_{,x} + \beta_p)\frac{T_{10}}{a_o}\delta(\mu\Omega R)\cos\psi]$$

$$+ \rho_A a_o C_f x(\theta_G + \phi)[- \frac{1}{2}c_{cs}\Omega\dot{w} - \frac{1}{2}c_{cs}\Omega^2 v(w_{,x} + \beta_p)$$

$$+ \frac{1}{4}(c_b + c_{cs})^2\Omega\frac{T_4}{a_o}\dot{\delta} - \frac{1}{2}c_{cs}\Omega(\lambda\Omega R) - \frac{1}{8}(2c_b + c_{cs})c_{cs}\Omega(\dot{\theta}_G + \dot{\phi})$$

$$- \frac{1}{2}c_{cs}\Omega(w_{,x} + \beta_p)(\mu\Omega R)\cos\psi]$$

$$+ \rho_A a_o \frac{C_{do}}{a_o}[- c_{cs}(\dot{v} + e\Omega)(\mu\Omega R)\sin\psi - c_{cs}v_{,x}(\mu\Omega R)^2\cos\psi\sin\psi$$

$$- \frac{1}{2}c_{cs}(\mu\Omega R)^2\sin^2\psi]$$

$$+ \rho_A a_o \frac{C_{do}}{a_o}x[- c_{cs}\Omega(\dot{v} + e\Omega) - c_{cs}\Omega v_{,x}(\mu\Omega R)\cos\psi - c_{cs}\Omega(\mu\Omega R)\sin\psi]$$

$$- \frac{1}{2}\rho_A a_o \frac{C_{do}}{a_o}x^2 c_{cs}\Omega^2 \qquad (3.119a)$$

$$p_{Acz5} =$$

$$\rho_A a_o C_f \{ - \frac{1}{4}(c_b + c_{cs})^2\Omega\frac{T_4}{a_o}\delta(\mu\Omega R)\cos\psi$$

$$+ [- \frac{1}{2}c_{cs}\dot{w} + 2(c_b + c_{cs})\dot{v}\frac{T_{10}}{a_o}\delta - \frac{1}{4}(c_b + c_{cs})^2\frac{T_4}{a_o}\dot{\delta}$$

$$+\frac{1}{8}(c_b+c_{cs})(2c_b+3c_{cs})\frac{T_{11}}{a_o}\dot{\delta}+2(c_b+c_{cs})e\Omega\frac{T_{10}}{a_o}\delta$$

$$-\frac{1}{2}c_{cs}(\lambda\Omega R)+\frac{1}{8}(2c_b+c_{cs})c_{cs}(\dot{\theta}_G+\dot{\phi})$$

$$+\frac{3}{4}(c_b+c_{cs})c_{cs}(\dot{\theta}_G+\dot{\phi})](\mu\Omega R)\sin\psi$$

$$+[2(c_b+c_{cs})v_{,x}\frac{T_{10}}{a_o}\delta-\frac{1}{2}c_{cs}(w_{,x}+\beta_p)](\mu\Omega R)^2\cos\psi\sin\psi$$

$$+(c_b+c_{cs})\frac{T_{10}}{a_o}\delta(\mu\Omega R)^2\sin^2\psi\}$$

$$+\rho_A a_o C_f(\theta_G+\phi)[\frac{1}{8}(2c_b+c_{cs})c_{cs}\Omega(\mu\Omega R)\cos\psi+c_{cs}(\dot{v}+e\Omega)(\mu\Omega R)\sin\psi$$

$$+c_{cs}v_{,x}(\mu\Omega R)^2\cos\psi\sin\psi+\frac{1}{2}c_{cs}(\mu\Omega R)^2\sin^2\psi]$$

$$+\rho_A a_o C_f x\{-\frac{1}{2}c_{cs}\Omega\dot{w}+2(c_b+c_{cs})\Omega\dot{v}\frac{T_{10}}{a_o}\delta-\frac{1}{4}(c_b+c_{cs})^2\Omega\frac{T_4}{a_o}\dot{\delta}$$

$$+\frac{1}{8}(c_b+c_{cs})(2c_b+3c_{cs})\Omega\frac{T_{11}}{a_o}\dot{\delta}+2(c_b+c_{cs})e\Omega^2\frac{T_{10}}{a_o}\delta$$

$$-\frac{1}{2}c_{cs}\Omega(\lambda\Omega R)+\frac{1}{8}(2c_b+c_{cs})c_{cs}\Omega(\dot{\theta}_G+\dot{\phi})$$

$$+\frac{3}{4}(c_b+c_{cs})c_{cs}\Omega(\dot{\theta}_G+\dot{\phi})$$

$$+[2(c_b+c_{cs})\Omega v_{,x}\frac{T_{10}}{a_o}\delta-\frac{1}{2}c_{cs}\Omega(w_{,x}+\beta_p)](\mu\Omega R)\cos\psi$$

$$+2(c_b+c_{cs})\Omega\frac{T_{10}}{a_o}\delta(\mu\Omega R)\sin\psi\}$$

$$+\rho_A a_o C_f x(\theta_G+\phi)[c_{cs}\Omega\dot{v}+c_{cs}e\Omega^2+c_{cs}\Omega v_{,x}(\mu\Omega R)\cos\psi+c_{cs}\Omega(\mu\Omega R)\sin\psi]$$

$$+\rho_A a_o C_f x^2(c_b+c_{cs})\Omega^2\frac{T_{10}}{a_o}\delta$$

$$+\frac{1}{2}\rho_A a_o c_{cs}\Omega^2 \qquad (3.119b)$$

From Eq. (3.99), the additional aerodynamic moment about the elastic axis in the "5" system due to the presence of the control surface is given by:

$$q_{Acx5} = C_f(\Delta M_{yNC} + \Delta M_{yC})$$

where the fact that the control surface is located outside the reverse flow region has been used (i.e. $R_D = R_{LM} = 1$). The control flap is assumed to be symmetric (i.e., uncambered).

Substituting Eqs. (3.115) and (3.116) into the previous expression yields:

$$\begin{aligned}
q_{Acx5} = \frac{C_f}{8}\rho_A a_o(c_b + c_{cs})^2\{ & -\frac{1}{32}c_{cs}(2c_b + c_{cs})(\ddot{\theta}_G + \ddot{\phi}) \\
& + c_{cs}[X_A - \frac{1}{4}(c_b + c_{cs})](\ddot{\theta}_G + \ddot{\phi}) \\
& - \frac{1}{2}c_{cs}[\dot{U}_T(\theta_G + \phi) - \dot{U}_P] \\
& - 2\frac{T_4}{a_o}U_T^2\delta - \frac{T_1}{a_o}(c_b + c_{cs})U_T\dot{\delta} \\
& + [\frac{T_8}{a_o}(c_b + c_{cs}) + (\frac{3}{2}c_b - 2X_A)\frac{T_4}{a_o}](\dot{U}_T\delta + U_T\dot{\delta}) \\
& + \frac{1}{2}(c_b + c_{cs})[\frac{T_7}{a_o}(c_b + c_{cs}) + (\frac{3}{2}c_b - 2X_A)\frac{T_1}{a_o}]\ddot{\delta}\} \\
+ \frac{C_f}{8}\rho_A a_o c_{cs}(2c_b + c_{cs})\{ & U_T^2(\theta_G + \phi) - U_T U_P \\
& - [(X_A - \frac{1}{4}c_b)^2 + \frac{1}{32}c_b^2](\ddot{\theta}_G + \ddot{\phi}) \\
& + (X_A - \frac{1}{4}c_b)[\dot{U}_T(\theta_G + \phi) - \dot{U}_P]\} \\
+ \frac{C_f}{2}\rho_A a_o(c_b + c_{cs})U_T[& \frac{3}{2}c_{cs}(\dot{\theta}_G + \dot{\phi}) + 2\frac{T_{10}}{a_o}U_T\delta
\end{aligned}$$

$$+\frac{1}{4}(2c_b+3c_{cs})\frac{T_{11}}{a_o}\dot{\delta}][X_A-\frac{1}{4}(c_b+2c_{cs})]$$

$$+\frac{C_f}{2}\rho_A a_o c_{cs} U_T[U_T(\theta_G+\phi)-U_P$$

$$-(X_A-\frac{1}{2}c_b)(\dot{\theta}_G+\dot{\phi})][X_A-\frac{1}{4}(3c_b+2c_{cs})]$$

Substituting the expressions for U_T and U_P given by Eqs. (3.88) into the above expression yields:

q_{Acx5} =

$$\rho_A a_o C_f\{\frac{1}{8}(c_b+c_{cs})^2\Omega\frac{T_{18}}{a_o}\delta+\frac{1}{8}(c_b+c_{cs})^2(X_A-\frac{5}{16}c_b-\frac{9}{32}c_{cs})(\ddot{\theta}_G+\ddot{\phi})$$

$$+\frac{1}{8}(c_b+c_{cs})^2\Omega\frac{T_{18}}{a_o}(\mu\Omega R)\cos\psi$$

$$+[2(c_b+c_{cs})(X_A-\frac{1}{4}c_b-\frac{1}{2}c_{cs})\dot{v}\frac{T_{10}}{a_o}\delta$$

$$+\frac{1}{8}(c_b+c_{cs})(2c_b+3c_{cs})(X_A-\frac{1}{4}c_b-\frac{1}{2}c_{cs})\frac{T_{11}}{a_o}\dot{\delta}$$

$$+2(c_b+c_{cs})(X_A-\frac{1}{4}c_b-\frac{1}{2}c_{cs})e\Omega\frac{T_{10}}{a_o}\delta+\frac{1}{8}(c_b+c_{cs})^2\frac{T_{18}}{a_o}\dot{\delta}$$

$$-\frac{1}{2}c_{cs}(X_A-\frac{3}{4}c_b-c_{cs})(\dot{w}+\lambda\Omega R)-\frac{1}{8}(2c_b+c_{cs})c_{cs}\dot{w}$$

$$-\frac{1}{2}(c_b+c_{cs})^2\dot{v}\frac{T_4}{a_o}\delta-\frac{1}{2}(c_b+c_{cs})^2e\Omega\frac{T_4}{a_o}\delta$$

$$-\frac{1}{8}(c_b+c_{cs})^3\frac{T_1}{a_o}\dot{\delta}-\frac{1}{8}(2c_b+c_{cs})c_{cs}(\lambda\Omega R)](\mu\Omega R)\sin\psi$$

$$+[2(c_b+c_{cs})(X_A-\frac{1}{4}c_b-\frac{1}{2}c_{cs})v_{,x}\frac{T_{10}}{a_o}\delta-\frac{1}{2}(c_b+c_{cs})^2v_{,x}\frac{T_4}{a_o}\delta$$

$$-\frac{1}{2}c_{cs}(X_A-\frac{3}{4}c_b-c_{cs})(w_{,x}+\beta_p)$$

$$- \frac{1}{8}(2c_b + c_{cs})c_{cs}(w_{,x} + \beta_p)](\mu\Omega R)^2 \cos\psi \sin\psi$$

$$+ [(c_b + c_{cs})(X_A - \frac{1}{4}c_b - \frac{1}{2}c_{cs})\frac{T_{10}}{a_o}\delta$$

$$- \frac{1}{4}(c_b + c_{cs})^2\frac{T_4}{a_o}\delta](\mu\Omega R)^2 \sin^2\psi\}$$

$$+ \rho_A a_o C_f(\theta_G + \phi)\{ - \frac{1}{16}(c_b + c_{cs})^2 c_{cs}\Omega(\mu\Omega R)\cos\psi$$

$$+ [c_{cs}(X_A - \frac{3}{4}c_b - c_{cs})\dot{v} + c_{cs}(X_A - \frac{3}{4}c_b - c_{cs})e\Omega$$

$$+ \frac{1}{4}(2c_b + c_{cs})c_{cs}\dot{v} + \frac{1}{4}(2c_b + c_{cs})c_{cs}e\Omega](\mu\Omega R)\sin\psi$$

$$+ [c_{cs}(X_A - \frac{3}{4}c_b - c_{cs})v_{,x} + \frac{1}{4}(2c_b + c_{cs})c_{cs}v_{,x}](\mu\Omega R)^2 \cos\psi \sin\psi$$

$$+ [\frac{1}{2}c_{cs}(X_A - \frac{3}{4}c_b - c_{cs}) + \frac{1}{8}(2c_b + c_{cs})c_{cs}](\mu\Omega R)^2 \sin^2\psi\}$$

$$+ \rho_A a_o C_f x\{2(c_b + c_{cs})(X_A - \frac{1}{4}c_b - \frac{1}{2}c_{cs})\Omega\dot{v}\frac{T_{10}}{a_o}\delta$$

$$+ \frac{1}{8}(c_b + c_{cs})(2c_b + 3c_{cs})(X_A - \frac{1}{4}c_b - \frac{1}{2}c_{cs})\Omega\frac{T_{11}}{a_o}\dot{\delta}$$

$$+ 2(c_b + c_{cs})(X_A - \frac{1}{4}c_b - \frac{1}{2}c_{cs})e\Omega^2\frac{T_{10}}{a_o}\delta + \frac{1}{8}(c_b + c_{cs})^2\Omega\frac{T_{18}}{a_o}\dot{\delta}$$

$$- \frac{1}{2}c_{cs}(X_A - \frac{3}{4}c_b - c_{cs})\Omega\dot{w} - \frac{1}{2}c_{cs}(X_A - \frac{3}{4}c_b - c_{cs})\Omega(\lambda\Omega R)$$

$$- \frac{1}{8}(2c_b + c_{cs})c_{cs}\Omega\dot{w} - \frac{1}{2}(c_b + c_{cs})^2\Omega\dot{v}\frac{T_4}{a_o}\delta - \frac{1}{2}(c_b + c_{cs})^2 e\Omega^2\frac{T_4}{a_o}\delta$$

$$- \frac{1}{8}(c_b + c_{cs})^3\Omega\frac{T_1}{a_o}\dot{\delta} - \frac{1}{8}(2c_b + c_{cs})c_{cs}\Omega(\lambda\Omega R)$$

$$+ [2(c_b + c_{cs})(X_A - \frac{1}{4}c_b - \frac{1}{2}c_{cs})\Omega v_{,x}\frac{T_{10}}{a_o}\delta - \frac{1}{2}(c_b + c_{cs})^2\Omega v_{,x}\frac{T_4}{a_o}\delta$$

$$- \frac{1}{2}c_{cs}(X_A - \frac{3}{4}c_b - c_{cs})\Omega(w_{,x} + \beta_p)$$

$$- \frac{1}{8}(2c_b + c_{cs})c_{cs}\Omega(w_{,x} + \beta_p)](\mu\Omega R)\cos\psi$$

$$+ [2(c_b + c_{cs})(X_A - \frac{1}{4}c_b - \frac{1}{2}c_{cs})\Omega\frac{T_{10}}{a_o}\delta$$

$$- \frac{1}{2}(c_b + c_{cs})^2\Omega\frac{T_4}{a_o}\delta](\mu\Omega R)\sin\psi\}$$

$$+ \rho_A a_o C_f x(\theta_G + \phi)\{c_{cs}(X_A - \frac{3}{4}c_b - c_{cs})\Omega\dot{v} + c_{cs}(X_A - \frac{3}{4}c_b - c_{cs})e\Omega^2$$

$$+ \frac{1}{4}(2c_b + c_{cs})c_{cs}\Omega\dot{v} + \frac{1}{4}(2c_b + c_{cs})e\Omega^2$$

$$+ [c_{cs}(X_A - \frac{3}{4}c_b - c_{cs})\Omega v_{,x} + \frac{1}{4}(2c_b + c_{cs})c_{cs}\Omega v_{,x}](\mu\Omega R)\cos\psi$$

$$+ [c_{cs}(X_A - \frac{3}{4}c_b - c_{cs})\Omega + \frac{1}{4}(2c_b + c_{cs})c_{cs}\Omega](\mu\Omega R)\sin\psi\}$$

$$+ \rho_A a_o C_f x^2[(c_b + c_{cs})(X_A - \frac{1}{4}c_b - \frac{1}{2}c_{cs})\Omega^2\frac{T_{10}}{a_o}\delta - \frac{1}{4}(c_b + c_{cs})^2\Omega^2\frac{T_4}{a_o}\delta]$$

$$+ \rho_A a_o C_f x^2(\theta_G + \phi)[\frac{1}{2}c_{cs}(X_A - \frac{3}{4}c_b - c_{cs})\Omega^2 + \frac{1}{8}(2c_b + c_{cs})c_{cs}\Omega^2]\} \qquad (3.120)$$

From Eq. (3.96) the aerodynamic hinge moment per unit span in the "5" system is given by

$$q_{Ahx5} = C_f(M_{hNC} + M_{hC})$$

where the multiplicative scaling factor C_f has been used to account for the over-prediction of the aerodynamic hinge moment by 2D quasisteady aerodynamics. Substituting Eqs. (3.72) and (3.73) into the previous expression yields:

$$q_{Ahx5} = -\frac{C_f}{4}\rho_A(c_b + c_{cs})^2\{U_T^2(\theta_G + \phi)T_{12} - U_T U_P T_{12}$$

$$+ [\frac{1}{2}(c_b + 3c_{cs}) - X_A](T_{12} - T_4)U_T(\dot{\theta}_G + \dot{\phi})$$

$$- \frac{1}{2}(c_b + c_{cs})(2T_9 + T_1)U_T(\dot{\theta}_G + \dot{\phi}) + \frac{1}{2}T_{13}(c_b + c_{cs})^2(\ddot{\theta}_G + \ddot{\phi})$$

$$+ \frac{1}{2}(c_b + c_{cs})[\dot{U}_P - \dot{U}_T(\theta_G + \phi)]T_1 + 2U_T^2\frac{T_{15}}{a_o}\delta$$

$$- (c_b + c_{cs})\frac{T_2}{a_o}\dot{U}_T\delta + \frac{1}{4}(2c_b + 3c_{cs})\frac{T_{11}}{a_o}(T_{12} - T_4)U_T\dot{\delta}$$

$$- \frac{1}{2}(c_b + c_{cs})^2\ddot{\delta}\frac{T_3}{a_o}\}$$

Substituting the expressions for U_T and U_P given by Eqs. (3.88) into the above expression yields:

$q_{Ahx5} =$

$$\rho_A C_f(c_b + c_{cs})^2\{ - \frac{1}{8}(c_b + c_{cs})\dot{w}T_1 + \frac{1}{4}\dot{v}\dot{w}T_{12} + \frac{1}{4}e\Omega\dot{w}T_{12} + \frac{1}{4}\dot{v}(\lambda\Omega R)T_{12}$$

$$+ \frac{1}{4}e\Omega(\lambda\Omega R)T_{12} - \frac{1}{8}(c_b + c_{cs})^2(\ddot{\theta}_G + \ddot{\phi})T_{13}$$

$$+ [\frac{1}{4}\dot{w}v_{,x}T_{12} + \frac{1}{4}v_{,x}(\lambda\Omega R)T_{12} + \frac{1}{4}\dot{v}(w_{,x} + \beta_p)T_{12} + \frac{1}{4}e\Omega(w_{,x} + \beta_p)T_{12}$$

$$+ \frac{1}{4}(c_b + c_{cs})\Omega\frac{T_2}{a_o}\delta - \frac{1}{8}(c_b + c_{cs})\dot{w}_{,x}T_1](\mu\Omega R)\cos\psi$$

$$+ [\frac{1}{4}(X_A - \frac{1}{2}c_b - \frac{3}{2}c_{cs})(T_{12} - T_4)(\dot{\theta}_G + \dot{\phi})$$

$$+ \frac{1}{8}(c_b + c_{cs})(2T_9 + T_1)(\dot{\theta}_G + \dot{\phi}) + \frac{1}{4}\dot{w}T_{12} - \dot{v}\frac{T_{15}}{a_o}\delta$$

$$+ \frac{1}{4}\Omega v(w_{,x} + \beta_p)T_{12} + \frac{1}{4}(\lambda\Omega R)T_{12} - \frac{1}{16}(2c_b + 3c_{cs})\frac{T_{16}}{a_o}\dot{\delta}$$

$$- e\Omega\frac{T_{15}}{a_o}\delta + \frac{1}{8}(c_b + c_{cs})\Omega(w_{,x} + \beta_p)T_1](\mu\Omega R)\sin\psi$$

$$+ [- v_{,x}\frac{T_{15}}{a_o}\delta + \frac{1}{4}(w_{,x} + \beta_p)T_{12}](\mu\Omega R)^2\cos\psi\sin\psi$$

$$+\frac{1}{4}v_{,x}(w_{,x}+\beta_p)T_{12}(\mu\Omega R)^2\cos^2\psi-\frac{1}{2}\frac{T_{15}}{a_o}\delta(\mu\Omega R)^2\sin^2\psi\}$$

$$+\rho_A C_f(c_b+c_{cs})^2(\theta_G+\phi)\{\frac{1}{8}(c_b+c_{cs})\dot{v}T_1-\frac{1}{4}\dot{v}^2T_{12}-\frac{1}{2}e\Omega\dot{v}T_{12}$$

$$-\frac{1}{4}e^2\Omega^2T_{12}$$

$$+[\frac{1}{8}(c_b+c_{cs})\dot{v}_{,x}T_1-\frac{1}{2}\dot{v}v_{,x}T_{12}-\frac{1}{2}e\Omega v_{,x}T_{12}$$

$$+\frac{1}{8}(c_b+c_{cs})\Omega T_1](\mu\Omega R)\cos\psi$$

$$+[-\frac{1}{2}\Omega vv_{,x}T_{12}-\frac{1}{8}(c_b+c_{cs})\Omega v_{,x}T_1+\frac{1}{2}\Omega w\beta_pT_{12}-\frac{1}{2}\dot{v}T_{12}$$

$$-\frac{1}{2}\Omega uT_{12}-\frac{1}{2}e\Omega T_{12}](\mu\Omega R)\sin\psi$$

$$-\frac{1}{2}v_{,x}T_{12}(\mu\Omega R)^2\cos\psi\sin\psi-\frac{1}{4}v_{,x}{}^2T_{12}(\mu\Omega R)^2\cos^2\psi$$

$$-\frac{1}{4}T_{12}(\mu\Omega R)^2\sin^2\psi\}$$

$$+\rho_A C_f(c_b+c_{cs})^2x\{\frac{1}{4}(X_A-\frac{1}{2}c_b-\frac{3}{2}c_{cs})(T_{12}-T_4)\Omega(\dot{\theta}_G+\dot{\phi})$$

$$+\frac{1}{8}(c_b+c_{cs})(2T_9+T_1)\Omega(\dot{\theta}_G+\dot{\phi})+\frac{1}{4}\Omega\dot{w}T_{12}$$

$$-\Omega\dot{v}\frac{T_{15}}{a_o}\delta+\frac{1}{4}\Omega^2v(w_{,x}+\beta_p)T_{12}+\frac{1}{4}\Omega(\lambda\Omega R)T_{12}$$

$$-\frac{1}{16}(2c_b+3c_{cs})\Omega\frac{T_{16}}{a_o}\dot{\delta}-e\Omega^2\frac{T_{15}}{a_o}\delta$$

$$+[-\Omega v_{,x}\frac{T_{15}}{a_o}\delta+\frac{1}{4}\Omega(w_{,x}+\beta_p)T_{12}](\mu\Omega R)\cos\psi$$

$$-\Omega\frac{T_{15}}{a_o}\delta(\mu\Omega R)\sin\psi\}$$

$$+ \rho_A C_f (c_b + c_{cs})^2 x(\theta_G + \phi)[- \frac{1}{2}\Omega^2 v v_{,x} T_{12} + \frac{1}{2}\Omega^2 w \beta_p T_{12} - \frac{1}{2}\Omega \dot{v} T_{12}$$

$$- \frac{1}{2}\Omega^2 u T_{12} - \frac{1}{2} e \Omega^2 T_{12}$$

$$- \frac{1}{2}\Omega v_{,x} T_{12}(\mu \Omega R)\cos\psi - \frac{1}{2}\Omega T_{12}(\mu \Omega R)\sin\psi]$$

$$- \frac{1}{2}\rho_A C_f (c_b + c_{cs})^2 x^2 \Omega^2 \frac{T_{15}}{a_o}\delta$$

$$- \frac{1}{4}\rho_A C_f (c_b + c_{cs})^2 x^2 (\theta_G + \phi)\Omega^2 T_{12} \qquad (3.121)$$

where

$$T_{15} = T_5 + T_{10}(T_{12} - T_4)$$

$$T_{16} = T_{11}(T_{12} - T_4)$$

$$T_{17} = T_7(c_b + c_{cs}) + (\frac{3}{2}c_b - 2X_A)T_1$$

$$T_{18} = T_8(c_b + c_{cs}) + (\frac{3}{2}c_b - 2X_A)T_4$$

The distributed aerodynamic loads acting on the control surface can be transformed from the "5" system to the "3" system, in which the equations of motion are formulated, using the coordinate transformation defined in Chapter 2. The distributed aerodynamic force acting on the control surface can be expressed in the "3" system as:

$$\vec{p}_{Ac} = p_{Acx3}\hat{e}_{x3} + p_{Acy3}\hat{e}_{y3} + p_{Acz3}\hat{e}_{z3}$$

where

$$p_{Acx3} = - v_{,x} p_{Acy5} - w_{,x} p_{Acz5} \qquad (3.122a)$$

$$p_{Acy3} = p_{Acy5} \qquad (3.122b)$$

$$p_{Acz3} = - v_{,x} w_{,x} p_{Acy5} + p_{Acz5} \qquad (3.122c)$$

Similarly, the distributed aerodynamic moment due to the control surface can be expressed in the "3" system as:

$$\vec{q}_{Ac} = q_{Acx3}\,\hat{e}_{x3} + q_{Acy3}\,\hat{e}_{y3} + q_{Acz3}\,\hat{e}_{z3}$$

where

$$q_{Acx3} = q_{Acx5} \tag{3.123a}$$

$$q_{Acy3} = v_{,x}\,q_{Acx5} \tag{3.123b}$$

$$q_{Acz3} = w_{,x}\,q_{Acx5} \tag{3.123c}$$

3.5 DAMPING LOADS

The structural damping present in the system is assumed to be of a viscous type. The structural damping is assumed to act on the blade only. The representation of the structural damping presented below is adopted from Ref. 38. The distributed damping force acting on the blade is defined as

$$\vec{p}_D = -g_{SL}\,\dot{v}\,\hat{e}_{y3} - g_{SF}\,\dot{w}\,\hat{e}_{z3} \tag{3.124}$$

Similarly, the distributed damping moment acting on the blade is defined as

$$\vec{q}_D = -g_{ST}\,\dot{\phi}\,\hat{e}_{x4}$$

which can be expressed in the "3" system as

$$\vec{q}_D = -g_{ST}\,\dot{\phi}(\hat{e}_{x3} - v_{,x}\,\hat{e}_{y3} - w_{,x}\,\hat{e}_{z3}) \tag{3.125}$$

3.6 TOTAL DISTRIBUTED LOADS

The total distributed loads are obtained by summing the inertial, gravitational, aerodynamic, and damping contributions.

The resultant distributed force acting on the blade is given by:

$$\vec{p}_b = \vec{p}_{Ib} + \vec{p}_{Gb} + \vec{p}_{Ab} + \vec{p}_D \tag{3.126}$$

which can be expressed in the "3" system as:

$$\vec{p}_b = p_{bx3}\,\hat{e}_{x3} + p_{by3}\,\hat{e}_{y3} + p_{bz3}\,\hat{e}_{z3}$$

where

$$p_{bx3} = p_{Ibx2} + p_{Gbx2} + \beta_p (p_{Ibz2} + p_{Gbz2})$$

$$- v_{,x}\, p_{Aby5} - w_{,x}\, p_{Abz5} \tag{3.127a}$$

$$p_{by3} = p_{Iby2} + p_{Gby2} + p_{Aby5} - g_{SL}\,\dot{v} \tag{3.127b}$$

$$p_{bz3} = -\beta_p (p_{Ibx2} + p_{Gbx2}) + p_{Ibz2} + p_{Gbz2}$$

$$- v_{,x} w_{,x}\, p_{Aby5} + p_{Abz5} - g_{SF}\,\dot{w} \tag{3.127c}$$

The total distributed moment acting on the blade is given by:

$$\vec{q}_b = \vec{q}_{Ib} + \vec{q}_{Gb} + \vec{q}_{Ab} + \vec{q}_D \tag{3.128}$$

which can be expressed in the "3" system as:

$$\vec{q}_b = q_{bx3}\,\hat{e}_{x3} + q_{by3}\,\hat{e}_{y3} + q_{bz3}\,\hat{e}_{z3}$$

where

$$q_{bx3} = q_{Ibx2} + q_{Gbx2} + \beta_p (q_{Ibz2} + q_{Gbz2}) + q_{Abx5} - g_{ST}\,\dot{\phi} \tag{3.129a}$$

$$q_{by3} = q_{Iby2} + q_{Gby2} + v_{,x}\, q_{Abx5} + g_{ST}\, v_{,x}\,\dot{\phi} \tag{3.129b}$$

$$q_{bz3} = -\beta_p (q_{Ibx2} + q_{Gbx2}) + q_{Ibz2} + q_{Gbz2} + w_{,x}\, q_{Abx5}$$

$$+ g_{ST}\, w_{,x}\, \dot{\phi} \tag{3.129c}$$

The resultant distributed force acting on the control flap is given by:

$$\vec{p}_c = \vec{p}_{Ic} + \vec{p}_{Gc} + \vec{p}_{Ac} \tag{3.130}$$

which can be expressed in the "3" system as:

$$\vec{p}_c = p_{cx3}\, \hat{e}_{x3} + p_{cy3}\, \hat{e}_{y3} + p_{cz3}\, \hat{e}_{z3}$$

where

$$p_{cx3} = p_{Icx3} + p_{Gcx3} + p_{Acx3}$$

$$p_{cy3} = p_{Icy3} + p_{Gcy3} + p_{Acy3}$$

$$p_{cz3} = p_{Icz3} + p_{Gcz3} + p_{Acz3} \tag{3.131}$$

The resultant distributed moment about the elastic axis of the blade due to the control flap loads are given by:

$$\vec{q}_c = \vec{q}_{Ic} + \vec{q}_{Ac} + \vec{q}_{Gc} \tag{3.132}$$

which can be expressed in the "3" system as:

$$\vec{q}_c = q_{cx3}\, \hat{e}_{x3} + q_{cy3}\, \hat{e}_{y3} + q_{cz3}\, \hat{e}_{z3}$$

where

$$q_{cx3} = q_{Icx3} + q_{Gcx3} + q_{Acx3} \tag{3.133a}$$

$$q_{cy3} = q_{Icy3} + q_{Gcy3} + q_{Acy3} \tag{3.133b}$$

$$q_{cz3} = q_{Icz3} + q_{Gcz3} + q_{Acz3} \tag{3.133c}$$

The resultant distributed moment about the control flap hinge is given by:

$$\vec{q}_h = \vec{q}_{Ih} + \vec{q}_{Gh} + \vec{q}_{Ah} \tag{3.134}$$

Chapter IV

OFFSET-HINGED SPRING RESTRAINED BLADE MODEL

In this chapter, the equations of motion of an isolated hingeless rotor blade are formulated using the offset-hinged spring restrained blade model. This model is used in the first stages of this study to gain physical insight into the problem of controlling helicopter vibrations using an actively controlled flap mounted on the blade. The key insights learned in the first stage are then used as a foundation for the second stage of this study, which focuses on practical issues concerning the control flap implementation.

4.1 THE BLADE MODEL

The offset-hinged spring restrained blade model was first used in Ref. 37 to study the flap-lag dynamics of a hingeless rotor blade in hover. Since then many good models have been derived[50,53] based on the spring restrained model to study the flap-lag-torsion dynamics and stability of hingeless rotor blades in forward flight. The simple spring restrained blade model is particularly convenient for developing explicit equations of motion for the blade dynamics. Valuable insight can be gained by examining the coupling between the flap, lead-lag and torsional dynamics, which is possible when an explicit formulation is used. Though the spring restrained blade model of a hingeless blade is not as refined or accurate as a fully flexible blade model, it is very useful for performing trend type studies. The essential features of the offset-hinged spring restrained blade model are discussed in the next section.

In the offset-hinged spring restrained blade model, the flexibility of the blade is concentrated at a single point called the hinge offset point, located a distance e from the hub; the blade outboard of the root is assumed to be completely rigid. An orthogonal triad of torsional root springs, oriented along the axes of the "S" system as shown in Fig. 2, is used to represent the flexibility of the blade in flap, lead-lag and torsion. It is assumed that the

orientation of the triad of root springs does not change as the blade deforms. This assumption is consistent with the modeling of an hingeless rotor blade which, being cantilevered at the blade root, undergoes no displacement or rotation at the root of the blade.

The elastic deformation of the spring restrained blade consists of the rigid rotation of the blade about the root springs in flap, lead-lag and torsion. The following deformation sequence is adopted in this study: 1) a flap rotation by the angle β clockwise about the y_3 axis; 2) a lead-lag rotation by the angle ζ counter-clockwise about the z_3 axis after is has been rotated by the angle β, and 3) a torsional rotation by the angle ϕ counter-clockwise about the x_3 axis after it has been rotated by the angle β and then ζ. These three angles completely describe the elastic deformation of the offset-hinged spring restrained blade, and thus represent the blade degrees of freedom for this blade model.

The elastic restoring moments about the blade root are obtained by resolving the total rotation resulting from the above sequence of rotations into components along the axes of the torsional root springs and then multiplying each component by the negative of the appropriate spring stiffness. In this study, the stiffnesses of the torsional root springs are selected so that the resulting uncoupled non-rotating frequencies of the rigid blade in flap, lead-lag and torsion match the corresponding uncoupled first non-rotating frequencies of the fully elastic blade.

The elastic restoring moments are combined with the moments about the blade root due to the distributed inertial, gravitational, damping and aerodynamic loads on the blade to obtain the resultant moment about the blade root. The equations of motion for the offset-hinged spring restrained blade model are obtained by setting this root moment to zero. This yields a set of three fully coupled nonlinear ordinary differential equations of motion, which are associated with the flap, lead-lag and torsional degrees of freedom of the blade. The resulting equations are nonlinear due to the assumption of moderate deflections, which introduces geometric nonlinearities into the expressions for the inertial, aerodynamic and structural loads, and couples the equations of motion as well.

4.2 DISTRIBUTED LOADS

General expressions for the distributed loads on the blade have been developed in Chapter 3 in terms of the three displacement quantities u, v and w and the rotational quantity ϕ. Before these loads can be integrated along the span of the blade, they must be expressed entirely in terms of the blade degrees of freedom of the spring restrained blade model, namely the flap angle β, the lead-lag angle ζ and the twist angle ϕ. The relationship between these two sets of variables can be determined by comparing the position vector of a point on the elastic axis of the blade described in terms of the blade degrees of freedom for the rigid blade model with the position vector defined in Chapter 3 in terms of u, v and w. In Chapter 3 the position vector of an arbitrary point on the elastic axis of the deformed blade was shown to be given by

$$\vec{r}_{EA} = e\,\hat{e}_{x2} + (x+u)\,\hat{e}_{x3} + v\,\hat{e}_{y3} + w\,\hat{e}_{z3} \tag{3.82}$$

For the offset-hinged spring restrained blade model, the position of an arbitrary point on the elastic axis of the deformed blade can be expressed as:

$$\vec{r}_{EA} = e\,\hat{e}_{x2} + x\,\hat{e}_{x4} \tag{4.1}$$

Transforming the unit vector $\hat{e}_{x4}$ to the "3" system using the appropriate coordinate transformation defined in Chapter 2 yields:

$$x\,\hat{e}_{x4} = x\,\hat{e}_{x3} + \zeta x\,\hat{e}_{y3} + \beta x\,\hat{e}_{z3} \tag{4.2}$$

Substituting the above expression into Eq. (4.1) yields:

$$\vec{r}_{EA} = e\,\hat{e}_{x2} + x\,\hat{e}_{x3} + \zeta x\,\hat{e}_{y3} + \beta x\,\hat{e}_{z3}$$

Comparing the previous expression with Eq. (3.82) reveals that

$$v = \zeta x \quad , \quad w = \beta x \tag{4.3a}$$

from which it follows immediately that

$$v_{,x} = \zeta \quad , \quad w_{,x} = \beta \tag{4.3b}$$

The axial displacement u(x) due to the flap and lead-lag angular displacements, β and ζ, can be expressed as:

$$u(x) = -\frac{1}{2}\int_0^x (\zeta^2 + \beta^2)\,dx = -\frac{1}{2}(\zeta^2 + \beta^2)x \tag{4.4}$$

Expressions for the distributed loads acting on the spring restrained blade model are obtained by substituting Eqs. (4.3) and (4.4) into the expressions for the distributed loads acting on the fully elastic blade model formulated in Chapter 3.

4.3 ROOT MOMENT DUE TO BLADE LOADING

The moments about the blade root due to the distributed inertial, gravitational and aerodynamic loads acting on the blade are obtained by integrating the distributed loads along the span of the blade. Since the blade outboard of the root is rigid, the geometry of the deformed blade is unchanged from the geometry of the undeformed blade, and is therefore known a priori. Furthermore, the distributed loads are separable in terms of their spatial and time dependencies, consisting of products of the blade degrees of freedom β, ζ and ϕ, which are functions of time only, and known x-dependent quantities, such as the mass, pretwist and principal cross-sectional inertia distributions of the blade. This separability permits the explicit integration of the distributed loads along the span of the blade, thereby eliminating the spatial degree of freedom in the equations of motion.

The integration along the blade span can be expressed symbolically as

$$\vec{M}_R = \int_0^{L_b} \vec{q}_b\,dx + \int_0^{L_b} x\,\hat{e}_{x4} \times \vec{p}_b\,dx$$

$$+ \int_{x_{cs}}^{x_{cs}+L_{cs}} \vec{q}_c\,dx + \int_{x_{cs}}^{x_{cs}+L_{cs}} x\,\hat{e}_{x4} \times \vec{p}_c\,dx \tag{4.5}$$

which can be expressed in the "3" system as:

$$\vec{M}_R = M_{Rx3}\,\hat{e}_{x3} + M_{Ry3}\,\hat{e}_{y3} + M_{Rz3}\,\hat{e}_{z3} \tag{4.6}$$

The evaluation of the various integrals appearing in Eq. (4.5) is too lengthy to be presented here, but is described in detail in Appendix C. The substitution of Eqs. (4.3) and (4.4) into the expressions for the distributed loads derived in Chapter 3, and the integrations in Eq. (4.5), are performed explicitly using the symbolic manipulation program MACSYMA. The application of MACSYMA in evaluating explicit integrals is described in Appendix B.

4.4 ELASTIC RESTORING MOMENTS

The elastic restoring moments are obtained by resolving the total rotation of the rigid blade about its root into components along the axes of the torsional root springs and then multiplying each component by the negative of the appropriate spring stiffness. The torsional root springs are oriented along the axes of the "S" system as shown in Fig. 2. The orientation of the triad is oriented by pilot input at an angle $R_C\theta_{Gr}$ about the x_3 axis, as shown in Fig. 2, where $\theta_{Gr} = \theta_G(x = 0)$ represents the total geometric pitch angle at the blade root. The elastic coupling parameter R_C was introduced in Ref. 50 to vary, in a simple manner, the amount of flap-lag elastic coupling present in the model. When $R_C = 1.0$, for example, there is full elastic coupling and the orientation of the root springs changes as the pitch of the blade changes in such a manner as to always remain parallel to the principal axes of the blade at the blade root. This case models a hingeless rotor system with all of the flexibility outboard of the pitch change bearing. When $R_C = 0$ the orientation of the root springs does not change as the blade pitch changes. This case models a rotor system with all the flexibility inboard of the pitch change bearing. Values of R_C between 0.0 and 1.0 represent varying amounts of flap-lag elastic coupling present in the helicopter model.

It is assumed that the orientation of the root springs does not change with the blade deformation. This is to be consistent with the modeling of a hingeless rotor blade, which is cantilevered at the blade root. The cantilevered boundary condition specifies a zero slope at the cantilevered end.

In order to evaluate the elastic restoring moments provided by the triad of root springs, it is necessary to calculate the total rotation about the blade root due the flap rotation β, the lead-lag rotation ζ, and the torsional rotation ϕ about the blade root. The evaluation of the total rotation is facilitated by the use of the transformation matrices defined below.

The transformation matrix associated with a rotation by the angle β clockwise about the y_i axis is given by

$$[T_\beta] = \begin{bmatrix} 1 & 0 & \beta \\ 0 & 1 & 0 \\ -\beta & 0 & 1 \end{bmatrix} \tag{4.7}$$

The transformation matrix associated with a rotation by the angle ζ counter-clockwise about the z_i axis is given by

$$[T_\zeta] = \begin{bmatrix} 1 & \zeta & 0 \\ -\zeta & 1 & 0 \\ 0 & 0 & 1 \end{bmatrix} \tag{4.8}$$

It should be noted that it has been assumed that β and ζ are small angles.

It is easily verified that, within the context of the small angle assumption, the inverse transformations can be obtained by matrix transpose

$$[T_\beta]^{-1} = [T_\beta]^T \tag{4.9a}$$

$$[T_\zeta]^{-1} = [T_\zeta]^T \tag{4.9b}$$

Assuming the angular rotations to be small, which is consistent with the ordering scheme used in this study, they may be treated as vectors oriented in the direction about which the rotation occurs. Using the transformation matrices defined above, the total rotation vector can be expressed in the "3" system as:

$$\begin{Bmatrix} \theta_{rx3} \\ \theta_{ry3} \\ \theta_{rz3} \end{Bmatrix} = \begin{Bmatrix} 0 \\ -\beta \\ 0 \end{Bmatrix} + [T_\beta]^T \begin{Bmatrix} 0 \\ 0 \\ \zeta \end{Bmatrix} + [T_\beta]^T [T_\zeta]^T \begin{Bmatrix} \phi \\ 0 \\ 0 \end{Bmatrix} \tag{4.10}$$

where the use of Eq. (4.9) has been used to define the inverse transformations. The negative sign on the flap angle β in the above expression is due to the fact that β has been defined in this study as positive clockwise.

Carrying out the matrix multiplications yields:

$$\theta_{rx3} = \phi - \beta\zeta \tag{4.11a}$$

$$\theta_{ry3} = -\beta + \phi\zeta \tag{4.11b}$$

$$\theta_{rz3} = \zeta + \phi\beta \tag{4.11c}$$

The total rotation vector may be transformed to the "S" system using the appropriate coordinate transformation defined in Chapter 2, yielding

$$\begin{Bmatrix} \theta_{rxS} \\ \theta_{ryS} \\ \theta_{rzS} \end{Bmatrix} = \begin{bmatrix} 1 & 0 & 0 \\ 0 & \cos(R_C\theta_{Gr}) & -\sin(R_C\theta_{Gr}) \\ 0 & \sin(R_C\theta_{Gr}) & \cos(R_C\theta_{Gr}) \end{bmatrix} \begin{Bmatrix} \theta_{r3x} \\ \theta_{r3y} \\ \theta_{r3z} \end{Bmatrix} \tag{4.12}$$

Carrying out the matrix multiplication, the components of the total rotation about the blade root in the "S" system are:

$$\theta_{rxS} = \phi - \beta\zeta \tag{4.13a}$$

$$\theta_{ryS} = (-\beta + \phi\zeta)\cos(R_C\theta_{Gr}) + (\zeta + \phi\beta)\sin(R_C\theta_{Gr}) \tag{4.13b}$$

$$\theta_{rzS} = (\zeta + \phi\beta)\cos(R_C\theta_{Gr}) - (-\beta + \phi\zeta)\sin(R_C\theta_{Gr}) \tag{4.13c}$$

Now that the total rotation vector due to the sequence of rigid rotations about the blade root has been resolved into components along the axes of the "S" system, the elastic restoring moment about the blade root in the "S" system can be expressed as:

$$\begin{Bmatrix} M_{ExS} \\ M_{EyS} \\ M_{EzS} \end{Bmatrix} = -\begin{bmatrix} K_\phi & 0 & 0 \\ 0 & K_\beta & 0 \\ 0 & 0 & K_\zeta \end{bmatrix} \begin{Bmatrix} \theta_{rxS} \\ \theta_{ryS} \\ \theta_{rzS} \end{Bmatrix} \tag{4.14}$$

where K_β, K_ζ and K_ϕ are the torsional spring stiffnessess in flap, lead-lag and torsion respectively.

Carrying out the matrix multiplication yields:

$$M_{ExS} = -K_{\phi}(\phi - \beta\zeta) \tag{4.15a}$$

$$M_{EyS} = -K_{\beta}[(-\beta + \zeta\phi)\cos(R_C\theta_{Gr}) + (\zeta + \beta\phi)\sin(R_C\theta_{Gr})] \tag{4.15b}$$

$$M_{EzS} = -K_{\zeta}[(\zeta + \beta\phi)\cos(R_C\theta_{Gr}) - (-\beta + \zeta\phi)\sin(R_C\theta_{Gr})] \tag{4.15c}$$

Finally the elastic restoring moment at the blade root may be expressed in the "3" system, in which the dynamic equations of motion are formulated, by transforming them from the "S" system to the "3" system using the appropriate coordinate transformation defined in Chapter 2

$$\begin{Bmatrix} M_{Ex3} \\ M_{Ey3} \\ M_{Ez3} \end{Bmatrix} = \begin{bmatrix} 1 & 0 & 0 \\ 0 & \cos(R_C\theta_{Gr}) & -\sin(R_C\theta_{Gr}) \\ 0 & \sin(R_C\theta_{Gr}) & \cos(R_C\theta_{Gr}) \end{bmatrix} \begin{Bmatrix} M_{ExS} \\ M_{EyS} \\ M_{EzS} \end{Bmatrix} \tag{4.16}$$

Carrying out the matrix multiplication yields the components of the total elastic restoring moment about the blade root in the "3" system:

$$M_{Ex3} = -K_{\phi}(\phi - \beta\zeta) \tag{4.17a}$$

$$\begin{aligned} M_{Ey3} = &-[K_{\beta}\cos^2(R_C\theta_{Gr}) + K_{\zeta}\sin^2(R_C\theta_{Gr})](-\beta + \zeta\phi) \\ &+ (K_{\zeta} - K_{\beta})\cos(R_C\theta_{Gr})\sin(R_C\theta_{Gr})(\zeta + \beta\phi) \end{aligned} \tag{4.17b}$$

$$\begin{aligned} M_{Ez3} = &-[K_{\zeta}\cos^2(R_C\theta_{Gr}) + K_{\beta}\sin^2(R_C\theta_{Gr})](\zeta + \beta\phi) \\ &+ (K_{\zeta} - K_{\beta})\cos(R_C\theta_{Gr})\sin(R_C\theta_{Gr})(-\beta + \zeta\phi) \end{aligned} \tag{4.17c}$$

The above expressions are identical to those derived in Refs. 38, 50 and 53. It is interesting to note from the above expressions that for a "matched stiffness" rotor blade (i.e. $K_{\beta} = K_{\zeta}$) that there is no elastic coupling even for $R_C > 0$

The spring stiffnesses K_{ϕ}, K_{β} and K_{ζ} are usually selected[38,50,53] such that the non-rotating flap, lead-lag and torsional frequencies of the rigid blade match the corresponding fundamental non-rotating flap, lead-lag and torsional frequencies of the actual blade which is being modeled. Denoting ω_{β}, ω_{ζ} and ω_{ϕ} as the fundamental non-rotating frequencies

of the blade in flap, lag and torsion, respectively, the torsional stiffnesses are defined as follows:

$$K_\beta = \omega_\beta^2(I_b + I_c) \tag{4.18a}$$

$$K_\zeta = \omega_\zeta^2(I_b + I_c) \tag{4.18b}$$

$$K_\phi = \omega_\phi^2(J_b + J_c) \tag{4.18c}$$

where I_b and I_c represent the flapping inertia about the blade root of the blade and control surface, respectively, and J_b and J_c represent the polar moments of inertia of the blade and control surface, respectively. The above expressions, without the control flap inertias terms, have been taken from Ref. 50.

Since the blade configuration is usually described by the fundamental rotating frequencies, it is desirable to define the relationship between the rotating frequencies, which characterize the blade configuration, and the non-rotating frequencies, which are used to obtain the spring stiffnesses. For the offset-hinged spring restrained blade model used in this study, the fundamental rotating frequencies of the blade can be expressed as:

$$\omega_{F1}^2 = \omega_\beta^2 + \Omega^2 + M_b\Omega^2 \frac{x_b e}{I_b} + (\omega_\zeta^2 - \omega_\beta^2)\sin^2(R_C\theta_{Gr}) \tag{4.19a}$$

$$\omega_{L1}^2 = \omega_\zeta^2 + M_b\Omega^2 \frac{x_b e}{I_b} + (\omega_\zeta^2 - \omega_\beta^2)\sin^2(R_C\theta_{Gr}) \tag{4.19b}$$

$$\omega_{T1}^2 = \omega_\phi^2 + \Omega^2 \frac{I_{mbr3} - I_{mbr2}}{J_b} \tag{4.19c}$$

where

$$\int_0^{L_b} (I_{MB2}\cos^2\theta_{pt} + I_{MB3}\sin^2\theta_{pt})\,dx = I_{mbr2}$$

$$\int_0^{L_b} (I_{MB2}\sin^2\theta_{pt} + I_{MB3}\cos^2\theta_{pt})\,dx = I_{mbr3}$$

Equations (4.19) were obtained from the linearized rotating free vibration problem for the offset-hinged spring restrained blade model[38,50,53].

Modifying Eqs. (4.19) to include the control flap inertia yields:

$$\omega_{F1}^2 = \omega_\beta^2 + \Omega^2 + M_b\Omega^2 \frac{x_b e}{I_b + I_c} + M_c\Omega^2 \frac{x_c e}{I_b + I_c}$$

$$+ (\omega_\zeta^2 - \omega_\beta^2)\sin^2(R_C\theta_{Gr}) \tag{4.20a}$$

$$\omega_{L1}^2 = \omega_\zeta^2 + M_b\Omega^2 \frac{x_b e}{I_b + I_c} + M_c\Omega^2 \frac{x_c e}{I_b + I_c}$$

$$+ (\omega_\zeta^2 - \omega_\beta^2)\sin^2(R_C\theta_{Gr}) \tag{4.20b}$$

$$\omega_{T1}^2 = \omega_\phi^2 + \Omega^2 \frac{I_{mbr3} - I_{mbr2}}{J_b + J_c} \tag{4.20c}$$

where M_c is the control flap mass, and x_c is the distance to the mass centroid of the control flap from the blade root. The above expressions have been obtained from the linearized rotating free vibration problem for the offset-hinged spring restrained blade model with a partial span trailing edge flap. These expressions were obtained using MACSYMA.

4.5 STRUCTURAL DAMPING LOADS

The structural damping incorporated in this analysis is of a viscous equivalent type, and is identical to that used in Refs. 38, 50 and 53. The damping moment about the blade root in the "3" system is defined as:

$$\vec{M}_D = M_{Dx3}\,\hat{e}_{x3} + M_{Dy3}\,\hat{e}_{y3} + M_{Dz3}\,\hat{e}_{z3}$$

where

$$M_{Dx3} = -C_\phi\,\dot{\phi} \tag{4.21a}$$

$$M_{Dy3} = C_\beta\,\dot{\beta} \tag{4.21b}$$

$$M_{Dz3} = -C_\zeta \dot{\zeta} \tag{4.21c}$$

C_β, C_ζ and C_ϕ are the damping coefficients in flap, lead-lag, and torsion, respectively.

4.6 EQUATIONS OF MOTION OF THE ISOLATED BLADE

The dynamic equations of motion of an isolated blade for the offset-hinged spring restrained blade model are formulated by summing the moments about the blade root and setting this sum to zero. The total moment about the blade root due to the inertial, gravitational and aerodynamic loads is countered by the elastic restoring moment and the viscous damping moment about the blade root. Summing the moments about the blade root and equating the resultant to zero yields:

$$\vec{M}_E + \vec{M}_D + \vec{M}_R = \vec{0} \tag{4.22}$$

Substituting Eqs. (4.6), (4.21) and (4.21) into the previous expression, and evaluating each component to zero, yields the equations of motion for the offset-hinged spring restrained blade model:

Flap Equation

$$\begin{aligned} &-[K_\beta \cos^2(R_C\theta_{Gr}) + K_\zeta \sin^2(R_C\theta_{Gr})](-\beta + \zeta\phi) \\ &+ (K_\zeta - K_\beta)\cos(R_C\theta_{Gr})\sin(R_C\theta_{Gr})(\zeta + \beta\phi) \\ &+ C_\beta \dot{\beta} + M_{Ry3} = 0 \end{aligned} \tag{4.23}$$

Lag Equation

$$\begin{aligned} &-[K_\zeta \cos^2(R_C\theta_{Gr}) + K_\beta \sin^2(R_C\theta_{Gr})](\zeta + \beta\phi) \\ &+ (K_\zeta - K_\beta)\cos(R_C\theta_{Gr})\sin(R_C\theta_{Gr})(-\beta + \zeta\phi) \\ &- C_\zeta \dot{\zeta} + M_{Rz3} = 0 \end{aligned} \tag{4.24}$$

Torsion Equation

$$-K_{\phi}(\phi - \beta\zeta) - C_{\phi}\dot{\phi} + M_{Rx3} = 0 \qquad (4.25)$$

Explicit expressions for M_{Rx3}, M_{Ry3} and M_{Rz3} are developed in Appendix C using MACSYMA.

Chapter V

FULLY ELASTIC BLADE MODEL

In this context, the blade is considered to be a deformable slender rod, made of linearly isotropic, homogeneous material. The analysis is restricted to the case of small strains and finite rotations (i.e. moderate deflections). In this study the Bernoulli-Euler hypothesis is assumed to apply. Furthermore, it is assumed that strains within the cross-section can be neglected.

The structural part of the model is taken from Ref. 46. In that reference a set of non-linear partial differential equations of motion was formulated for an isotropic blade with fully coupled flap-lag-torsional dynamics undergoing moderate deflections. The distributed inertial, gravitational and aerodynamic loads acting on the blade have already been developed in Chapter 3. These loads have been formulated in terms of the elastic displacements u, v, and w and the elastic twist ϕ. The inextentionality assumption is used to eliminate the axial deformation u(x) from the expressions. For an inextensional beam cantilevered at $x=0$, the axial displacement at a spanwise location x is given by

$$u(x) = -\frac{1}{2}\int_0^x (v^2{}_{,x} + w^2{}_{,x})\, dx \tag{5.1}$$

This relation is frequently denoted as the shortening effect due to bending deformation.

The spatial dependence of the equations of motion is removed using Galerkin's method of weighted residuals. Two torsional, two lead-lag, and three flap free vibration modes of the rotating blade are used to represent the blade flexibility. The rotating mode shapes are obtained using the first nine exact nonrotating modes of an uniform cantilevered beam.

5.1 EQUATIONS OF MOTION OF THE FLEXIBLE BLADE

The formulation of the mathematical model for the fully elastic blade problem is based upon a set of consistently derived, non-linear partial differential equations describing the coupled flap-lag-torsional dynamics of an isolated rotor blade in forward flight, formulated in the undeformed reference frame assuming moderate deflections. A general version of these equations, with the distributed loads left in general symbolic form has been presented in Ref. 47. The general blade aeroelastic equations in forward flight presented in Ref. 47 are based on the formulation of Ref. 46.

The equations of equilibrium which serve as the starting point in this study are given by Eqs. (5)-(7) of Ref. 47 and are presented below. These equations were formulated using the deformation sequence lag-flap-torsion.

Flap Equation

$$
\begin{aligned}
&-[(EI_{\zeta\zeta}-EI_{\eta\eta})\sin\theta_G\cos\theta_G(v_{,xx}+2\phi w_{,xx})+(EI_{\zeta\zeta}-EI_{\eta\eta})\phi v_{,xx}\cos 2\theta_G \\
&\quad+(EI_{\zeta\zeta}\sin^2\theta_G+EI_{\eta\eta}\cos^2\theta_G)w_{,xx} \\
&\quad-TX_{IIb}(\sin\theta_G+\phi\cos\theta_G)]_{,xx} \\
&\quad+(GJ_b\phi_{,x}v_{,xx})_{,x}+(w_{,x}T)_{,x}-(v_{,x}q_{x3})_{,x}+q_{y3,x}+p_{z3}=0
\end{aligned}
\tag{5.2}
$$

Lag Equation

$$
\begin{aligned}
&-[(EI_{\zeta\zeta}\cos^2\theta_G+EI_{\eta\eta}\sin^2\theta_G)v_{,xx}+(EI_{\zeta\zeta}-EI_{\eta\eta})\phi w_{,xx}\cos 2\theta_G \\
&\quad+(EI_{\zeta\zeta}-EI_{\eta\eta})\sin\theta_G\cos\theta_G(w_{,xx}-2\phi v_{,xx}) \\
&\quad-TX_{IIb}(\cos\theta_G-\phi\sin\theta_G)]_{,xx} \\
&\quad-(GJ_b\phi_{,x}w_{,xx})_{,x}+(v_{,x}T)_{,x}+(w_{,x}q_{x3})_{,x}-q_{z3,x}+p_{y3}=0
\end{aligned}
\tag{5.3}
$$

Torsion Equation

$$
\begin{aligned}
&[GJ_b(\phi_{,x}+v_{,xx}w_{,x})]_{,x} \\
&\quad+(EI_{\zeta\zeta}-EI_{\eta\eta})[(v^2{}_{,xx}-w^2{}_{,xx})\sin\theta_G\cos\theta_G-v_{,xx}w_{,xx}\cos 2\theta_G]
\end{aligned}
$$

$$+ TX_{IIb}(w_{,xx}\cos\theta_G - v_{,xx}\sin\theta_G)$$

$$+ q_{x3} + v_{,x}q_{y3} + w_{,x}q_{z3} = 0 \tag{5.4}$$

where X_{IIb} is the offset of the tension center from the elastic axis, and

$$\vec{p} = p_{x3}\hat{e}_{x3} + p_{y3}\hat{e}_{y3} + p_{z3}\hat{e}_{z3} \tag{5.5a}$$

$$\vec{q} = q_{x3}\hat{e}_{x3} + q_{y3}\hat{e}_{y3} + q_{z3}\hat{e}_{z3} \tag{5.5b}$$

represent the total distributed force and moment, respectively, acting at the elastic axis of the blade, expressed in the undeformed reference frame ("3" system).

The quantity GJ_b is the torsional stiffness of the blade

$$GJ_b = \int_A G(y_0^2 + z_0^2)\,dy_0\,dz_0 \tag{5.6}$$

and $EI_{\zeta\zeta}$ and $EI_{\eta\eta}$ represent the principal bending stiffnesses of the blade cross-section

$$EI_{\eta\eta} = \int_A E\zeta_b^2\,dA \tag{5.7a}$$

$$EI_{\zeta\zeta} = \int_A E\eta_b^2\,dA \tag{5.7b}$$

The boundary conditions associated with Eqs. (5.2) – (5.4) are:

$$\text{at } x = 0: \quad v = w = \phi = v_{,x} = w_{,x} = 0 \tag{5.8a}$$

$$\text{at } x = L_b: \quad v_{,xx} = v_{,xxx} = w_{,xx} = w_{,xxx} = \phi_{,x} = T = 0 \tag{5.8b}$$

The first set of boundary conditions is associated with the cantilevered root at $x = 0$, and the second set is associated with the free end at $x = L_b$.

The equations of motion represented by Eqs. (5.2) – (5.4) were formulated using the deformation sequence lag-flap-torsion. This differs from the deformation sequence flap-lag-torsion adopted in this study in the derivation of the distributed loads acting on the blade. To formulate a consistent set of equations it is necessary to adopt and maintain a

single deformation sequence. Therefore, to avoid rederiving the distributed loads, a set of equations analogous to Eqs. (5.2) – (5.4) is developed in this section for the sequence flap-lag-torsion.

Equations (5.2) – (5.4) were obtained from a general set of expressions developed in Ref. 46 in which the transformation from the undeformed to the deformed reference frame was left in symbolic form. The transformation from the undeformed reference frame ("3" system) to the deformed reference frame ("4" system) was represented symbolically as:

$$\begin{Bmatrix} \hat{e}_{x4} \\ \hat{e}_{y4} \\ \hat{e}_{z4} \end{Bmatrix} = \begin{bmatrix} 1 & S_{12} & S_{13} \\ S_{21} & 1 & S_{23} \\ S_{31} & S_{32} & 1 \end{bmatrix} \begin{Bmatrix} \hat{e}_{x3} \\ \hat{e}_{y3} \\ \hat{e}_{z3} \end{Bmatrix} \tag{5.9}$$

The general set of equations, based on this transformations, are represented by Eqs. (C-24) of Ref. 46:

Flap Equation

$$\{M_{y\cdot x} + (S_{12})_{,x} M_x + [(S_{32})_{,x} - S_{12}(S_{31})_{,x}]M_z - S_{23} M_{z\cdot x}\}_{,x}$$

$$+ (S_{13} T)_{,x} - (S_{12} q_{x3})_{,x} + q_{y3\cdot x} + p_{z3} = 0 \tag{5.10}$$

Lag Equation

$$- \{M_{z\cdot x} + (S_{13})_{,x} M_x + [(S_{23})_{,x} - S_{13}(S_{21})_{,x}]M_y - S_{32} M_{y\cdot x}\}_{,x}$$

$$+ (S_{12} T)_{,x} - q_{z3\cdot x} + (S_{13} q_{x3})_{,x} + p_{y3} = 0 \tag{5.11}$$

Torsion Equation

$$M_{x\cdot x} + [(S_{21})_{,x} + S_{13}(S_{23})_{,x}]M_y + [(S_{31})_{,x} + S_{12}(S_{32})_{,x}]M_z$$

$$+ q_{x3} + S_{12} q_{y3} + S_{13} q_{z3} = 0 \tag{5.12}$$

where

$$M_x = GJ_b \tau \tag{5.13a}$$

$$M_y = - EI_{yz} \kappa_y - EI_{yy} \kappa_z + T z_A \tag{5.13b}$$

$$M_z = EI_{zz}\,\kappa_y + EI_{yz}\,\kappa_z - T\,y_A \tag{5.13c}$$

represent the components of the elastic restoring moment acting on the cross-section of the deformed blade. The bending stiffnesses are defined as:

$$EI_{zz} = \int_A E\,(y_A - y_0)^2\,dy_0\,dz_0$$

$$EI_{yz} = \int_A E\,(y_A - y_0)(z_A - z_0)\,dy_0\,dz_0$$

$$EI_{yy} = \int_A E\,(z_A - z_0)^2\,dy_0\,dz_0$$

The coordinate pair (y_A, z_A) represents the coordinates of the area centroid of the blade cross-section, i.e.

$$\int_{A_b} y_0\,dy_0\,dz_0 = y_A\,A_b$$

$$\int_{A_b} z_0\,dy_0\,dz_0 = z_A\,A_b$$

where A_b is the area of the blade cross-section.

For a symmetric blade cross-section:

$$EI_{zz} = EI_{\zeta\zeta}\cos^2\theta_G + EI_{\eta\eta}\sin^2\theta_G \tag{5.14a}$$

$$EI_{yz} = (EI_{\zeta\zeta} - EI_{\eta\eta})\sin\theta_G\cos\theta_G \tag{5.14b}$$

$$EI_{yy} = EI_{\zeta\zeta}\sin^2\theta_G + EI_{\eta\eta}\cos^2\theta_G \tag{5.14c}$$

Furthermore,

$$y_A = X_{IIb}\cos\theta_G \;\;;\;\; z_A = X_{IIb}\sin\theta_G$$

for a symmetric blade.

The quantities denoted by κ_y and κ_z in Eqs. (5.13) represent the bending curvatures of the blade and τ is the rate of twist. These quantities are defined in Ref. 54 by:

$$\kappa_y = \hat{e}_{y4} \cdot \hat{e}_{x4,x} = -\hat{e}_{x4} \cdot \hat{e}_{y4,x}$$

$$\kappa_z = \hat{e}_{z4} \cdot \hat{e}_{x4,x} = -\hat{e}_{x4} \cdot \hat{e}_{z4,x}$$

$$\tau = \hat{e}_{z4} \cdot \hat{e}_{y4,x} = -\hat{e}_{y4} \cdot \hat{e}_{z4,x}$$

The bending curvatures and the twist of the blade depend upon the transformation from the undeformed to the deformed coordinate system. Making use of Eq. (5.9), general expressions for the curvature and twist are

$$\kappa_y = (S_{12})_{,y} + S_{23}(S_{13})_{,x} \tag{5.15a}$$

$$\kappa_z = S_{32}(S_{12})_{,x} + (S_{13})_{,x} \tag{5.15b}$$

$$\tau = S_{31}(S_{21})_{,x} + (S_{23})_{,x} \tag{5.15c}$$

A detailed derivation of the equations of motion for the deformation sequence lag-flap-torsion represented by Eqs. (5.2) – (5.4) from the general expressions given by Eqs. (5.10) – (5.12) and (5.15) is presented in Ref. 46. For this sequence the transformation from the undeformed to the deformed reference frame is given by:

$$\begin{Bmatrix} \hat{e}_{x4} \\ \hat{e}_{y4} \\ \hat{e}_{z4} \end{Bmatrix} = \begin{bmatrix} 1 & v_{,x} & w_{,x} \\ -(v_{,x} + \phi w_{,x}) & 1 & \phi \\ -(w_{,x} - \phi v_{,x}) & -(\phi + v_{,x} w_{,x}) & 1 \end{bmatrix} \begin{Bmatrix} \hat{e}_{x3} \\ \hat{e}_{y3} \\ \hat{e}_{z3} \end{Bmatrix} \tag{5.16}$$

Using Eqs. (5.15), the expressions for the bending curvatures and twist for the case lag-flap-torsion are:

$$\kappa_y = v_{,xx} + \phi w_{,xx} \tag{5.17a}$$

$$\kappa_z = w_{,xx} - \phi v_{,xx} \tag{5.17b}$$

$$\tau = \phi_{,x} + v_{,xx} w_{,x} \tag{5.17c}$$

The ordering scheme has been used to neglect the higher order terms in the above expressions. In Ref. 46 Eqs. (5.17) were substituted into Eqs. (5.10) – (5.12) to obtain the equations of motion represented by Eqs. (5.2) – (5.4).

For the deformation sequence flap-lag-torsion, the transformation from the undeformed to the deformed reference frame is given by:

$$\begin{Bmatrix} \hat{e}_{x4} \\ \hat{e}_{y4} \\ \hat{e}_{z4} \end{Bmatrix} = \begin{bmatrix} 1 & v_{,x} & w_{,x} \\ -(v_{,x} + \phi w_{,x}) & 1 & (\phi - v_{,x} w_{,x}) \\ -(w_{,x} - \phi v_{,x}) & -\phi & 1 \end{bmatrix} \begin{Bmatrix} \hat{e}_{x3} \\ \hat{e}_{y3} \\ \hat{e}_{z3} \end{Bmatrix} \tag{5.18}$$

Using Eqs. (5.15) the bending curvatures and twist for this case are:

$$\kappa_y = v_{,xx} + \phi w_{,xx} \tag{5.19a}$$

$$\kappa_z = w_{,xx} - \phi v_{,xx} \tag{5.19b}$$

$$\tau = \phi_{,x} - v_{,x} w_{,xx} \tag{5.19c}$$

It is interesting to note that the expressions obtained for κ_y and κ_z are the same for the two deformation sequences. Though the expressions obtained for the twist τ are not the same, the leading orders terms are identical. This can be attributed to the fact that the only differences between coordinate transformations given by Eqs. (5.16) and (5.18) are in the S_{23} and the S_{32} terms.

Substituting the flap-lag-torsion coordinate transformation given by Eq. (5.18) and the curvatures and twist given by Eqs. (5.19) into Eqs. (5.10)-(5.12) yields the following set of equations of motion for the deformation sequence flap-lag-torsion:

Flap Equation

$$\begin{aligned} &-[(EI_{\zeta\zeta} - EI_{\eta\eta}) \sin\theta_G \cos\theta_G (v_{,xx} + 2\phi w_{,xx}) + (EI_{\zeta\zeta} - EI_{\eta\eta})\phi v_{,xx} \cos 2\theta_G \\ &\quad + (EI_{\zeta\zeta} \sin^2\theta_G + EI_{\eta\eta} \cos^2\theta_G) w_{,xx} \\ &\quad - TX_{IIb}(\sin\theta_G + \phi \cos\theta_G)]_{,xx} \\ &\quad + (GJ_b \phi_{,x} v_{,xx})_{,x} + (w_{,x} T)_{,x} - (v_{,x} q_{x3})_{,x} + q_{y3,x} + p_{z3} = 0 \end{aligned} \tag{5.20}$$

Lag Equation

$$
\begin{aligned}
&-[(EI_{\zeta\zeta}\cos^2\theta_G + EI_{\eta\eta}\sin^2\theta_G)v_{,xx} + (EI_{\zeta\zeta} - EI_{\eta\eta})\phi w_{,xx}\cos 2\theta_G \\
&\quad + (EI_{\zeta\zeta} - EI_{\eta\eta})\sin\theta_G\cos\theta_G(w_{,xx} - 2\phi v_{,xx}) \\
&\quad - TX_{IIb}(\cos\theta_G - \phi\sin\theta_G)]_{,xx} \\
&\quad - (GJ_b\phi_{,x}w_{,xx})_{,x} + (v_{,x}T)_{,x} + (w_{,x}q_{x3})_{,x} - q_{z3,x} + p_{y3} = 0
\end{aligned}
\tag{5.21}
$$

Torsion Equation

$$
\begin{aligned}
&[GJ_b(\phi_{,x} - v_{,x}w_{,xx})]_{,x} \\
&\quad + (EI_{\zeta\zeta} - EI_{\eta\eta})[(v^2{}_{,xx} - w^2{}_{,xx})\sin\theta_G\cos\theta_G - v_{,xx}w_{,xx}\cos 2\theta_G] \\
&\quad + TX_{IIb}(w_{,xx}\cos\theta_G - v_{,xx}\sin\theta_G) \\
&\quad + q_{x3} + v_{,x}q_{y3} + w_{,x}q_{z3} = 0
\end{aligned}
\tag{5.22}
$$

Comparing Eqs. (5.2) - (5.4) with Eqs. (5.20) - (5.22) reveals that the structural part of the flap and lag equations are identical for the two deformation sequences. This can be attributed to the fact that the expressions for the curvatures of the blade are the same for the two deformation sequences. The only difference evident in the structural part of the torsion equations given by Eqs. (5.4) and (5.22) is in the first term. The quantity in parenthesis multiplied by the torsional stiffness of the blade GJ_b in each of these equations can be recognized as the twist of the blade τ, which has been shown to be different for the two deformation sequences. It should be noted that the boundary conditions given by Eqs. (5.8) are also the same for the two deformation sequences. The boundary conditions together with (5.20) – (5.22) , are used in this study to develop explicit expressions for the equations of motion of the flexible blade.

The tension T is eliminated from the flap, lag and torsional equations in a manner similar the approach used in Ref. 47 where, after neglecting higher order terms, the axial tension equation is expressed as

$$T_{,x} = -p_{Ix3} \tag{5.23}$$

where p_{Ix3} represents the axial load at the elastic axis of the blade due to the rotation of the blade. Integrating Eq. (5.23) with respect to x and using the boundary condition $T(x = L_b) = 0$ yields:

$$T(x) = -\int_x^{L_b} T_{,x}\, dx = -\left[\int_0^{L_b} T_{,x}\, dx - \int_0^x T_{,x}\, dx\right]$$

$$= \int_0^{L_b} p_{Ix3}\, dx - \int_0^x p_{Ix3}\, dx \tag{5.24}$$

The system of coupled partial differential equations of motion represented by Eqs. (5.20) – (5.22) is transformed to a system of ordinary nonlinear ordinary differential equations using Galerkin's method to eliminate the spatial variable x. In this study, the first two torsional modes, the first two lead-lag bending modes, and the first three flap bending modes of a rotating uniform cantilevered beam are used as comparison functions, i.e.

$$w \cong \tilde{w} = \sum_{i=1}^{3} q_{wi}(\psi)\, W_i(x) \tag{5.25a}$$

$$v \cong \tilde{v} = \sum_{i=1}^{2} q_{vi}(\psi)\, V_i(x) \tag{5.25b}$$

$$\phi \cong \tilde{\phi} = \sum_{i=1}^{2} q_{\phi i}(\psi)\, \Phi_i(x) \tag{5.25c}$$

where $W_i(x)$, $V_i(x)$ and $\Phi_i(x)$ represent the i-th flap, lead-lag and torsional uncoupled rotating mode shape, respectively. The participation coefficients $q_{\phi 1}$, $q_{\phi 2}$, q_{v1}, q_{v2}, q_{w1}, q_{w2} and q_{w3} represent the seven generalized degrees of freedom of the fully flexible blade model.

The uncoupled rotating mode shapes are generated using the first nine exact modes of a nonrotating uniform beam. The analytical expressions for the nonrotating mode shapes are taken from Ref. 1. The integrals required to calculate the mass and stiffness

matrices of the free-vibration problem for the rotating beam are evaluated numerically using 20-point Gaussian quadrature. This free vibration problem is solved separately, before embarking on the aeroelastic computations, and thus it essentially represents a preprocessing stage.

To apply Galerkin's method the error residuals associated with the use of Eqs. (5.25) in the equations of motion must be formed. These are then multiplied by the appropriate mode shape and integrated over the span of the blade. Galerkin's method consists of setting each of these integrals to zero and solving for modal participation coefficients, which represent the generalized coordinates of the problem.

Multiplying each error residual by the appropriate mode shape and integrating over the span of the blade yields:

Flap Equation (i = 1,2,3)

$$\int_0^{L_b} \{ -[(EI_{\zeta\zeta} - EI_{\eta\eta}) \sin\theta_G \cos\theta_G (\tilde{v}_{,xx} + 2\tilde{\phi}\tilde{w}_{,xx})$$

$$+ (EI_{\zeta\zeta} - EI_{\eta\eta})\tilde{\phi}\tilde{v}_{,xx} \cos 2\theta_G + (EI_{\zeta\zeta} \sin^2\theta_G + EI_{\eta\eta} \cos^2\theta_G)\tilde{w}_{,xx}$$

$$- TX_{IIb}(\sin\theta_G + \tilde{\phi} \cos\theta_G)]_{,xx}$$

$$+ (GJ_b\tilde{\phi}_{,x}\tilde{v}_{,xx} + \tilde{w}_{,x}T - \tilde{v}_{,x}\tilde{q}_{x3} + \tilde{q}_{y3})_{,x} + \tilde{p}_{z3}\} W_i(x)\, dx = 0 \qquad (5.26)$$

Lag Equation (i = 1,2)

$$\int_0^{L_b} \{ -[(EI_{\zeta\zeta} \cos^2\theta_G + EI_{\eta\eta} \sin^2\theta_G)\tilde{v}_{,xx} + (EI_{\zeta\zeta} - EI_{\eta\eta})\tilde{\phi}\tilde{w}_{,xx} \cos 2\theta_G$$

$$+ (EI_{\zeta\zeta} - EI_{\eta\eta}) \sin\theta_G \cos\theta_G (\tilde{w}_{,xx} - 2\tilde{\phi}\tilde{v}_{,xx})$$

$$- TX_{IIb}(\cos\theta_G - \tilde{\phi} \sin\theta_G)]_{,xx}$$

$$+ (-GJ_b\tilde{\phi}_{,x}\tilde{w}_{,xx} + \tilde{v}_{,x}T + \tilde{w}_{,x}\tilde{q}_{x3} - \tilde{q}_{z3})_{,x} + \tilde{p}_{y3}\} V_i(x)\, dx = 0 \qquad (5.27)$$

Torsion Equation (i = 1,2)

$$\int_0^{L_b} \{[GJ_b(\tilde{\phi}_{,x} - \tilde{v}_{,x}\tilde{w}_{,xx})]_{,x}$$

$$+ (EI_{\zeta\zeta} - EI_{\eta\eta})[(\tilde{v}^2_{,xx} - \tilde{w}^2_{,xx}) \sin\theta_G \cos\theta_G - \tilde{v}_{,xx}\tilde{w}_{,xx} \cos 2\theta_G]$$

$$+ TX_{IIb}(\tilde{w}_{,xx} \cos\theta_G - \tilde{v}_{,xx} \sin\theta_G)$$

$$+ \tilde{q}_{x3} + \tilde{v}_{,x}\tilde{q}_{y3} + \tilde{w}_{,x}\tilde{q}_{z3}\} \Phi_i(x)\, dx = 0 \qquad (5.28)$$

where the tilde over the distributed loads indicates that $\tilde{v}$, $\tilde{w}$ and $\tilde{\phi}$ given by Eqs. (5.25) have been substituted into the expressions.

It is well known that when approximations such as Eqs. (5.25) are used to obtain approximations for the spatial derivatives of w, v and ϕ, the quality of the approximations deteriorates quickly as the order of the derivative increases. This is due to the fact that with each successive spatial differentiation the errors inherent in the approximations are amplified. Thus all spatial derivatives higher than second order are eliminated from Eqs. (5.26)-(5.28) by integrating by parts twice using the boundary conditions given by Eqs. (5.8).

Integrating the first integrand in Eqs. (5.27) and (5.26) by parts twice, integrating the second integrand in Eqs. (5.27) and (5.26) and the first integrand in Eq. (5.28) by parts once, and making use of the boundary conditions given by Eqs. (5.8), yields:

Flap Equation (i = 1,2,3)

$$\int_0^{L_b} \{ - [(EI_{\zeta\zeta} - EI_{\eta\eta}) \sin\theta_G \cos\theta_G(\tilde{v}_{,xx} + 2\tilde{\phi}\tilde{w}_{,xx})$$

$$+ (EI_{\zeta\zeta} - EI_{\eta\eta})\tilde{\phi}\tilde{v}_{,xx} \cos 2\theta_G + (EI_{\zeta\zeta} \sin^2\theta_G + EI_{\eta\eta} \cos^2\theta_G)\tilde{w}_{,xx}$$

$$- TX_{IIb}(\sin\theta_G + \tilde{\phi} \cos\theta_G)]\, W_{i,xx}$$

$$+ (GJ_b\tilde{\phi}_{,x}\tilde{v}_{,xx} + \tilde{w}_{,x}T - \tilde{v}_{,x}\tilde{q}_{x3} + \tilde{q}_{y3})\, W_{i,x} + \tilde{p}_{z3}\, W_i\}\, dx = 0 \qquad (5.29)$$

Lag Equation (i = 1,2)

$$\int_0^{L_b} \{ - [(EI_{\zeta\zeta} \cos^2\theta_G + EI_{\eta\eta} \sin^2\theta_G)\tilde{v}_{,xx} + (EI_{\zeta\zeta} - EI_{\eta\eta})\tilde{\phi}\tilde{w}_{,xx} \cos 2\theta_G$$

$$+ (EI_{\zeta\zeta} - EI_{\eta\eta}) \sin\theta_G \cos\theta_G(\tilde{w}_{,xx} - 2\tilde{\phi}\tilde{v}_{,xx})$$

$$- TX_{IIb}(\cos\theta_G - \tilde{\phi} \sin\theta_G)] V_{i,xx}$$

$$+ (- GJ_b\tilde{\phi}_{,x}\tilde{w}_{,xx} + \tilde{v}_{,x}T + \tilde{w}_{,x}\tilde{q}_{x3} - \tilde{q}_{z3}) V_{i,x} + \tilde{p}_{y3}V_i\} dx = 0 \qquad (5.30)$$

Torsion Equation (i = 1,2)

$$\int_0^{L_b} \{[GJ_b(\tilde{\phi}_{,x} - \tilde{v}_{,x}\tilde{w}_{,xx})] \Phi_{i,x}$$

$$+ (EI_{\zeta\zeta} - EI_{\eta\eta})[(\tilde{v}^2_{,xx} - \tilde{w}^2_{,xx}) \sin\theta_G \cos\theta_G - \tilde{v}_{,xx}\tilde{w}_{,xx} \cos 2\theta_G] \Phi_i$$

$$+ TX_{IIb}(\tilde{w}_{,xx} \cos\theta_G - \tilde{v}_{,xx} \sin\theta_G) \Phi_i$$

$$+ (\tilde{q}_{x3} + \tilde{v}_{,x}\tilde{q}_{y3} + \tilde{w}_{,x}\tilde{q}_{z3}) \Phi_i\} dx = 0 \qquad (5.31)$$

After carrying out the integrations over the blade span, the resulting set of equations represent a set of seven second order nonlinear coupled ordinary differential equations in terms of the modal participation coefficients q_{w1}, q_{w2}, q_{w3}, q_{v1}, q_{v2}, $q_{\phi 1}$ and $q_{\phi 2}$. The integrations of the error residuals over the blade span is performed using 20-point Gaussian quadrature. The expressions for $\tilde{w}$, $\tilde{v}$ and $\tilde{\phi}$ given by Eqs. (5.25) are substituted into the equations of motion but are not expanded. Instead, they are evaluated numerically at each blade station required in the numerical integration procedure.

It is important to recognize that up to this point the presence of a partial span trailing edge flap on the blade span has not been explicitly accounted for in equations of motion of the flexible blade represented by Eqs. (5.29) – (5.31). The incorporation of the effects due to an actively controlled flap into the equations of motion is described in the next section.

5.2 INCORPORATION OF THE CONTROL FLAP

An aerodynamic surface, modeled as a partial span trailing edge flap located on the outboard sections of the blade, as shown in Fig. 3, is considered to be an integral part of the blade. The control surface has a chord length of c_{cs} and a span of L_{cs}, with the inboard edge located a distance x_{cs} from the blade root. The control surface is attached to the trailing edge of the blade by a series of hinges located at a finite number of discrete points (referred to as "hinge points") along the trailing edge of the blade. It is assumed that each hinge is rigid in all directions except about the hinge axis, about which the control surface rotates. The hinges adequately constrain the control surface cross-section to a pure rotation in the plane of the blade cross-section.

The presence of actively controlled flap on the blade span must be appropriately incorporated into the equations of motion. In this study, the inertial, gravitational, and aerodynamic effects are included, but the structural effects of the control flap are neglected. It is assumed that the additional stiffness provided by the presence of a relatively small control flap, on the outboard sections of the blade, has a negligible effect on the blade deformation. The increase in the local bending and torsional stiffness of blade cross-sections incorporating a trailing edge flap only directly affects the deformation of the blade sections outboard of the inboard edge of the control flap; and since the curvature and rate of twist of these blade sections near the tip are small compared to those at the root, changes in the curvature and rate of twist due to control flap stiffness are assumed to be negligible. Thus one may assume that the presence of the flap has a negligible effect the bending deformation of the blade; and the elastic twist is significantly altered only for blades relatively soft in torsion. Despite its relatively small size, however, the inertial effects are included since the mass is located at a considerable distance from the hub and thus can influence the blade root moment.

The effects of the control flap are accounted for by transferring the distributed loads acting on the control flap to the elastic axis of the blade. The total distributed force acting on the blade can be expressed as:

$$\vec{p} = \begin{cases} \vec{p}_b & \text{for} \quad 0 < x < x_{cs} \\ \vec{p}_b + \vec{p}_c & \text{for} \quad x_{cs} < x < x_{cs} + L_{cs} \\ \vec{p}_b & \text{for} \quad x_{cs} + L_{cs} < x < L_b \end{cases} \tag{5.32}$$

where

$$\vec{p}_b = p_{bx3}\,\hat{e}_{x3} + p_{by3}\,\hat{e}_{y3} + p_{bz3}\,\hat{e}_{z3} \tag{5.33}$$

is the distributed force due to the blade loads, and

$$\vec{p}_c = p_{cx3}\,\hat{e}_{x3} + p_{cy3}\,\hat{e}_{y3} + p_{cz3}\,\hat{e}_{z3} \tag{5.34}$$

is the distributed force due to the presence of the control flap. The components of $\vec{p}_b$ are defined by Eqs. (3.127), and the components of $\vec{p}_c$ are defined by Eqs. (3.131).

Similarly, the total distributed moment can be expressed as:

$$\vec{q} = \begin{cases} \vec{q}_b & \text{for} \quad 0 < x < x_{cs} \\ \vec{q}_b + \vec{q}_c & \text{for} \quad x_{cs} < x < x_{cs} + L_{cs} \\ \vec{q}_b & \text{for} \quad x_{cs} + L_{cs} < x < L_b \end{cases} \tag{5.35}$$

where

$$\vec{q}_b = q_{bx3}\,\hat{e}_{x3} + q_{by3}\,\hat{e}_{y3} + q_{bz3}\,\hat{e}_{z3} \tag{5.36}$$

is the distributed moment due to the blade loads, and

$$\vec{q}_c = q_{cx3}\,\hat{e}_{x3} + q_{cy3}\,\hat{e}_{y3} + q_{cz3}\,\hat{e}_{z3} \tag{5.37}$$

is the distributed moment due to the presence of a control flap. The components of $\vec{q}_b$ are defined by Eqs. (3.129), and the components of $\vec{q}_c$ are defined by Eqs. (3.133).

Substituting Eqs. (5.32) and (5.35) into the Eqs. (5.29)-(5.31) yields:

Flap Equation (i = 1,2,3)

$$\int_0^{L_b} \{ - [(EI_{\zeta\zeta} - EI_{\eta\eta}) \sin\theta_G \cos\theta_G (\tilde{v}_{,xx} + 2\tilde{\phi}\tilde{w}_{,xx})$$

$$+ (EI_{\zeta\zeta} - EI_{\eta\eta})\tilde{\phi}\tilde{v}_{,xx} \cos 2\theta_G + (EI_{\zeta\zeta} \sin^2\theta_G + EI_{\eta\eta} \cos^2\theta_G)\tilde{w}_{,xx}$$

$$- TX_{IIb}(\sin \theta_G + \tilde{\phi} \cos \theta_G)] W_{i,xx}$$

$$+ (GJ_b\tilde{\phi}_{,x}\tilde{v}_{,xx} + \tilde{w}_{,x}T - \tilde{v}_{,x}\tilde{q}_{bx3} + \tilde{q}_{by3}) W_{i,x} + \tilde{p}_{bz3} W_i\} dx$$

$$+ \int_{x_{cs}}^{x_{cs} + L_{cs}} [(-\tilde{v}_{,x}\tilde{q}_{cx3} + \tilde{q}_{cy3}) W_{i,x} + \tilde{p}_{cz3} W_i] dx = 0 \qquad (5.38)$$

Lag Equation (i = 1,2)

$$\int_0^{L_b} \{ - [(EI_{\zeta\zeta} \cos^2\theta_G + EI_{\eta\eta} \sin^2\theta_G)\tilde{v}_{,xx} + (EI_{\zeta\zeta} - EI_{\eta\eta})\tilde{\phi}\tilde{w}_{,xx} \cos 2\theta_G$$

$$+ (EI_{\zeta\zeta} - EI_{\eta\eta}) \sin \theta_G \cos \theta_G(\tilde{w}_{,xx} - 2\tilde{\phi}\tilde{v}_{,xx})$$

$$- TX_{IIb}(\cos \theta_G - \tilde{\phi} \sin \theta_G)] V_{i,xx}$$

$$+ (-GJ_b\tilde{\phi}_{,x}\tilde{w}_{,xx} + \tilde{v}_{,x}T + \tilde{w}_{,x}\tilde{q}_{bx3} - \tilde{q}_{bz3}) V_{i,x} + \tilde{p}_{by3}V_i\} dx$$

$$+ \int_{x_{cs}}^{x_{cs} + L_{cs}} [(\tilde{w}_{,x}\tilde{q}_{cx3} - \tilde{q}_{cz3}) V_{i,x} + \tilde{p}_{cy3}V_i] dx = 0 \qquad (5.39)$$

Torsion Equation (i = 1,2)

$$\int_0^{L_b} \{[GJ_b(\tilde{\phi}_{,x} - \tilde{v}_{,x}\tilde{w}_{,xx})] \Phi_{i,x}$$

$$+ (EI_{\zeta\zeta} - EI_{\eta\eta})[(\tilde{v}_{,xx}^2 - \tilde{w}_{,xx}^2) \sin \theta_G \cos \theta_G - \tilde{v}_{,xx}\tilde{w}_{,xx} \cos 2\theta_G] \Phi_i$$

$$+ TX_{IIb}(\tilde{w}_{,xx} \cos \theta_G - \tilde{v}_{,xx} \sin \theta_G) \Phi_i$$

$$+ (\tilde{q}_{bx3} + \tilde{v}_{,x}\tilde{q}_{by3} + \tilde{w}_{,x}\tilde{q}_{bz3}) \Phi_i\} dx$$

$$+ \int_{x_{cs}}^{x_{cs} + L_{cs}} [(\tilde{q}_{cx3} + \tilde{v}_{,x}\tilde{q}_{cy3} + \tilde{w}_{,x}\tilde{q}_{cz3}) \Phi_i] dx = 0 \qquad (5.40)$$

Chapter VI

METHOD OF SOLUTION

For both blade models, the system of nonlinear ordinary differential equations of motion of the isolated blade can be represented by the following vector of size N_{DOF}, the number of blade degrees of freedom in the model:

$$\vec{f}_b(\vec{q}_b, \dot{\vec{q}}_b, \ddot{\vec{q}}_b, \vec{q}_t, \delta; \psi) = \vec{0} \tag{6.1}$$

The vector $\vec{q}_b$ contains the blade degrees of freedom and $\vec{q}_t$ is a vector containing the trim variables of the problem. Each row of $\vec{f}_b$ represents the equation of motion associated with a particular degree of freedom in $\vec{q}_b$.

In the formulation of the equations of motion, the following quantities were assumed to be known: the inflow ratio λ; the rotor angle of attack α_R ; the collective pitch angle θ_0; the cyclic cosine pitch input θ_{1c}; and the cyclic sine pitch input θ_{1s}. These five quantities collectively represent the trim settings of the helicopter and appear explicitly in the blade equations of motion. Therefore, the blade equations equations can not be solved until these five quantities have been determined.

The trim vector appearing in Eq. (6.1), defined as:

$$\vec{q}_t = \{\lambda, \alpha_R, \theta_0, \theta_{1c}, \theta_{1s}\}^T \tag{6.2}$$

represents the solution to a set of nonlinear trim equations which can be expressed in the following vector form:

$$\vec{f}_t(\vec{q}_b, \dot{\vec{q}}_b, \ddot{\vec{q}}_b, \vec{q}_t, \delta; \psi) = \vec{0} \tag{6.3}$$

The system of trim equations represented by Eq. (6.3) is obtained by enforcing the overall force and moment equilibrium of the helicopter in steady, level forward flight. The vector $\vec{f}_t$ also contains an inflow equation. The process of determining the trim variables is re-

ferred to as the "trim analysis". Before equilibrium can be enforced at the hub, it is necessary to evaluate the forces and moments at the hub due to blade loading and due to the forces and moments acting on the fuselage during forward flight.

6.1 ROTOR HUB LOADS

The total force and moment at the hub due to blade loading are obtained by integrating the distributed loads along the span of the isolated blade in the rotating frame ("2" system), transforming them to the non-rotating hub-fixed reference frame ("1" system), and then summing the contribution at the hub from each blade in the rotor.

The total force and moment at the blade root due to the inertial gravitational, damping and aerodynamic loads on the k-th blade, obtained by integrating the distributed loads along the span of the blade, can be expressed in the "2" system by:

$$\vec{F}_R(\psi_k) = F_{Rx2}(\psi_k)\hat{e}_{x2} + F_{Ry2}(\psi_k)\hat{e}_{y2} + F_{Rz2}(\psi_k)\hat{e}_{z2}$$

and

$$\vec{M}_R(\psi_k) = M_{Rx2}(\psi_k)\hat{e}_{x2} + M_{Ry2}(\psi_k)\hat{e}_{y2} + M_{Rz2}(\psi_k)\hat{e}_{z2}$$

respectively, where

$$\psi_k = \psi + \frac{2\pi(k-1)}{N_b} \tag{6.4}$$

is the azimuth angle of the k-th blade.

Transforming the root force $\vec{F}_R$ to the "1" system using the coordinate transformations defined in Chapter 2 by Eq. (2.5), yields the force at the hub due to the k-th blade

$$\vec{F}_{Hk}(\psi_k) = F_{Hkx1}(\psi_k)\hat{e}_{x1} + F_{Hky1}(\psi_k)\hat{e}_{y1} + F_{Hkz1}(\psi_k)\hat{e}_{z1}$$

where

$$F_{Hkx1}(\psi_k) = F_{Rx2}(\psi_k)\cos\psi_k - F_{Ry2}(\psi_k)\sin\psi_k$$

$$F_{Hky1}(\psi_k) = F_{Rx2}(\psi_k) \sin\psi_k + F_{Ry2}(\psi_k) \cos\psi_k$$

$$F_{Hkz1}(\psi_k) = F_{Rz2}(\psi_k)$$

The total force at the hub due to N_b blades is obtained by summing the contribution of each blade

$$\vec{F}_H(\psi) = \sum_{k=1}^{N_b} \vec{F}_{Hk}(\psi_k)$$

which can be expressed as:

$$\vec{F}_H(\psi) = F_{Hx1}(\psi)\,\hat{e}_{x1} + F_{Hy1}(\psi)\,\hat{e}_{y1} + F_{Hz1}(\psi)\,\hat{e}_{z1}$$

where

$$F_{Hx1}(\psi) = \sum_{k=1}^{N_b} [F_{Rx2}(\psi_k) \cos\psi_k - F_{Ry2}(\psi_k) \sin\psi_k]$$

$$F_{Hy1}(\psi) = \sum_{k=1}^{N_b} [F_{Rx2}(\psi_k) \sin\psi_k + F_{Ry2}(\psi_k) \cos\psi_k]$$

$$F_{Hz1}(\psi) = \sum_{k=1}^{N_b} F_{Rz2}(\psi_k)$$

The moment at the hub due to the k-th blade is given by:

$$\vec{M}_{Hk}(\psi_k) = \vec{M}_R(\psi_k) + e\,\hat{e}_{x2} \times \vec{F}_R(\psi_k)$$

which can be expressed in the "1" system as:

$$\vec{M}_{Hk}(\psi_k) = M_{Hkx1}(\psi_k)\,\hat{e}_{x1} + M_{Hky1}(\psi_k)\,\hat{e}_{y1} + M_{Hkz1}(\psi_k)\,\hat{e}_{z1}$$

Carrying out the cross-product yields

$$M_{Hkx1}(\psi_k) = M_{Rx2}(\psi_k) \cos\psi_k - [M_{Ry2}(\psi_k) - e\,F_{Rz2}(\psi_k)] \sin\psi_k$$

$$M_{Hky1} = M_{Rx2}(\psi_k) \sin\psi_k + [M_{Ry2}(\psi_k) - e\,F_{Rz2}(\psi_k)] \cos\psi_k$$

$$M_{Hkz1}(\psi_k) = M_{Rz2}(\psi_k) + e\, F_{Ry2}(\psi_k)$$

The total hub moment due to N_b blades is obtained by summing the contribution from each blade

$$\vec{M}_H(\psi) = \sum_{k=1}^{N_b} \vec{M}_{Hk}(\psi_k)$$

which can be expressed as:

$$\vec{M}_H(\psi) = M_{Hx1}(\psi)\,\hat{e}_{x1} + M_{Hy1}(\psi)\,\hat{e}_{y1} + M_{Hz1}(\psi)\,\hat{e}_{z1}$$

where

$$M_{Hx1}(\psi) = \sum_{k=1}^{N_b} \{M_{Rx2}(\psi_k)\cos\psi_k - [M_{Ry2}(\psi_k) - e\, F_{Rz2}(\psi_k)]\sin\psi_k\}$$

$$M_{Hy1}(\psi) = \sum_{k=1}^{N_b} \{M_{Rx2}(\psi_k)\sin\psi_k + [M_{Ry2}(\psi_k) - e\, F_{Rz2}(\psi_k)]\cos\psi_k\}$$

$$M_{Hz1}(\psi) = \sum_{k=1}^{N_b} [M_{Rz2}(\psi_k) + e\, F_{Ry2}(\psi_k)]$$

In this study it is assumed that there are four blades in the rotor (i.e. $N_b = 4$) and therefore the azimuth angle of the k-th blade is given by:

$$\psi_k = \psi + \frac{\pi}{2}(k-1)$$

6.2 ROTOR AERODYNAMIC THRUST

The total aerodynamic thrust produced by the rotor is required in the inflow equation to calculate the inflow. The thrust of the rotor is defined as the total aerodynamic force parallel to the rotor shaft, and is obtained by summing the contribution from each blade. The z_2 axis is parallel to the shaft axis; thus the total aerodynamic thrust is given by:

$$T_R = \sum_{k=1}^{N_b=4} F_{Az2}(\psi_k) \tag{6.5}$$

where $F_{Az2}(\psi_k)$ represents the z_2 component of the aerodynamic force at the blade root of the k-th blade.

6.3 FUSELAGE FORCES AND MOMENTS

The fuselage weight and the aerodynamic drag acting on the fuselage in forward flight produce forces and moments at the hub which must be in equilibrium with the rotor hub loads in order to maintain steady level flight. The forces and moments at the hub for a helicopter with weight coefficient C_W and an equivalent fuselage flat plate drag area of fC_{df} are described next.

6.3.1 *Forces and Moments Due to Fuselage Weight*

Given the weight of the helicopter,

$$W = C_W \pi R^2 \rho_A \Omega^2 R^2 \tag{6.6}$$

the weight of the fuselage can be obtained by subtracting the weight of the rotor blades, which are already accounted for in the gravitational loads. Thus the fuselage weight is given by:

$$W_f = C_W \pi R^2 \rho_A \Omega^2 R^2 - g N_b M_b \tag{6.7}$$

The weight acts in the direction of the gravitational vector, which is oriented parallel to the negative z_0 axis. The force due to fuselage weight can be expressed in the "1" system as:

$$\vec{F}_{Wf} = -W_f(\sin \alpha_R \hat{e}_{x1} + \cos \alpha_R \hat{e}_{z1}) \tag{6.8}$$

where the angle α_R is the trim rotor angle of attack.

This force is assumed to act at the fuselage center of gravity, which is located a distance Z_{FC} below the hub along the negative z_1 axis, and a distance X_{FC} in front of the hub along the negative x_1 axis, as shown in Fig. 5. The position vector of the fuselage center of gravity relative to the hub center can be expressed as:

$$\vec{r}_{FC} = -X_{FC}\hat{e}_{x1} - Z_{FC}\hat{e}_{z1} \tag{6.9}$$

The fuselage weight produces a pitching moment about the hub given by:

$$M_{Wf}\hat{e}_{y1} = \vec{r}_{FC} \times \vec{F}_{Wf} \tag{6.10}$$

Using Eqs. (6.8) – (6.10) yields:

$$M_{Wf} = -W_f(-X_{FC}\cos\alpha_R + Z_{FC}\sin\alpha_R) \tag{6.11}$$

6.3.2 *Forces and Moments Due to Fuselage Drag*

The parasitic drag acting on the fuselage is given by:

$$D_f = \frac{1}{2}\rho_A V_{Af}^2 fC_{df} \tag{6.12}$$

where V_{Af} represents the magnitude of the resultant air velocity employed in calculating fuselage drag, and fC_{df} is the area used for the drag calculation. A value of $fC_{df} \cong 0.01A_R$ is frequently used in helicopter studies[45], where $A_R = \pi R^2$ is the rotor disk area.

Since, for a single rotor helicopter, a substantial portion of the fuselage is beneath the rotor disk, the effect of rotor downwash is included in defining the total air velocity used in the fuselage drag calculation. Thus the total air velocity is given by

$$\vec{V}_{Af} = \Omega R(\mu\hat{e}_{x1} - \lambda\hat{e}_{z1}) \tag{6.13}$$

It is assumed that the drag force acts parallel to $\vec{V}_{AF}$, which is oriented along the unit vector

$$\frac{\vec{V}_{Af}}{|\vec{V}_{Af}|} = \frac{\mu}{\sqrt{\mu^2+\lambda^2}}\hat{e}_{x1} - \frac{\lambda}{\sqrt{\mu^2+\lambda^2}}\hat{e}_{z1} \tag{6.14}$$

Using Eq. (6.12) and (6.14), the drag force acting on the fuselage can be expressed as:

$$\vec{F}_{Df} = \frac{D_f}{\sqrt{\mu^2+\lambda^2}}(\mu\hat{e}_{x1} - \lambda\hat{e}_{z1}) \tag{6.15}$$

where from Eq. (6.12) and (6.13)

$$D_f = \frac{1}{2}\rho_A\Omega^2R^2(\mu^2+\lambda^2)fC_{df} \tag{6.16}$$

The center of drag of the fuselage is assumed to be located a distance Z_{FA} below the hub along the negative z_1 axis, and a distance X_{FA} behind the rotor along the x_1 axis, as shown in Fig. 5. The position vector from the hub center to center of drag is given by:

$$\vec{r}_{FA} = X_{FA}\hat{e}_{x1} - Z_{FA}\hat{e}_{z1} \tag{6.17}$$

The fuselage drag force causes a pitching moment about the hub center given by:

$$M_{Df}\hat{e}_{y1} = \vec{r}_{FA} \times \vec{F}_{Df} \tag{6.18}$$

Making use of Eqs. (6.15) – (6.18) yields:

$$M_{Df} = \frac{1}{2}\rho_A(\Omega R)^2\sqrt{\mu^2+\lambda^2}\, fC_{df}(\lambda X_{FA} - \mu Z_{FA}) \tag{6.19}$$

6.4 TRIM ANALYSIS

The blade equations formulated in this study represent the equations of motion of an isolated blade of a hingeless fixed-hub rotor configuration. In order to generate realistic values of the vibratory hub loads, the rotor angle of attack and the pitch settings of the rotor must represent meaningful values corresponding to those encountered by a helicopter in steady forward flight. The trim variables must be selected such that the rotor generates the forces and moments required by a helicopter with weight coefficient C_W and equivalent

fuselage flat plate drag area fC_{df} to maintain steady, level flight for an advance ratio μ. This is accomplished by enforcing overall force and moment equilibrium of the helicopter for any given flight condition. This is usually denoted as propulsive trim[11].

A helicopter in free flight has a total of six degrees of freedom, three translational and three rotational; consequently, three force and three moment equilibrium equations have to be satisfied. In this study, however, the tail rotor is not modeled; therefore the tail rotor pitch setting is not considered as a trim variable, and lateral force and yawing moment equilibrium are not enforced. It is assumed that the tail rotor pitch setting can be specified such that yaw equilibrium and lateral force equilibrium are maintained. Furthermore, the main rotor shaft angle in the lateral plane (i.e. ϕ_s, the sideways tilt of the rotor axis) is excluded as a trim variable since it has very little influence on helicopter vibrations[45].

Thus, only four equilibrium equations: two force equilibrium equations, one in the vertical (z_1) direction and one in the longitudinal (x_1) direction; and two moment equilibrium equations, one in roll (about the x_1 axis) and one in pitch (about the y_1 axis); have to be satisfied. The equilibrium equations are formulated in the "1" system with its origin at the hub center O_H, which represents the non-rotating, hub-fixed reference system (see Fig. 6). Together with the inflow equation, there are a total of five trim equations which must be solved for the trim variables in Eq. (6.2). These equations are assembled into the vector of trim equations represented by Eq. (6.3).

The five trim equilibrium equations are:

(1) The inflow equation for a helicopter rotor in forward flight

$$f_i(1) = C_T + 2\sqrt{\mu^2 + \lambda^2}\,(\mu \tan \alpha_R - \lambda) = 0 \tag{6.20}$$

where constant inflow is assumed in this study for convenience. Equation (6.20) is a steady state result from the steady far field momentum equation[25].

The thrust coefficient is defined as:

$$C_T = \frac{T_R}{\pi R^2 \rho_A R^2 \Omega^2} \tag{6.21}$$

where T_R is the total thrust produced by the rotor, and is given by Eq. (6.5).

(2) The rolling moment equation is obtained by setting the total rolling moment to zero

$$f_t(2) = M_{Hx1} = 0 \tag{6.22}$$

This is justified, since the rotor tilt angle in the lateral plane and the tail rotor are both not modeled.

(3) The pitching moment equation is obtained by enforcing pitching moment equilibrium about the hub

$$f_t(3) = M_{Hy1} + M_{Df} + M_{Wf} = 0$$

where M_{Hy1} is the total hub moment due to blade loads, M_{Df} is the pitching moment due to the fuselage drag given by Eq. (6.19) and M_{Wf} is the pitching moment due to the fuselage weight given by Eq. (6.11). Substituting Eq. (6.19) and (6.11) into the pitching moment equation yields:

$$f_t(3) = M_{Hy1} - W_f(-X_{FC}\cos\alpha_R + Z_{FC}\sin\alpha_R)$$

$$+ \frac{1}{2}\rho_A\Omega^2R^2fC_{df}\sqrt{\mu^2+\lambda^2}\,(\lambda X_{FA} - \mu Z_{FA}) = 0 \tag{6.23}$$

(4) The vertical force equation is obtained by enforcing force equilibrium in the z_1 direction. Using Eqs. (6.8) and (6.15), the vertical force equation can be expressed as

$$f_t(4) = F_{Hz1} - W_f\cos\alpha_R - D_f\frac{\lambda}{\sqrt{\mu^2+\lambda^2}} = 0$$

where the fuselage weight W_f is given by Eq. (6.7) and the fuselage drag force D_f is given by Eq. (6.12) . Substituting Eq. (6.12) for the fuselage drag into the vertical force equation yields:

$$f_t(4) = F_{Hz1} - W_f\cos\alpha_R - \frac{1}{2}\rho_A\Omega^2R^2fC_{df}\,\lambda\sqrt{\mu^2+\lambda^2} = 0 \tag{6.24}$$

(5) The longitudinal force equation is obtained by enforcing force equilibrium in the x_1 direction (see Fig. 6). Using Eqs. (6.8) and (6.15), the longitudinal force equation can be expressed as

$$f_t(5) = F_{Hx1} + D_f \frac{\mu}{\sqrt{\mu^2 + \lambda^2}} - W_f \sin\alpha_R = 0$$

where F_{Hx1} is the longitudinal hub force due to blade loading. Substituting the fuselage drag given by Eq. (6.12) into the longitudinal force equation yields

$$f_t(5) = F_{Hx1} + \frac{1}{2}\rho_A \Omega^2 R^2 f C_{df} \mu \sqrt{\mu^2 + \lambda^2} - W_f \sin\alpha_R = 0 \tag{6.25}$$

It is important to emphasize at this point that only the constant part of the rotor loads (i.e. their average value over one rotor revolution) needs to be in equilibrium with the fuselage forces and moments for trim to be established. This aspect of trim is discussed in greater detail in the section of this Chapter describing the solution procedure used in this study.

It is evident from Eqs. (6.20) – (6.25) that the trim solution of the helicopter depends upon the blade degrees of freedom through the rotor forces and moments, which are functions of the blade response. Therefore the trim and response problems are closely coupled and cannot be solved independently. One possible approach involves solving each set of equations separately, but in a coupled manner, using successive approximations for the solution of the other set of equations. This is an iterative procedure in which an approximation of the blade response is used to solve for an approximate trim solution. This trim solution is then substituted back into the blade equations to obtain an improved approximation of the blade response. This procedure is continued until the trim and response solutions converge. Previous research at UCLA has shown that this iterative procedure may be inefficient[50,45].

Therefore in this study an alternative procedure for solving the coupled trim aeroelastic response solution is used. The trim and response solutions are obtained simultaneously

by the harmonic balance technique. This analysis procedure is very similar to the procedure initially used in Ref. 50.

6.5 COUPLED TRIM AND RESPONSE CALCULATION USING THE HARMONIC BALANCE TECHNIQUE

In the harmonic balance technique, the solution of a periodic system of ordinary differential equations in the time domain is replaced by a solution in the frequency domain. Replacing the time domain solution by a frequency domain solution is justified, since only the periodic nonlinear steady state response of the system is required. The harmonic balance technique enables one to replace a system of ordinary differential equations of motion in the time domain by a system of algebraic equations with constant coefficients in the frequency domain. The transformation to the frequency domain is accomplished by carrying out a Fourier series expansion of each differential equation and each corresponding blade degree of freedom. Since a Fourier series expansion is only strictly valid for periodic functions, the harmonic balance technique is suitable for periodic systems only. The equations of motion of an isolated blade, in steady forward flight, represent a periodic system; thus the harmonic balance technique can be applied to the problem of determining the steady state trim and aeroelastic response solution under steady flight conditions. The harmonic balance technique is not applicable to flight conditions involving transient flight maneuvers or gusts.

Any periodic function with a fundamental frequency of 1/rev (i.e. $f(\psi + 2\pi) = f(\psi)$) can be represented exactly by an infinite Fourier series expansion of the form

$$f(\psi) = f_0 + \sum_{n=1}^{\infty} [f_{nc} \cos(n\psi) + f_{ns} \sin(n\psi)] \tag{6.26}$$

where

$$f_0 = \frac{1}{2\pi} \int_0^{2\pi} f(\psi)\, d\psi \tag{6.27a}$$

$$f_{nc} = \frac{1}{\pi}\int_0^{2\pi} f(\psi)\cos(n\psi)\,d\psi \qquad n = 1, 2, \ldots, \infty \tag{6.27b}$$

$$f_{ns} = \frac{1}{\pi}\int_0^{2\pi} f(\psi)\sin(n\psi)\,d\psi \qquad n = 1, 2, \ldots, \infty \tag{6.27c}$$

represent the Fourier coefficients of the series expansion and can be derived from Eq. (6.26) using the orthogonality of cosine and sine functions.

It is usually both impractical and unnecessary to use the infinite series expansion represented by Eq. (6.26) to capture the behavior of the periodic function $f(\psi)$. Usually, very good approximations can be obtained by truncating the expansion to a sufficient number of terms

$$f(\psi) \cong f_0 + \sum_{n=1}^{N_H}[f_{nc}\cos(n\psi) + f_{ns}\sin(n\psi)] \tag{6.28}$$

The number of harmonics retained N_H determines the quality of the approximation. Often the higher harmonics are small and can be neglected. However, when Eq. (6.28) is employed in the solution of a periodic system, the number of harmonics retained in the solution must be at least as large as the highest harmonic present in the periodic forcing function. Equation (6.28) enables one to represent of a scalar function of ψ by a set of $(1 + 2N_H)$ coefficients. Equations (6.28) and (6.27), which can be extended to the vector case, are used to develop the harmonic balance technique.

In steady forward flight the blade response is periodic with a fundamental frequency of 1/rev (i.e. $\vec{q}_b(\psi) = \vec{q}_b(\psi + 2\pi)$) and thus it can be approximated by a Fourier series expansion containing N_H harmonics

$$\vec{q}_b \cong \vec{q}_{b0} + \sum_{n=1}^{N_H}[\vec{q}_{bnc}\cos(n\psi) + \vec{q}_{bns}\sin(n\psi)] \tag{6.29}$$

where $\vec{q}_{b0}$ represents the constant part of $\vec{q}_b$ and $\vec{q}_{bnc}$ and $\vec{q}_{bns}$ represent the cosine and sine amplitudes, respectively, of the n/rev harmonics. Collectively $\vec{q}_{b0}$, $\vec{q}_{bnc}$ and $\vec{q}_{bns}$ represent a total of $(1 + 2N_H)$ vectors, each containing a total of N_{DOF} coefficients. These

vectors can be considered as the coefficient vectors of the Fourier expansion of the blade degrees of freedom.

The number of harmonics N_H retained in the expansion of the blade degrees of freedom determines the accuracy of the response solution. There are two primary factors which must be considered when selecting N_H: First, since the response solution is used to determine the vibratory hub loads, which are predominantly N_b/rev, at least N_b four harmonics must be retained; and secondly, to properly capture the effects of the various N/rev harmonic control inputs used to reduce vibrations, N_H should be at least one greater than the highest harmonic used in the control input N_{max}. Thus, the number of harmonics retained is determined from the following expression:

$$N_H = \max(N_b, N_{max}) + 1$$

From Eq. (6.29), the first and second derivatives of $\vec{q}_b$ can be expressed as:

$$\dot{\vec{q}}_b \cong \sum_{n=1}^{N_H} [-n\vec{q}_{bnc} \sin(n\psi) + n\vec{q}_{bns} \cos(n\psi)] \tag{6.30a}$$

$$\ddot{\vec{q}}_b \cong \sum_{n=1}^{N_H} [-n^2 \vec{q}_{bnc} \cos(n\psi) - n^2 \vec{q}_{bns} \sin(n\psi)] \tag{6.30b}$$

Thus the blade response can be completely described in terms of the $(1 + 2N_H)$ coefficient vectors represented by $\vec{q}_{b0}$, $\vec{q}_{bnc}$ and $\vec{q}_{bns}$. These vectors collectively represent a total of $(1 + 2N_H)N_{DOF}$ coefficients and represent the new degrees of freedom of the problem. The blade response solution in the frequency domain consists of finding the coefficient vectors $\vec{q}_{b0}$, $\vec{q}_{bnc}$ and $\vec{q}_{bns}$ such that Eq. (6.1) is satisfied, which is coupled with finding the vector of trim variables $\vec{q}_t$ such that Eq. (6.3) is satisfied.

The blade equations and trim equations can be expressed explicitly in terms of the blade expansion coefficients by substituting Eqs. (6.29) and (6.30) directly into Eqs. (6.1) and (6.3). After performing various trigonometric and algebraic manipulations, collecting the constant part and the various harmonics for each equation and putting them in a series representation, the trim and blade equations can each be expressed in the form:

$$\vec{f}_t = \vec{f}_{t0} + \sum_{n=1}^{N_{Ht}} [\vec{f}_{tnc} \cos(n\psi) + \vec{f}_{tns} \sin(n\psi)] = \vec{0} \tag{6.31}$$

$$\vec{f}_b = \vec{f}_{b0} + \sum_{n=1}^{N_{Hb}} [\vec{f}_{bnc} \cos(n\psi) + \vec{f}_{bns} \sin(n\psi)] = \vec{0} \tag{6.32}$$

The integers N_{Ht} and N_{Hb} represent the number of harmonics which arise in the trim and response equations, respectively, from the substitution of the Fourier series expansion for the blade degrees of freedom given by Eq. (6.29) into the equations. The product of two harmonic signals with frequencies ω_1 and ω_2, respectively, can be expressed as a sum of two harmonic signals with the respective frequencies $(\omega_2 + \omega_1)$ and $(\omega_2 - \omega_1)$; since the trim and blade equations contain products of the blade degrees of freedom, the integers N_{Ht} and N_{Hb} will generally be larger than N_H.

As stated previously, trimming the vehicle only involves enforcing the equilibrium of the constant part of the forces and moments acting on the vehicle, thus only the constant part of Eq. (6.31) needs to be satisfied

$$\vec{f}_{t0} = \vec{0} \tag{6.33}$$

Equation (6.33) represents a system of five algebraic equations in terms of the five trim variables and the $N_{DOF}(1 + 2N_H)$ blade response coefficients.

However, in order to satisfy Eq. (6.32), it is necessary that the constant part and the various n/rev harmonics be set equal to zero, i.e.

$$\vec{f}_{b0} = \vec{0} \tag{6.34a}$$

$$\vec{f}_{bnc} = \vec{f}_{bns} = \vec{0} \; ; \qquad n = 1, 2, \ldots, N_{Hb} \tag{6.34b}$$

Equations (6.34) represents a set of $N_{DOF}(1 + 2N_{Hb})$ coupled nonlinear algebraic equations in terms of the five trim variables and the $N_{DOF}(1 + 2N_H)$ blade response coefficients. To ensure that the number of equations is equal to the number of unknowns, N_{Hb} is set equal to N_H. Thus Eqs. (6.33) and (6.34) collectively represent a coupled system of

$[5 + N_{DOF}(1 + 2N_H)]$ algebraic equations in terms of $[5 + N_{DOF}(1 + 2N_H)]$ trim and blade expansion coefficients variables. Through the use of harmonic balance technique, the solution of a coupled system of N_{DOF} ordinary differential equations and five trim equations in the time domain has been transformed to the solution of a coupled system of $[5 + N_{DOF}(1 + N_H)]$ algebraic equations in the frequency domain. Though the dimension of the problem has increased substantially, it is generally much easier to solve a coupled system of nonlinear algebraic equations than a smaller system of coupled nonlinear periodic ordinary differential equations. There are many packaged programs available which solve systems of nonlinear algebraic equations. In this study the IMSL[58] subroutine DNEQNF, a Newton based method which uses finite differences to form the Jacobian, is used to obtain the coupled trim and response solution.

Unfortunately, the formation of the explicit expansions given by Eqs. (6.31) and (6.32) represents a formidable task (even by computer algebra) due to the plethora of higher order terms involving products of the blade degrees of freedom resulting from the assumption of moderate deflections. Therefore, the formation of Eqs. (6.31) and (6.32) is done numerically. Examination of these two expressions reveals that they represent Fourier expansions of the trim and response equations. Therefore the expansion coefficients in Eqs. (6.31) and (6.32) represent Fourier coefficients; use of the definition of these coefficients presented in Eqs. (6.27) can be used to numerically determine the value of each of these coefficients. Therefore, Eqs. (6.33) and (6.34) can be expressed as

$$\vec{f}_{t0} = \frac{1}{2\pi}\int_0^{2\pi} \vec{f}_t(\vec{q}_b, \dot{\vec{q}}_b, \ddot{\vec{q}}_b, \vec{q}_t, \delta; \psi)\, d\psi = \vec{0} \tag{6.35a}$$

$$\vec{f}_{b0} = \frac{1}{2\pi}\int_0^{2\pi} \vec{f}_b(\vec{q}_b, \dot{\vec{q}}_b, \ddot{\vec{q}}_b, \vec{q}_t, \delta; \psi)\, d\psi = \vec{0} \tag{6.35b}$$

$$\vec{f}_{bnc} = \frac{1}{\pi}\int_0^{2\pi} \vec{f}_b(\vec{q}_b, \dot{\vec{q}}_b, \ddot{\vec{q}}_b, \vec{q}_t, \delta; \psi)\cos(n\psi)\, d\psi = \vec{0} \quad n = 1,2,\ldots,N_H \tag{6.35c}$$

$$\vec{f}_{bns} = \frac{1}{\pi}\int_0^{2\pi} \vec{f}_b(\vec{q}_b, \dot{\vec{q}}_b, \ddot{\vec{q}}_b, \vec{q}_t, \delta; \psi)\sin(n\psi)\,d\psi = \vec{0} \quad n = 1,2,\ldots,N_H \tag{6.35d}$$

Gaussian quadrature is used to evaluate the integrals in Eqs. (6.35), because it minimizes the number of integration points for a given accuracy[2]. The expansion of the blade degrees of freedom represented by Eqs. (6.29) is substituted into Eqs. (6.35), but is not expanded; instead, it is evaluated numerically at each azimuth angle ψ required in the numerical integration scheme. In this study, 30 Gaussian integration points are used to integrate over one rotor revolution.

6.6 CALCULATION OF THE 4/REV HUB SHEARS AND MOMENTS

For a four bladed rotor in steady flight, the vibratory hub loads are predominantly 4/rev in the fixed system. In this study, various optimal control strategies are employed to simultaneously reduce the 4/rev hub shears and moments. The amplitudes of the 4/rev vibration components are obtained from a harmonic analysis of the hub loads. If $\vec{F}_H(\psi)$ and $\vec{M}_H(\psi)$ represent the total force and moment, respectively, at the hub obtained by summing the contribution from each blade in the fixed system, then

$$\vec{F}_{H4c} = \frac{1}{\pi}\int_0^{2\pi} \vec{F}_H(\psi)\cos 4\psi\,d\psi \tag{6.36a}$$

$$\vec{F}_{H4s} = \frac{1}{\pi}\int_0^{2\pi} \vec{F}_H(\psi)\sin 4\psi\,d\psi \tag{6.36b}$$

represent the cosine and sine amplitudes, respectively, of the 4/rev hub shears. Similarly,

$$\vec{M}_{H4c} = \frac{1}{\pi}\int_0^{2\pi} \vec{M}_H(\psi)\cos 4\psi\,d\psi \tag{6.37a}$$

$$\vec{M}_{H4s} = \frac{1}{\pi}\int_0^{2\pi} \vec{M}_H(\psi)\sin 4\psi\,d\psi \tag{6.37b}$$

represent the cosine and sine amplitudes, respectively, of the 4/rev hub moments.

6.7 LINEARIZED STABILITY

In this study the stability of the periodic system, linearized about the time-dependent equilibrium position, is determined from Floquet theory[13]. Linearizing the blade equations about the nonlinear time-dependent equilibrium position yields

$$\vec{f}_b(\vec{q}_b + \Delta\vec{q}_b) = [M(\vec{q}_b)]\Lambda\ddot{\vec{q}}_b + [C(\vec{q}_b)]\Lambda\dot{\vec{q}}_b + [K(\vec{q}_b)]\Lambda\vec{q}_b + \text{h.o.t.} = \vec{0} \tag{6.38}$$

where the fact that $\vec{f}_b(\vec{q}_b) = \vec{0}$ has been used. The quantity $\Lambda\vec{q}_b$ represents a small perturbation from the time dependent equilibrium position, and

$$[M] = \partial\vec{f}_b/\partial\ddot{\vec{q}}_b$$

$$[C] = \partial\vec{f}_b/\partial\dot{\vec{q}}_b$$

$$[K] = \partial\vec{f}_b/\partial\vec{q}_b$$

are the mass, damping, and stiffness matrices, respectively, of the linearized system.

The linearized system given by Eq. (6.38) can be expressed in the first order state space form

$$\dot{\vec{y}} = [A]\vec{y} \tag{6.39}$$

where the state vector $\vec{y}$ is defined as

$$\vec{y} = \{\Lambda\vec{q}_b^T \quad \Lambda\dot{\vec{q}}_b^T\}^T$$

and the system matrix [A] is defined as

$$[A] = \begin{bmatrix} [0] & [I] \\ -[M]^{-1}[K] & -[M]^{-1}[C] \end{bmatrix}$$

In hover, the system matrix [A] is constant, and thus the eigenvalues of [A] determine system stability. If $\lambda_j = \zeta_j \pm i\omega_j$ is the j-th eigenvalue of [A], then the system is assymptotically stable if $\zeta_j < 0$ for all j.

In forward flight, however, the system matrix [A] is periodic with a period of one rotor revolution (i.e., $[A(\psi)] = [A(\psi + 2\pi)]$). The stability of the periodic system can be determined using Floquet theory from the eigenvalues of the state transition matrix at the end of one period. According the Floquet theory[13], the characteristic exponents $\lambda_j = \zeta_j \pm i\,\omega_j$ of the periodic system are related to the characteristic multipliers $\Lambda_j = Z_j \pm i\,\Omega_j$ of the state transition matrix at the end of one period $[\Phi(2\pi, 0)]$ as follows:

$$\zeta_j = \frac{1}{2\tau} \ln(Z_j^2 + \Omega_j^2)$$

$$\omega_j = \frac{1}{\tau} \tan^{-1}\left(\frac{\Omega_j}{Z_j}\right) \tag{6.40}$$

where $\tau = 2\pi$ is the non-dimensional rotor period. The linearized periodic system is assymptotically stable if $\zeta_j < 0$ for all j.

The state transition matrix at the end of one period can be calculated by numerically integrating Eq. (6.39) over one revolution n times, where $n = 2N_{DOF}$ is the dimension of the linearized system in state space form, using the initial conditions

$$\vec{y}_j(0) = \{\delta_{1j}\ \delta_{2j}\ \ldots\ \delta_{nj}\}^T \quad \text{for } j = 1,\ 2,\ \ldots,\ n \tag{6.41}$$

The quantity δ_{ij} is unity when i = j and zero otherwise. Solving the system given by Eq. (6.39) using the initial condition vector $\vec{y}_j(0)$ yields the j-th column of the state transition matrix.

For numerical efficiency, the task of integrating the system is done so that the n integration passes are carried out simultaneously; this approach is commonly denoted the single-pass method[4]. The single-pass version of the classic n-pass algorithm consists of numerically integrating over one revolution the n^2 system represented by

$$\dot{\vec{Y}} = \begin{bmatrix} [A] & [0] & \cdot & \cdot \\ [0] & [A] & \cdot & \cdot \\ \cdot & \cdot & \cdot & \cdot \\ \cdot & \cdot & [A] & [0] \\ \cdot & \cdot & [0] & [A] \end{bmatrix} \vec{Y} \tag{6.42}$$

using the initial condition vector

$$\vec{Y}(0) = \{\vec{y}_1^T(0)\ \vec{y}_2^T(0)\ \ldots\ \vec{y}_n^T(0)\}^T \tag{6.43}$$

where $\vec{y}_j(0)$ is defined by Eq. (6.41). The solution of the system represented by Eq. (6.42) using the initial condition vector given by Eq. (6.43) yields all n columns of the state transition matrix simultaneously.

In this study the numerical integration of the system given by Eq. (6.42) is accomplished using DE/STEP, a general purpose Adams-Bashforth ODE solver[48]. It is important to note that the implementation of the single-pass algorithm does not require the coding of the $n^2 \times n^2$ matrix in Eq. (6.42), but only the coding of the $n \times n$ system matrix [A].

Chapter VII

VIBRATION REDUCTION USING ACTIVE CONTROLS

The vast majority of helicopter vibration reduction studies [5,23,27,34,40, 43,44, 49,50,51,56,57] to date have employed control strategies based on frequency domain formulations of the control problem. The periodic nature of the blade response in forward flight is used to transfer the control problem from the time domain, where it is described by a set of differential equations with periodic coefficients, to the frequency domain, where it is governed by a set of algebraic equations with constant coefficients. However, since the periodic assumption is only valid under steady state conditions, the control solutions obtained are only applicable toward the reduction of the vibration levels experienced in steady flight.

The control strategies are generally based on the minimization of a performance index that is a quadratic function of the vibration magnitudes and control input amplitudes.

$$J = \vec{Z}_i^T [W_Z]\vec{Z}_i + \vec{u}_i^T [W_U]\vec{u}_i + \Delta\vec{u}_i^T [W_\Delta]\Delta\vec{u}_i \tag{7.1}$$

where $\Delta\vec{u}_i = \vec{u}_i - \vec{u}_{i-1}$. The vectors $\vec{Z}_i$ and $\vec{u}_i$ contain the cosine and sine amplitudes of the vibration and control input harmonics, respectively, during the i-th control step. The indices on both the vibrations and control reflect the discrete-time nature of control strategies based on frequency domain formulations of the control problem. The time increment (or control step) $t_s = \Delta t$ between control updates must be sufficient to allow the system to return to a steady state condition. In a real-time application of feedback control on an actual helicopter, t_s must provide a long enough time sample of the vibration levels to properly measure their cosine and sine amplitudes, which are used as feeback to the controller. Generally, the time increment is at least one rotor revolution[24,45].

The matrices $[W_Z]$, $[W_U]$ and $[W_\Delta]$ in Eq. (7.1) are weighting matrices on the vibrations, control and rate of change of control, respectively. Constraints may be placed on the

magnitude of the control update $\Delta\vec{u}i$ to ensure controller stability under rapidly changing conditions. The weighting matrices are typically diagonal, in which case J represents the weighted sum of the mean squares of the vibrations and control. The relative weightings on each of the parameters can be changed to vary their relative importance.

The optimum control law is obtained by taking the gradient of J given by Eq. (7.1) with respect to the control $\vec{u}_i$ and setting the gradient equal to zero

$$\frac{\partial J}{\partial \vec{u}_i} = \vec{0} \tag{7.2}$$

The resulting set of equations are solved for the optimal control denoted by $\vec{u}_i^*$, where "optimal" refers to the control input which minimizes J during each control step.

In the case where all the parameters in the model are known, a deterministic optimal control strategy is obtained from the solution of Eq. (7.2). However, with unknown, estimated parameters, the certainty-equivalence principle may be applied: the deterministic control solution is used with the estimated parameter values; otherwise, a cautious controller is obtained by minimizing the expected value of the performance index J with respect to the control. In this study, only deterministic controllers are considered; i.e., it is assumed that both the control input and the resulting vibration levels are known without error.

Before J can be minimized with respect to the control input, it is necessary to first obtain a model of the system response, represented by $\vec{Z}$, to the control. Two linear, quasi-static, frequency domain representations of the helicopter response to control are commonly used[5,23,27,34,40, 43,44, 49,50,51,56,57]. The first is a global model which assumes linearity of the system over the entire range of control application; and the second is a local model which is based on a linearization of the system about the current control. Both models utilize a transfer matrix, usually denoted as [T] , to relate the cosine and sine amplitudes of the control harmonics to the cosine and sine amplitudes of the vibration harmonics. This concept of a linear, quasi-static, frequency domain representation of the relationship between harmonics of the vibratory response and the harmonics of the control

input was first introduced in Ref. 30, where the notation [T] for the transfer matrix was first used.

The transfer matrix can be interpreted as the Jacobian of the system response to the control input which is required in a Taylor series expansion of the response about some control input $\vec{u}_o$

$$\vec{Z}(\vec{u}) = \vec{Z}(\vec{u}_o) + [T(\vec{u}_o)](\vec{u} - \vec{u}_o) + \text{h.o.t.}$$

where

$$[T] = \frac{\partial \vec{Z}}{\partial \vec{u}}$$

In the global model, where linearity is assumed over the entire range of control application, the Taylor series expansion is evaluated about a zero control input (i.e., $\vec{u}_o = \vec{0}$)

$$\vec{Z}_i = \vec{Z}_0 + [T_0]\vec{u}_i \tag{7.3}$$

where $\vec{Z}_0$ represents the baseline (uncontrolled) vibration levels. In this model the transfer matrix is evaluated about a zero control input, and is assumed to be constant over the entire range of control application.

Substituting Eq. (7.3) into Eq. (7.1) and minimizing with respect to the control yields the global controller

$$\vec{u}_i^* = -[D_0]^{-1}\{[T_0]^T[W_Z]\vec{Z}_0 - [W_\Delta]\vec{u}_{i-1}^*\} \tag{7.4}$$

where

$$[D_0] = [T_0]^T[W_Z][T_0] + [W_u] + [W_\Delta] \tag{7.5}$$

Equation (7.4) is in the form of an open-loop controller[24] where the control during each control step is determined by the uncontrolled vibration levels $\vec{Z}_0$. In the case where the rate of change of control is not penalized (i.e., $[W_\Delta] = [0]$) the controller converges in a single step.

Feedback can be introduced into the global controller by expressing the global system model in the equivalent form

$$\vec{Z}_i = \vec{Z}_{i-1} + [T_0](\vec{u}_i - \vec{u}_{i-1}) \tag{7.6}$$

which was obtained by evaluating Eq. (7.3) for two successive control steps and subtracting the two expressions.

Substituting Eq. (7.6) into the performance index J and minimizing with respect to control yields

$$\vec{u}_i^* = -[D_0]^{-1}\{[T_0]^T[W_Z]\vec{Z}_{i-1} - [W_\Delta]\vec{u}_{i-1}^* - [T_0]^T[W_Z][T_0]\vec{u}_{i-1}^*\} \tag{7.7}$$

where $[D_0]$ is given by Eq. (7.5). Equation (7.7) is in the form of a closed-loop controller where the control input during each control step is determined by feedback of the measured vibration levels of the previous control step. Equation (7.7) is denoted as the feedback form of the global controller.

If the system were truly linear, then the open-loop form of the global controller given by Eq. (7.4) would yield the true "optimal" input (in the sense that J is minimized). However, the system represented by a helicopter in forward flight is inherently nonlinear due to moderate blade deflections, which introduces geometric nonlinearities into the system. The use of the feedback form of the global controller given by Eq. (7.7) should yield better vibration reduction in the presence of system nonlinearities. However, it is reasonable to expect that a controller based on a local system model, which is based on a linearization about the control, would produce the best vibration reduction.

The local system model is obtained by linearizing the system about the current control input

$$\vec{Z}_i = \vec{Z}_{i-1} + [T_{i-1}](\vec{u}_i - \vec{u}_{i-1}) \tag{7.8}$$

In this case the transfer matrix is assumed to be a function of the current control input $\vec{u}_{i-1}$.

Substituting the local system model into the performance index and minimizing with respect to the control yields the local controller

$$\vec{u}_i^* = -[D_{i-1}]^{-1}\{[T_{i-1}]^T[W_Z]\vec{Z}_{i-1} - [W_\Lambda]\vec{u}_{i-1}^* - [T_{i-1}]^T[W_Z][T_{i-1}]\vec{u}_{i-1}^*\} \tag{7.9}$$

where

$$[D_{i-1}] = [T_{i-1}]^T[W_Z][T_{i-1}] + [W_U] + [W_\Lambda] \tag{7.10}$$

Equation (7.9) is in the form of a closed-loop controller[24] where the control input during each control step is determined by feedback of the measured response during the previous control step. Comparison of Eq. (7.9) with the feedback form of the global controller given by Eq. (7.7) reveals that the only difference between the two controllers is that the transfer matrix [T] must be updated after each control step in the case of the local controller. Updating the transfer matrix should improve the controller performance due to the nonlinearity of the system.

Detailed derivations of the global and local controllers presented above, along with their cautious counterparts, are presented in Ref. 24.

7.1 REDUCTION OF THE 4/REV HUB SHEARS AND MOMENTS

In this study, the deterministic global and local controllers are employed to produce simultaneous reduction in the 4/rev hub shears and moments. In this case the vibration vector $\vec{Z}_i$ contains the cosine and sine amplitudes of the 4/rev hub shears and moments

$$\vec{Z} = \begin{Bmatrix} \vec{Z}_F \\ \vec{Z}_M \end{Bmatrix} \tag{7.11}$$

where

$$\vec{Z}_F = \begin{Bmatrix} \vec{F}_{H4c} \\ \vec{F}_{H4s} \end{Bmatrix} , \quad \vec{Z}_M = \begin{Bmatrix} \vec{M}_{H4c} \\ \vec{M}_{H4s} \end{Bmatrix}$$

7.2 CONTROL INPUT FOR VIBRATION REDUCTION

In the present study, vibration reduction in forward flight is uniquely implemented through an actively controlled trailing edge flap on the blade. To guarantee a periodic blade response, only periodic control inputs with a fundamental frequency of Ω are considered. In this case the control flap deflection angle of the k-th blade can be expressed as a sum of harmonic signals with frequencies that are integer multiples of the rotor frequency

$$\delta(\psi_k) = \sum_{N=2}^{N_{max}} [\delta_{Nc} \cos(N\psi_k) + \delta_{Ns} \sin(N\psi_k)] \tag{7.12}$$

where N_{max} represents the highest harmonic used in the control input signal. The 1/rev input harmonic is intensionally excluded since it was decided to not disturb the trim cyclic pitch inputs.

In the present study, the four blades are assumed to be identical. To ensure that all four blades track, it is assumed that the control flap on each blade executes the same motion, but shifted in phase by the angle between the blades (ninety degrees in the case of a four bladed rotor.) Thus the control input for vibration reduction using the global or local controllers can be represented by the vector containing the cosine and sine amplitudes of the various N/rev input harmonics

$$\vec{u} = \{\delta_{Nc}, \delta_{Ns}, \cdots, \delta_{(Nmax)c}, \delta_{(Nmax)s}\}^T \tag{7.13}$$

Conventional individual blade control (IBC), which relies on oscillating the entire blade, is also implemented in this study, purely for comparison purposes. In the IBC case the total pitch input is given by

$$\theta_{pc}(\psi_k) = \theta_0 + \theta_{1c} \cos(\psi_k) + \theta_{1s} \sin(\psi_k) + \theta_{IBC}(\psi_k) \tag{7.14}$$

where

$$\theta_{IBC}(\psi_k) = \sum_{N=2}^{N_{max}} [\theta_{Nc} \cos(N\psi_k) + \theta_{Ns} \sin(N\psi_k)] \tag{7.15}$$

is the IBC pitch input. The control input vector for IBC is defined as

$$\vec{u} = \{\theta_{Nc}, \theta_{Ns}, \cdots, \theta_{(Nmax)c}, \theta_{(Nmax)s}\}^T \tag{7.16}$$

7.3 TRANSFER MATRIX CALCULATION

As mentioned previously, the transfer matrix [T] can be interpreted as the Jacobian of the vibratory response with respect to the control input. Since the blade response solution and the vibration levels are obtained numerically, the sensitivity of the system to control must also be determined numerically. Thus, in this study, the transfer matrix is calculated numerically one column at a time using finite differences. If the small change in the blade response due to a small perturbation in the control input was neglected, however, approximate analytical expressions for the elements of the [T] matrix could be developed.

In the case of the global controller, the transfer matrix is evaluated about a zero control input. The j-th column of the transfer matrix is formed by setting all elements of the control input vector to zero except the j-th element, which is set to some small value, say 0.01 radians. The resulting change in the 4/rev vibration levels from their baseline values is calculated and then divided by the magnitude of the control input, 0.01 radians, yielding the j-th column of the transfer matrix.

In the case of the local controller, which is based on a linearization of the system about the control, the transfer matrix is evaluated about the current control. The j-th column of the transfer matrix is calculated by adding a small increment, say 0.01 radians, to the j-th element of the current control vector. The resulting change in the vibration vector is divided by the value of the small increment, 0.01 radians, yielding the j-th column of the transfer matrix.

7.4 CONTROL POWER REQUIREMENTS

Operating the control surface actuators for vibration reduction will of course require power from the helicopter powerplant. It was postulated that a suitable measure of the power required will be provided by the instantaneous power required to drive a single control flap, averaged over one rotor revolution, and multiplied by the number of blades. The instantaneous power consists of the product of the instantaneous values of the control surface hinge moment $M_\delta(\psi_k)$ and the angular velocity of the control surface about its hinge $\dot{\delta}(\psi_k)$. Thus the power required to implement control using an active control surface on each blade is defined as:

$$P_{cs} = \sum_{k=1}^{N_b=4} \frac{1}{2\pi} \int_0^{2\pi} [-M_\delta(\psi_k)\,\dot{\delta}(\psi_k)]\,d\psi_k \tag{7.17}$$

The negative sign in Eq. (7.17) accounts for the fact that the instantaneous power is defined as positive when the required control torque and the angular velocity are in the same direction. The hinge moment M_δ has been defined as the net moment about the control surface hinge due to the loads on the control surface. Thus the actuator must supply a counter torque equal to $-M_\delta(\psi_k)$ in order to implement the control.

Both $M_\delta(\psi_k)$ and $\dot{\delta}(\psi_k)$ represent harmonic signals, and when there is a phase difference between these two harmonic signals (which will generally be the case), then the instantaneous power will be negative over some portions the cycle. Negative power has no meaning in this context, however, since the helicopter powerplant cannot accumulate power. Therefore, for the regions in which the integrand in Eq. (7.17) is negative, which can occur over a significant portion of the rotor revolution[44,45], the integrand is set equal to zero.

In addition to the power required to drive the control surfaces, additional power may be required to drive the rotor. It is noteworthy that introduction of the control inputs to the blade will modify the blade loads and thus the required rotor torque can also be affected. Furthermore, the implementation of control could reduce the rotor power requirements. In the flight tests conducted in Ref. 57, a small decrease in rotor power was observed when

HHC was implemented. This saving in power may offset the power required to drive the control surfaces. The rotor power is defined as the average power over one rotor revolution required to drive the rotor at a constant angular velocity Ω

$$P_R = \frac{\Omega}{2\pi}\int_0^{2\pi} [-M_{Hz1}(\psi)]\, d\psi \tag{7.18}$$

where $M_{Hz1}(\psi)$ is the total yawing moment about the hub. The negative sign in front of $M_{Hz1}(\psi)$ is due to the fact that it represents the torque about the rotor shaft due to the loading on the blades, and therefore the power plant must supply a torque equal to $(-M_{Hz1})$ to maintain a constant angular velocity. Equation (7.18) can be used to calculate the rotor power in absence of flap control inputs as well as when the control is implemented to determine any changes in rotor power.

A third kind of power requirement must also be considered. Since the blade loads are affected by the flap inputs, the power required to drive the pitch link actuators for helicopter control may also be affected. Therefore, the change in power required for helicopter control must also be taken into account. The power required for helicopter trim (i.e. trim power) is defined as:

$$P_{trim} = \sum_{k=1}^{N_b=4} \frac{1}{2\pi}\int_0^{2\pi} [-M_{Rx3}(\psi_k)\dot{\theta}_{pc}(\psi_k)]\, d\psi_k \tag{7.19}$$

where $M_{Rx3}(\psi_k)$ represents the torsional moment about the root of the k-th blade. For the regions in which the integrand in the above expression is negative, the integrand is set equal to zero. Equation (7.19) can be used to calculate the trim power both with and without flap control inputs to determine any changes in trim power requirements.

Chapter VIII

MODEL VERIFICATION

Before pursuing the principal goals of any analytical study it is crucial to first validate the analytical model and solution procedure developed in the study. This is best accomplished through comparisons with other investigations with comparable analytical models. In the present study, comparison of trim and blade response results can be used to test both the validity of the equations of motion as well as the solution procedure implemented. Furthermore, for equations of motion presented in explicit form, as they are in this study, a direct term by term comparison can be made in order to verify the expressions and identify any differences which might affect the results.

In addition to trim and response results, comparisons of blade stability results in forward flight can also be used as a reliable test of the accuracy of the equations of motion. It is well known that blade stability results are much more sensitive to the higher order terms in the equations of motion than the trim and response results. Since the vibratory hub loads can also be very sensitive to these higher order terms, it is important to carry out stability comparisons to properly ensure the validity of the analytical model employed in this study before proceeding to the calculation of the vibratory hub loads.

There are no results available in the literature against which blade response and stability, including the effect of the control surface, could be validated. Though the controllable twist rotor investigated in Ref. 28 utilized a servo flap, it was implemented on an articulated blade, in contrast to the hingeless blade modeled in the present study. Thus, validation of the blade model without the control flap is the best that can be conducted at present. But since the control flap is incorporated into the blade model in a manner consistent with the overall problem formulation, model validation without the flap should still lend credence to the entire blade model.

8.1 VALIDATION OF THE OFFSET-HINGED SPRING RESTRAINED BLADE MODEL

The offset-hinged spring restrained blade model utilized in Ref. 50 to investigate the active control of helicopter aeromechanical and aeroelastic instabilities is almost identical to the model used in the present study. The inertial loads were obtained using D'Alembert's principle and Greenberg quasisteady aerodynamics are used to calculate the aerodynamic loads. However, the reverse flow model and solution procedure used in Ref. 50 differ from those used in the present study. In Ref. 50 the sign on both the drag and the lift switch sign inside the reverse flow region, as opposed to setting the lift to zero, which is done in this study. Flap trim and quasilinearization was used in Ref. 50 to obtain the majority of the trim and response results. However, a version of the harmonic balance technique, similar to the procedure used in this study, was also employed to investigate the effect of the solution procedure on the trim and response results.

Although the model of Ref. 50 incorporates a rigid fuselage to investigate coupled rotor/fuselage instabilities, the fuselage degrees of freedom were set to zero in the trim and response solutions. Though the solution procedure used in Ref. 50 differs from the method used in this study, the equations of motion were essentially identical; therefore the trim and response results obtained in Ref. 50 should be comparable to those obtained in the present study.

Blade stability results were also obtained in Ref. 50. It is well known that such results are a good indicator of the accuracy of the mathematical model, because blade stability is sensitive to higher order terms. The method used to compute the stability results in Ref. 50 was similar to that employed in the present study.

In Ref. 50 the forces and moments acting on the blade were formulated explicitly, thus allowing a direct term by term comparison with the expressions of this study. Comparison of these expressions reveals that the two sets of expressions are almost identical except for a few terms of the highest order retained in the ordering scheme. While the ordering scheme used by Ref. 50 was identical to the one used in this study, there are a few terms that were not included in the expressions of Ref. 50 which should have been retained based on a consistent application of the ordering scheme. However, these terms are very small

and have little or no effect on the trim and blade response solution; but they may have a minor effect on the blade stability results.

To ensure that the explicit expressions are implemented correctly in the computer analysis program, trim, blade response, and stability results were generated and compared with those of Ref. 50. First the coupled flap-lag portion of the blade model is validated by comparing it to the coupled flap-lag stability boundaries in hover and the coupled flap-lag response solution in forward flight. Next, the coupled flap-lag-torsion problem is validated by comparing it to the coupled flap-lag-torsional trim and blade response results in forward flight. Finally, stability results are compared.

8.1.1 *Coupled Flap-Lag Problem*

Reference 50 compared flap-lag trim, blade response, and stability results with Ref. 8 to validate the flap-lag portion of the blade model. In the investigation of the effects of unsteady aerodynamics in rotary-wing aeroelasticity presented in Ref. 8, an offset-hinged spring restrained blade model was utilized with flap and lead-lag dynamics only. The aerodynamic loads were based on both Greenberg unsteady and quasi-steady aerodynamics, but with the noncirculatory portion of the lift and moment excluded. The blade model of Ref. 8 should be similar to the model of this study with the torsional degree of freedom and the noncirculatory portion (apparent mass terms) of the aerodynamic loads removed; this was also concluded in Ref. 50. Therefore, flap-lag results generated using the model of the present study are also compared with the results presented in Ref. 8.

By setting the non-dimensional fundamental rotating torsional frequency of the blade equal to a sufficiently high value, i.e. $\omega_{T1} \geq 10$, the torsional degree of freedom can be removed. However, the noncirculatory portion of the aerodynamic loads could not be removed as easily. For the purposes of making comparisons with Ref. 8, a second set of equations of motion were derived for this study in which the noncirculatory lift and moment were not included.

8.1.1.1 Stability Boundaries in Hover

The data for the hover case is shown in Table 1 and was taken from Ref. 8. The data presented in this table have been non-dimensionalized using R, M_b and $(1/\Omega)$ for length, mass and time, respectively. The inflow equation used in Ref. 8 to calculate the hover stability boundaries is given by

$$\lambda = \frac{a_o\sigma}{16}\left(\sqrt{1 + \frac{24\theta_G}{a_o\sigma}} - 1\right) \tag{8.1}$$

TABLE 1

Non-dimensional data for the calculation of the coupled flap-lag stability boundaries in hover

Flight Data	
$\mu = 0.0$	
Rotor Data	
$c_b = 2b = 0.03927$	$\omega_{T1} = 10$
$L_b = 1.0$	ω_{F1} = variable
$e = 0.0$	ω_{L1} = variable
$\beta_p = 0.0$	$C_\phi = 0.0$
$\theta_{pt} = 0.0$	$C_\beta = 0.0$
$R_C = 0.0$	$C_\zeta = 0.0$
$\theta_G = 0.25$	$a_o = 2\pi$
$x_b = 0.5$	$C_{d0} = 0.01$
$I_b = 0.3333333$	$C_{m0} = 0.0$
$J_b = 0.0002572$	$N_b = 4$
$X_{Ib} = 0.0$	$\sigma = 0.05$
$X_A = 0.0$	$\gamma = 5.0$
Fuselage Data	
$X_{FA} = 0.0$	$Z_{FA} = 0.0$
$X_{FC} = 0.0$	$Z_{FC} = 0.0$

A comparison of the coupled flap-lag stability boundaries in hover generated using the model developed in this study, together with the models employed in Refs. 8 and 50, is presented in Fig. 13. The overall comparison of the results with both references is quite good. Clearly the stability results of this study compare most favorably with the results of Ref. 50, though there is some minor disagreement at the lower blade frequencies. As mentioned previously, a direct comparison of the explicit expressions developed in this study with those of Ref. 50 revealed a slight discrepancy in the higher order terms. Due

to the sensitivity of stability results to higher order terms, it was concluded that this small discrepancy was the primary cause of the minor disagreement between the two sets of results.

8.1.1.2 Response Solution in Forward Flight

The non-dimensional data for this model is presented in Table 2 and corresponds to the "C" model used in Ref. 8, which represents a soft-in-plane hingeless rotor blade with uniform properties. The data have been non-dimensionalized using the dimensional parameters listed in the previous section.

TABLE 2

Non-dimensional data for the calculation of the coupled flap-lag response in forward flight

Flight Data	
$\mu = 0.4$	
Rotor Data	
$c_b = 2b = 0.05498$	$\omega_{T1} = 10$
$L_b = 1.0$	$\omega_{F1} = 1.125$
$e = 0.0$	$\omega_{L1} = 0.732$
$\beta_p = 0.0$	$C_\phi = 0.0$
$\theta_{pt} = 0.0$	$C_\beta = 0.0$
$R_C = 1.0$	$C_\zeta = 0.0$
$x_b = 0.5$	$a_o = 2\pi$
$I_b = 0.3333333$	$C_{d0} = 0.01$
$J_b = 0.0002572$	$C_{m0} = 0.0$
$X_{Ib} = 0.0$	$N_b = 4$
$X_A = 0.0$	$\sigma = 0.07$
	$\gamma = 5.5$
Helicopter Data	
$C_W = 0.005$	$fC_{df} = 0.01A_R$
$X_{FA} = 0.0$	$Z_{FA} = 0.0$
$X_{FC} = 0.0$	$Z_{FC} = 0.0$

The reverse flow model used in Refs. 8 and 50 differs from the model used in this study. In the reverse flow model used in these two references, the sign of the drag and lift was switched inside the reverse flow region. Therefore, when generating the results in this section, the reverse flow model employed in Refs. 50 and 8 was adopted.

For the coupled flap-lag case the comparison of the flap and lead-lag response, at the blade tip, is presented in Fig. 14. The response solutions given in Refs. 8 and 50 were

obtained using the flap trim and quasi-linearization method; however, the response solution for the present study was obtained using the full trim harmonic balance technique with three harmonics (i.e. $N_H = 3$). Though the flap-lag response solution of this study is very similar to the solutions of Ref. 50 and 8, there is a marked difference. This can be attributed to the difference in solution methods; since only the flap response was used to obtain the trim solution in Refs. 50 and 8, it differs from the trim solution used in this study in which the full coupled flap-lag response solution is solved in a coupled manner with propulsive trim. Therefore the blade response solutions of Refs. 50 and 8, shown in Fig. 14, were calculated for a somewhat different trim state from that used in this study. This observation was also made in Ref. 50 where it was discovered that the deviation in the trim variables calculated using flap trim from those using a fully coupled trim/aeroelastic analysis could produce a significant difference in the respective equilibrium solutions.

Despite the fairly small disagreement between the coupled flap-lag blade response solution obtained in this study and those generated in Refs. 50 and 8, which can most likely be attributed to the difference in solution procedures, the comparisons were deemed close enough to lend credence to the flap-lag portion of the mathematical model and solution procedure.

8.1.2 *Coupled Flap-Lag-Torsion Problem*

In this section the complete coupled flap-lag-torsional equations of motion together with solution procedure are verified by comparing the trim, response and stability results in forward flight those obtained in Ref. 50. The non-dimensional data for the blade configuration used in these comparisons is given in Table 3 and corresponds to a soft-in-plane matched stiffness (i.e. $K_\beta = K_\zeta$) rotor blade with uniform properties. The data in Table 3 has been non-dimensionalized using R, M_b and $(1/\Omega)$ for length, mass and time, respectively. The trim and response solutions of the blade in forward flight are compared first, and next the lead-lag damping values in forward flight are also compared.

TABLE 3

Non-dimensional data used in calculating the coupled flap-lag-torsion results in forward flight

Flight Data

$\mu = 0.3$

Rotor Data

$c = 2b = 0.03927$	$\omega_{T1} = 2.5, 5.0$
$L_b = 1.0$	$\omega_{F1} = 1.15$
$e = 0.0$	$\omega_{L1} = 0.57$
$\beta_p = 0.0$	$C_\phi = 0.0$
$\theta_{pt} = 0.0$	$C_\beta = 0.0$
$R_C = 0.0$	$C_\zeta = 0.0$
$x_b = 0.5$	$a_o = 5.70$
$I_b = 0.3333$	$C_{d0} = 0.01$
$J_b = 0.0001$	$C_{m0} = -0.02$
$X_{Ib} = 0.0$	$N_b = 4$
$X_A = 0.0$	$\sigma = 0.05$
	$\gamma = 5.0$

Helicopter Data

$C_W = 0.005$	$fC_{df} = 0.01A_R$
$X_{FA} = 0.0$	$L_{FA} = 0.2$
$X_{FC} = 0.0$	$L_{FC} = 0.2$

8.1.2.1 Trim Solution in Forward Flight

Though flap trim combined with the quasilinearization procedure was used to obtain most of the trim and response results in Ref. 50, a small set of results were presented which were obtained using the harmonic balance technique described in this study. The trim and response results obtained in Ref. 50 by employing the harmonic balance technique are compared in this section to similar results calculated in the present study. The results presented in this section were generated by retaining three harmonics ($N_H = 3$) in the expansion of the blade degrees of freedom.

The first comparison presented is between the trim variables obtained in this study with those of Ref. 50, calculated at two different blade torsional frequencies. Figure 15 presents the comparison between the rotor plane angles of attack and inflow ratios, and Fig. 16 compares the collective and cyclic pitch inputs. It should be noted that these results were generated without the reverse flow model. The comparison of the trim results is quite good, though the trim solutions tend to diverge slightly at the higher advance ratios. The

exact reason for this was not found, however the discrepancy between the trim solutions is sufficiently small to conclude that overall the comparisons are very good.

8.1.2.2 Response Solution in Forward Flight

A comparison of the flap, lead-lag and torsional responses are presented in Fig. 17 for an advance ratio of $\mu = 0.3$ and rotating nondimensional torsional frequency of 5.0/rev. The lead-lag and torsional responses obtained in this study are almost identical to those in Ref. 50. However, there is a small but noticeable difference between the flap responses. The flap response of this study has two even peaks, while the two peaks of Ref. 50 are slightly uneven; the first peak being slightly smaller than the second. The cause of this slight discrepancy is unclear, but may be related to the small discrepancy between the higher order terms present in this study which were not present in Ref. 50, as noted earlier. However, this minor variance between the two flap responses firmly supports the validity of the trim and response solution procedure used in this study.

8.1.2.3 Stability in Forward Flight

Comparison of stability information is based upon the real part of the characteristic exponent for the lag degree of freedom, which is the degree of freedom which has the potential for becoming unstable in forward flight. Comparison of this information with that obtained in Ref. 50 is presented in Fig. 18. The comparison with Ref. 50 is very good over the entire range of advance ratios, thus lending credence to the validity of the coupled flap-lag-torsional model and solution procedure employed in this study.

8.2 VALIDATION OF THE FULLY ELASTIC BLADE MODEL

Verification of fully elastic blade model developed in this study is based on comparison with the results obtained in Refs. 38 and 45. In the study of coupled rotor/fuselage vibration reduction in forward flight using higher harmonic control presented in Ref. 38, a fully flexible blade model and solution procedure was employed which is identical to the one used

in this study. Though Ref. 38 incorporated a flexible fuselage in the mathematical model, trim and response results were presented for the isolated blade case for validation of the flexible blade model. However, since Ref. 38 does not present any stability results, comparisons with that reference could only be used to validate the trim and response portion of the model used in this study.

Stability results in forward flight which can be used for model verification can be found in Ref. 45. The fully elastic blade model utilized in Ref. 45 to study vibration reduction on isolated rotor blades in forward flight using higher harmonic control, is based on the same set of equations of motion used in this study. However, a Galerkin type finite-element method combined with an implicit formulation was used in Ref. 45. Cubic interpolation polynomials were used for the modeling of flap and lag bending, and a quadratic interpolation polynomial was used for the modeling of torsion. Each finite-element therefore has a total of 11 degrees of freedom: displacement and slope at each end of the element for flap and lag bending; and rotation at each end of the element and also at a midelement node for torsion. A normal mode coordinate transformation based upon one torsional, two lag and three flap rotating coupled modes, was used to reduce the number of degrees of freedom.

Furthermore, Ref. 45 employed an implicit unsteady aerodynamic formulation based upon a finite-state, time-domain model for the unsteady aerodynamic effects. A simple reverse flow model was used in which both the drag and the lift change sign inside the reverse flow region. Flap trim and quasilinearization were used to obtain the trim and blade response. Since an implicit aerodynamic formulation is employed, the derivatives of the aerodynamic loads required for the stability analysis were calculated using finite differences.

While there are significant differences between the aeroelastic analysis used in Ref. 45 and the analysis presented in this study, it was reasonable to expect similar results from the two approaches since they are based upon very similar equations of motion. Furthermore, Ref. 45 contains some results generated using full propulsive trim and quasisteady aerodynamics; although the apparent mass terms were neglected in the calculations.

Therefore comparison with selected results from Ref. 45 was deemed to play a useful role in validating the fully elastic blade model developed in this study.

The blade configuration used for model verification is presented in Table 4. The data in that table have been non-dimensionalized using M_b , R and $(1/\Omega)$ for mass, length and time, respectively. The configuration represents a uniform soft-in-plane rotor blade model with the center-of-gravity of the fuselage located a distance 0.5R below the hub and with the fuselage drag center located a distance 0.25R below the hub.

TABLE 4

Soft-in-plane fully elastic blade configuration

Flight Data	
μ = variable	
Rotor Data	
$N_b = 4$	
$c_b = 2b = 0.05498$	$L_b = 1.0$
$e = 0$	$\theta_{pt} = 0$
$\omega_F = 1.123, 3.41, 7.65$	$a_o = 2\pi$
$\omega_L = 0.732, 4.485$	$C_{do} = 0.01$
$\omega_{T1} = 3.17$	$C_{mo} = 0.0$
$\gamma = 5.5$	$\sigma = 0.07$
Helicopter Data	
$C_W = 0.005$	$fC_{df} = 0.01A_R$
$X_{FA} = 0.0$	$Z_{FA} = 0.25$
$X_{FC} = 0.0$	$Z_{FC} = 0.5$

8.2.1 *Trim Solution in Forward Flight*

A comparison of the trim state of the rotor at different advance ratios with the results obtained in Refs. 38 and 45 is presented in Figs. 19 and 20. Two sets of trim results which were obtained in Ref. 45 are presented. The first set of trim results was generated in Ref. 45 using flap trim, which represents a propulsive trim procedure in which the blade flexibility is modeled with a linear flapping equation of motion for the first flap mode only. The second set of trim results was obtained in Ref. 45 using a propulsive trim procedure in which all blade degrees of freedom are included; however only the constant and first harmonics of the blade response are used to calculate the trim variables. For both sets of trim

results from Ref. 45, a simplified version of the aeroelastic model is used, in which only four rotating coupled modes are used to represent the flexibility of the blade and the mode shapes are calculated using only two finite elements. In addition, quasisteady aerodynamics (without apparent mass terms) was used and constant inflow was assumed.

The trim results from Ref. 38 compare very favorably with the results of this study. This is to be expected since the blade models and solution procedures are essentially identical. However, the two sets of results from Ref. 45 do not compare as favorably. Of the two sets, the set of results obtained using flap trim compare more favorably, especially in the rotor angle of attack and the sine cyclic pitch input. One would expect that the propulsive trim results would compare better than the flap trim results, however recall that only the constant and first harmonics of the blade response were retained in the calculation of the trim state by Ref. 45, while the constant part and the first five harmonics ($N_H = 5$) are retained in this study. The full trim procedure used by Ref. 45 represents an improvement over the flap trim procedure, though it is not as complete as the one used in this study. Reference 45 also employed a different reverse flow model from that used in this study, which can also significantly influence the trim results. Recall that in Ref. 45 the sign on both the drag and the lift was switched inside the reverse flow region, while in this study the lift was set to zero.

8.2.2 *Response Solution in Forward Flight*

A comparison of tip response results for an advance ratio of $\mu = 0.3$ is presented in Fig. 21. The tip response has been non-dimensionalized with respect to the radius of the blade. Since the flap trim results of Ref. 45 compared better than the full trim results to the results of this study, the tip response plotted in Fig. 21 represents the response obtained using flap trim. The blade response in Ref. 45 was obtained using quasilinearization. It should be emphasized that the results in Ref. 45 were calculated using unsteady aerodynamics.

Once again very good agreement with Ref. 38 is obtained. However there is a significant discrepancy between the results obtained in this study and the response found in Ref. 45. While the response in Ref. 45 was obtained for a slightly different trim state, the discrepancy in the blade response can be primarily attributed to the difference in the reverse flow models. The sign on the lift is switched inside the reverse flow region in Ref. 45, instead of being set equal to zero as done in this study. This produces a greater imbalance in the aerodynamic loads acting on the advancing and the retreating side of the rotor disk, which in turn results in a much lower flap response in Ref. 45. Comparison of the flap responses presented in Fig. 21 reveals that on the advancing side of the rotor disk the flap responses are very similar, however the responses diverge on the retreating side, the response in Ref. 45 exhibits much smaller flap angles. Thus variations in the amplitude of the flap response in Ref. 45 are considerably greater than those observed in this study.

8.2.3 *Stability Results in Forward Flight*

A comparison of the stability results calculated in the present study is compared with those obtained in Ref. 45. Results are obtained using both the soft-in-plane blade ($\omega_{L1} = 0.732$/rev) presented in Table 4, and the stiff-in-plane blade configuration ($\omega_{L1} = 1.42$/rev) presented in Table 5.

The stability results in Ref. 45 were obtained assuming quasisteady aerodynamics (without apparent mass terms) using flap trim combined with a quasilinearization procedure to obtain the time dependent equilibrium position. Finite differences were used to obtain the stability derivatives of the aerodynamic loads. Floquet theory was used to obtain the characteristic exponents of the linearized system from the value of the state transition matrix at the end of one period; which in turn was obtained in a single-pass using DE/STEP.

A comparison of the real part of the characteristic exponents associated with each mode is plotted versus advance ratio in Figs. 23 through 24 for the soft-in-plane blade case. Overall the comparisons are favorable, though there are small differences for each of the modes. Since it is the lag degree-of-freedom which is the critical degree-of-freedom for

TABLE 5

Stiff-in-plane fully elastic blade configuration

Flight Data	
μ = variable	
Rotor Data	
$N_b = 4$	
$c_b = 2b = 0.05498$	$L_b = 1.0$
$e = 0$	$\theta_{pt} = 0$
$\omega_F = 1.123, 3.41, 7.65$	$a_o = 2\pi$
$\omega_L = 1.42, 8.75$	$C_{do} = 0.01$
$\omega_{T1} = 3.17$	$C_{mo} = 0.0$
$\gamma = 5.5$	$\sigma = 0.07$
Helicopter Data	
$C_W = 0.005$	$fC_{df} = 0.01A_R$
$X_{FA} = 0.0$	$Z_{FA} = 0.25$
$X_{FC} = 0.0$	$Z_{FC} = 0.5$

stability, the real part of the characteristic exponent of the first and second lag modes are plotted separately from the other modes in Fig. 22. The real part of the characteristic exponent is a measure of the damping of that mode. It is evident from Figs. 22 and 23 that the damping in lag is the lowest and therefore it is the lag mode which can potentially become unstable first. The comparison of the real part of the characteristic exponents for the first two lag modes with Ref. 45 is favorable, though there is a small discrepancy between the first lag mode results at the higher advance ratios, and between the second lag mode results at the lower advance ratios. There are three probable sources for these discrepancies: 1) the difference in the reverse flow models; 2) the difference in the trim procedures; and 3) the fact that in Ref. 45 the apparent mass terms are neglected in the quasisteady aerodynamics. The apparent mass terms introduce various higher order terms; and thus they may have an effect on blade stability, which is sensitive to higher order terms. These apparent mass terms become more important as the advance ratio increases, and thus may partially explain the discrepancy between the first lag mode results evident at the higher advance ratios. Another factor which could explain the difference in the first lag mode results is the difference in the reverse flow models. It should be noted that this difference increases at the higher advance ratios. However, this cannot explain

the difference displayed in the second lag mode stability results at low advance ratios. One possible explanation for this discrepancy is related to the use of finite differences to obtain the stability derivatives of the aerodynamic loads in Ref. 45. Since the real part of the characteristic exponent of the second lag mode is very small, its value can be very sensitive to the accuracy of the finite difference approximation for this stability derivative.

A comparison of the real part of the characteristic exponents for the first two flap modes is presented in Fig. 23, and similar information is presented for the third flap mode and the fundamental torsional mode in Fig. 24. The results compare well with those obtained in Ref. 45, but there are some small differences. Again these minor differences can be attributed to the difference in trim procedures, reverse flow models, and, to a lesser extent, on the absence of apparent mass terms in the expressions for the aerodynamic loads used by Ref. 45.

A comparison of the real part of the characteristic exponents calculated in this study with the results obtained in Ref. 45 for the stiff-in-plane blade case (ω_{L1} = 1.42/rev) is presented in Figs. 25 through 27. Comparison of the real part of the characteristic exponents for the first two lag modes are presented in Fig. 25, for the first two flap modes in Fig. 26, and for the third flap and first torsion modes in Fig. 27. Overall the comparisons are favorable, except that Ref. 45 predicts an instability in the fundamental lag mode for advance ratios greater than 0.4 which was not observed in the model of this study. The reason Ref. 45 obtained this instability is not known. It should be noted, however, that comparisons which were made recently[16] with an independent researcher employing a similar blade model and solution procedure, verified the stiff-in-plane results obtained in the present study.

8.2.4 *Vibratory Response in Forward Flight.*

Results for the 4/rev vibratory hub shears and hub moments in forward flight were presented in Ref. 45. It is useful to also compare vibratory loads between various studies before embarking on research aimed at reducing these vibratory loads.

The 4/rev vibratory hub shears and moments calculated in Ref. 45, for the case of quasisteady aerodynamics, were obtained using flap trim and quasilinearization, instead of the full trim harmonic balance procedure used in the present study. Furthermore, the integration around the azimuth, required in the harmonic analysis of the vibratory hub loads, was performed in Ref. 45 using a trapezoidal integration scheme, in contrast to 30-point Gaussian quadrature used in this study. It was not stated in Ref. 45 how many points around the azimuth were used in the integration scheme.

A comparison of the magnitudes of the 4/rev vibratory hub shear and moment components calculated in this study with results obtained from Ref. 45 are plotted in Figs. 28 through 30 for the soft-in-plane blade case. It should be noted that the results presented in Ref. 45 represented peak-to-peak values and were scaled by dividing by the non-dimensional flapping inertia I_b which is equal to 1/3 for an uniform blade. Therefore in order to compare them with the results in this study the values from Ref. 45 were divided by two and multiplied by I_b.

For each component, the amplitude of the hub shears obtained in this study are smaller than those obtained in Ref. 45, especially the vertical component, and the amplitudes of the hub moments are slightly larger. The difference in the amplitudes can be attributed to the difference in the reverse flow models and the trim procedures. Recall from the comparison of the blade tip response in forward flight presented earlier, the flap response obtained in Ref. 45 was greater due to the different reverse flow model and trim solution used by that reference. It should be noted that as the advance ratio increases, the effects of the difference in the reverse flow model becomes more important.

Comparisons of the 4/rev hub shear and moment amplitudes with Ref. 45 for the case of the stiff-in-plane blade are presented in Figs. 31 through 33. Examination of these figures

shows that the correlation of hub loads with Ref. 45 is better in the case of the stiff-in-plane blade.

Overall, the comparisons with both Ref. 38 and 45 are considered to be quite reasonable, thus lending credence to both the blade model and solution procedure used in this study. Even though there exist some important differences between the aeroelastic analysis of Ref. 45 and the one used in this study, the comparisons presented here are considered to more than adequately justify the validity of the present aeroelastic analysis.

Chapter IX

CONTROL STUDIES USING THE OFFSET-HINGED SPRING RESTRAINED BLADE MODEL

In this chapter, the global and local deterministic controllers, implemented through an individually controlled aerodynamic surface on each blade are employed to achieve simultaneous reduction of the vibratory hub shears and hub moments in forward flight. To demonstrate the effectiveness of this control approach in reducing vibrations, the degree of vibration reduction achieved is compared with conventional IBC, in which the entire blade is oscillated. Comparisons of the control input amplitudes and power required to implement control for the two control approaches, are also made. Furthermore, these comparisons are studied for a reasonably wide range of blade fundamental rotating torsional frequencies, to assess the influence of blade torsional flexibility on the vibration reduction potential of this new approach.

9.1 SIMULTANEOUS REDUCTION OF THE VIBRATORY HUB SHEARS AND MOMENTS

For the results presented in this chapter, only the vibration magnitudes were penalized in the quadratic cost functional

$$J = \vec{Z}_i^T [W_Z] \vec{Z}_i \tag{9.1}$$

For this case the quadratic cost functional J consists of the weighted sum of the squares of the amplitudes of the hub shears and moments

$$J = W_F \vec{Z}_F^T \vec{Z}_F + W_M \vec{Z}_M^T \vec{Z}_M$$

and consequently represents a measure of the vibration levels experienced during the ith step. All six components of the vibratory hub loads are considered to be of equal importance in terms of reduction. However, due to the non-dimensionalization scheme used in this study, the relative magnitude of the amplitudes of the baseline vibratory hub moments

are an order of magnitude smaller than the amplitudes of the baseline vibratory hub shears. Therefore, in this trend type of study, to ensure that an equivalent level of vibration reduction is achieved in both the hub shears and hub moments, the weighting W_M on the squares of the hub moment amplitudes was scaled up by a factor of 10 relative to the weighting W_F on the squares of the hub shear amplitudes.

The global controller for the case when only the vibrations are penalized is obtained by substituting $[W_u] = [W_\Delta] = [0]$ into Eq. (7.4) to yield

$$\vec{u}_1^* = -[D_0]^{-1}[T_0]^T[W_Z]\vec{Z}_0 \tag{9.2}$$

where

$$[D_0] = [T_0]^T[W_Z][T_0] \tag{9.3}$$

It is evident from Eq. (9.2) that in this case the global controller converges in a single step. However, the control input given by Eq. (9.2) represents the true "optimal" input only if the system is truly linear. Since the assumption of moderate deflections made in the problem formulation introduces geometric nonlinearities into the problem, the system is nonlinear and therefore the local controller, which is based on a linearization of the problem about the current control, must be used in order to obtain the true "optimal" control input.

The local controller for this case is obtained by substituting $[W_u] = [W_\Delta] = [0]$ into Eq. (7.9) to yield

$$\vec{u}_1^* = -[D_{1-1}]^{-1}[T_{1-1}]^T[W_Z]\vec{Z}_{1-1} + \vec{u}_{1-1}^* \tag{9.4}$$

where

$$[D_{1-1}] = [T_{1-1}]^T[W_Z][T_{1-1}] \tag{9.5}$$

Equation (9.4) is in the form of a closed-loop controller where feedback of the measured vibration levels is used to determine the control input during each control step. Thus the local controller represents an iterative scheme and should converge to the true "optimal" control input for the nonlinear system represented by the helicopter.

The blade data employed in the vibration reduction studies presented in this chapter is given in Table 6. Except for the parameters C_W, γ and σ, the data in the table has been non-dimensionalized using the dimensional parameters R, M_b and $(1/\Omega)$ for length, mass and time, respectively. Furthermore, all results presented in this chapter are non-dimensionalized using these characteristic parameters. The data in Table 6 corresponds to a soft-in-plane uniform blade configuration which is used in the active control studies involving conventional IBC. The data employed in the studies of control implemented through an actively controlled flap on each blade is the same as presented in Table 6 except that each blade incorporates a 20% span, 1/4 chord partial span trailing edge flap centered about the 75% span blade station. In addition, to account for the 5% higher effective solidity due to the presence of a trailing edge flap on each blade, the weight coefficient C_W is increased by 5%. This ensures that the two blade configurations have roughly equivalent blade loading, as represented by C_T/σ.

TABLE 6

Spring restrained blade data

Flight Data

$\mu = 0.3$

Rotor Data

$c_b = 2b = 0.03927$	$2.5 \leq \omega_{T1} \leq 5.0$
$L_b = 1.0$	$\omega_{F1} = 1.15$
$e = 0.0$	$\omega_{L1} = 0.57$
$\beta_p = 0.0$	$C_\phi = 0.0$
$\theta_{pt} = 0.0$	$C_\beta = 0.0$
$R_C = 0.0$	$C_\zeta = 0.0$
$X_{Ib} = 0.0$	$a_o = 5.70$
$X_A = 0.0$	$C_{d0} = 0.01$
$x_b = 0.5$	$C_{m0} = -0.02$
$I_b = 0.3333$	$N_b = 4$
$J_b = 0.0001$	$\gamma = 5.0$
$X_{Ic} = 0.0$	$\sigma = 0.05$

Helicopter Data

$C_w = 0.005$	$fC_{df} = 0.01A_R$
$X_{FA} = 0.0$	$Z_{FA} = 0.2$
$X_{FC} = 0.0$	$Z_{FC} = 0.2$

The uncontrolled (baseline) value of the quadratic cost functional obtained using the blade configuration incorporating a trailing edge flap is compared in Fig. 34 to the value

obtained using the conventional blade configuration. The reason for the small difference in the uncontrolled vibration levels evident in the figure is due to the minor difference in the blade configurations. However, since the controlled vibration levels achieved by implementing the two control approaches are a small fraction of their uncontrolled values, this difference is considered to be unimportant.

Examination of Fig. 34 reveals that the highest uncontrolled vibration levels are obtained for the case of the torsionally soft blade with $\omega_{T1} = 2.5$/rev. As the torsional frequency of the blade is increased above 2.5/rev, the vibration levels decrease sharply until they reach a fairly constant level around $\omega_{T1} = 4$/rev. This sensitivity of the vibration levels to changes in the torsional stiffness of the blade can be attributed to the sensitivity of the aerodynamic loads to changes in the angle of attack of the blade. As the blade becomes stiffer in torsion, the blade torsional response decreases in magnitude, resulting in lower vibratory loads. in this case.

The control studies presented in this chapter were based upon a control input signal consisting of a combination of a 2, 3, 4 and 5/rev harmonic input signal (i.e. $N_{max} = 5$). The 3, 4, and 5/rev input frequencies were selected since a 4/rev input signal introduced in the nonrotating system through a conventional swashplate, which is frequently used in HHC studies on four bladed rotors, generates a signal with 3, 4 and 5/rev components in the rotating reference frame. The 2/rev input frequency was added to this set since it was found to be approximately as effective as the other frequencies in achieving vibration reduction[39]. Input harmonics greater than 5/rev were rejected since it was found that these higher input harmonics adversely affected the 8/rev vibration levels, the next greatest vibration component after the 4/rev vibrations in a four-bladed rotor.

The (2, 3, 4, 5/rev) frequency combination was selected after comparing the effectiveness of various input frequency combinations in reducing the 4/rev vibration levels, as well as their impact on the 8/rev vibrations. This set of input frequencies was found to produce the greatest level of reduction in the 4/rev vibrations without unacceptable increases in the 8/rev vibration levels. This is demonstrated in Figs. 35 through 38, which depict the level of vibration reduction achieved in the 4/rev hub shears and moments using various input

frequency combinations, and the resulting impact on the 8/rev hub loads. The results in the figures were obtained by employing the global control using the input frequency combinations (3, 4, 5/rev), (2, 3, 4, 5/rev), and (2, 3, 4, 5, 6/rev) on a blade with a fundamental rotating torsional frequency of $\omega_{T1} = 3.0/\text{rev}$. Figures 35 and 36 demonstrate the effectiveness of these three input frequency combinations in reducing the 4/rev hub loads, and the resulting impact on the 8/rev vibrations, when control is implemented through the actively controlled flap. Figures 37 and 38 represent comparisons obtained using conventional IBC. These two sets of figures clearly demonstrate that the addition of the 2/rev input frequency to the (3, 4, 5/rev) frequency combination results in a significant improvement in the effectiveness of both control approaches. However, when the 6/rev input frequency is included, the small additional decrease obtained in the 4/rev vibrations is more than cancelled out by the significant increase observed in the 8/rev vibration levels.

The global and local controllers were employed to reduce simultaneously the 4/rev hub shears and hub moments. Control was implemented through the actively controlled flap, and also using conventional IBC, primarily for comparison purposes. In the present case, where only the vibration magnitudes were penalized, the global controller always converged in a single step. However the local controller, which is based on a linearization about the current control, required a number of iterations to converge. Typical iteration histories of the local controller are presented in Figs. 39 through 42 for both control approaches. The results were obtained using a blade with a torsional frequency of $\omega_{T1} = 3/\text{rev}$. These figures show that the controlled cost functional, plotted in Fig. 39, and the controlled hub shears and moments, plotted in Figs. 40 through 41, converge to steady values by the fourth iteration. Convergence was assumed to have occurred when the change in the cost functional from the previous step was less than 1%. It was found that the local controller always converged within three to four iterations over the entire range of blade torsional frequencies considered.

A comparison of the controlled values of the quadratic cost functional obtained when employing the global and local controllers is presented in Fig. 43 for both control approaches. In each case the converged value of the controlled cost functional is plotted as

a percentage of the baseline value. It is evident from the figure that very substantial vibration reduction was achieved by both conventional IBC and the actively controlled flap over the entire range of blade torsional frequencies considered. The local controller performed better than the global controller in each case. In the case of conventional IBC, the local controller successfully reduced the cost functional by at least 99.75% over the entire range of blade torsional frequencies considered, compared to a reduction by only about 97.5% achieved by employing the global controller. For the case when the control was implemented through an actively controlled flap, the local controller was able to increase the degree of vibration reduction from 98.25%, achieved by the global controller, to at least 99% over the entire range of torsional frequencies.

In the case considered here, where only the vibration magnitudes are penalized, the global controller simply represents the first control step of the local controller. However, the problem is inherently nonlinear due to the assumption of moderate deflections, and thus the introduction of feedback will of course increase the degree of vibration reduction which can be achieved. It is interesting to note from Fig. 43 that as the blade becomes relatively stiff in torsion very little improvement in the vibration reduction effectiveness is achieved in either control approach when the local controller is employed. This can be attributed to the fact that the nonlinearity inherent in the system is due to the sensitivity of the blade vibratory response to control. As the torsional stiffness of the blade is increased, this sensitivity diminishes, reducing the strength of the nonlinearity inherent in the system. Therefore, as long as the system parameters (i.e., the elements of the [T] matrix) are known without error, little improvement in vibration reduction is to be expected from the introduction of feedback in the case of torsionally stiff blades.

In order to examine the degree of reduction achieved in each of the vibratory hub load components, the vertical hub vertical hub shear component is selected as a representative indicator of all six vibratory hub load components. A plot of the baseline value of the 4/rev vertical hub shear versus blade torsional frequency is presented in Fig. 44 for the two blade configurations. The figure reveals that the presence of a trailing edge flap on the blade has a very small effect on this vibratory component, as seen from the present results.

Comparison of the controlled value of the 4/rev vertical hub shear obtained by employing the global and local controllers is presented in Fig. 45 for both control approaches. The figure reveals that very substantial reduction in the amplitude of the 4/rev vertical hub shear was achieved by both conventional IBC and the actively controlled flap. In both cases the best reduction was obtained by employing the local controller. Using the local controller, the vertical hub shear was reduced by at least 97.5% by conventional IBC and by at least 95% using the actively controlled flap over the entire range of blade torsional frequencies considered. Very similar results were obtained for the other five components of the vibratory hub loads. Overall, it appears that conventional IBC is slightly more effective in reducing the vibratory hub loads; however, the difference in the degree of vibration reduction achieved by the two control approaches is small.

Comparisons of the baseline and controlled values of the 4/rev hub shears and moments achieved using the actively controlled flap and conventional IBC are presented in Figs. 46 through 49. The behavior of both a blade relatively soft in torsion, with ω_{T1} = 2.5/rev. and for a blade relatively stiff in torsion, with ω_{T1} = 5/rev, are compared. The degree of reduction achieved in the 4/rev hub shears and moments using the actively controlled flap and using conventional IBC is presented in Figs. 46 and 48, respectively, for the case of the torsionally soft blade, and in Figs. 47 and 49, respectively, for the case of the torsionally stiff blade. The two sets of figures show that very substantial reduction in the 4/rev hub shear and moment components was achieved by both control approaches. In each case the local controller achieved a greater degree of vibration reduction in each of the vibratory hub load components.

9.1.1 *Control Power Requirements*

A comparison of the average power required (per revolution) for the implementation of the vibration reduction using the two control approaches is presented in Fig. 50. The power required for conventional IBC is defined as the average power needed to drive the blade root pitch actuators during one revolution:

$$P_{IBC} = \sum_{k=1}^{N_b=4} \frac{1}{2\pi} \int_0^{2\pi} [- M_{Rx3}(\psi_k)\, \dot{\theta}_{IBC}(\psi_k)]\, d\psi_k \qquad (9.6)$$

where $\theta_{IBC}(\psi_k)$ represents the instantaneous additional IBC pitch input of the k-th blade and $M_{Rx3}(\psi_k)$ represents the instantaneous blade root feathering moment.

Examination of Fig. 50 reveals that substantially more power is required to implement vibration reduction using the conventional IBC approach than for vibration reduction based on the actively controlled flap. Vibration reduction using conventional IBC required about 12 times more power at the lower blade torsional frequencies, and about 7 times more power at the higher blade torsional frequencies. These higher power requirements appear to be associated with the need to drive harmonically the fairly large and coupled elastic system represented by the entire blade, as opposed to being required to drive harmonically a relatively small aerodynamic surface. It is also evident from this figure that as the torsional frequency the blade increases, the power required to implement the control increases for both control approaches.

9.1.2 *Control Input Requirements*

A comparison of the maximum amplitudes of the optimal control input required for vibration reduction by the two control approaches is presented in Fig. 51. Of course larger control input amplitudes are required for vibration reduction when using the actively controlled flap, but these angles are quite reasonable; over the entire range of blade torsional frequencies investigated, the largest control flap deflection angle required is only 8 degrees. It is evident from Fig. 51 that in both control approaches, the required control input amplitudes increase with increasing blade torsional stiffness. As the blade becomes stiffer in torsion, the sensitivity of the system to control diminishes, thus requiring larger control input amplitudes to achieve roughly the same degree of vibration reduction. This important influence of the blade fundamental torsional frequency on vibration reduction is also consistent with the findings presented in Ref. 28.

9.2 EFFECT OF MASS UNBALANCE

The results presented so far have been generated using a mass balanced flap, i.e. the offset X_{lc} between the hinge point and the center of gravity of the control flap is zero. When this is true the inertial moment about the control flap hinge is due only to the polar moment of inertia of the control flap, denoted as J_c. Moving the center of gravity of the control flap aft of the hinge point increases the rotational inertia and thus can have a significant impact on the hinge moment and the amount of power required to drive the control flap. The effect of using a mass unbalanced flap is investigated in this section by moving the control flap center of gravity aft of the hinge point by one quarter of the control flap chord length, i.e. $X_{lc} = (1/4)c_{cs}$.

A comparison of the uncontrolled vibration levels obtained using a mass balanced and an unbalanced control flap is presented in Fig. 52. The figure shows that almost no change is observed in the uncontrolled vibration levels when a mass unbalanced trailing edge flap is used. Furthermore, it is evident from Fig. 53 that the impact on the controlled vibration levels is also very small. Finally, examination of the required control input amplitudes presented in Fig. 54 shows that the use of a mass unbalanced trailing edge flap has no effect on the input amplitudes either. Thus, shifting the mass center of the control flap aft of the hinge point has virtually no effect on the vibration levels or on its potential to reduce them.

However, a comparison of the control power requirements of the mass balanced and unbalanced control flap presented in Fig. 55 reveals that a substantial reduction in power requirements can be obtained by using an unbalanced flap. The figure depicts a 50% (at the higher blade torsional frequencies) to 80% (at the lower blade torsional frequencies) reduction in power requirements for the unbalanced flap. Thus the flapping and twisting motions of the blade, which provide inertial moments about the control surface hinge when $X_{lc} > 0$. help drive the control flap which reduces the load on the control flap servo-actuator.

Chapter X

CONTROL STUDIES USING THE FULLY ELASTIC BLADE MODEL

The results obtained using the flexible blade model are presented in this chapter. The nominal data for the elastic blade configuration employed in this study is presented in Table 7 and corresponds to a soft-in-plane blade with uniform mass and stiffness. The data resembles approximately an MBB-105 helicopter. The data in the table (exept for C_W, γ and σ) have been nondimensionalized using M_b, L_b and $(1/\Omega)$ for mass, length, and time respectively.

TABLE 7

Elastic blade configuration used in control studies

Dimensional Data

$R = 4.91m$
$\Omega = 425RPM$
$M_b = 52kg$

Nondimensional Data

Flight Data

$\mu = 0.3$

Rotor Data

$N_b = 4$	$L_b = 1.0$
$\gamma = 5.5$	$\sigma = 0.07$
$c_b = 2b = 0.05498$	$e = 0$
$X_A = 0.0$	$X_{lb} = 0.0$
$I_{MB2} = 0.0000$	$\theta_{pt} = 0.0$
$I_{MB3} = 0.0004$	$a_o = 2\pi$
$\omega_F = 1.123, 3.41, 7.62$	$C_{do} = 0.01$
$\omega_L = 0.732, 4.46$	$C_{mo} = 0.0$
$2.5 \leq \omega_{T1} \leq 5.0$	

Helicopter Data

$C_W = 0.005$	$fC_{df} = 0.01A_R$
$X_{FA} = 0.0$	$Z_{FA} = 0.3$
$X_{FC} = 0.0$	$Z_{FC} = 0.3$

The blade data in Table 7 corresponds to a conventional blade configuration (i.e., no trailing edge flap) that is utilized in the control studies involving conventional IBC. In the studies of control implemented through an actively controlled flap, the same blade data is

used, except that each blade incorporates a partial span trailing edge flap which is 12% of the blade span, 1/4 of the blade chord, and centered about the 75% blade span position. The addition of the trailing edge flap to the blade span alters the mass distribution of the blade, which changes the natural frequencies of vibration. In this study, the bending and torsional stiffnesses of the flexible blade incorporating the control flap were increased (slightly) to compensate for the additional mass, such that the resulting fundamental frequencies match those of the conventional blade configuration presented in Table 7. This was done to similate the BO-105 blade, as it exists. However, to account for the 3% higher effective rotor solidity due to the presence of a trailing edge flap on each blade, the value of the weight coefficient C_W used in the control studies involving the control flap is 3% larger than the value shown in Table 7. This ensures that the two blade configurations have roughly equivalent blade loading, as represented by C_T/σ .

The local controller represented by Eq. (7.9) was employed to produce simultaneous reduction in the vibratory hub shears and moments using the actively controlled flap. Conventional IBC was also implemented for comparison purposes. In both control approaches an input signal consisting of 2, 3, 4, and 5/rev harmonic components in the rotating reference frame was utilized. This combination of frequencies was found to produce the greatest degree of reduction in the 4/rev hub loads without causing a significant increase in the 8/rev hub loads, which are the next largest component of the vibratory loads in a four-bladed rotor.

In the active control studies presented in this chapter only the vibration levels are penalized (i.e., $[W_U] = [W_\Lambda] = [0]$) . In this case the quadratic cost functional J consists of the weighted sum of the squares of the amplitudes of the hub shears and hub moments, and thus represents a measure of the vibration levels experienced during the i-th control step. The weightings on the squares of the hub moment amplitudes were scaled by a factor of ten relative to the weightings on the squares of the hub shear amplitudes. This was found to be necessary in order to achieve roughly the same degree of reduction in the vibratory hub shear and hub moment components.

A comparison of the uncontrolled (baseline) values of the quadratic cost functional for a conventional blade and a blade incorporating a trailing edge flap is presented in Fig. 56. The comparison is conducted over a range of blade fundamental rotating torsional frequencies, starting from a blade which is relatively soft in torsion, $\omega_{T1} = 2.5$/rev, to a blade which is relatively stiff in torsion $\omega_{T1} = 5.0$/rev . Figure 56 reveals that the addition of a relatively small trailing edge flap to the outboard sections of the blade span results in a 25-40% decrease in the baseline value of the cost functional, representing a 13-23% reduction in the 4/rev hub load magnitudes. It should be noted that the offset between the center of gravity of the blade cross-section and the elastic axis is zero for this case. The presence of a trailing edge flap on the blade shifts the center of gravity behind the elastic axis, which has the effect of increasing the inertial coupling between the flapping and twisting motions of the blade. This coupling appears to have a beneficial effect on the vibration levels in this case. *Thus in effect, the mass of the trailing edge flap may be acting like a tuning mass, which is sometimes used to tailor the blade vibratory response.*

The minimum value of the quadratic cost functional achieved by employing the local controller implemented through the actively controlled flap is presented in Fig. 57. The results obtained using conventional IBC are presented for comparison. The figure shows that very substantial vibration reduction was achieved by both control approaches over the entire range of torsional frequencies considered, and that the level of reduction produced by the actively controlled flap is comparable to conventional IBC. In fact, for blades with a torsional frequency in range $3.1 \leq \omega_{T1} \leq 3.7$, the level of vibration reduction produced by oscillating the relatively small trailing edge flap exceeds that achieved by oscillating the entire blade. This occurs when the torsional frequency of the blade ω_{T1} is close to the rotating frequency of the second flap bending mode, which is given by $\omega_{F2} = 3.7$/rev when $x_c = 0.75R$.

A very important capability lacking in conventional IBC, where the entire blade undergoes a uniform pitch change about the blade root, is the ability to cyclically vary the twist distribution of the blade. It was shown by Lemnios and Smith[28] in their study of a controllable twist rotor (CTR) configuration that improvements in rotor performance, and sig-

nificant decreases in blade bending amplitudes, could be achieved by cyclically varying the twist distribution of the blade. In their study, a servo-flap similar to the one used in this study to produce the external torsional moments needed to alter the twist distribution of the blade. Thus the ability of the actively controlled flap to affect the blade's twist may help explain its superior performance compared to conventional IBC for blades with a torsional frequency near the frequency of the second flap bending mode. The increase in coupling between these two modes should increase the potential of the actively controlled flap to affect the vibratory response of the blade, and hence the vibration levels.

Examination of Fig. 57 shows that the effectiveness of conventional IBC is relatively insensitive to variations in the torsional stiffness of the blade, while the figure depicts a decrease in control flap effectiveness at the higher blade torsional frequencies. As the blade becomes stiffer in torsion, the ability of the control flap to affect the twist distribution of the blade is reduced, thus reducing its effectiveness in controlling vibrations. Practically, though, the optimal cost functional at the higher torsional frequencies is still very small.

The degree of reduction achieved in each of the 4/rev hub load components by the two control approaches is shown in Figs. 58 through 63 by comparing the reduced hub shear and moment amplitudes with their baseline values. Comparisons are presented for the torsional frequencies $\omega_{T1} = 2.5,\ 3.0,\ 3.5,\ 4.0,\ 4.5$ and 5.0/rev. Examination of these figures reveals that the actively controlled flap successfully reduced the hub shears the hub shear components by at least 80% over the entire range of torsional frequencies, and reduced the hub moment components by at least 50%. The best performance of the actively controlled flap, obtained at $\omega_{T1} = 3.5$/rev, consisted of a 98% reduction in the hub shear components, and a 92% reduction in the hub moment components. The effectiveness of conventional IBC was fairly constant over the entire range of torsional frequencies considered, reducing the hub shears by at least 97%, and the hub moments by at least 87%.

A comparison of the maximum control input amplitudes required for vibration reduction by the two control approaches is presented in Fig. 64. Of course the input angles required by the actively controlled flap were much larger than the IBC pitch angles, but these deflection angles were quite reasonable: over the entire range of blade torsional frequencies

investigated, the largest control flap deflection angle required was only ten degrees. An increase in control amplitudes with increasing torsional stiffness is evident for both control approaches; however the greatest increase is in the required control flap deflection angles. This can be attributed to the fact that as the blade becomes stiffer in torsion, much larger input angles are required to affect changes in the twist distribution of the blade.

Finally, a comparison of the power required to implement control through the actively controlled flap and conventional IBC is presented in Fig. 65. The power required to drive the control surface actuators is defined by Eq. (7.17) and the power required to implement conventional IBC is defined by Eq. (9.6). Figure 65 reveals that oscillating the entire blade requires considerably more power than oscillating the relatively small trailing edge flap; conventional IBC requires anywhere from 3 times (on a torsionally stiff blade) to 10 times (on a torsionally soft blade) the power for its implementation. The power requirements of both control approaches increase as the blade becomes stiffer in torsion, as shown in Fig. 65. As the blade becomes stiffer in torsion, it becomes more difficult, and hence more costly, to alter the vibratory response of the blade.

10.1 COMPARISONS WITH THE SPRING RESTRAINED BLADE MODEL

In this section results generated using the fully elastic blade model are compared with results obtained using the simple offset-hinged spring restrained blade model to determine the effect of the refined blade model on the dynamic behavior of the blade. The elastic blade data presented in Table 7 is employed to obtain the results using the simple spring restrained blade model. To provide valid comparisons between the two blade models, the stiffnesses of the torsional root springs are set such that the resulting rotating frequencies in flap, lead-lag and torsion match the fundamental rotating frequencies of the flexible blade. There is no unique combination of the root offset and spring stiffnesses which yields the appropriate fundamental rotating frequencies. Thus, to obtain a unique set of spring stiffnesses, the root offset in the spring restrained blade model is set to zero, which is the value of e used in the flexible blade model.

10.1.1 *Trim and Response Solution in Forward Flight*

The trim state of the rotor obtained using the two blade models is plotted versus advance ratio in Figs. 66 and 67 for a blade with a torsional frequency of $\omega_{T1} = 3.17$/rev. The inflow ratio and rotor angle of attack are plotted in Fig. 66 and the trim pitch settings are depicted in Fig. 67. Examination of these two figures reveals that the use of a more realistic dynamic model, as represented by the fully elastic blade model, has very little impact on the trim results. Except for the collective pitch angle, which is slightly larger in the case of the flexible blade model, the trim results are almost identical. However, a comparison of the blade tip response results presented in Fig. 68, reveals a considerable difference in response solutions. Though the character of the response solutions are very similar between the two blade models, as seen in Fig. 68, the tip deflection amplitudes obtained using the flexible blade model are larger. The greatest difference is evident in the twist deflection of the blade, which may explain the slightly higher collective pitch settings required by the flexible blade model seen in Fig. 67. A higher pitch setting would be required to offset the larger negative elastic twist of the flexible blade model.

10.1.2 *Vibratory Hub Loads*

The importance of the modeling of the blade flexibility when calculating vibration levels was investigated by comparing the amplitudes of the 4/rev hub shears and moments obtained using the simple offset-hinged spring restrained blade model with those obtained using the more realistic flexible blade model. The vibration magnitudes, calculated for a blade with a torsional frequency of $\omega_{T1} = 3.17$/rev, are plotted at different advance ratios in Figs. 69 through 71. The results demonstrate that the improvement in the dynamic modeling capability afforded by the fully elastic blade model results in a dramatic increase in the calculated values of the vibratory hub loads. Except in the case of the vertical hub shear component, which is almost identical for the two blade models, the amplitudes of the 4/rev hub loads obtained using the fully elastic blade model are much greater than those predicted by the spring restrained blade model: the longitudinal and lateral hub shear

amplitudes are about 100% larger, and the hub moment amplitudes are more than 200% larger. This dramatic increase in the vibratory hub loads can be attributed at least in part to the larger response amplitudes obtained using the flexible blade model, depicted in Fig. 68. The greatest difference is evident in the torsional deflection of the blade, which can have a substantial impact on the vibratory aerodynamic loads.

10.1.3 *Active Control Studies*

The uncontrolled (baseline) values of the quadratic cost functional obtained using the two blade models are compared in Fig. 72. The figure depicts significantly higher vibration levels for the flexible blade model. This can be attributed to the fact that the 4/rev hub loads obtained using the flexible blade model are much larger than those predicted by the simple spring restrained blade model, as shown in Figs. 69 through 71. Recall that the greatest difference was evident in the hub moment components, which have been weighted more heavily in the quadratic cost functional than the hub shear components. It is interesting to note from Fig. 72 for the simple spring restrained blade model, almost no change is evident in the vibration levels due to the addition of a trailing edge flap to the blade span.

The minimum value of the quadratic cost functional achieved using the actively controlled flap and conventional IBC implemented on the spring restrained blade model is compared in Fig. 73 with the results obtained using the fully elastic blade model. The figure demonstrates that, despite the substantially greater vibration levels obtained using the flexible blade, both control approaches implemented on the flexible blade were still very effective in achieving substantial vibration reduction. In fact, comparison of the results obtained using the two blade models reveals that better vibration reduction was achieved in the case of the flexible blade model. It appears that the improvement in the dynamic modeling capability provided by the flexible blade model results in an increase in the potential of either control approach to reduce vibrations.

The most important difference between the two blade models evident in Fig. 73 is the difference in the degree of degradation displayed in the effectiveness of the actively con-

trolled flap at the higher blade torsional frequencies. The severity of the reduction in control flap effectiveness displayed in the simple spring restrained blade model may be attributable to the fact that this model, in which the blade flexibility is assumed to be concentrated at the blade root, is unable to model changes in twist distribution.

The maximum control input amplitudes obtained using the two blade models are compared in Fig. 74. The figure reveals that, despite the much larger uncontrolled vibration levels observed in the flexible blade model, the required conventional IBC pitch input amplitudes are almost identical for the two blade models. This is not true in the case of the actively controlled flap; except for blades relatively soft in torsion ($\omega_{T1} \leq 3.5$/rev), much larger control flap deflection angles are required to reduce vibrations in the case of the flexible blade model, in some cases as much as 50% larger.

The power requirements obtained using the two blade models are compared in Fig. 75. The figure shows that the difference in power requirements between the two control approaches is very similar between the two blade models.

10.2 IMPORTANCE OF THE CONTROL FLAP SPANWISE LOCATION

In the nominal configuration the trailing edge flap is centered about the 75% span position (i.e., $x_c = 0.75R$), which is very close to the node location of the second flap and lag bending modes. It was postulated that centering the trailing edge flap about this node point would minimize its potential for exciting the second bending modes of the flexible blade. The effect of locating the centroid of the trailing edge flap away from this node point was investigated by moving the centroid of the control flap outboard to the 85% span position ($x_c = 0.85R$). The effect on the uncontrolled vibration levels is shown in Fig. 76 by comparing the baseline value of the cost functional J for $x_c = 0.75R$ and $x_c = 0.85R$. The figure reveals that moving the trailing edge flap outboard of the node results in a 50% decrease in the baseline value of J, which represents about a 30% reduction in the baseline vibrations.

The effect of moving the trailing edge flap outboard on its ability to reduce vibrations is shown in Fig. 77. One might expect that moving the control flap outboard on the blade span, in the direction of greater effective air speeds, would have a beneficial effect on the vibration reduction potential of the actively controlled flap. However, Fig. 77 depicts a significant reduction in control flap effectiveness when the flap is moved outboard, for blades with a fundamental rotating torsional frequency in the vicinity of 4/rev. It is interesting to note that this is very close to the rotating frequency of the second flap mode, which is given by $\omega_{F2} = 3.97$/rev when $x_c = 0.85R$. Thus it appears that moving the centroid of the trailing edge flap away from the node location of the second flap mode, where the interaction between the second flap mode and the fundamental torsional mode is minimized, has a detrimental effect on the vibration reduction potential of the actively controlled flap when the frequencies of the two modes are close. However, Fig. 77 shows a substantial increase in the vibration reduction effectiveness of the control flap for blades relatively stiff in torsion when $x_c = 0.85R$.

The effect of moving the centroid of the control flap outboard on the required control flap deflection angles is depicted in Fig. 78. The figure reveals that the decrease in control flap effectiveness in the vicinity of $\omega_{T1} = 4$/rev is accompanied by a small increase in control input amplitudes, while a minor decrease in control angles is observed in the vicinity of $\omega_{T1} = 4.5$/rev. It should be noted that $\omega_{T1} = 4.5$/rev is very close to the rotating frequency of the second lag mode, which in this case is given by $\omega_{L2} = 4.48$/rev.

Finally, the effect on the power requirements of the actively controlled flap when it is moved outboard is presented in Fig. 79. The figure shows that the increase in control angles in the vicinity of $\omega_{T1} = 4$/rev is accompanied by about a 100% increase in the power required to actuate the control flap. However, for blades relatively stiff in torsion ($\omega_{T1} > 4.5$/rev), there is about a 70% reduction in the power required.

Figures 77 through 78 demonstrate that, in the present case, coupling of the fundamental torsional mode with the second flap bending mode has a detrimental impact on control flap performance. On the other hand, coupling with the second lead-lag mode appears to have a beneficial impact on control flap performance. Finally, moving the control

flap outboard on torsionally stiff blades improves its vibration reduction effectiveness and results in a significant decrease in power consumption.

10.3 EFFECT OF HINGE MOMENT CORRECTION

The influence of changes in the value of the aerodynamic hinge moment correction factor C_f on the performance of the actively controlled flap was studied using the flexible blade model, by changing the nominal value of $C_f = 0.6$, used up until this point, to the more conservative value of $C_f = 0.5$. Recall that C_f is used not only to scale the aerodynamic hinge moment, but also to scale the additional aerodynamic lift and pitching moment produced by the partial span trailing edge flap. A comparison of the degree of vibration reduction achieved using the actively controlled flap for the two different values of C_f is presented in Fig. 80. The figure shows that decreasing the value of C_f by about 15% has almost no effect on the potential of the actively controlled flap to reduce vibrations. However, a comparison of the control input requirements, shown in Fig. 81, and the power requirements, shown in Fig. 82, reveal that decreasing C_f by about 15% results in a corresponding increase in both the input angles and power requirements to implement control.

10.4 EFFECT OF COMPRESSIBILITY CORRECTION

The effect of introducing compressibility correction was also studied using the flexible blade model. Compressibility effects are accounted for using the Prandtl-Glauert correction factor, defined as

$$\beta = \sqrt{1 - M_{x,\psi}^2} \tag{10.7}$$

to obtain the compressible lift curve slope:

$$a = \frac{a_o}{\beta} = \frac{a_o}{\sqrt{1 - M_{x,\psi}^2}} \tag{10.8}$$

where $M_{x,\psi}$ is the local Mach number at x, ψ. The local Mach number on the blade can be expressed as

$$M_{x,\psi} = \frac{\sqrt{U_T^2 + U_P^2}}{c_a}$$

where c_a represents the speed of sound in air. If the dynamics of the blade are neglected, then the local Mach number can be approximated as[25]

$$M_{x,\psi} = M_{tip}\left(\frac{x}{L_b} + \mu \sin\psi\right) \tag{10.9}$$

where $M_{tip} = (\Omega R)/c_a$ represents the Mach number at the blade tip in hover. In the results presented in this section the compressible lift curve slope was obtained using the value $M_{tip} = 0.65$, which is a typical value associated with modern helicopter rotors[24].

Figure 83 presents comparisons of the baseline (uncontrolled) values of the cost functional obtained using the incompressible and the compressible lift curve slopes. The comparisons are presented for both the conventional blade configuration and the blade configuration incorporating the trailing edge flap. It is evident from the figure that overall the introduction of compressibility has a small but significant effect on the uncontrolled vibration levels. The introduction of compressibility correction results in a small decrease in the vibration levels obtained in the case of the conventional blade configuration (i.e. no control flap). It is interesting to note that when compressibility effects are accounted for, the impact on the uncontrolled vibration levels due to the addition of the trailing edge flap to the blade is reduced, resulting in very similar vibration levels for the two blade configurations.

The effect of compressibility correction on the vibration reduction effectiveness of the actively controlled flap and conventional IBC is presented in Fig. 84. In both cases the introduction of compressibility correction results in a small decrease in effectiveness for blades relatively soft in torsion, and a small increase for blades relatively stiff in torsion. Otherwise, there is little impact on the vibration reduction potential of either control approach.

The effect of compressibility correction on the maximum input angles required by the two control approaches is investigated in Fig. 85. Only small changes in the control input requirements of conventional IBC can be observed. In the case of the actively controlled flap, there is no significant change in control input requirements other than a small increase (about two degrees) for blades relatively stiff in torsion.

The effect of compressibility correction on the power required to implement the two control approaches is investigated in Fig. 86. A small decrease in power requirements, ranging from 16-19%, is observed for both control approaches when compressibility effects are included. Since the percent decrease is roughly the same for both the actively controlled flap and conventional IBC, the difference in power requirements between the two control approaches is essentially unchanged from the incompressible case.

When considering Figs. 83 through 86, it should be kept in mind that the introduction of compressibility is accomplished by scaling the incompressible lift curve slope by the factor $(1/\beta)$, which is greater than one. Thus the introduction of compressibility results in an effective increase in the sensitivity of the aerodynamic loads to changes in both the pitch angle of the blade and the deflection angle of the trailing edge flap. However, for an advance ratio of $\mu = 0.3$ and a tip Mach number of $M_{tip} = 0.65$, which has been used in the present case, it can be determined from Eq. (10.9) that $(1/\beta)$ ranges between $1.03 \leq \frac{1}{\beta} \leq 1.44$ over the span of the trailing edge flap, and between $1.02 \leq \frac{1}{\beta} \leq 1.87$ over the span of the entire blade. The value of $(1/\beta)$ does not deviate too far from unity in the present case ($M_{tip} = 0.65$ and $\mu = 0.3$), and thus the introduction of compressibility has a minor effect on the results. However, if either M_{tip} or μ were increased, then a larger portion of the blade span would be in the transonic range over a greater portion of each revolution, and therefore the effects of compressibility would be more pronounced.

Chapter XI

TIME DOMAIN SOLUTION OF THE EQUATIONS OF MOTION

The results presented so far have been obtained using the harmonic balance technique to extract the trim state and blade response in a completely coupled manner. This technique is based upon the assumption of a periodic steady state response solution under fixed-hub steady flight conditions. The periodic assumption allows the transformation of the system of nonlinear ordinary differential equations in the time domain to a set of nonlinear algebraic equations in the frequency domain. Though this transformation increases the order of the system by a factor of $(1 + 2N_H)$, there are many packaged subroutines available which efficiently solve large systems of nonlinear algebraic equations. In addition, the transformation of the aeroelastic response problem to the frequency domain permits its simultaneous solution with the trim problem, which is generally formulated in the frequency domain for steady flight conditions.

Another approach for generating the trim and aeroelastic response solution involves a two step procedure; where a simplified aeroelastic response analysis is used first to obtain the trim state of the rotor, which is subsequently used in the solution of the full aeroelastic response problem in the time domain using quasilinearization. This method requires the linearization of the blade equations about a k-th iteration, which when written out in first order form read[3,50]

$$\dot{\vec{y}}_{k+1} = [A_k(\psi)]\,\vec{y}_{k+1} + \vec{f}_k(\psi) \tag{11.1}$$

where the vector of states is defined as

$$\vec{y} = \{\vec{q}_b^{\,T} \quad \dot{\vec{q}}_b^{\,T}\}^T \tag{11.2}$$

The matrix $[A_k]$ and the vector $\vec{f}_k$ for the k-th iteration are defined as

$$[A_k] = \begin{bmatrix} [0] & [I] \\ -[M_k]^{-1}[K_k] & -[M_k]^{-1}[C_k] \end{bmatrix}$$

$$\vec{f}_k = \begin{Bmatrix} \vec{0} \\ -[M_k]^{-1}([M]\ddot{\vec{q}}_b + [C]\dot{\vec{q}}_b + [K]\vec{q}_b - \vec{f}_b)_k \end{Bmatrix}$$

where the subscript k indicates the term is evaluated at the k-th iteration. In the above expressions

$$[M] = \partial \vec{f}_b / \partial \ddot{\vec{q}}_b \tag{11.3}$$

$$[C] = \partial \vec{f}_b / \partial \dot{\vec{q}}_b \tag{11.4}$$

$$[K] = \partial \vec{f}_b / \partial \vec{q}_b \tag{11.5}$$

Quasilinearization generates the nonlinear solution iteratively through successive linear approximations of the system. Each stage of the procedure begins by linearizing the system about some periodic solution $\vec{y}_k$. The transition matrix $[\Phi_k(2\pi)]$ at the end of one period is obtained from the homogeneous linearized system and the solution $\vec{y}_k(2\pi)$ corresponding to a zero initial state is obtained from the nonhomogeneous linearized system. These are then used in the following result from linear periodic system theory[3.50]

$$\vec{y}_k(0) = ([I] - [\Phi_k(2\pi)])^{-1} \vec{y}_k(2\pi)$$

to obtain the initial conditions corresponding to the converged steady state periodic response of the forced linearized system. Generating the periodic response with this initial condition gives the periodic solution for the next iteration. The procedure is continued until no change is observed in the periodic solution between two successive iterations.

Solving the response problem directly in the time domain has the advantage that the order of the system is only doubled, thus requiring much less memory than the harmonic balance technique. However, the quasilinearization procedure has the disadvantage of being computationally intensive. Considerable effort must be expended during each stage

of the iteration to linearize the system about the current solution and to obtain the transition matrix at the end of one period. Evaluation of the transition matrix requires the solution of the homogeneous linearized system either n times (where n is the order of the problem) as in the n-pass method, or the solution of an equivalent n^2 order system a single time as in the single pass method[50]. Furthermore, there are two convergence loops associated with quasilinearization: one associated with each of the linearized systems, and one associated with the solution of the nonlinear system.

A more straightforward approach to obtaining the nonlinear system response involves solving the nonlinear ordinary differential equations of motion directly in the time domain. This can be accomplished by using a general purpose ordinary differential equation (ODE) solver capable of handling nonlinear system of equations. This approach retains the low workspace requirements of quasilinearization but eliminates the need to successively linearize the system and evaluate the transition matrix, thus saving considerable time and computational effort. Furthermore, there is only a single convergence loop.

The only possible drawback to this approach is that it may be necessary to solve the trim and response problems separately. However, it has been shown in this study that the simple spring restrained blade model is adequate to obtain the trim state of the rotor. Comparisons between the trim state obtained using this simple model with that obtained using the fully elastic blade model showed that the trim solutions differed by less than 5% (see Figs. 66 and 67). Thus it is assumed in the solution of the equations of motion of the blade in the time domain that the trim state of the rotor is known beforehand with sufficient accuracy.

11.1 GENERAL PURPOSE ODE SOLVER DE/STEP

In this study the nonlinear ordinary differential equations of motion are integrated numerically in time using the general purpose Adams-Bashforth ODE solver DE/STEP[48]. The code as well as the theory behind its development is presented in detail in Ref. 48.

In order to use the ODE solver, the equations of motion must be expressed in first order form[48]:

$$\dot{\vec{y}} = \vec{F}(\vec{y}; t) \tag{11.6}$$

where the function $\vec{F}$ can be a nonlinear function of $\vec{y}$ and time.

However, the equations of motion of the isolated blade have been formulated as a set of fully coupled, nonlinear, second order ordinary differential equations:

$$\vec{f}_b(\vec{q}_b, \dot{\vec{q}}_b, \ddot{\vec{q}}_b, \vec{q}_t; t) = \vec{0}$$

In order to express the blade equations in first order state variable form it is necessary to first decompose the equations into the form:

$$\vec{f}_b = \vec{g}_b(\vec{q}_b, \dot{\vec{q}}_b, \vec{q}_t; t) + [M(\vec{q}_b, \vec{q}_t; t)]\ddot{\vec{q}}_b = \vec{0} \tag{11.7}$$

where [M] represents the mass matrix defined by Eq. (11.3). In general this matrix has off-diagonal terms due to the assumption of moderate deflections, which couples the equations. In this study explicit expressions for $\vec{g}_b$ and [M] were obtained using the MACSYMA symbolic manipulation program.

Solving Eq. (11.7) for the vector of generalized accelerations yields:

$$\ddot{\vec{q}}_b = -[M]^{-1}\vec{g}_b \tag{11.8}$$

Using the above expression, the system of blade equations can be written in first order state-variable form:

$$\dot{\vec{y}} = \begin{bmatrix} [0] & [I] \\ [0] & [0] \end{bmatrix} \vec{y} + \begin{Bmatrix} [0] \\ -[M]^{-1}\vec{g}_b \end{Bmatrix} \tag{11.9}$$

where [I] represents an ($N_{DOF} \times N_{DOF}$) identity matrix. The above first order system is nonlinear through the $[M]^{-1}\vec{g}_b$ term. It should be emphasized that the matrix inverse represented by $[M]^{-1}$ is performed numerically in the FORTRAN program.

11.1.1 *Numerical Integration Error Control*

The ODE solver DE/STEP attempts at each internal step to control each component of the local error vector so that

$$|\vec{e}_{local}(i)| \leq \text{RELERR} \times |\vec{y}(i)| + \text{ABSERR}$$

where RELERR and ABSERR are the relative and absolute error bounds, respectively, specified by the user. This is a mixed relative-absolute error criterion that includes, as special cases, pure absolute error (RELERR = 0) and pure relative error (ABSERR = 0). The code does not attempt to control the global error directly, so it is not necessarily true that

$$|\vec{e}_{global}(i)| \leq \text{RELERR} \times |\vec{y}(i)| + \text{ABSERR}$$

at the end of the integration. For most practical problems this inequality is approximately true and RELERR and ABSERR are chosen accordingly.

In choosing an error criterion, Ref. 48 suggests the following rules of thumb: "If the solution changes a great deal in magnitude during the integration, and you wish to see this change, use relative error. But use caution, since pure relative error is not defined when the solution vanishes. If the solution does not vary much, or if you are not interested in it when it is small, use absolute error. A mixed criterion is probably best and safest choice."

In this study a mixed criterion is used in which the absolute error is set equal to the relative error (i.e., ABSERR = RELERR).

11.1.2 *Workspace Requirements*

The workspace requirements are defined as the length of the WORK array required by the solution subroutines to store all the information necessary to obtain the solution. The workspace requirements of DE/STEP are approximately 100 + 21*N, where $N = 2N_{DOF}$ is the number of equations. This is considerably smaller than the workspace requirements of the IMSL subroutine DNEQNF, which are roughly 3*N**2 + 15*N where $N = N_{DOF}(1 + 2N_H)$ is the number of equations. When seven rotating mode shapes are used to represent the blade flexibility (i.e., $N_{DOF} = 7$), the workspace requirements of DE/STEP are approximately 394. The workspace requirements of DNEQNF in this case are at least 19,000 (for $N_H = 5$). Thus the memory requirements of DE/STEP are less than 2% of those of DNEQNF.

11.2 VALIDATION OF THE TIME DOMAIN SOLUTION PROCEDURE

In order to validate the numerical integration procedure (DE/STEP) used in this study, the converged steady state solution obtained by numerically integrating the equations of motion is compared with the results obtained using the harmonic balance technique. Comparisons are made using the flexible blade configuration presented in Table 8, which represents a soft-in-plane rotor blade with uniform mass and stiffness.

As a first check of the ODE solver, the steady state trim and response solution obtained using the harmonic balance technique is used as input for the numerical integration procedure. Assuming the state space equations represented by Eq. (11.9) have been formulated correctly, the integrated response solution should compare very favorably with the harmonic balance result. Any differences displayed in the response results can be attributed to numerical integration error. Thus comparisons of the integrated response solution obtained using steady state initial conditions with the periodic response solution obtained using the harmonic balance technique should reveal the magnitude of the integration errors. Knowledge of the level of accuracy achieved by the numerical integration procedure is essential to properly select the magnitude of the error tolerance required by DE/STEP.

TABLE 8

Elastic blade data used in time domain integration

Dimensional Data

$R = 4.91m$
$\Omega = 425RPM$
$M_b = 53kg$

Nondimensional Data

Flight Data

$\mu = 0.3$

Rotor Data

$N_b = 4$	
$c_b = 2b = 0.05498$	$L_b = 1.0$
$X_A = 0.0$	$X_{lb} = 0.0$
$I_{MB2} = 0.0000$	$e = 0.0$
$I_{MB3} = 0.0004$	$\theta_{pt} = 0.0$
$\omega_F = 1.123, 3.41, 7.62$	$a_o = 2\pi$
$\omega_L = 0.732, 4.46$	$C_{do} = 0.01$
$\omega_T = 3.00, 8.55$	$C_{mo} = 0.0$
$\gamma = 5.5$	$\sigma = 0.07$

Helicopter Data

$C_W = 0.005$	$fC_{df} = 0.01A_R$
$X_{FA} = 0.0$	$Z_{FA} = 0.3$
$X_{FC} = 0.0$	$Z_{FC} = 0.3$

The deviation of the integrated response solution from the steady state solution was examined for three error tolerances: RELERR = ABSERR = 10^{-3}, 10^{-4} and 10^{-5}. The deviations in the tip displacements at the end of one revolution from their appropriate steady state values are shown in Fig. 87 for all three error tolerances. The deviations in the tip velocities are shown in Fig. 88. As expected the smallest deviations were obtained when using the smallest error tolerance 10^{-5}. Figures 87 and 88 reveal that the tip velocities deviate more significantly than the displacements from the appropriate steady state values. The magnitude of the deviation of the displacements was less than 1% for all three error tolerances. But only at the smallest error tolerance (10^{-5}) was the deviations in all three velocities under 1%. It should be noted, however, that the flap and lead-lag velocities are smaller in magnitude than the tip displacements, and thus exhibit higher relative error. This could be avoided using pure relative error (i.e., ABSERR = 0), but this would create problems if any of the state variables approached zero.

The number of integration steps and corresponding integration times per revolution required by DE/STEP to achieve a given error tolerance was also examined. The number of integration steps per revolution is presented in Fig. 89 for all three error tolerances considered. The corresponding integration times (CPU seconds) per revolution are shown in Fig. 90. These execution times are for an IBM ES9000 model 900 mainframe computer. As expected significantly more integration steps and longer integration times are required to obtain higher levels of numerical accuracy. It is interesting to note from Figs. 87 and 90 that a significant increase in numerical accuracy can be achieved by decreasing the error tolerance from 10^{-3} to 10^{-4} without incurring a substantial increase in integration time. However, decreasing the error tolerance further to 10^{-5} results in a relatively minor increase in numerical accuracy but a relatively large increase (by about 45%) in integration time.

Based on the comparison studies conducted, which are described above, the error tolerance ABSERR = RELERR = 10^{-4} was selected as a good compromise between numerical accuracy and integration time. Unless stated otherwise, this error tolerance is used throughout the rest of this study dealing with the numerical integration of the equations of motion. The level of numerical accuracy achieved using this error tolerance is considered to be acceptable; the tip displacements at the end of each revolution deviate from their steady state values by less than 0.25%, and the tip velocities deviate by less than 3%. A 3% deviation in the lead-lag velocity is considered acceptable due to the relatively small magnitude of this velocity component. The small increase in accuracy which could be achieved using the error tolerance 10^{-5} does not justify the substantial increase in required integration time.

The integrated response solution obtained using steady state initial conditions and an error tolerance of 10^{-4} is compared in Fig. 91 with the harmonic balance response solution. The figure shows that the response solutions are essentially identical, thus validating both the numerical integration procedure DE/STEP and the state-space form of the equations represented by Eq. (11.9).

As mentioned previously, the ODE solver DE/STEP does not attempt to control the global error directly, but only places constraints on the local error during each integration step. To demonstrate that the global error is bounded, and also to verify that the periodic response in Fig. 91 truly represents the converged solution, the deviation in the tip displacements and velocities at the end of each revolution are presented in Figs. 92 and 93, respectively, for the first ten rotor revolutions. It is evident from these two figures that the errors in the displacements and velocities remain bounded during the ten revolutions; the tip displacements at the end of each revolution differ from the steady state values by less than 0.5%, and the tip velocities differ by not much more than 3%. Therefore the steady state response solution obtained using the harmonic balance technique truly represents the converged periodic solution.

11.2.1 *Convergence to a Steady State Condition*

It was demonstrated in the previous section that the numerical integration procedure reproduces the steady state solution indefinitely when steady state conditions are used as input. The convergence of the numerical integration procedure to the appropriate steady state solution is investigated by starting the integration procedure at conditions which differ greatly from steady state conditions. This will also reflect upon the robustness of the integration procedure as far as numerical stability is concerned.

Implicit in the application of the harmonic balance technique is the assumption of a globally stable system. Although the stability of the system is investigated for small perturbations about the steady state condition, the stability of the system in the presence of large disturbances is not addressed. This may lead to doubts concerning whether the system will indeed approach a steady state condition without passing through an unstable region. Therefore in this section the equations of motion are integrated numerically in time using a zero initial condition vector to verify convergence to a steady state periodic solution when the initial conditions are far from the steady state values. This will also provide

a check on the convergence of the numerical integration procedure to a steady state solution.

When using a numerical integration scheme such as DE/STEP to obtain the steady state response solution it is necessary to define the convergence criteria used to determine when a steady state solution has been reached. Since a periodic solution is being sought, the blade response can be assumed to have converged when the no change is observed in the response over two successive revolutions. Recognizing the fact that the blade response during a given revolution is determined completely by the value of the state vector at the beginning of the revolution, the solution can be considered to have converged when the state vector at the end of the revolution matches its value at the beginning of the revolution. Since this will never be true exactly due to numerical integration errors (see Figs. 92 and 93), it is necessary to define acceptable levels of variation in the state vector of the converged solution from one revolution to the next. It is not necessary to examine each element of the state vector (which contains a total of seven generalized displacements and seven generalized velocities), but only the tip displacements and tip velocities.

In this study the response is assumed to have converged to a steady state solution when the maximum deviation in the tip displacements from one revolution to the next is no greater than 1%, and the maximum deviation observed in the tip velocities is no greater than 5%. These tolerances were established based on consideration of Figs. 92 and 93 for the error tolerance 10^{-4} .

The tip response solution obtained by integrating from a zero initial state vector is compared in Fig. 94 with the steady state response solution for the first two rotor revolutions. The figure shows that the flap and torsional responses quickly approach their steady state solutions, deviating only slightly by the end of the second revolution. However, the lead-lag responses differ considerably during the two revolutions; this is a well known behavior which is a result of the low levels of damping associated with this degree of freedom.

To examine more closely the rate of convergence of the integrated response solution to steady state conditions, the flap, lead-lag and torsional tip delflections at the end of each

rotor period are plotted in Fig. 95 for the first thirty revolutions. The tip deflections can be seen to oscillate about their steady state values with decaying amplitudes. These oscillations are due to the presence of transient blade dynamics with frequencies which are not integer multiples of the rotor frequency Ω. The rate at which these transients die out depends on their frequency and damping. The flap and torsional modes are very highly damped with frequencies greater than the rotor frequency Ω. Thus the flap and torsional responses converge fairly quickly (in about six revolutions) to their steady state solutions, as shown in Fig. 95. The lead-lag modes, on the other hand, are very lightly damped. Furthermore, the fundamental lead-lag mode has a rotating frequency much lower than the the rotor frequency. Therefore many rotor revolutions (about thirty) are required for the lead-lag transients to die out, which is quite evident from Fig. 95.

The number of integration steps required by DE/STEP during each of the first ten revolutions to integrate from a zero initial state is investigated in Fig. 96. The corresponding integration times (executed on the IBM ES9000 mainframe) are shown in Fig. 97. Though only an error tolerance of 10^{-4} has been used to obtain the blade response, required integration steps and times per revolution are also presented for error tolerances of 10^{-3} and 10^{-5} for comparison. The two figures show that many more integration steps and much longer integration times are required during the first few revolutions, when large changes in the blade response are occurring. After the first two revolutions the number of integration steps and integration time per revolution quickly approach the values associated with the converged solution, as shown in Figs. 87 and 88. It should be kept in mind that the steady state solution is periodic with many higher harmonic components. Thus even after convergence has occurred, many steps are required per revolution to properly capture its time varying nature.

Using the convergence criteria defined earlier in this section, the response of the system can be considered to have converged to a steady state solution from zero initial conditions in about thirty revolutions. DE/STEP required about 3,300 integration steps and an execution time of 23 CPU seconds (on the IBM ES9000 mainframe) for the error tolerance of 10^{-4}. This is comparable to the 21 CPU seconds required by the IMSL subroutine

DNEQNF when six harmonics are used. It should be noted, however, that while the convergence time of DNEQNF is relatively insensitive to the initial guess used, convergence of the integration procedure can be greatly accelerated through a more judicious selection of the initial condition vector.

The convergence to a trimmed rotor condition from a zero initial state is investigated in Figs. 98 and 99. The average values of the longitudinal and lateral hub shears over the first thirty revolutions are compared in Fig. 98 with the steady state (trimmed) values obtained using the harmonic balance technique. The average values of the rolling and pitching moments are likewise compared in Fig. 99. The comparisons reveal that, although there is significant deviation from a trimmed flight condition during the first few revolutions, force equilibrium is attained fairly quickly. Moment equilibrium appears to take much longer, but this is due to the fact that the moments are much smaller in magnitude and thus more sensitive to numerical errors.

Finally, the convergence of the 4/rev hub shears and moments to steady state values is investigated in Figs. 100 through 102. The amplitudes of the 4/rev hub loads during the first thirty revolutions are compared in these figures with the steady state values calculated using the harmonic balance technique. Examination of Figs. 100 through 102 reveals that the vibration magnitudes deviate substantially during the first few revolutions, when large changes in the blade response are taking place. These large deviations can be attributed to the presence of transient vibrations resulting from the transient blade dynamics. As these transients die out, the vibration levels eventually converge to the appropriate steady state values, as shown in Figs. 100 through 102.

11.3 TIME DOMAIN RESPONSE TO CONTROL

The optimal control strategy used in this study is based on a quasistatic frequency domain representation of the helicopter response to control. This representation is only strictly valid when relating the steady state response of the system to a periodic control input, and thus the resulting control strategy only addresses the reduction of the steady

state vibration levels. The need to address the transient vibrations is commonly eliminated by the quasistatic assumption, which assumes the system response is immediate with no time lag or transient dynamics. This is commonly justified by one or more of the following assumptions: 1) the magnitude of the transient vibrations are small compared to the steady state levels so they may be neglected; or 2) the transients are sufficiently damped and of high enough frequency (compared to Ω) such that the transient vibrations die out fairly quickly; or 3) the resulting control strategy will also produce reductions in the transient vibration levels. Figures 100 through 102 demonstrate that the transient vibrations are neither small nor do they die out very quickly. In addition, since the transient vibrations are generally not 4/rev in the fixed frame, it is unreasonable to expect them to respond to control in the same manner as the 4/rev steady state vibrations.

The validity of the optimal control strategy used in this study to control the steady state vibration levels, as well as the validity of the quasistatic assumption, is investigated in this section by implementing the control solution obtained in the frequency domain in the time domain. This is accomplished by numerically integrating the equations of motion in time from steady state initial conditions while applying the optimal control solution in open-loop mode starting at $\psi = (\Omega t) = 0$. The magnitudes of the 4/rev hub shears and moments during the first thirty revolutions are plotted in Figs. 103 through 105. Except for the yawing moment component, which shows a slight increase (by about 3%) during the first revolution, the figures depict immediate reductions in each of the 4/rev hub load components. After only two revolutions all vibration components have decreased to levels substantially below their baseline values. By the third revolution the vibration levels (excluding the yawing moment) are reduced to less than 20% of their baseline values, and to less than 10% by the tenth revolution. The smaller degree of reduction achieved in the 4/rev yawing moment is due to its relatively small baseline value.

It is evident from Figs. 103 through 105 that the controlled vibration levels do not immediately attain their final values when the control is applied. This is due to the presence of transient blade dynamics initiated by the change in the control input (from a zero control input to the optimal control input). This change alters the condition of the blade and thus

its steady state response. However, this new response cannot be attained instantaneously. The transient blade dynamics can be considered to "transport" the blade to the new steady state response. Thus the measured vibration levels will not attain their final values until all transients have died out. This must be kept in mind when implementing the control strategy in the closed-loop mode. Sufficient time must be allowed to elapse between control steps to allow the vibration levels to settle down to their steady state values each time the control is updated. Otherwise the feed-back controller could cause the system to become unstable.

Figures 103 through 105 demonstrate that the optimal control solution based on a linear, quasistatic frequency domain representation of the helicopter response to control produces substantial reduction in the vibration levels when applied in the open-loop mode in the time domain. However, these figures show that the system response is not immediate; quite a few rotor revolutions, around ten in the present case, must transpire before transient effects can be ignored. The quasistatic assumption may be considered to be valid when devising control strategies for controlling vibrations experienced in steady level flight, but an unsteady time domain control approach would be better suited to deal with the transient vibrations produced by sudden changes in flight condition or gusts.

Chapter XII

CONCLUDING REMARKS

This study has developed a rotor aeroelastic analysis capable of modeling the effects of individual blade control (IBC) in forward flight implemented through an actively controlled partial span trailing edge flap on each blade capable of introducing control for vibration reduction directly in the rotating reference frame. The analysis program also posseses the capability to implement conventional IBC, in which the pitch angle of each blade is controlled independently in the rotating frame for vibration reduction.

Two blade models incorporating fully coupled flap-lag-torsional dynamics were utilized to represent an isolated hingeless rotor blade. In the first stage of this research the feasibility of this new control approach was investigated using a simple offset-hinged spring restrained blade model blade model with three degrees-of-freedom representing the dynamics of the isolated blade. In the second stage, in which the practical aspects of implementation on a real rotor blade were studied, a realistic fully elastic blade model with seven rotating coupled modes representing blade flexibility was employed. In both cases the inertial loads were formulated in a straightforward manner using D'Alembert's principle, and an extention of Greenberg quasisteady aerodynamics which includes the effects of a flap were used to formulate the aerodynamic loads. Four blades were combined to represent a four-bladed hingeless rotor configuration in steady level flight. A fully coupled trim and response analysis was used based upon the harmonic balance technique.

Simultaneous reduction of the vibratory hub shears and moments was achieved by minimizing a quadratic cost functional consisting of the weighted sum of the squares of the vibration magnitudes and control input amplitudes. Two linear quasistatic frequency domain representations of the helicopter vibratory response to control were considered: a global model which assumed linearity over the entire range of control; and a local model based on a linearization of the system about the current control.

The most important conclusions obtained in this analytical study using the two blade models are presented below. These conclusions should be considered within the framework of the simplifying assumptions upon which the aeroelastic simulation was based.

Spring Restrained Blade Model

The global and local controllers implemented through an actively controlled flap located on each blade were employed to produce simultaneous reduction in the vibratory hub shears. The effectiveness of the actively controlled flap to reduce vibrations and the required control input angles and power expenditures were investigated. Comparisons with conventional IBC were carried out to determine the relative effectiveness and efficiency of the two approaches. The investigations were carried out over a range of blade fundamental rotating torsional frequencies. The most important conclusions are presented below.

(1) Comparisons of the relative vibration reduction effectiveness of control implemented through the actively controlled partial span trailing edge flap with conventional IBC revealed that comparable levels of vibration reduction can be achieved by the two control approaches. Thus the actively controlled flap is a very attractive device because it has no effect on the airworthiness when compared to conventional IBC.

(2) Comparisons of the maximum input angles and the power requirements needed to implement both contol approaches were conducted. Obviously larger control angles were required for the actively controlled flap, however these angles were quite practical. The power required to implement conventional IBC was between 7 to 12 times larger than that required for the actively controlled flap. Therefore the actively controlled flap is a much more efficient means for vibration reduction in helicopters than conventional IBC.

(3) The vibration reduction characteristics of both global and local controllers were considered. While both controllers were effective in producing substantial vibration reduction, the local controller provided better vibration reduction in each case.

(4) A detailed examination of the influence of the torsional stiffness of the blade on vibration reduction effectiveness was conducted. It was found that as the torsional stiffness

of the blade is increased, larger control input angles and more power were required to achieve roughly the same degree of vibration reduction. The best vibration reduction was achieved for a fairly flexible blade configuration in torsion. This observation is consistent with the findings of Ref. 28.

Fully Elastic Blade Model

The local controller was employed to simultaneously reduce the vibratory hub shears and moments using the actively controlled flap and conventional IBC. Practical issues concerning the implementation of control through an actively controlled flap on a flexible blade were considered. These included: (a) the specific spanwise location of the trailing edge flap; (b) the effect of hinge moment correction; (c) the effects of compressibility, and (d) the importance of the span and chord length of the trailing edge flap. These investigations were carried out over a range of blade torsional frequencies. The most important conclusions obtained in this analytical study are presented below.

(1) Comparing the vibration reduction effectiveness of the actively controlled flap with conventional IBC revealed that approximately the same degree of vibration reduction can be achieved using either approach when implemented on the fully elastic blade. Furthermore, comparisons of power requirements demonstrated that the actively controlled flap required substantially less power, between 4% and 16% of the power required to implement conventional IBC. Thus the comparisons performed using the flexible blade model validate the results of the first stage of the feasibility study that *the actively controlled flap is a very attractive device for vibration reduction, both due to its power efficiency and because it has no effect on the airworthiness when compared to conventional IBC.*

(2) The uncontrolled vibration levels obtained using the fully elastic blade model and the spring restrained blade model were compared. It was found that the increase in the dynamic modeling capability available with the fully elastic blade model results in a dramatic increase in the calculated amplitudes of the vibratory hub loads. Comparing the control studies performed using the two blade models, however, revealed that despite the much higher vibration levels in the case of the flexible blade model, both control approaches

were still very effective in reducing the vibrations, without significant increases in the input amplitudes or power consumption compared to the spring restrained blade model.

(3) A detailed examination of the influence of the blade torsional stiffness on the vibration reduction potential of the actively controlled trailing edge flap was conducted using both blade models. It was found that as the torsional stiffness of the blade increased, both blade models exhibited a decrease in the effectiveness of the control flap and an accompanying increase in power requirements. However, the decrease in the effectiveness and increase in power requirements evident in the flexible blade model is much less severe than that observed using the spring restrained blade model.

(4) The importance of the spanwise location of the control flap was also considered. It was found that the vibration reduction effectiveness and power requirements of the control flap are strongly influenced by its spanwise location on the flexible blade. Thus the specific spanwise location of the actively controlled flap on the blade span is a very important design consideration. This sensitivity to the spanwise location of the control flap, which results from the interaction of the fundamental torsional mode and the second flap and lead-lag bending modes of the blade, is not displayed in the spring restrained blade model. Thus the flexible blade model provides a much better representation of the dynamics of a real helicopter blade.

(5) The importance of the aerodynamic hinge moment correction factor and compressibility correction in the vibration reduction potential of the actively controlled flap were investigated using the flexible blade model. It was found that these two parameters play a small but potentially significant role.

(6) The effect of varying the span and chord length of the trailing edge flap was investigated. It was found that in most cases changing the size of the control flap had little effect on its potential to reduce vibrations, but had a substantial impact on the associated power requirements and control input amplitudes.

Time Domain Solution

In the final stage of this study, the nonlinear equations of motion of the fully elastic blade model were integrated directly in time to validate the results obtained in the frequency domain. The most important conclusions are presented below.

(1) Solution of the aeroelastic response problem through direct numerical integration of the nonlinear equations of motion in the time domain is more efficient in terms of memory usage than the harmonic balance technique, but is about as computationally intensive, in terms of CPU time.

(2) The optimal control solution obtained from the frequency domain successfully reduces the steady state vibration levels when implemented in the time domain.

(3) The quasistatic assumption made in the representation of the steady state response of the helicopter to periodic control is adequate for controlling steady state vibrations, but is not valid when attempting to control transient vibrations.

REFERENCES

1. Blevins, R.D., Formulas for Natural Frequency and Mode Shape, Van Nostrand Reinhold Company, 1979.

2. Carnahan, B., Luther, H.A., and Wilkes, J.O., " Applied Numerical Methods , " John Wiley and Sons, Inc., New York, 1969.

3. Celi, R., " Aeroelasticity and Structural Optimization of Helicopter Rotor Blades With Swept Tips, " Ph.D. Dissertation, Mechanical, Aerospace, and Nuclear Engineering Department, University of California, Los Angeles, California, October 1987.

4. Celi, R. and Friedmann, P.P., " Rotor Blade Aeroelasticity in Forward Flight with an Implicit Aerodynamic Formulation, " AIAA Journal , Vol. 26, No. 12, December 1988, pp. 1425-1433.

5. Chopra, I., and McCloud, J.L., " A Numerical Simulation Study of Open-Loop, Closed-Loop and Adaptive Multicyclic Control Systems, " AHS Journal , Vol. 28, No. 1, January 1983, pp 63-67.

6. Crespo Da Silva, M.R.M. and Hodges, D.H., " The Role of Computerized Symbolic Manipulations in Rotorcraft Dynamic Analysis, " Computer and Mathematics with Application 12A, pp 161-172, 1986.

7. Davis, M.W., " Refinement and Evaluation of Helicopter Real-Time Self-Adaptive Active Vibration Control Algorithms, " NASA CR 3821, August 1984.

8. Dinyavari, M.A.H., " Unsteady Aerodynamics in Time and Frequency Domains for Finite-Time Arbitrary Motion of Rotary Wings Blade Aeroelasticity, " Ph.D. Dissertation, Mechanical, Aerospace and Nuclear Engineering Department, UCLA, December 1984.

9. Friedmann, P.P., " Recent Trends in Rotary-Wing Aeroelasticity, " Vertica , Vol. 11, No. 1/2, pp 139-170, 1987.

10. Friedmann, P., " Helicopter Vibration Reduction Using Structural Optimization With Aeroelastic/Multidisciplinary Constraints - A Survey, " Journal of Aircraft , Vol. 28, No. 1, January 1991, pp 8-21.

11. Friedmann, P.P., " Formulation and Solution of Rotary-Wing Aeroelastic Stability and Response Problems, " Vertica , Vol. 7, No. 2, 1983, pp 101-141.

12. Friedmann, P. and Kottapalli, S.B.R., " Coupled Flap-Lag-Torsional Dynamics of Hingeless Rotor Blade in Forward Flight. " Journal of the American Helicopter Society , Vol. 27, No. 4, Oct. 1982, pp. 28-36.

13. Friedmann, P., Hammond, C.E., and Woo, T., " Efficient Numerical Treatment of Periodic Systems with Application to Stability Problems, " International Journal of Numerical Methods in Engineering , No. 11, 1977, pp 1117-1136.

14. Friedmann, P.P. and Hodges, D.H., " Rotary-Wing Aeroelasticity with Application to VTOL Vehicles, " Flight-Vehicle Materials, Structures, and Dynamics, Vol. 5, Structural Dynamics and Aeroelasticity , A.K. Noor and S.L. Venneri Editors, published by ASME 1993, pp. 299-391.

15. Friedmann, P. and Yuan, C., " Effect of Modified Aerodynamic Strip Theories on Rotor Blade Aeroelastic Stability, " AIAA Journal , Vol. 15, No. 7, July 1977, pp. 932-940.

16. Friedmann, P., Yuan, K., Millott, T., and Venkatesan, C., "Aeroelastic Response and Stability Correlation Studies for Hingeless Rotors in Forward Flight," to be published as AIAA paper No. 94-1722 in the proceedings of the AIAA Dynamics Specialists Conference, Hilton Head, South Carolina, April 21-22, 1994.

17. Gray, R., and Davies, D.E., " Comparison of Experimentally and Theoretically Determined Values of Oscillatory Aerodynamic Control Surface Hinge Moment Coefficients, " RAE Technical Report 72023, March 1972.

18. Greenberg, J.M., " Airfoil in Sinusoidal Motion in a Pulsating Stream, " NACA-TN 1326, 1947.

19. Greenwood, D.T., Principles of Dynamics , Prentice-Hall, Inc., 1988.

20. Ham, N., " Helicopter Individual-Blade Control and its Applications, " 39th AHS Forum, St. Louis, Missouri, May 1983.

21. Ham, N.D., " Helicopter Individual-Blade-Control Research at MIT 1977-1985, " Vertica , Vol. 11, No. 1/2, pp. 109-122, 1987.

22. Jacklin, S.A., Leyland, J.A. and Blaas, A., " Full-Scale Wind Tunnel Investigation of a Helicopter Individual Blade Control System, " AIAA Paper 93-1361 CP, Proceedings of the 34th AIAA/ASME/ASCE/AHS/ASC Structures, Structural Dynamics and Materials Conference, La Jolla, CA, April 19-22, 1993, pp 576-582.

23. Jacob, H.G., and Lehmann, G., " Optimization of Blade Pitch Angle for Higher Harmonic Rotor Control, " Vertica , Vol. 7, No. 3, 1983, pp 271-286.

24. Johnson, W., " Self-Tuning Regulators for Multicyclic Control of Helicopter Vibrations, " NASA Technical Paper 1996, 1982.

25. Johnson, W., Helicopter Theory , Princeton University Press, 1980.

26. Kretz, M., " Research in Multicyclic and Active Control of Rotary-Wings, " Vertica , Vol. 1, No. 1/2, pp. 95-105, 1986.

27. Lehmann, G., " The Effect of Higher Harmonic Control (HHC) on a Four-Bladed Hingeless Model Rotor, " Vertica , Vol. 9, No. 3, 1985, pp 273-284.

28. Lemnios, A.Z., Smith, A.F., " An Analytical Evaluation of the Controllable Twist Rotor Performance and Dynamic Behavior, " Kaman Report R-794, 1972.

29. Loewy, R.G., " Helicopter Vibrations: A Technological Perspective, " AHS Journal . Vol. 29, October 1984, pp 4-30.

30. McCloud, J.L. III, and Kretz, M., " Multicyclic Jet-Flap Control for Alleviation of Helicopter Blade Stresses and Fuselage Vibration, " Rotorcraft Dynamics, NASA SP-352, 1974, pp 233-238.

31. Miao, W., Kottapalli, S.B.R., and Frye, H.M., " Flight Demonstration of Higher Harmonic Control (HHC) on S-76, " 42nd AHS Forum, Washington, D.C., June 1986, pp. 777-791.

32. Millott, T., and Friedmann, P., "Vibration Reduction in Helicopter Rotors Using an Active Control Surface Located on the Blade," AIAA paper No. 92-2451, Proceedings of the 33rd AIAA/ASME/ASCE/AHS Structures, Structural Dynamics and Materials Conference, Dallas, Texas, April 1992, pp 1975-1988.

33. Miura, H., " Application of Numerical Optimization Methods to Helicopter Design Problems-A Survey, " Vertica , Vol. 9, No. 2, 1985, pp 141-154.

34. Molusis, J.A., " The Importance of Nonlinearity on the Higher Harmonic Control of Helicopter Vibration, " 39th AHS Forum, St. Louis, Missouri, May 1983.

35. Molusis, J.A., Hammond, C.E., and Cline, J.H., " A Unified Approach to the Optimal Design of Adaptive and Gain Scheduled Controllers to Achieve Minimum Helicopter Vibration, " AHS Journal , Vol. 28, No. 2, April 1983, pp 9-18.

36. Nguyen, K., and Chopra, I., " Application of Higher Harmonic Control (HHC) to Rotors Operating at High Speed and Thrust, " Journal of the American Helicopter Society , Vol. 35, No. 3, July 1990, pp 78-89.

37. Ormiston, R.A. and Hodges, D.H., " Linear Flap-Lag Dynamics of Hingeless Helicopter Rotor Blades in Hover, " Journal of the American Helicopter Society , Vol. 17, No. 2, pp. 2-15, April 1972.

38. Papavassiliou, I., " Nonlinear Coupled Rotor-Fuselage Vibration Analysis and Higher Harmonic Control Studies for Vibration Reduction in Helicopters, " Ph.D. Dissertation, Mechanical, Aerospace and Nuclear Engineering Department, University of California, Los Angeles, California, 1991.

39. Papavassiliou, I., Friedmann, P.P., and Venkatesan, C., " Coupled Rotor/Fuselage Vibration Reduction Using Multiple Frequency Blade Pitch Control, " Paper No. 91-76, Proceedings of the Seventeenth European Rotorcraft Forum, September 24-26, Berlin; Germany, pp 91-76.1 - 91-76.44.

40. Polychroniadis, M., and Achache, M., " Higher Harmonic Control: Flight Tests of an Experimental System on SA 349 Research Gazelle, " 42nd AHS Forum, Washington, D.C., June 1986.

41. Reichert, G., " Helicopter Vibration Control-A Survey, " Vertica , Vol. 5, No 1, pp 1-20, 1981.

42. Richer, P., Eisbrecher, H.H., and Kloppel, V., " Design and First Tests of Individual Blade Control Actuators, " Proceedings of the 16th European Rotorcraft Forum, Sept. 18-20, 1990, Glasgow, United Kingdom, pp III 6.3.1 - III 6.3.9.

43. Robinson, L., and Friedmann, P.P., " Analytical Simulation of Higher Harmonic Control Using a New Aeroelastic Model, " Proceedings of the 30th AIAA/ASME/ASCE/AHS/ACS Structures, Structural Dynamics and Matrerials Conference, Mobile, Alabama, April 1989. AIAA Paper No. 89.1321.

44. Robinson, L., and Friedmann, P.P., " A Study of Fundamental Issues in Higher Harmonic Control Using Aeroelastic Simulation, " Journal of the American Helicopter Society , Vol. 36, No. 2, April 1991, pp 32-43.

45. Robinson, L.H., " Aeroelastic Simulation of Higher Harmonic Control, " Ph.D. Dissertation, Mechanical, Aerospace and Nuclear Engineering Department, UCLA, December 1989.

46. Rosen, A., and Friedmann, P.P., " Nonlinear Equations of Equilibrium for Elastic Helicopter or Wind Turbine Blades Undergoing Moderate Deformations, " NASA CR-159478, December 1978.

47. Shamie, J., and Friedmann, P., " Effect of Moderate Deflections on the Aeroelastic Stability of a Rotor Blade in Forward Flight, " Paper No. 24, Proceedings of the 3rd European Rotorcraft and Powered Lift Aircraft Forum, Aix-en-Provence, France, September 1977.

48. Shampine, L.F. and Gordon, M.K., Computer Solution of Ordinary Differential Equations-The Initial Value Problem , W.H. Freeman and Co., San Francisco, CA, 1975.

49. Shaw, J., Albion, A., Hanker, E.J., and Teal, R., " Higher Harmonic Control: Wind Tunnel Demonstration of Fully Effective Vibratory Hub Force Suppression, " AHS Journal , Vol. 34, No. 1, January 1989, pp 14-25.

50. Takahashi, M.D. " Active Control of Helicopter Aeromechanical and Aeroelastic Instabilities, " Ph.D. Dissertation, Mechanical, Aerospace and Nuclear Engineering Department, UCLA, June 1988.

51. Taylor, R.B., Farrar, F.A., and Miao, W., " An Active Control System for Helicopter Vibration Reduction by Higher Harmonic Pitch, " AIAA paper No. 80-0672, 36th AHS Forum, Washington, D.C., May 1980.

52. Theodorsen, T., " General Theory of Aerodynamic Instability and the Mechanism of Flutter, " NACA Report No. 496, 1935.

53. Venkatesan, C., and Friedmann, P., " Aeroelastic Effects in Multi-Rotor Vehicles With Application to a Hybrid Heavy Lift System. Part I: Formulation of Equations of Motion, " NASA Contractor Report 3822, August 1984.

54. Wempner, G., Mechanics of Solids with Application to Thin Bodies , McGraw-Hill, Inc., 1973.

55. White, R.B., and Landahl, M., " Effect of Gaps on the Loading Distribution of Planar Lifting Surfaces, " AIAA Journal , Vol. 6, No. 4, 1968, pp 626-631.

56. Wood, E.R., and Powers, J.H., " Practical Design Considerations for a Flightworthy Higher Harmonic Control System, " 36th AHS Forum. Washington, D.C., May 1980.

57. Wood, E.R., Powers, J.H., Cline, J.H., and Hammond, C.E., " On Developing and Flight Testing a Higher Harmonic Control System, " AHS Journal , Vol. 30, No. 1, January 1985, pp 3-20.

58. _____, " IMSL Library: Reference Manual, " IMSL Inc., Houston, Texas, 1980.

59. _____, " MACSYMA: Reference Manual, " Symbolics Inc., June 1986.

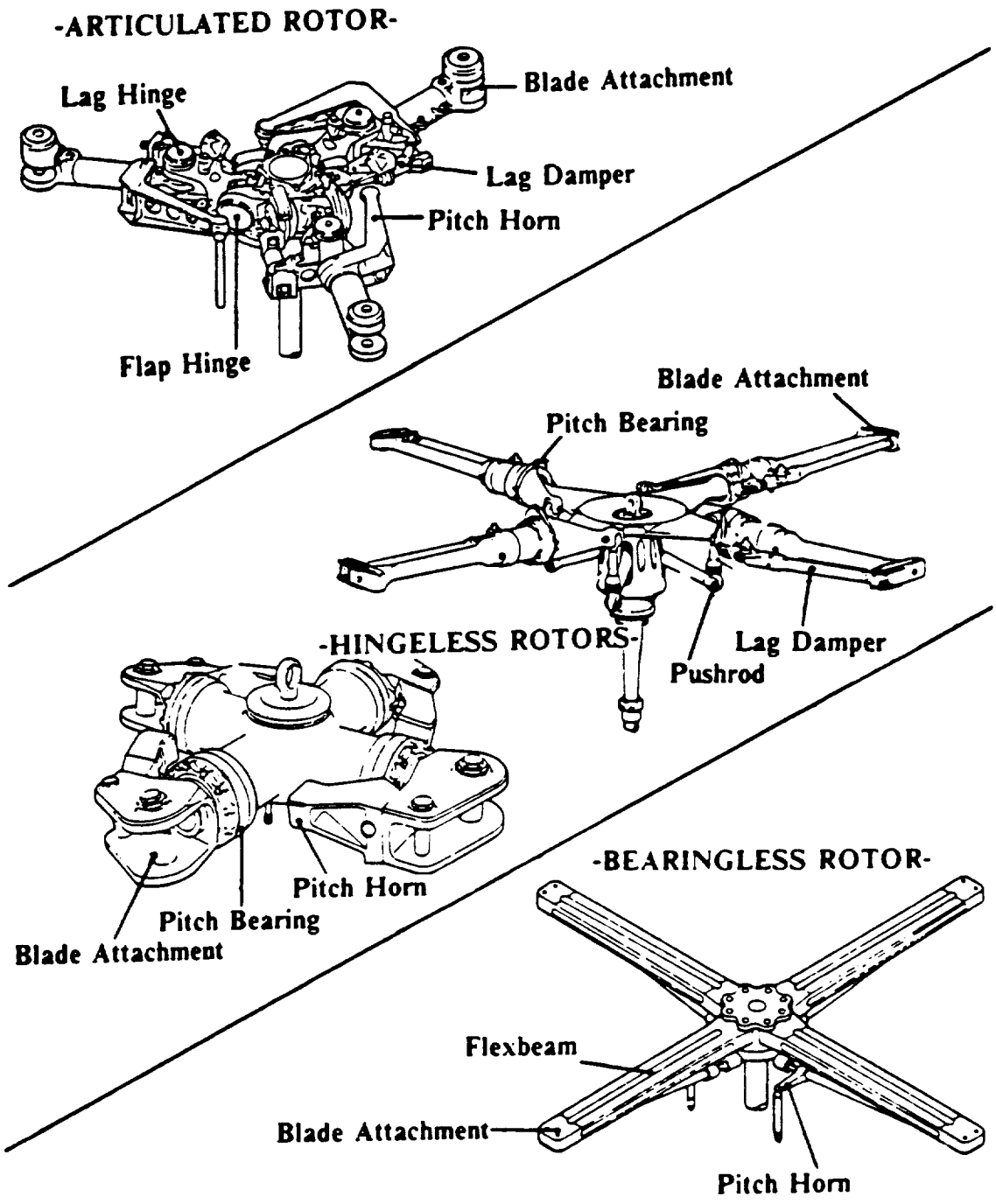

Figure 1: Schematics of typical articulated, hingeless and bearingless rotors

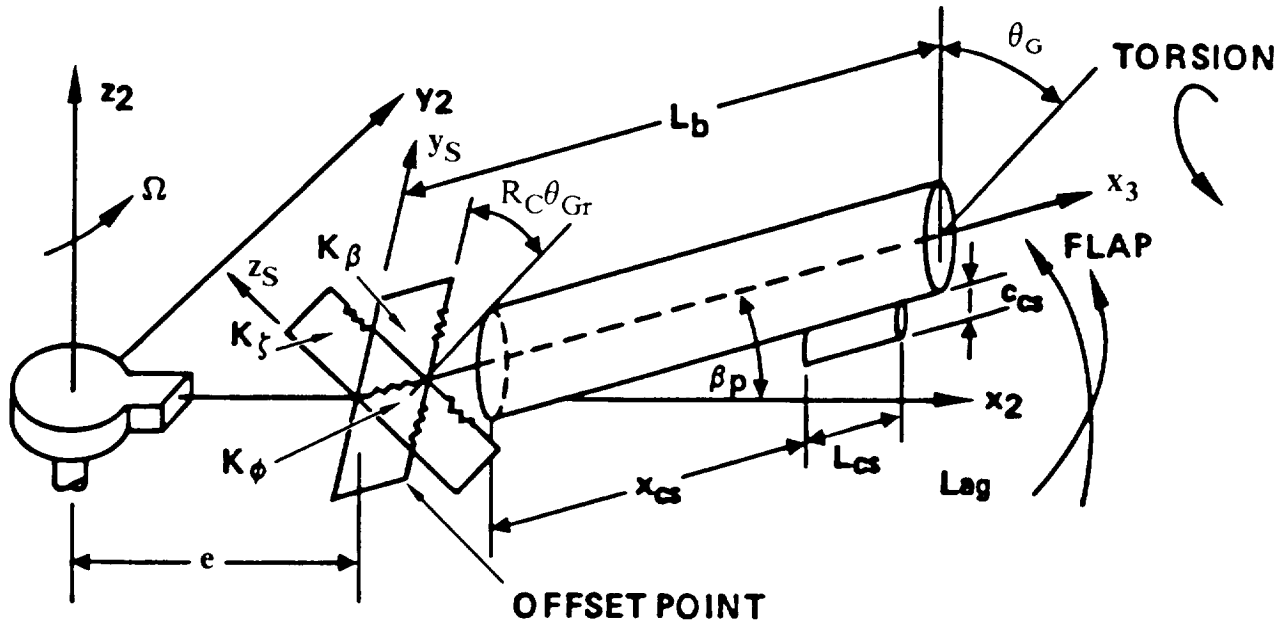

Figure 2: Offset-hinged spring restrained blade model incorporating a partial span trailing edge flap

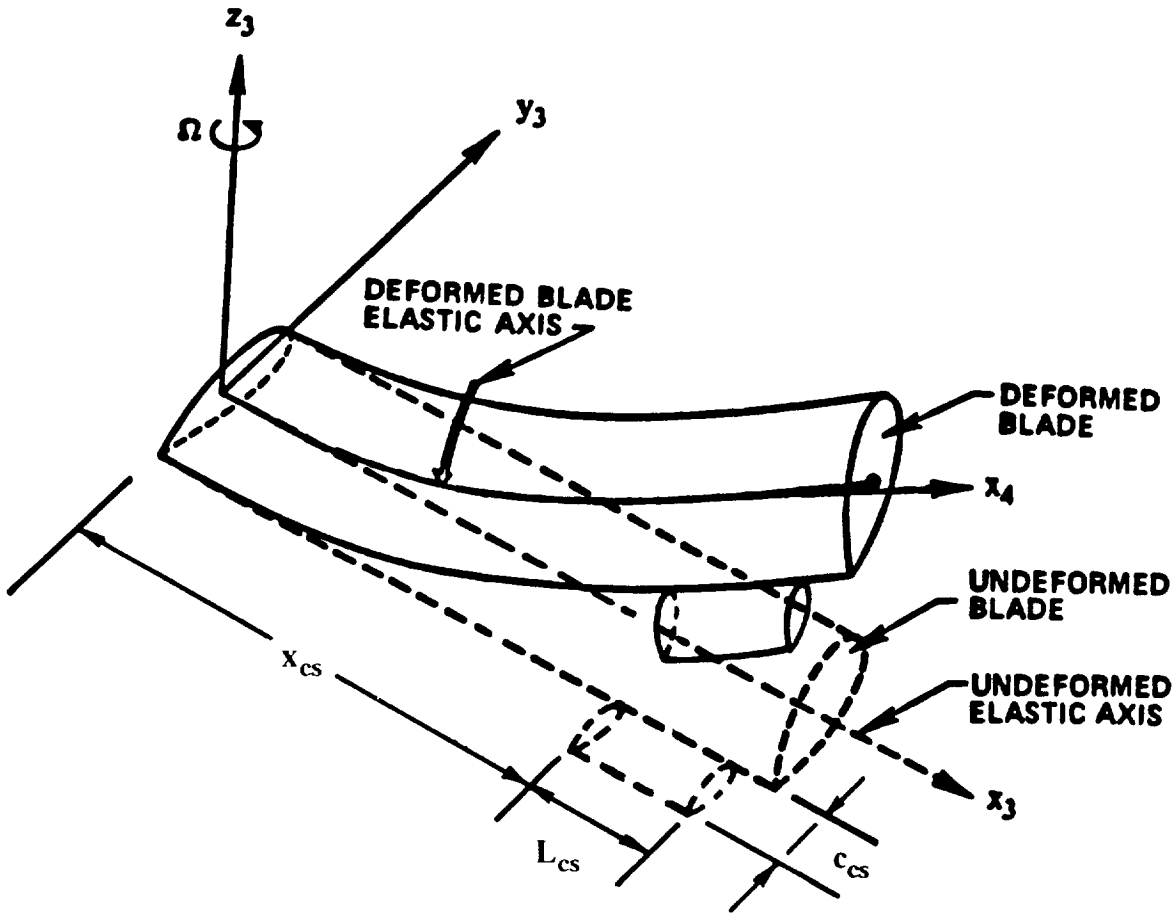

Figure 3: Fully elastic blade model incorporating a partial span trailing edge flap

O_H - **Hub Center**

E - Hinge Offset Point

C.G.- Fuselage Center of Mass

A.C.- Aerodynamic Drag Center of the Fuselage

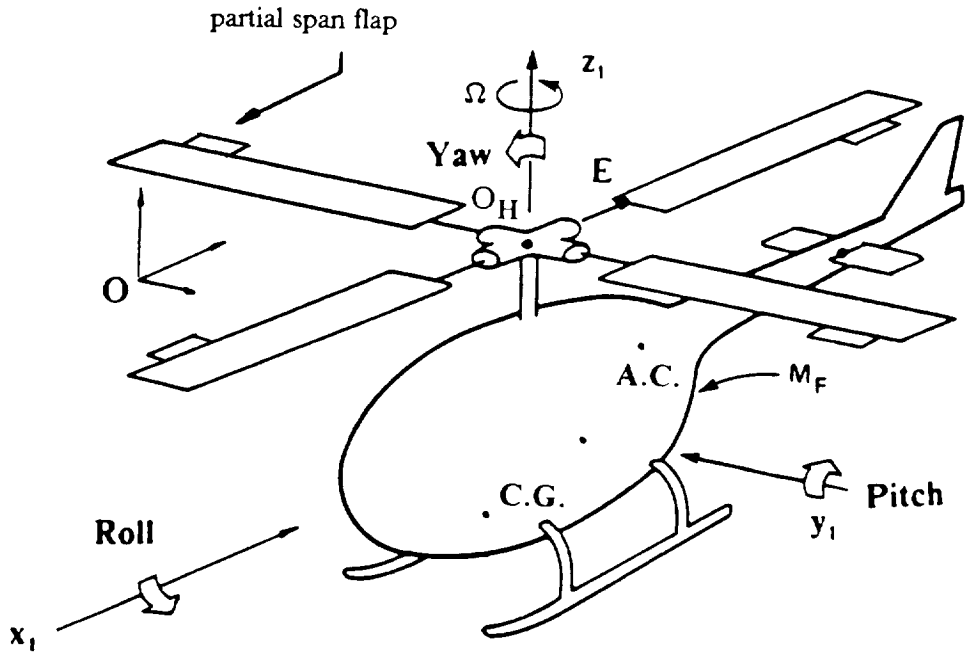

Figure 4: Schematic of a four-bladed helicopter

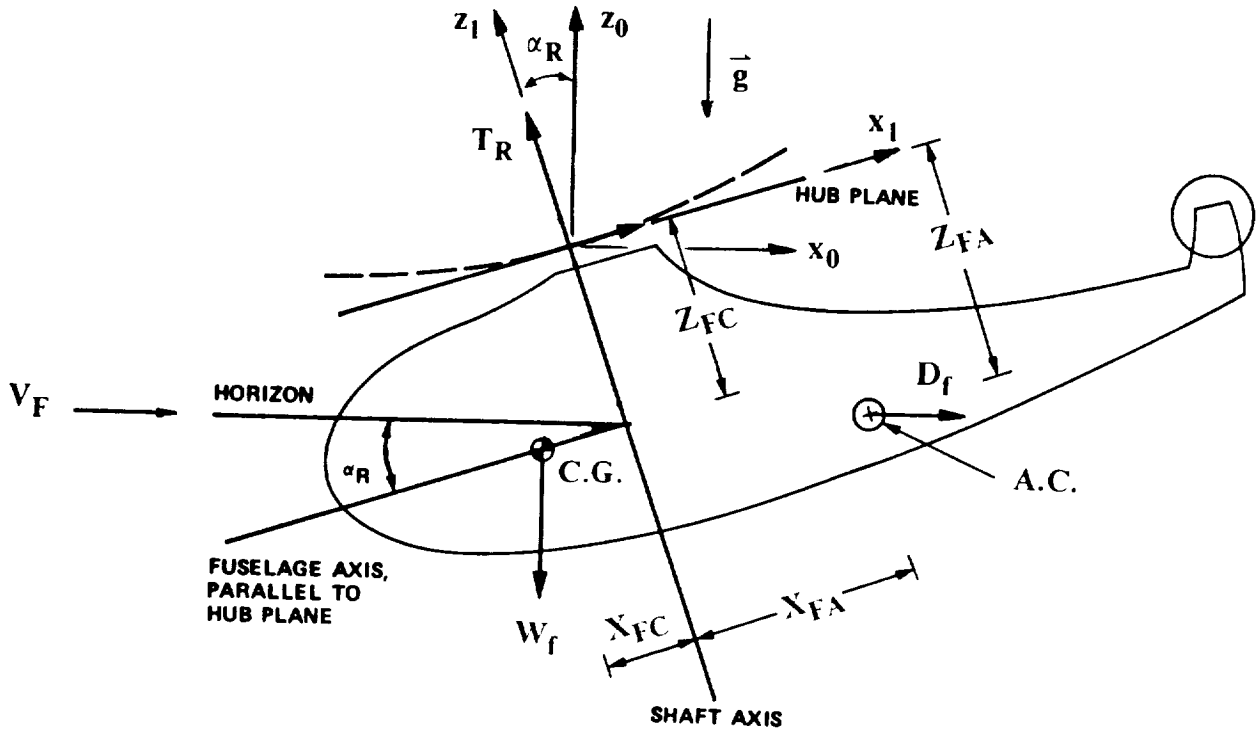

Figure 5: Schematic of helicopter in level forward flight

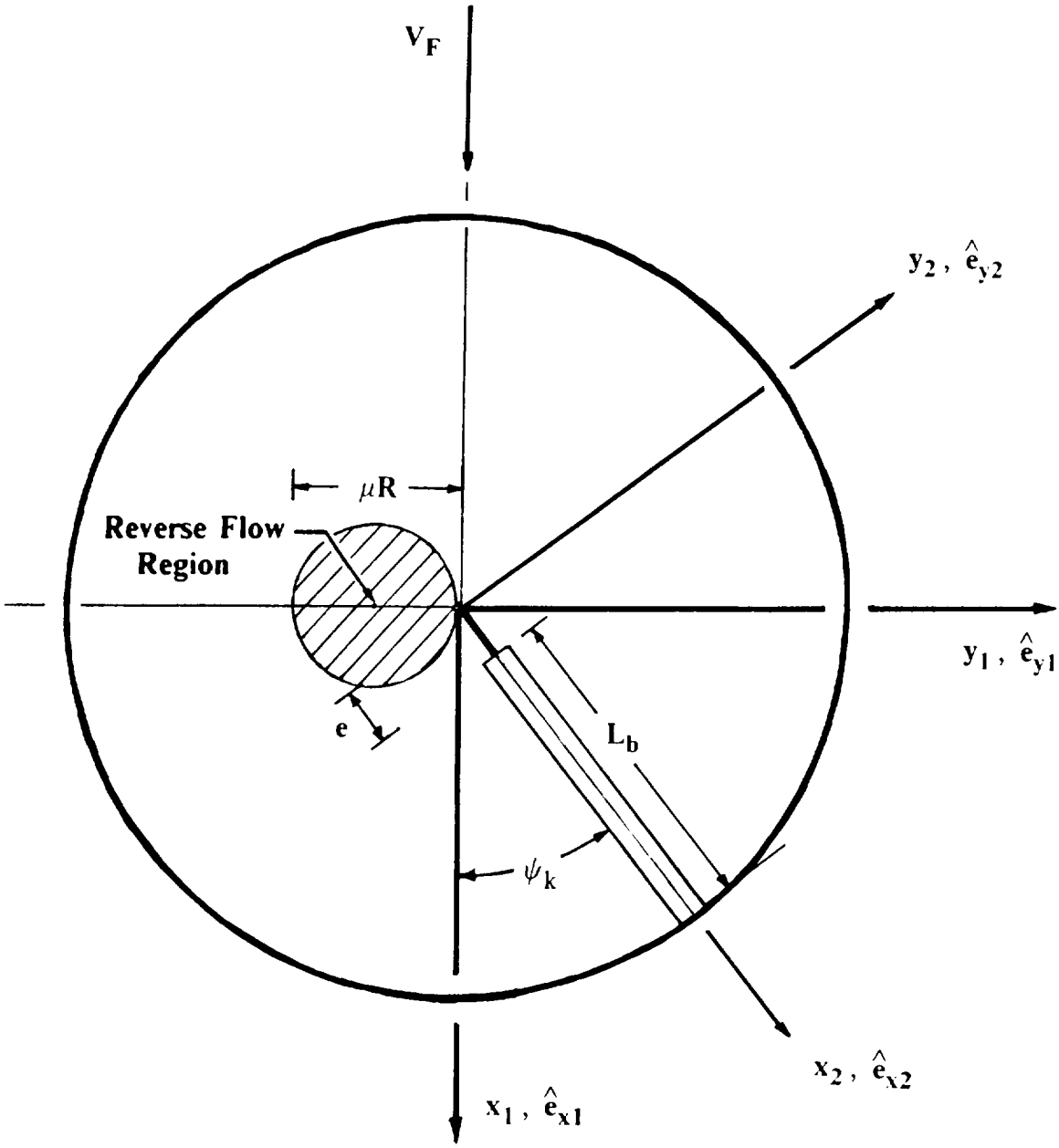

Figure 6: Schematic of the hub-fixed non-rotating reference frame and the blade fixed rotating reference frame

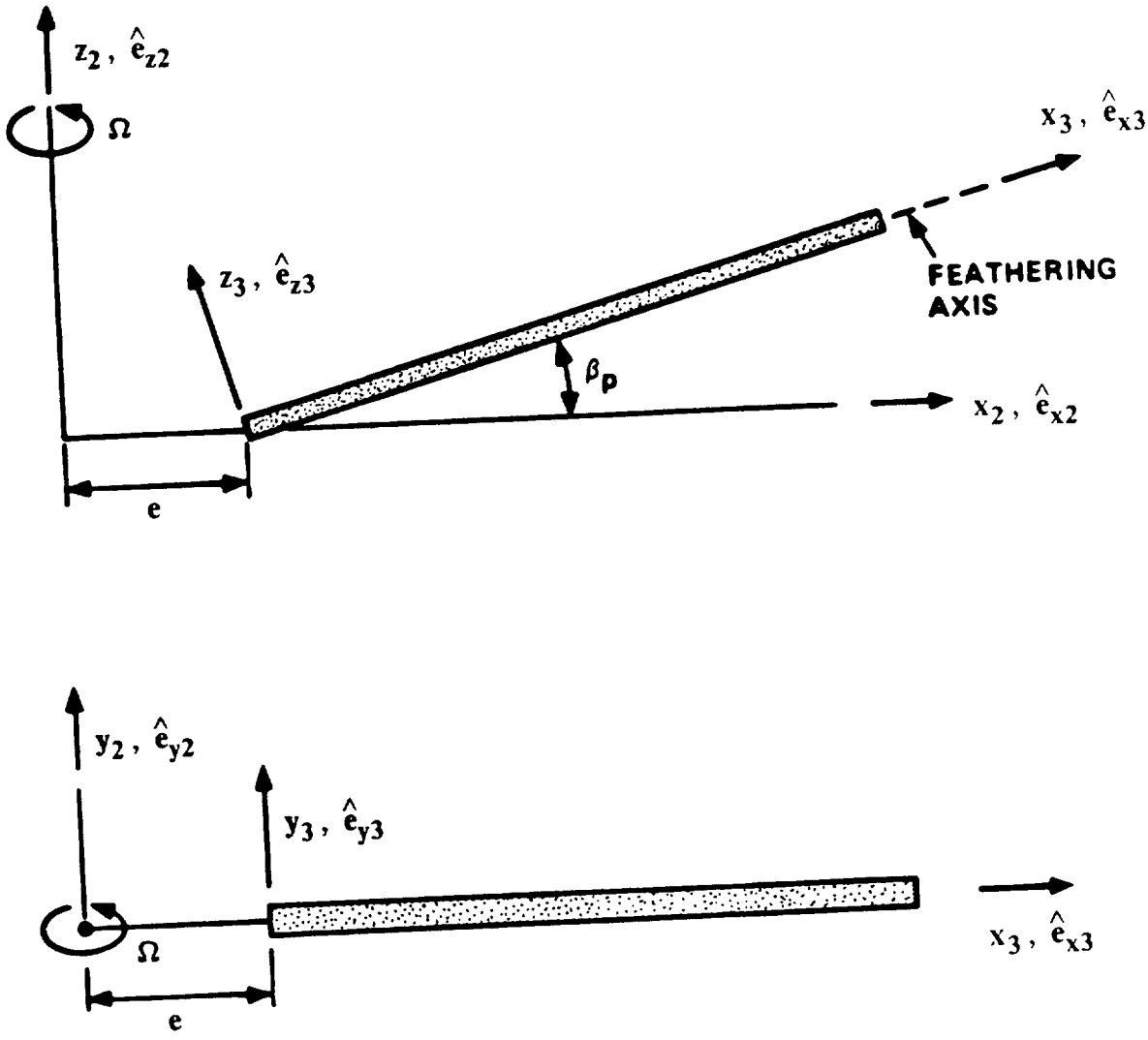

Figure 7: Geometry of the undeformed blade in the rotating reference frame

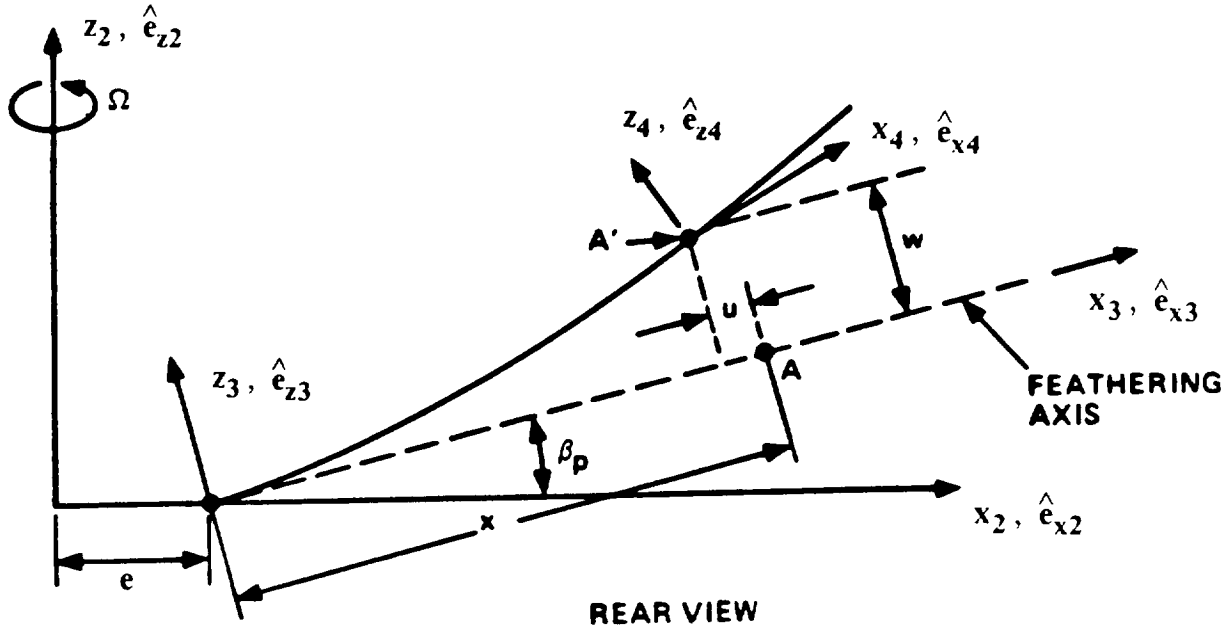

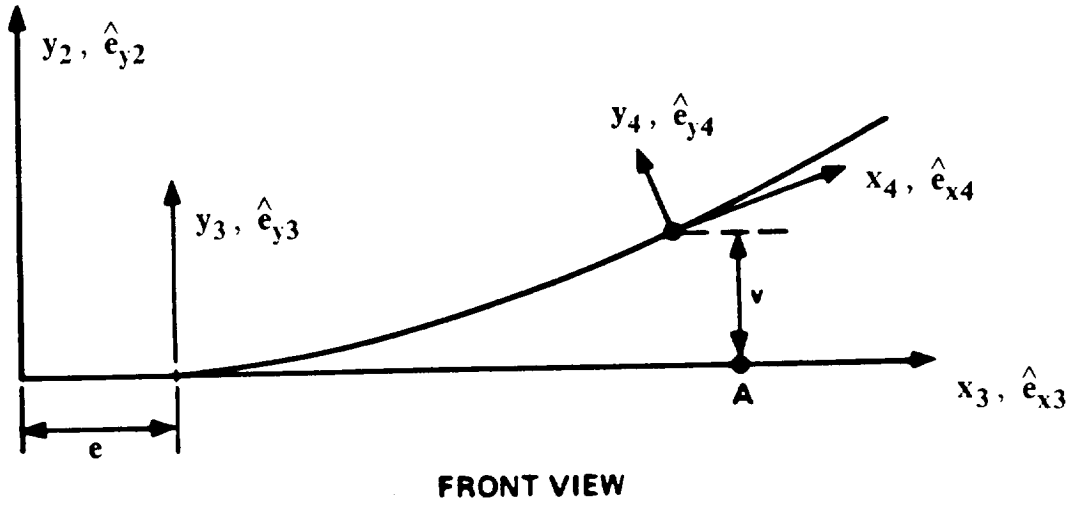

Figure 8: Geometry of the undeformed and deformed elastic axis of the blade

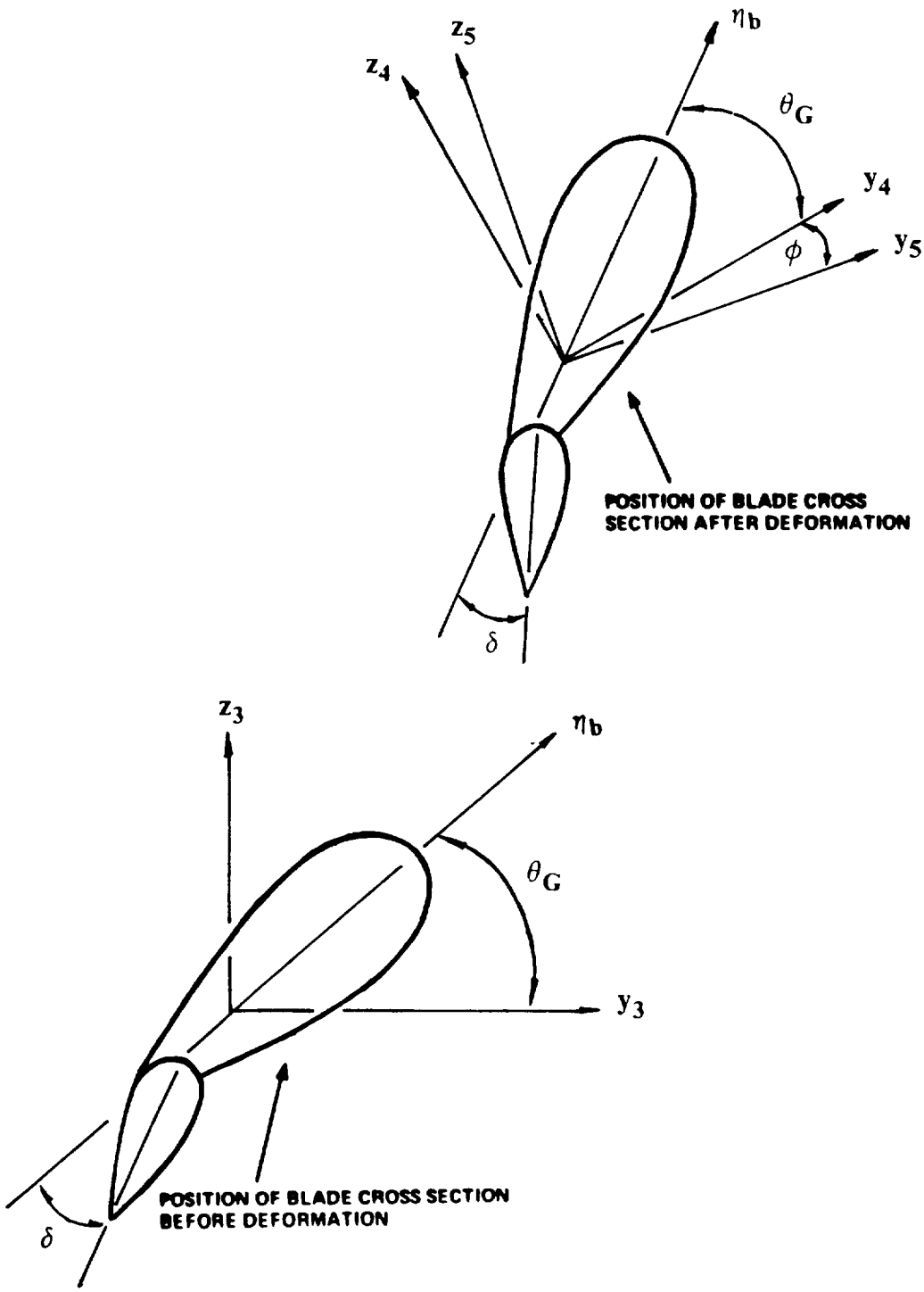

Figure 9: Geometry of the undeformed and deformed blade cross-section

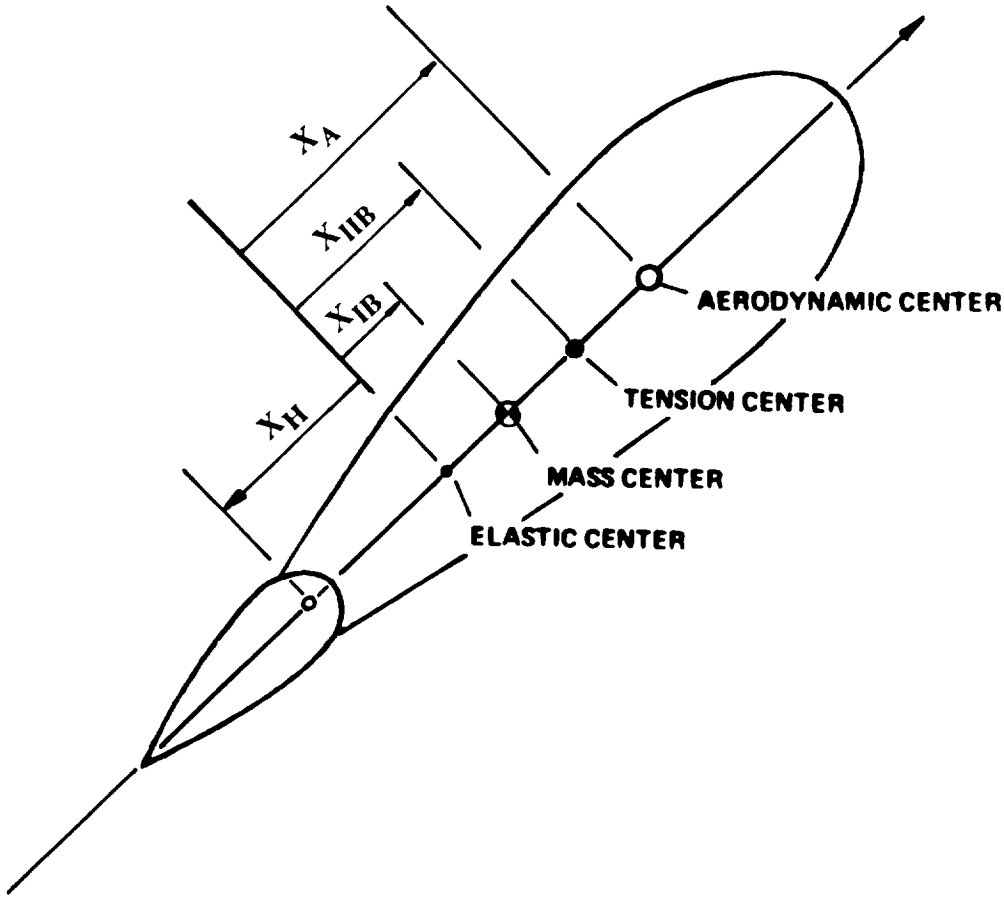

Figure 10: Schematic of various points on the blade cross-section

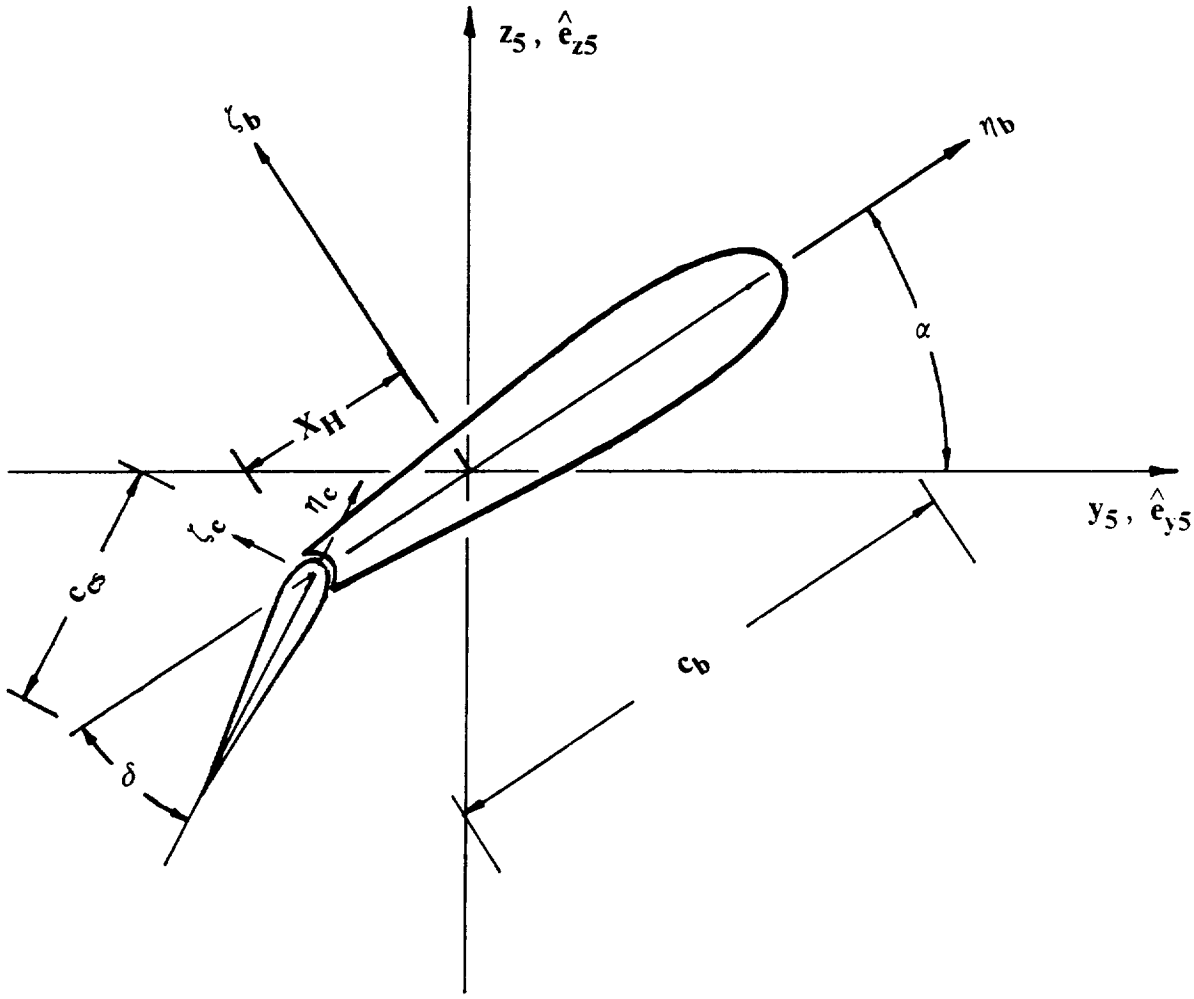

Figure 11: Schematic of the blade cross-section incorporating a trailing edge flap

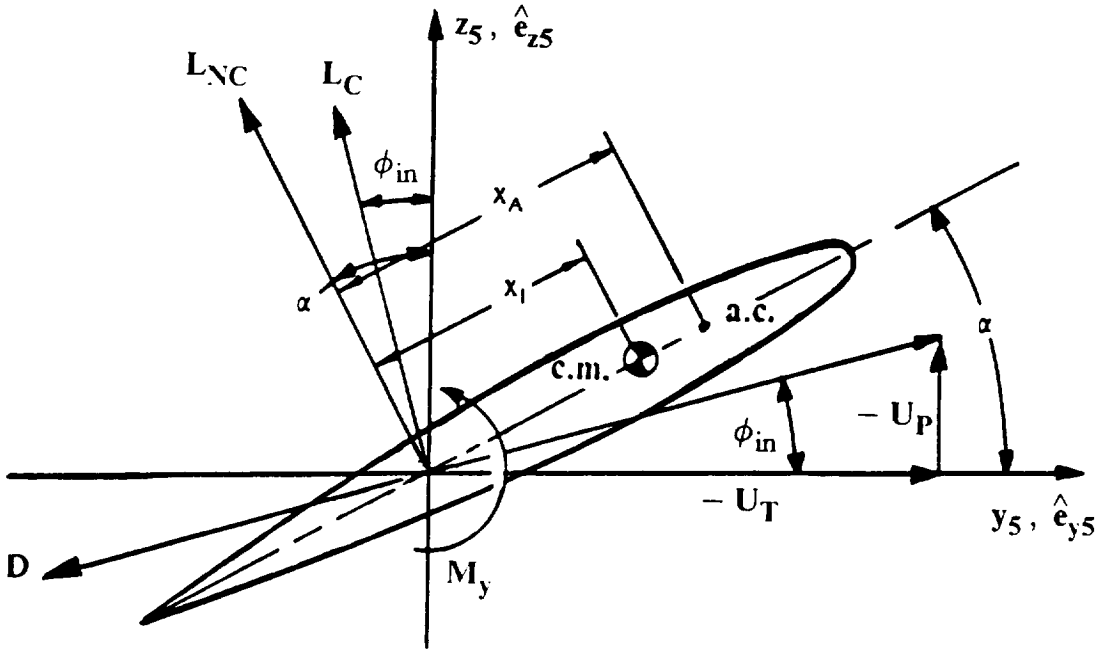

Figure 12: Schematic showing orientation of tangential and perpendicular air velocities and aerodynamic loads

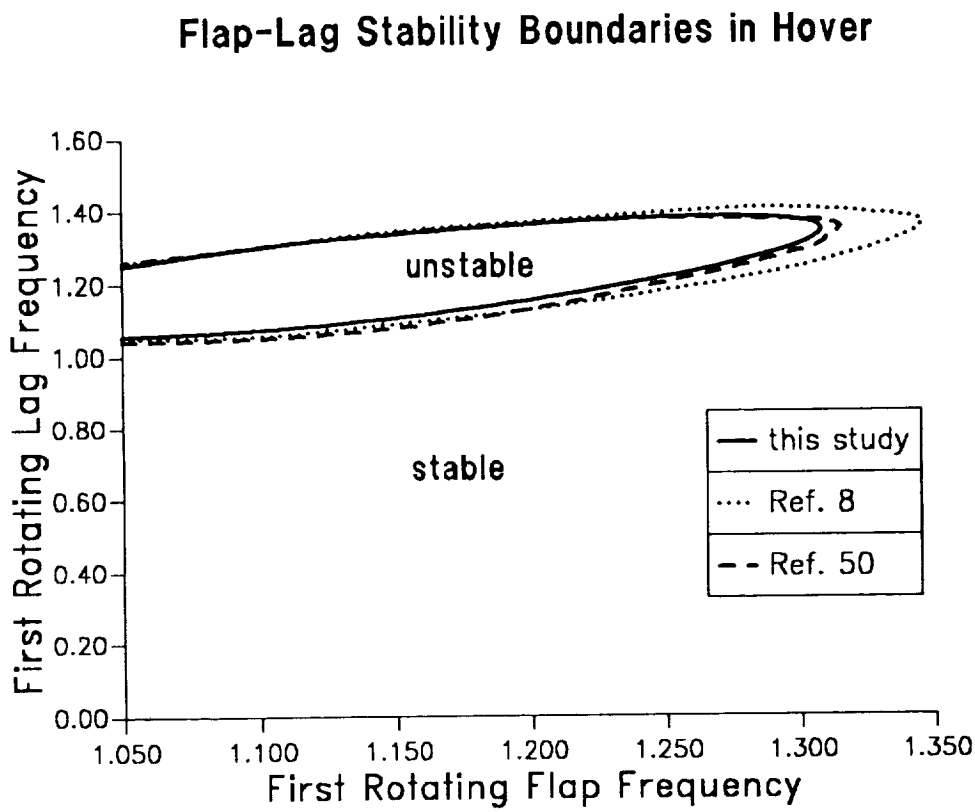

Figure 13: Flap-lag stability boundaries in hover for the offset-hinged spring restrained blade model

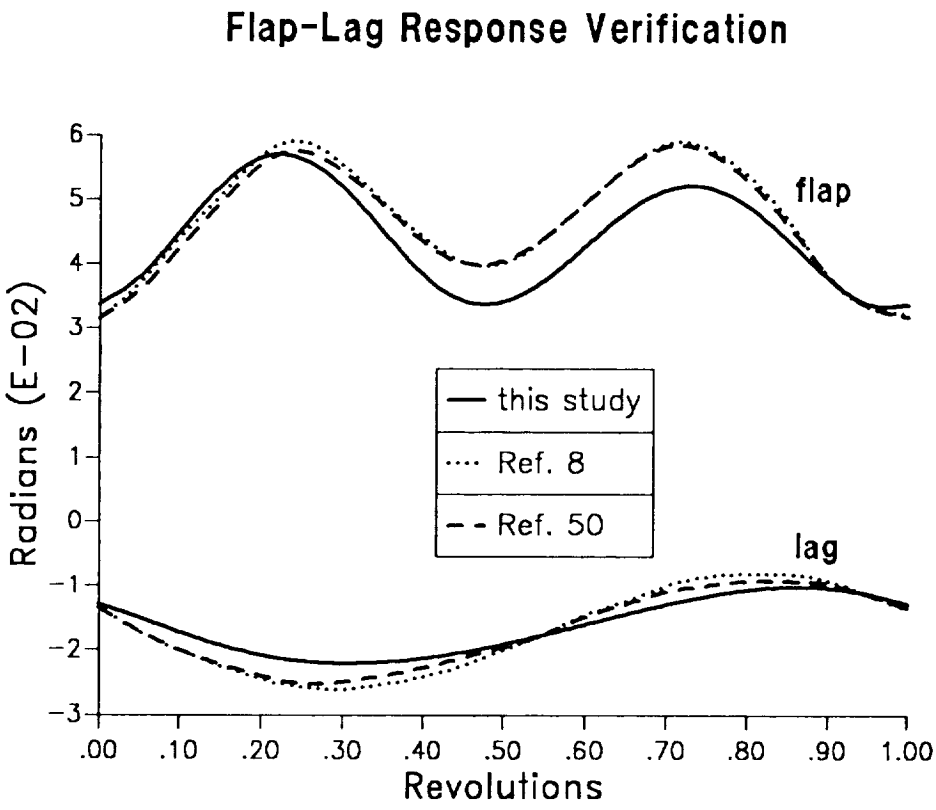

Figure 14: Coupled flap-lag response solution obtained using the offset-hinged spring restrained blade model

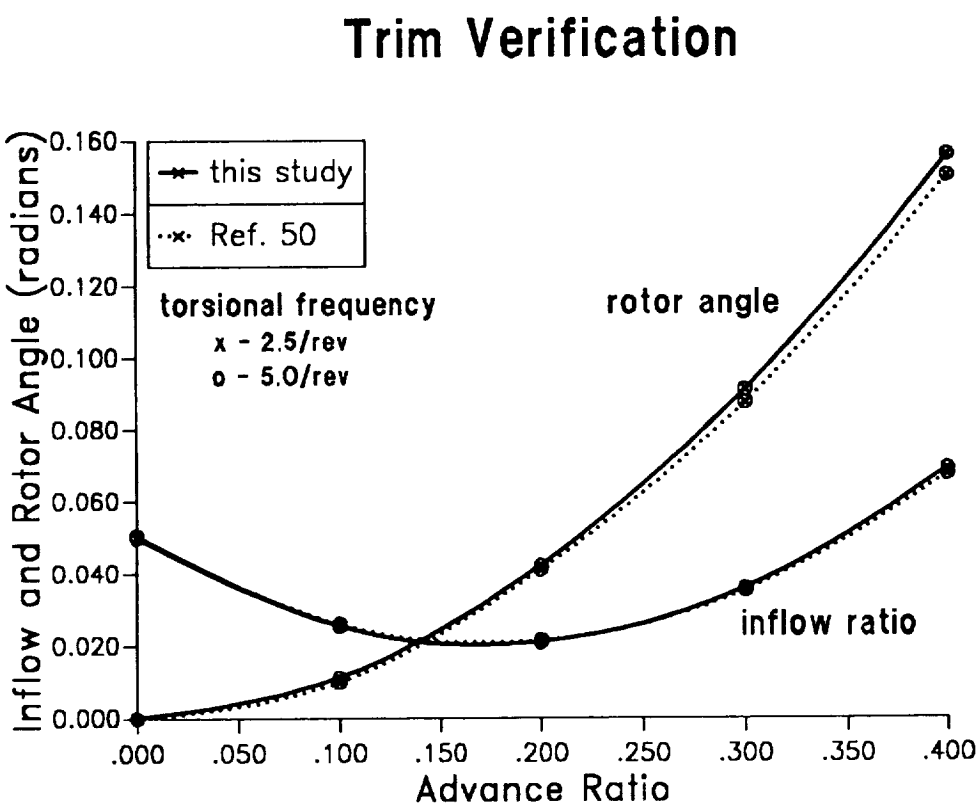

Figure 15: Trim results obtained using the offset-hinged spring restrained blade model, inflow and rotor angle of attack

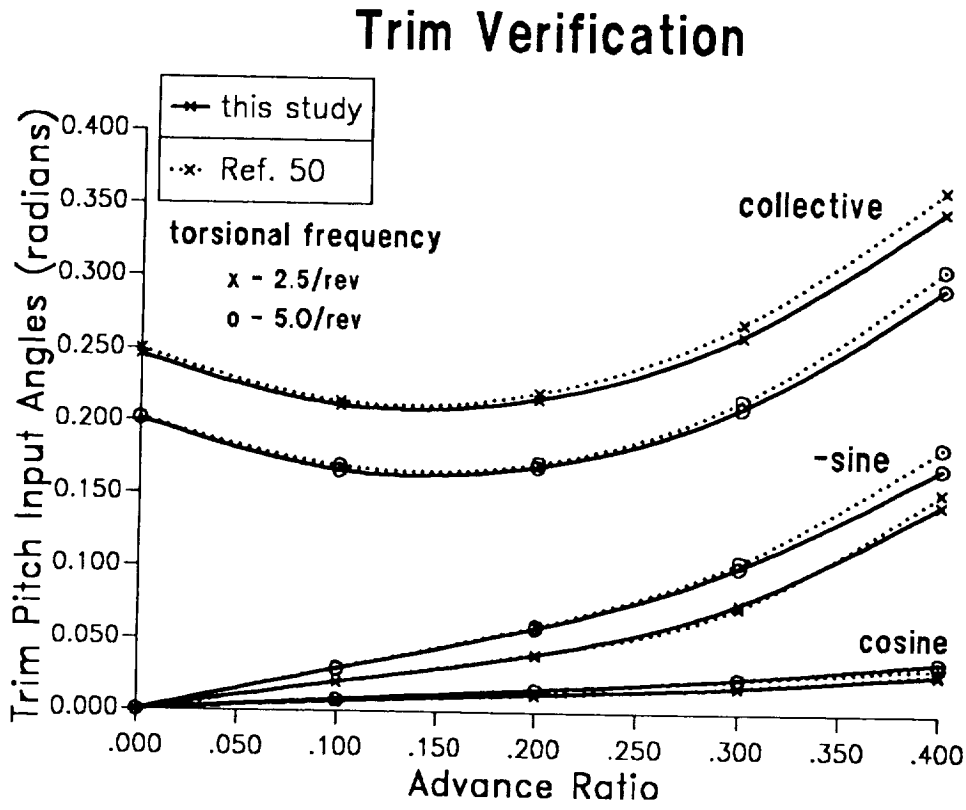

Figure 16: Trim results obtained using the offset-hinged spring restrained blade model, pitch inputs

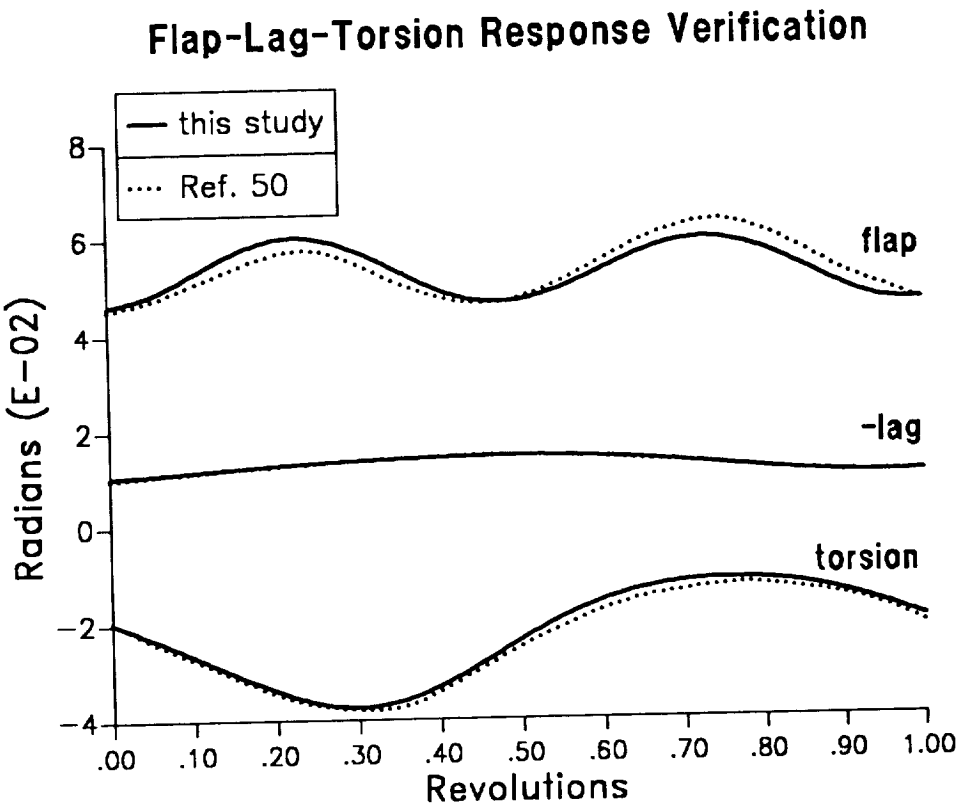

Figure 17: Coupled flap-lag-torsional response solution obtained using the offset-hinged spring restrained blade model

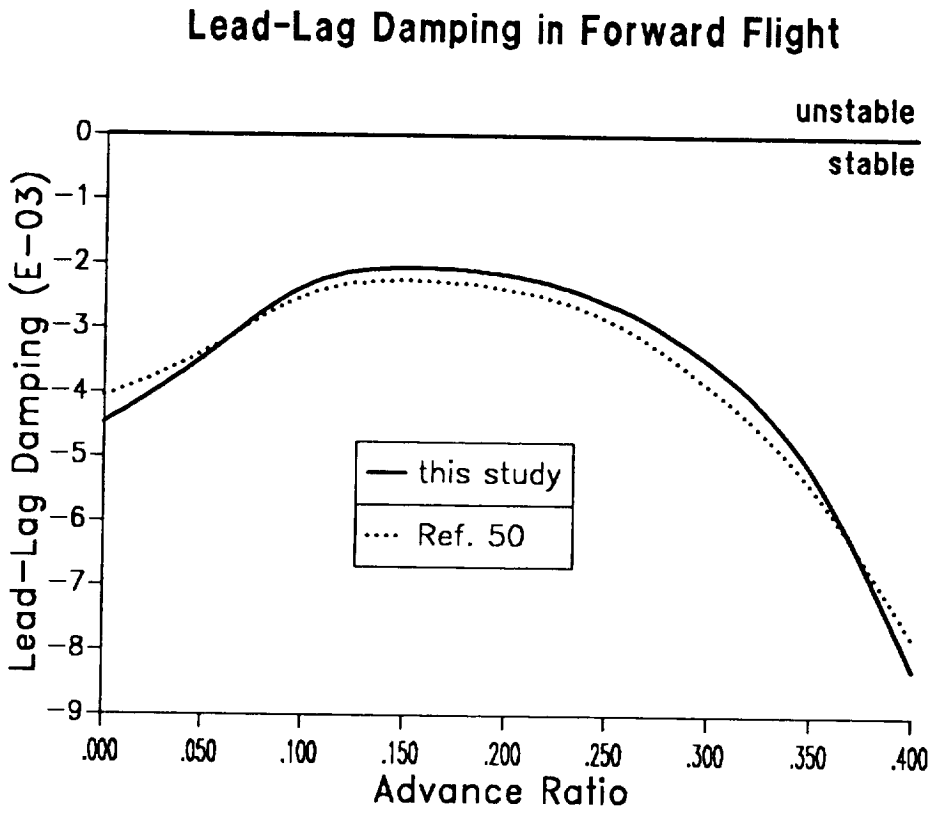

Figure 18: Coupled flap-lag-torsion lead-lag damping in forward flight obtained using the offset-hinged spring restrained blade model

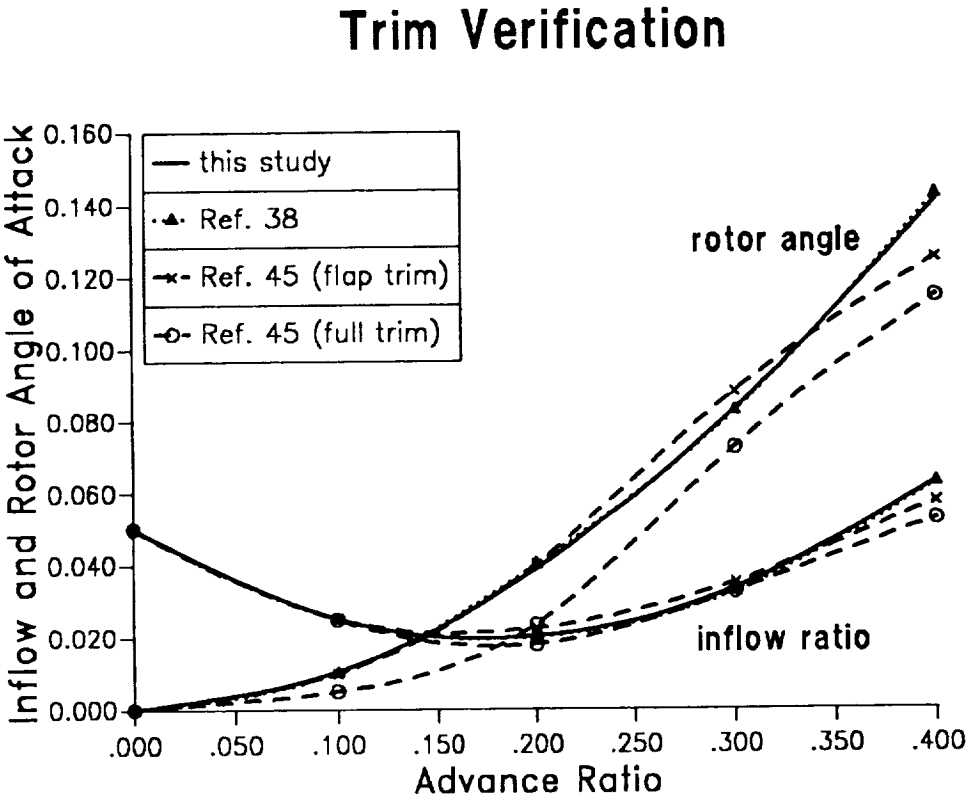

Figure 19: Trim results obtained using the fully elastic blade model, inflow and rotor angle of attack

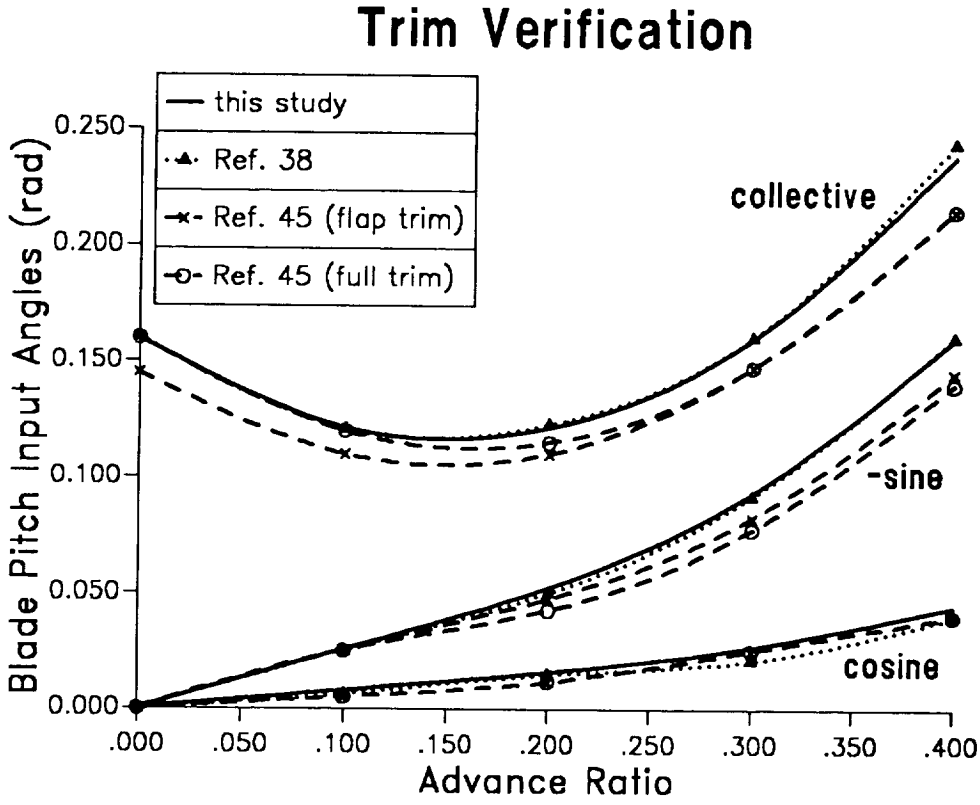

Figure 20: Trim results obtained using the fully elastic blade model, pitch setting

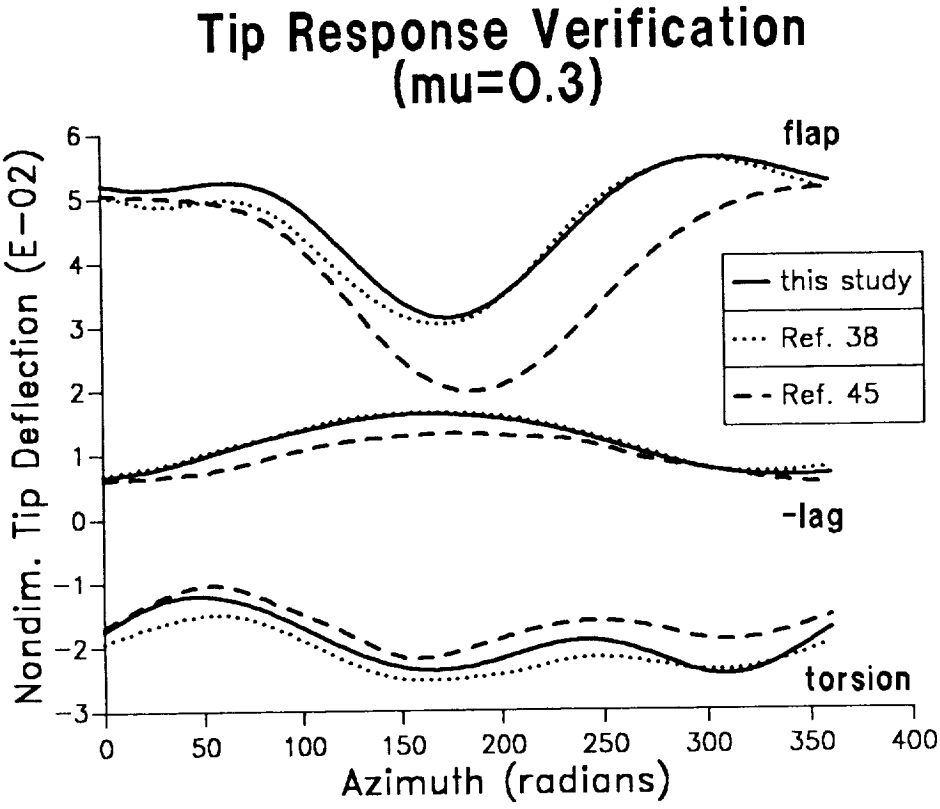

Figure 21: Blade tip response obtained using the fully elastic blade model

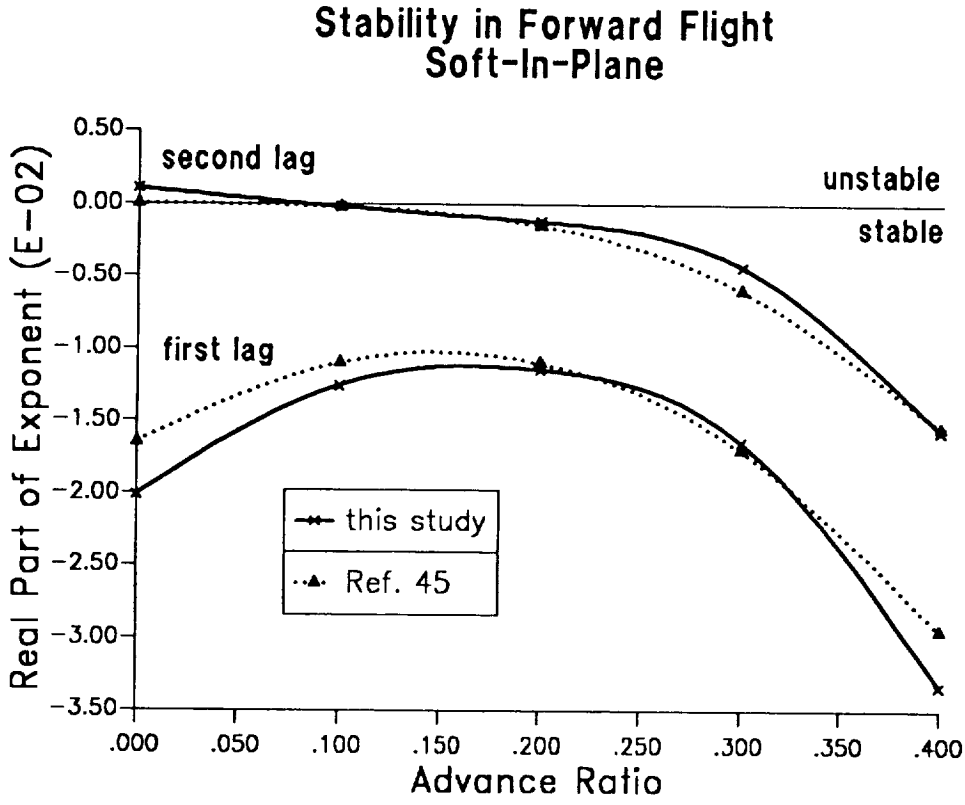

Figure 22: Lead-lag damping in forward flight, soft-in-plane blade

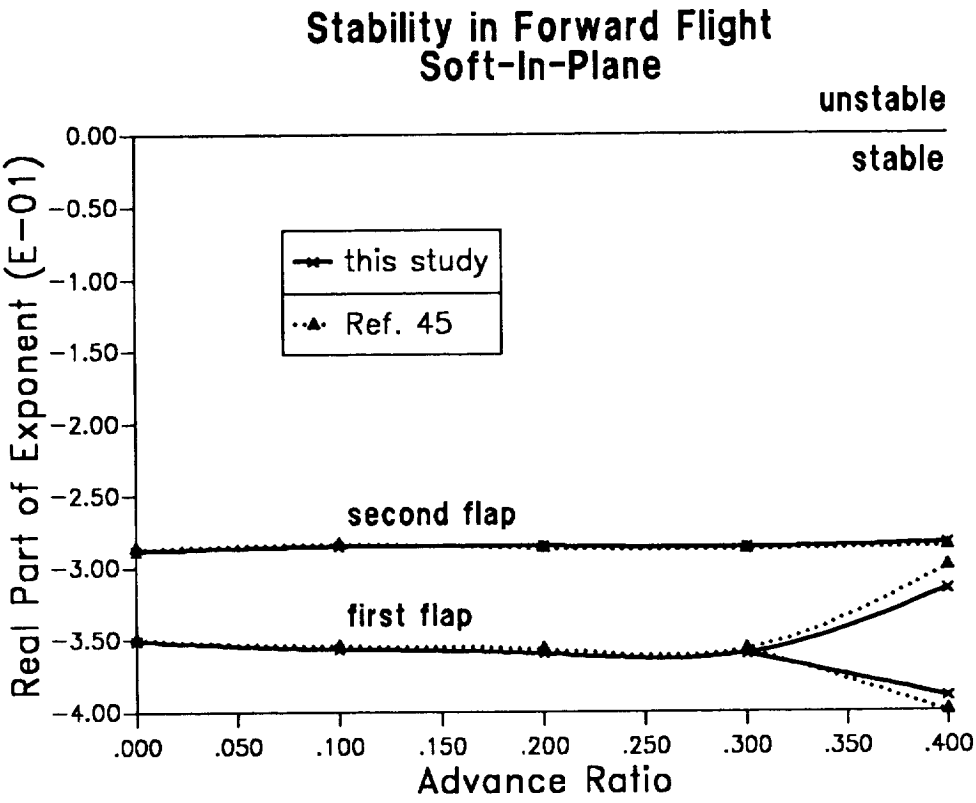

Figure 23: Flap damping in forward flight, soft-in-plane blade

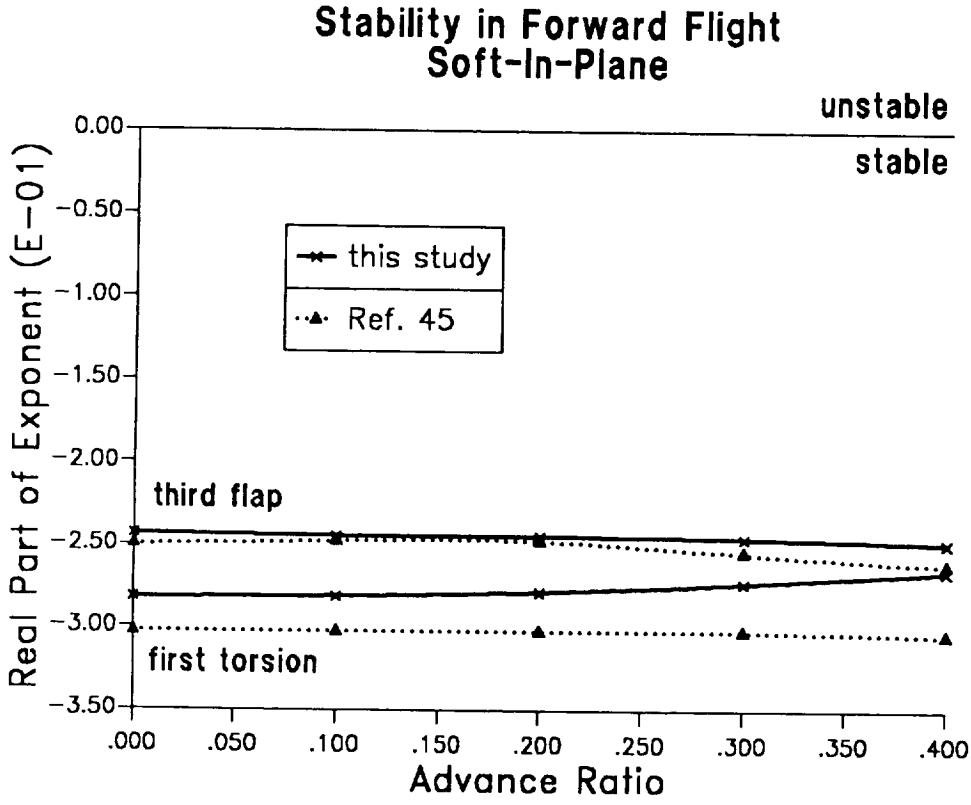

Figure 24: Flap and torsional damping in forward flight, soft-in-plane blade

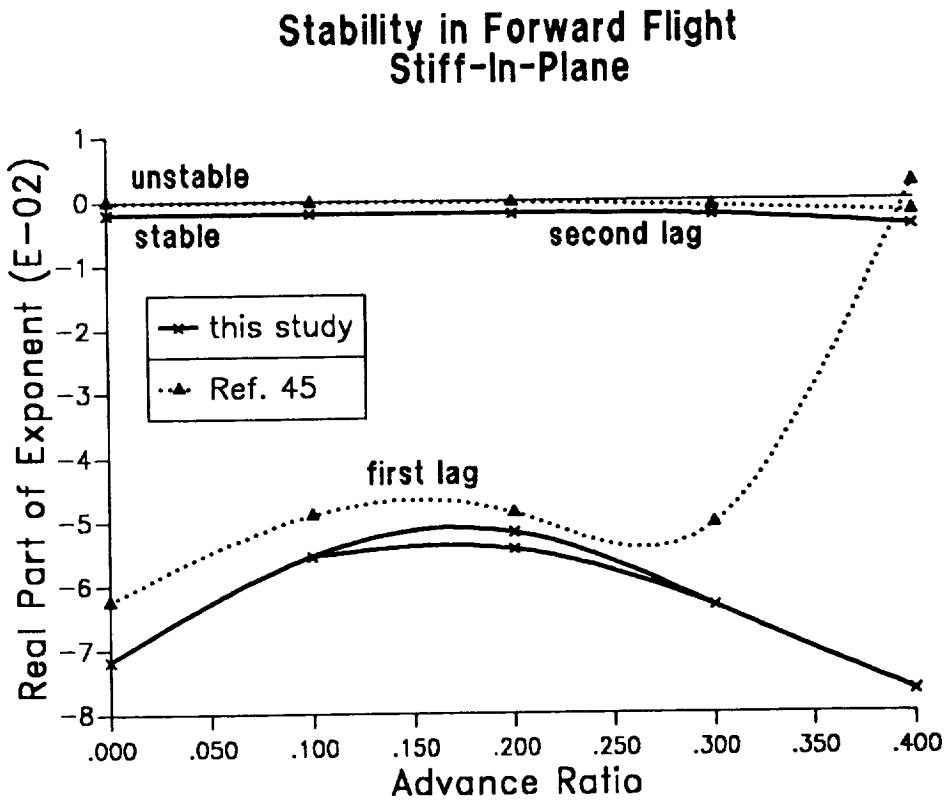

Figure 25: Lead-lag damping in forward flight, stiff-in-plane blade

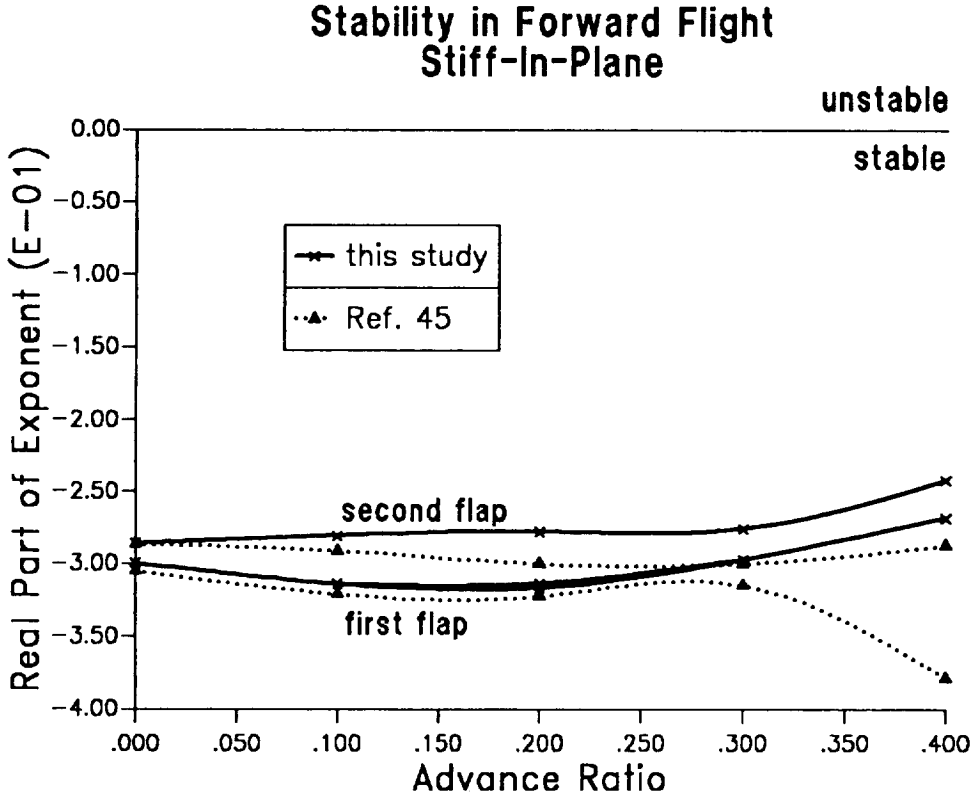

Figure 26: Flap damping in forward flight, stiff-in-plane blade

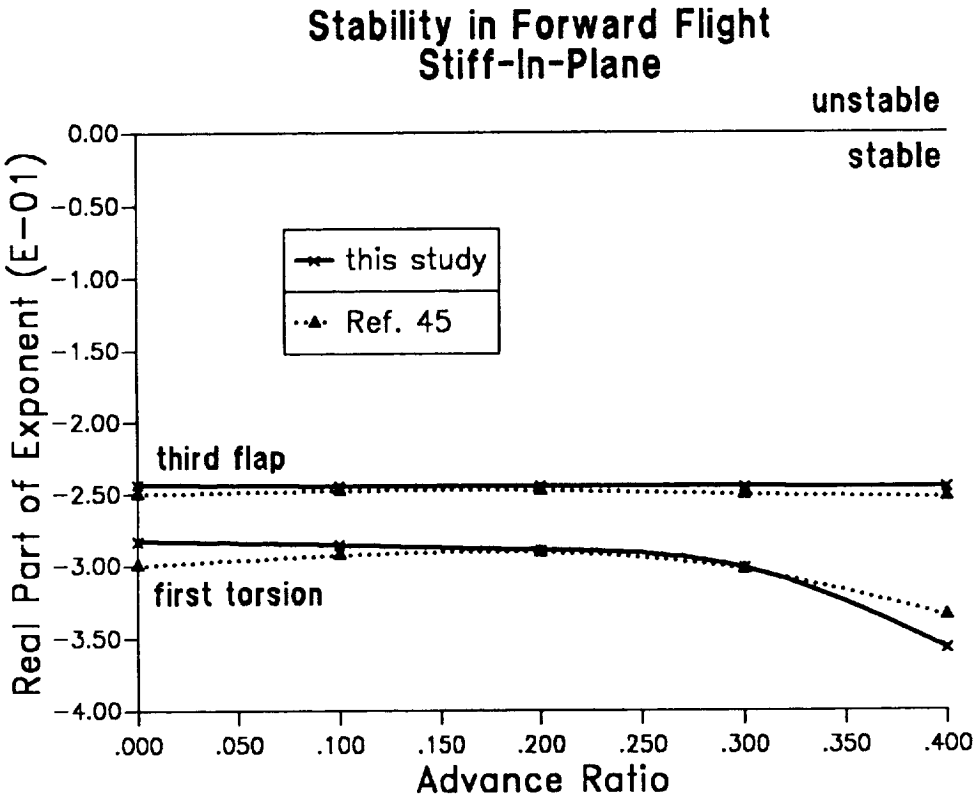

Figure 27: Flap and torsional damping in forward flight, stiff-in-plane blade

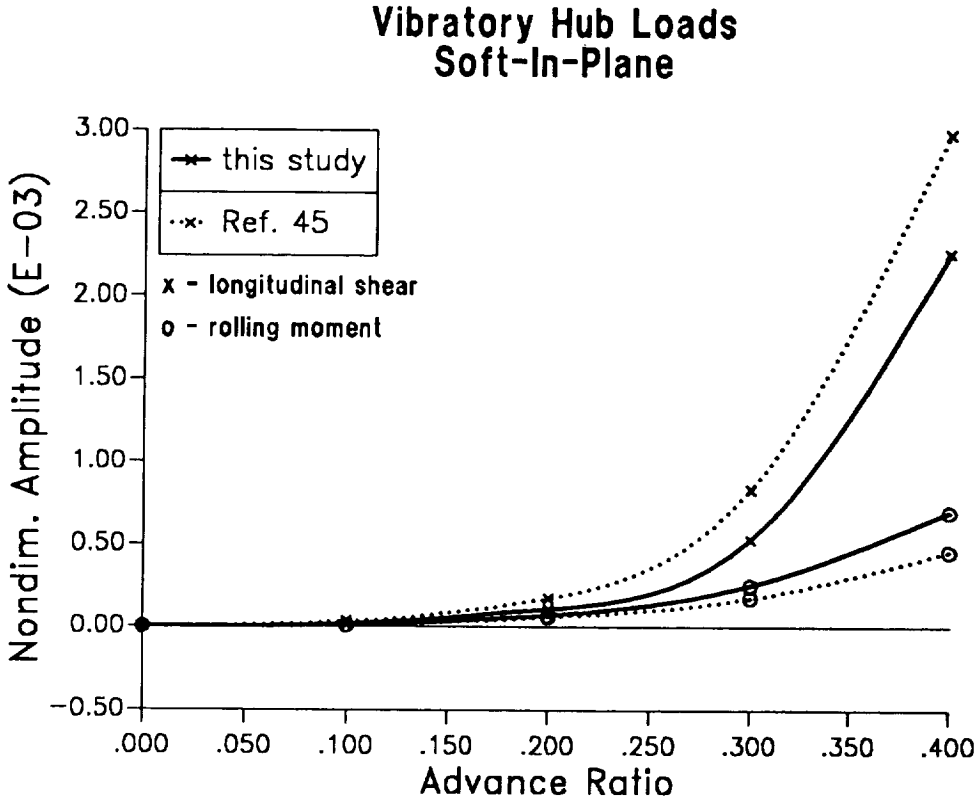

Figure 28: 4/rev longitudinal hub shear and rolling moment, soft-in-plane blade

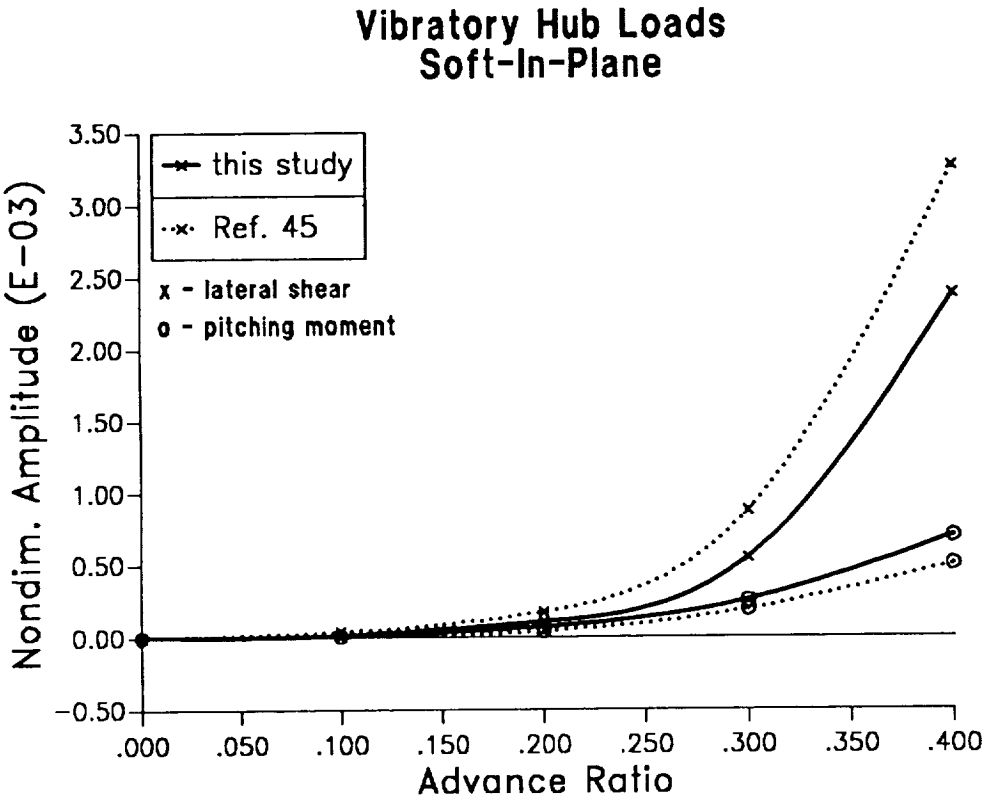

Figure 29: 4/rev lateral hub shear and pitching moment, soft-in-plane blade

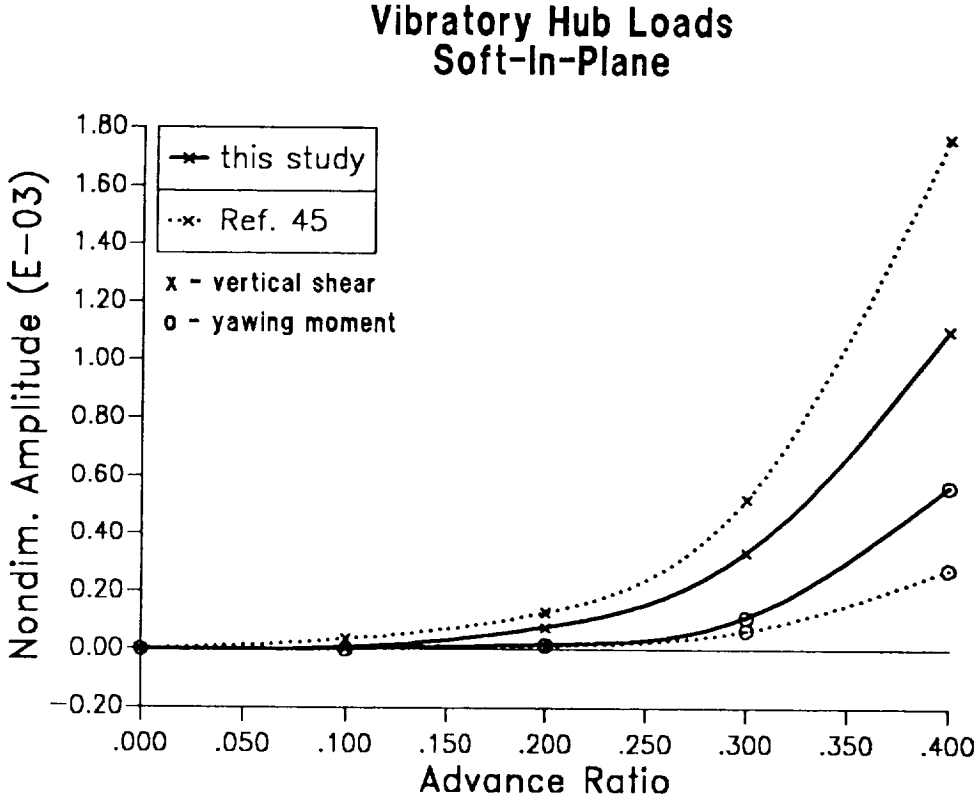

Figure 30: 4/rev vertical hub shear and yawing moment, soft-in-plane blade

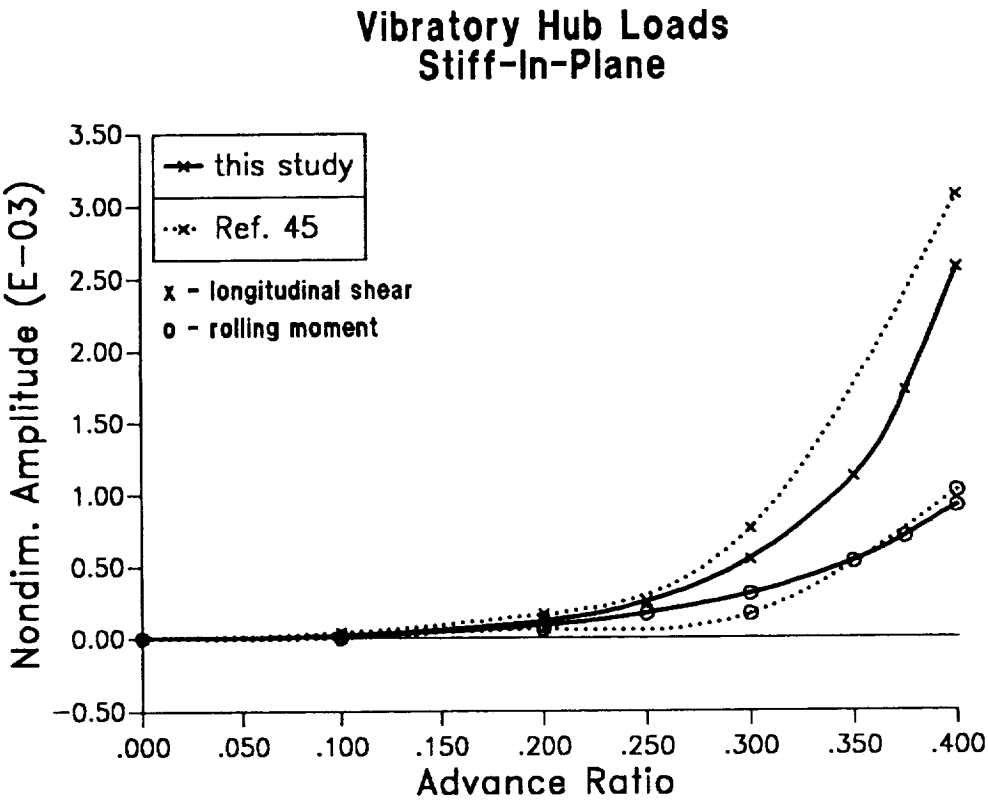

Figure 31: 4/rev longitudinal hub shear and rolling moment, stiff-in-plane blade

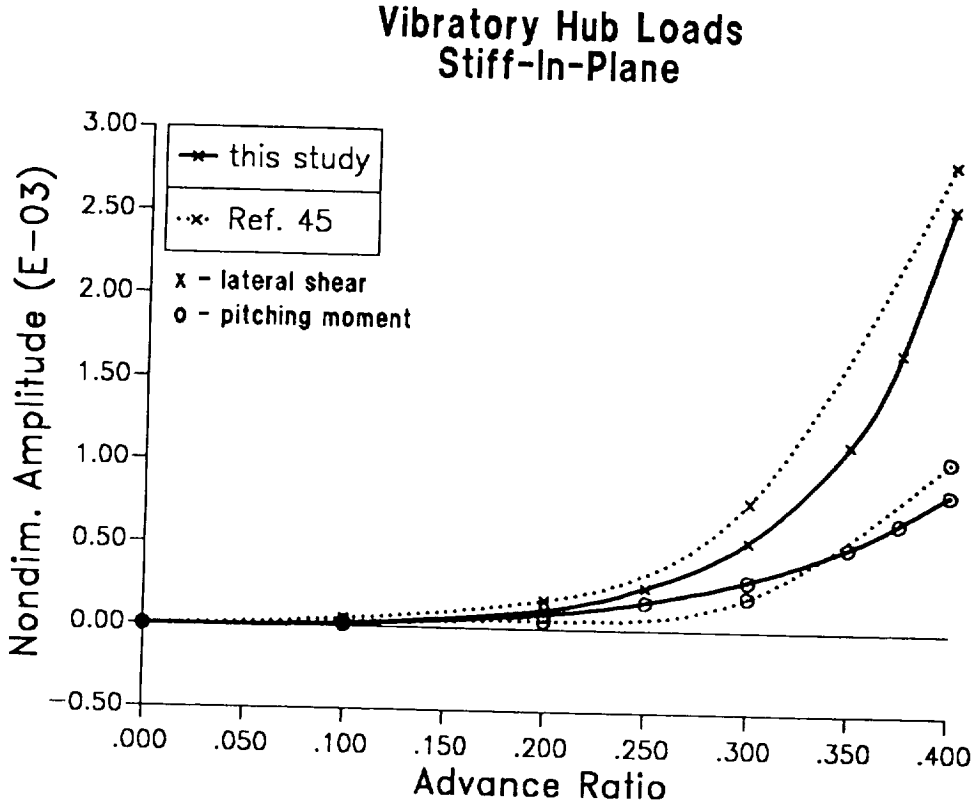

Figure 32: 4/rev lateral hub shear and pitching moment, stiff-in-plane blade

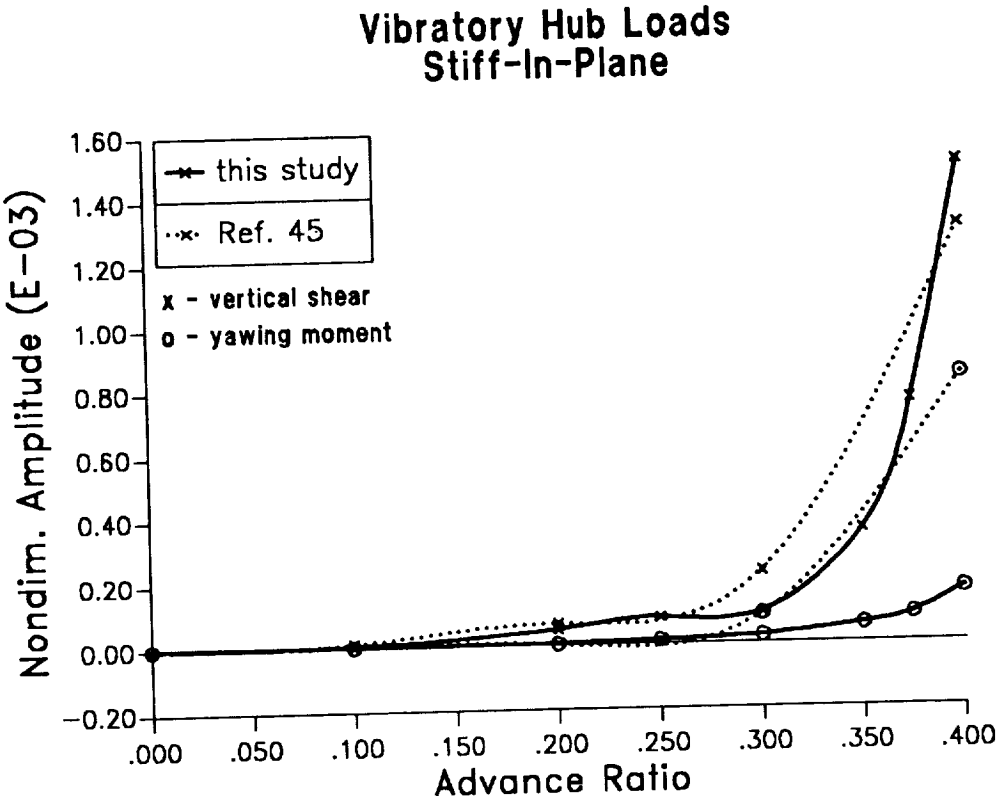

Figure 33: 4/rev vertical hub shear and yawing moment, stiff-in-plane blade

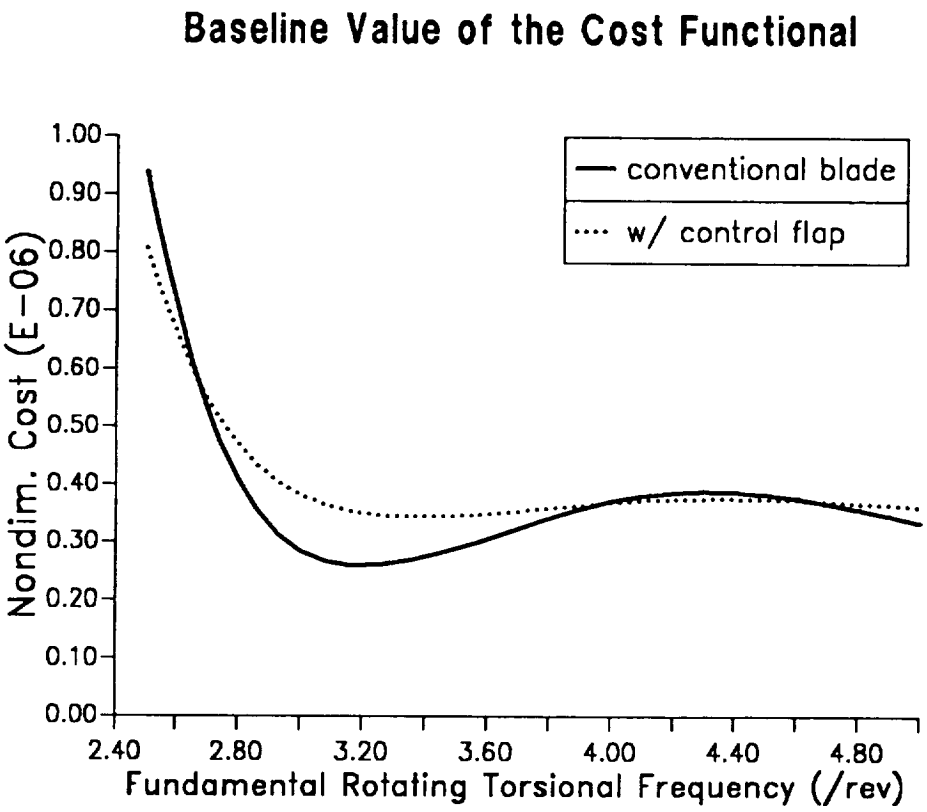

Figure 34: Baseline value of the quadratic cost functional for the spring restrained blade model

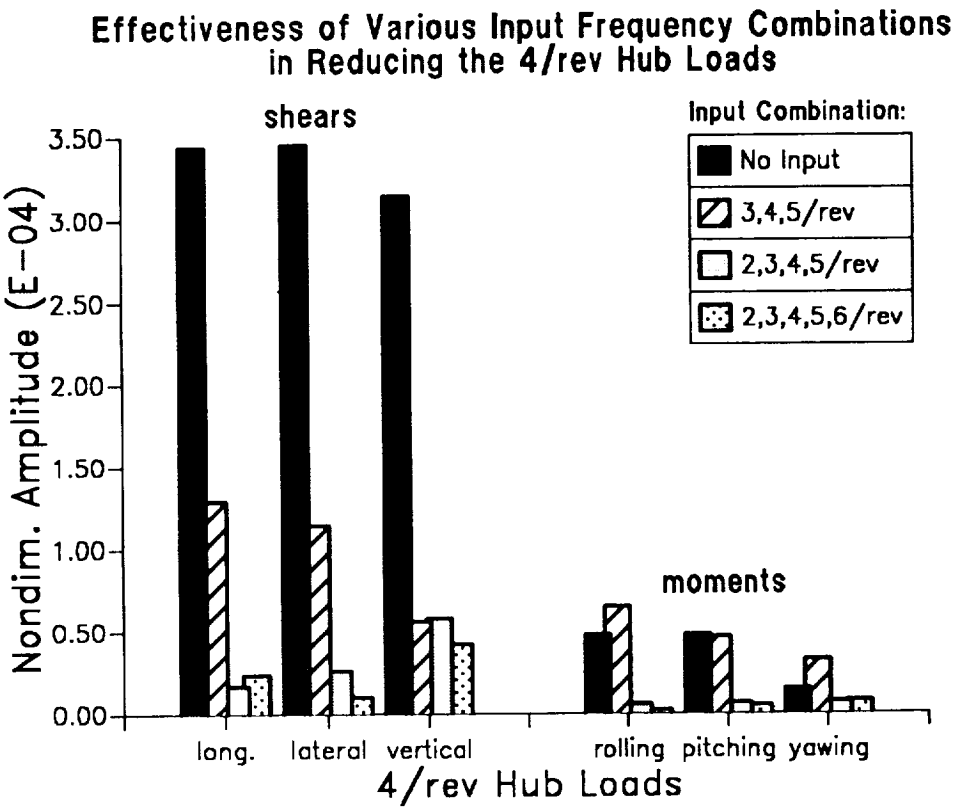

Figure 35: Effectiveness of various input frequency combinations in reducing the 4/rev hub loads using a control flap

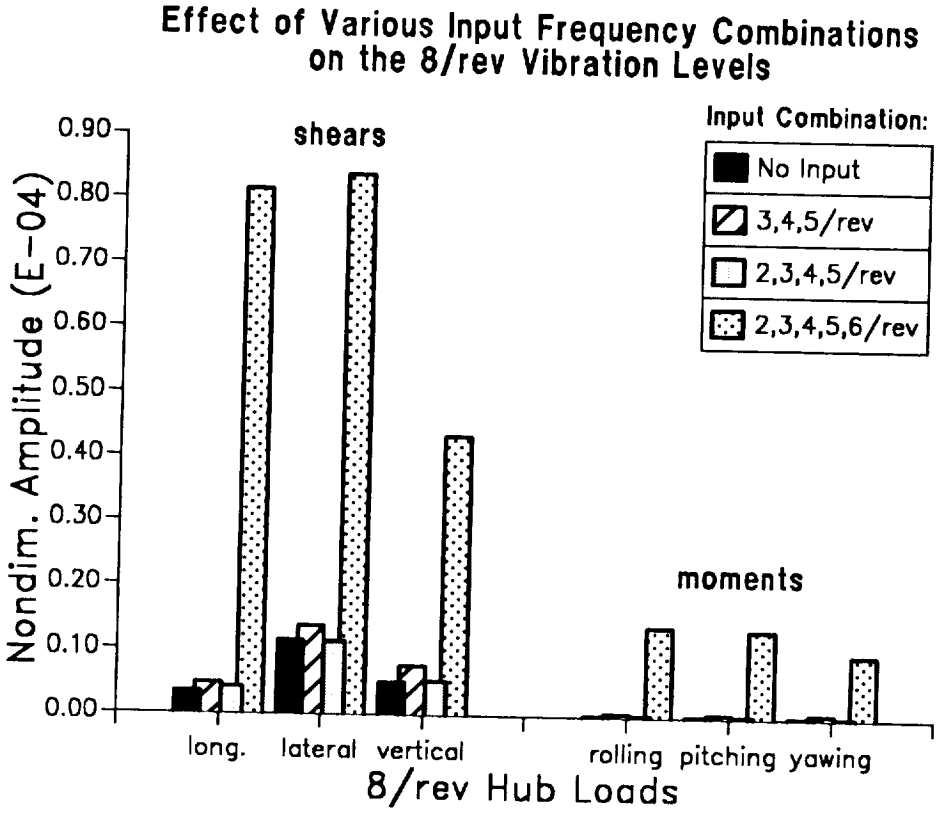

Figure 36: Effect of various input frequency combinations on the 8/rev hub loads for the control flap

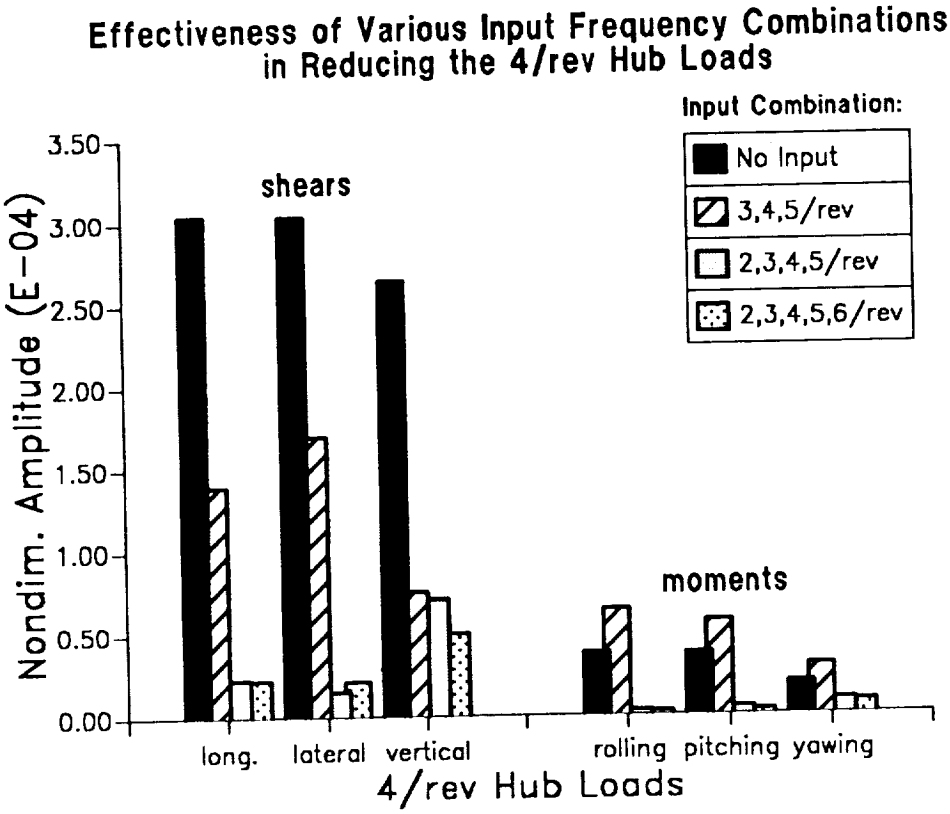

Figure 37: Effectiveness of various input frequency combinations in reducing the 4/rev hub loads using conventional IBC

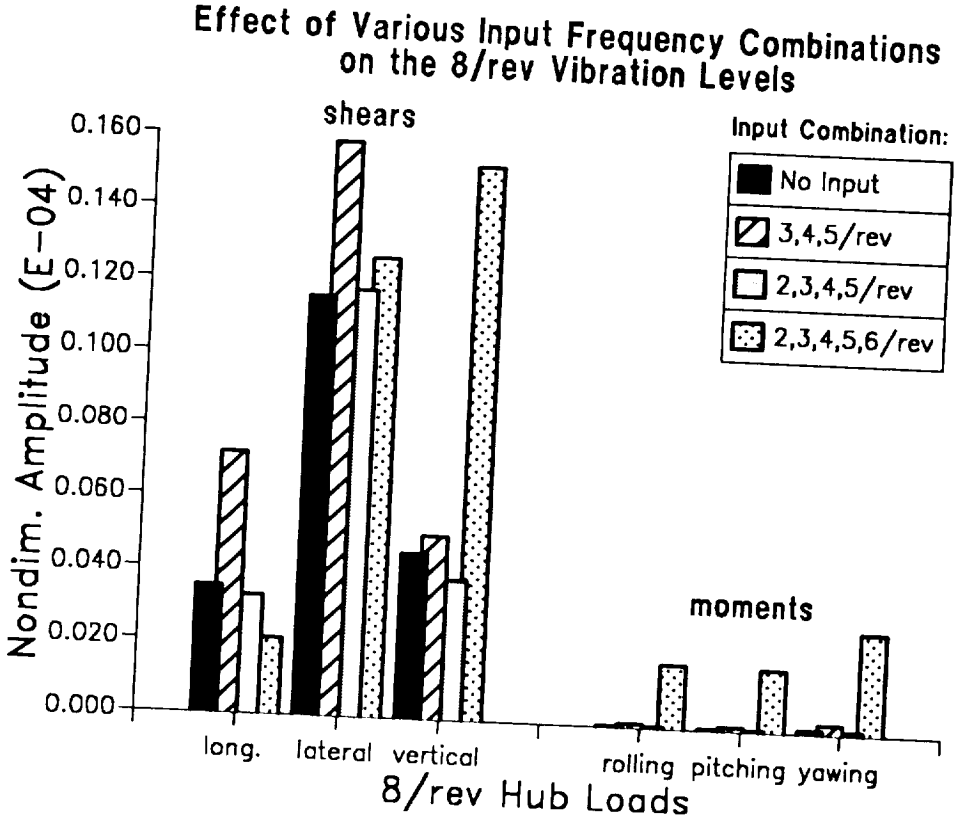

Figure 38: Effect of various input frequency combinations on the 8/rev hub loads for conventional IBC

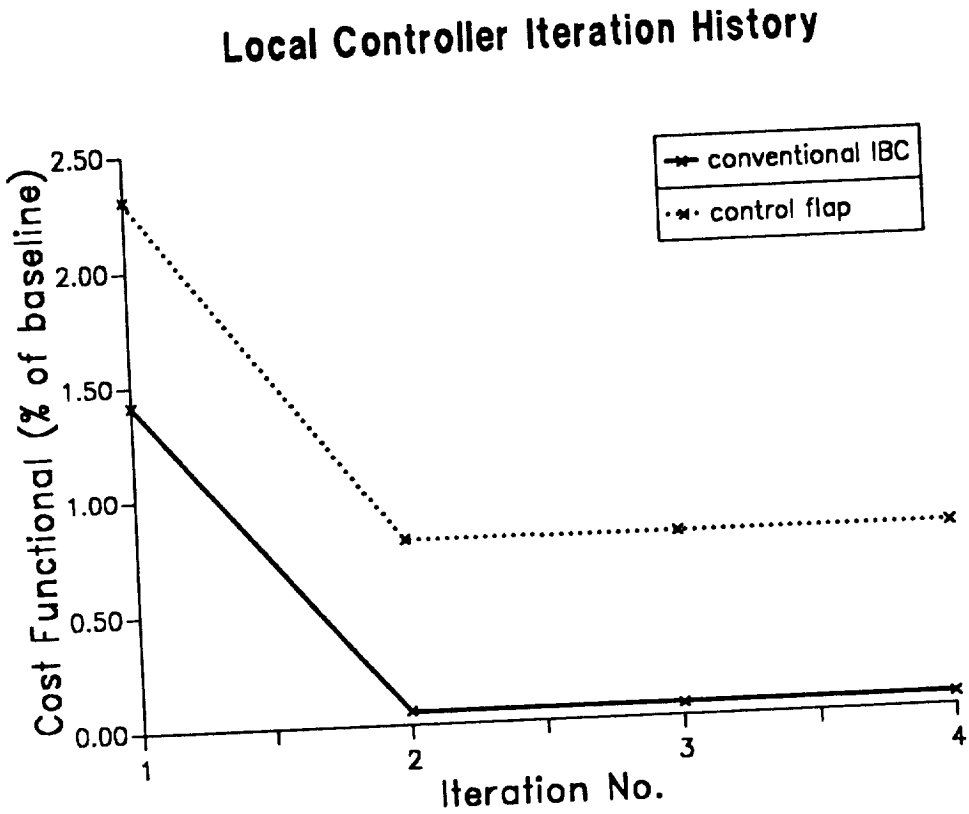

Figure 39: Iteration history of the local controller: cost functional

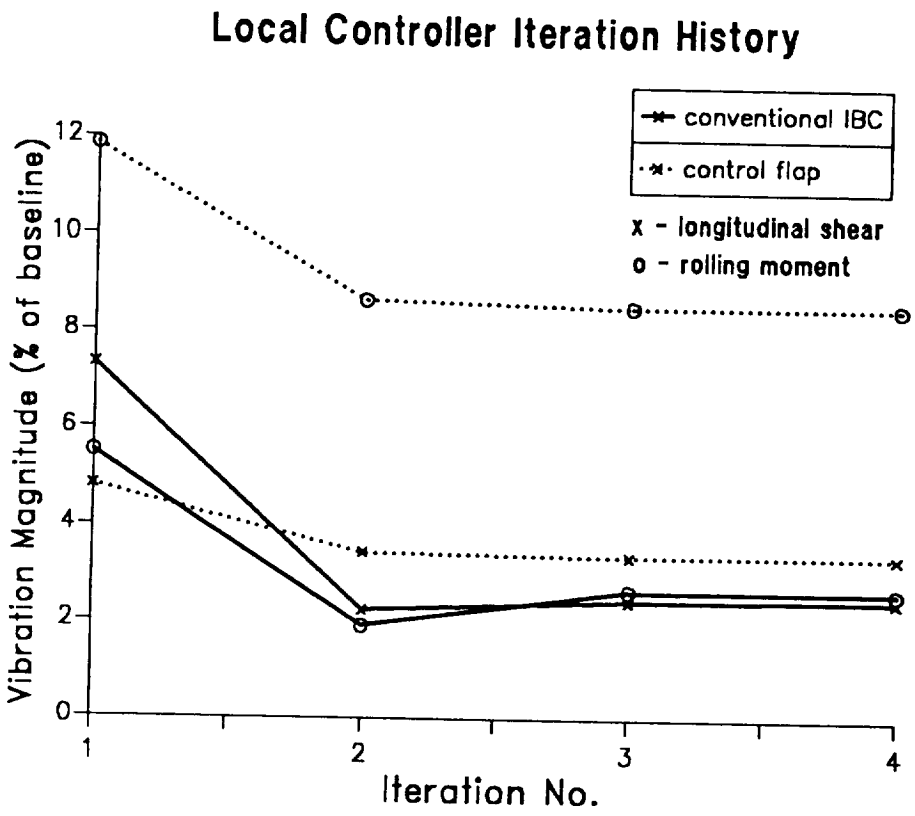

Figure 40: Iteration history of the local controller: 4/rev longitudinal shear and rolling moment

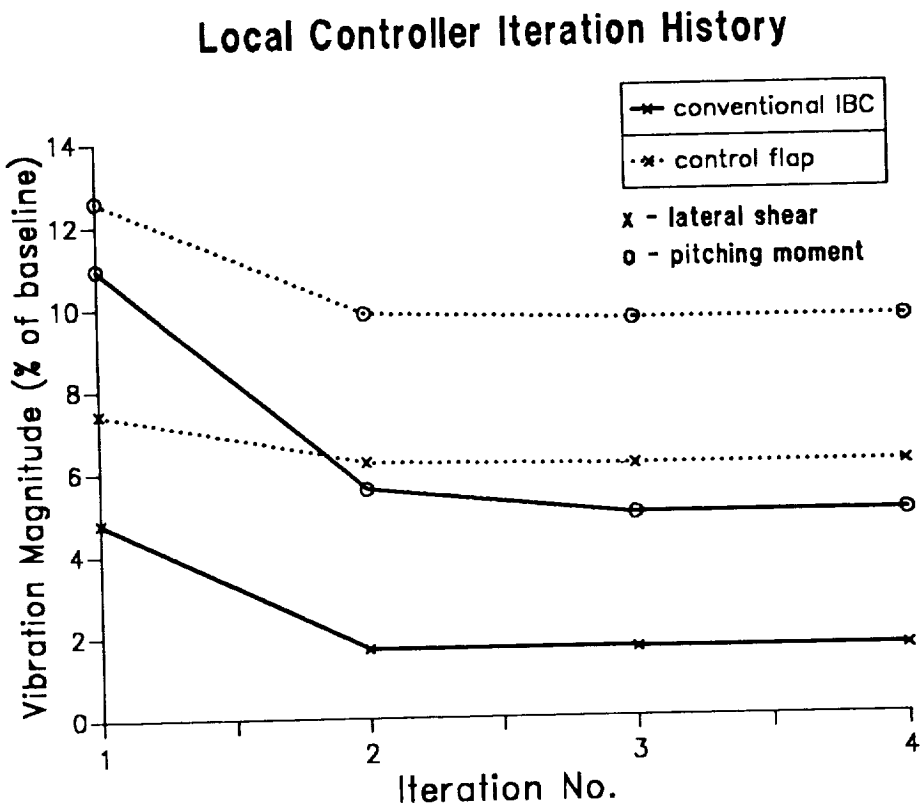

Figure 41: Iteration history of the local controller: 4/rev lateral shear and pitching moment

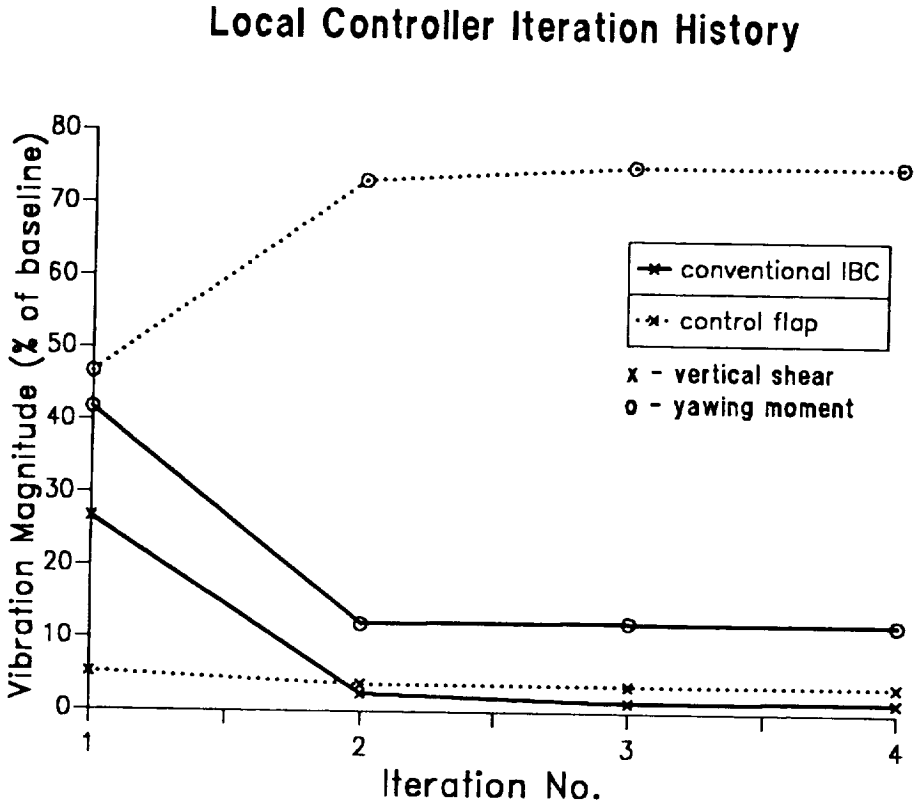

Figure 42: Iteration history of the local controller: 4/rev vertical shear and yawing moment

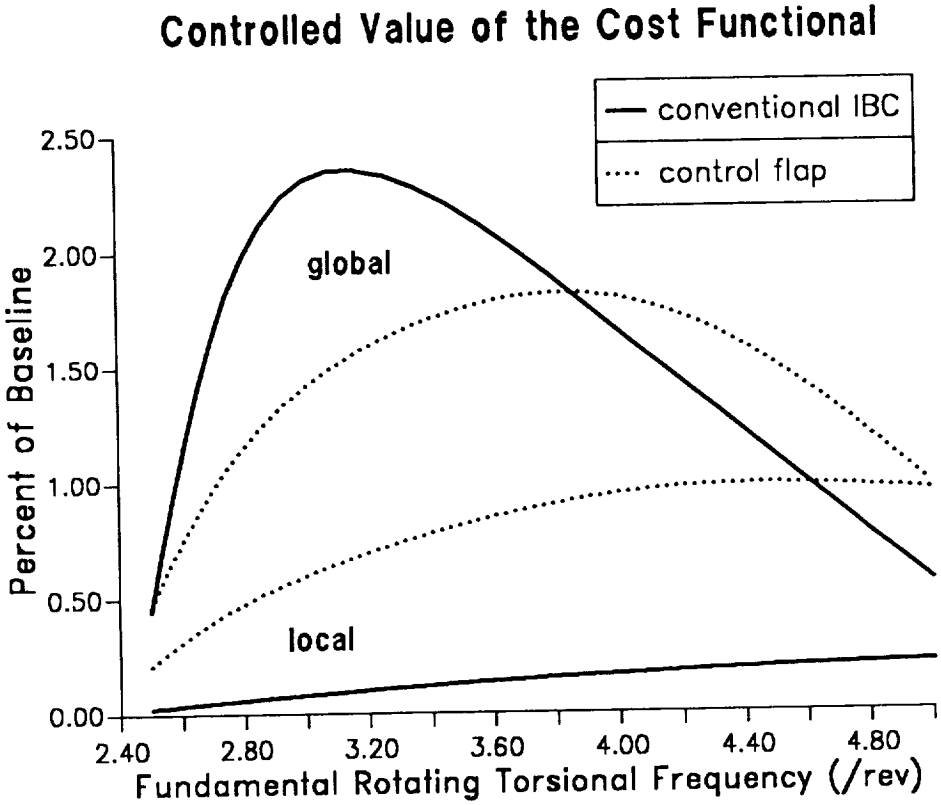

Figure 43: Controlled values of the quadratic cost functional for the spring restrained blade model

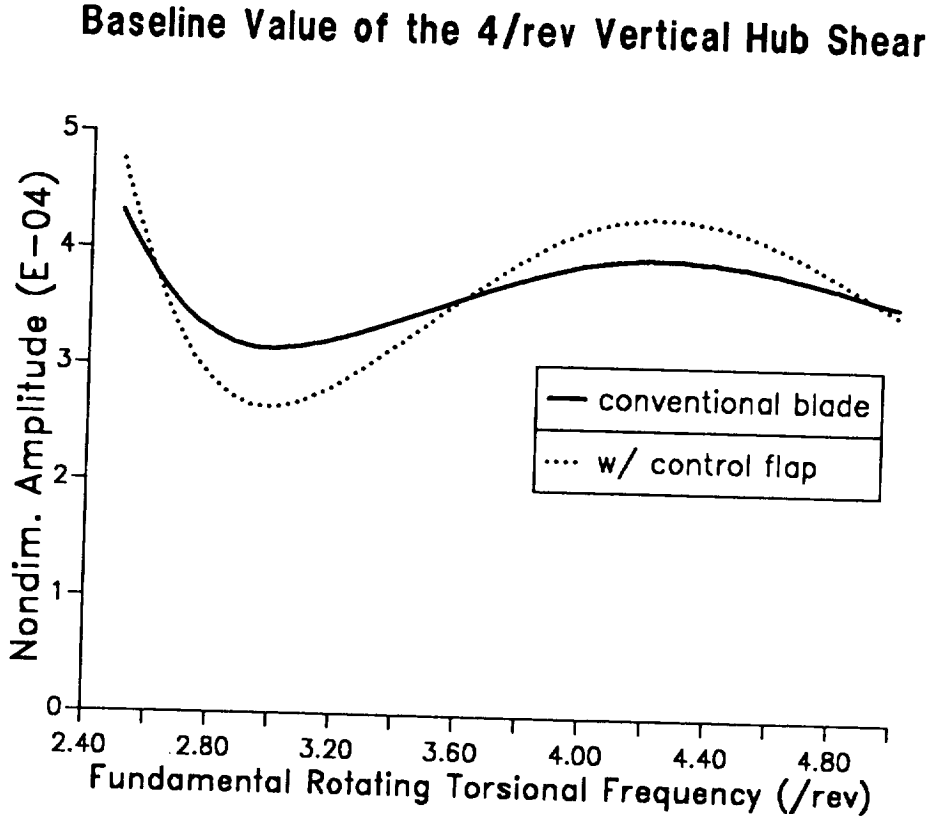

Figure 44: Baseline value of the 4/rev vertical hub shear for the spring restrained blade model

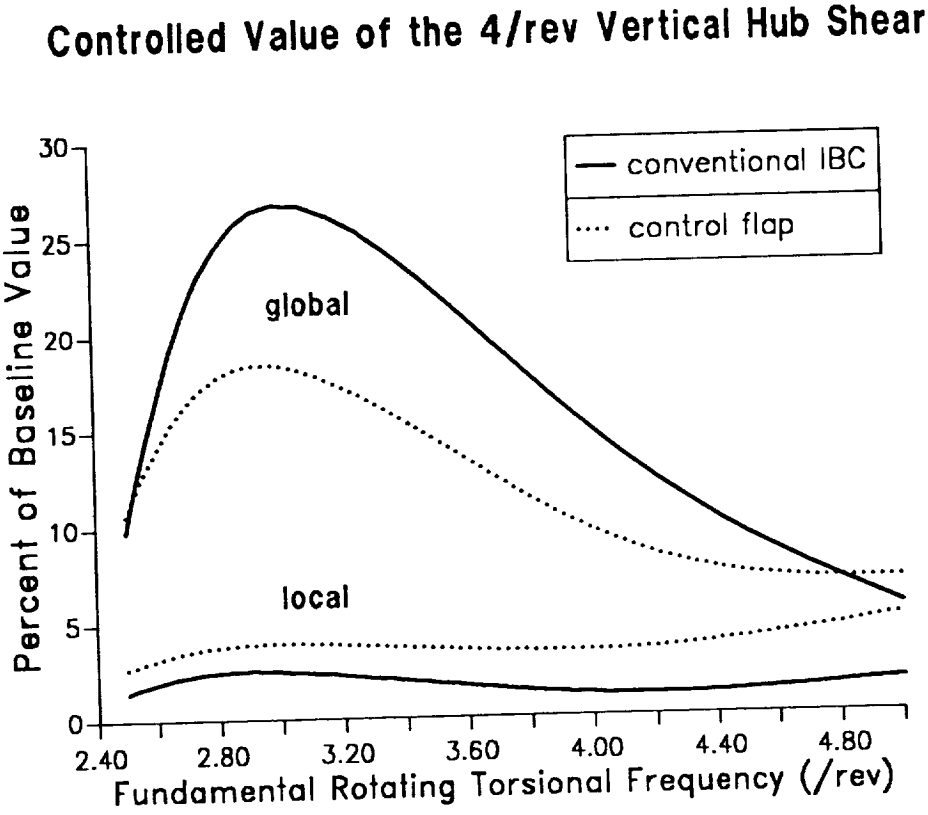

Figure 45: Controlled value of the 4/rev vertical hub shear for the spring restrained blade model

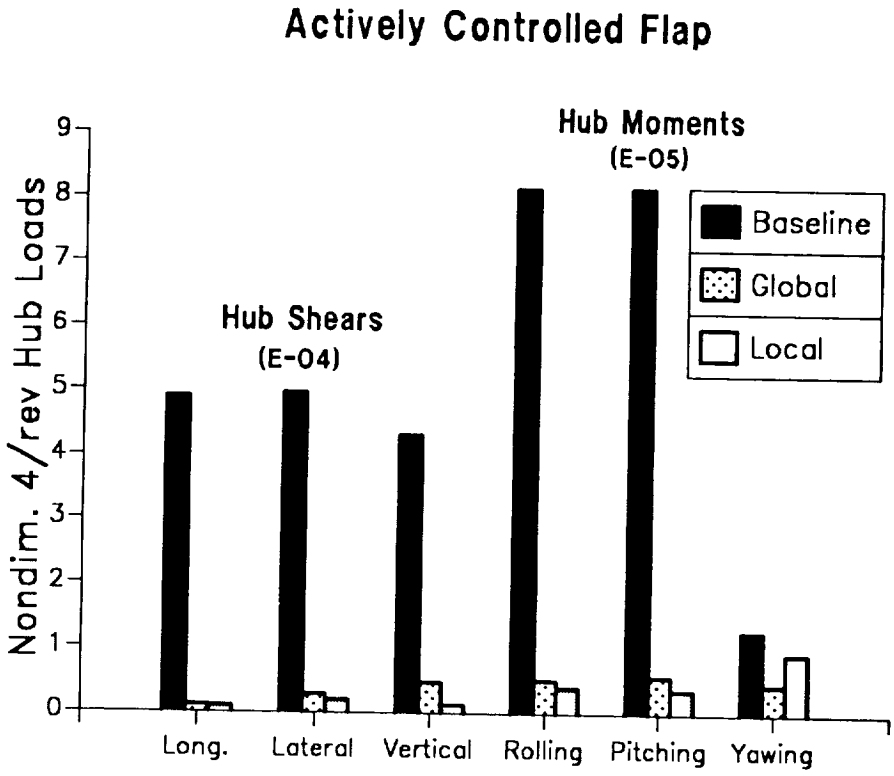

Figure 46: Simultaneous reduction of 4/rev hub shears and hub moments using a control flap, torsionally soft blade

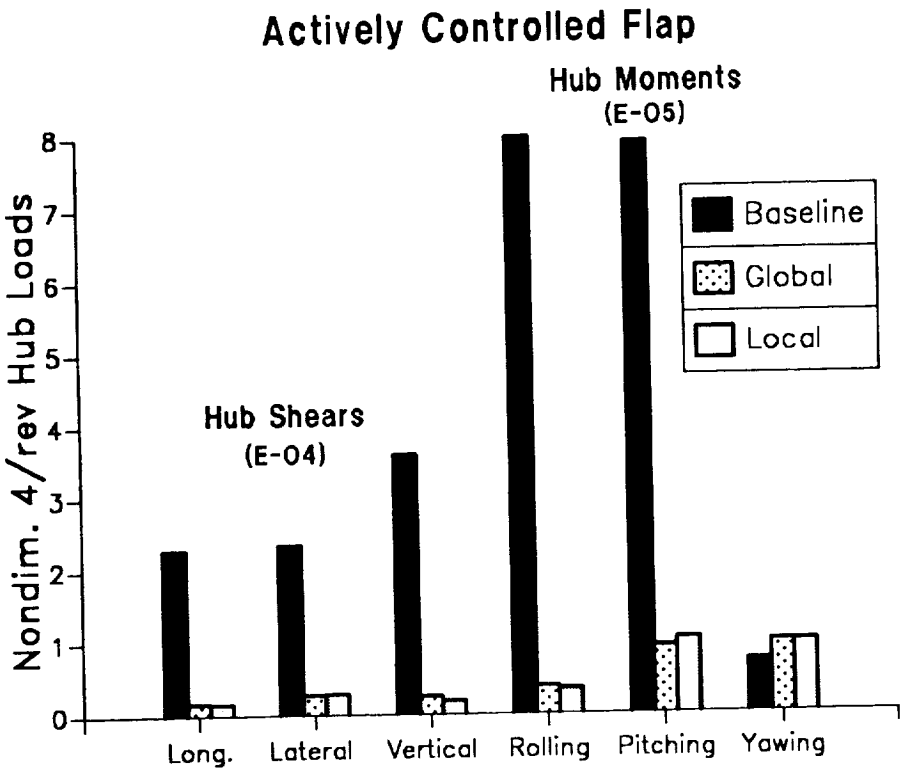

Figure 47: Simultaneous reduction of 4/rev hub shears and moments using a control flap, torsionally stiff blade

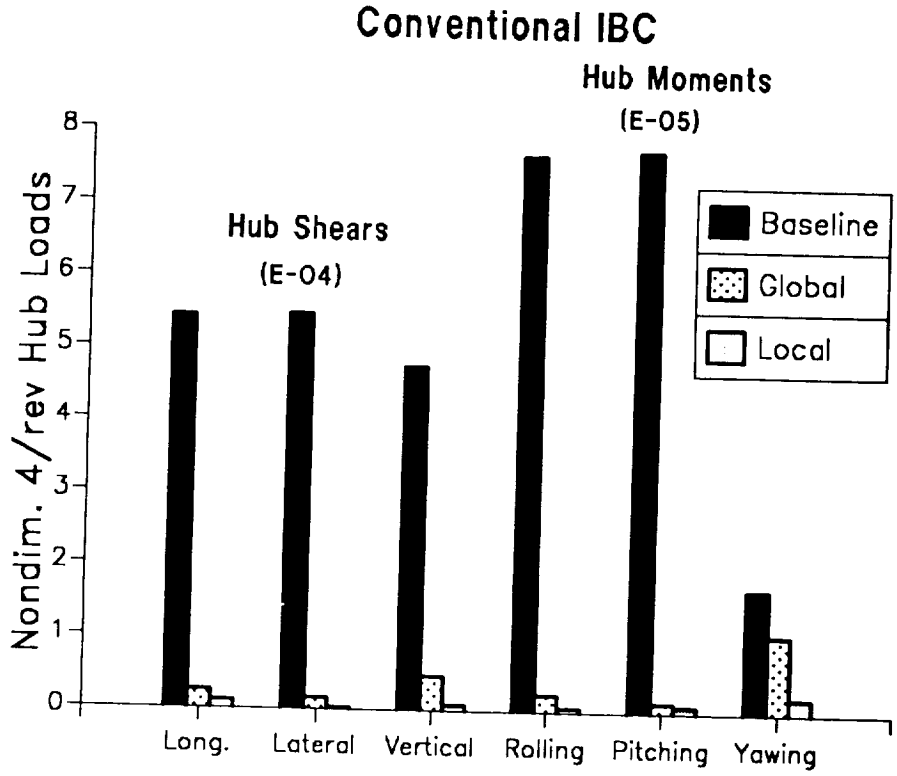

Figure 48: Simultaneous reduction of 4/rev hub shears and moments using conventional IBC, torsionally soft blade

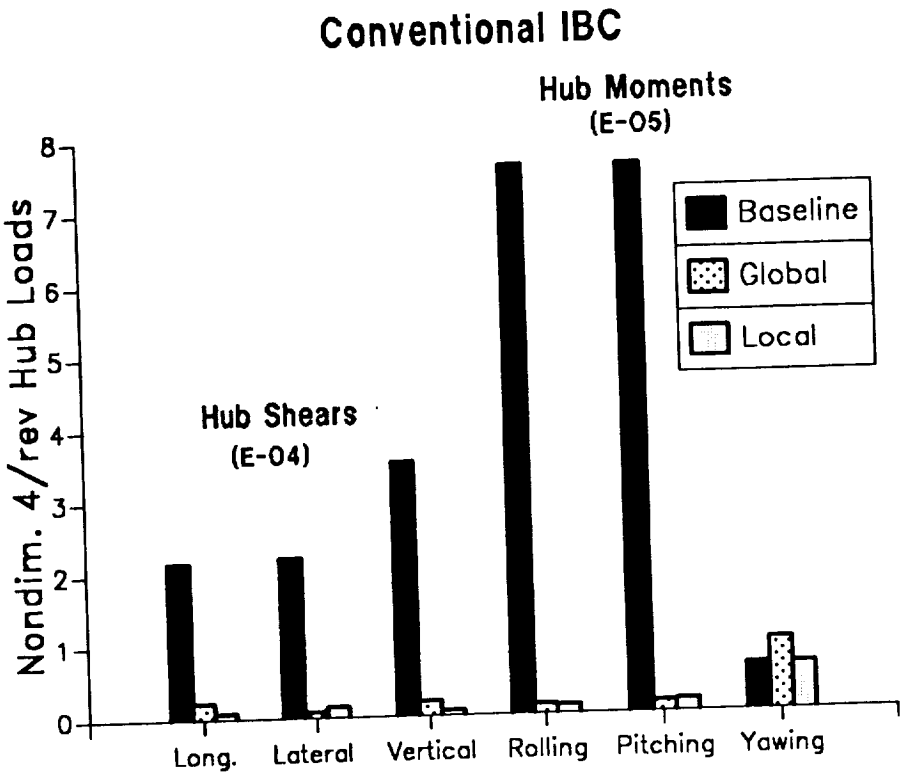

Figure 49: Simultaneous reduction of 4/rev hub shears and moments using conventional IBC, torsionally stiff blade

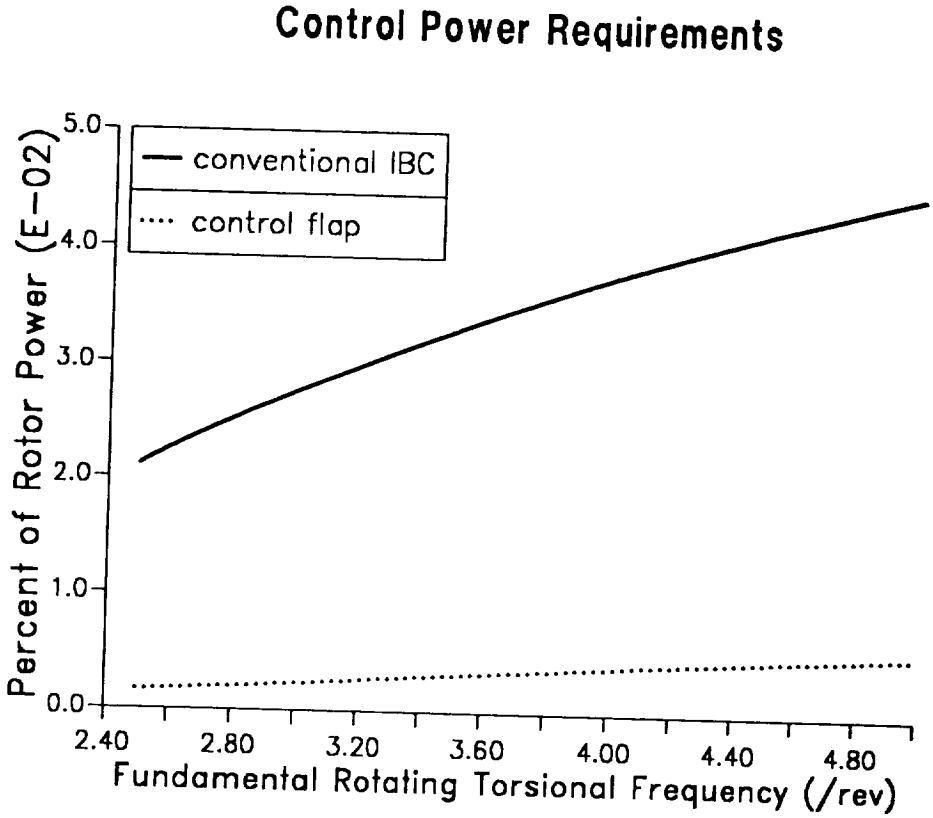

Figure 50: Control power requirements for the offset-hinged spring restrained blade model

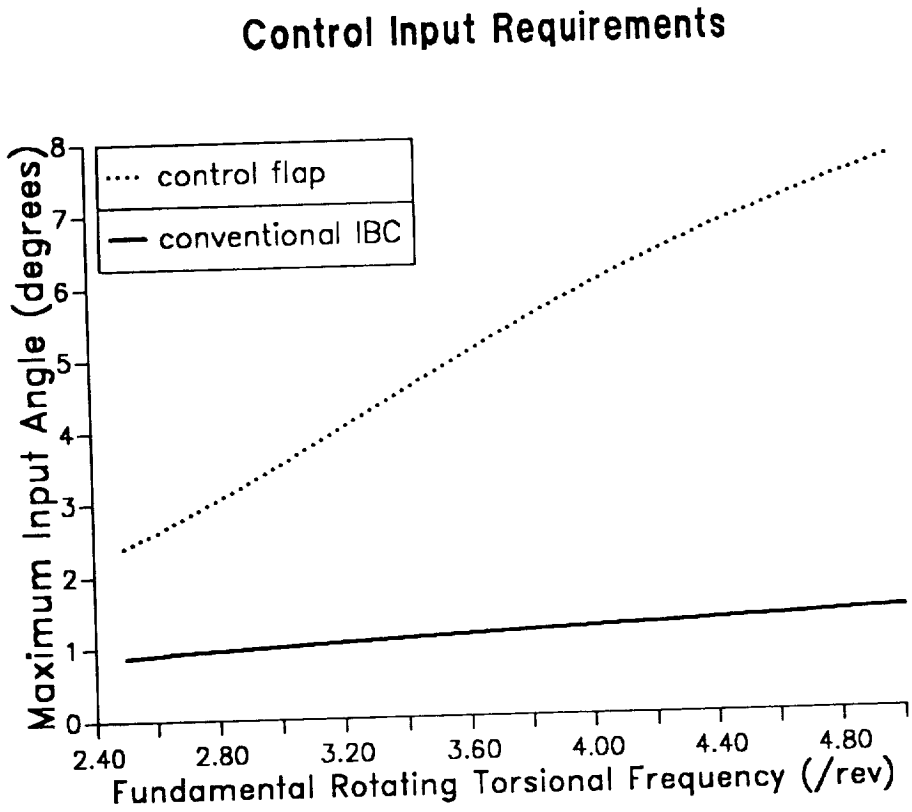

Figure 51: Control input for vibration reduction for the spring restrained blade model

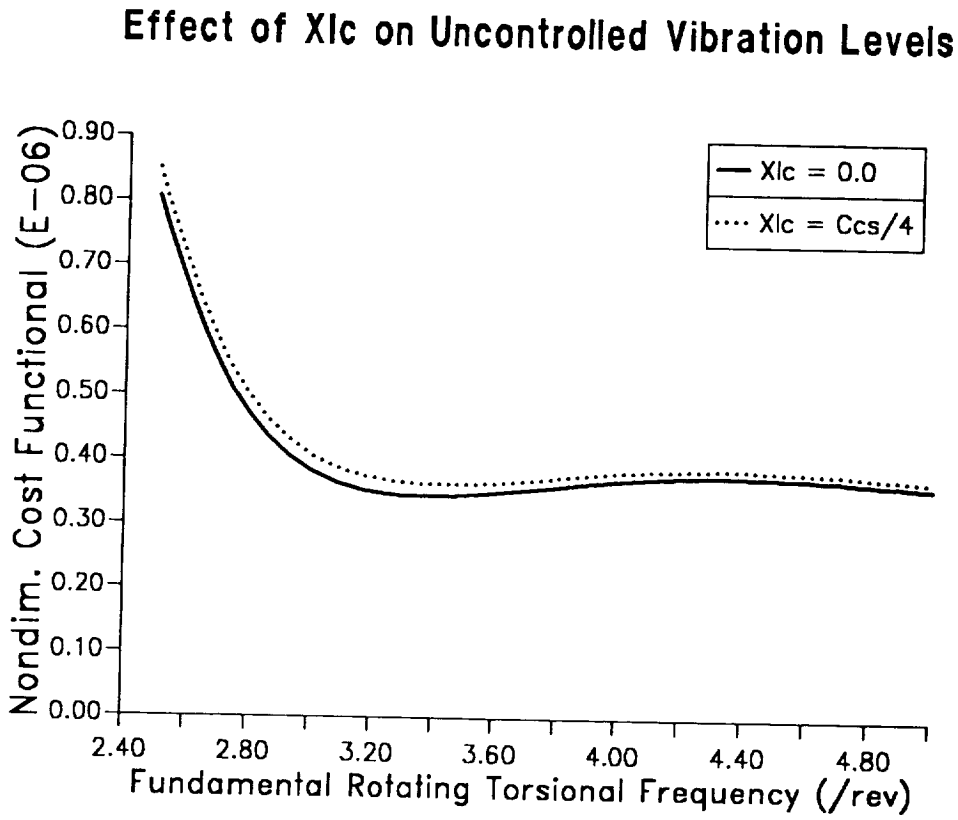

Figure 52: Effect of a mass unbalanced trailing edge flap on the uncontrolled vibration levels

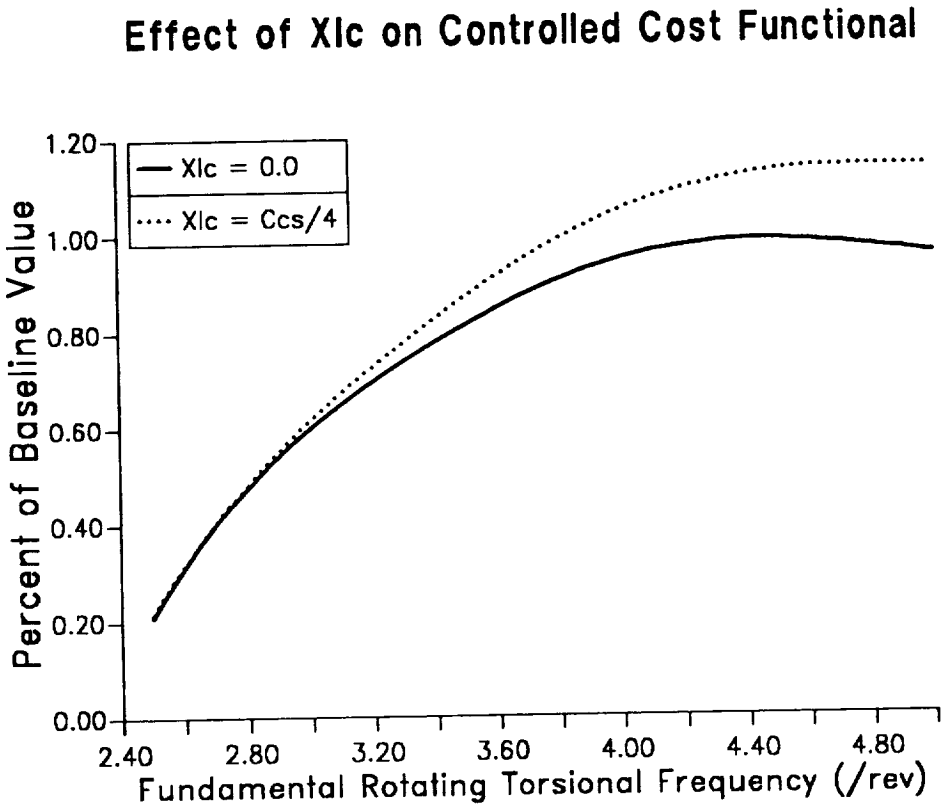

Figure 53: Effect of a mass unbalanced trailing edge flap on the controlled vibration levels

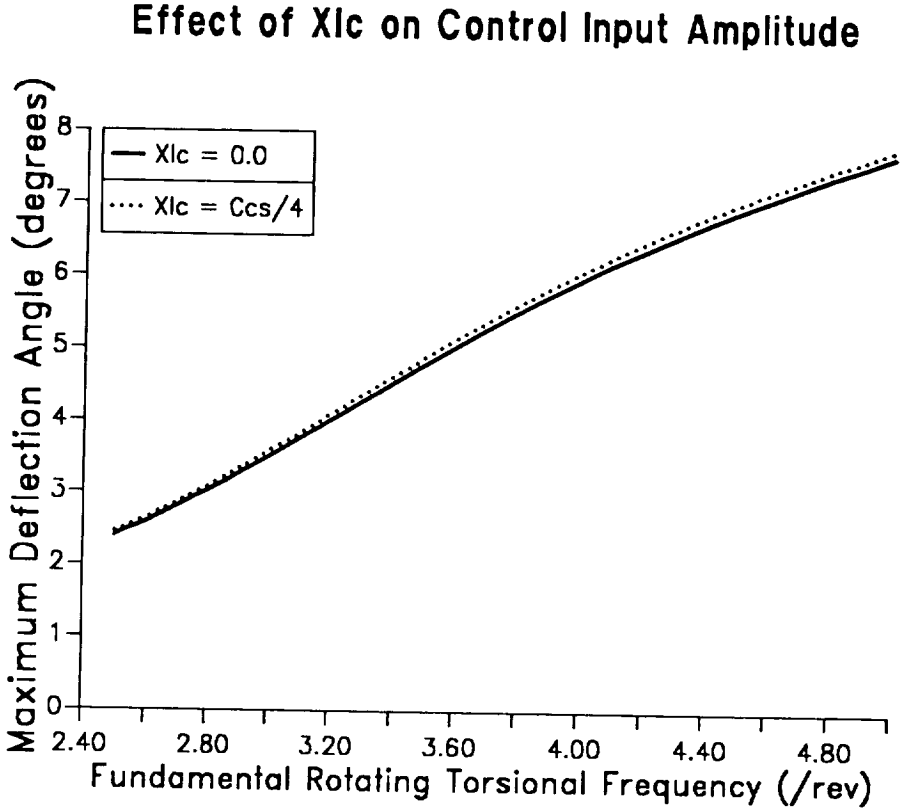

Figure 54: Effect of a mass unbalanced trailing edge flap on the control input amplitudes

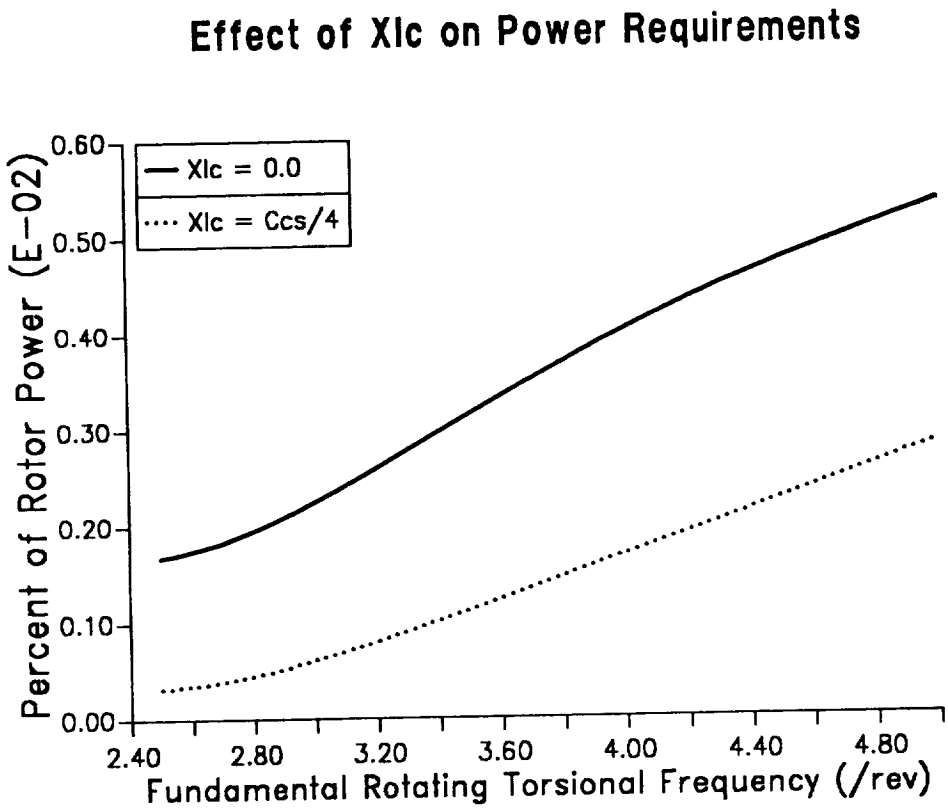

Figure 55: Effect of a mass unbalanced trailing edge flap on the control power requirements

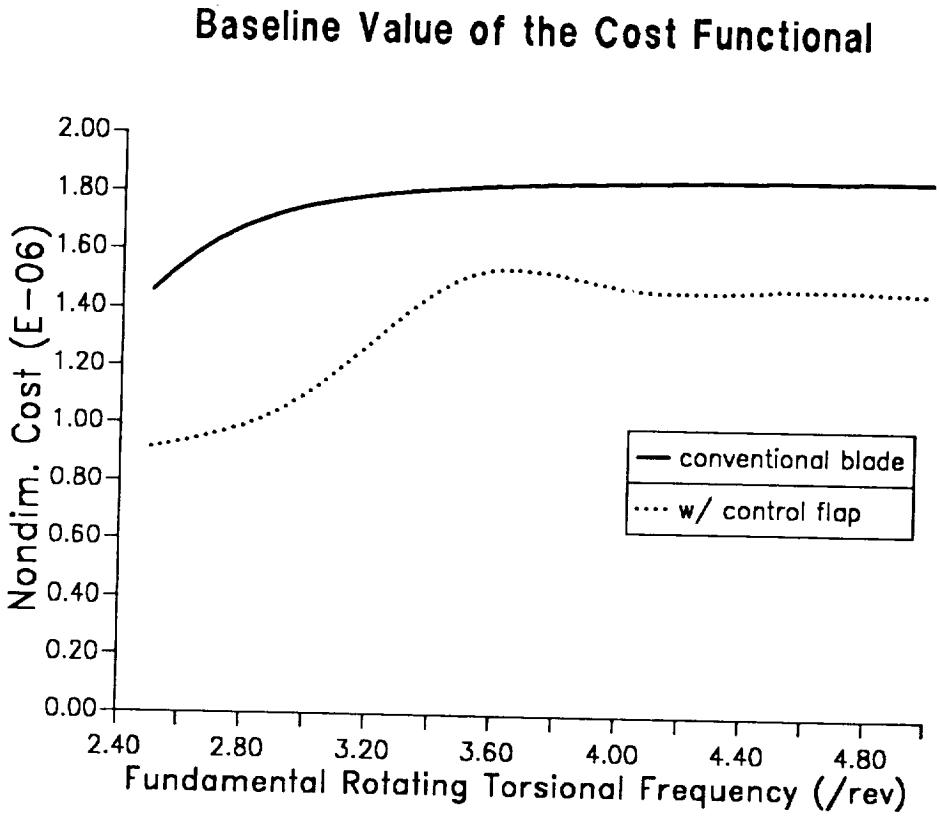

Figure 56: Uncontrolled value of the quadratic cost functional

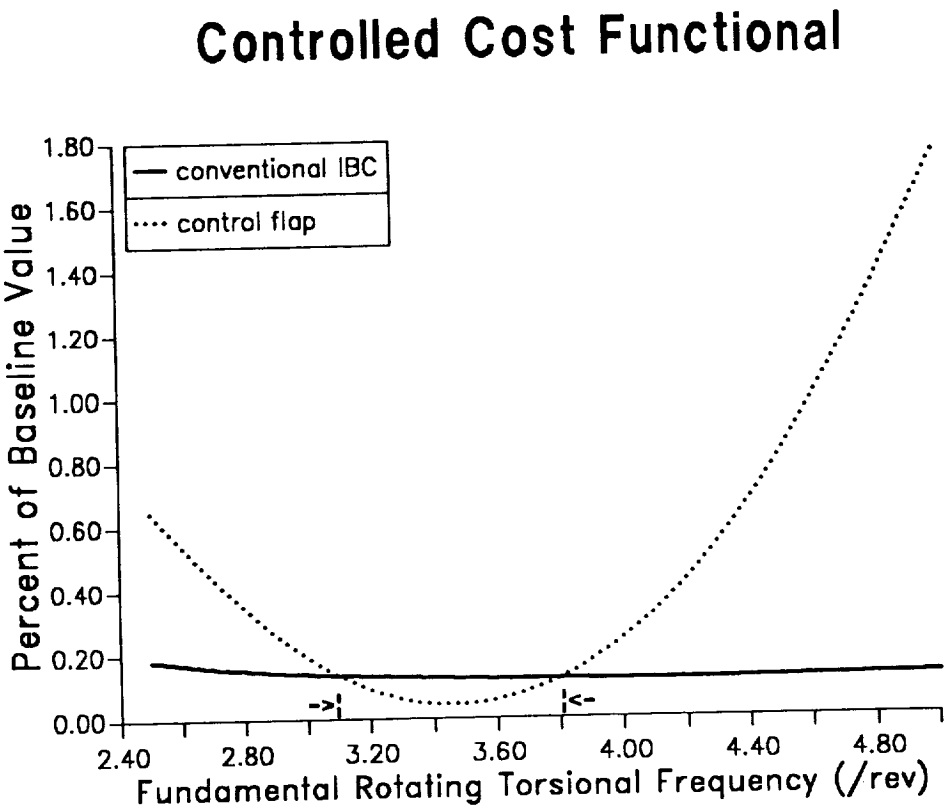

Figure 57: Minimized value of the quadratic cost functional

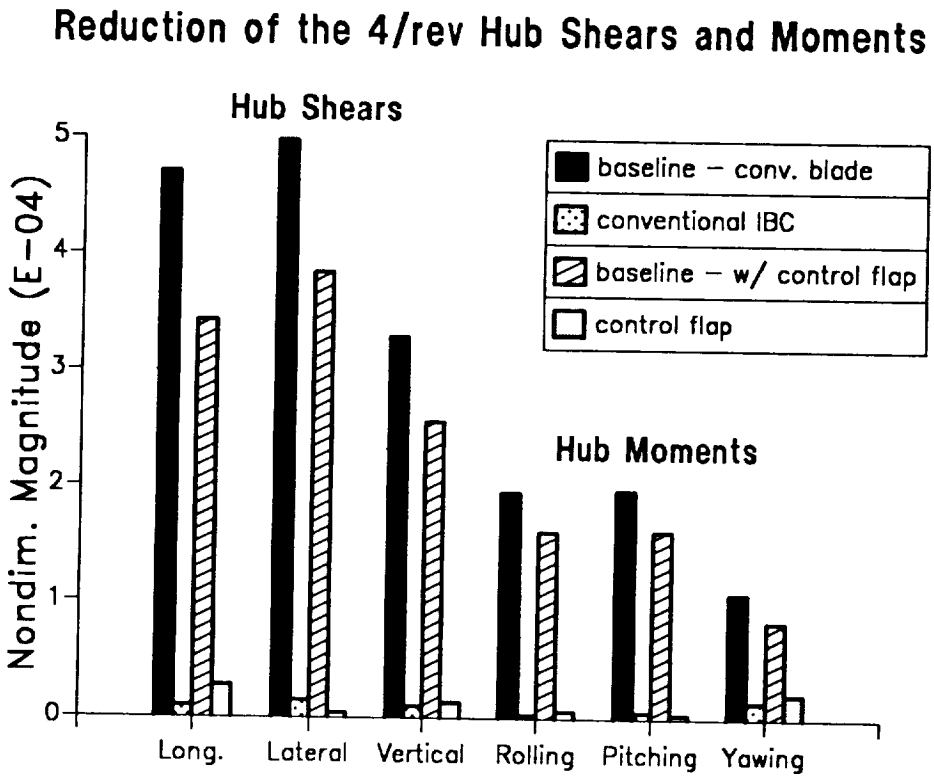

Figure 58: Simultaneous reduction of the 4/rev hub shears and moments, $\omega_{T1} = 2.5$/rev

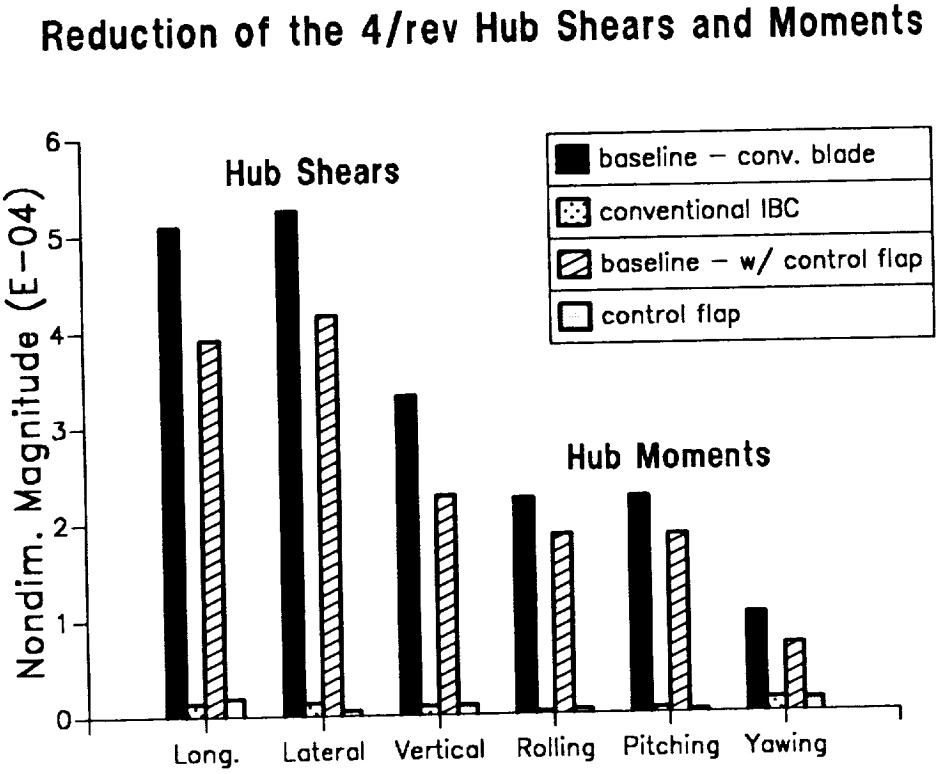

Figure 59: Simultaneous reduction of the 4/rev hub shears and moments, ω_{T1} = 3/rev

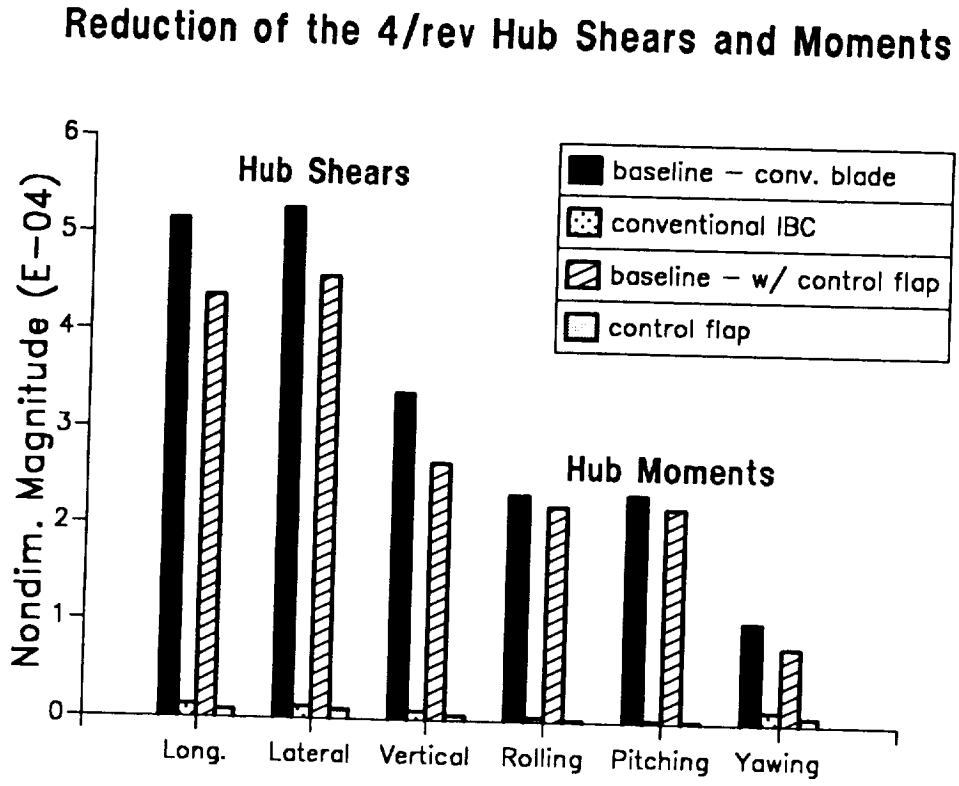

Figure 60: Simultaneous reduction of the 4/rev hub shears and moments, $\omega_{T1} = 3.5$/rev

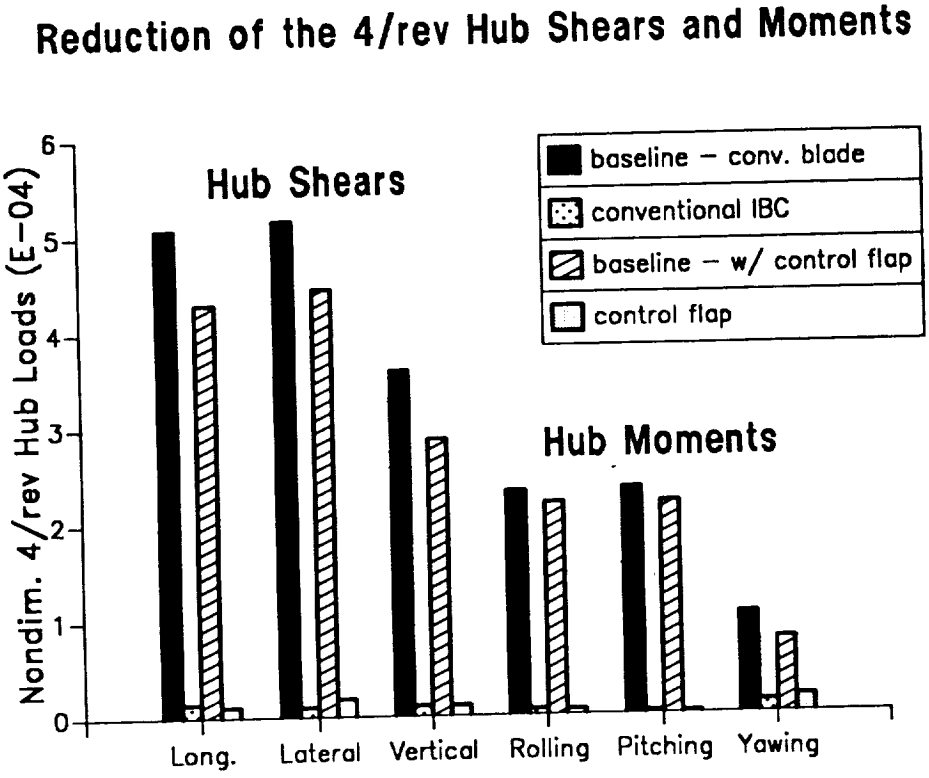

Figure 61: Simultaneous reduction of the 4/rev hub shears and moments, ω_{T1} = 4/rev

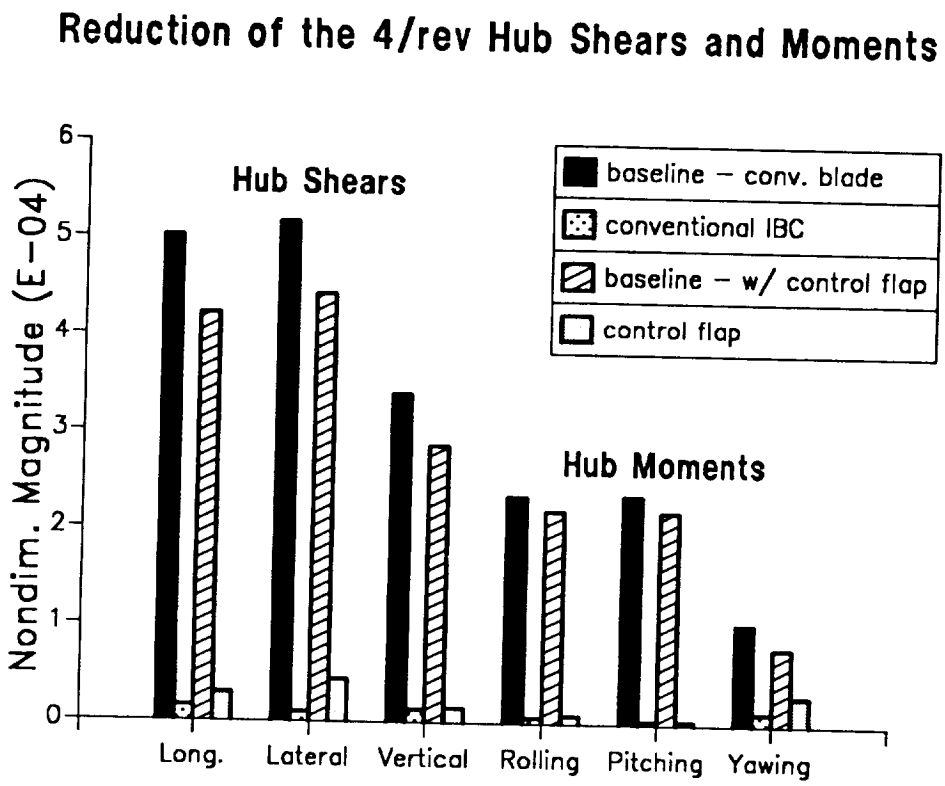

Figure 62: Simultaneous reduction of the 4/rev hub shears and moments, ω_{T1} = 4.5/rev

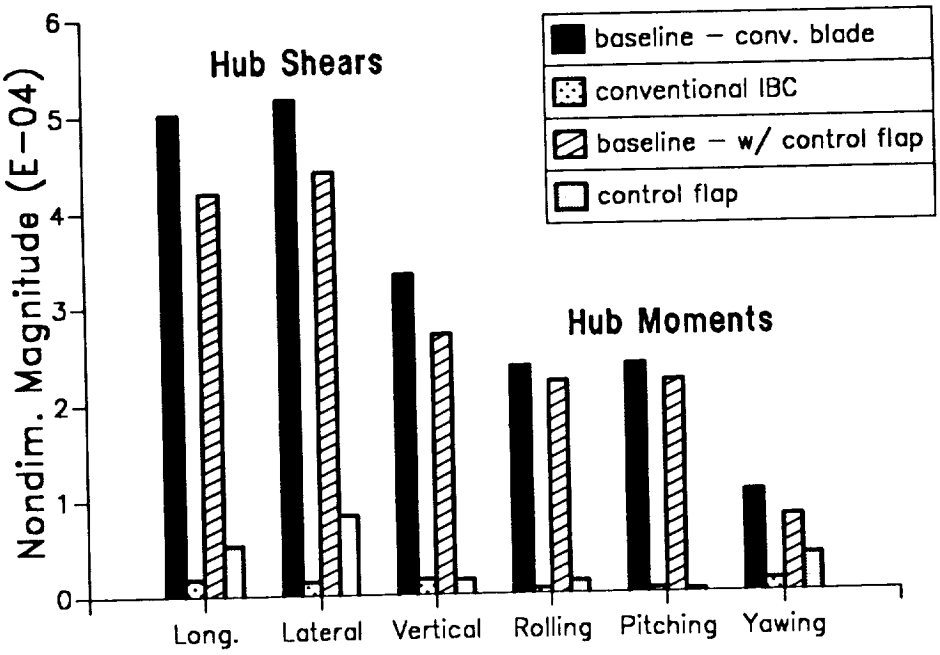

Figure 63: Simultaneous reduction of the 4/rev hub shears and moments, $\omega_{T1} = 5$/rev

Q-4.

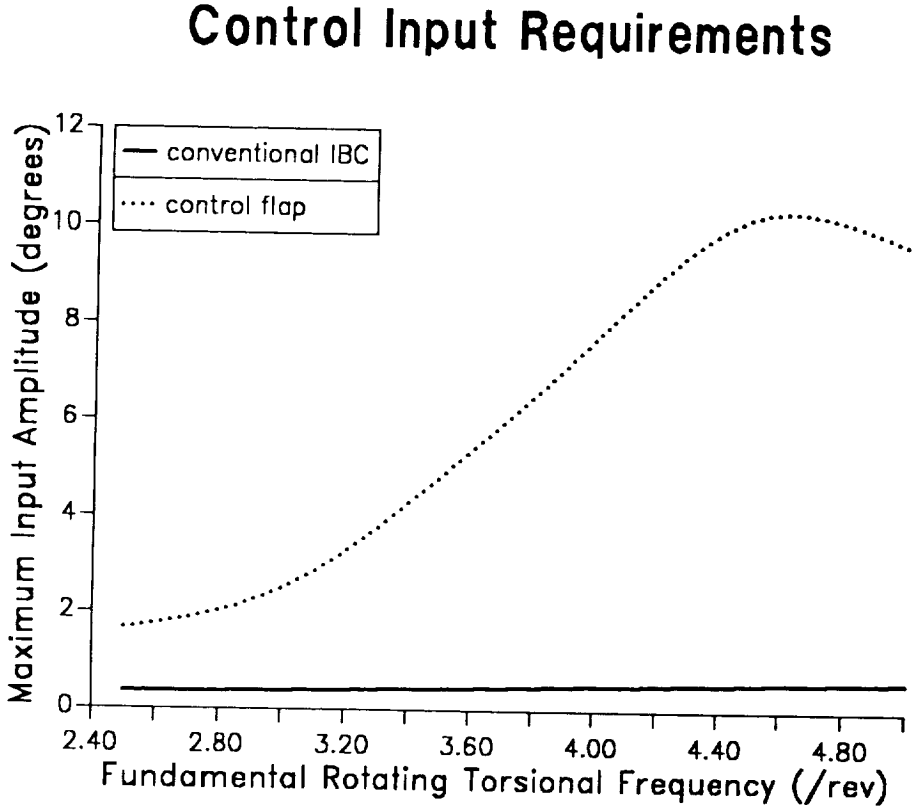

Figure 64: Control input requirements for conventional IBC and the actively controlled flap

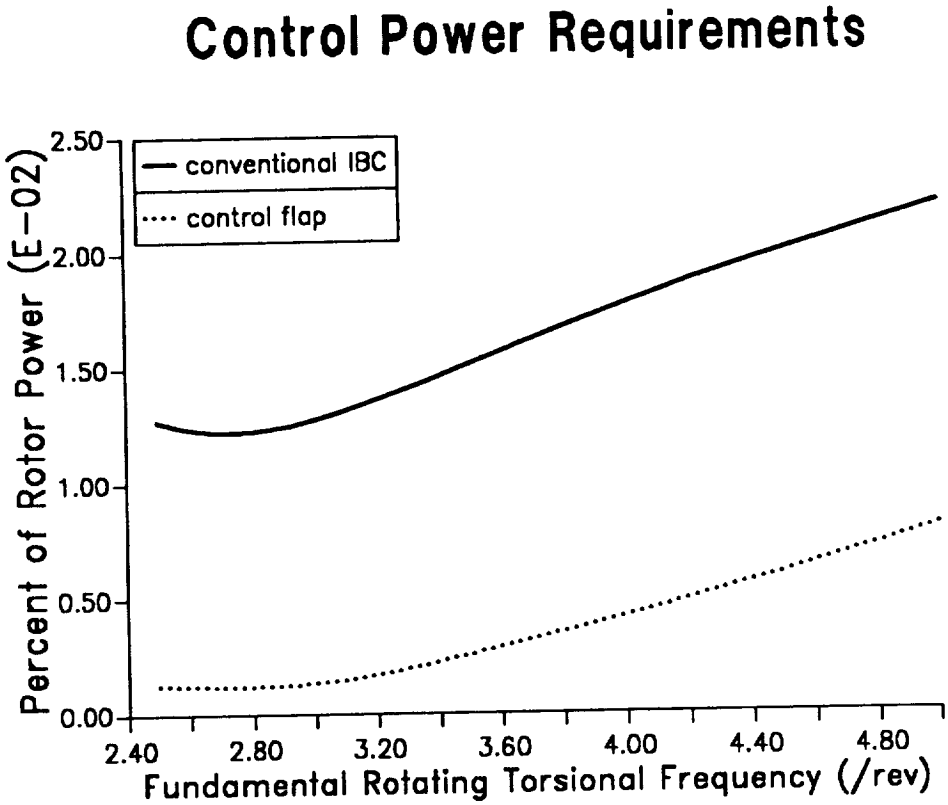

Figure 65: Power Requirements

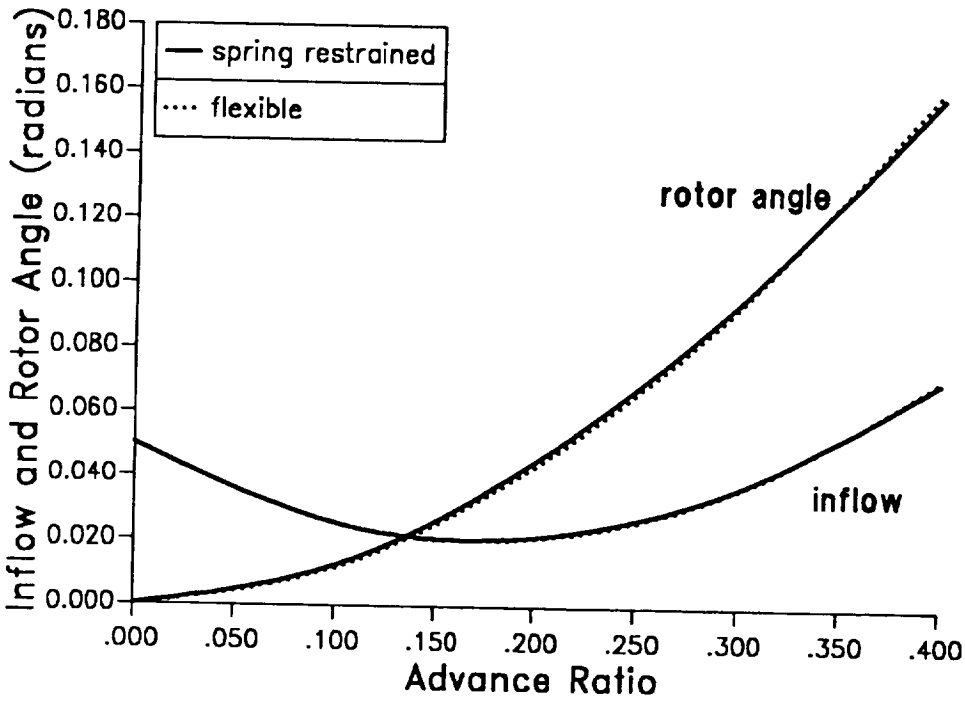

Figure 66: Trim results: inflow and rotor angle of attack

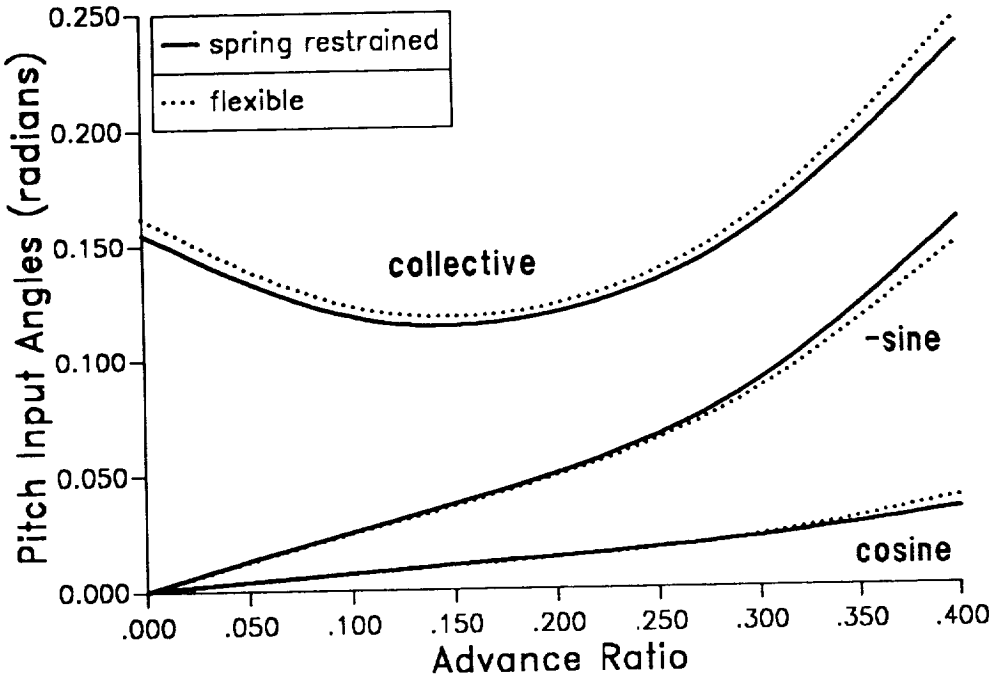

Figure 67: Trim results: pitch inputs

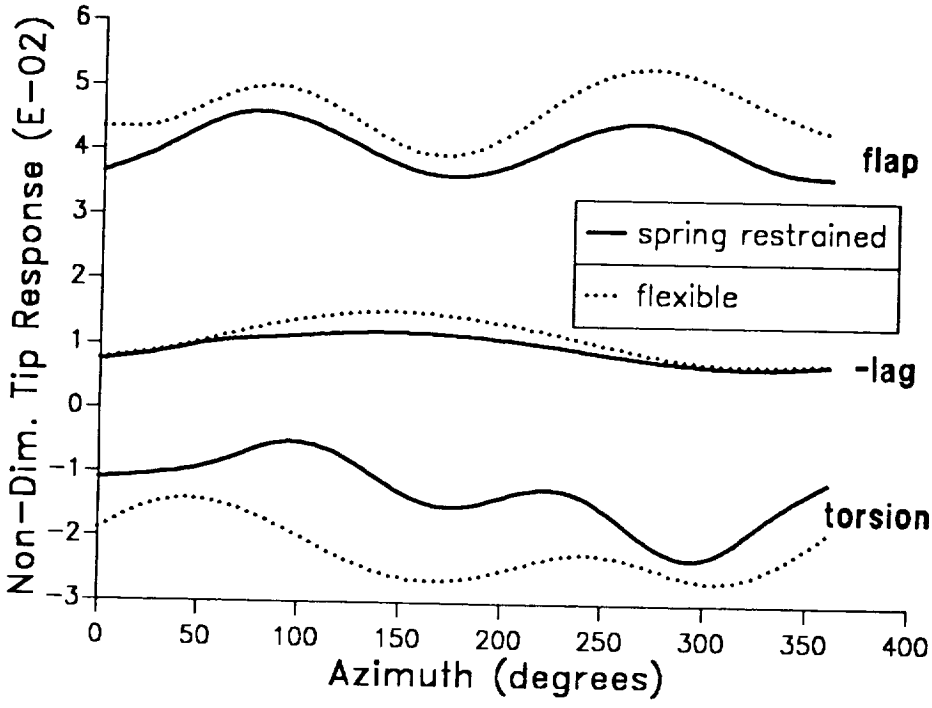

Figure 68: Tip response results

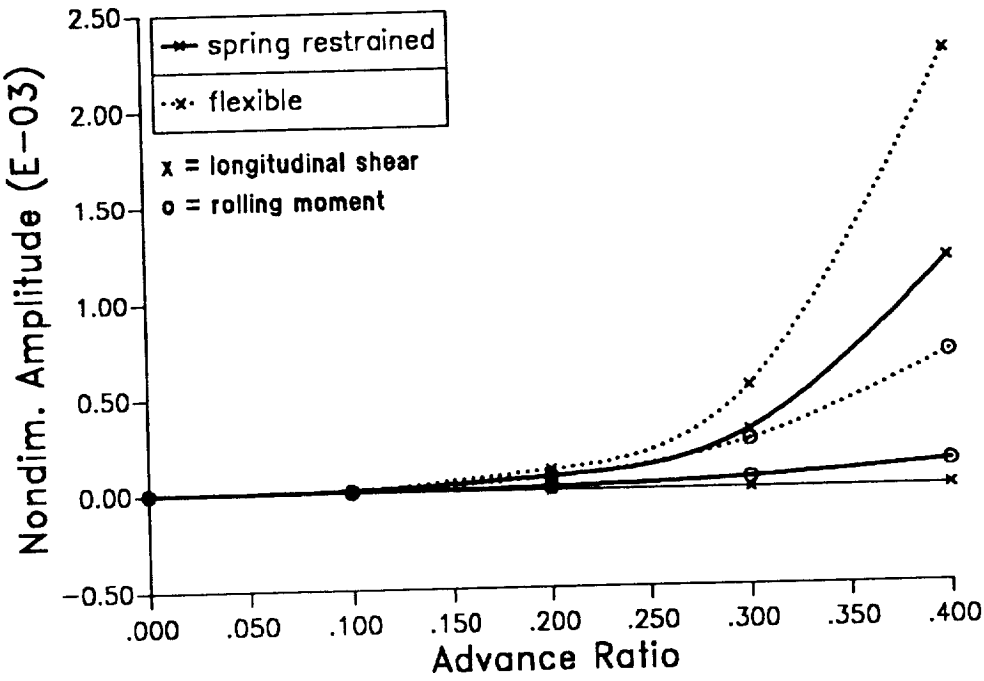

Figure 69: 4/rev longitudinal hub shear and rolling moment

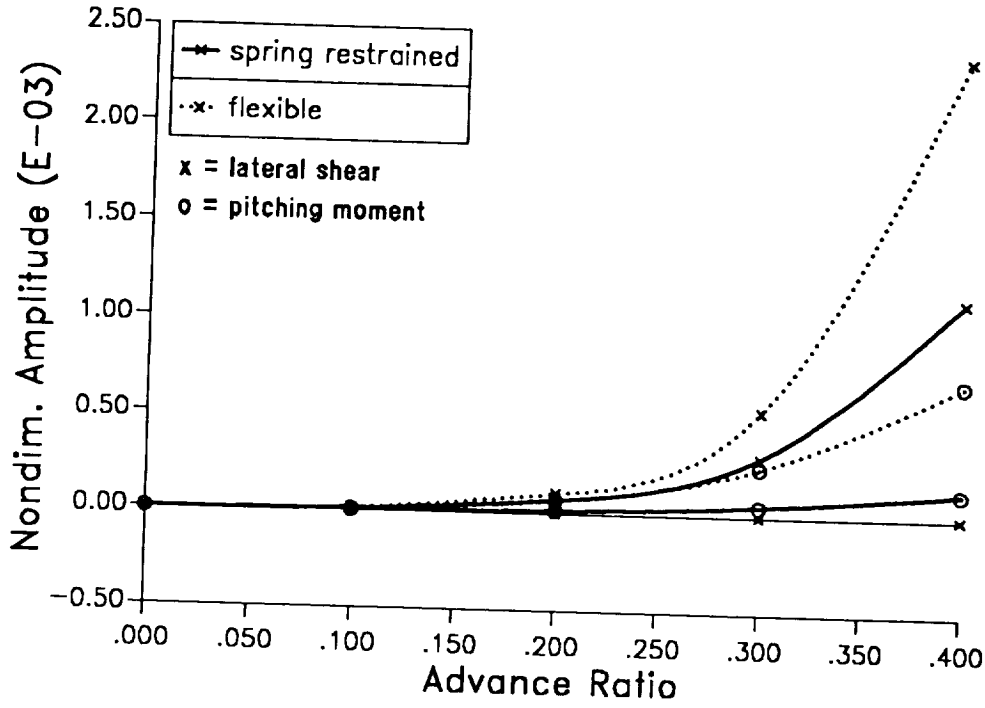

Figure 70: 4/rev lateral hub shear and pitching moment

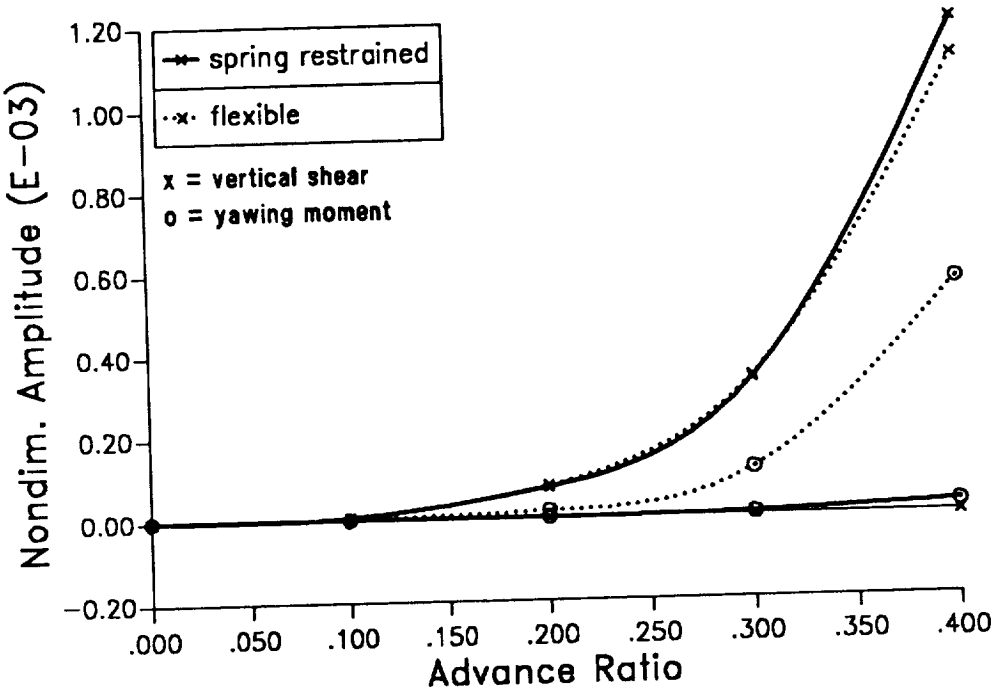

Figure 71: 4/rev vertical hub shear and yawing moment

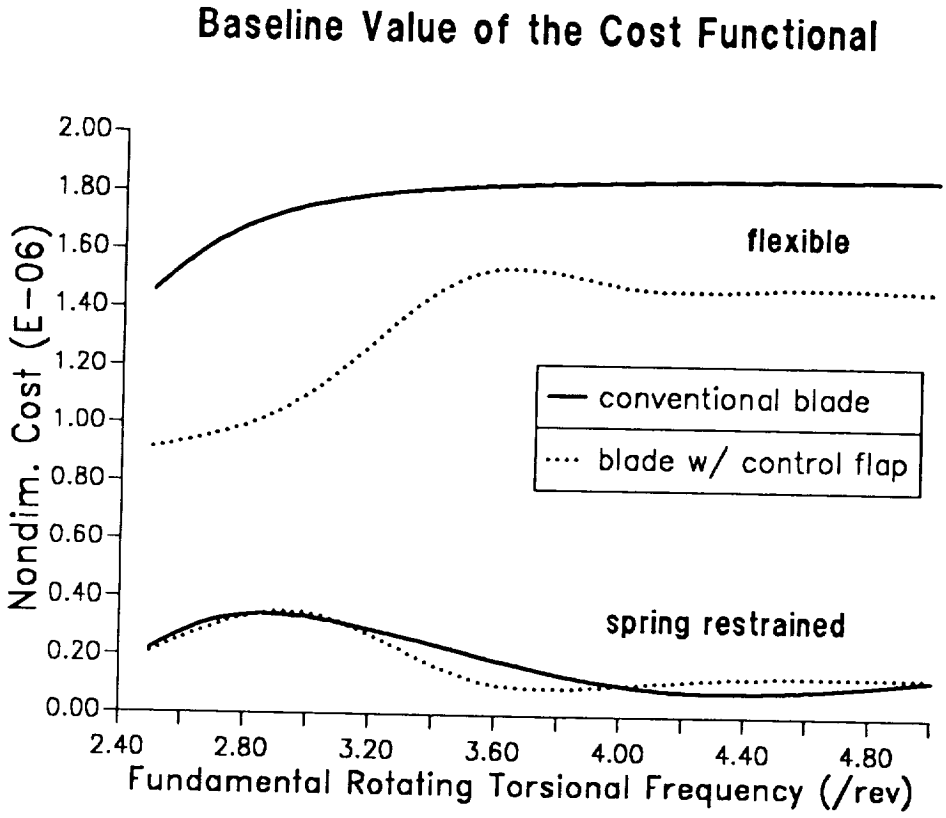

Figure 72: Uncontrolled value of the quadratic cost functional

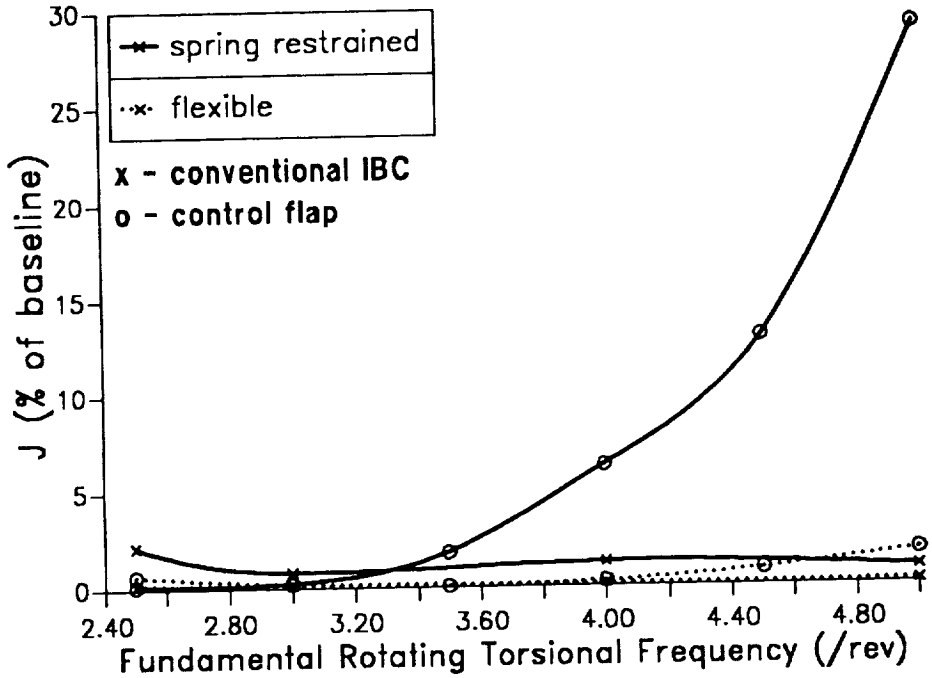

Figure 73: Minimized value of the quadratic cost functional

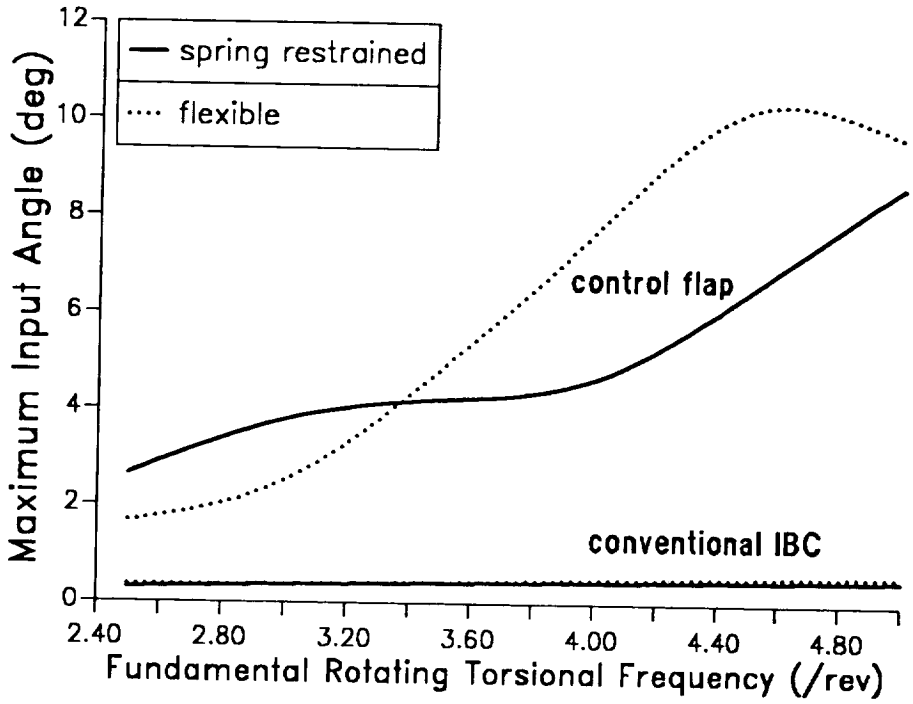

Figure 74: Control input requirements for conventional IBC and the actively controlled flap

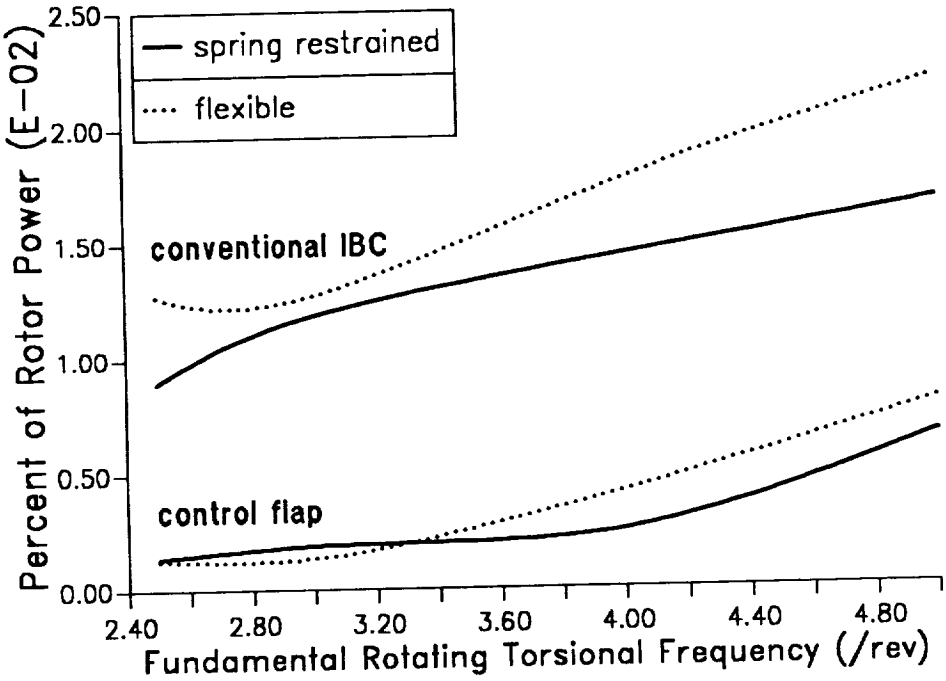

Figure 75: Power Requirements

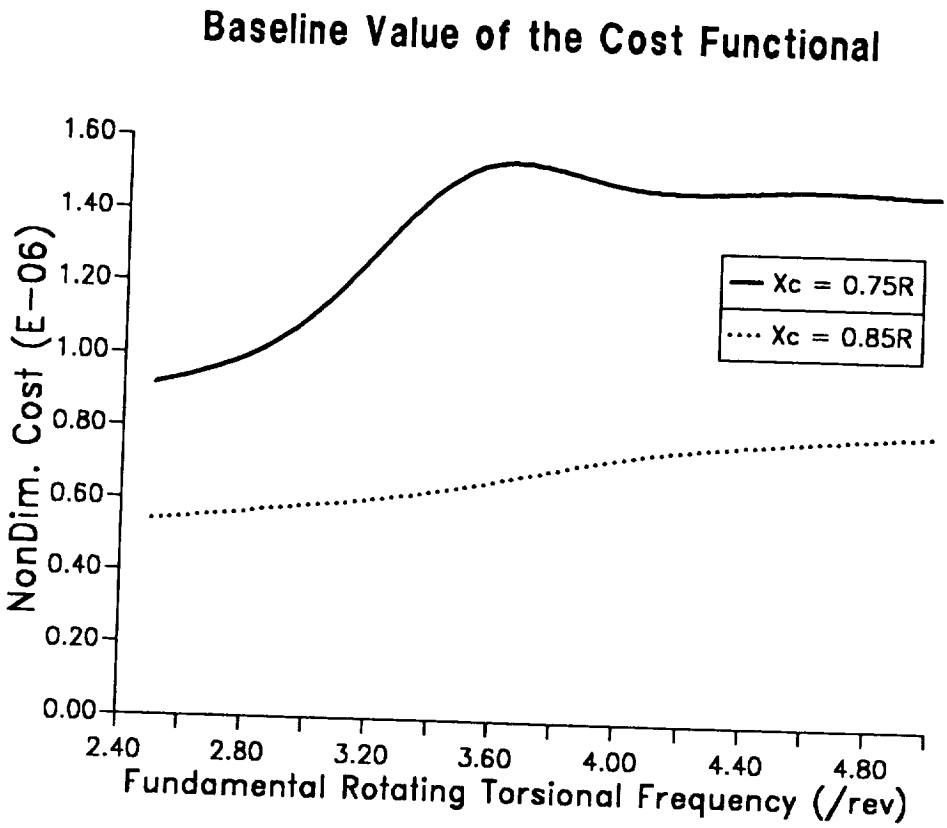

Figure 76: Effect of the spanwise location of the control flap on the uncontrolled value of the cost functional

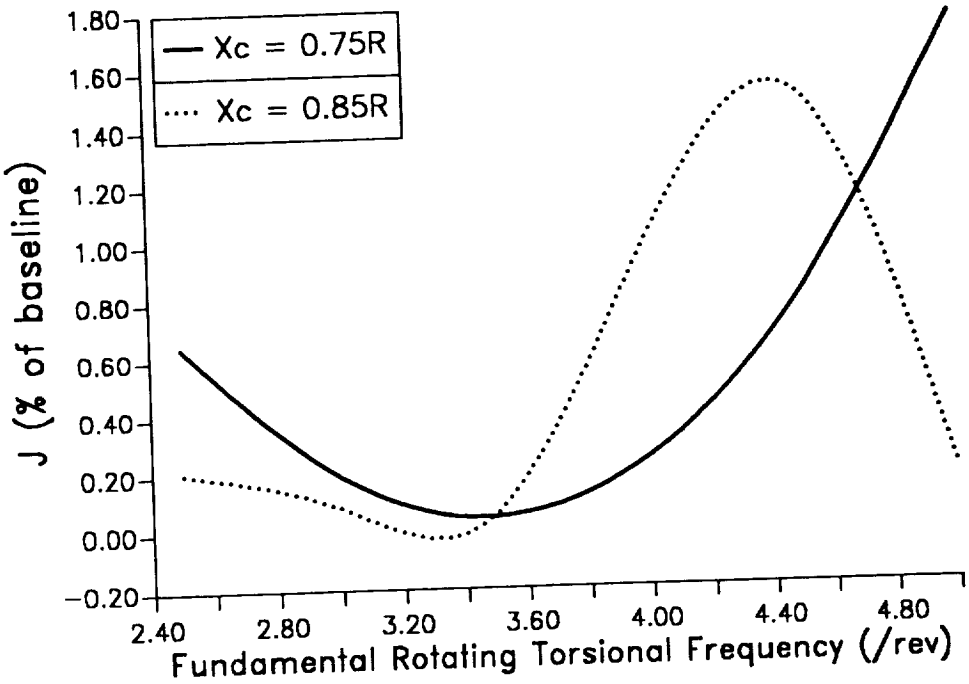

Figure 77: Effect of the spanwise location of the control flap on its vibration reduction effectiveness

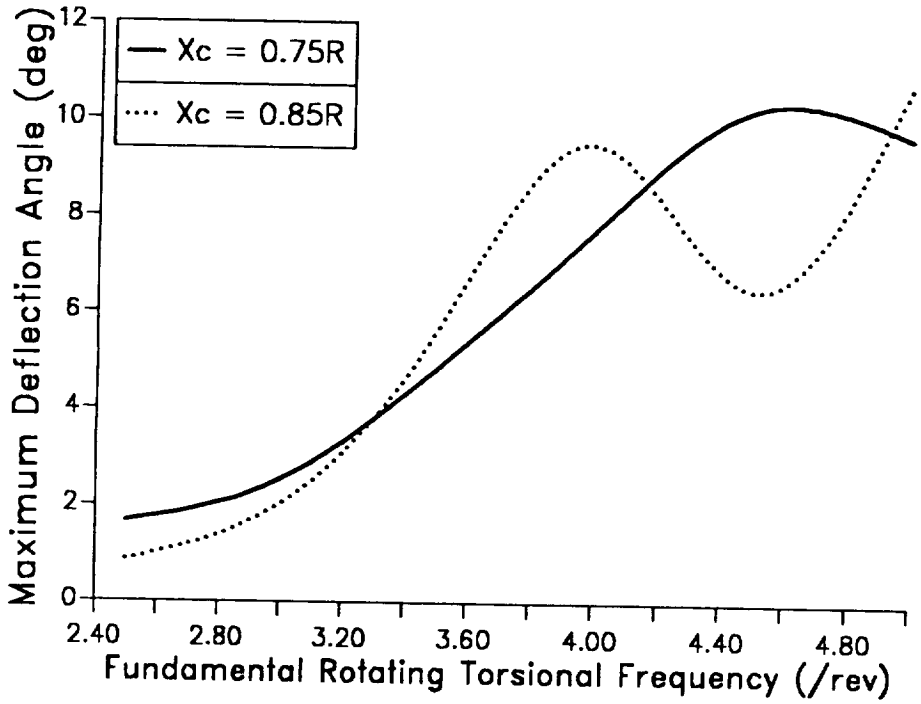

Figure 78: Effect of the spanwise location of the control flap on the control input requirements

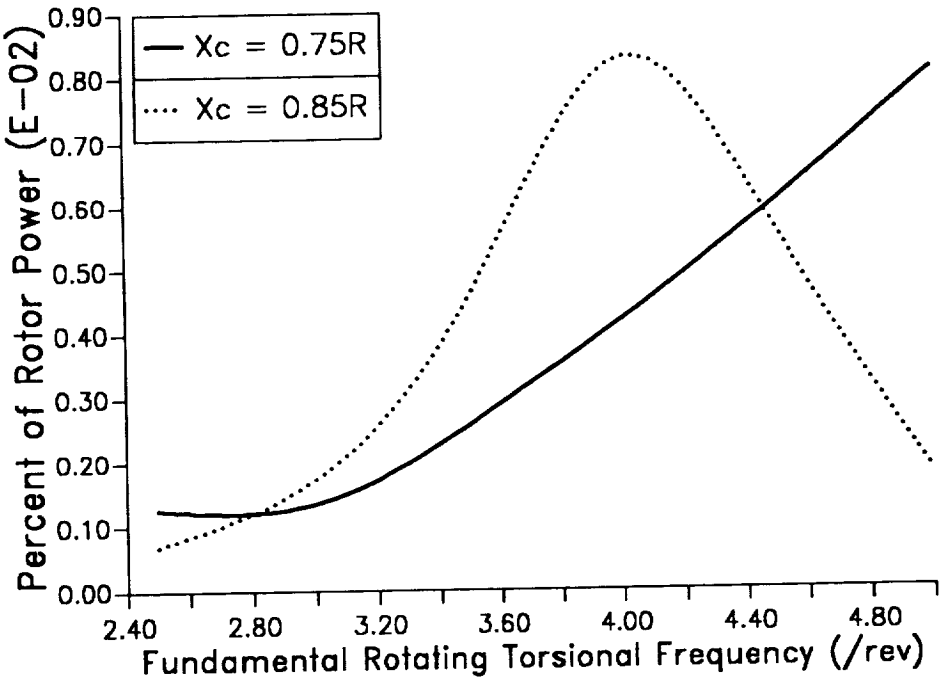

Figure 79: Effect of the spanwise location of the control flap on the power requirements

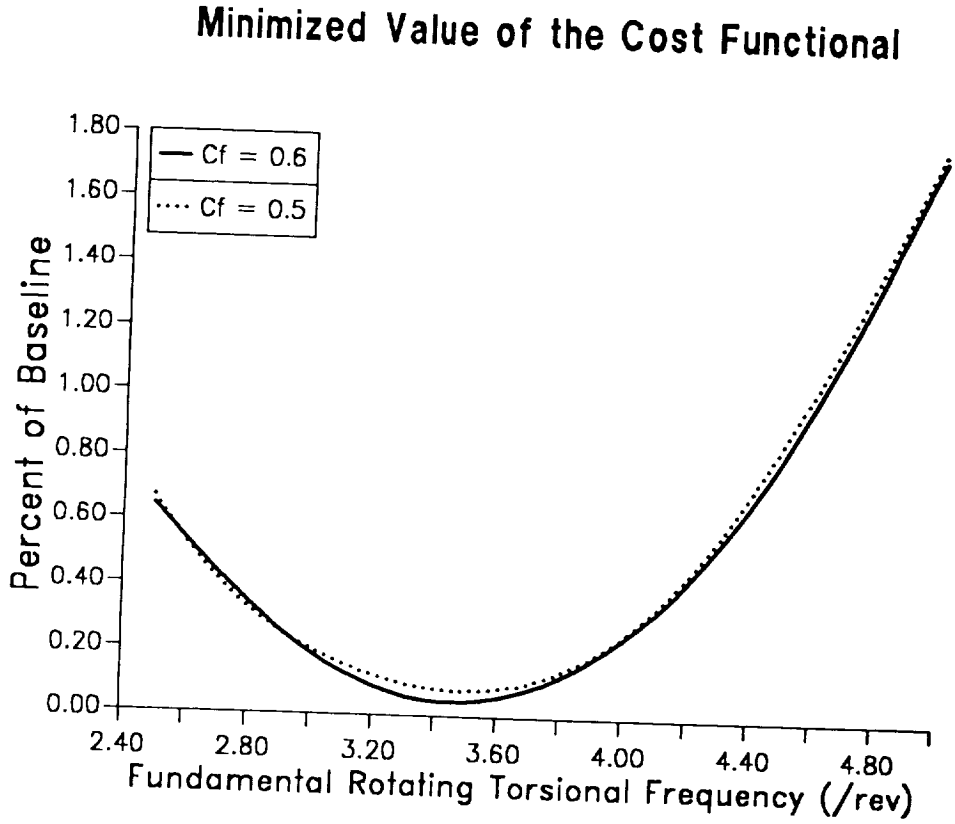

Figure 80: Effect of hinge moment correction on vibration reduction effectiveness of the control flap

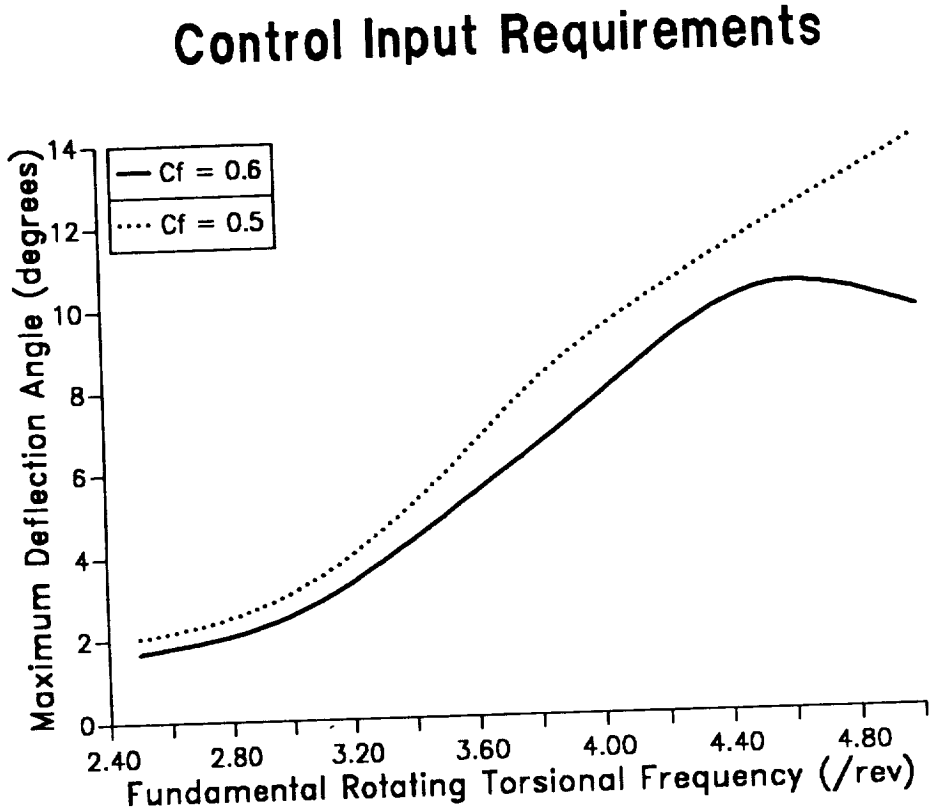

Figure 81: Effect of hinge moment correction on the control input requirements of the control flap

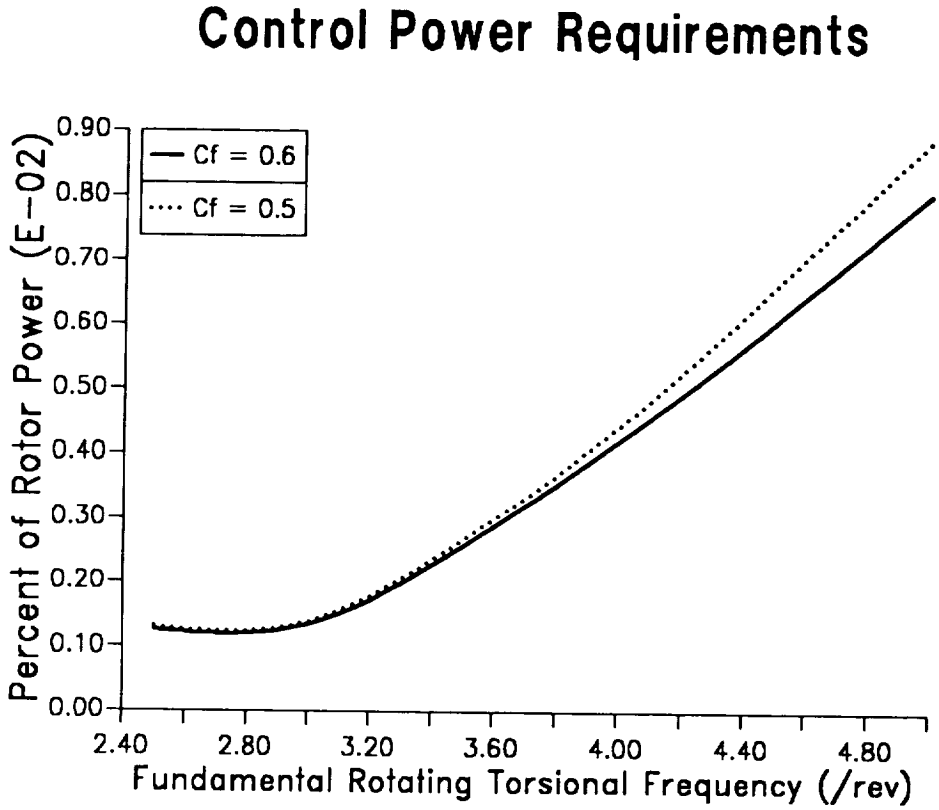

Figure 82: Effect of hinge moment correction on the power requirements of the control flap

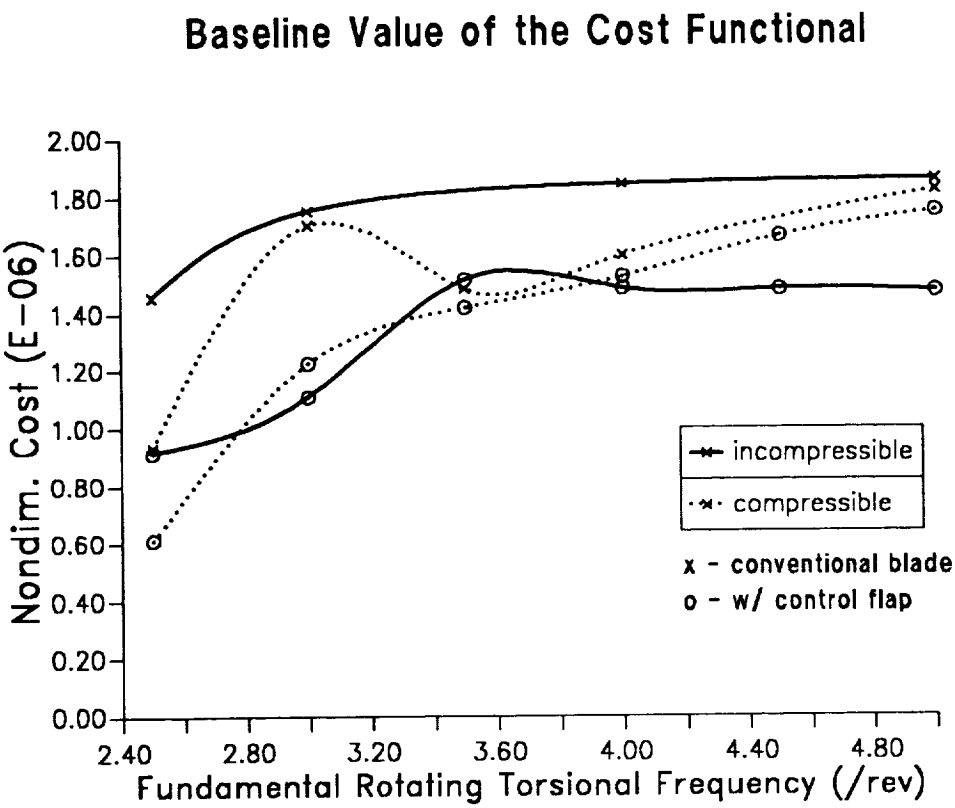

Figure 83: Effect of compressibility on the uncontrolled value of the cost functional

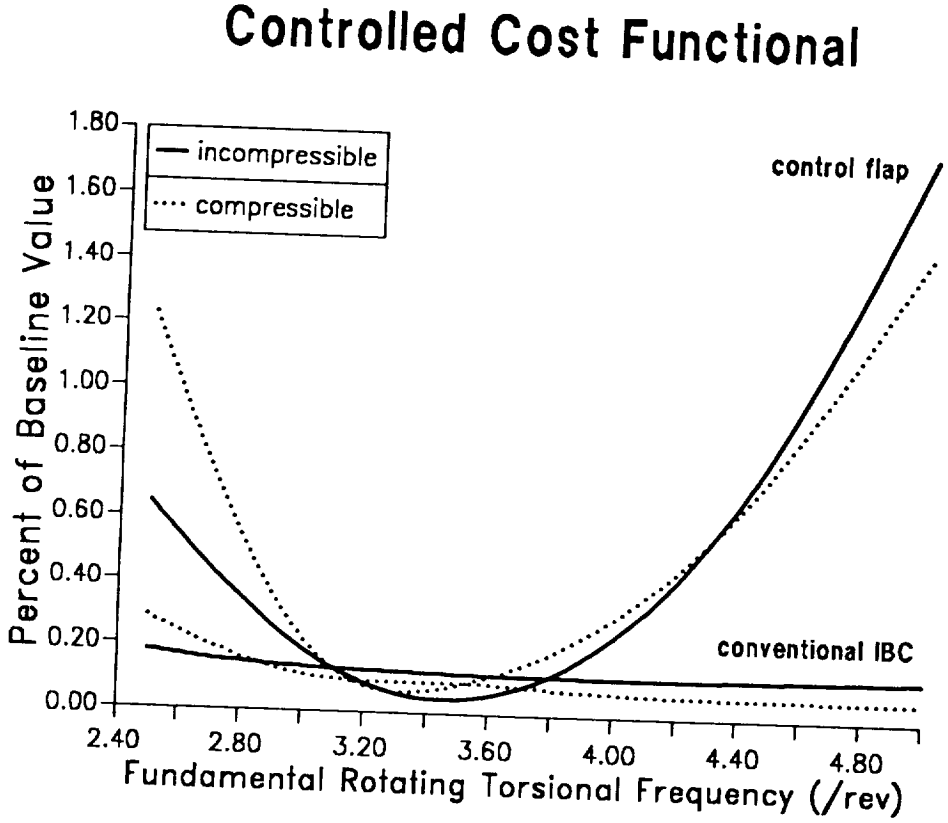

Figure 84: Effect of compressibility on vibration reduction effectiveness

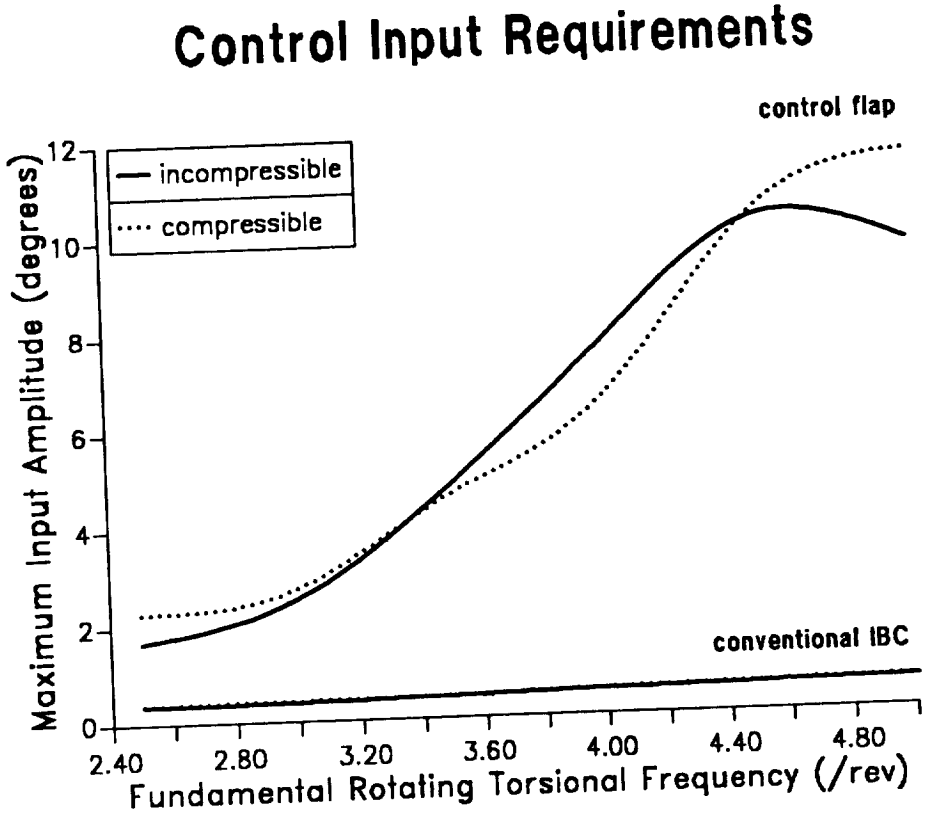

Figure 85: Effect of compressibility on control input requirements

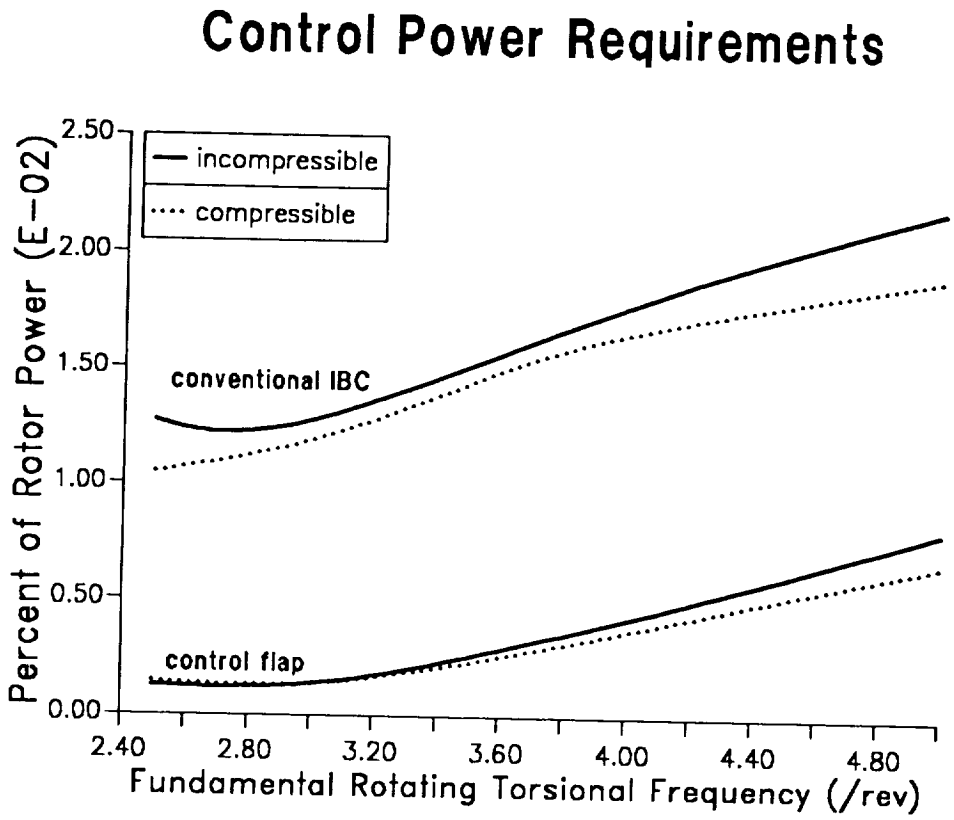

Figure 86: Effect of compressibility on power requirements

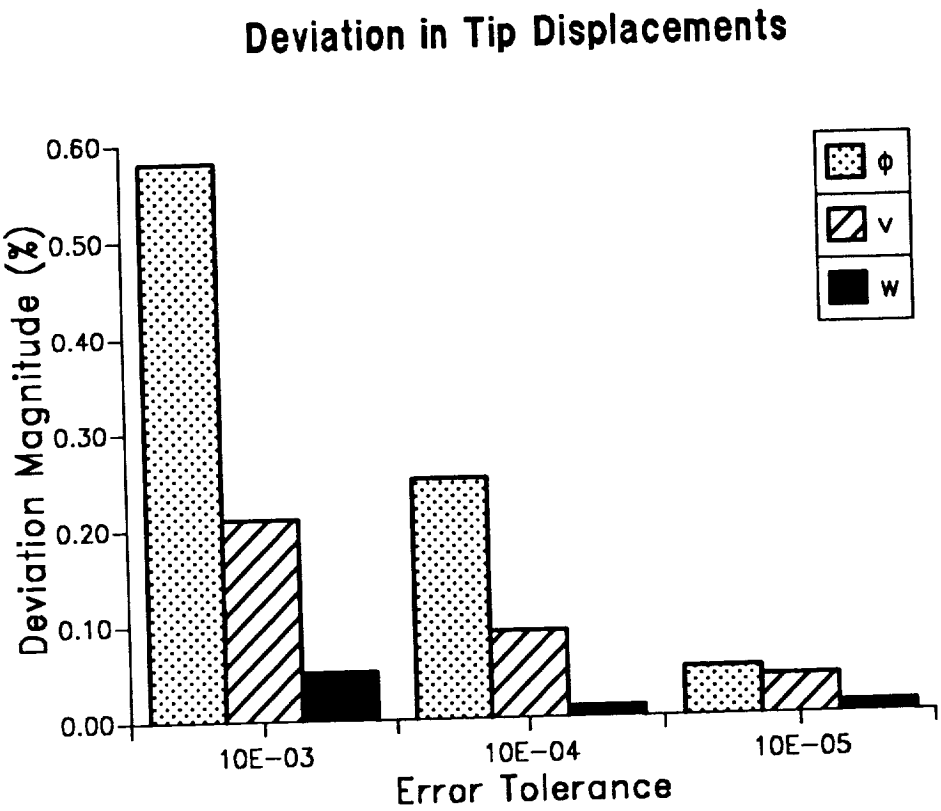

Figure 87: Deviation of tip displacements from steady state values at the end of one rotor revolution, converged solution

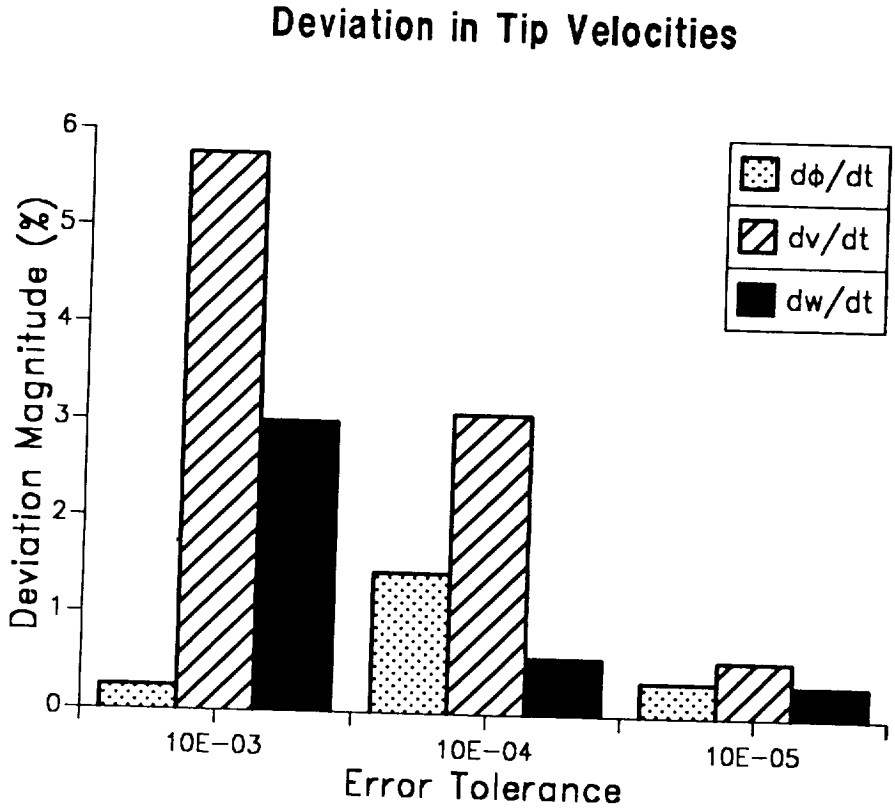

Figure 88: Deviation of tip velocities from steady state values at the end of one rotor revolution, converged solution

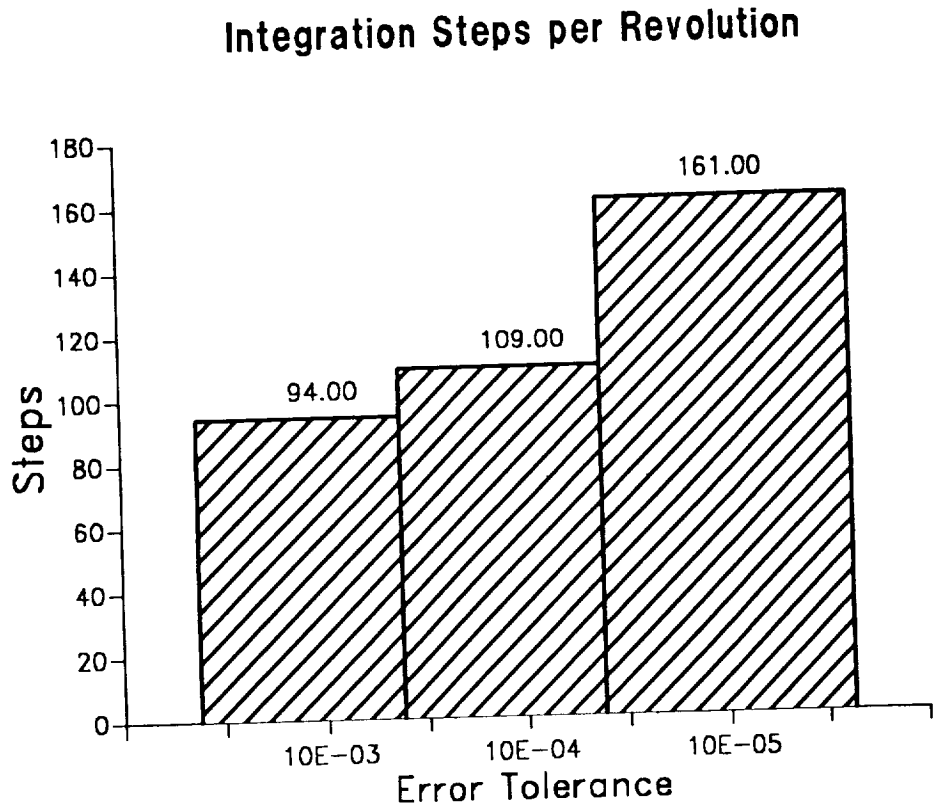

Figure 89: Number of integration steps per revolution, converged solution

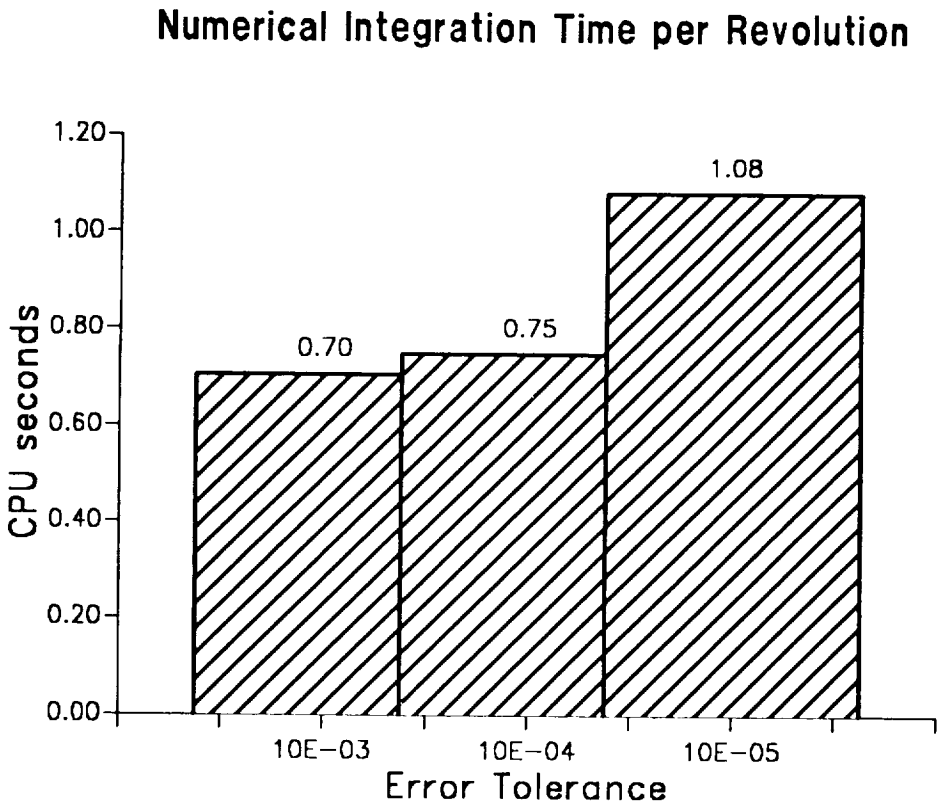

Figure 90: Integration time per revolution, converged solution

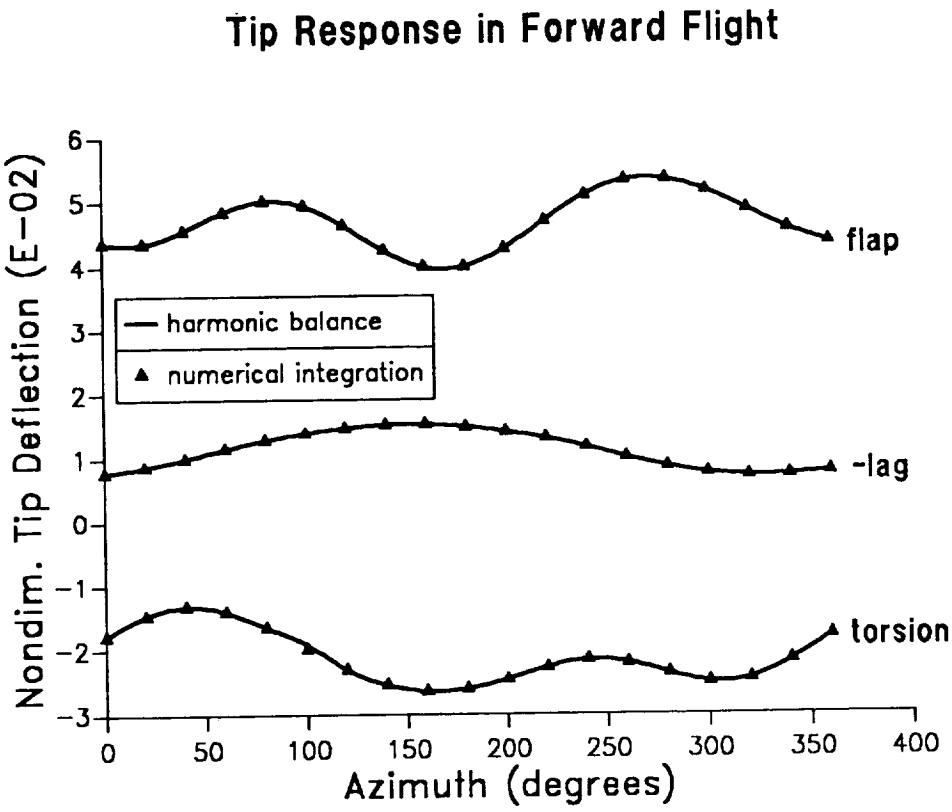

Figure 91: Verification of the steady state tip response solution

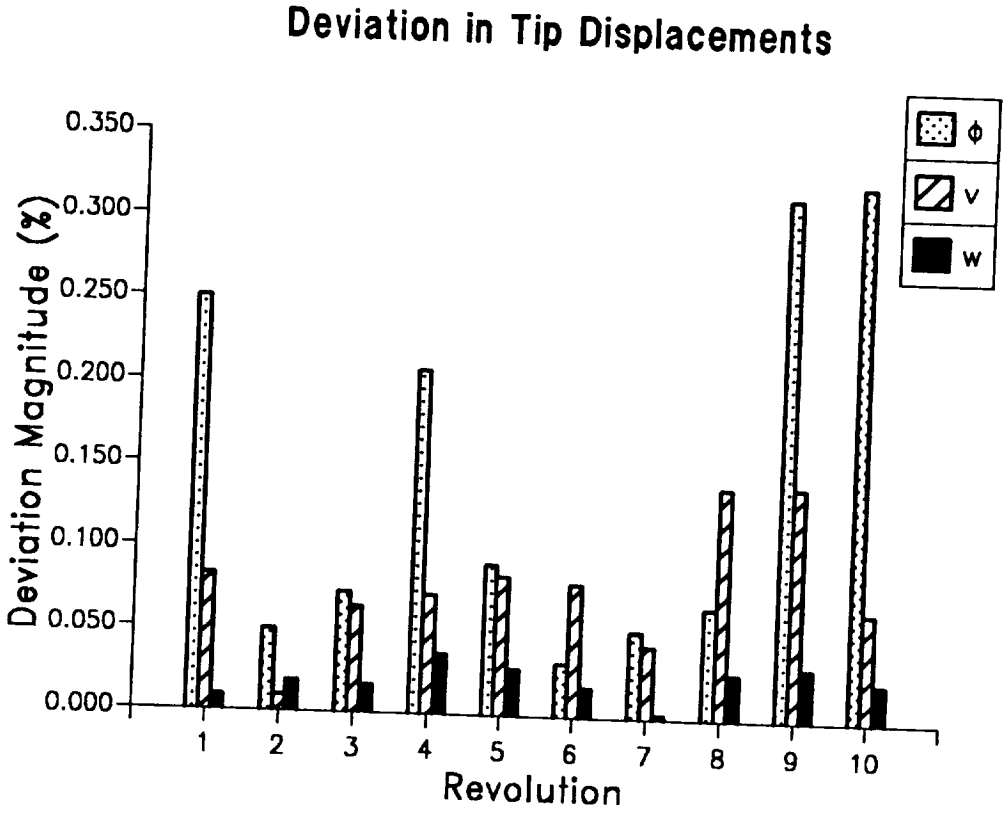

Figure 92: Deviation of tip displacements at the end of each revolution from the steady state values

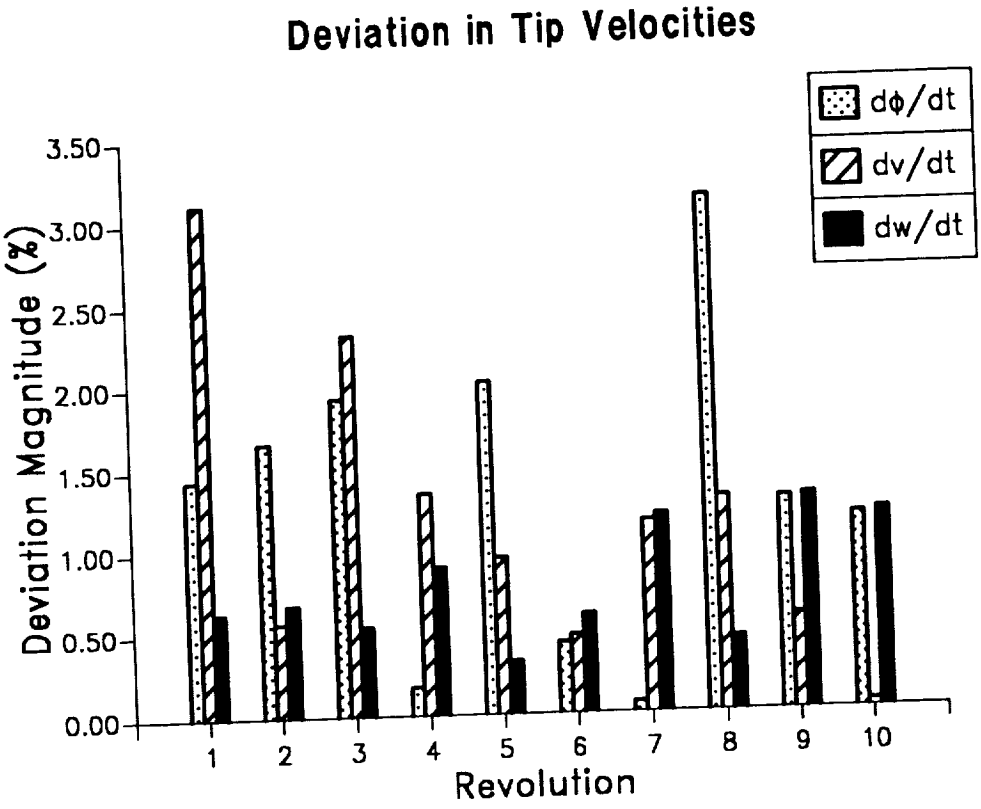

Figure 93: Deviation of the tip velocities at the end of each revolution from the steady state values

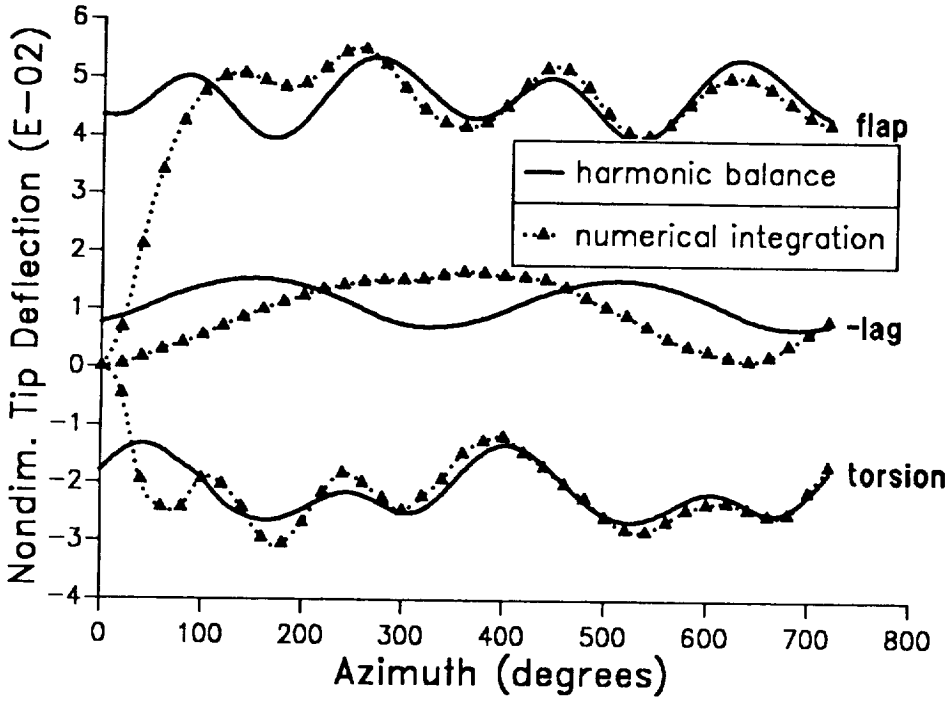

Figure 94: Tip response when the initial conditions are far from the steady state values

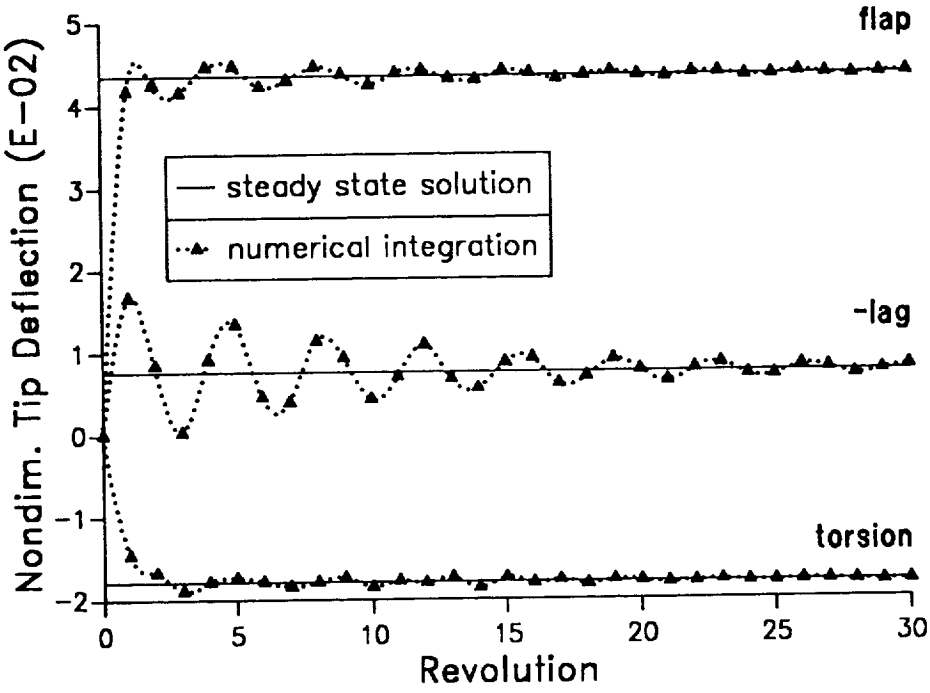

Figure 95: Convergence to a steady state tip response solution

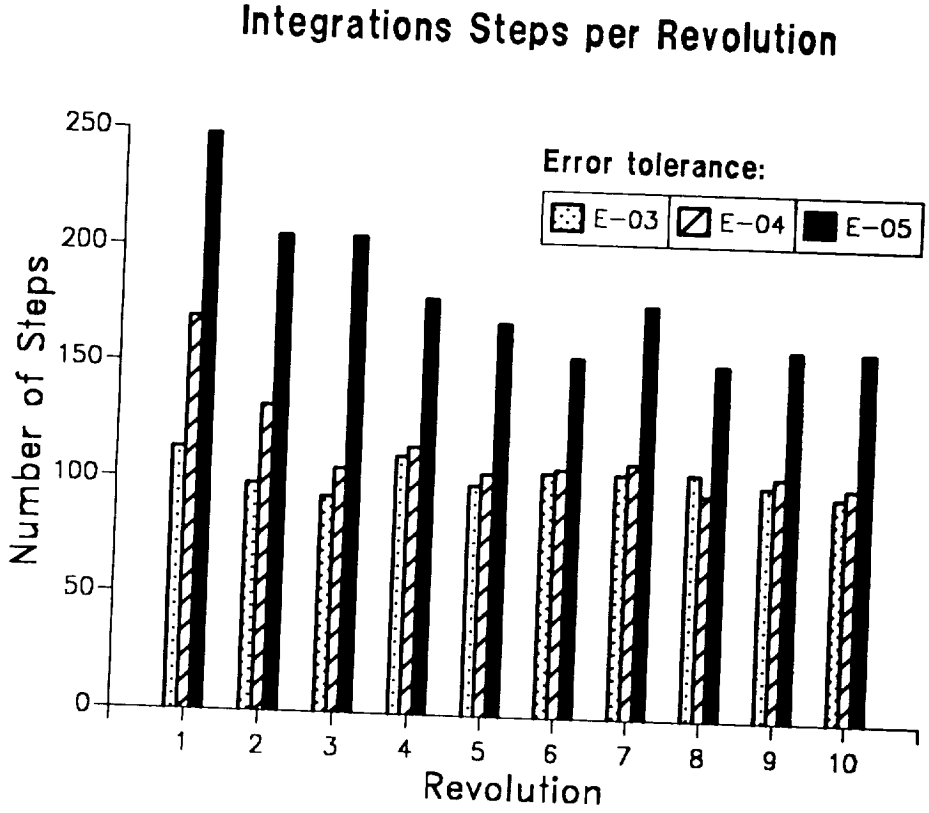

Figure 96: Number of integration steps per revolution when the initial state is far from periodic conditions

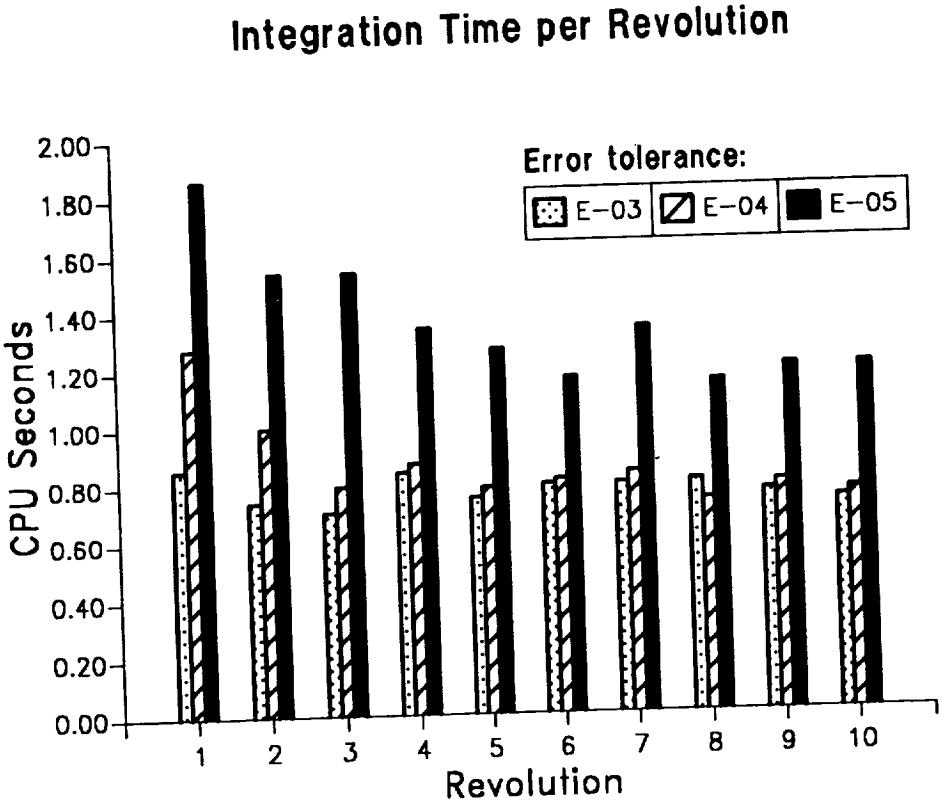

Figure 97: Integration time per revolution when the initial state is far from periodic conditions

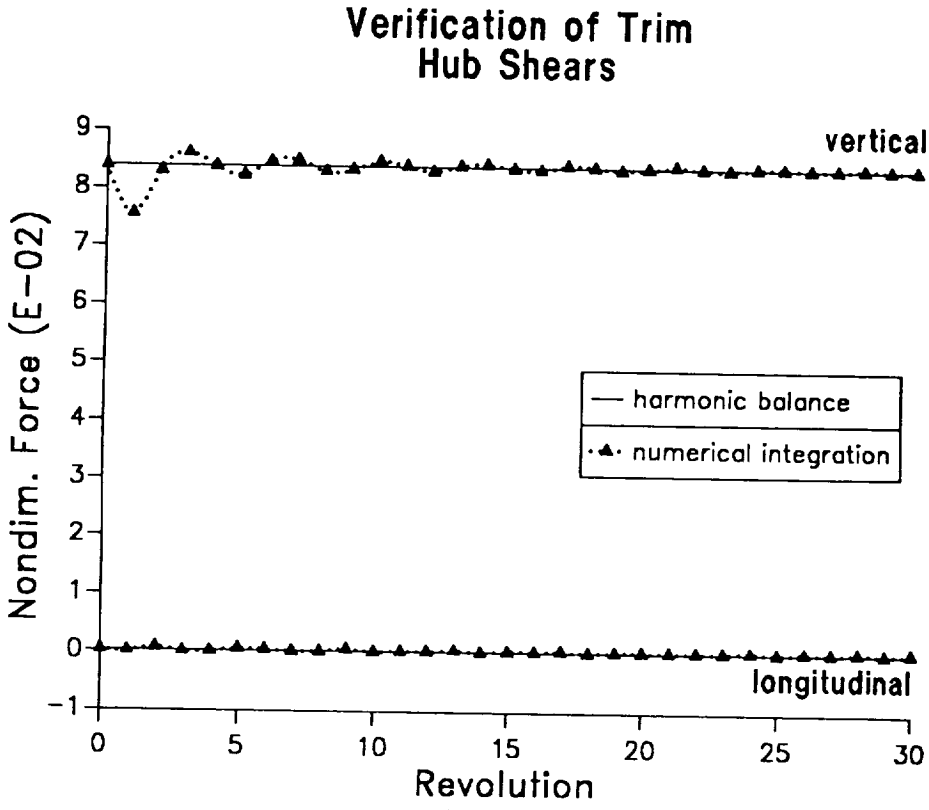

Figure 98: Convergence of trim solution: longitudinal and vertical forces

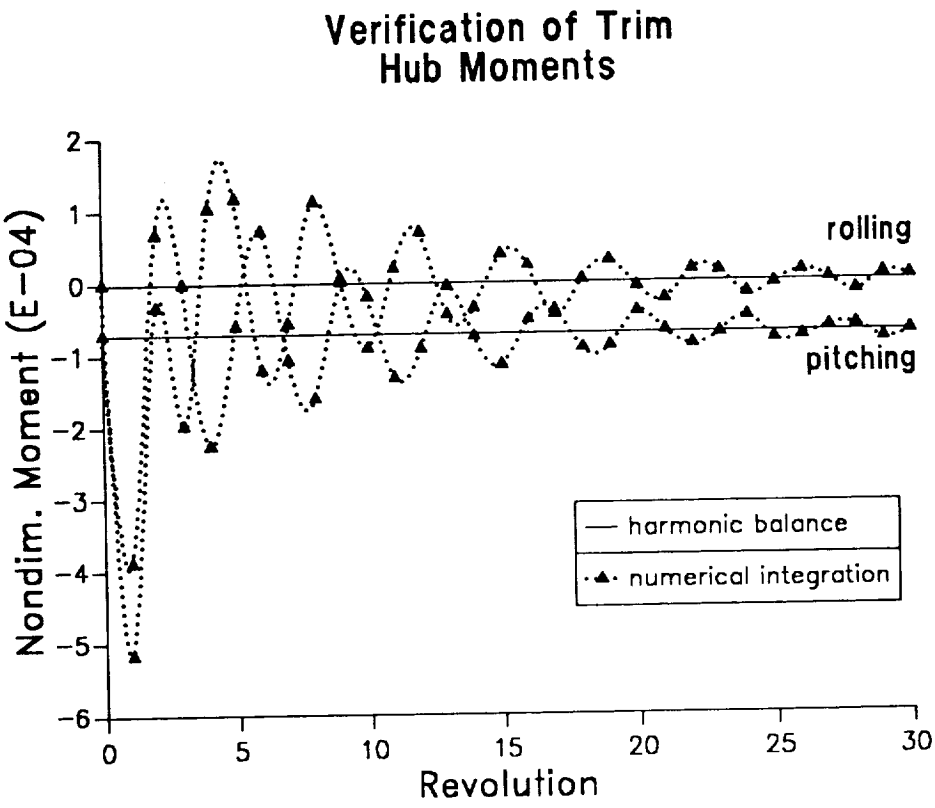

Figure 99: Convergence of trim solution: rolling and pitching moments

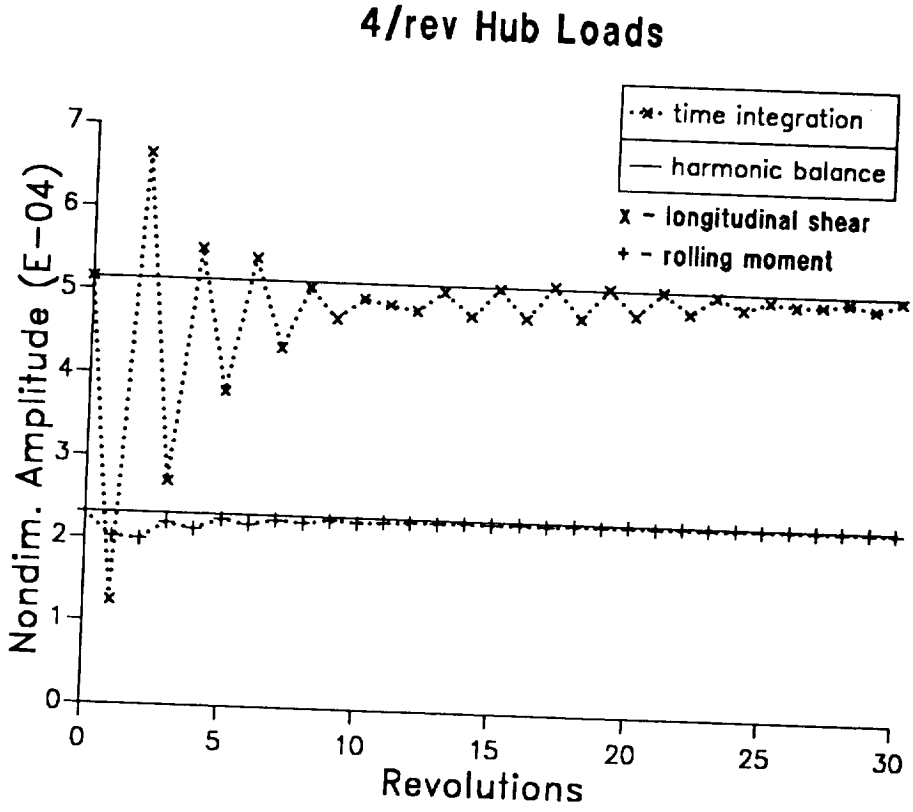

Figure 100: Convergence of vibratory hub loads to steady state: 4/rev longitudinal hub shear and rolling moment

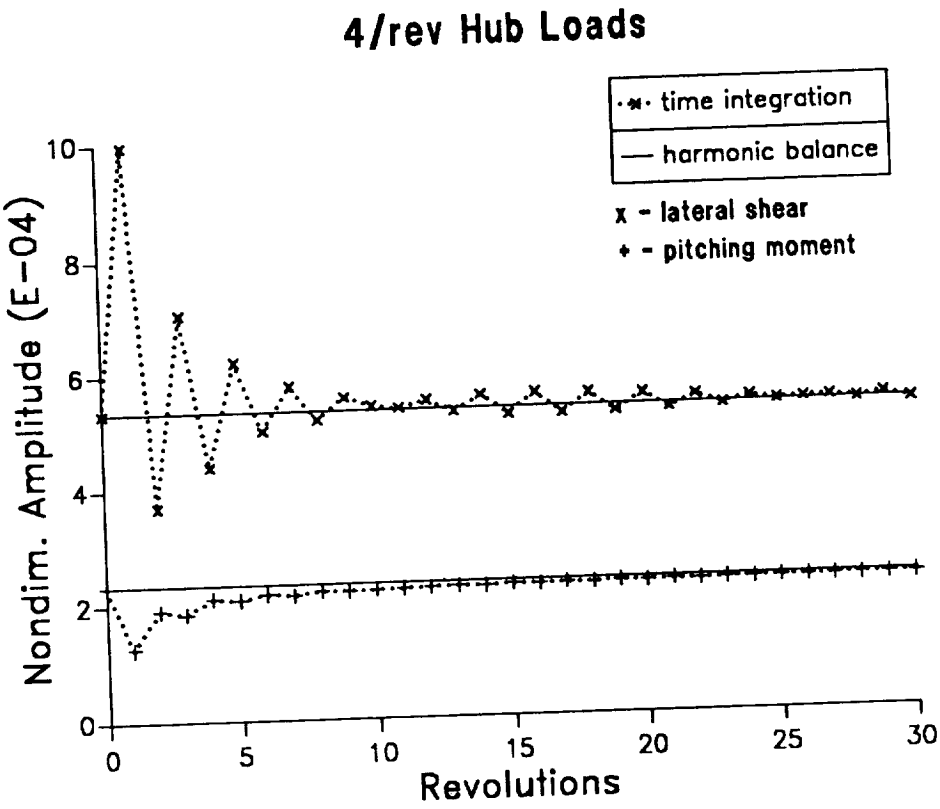

Figure 101: Convergence of vibratory hub loads to steady state: 4/rev lateral hub shear and pitching moment

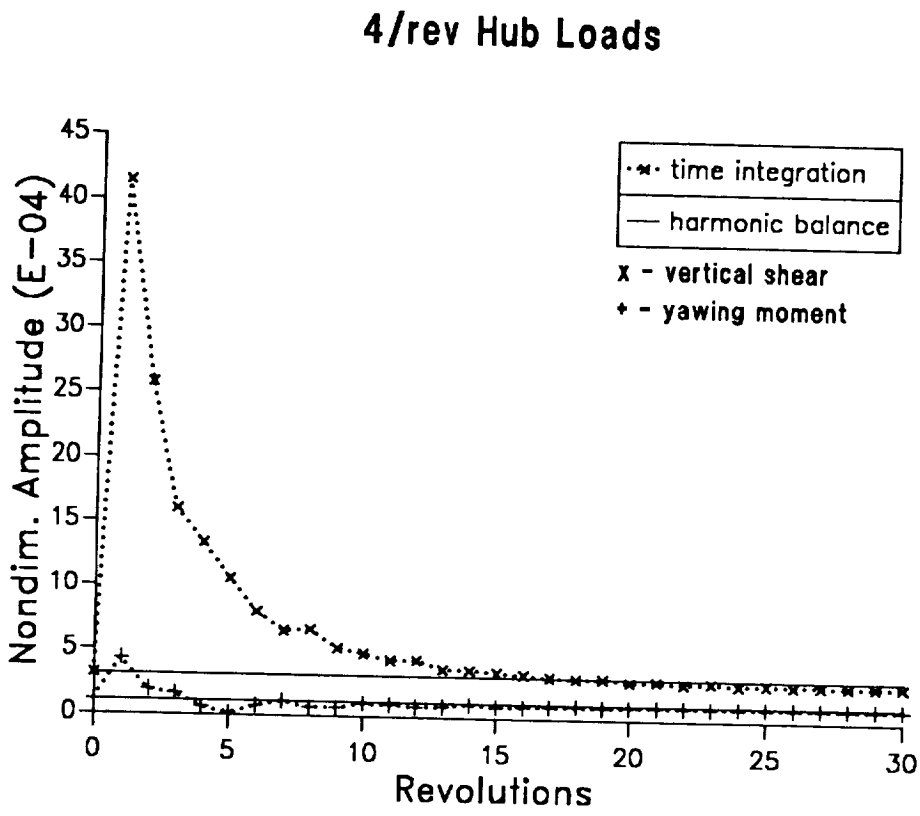

Figure 102: Convergence of vibratory hub loads to steady state: 4/rev vertical hub shear and yawing moment

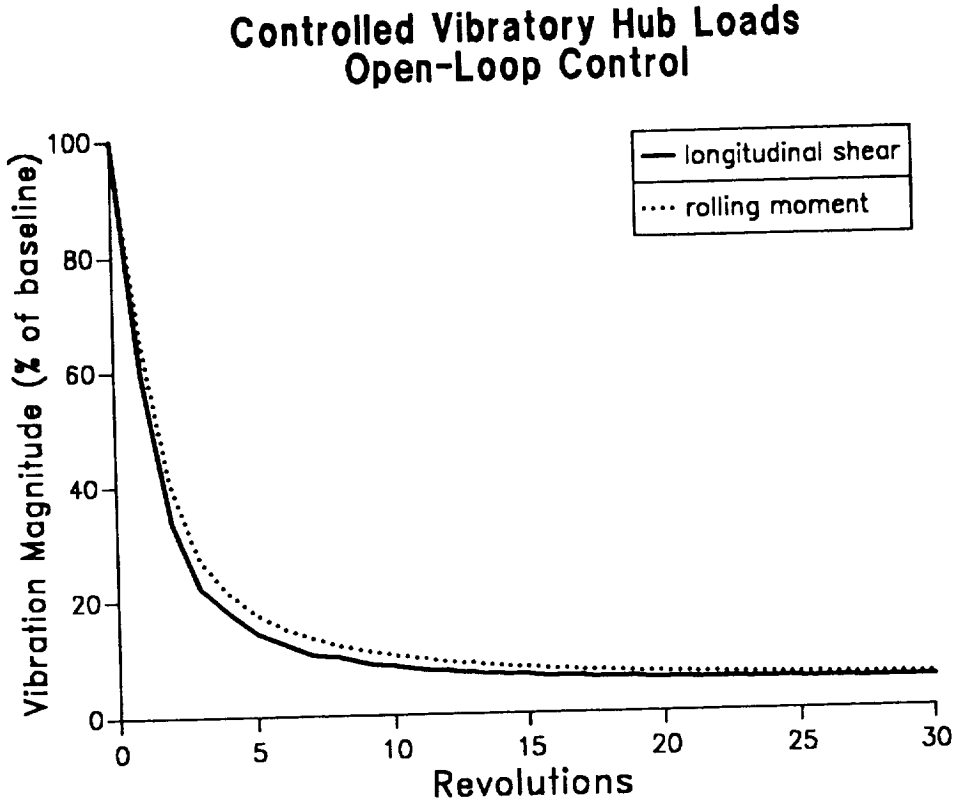

Figure 103: Time history of controlled vibration levels: 4/rev longitudinal hub shear and rolling moment

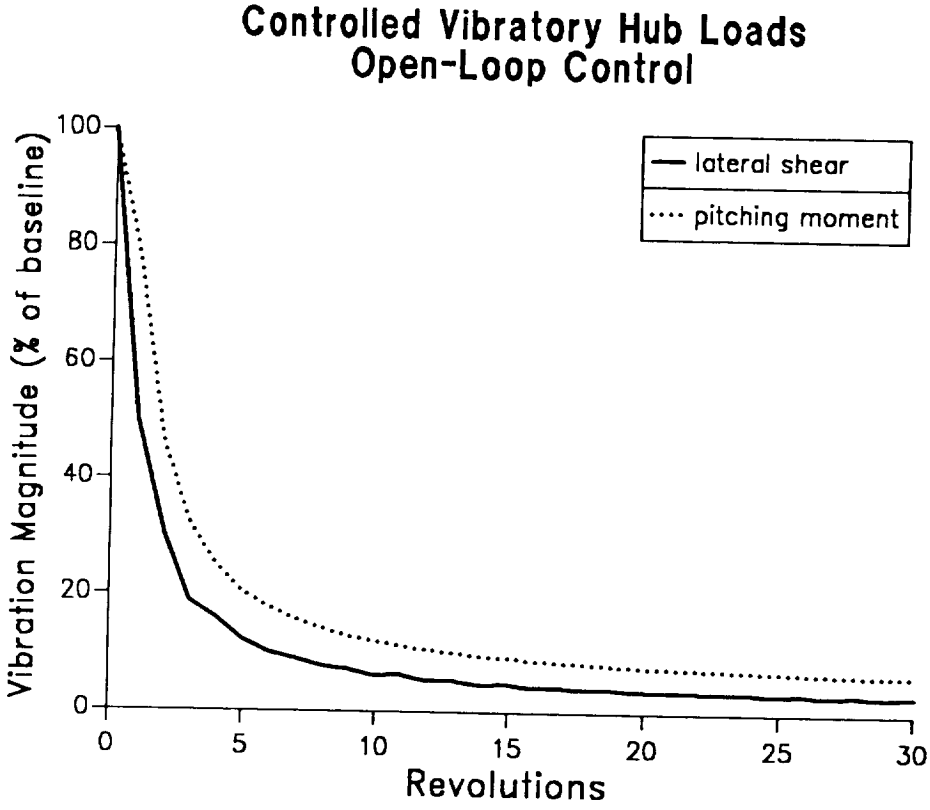

Figure 104: Time history of controlled vibration levels: 4/rev lateral hub shear and pitching moment

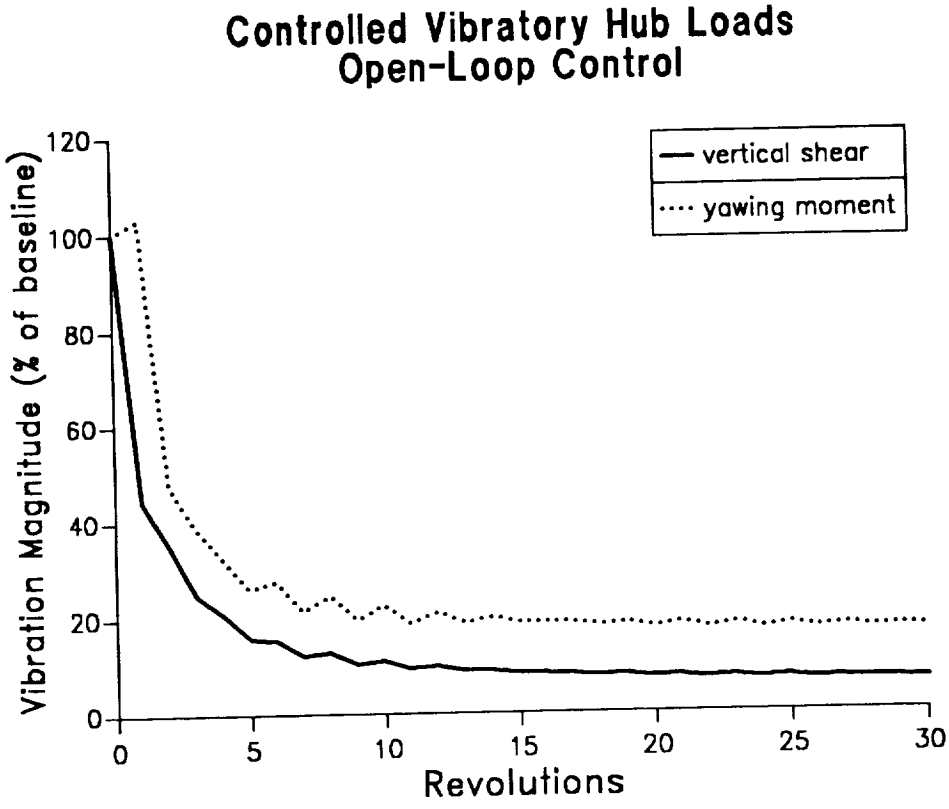

Figure 105: Time history of controlled vibration levels: 4/rev vertical hub shear and yawing moment

Appendix A

MODIFICATION OF THE QUASISTEADY AERODYNAMIC LOADS

The expressions used in this study to approximate the aerodynamic forces and moments per unit span on a rotor blade with a trailing edge flap are derived in this Appendix. The aerodynamic loads are based on a modification of Theodorsen's classical unsteady aerodynamic theory[52] to include the rotary-wing aerodynamic effects of time varying oncoming flow and variable inflow.

In the derivation of his unsteady aerodynamic theory, Theodorsen[52] includes the effects of a trailing edge flap with an arbitrary deflection angle. Thus the total lift and moment per unit span for a wing-aileron combination, together with the hinge moment per unit span about the flap hinge, are provided in Ref. 52. Theodorsen's theory is not suitable for rotor blades undergoing coupled flap-lag-torsional motion, and which are usually operating at constant or time varying geometric pitch angles[11,14]. Modifications to Theodorsen's theory to account for time varying oncoming flow and constant angle of pitch have been derived by Greenberg[18]. The adaptation of Greenberg's theory to rotary-wing problems and the correction for time varying inflow has been first derived in Ref. 15. Unfortunately, these modifications do not include the effects of a control flap. Thus Theodorsen's classical theory will serve as the point of departure in the present derivation.

A.1 THEODORSEN UNSTEADY AERODYNAMICS

Theodorsen's classical theory formulates the solution for the two-dimensional force and moment on a thin airfoil-aileron combination undergoing simple harmonic pitching and plunging motions in a uniform, steady flow field. The airfoil moves in vertical translation h(t) and rotates through the angle $\alpha(t)$ about an axis located a distance $\bar{x} = ba$ behind the midpoint of the total chord of the airfoil-aileron combination, and the (aerodynamically unbalanced) trailing edge flap rotates about an axis at $\bar{x} = bc$ through the angle $\delta(t)$ relative

to the airfoil chordline, as shown in Fig. A.1. The plunging motion h(t) is taken as positive down, and the pitching motions of the airfoil and control flap are positive trailing edge down (see Fig. A.1).

Theodorsen's classical theory formulates the solution for Laplace's equation

$$\nabla^2\phi = 0$$

in terms of the disturbance velocity potential ϕ subject to the two dimensional boundary condition that the airfoil chordline is a streamline of the flow, and subject to Kutta's hypothesis of finite, continuous velocities and pressures at the trailing edge.

Theodorsen separates the solution of the problem into two parts. First, an appropriate distribution of sources and sinks is placed just above and below the airfoil chordline such that the two dimensional boundary condition that the chordline is a streamline of the flow is satisfied. The disturbance velocity potential due to the sources and sinks represents the noncirculatory portion of the flow and is used to determine the noncirculatory aerodynamic loads acting on the airfoil. A pattern of vortices is then superimposed on the chordline, with counter-vortices along the wake to infinity, such that the Kutta condition at the trailing edge is satisfied. The disturbance velocity potential due to the pattern of vortices represents the circulatory portion of the flow and is used to determine the circulatory aerodynamic loads acting on the airfoil. Small disturbances are assumed, resulting in a linear theory.

A.2 INCLUSION OF ROTARY-WING AERODYNAMIC EFFECTS

Theodorsen's classical theory is modified in this section to include the effects of a time varying free stream velocity and variable inflow for the purposes of approximating the aerodynamic forces and moments on a rotor blade. The effect of time varying oncoming flow is accounted for by retaining all time derivatives of the free stream velocity U(t), which Theodorsen equates to zero. The effect of a time varying inflow velocity $v(t)$, shown in Fig. A.1, is included using the principle of superposition, which is valid in the context of a linear

aerodynamic theory. The effect of a constant component of the total pitch $\alpha(t)$ is not explicitly provided for, since this can be handled by steady-flow theory and the result afterwards superimposed on the solution.

The modifications to the noncirculatory and circulatory aerodynamic loads are discussed separately in the following two sections.

A.2.1 *Noncirculatory Lift and Moment*

From Ref. 52, for the noncirculatory portion of the flow, the lift (positive up), pitching moment (clockwise positive), and control flap hinge moment (clockwise positive), respectively, for the entire wing-aileron system are obtained by evaluating the following integrals:

$$L_{NC} = 2\rho b \int_{-1}^{+1} \dot{\phi}\, dx \tag{A.1}$$

$$M_{yNC} = -2\rho b^2 \int_{-1}^{+1} \dot{\phi}\,(x-c)\,dx + 2\rho U b \int_{-1}^{+1} \phi\, dx - b(c-a)\,L_{NC} \tag{A.2}$$

$$M_{hNC} = -2\rho b \int_{c}^{1} \dot{\phi}\,(x-c)\,dx + 2\rho U b \int_{c}^{1} \phi\, dx \tag{A.3}$$

where $x = \bar{x}/b$ is the nondimensional distance from the midpoint of the total chord of the airfoil-control flap combination. Also, $a = ba/b$ and $c = bc/b$.

The quantity $\phi(x,t)$ in Eqs. (A.1) – (A.3) is the velocity potential at a point x on the airfoil due to an appropriate distribution of sources and sinks just above and below the airfoil chord such that the two-dimensional boundary condition that the airfoil boundary is a streamline of the flow is satisfied. The velocity potentials due to position and velocity of the individual components of the wing-aileron system which together satisfy this condition[52] are:

$$\phi_\alpha = U\alpha b\sqrt{1-x^2}$$

$$\phi_h = \dot{h} b\sqrt{1-x^2}$$

$$\phi_{\dot{\alpha}} = \dot{\alpha} b^2 \left(\frac{1}{2}x - a\right)\sqrt{1-x^2}$$

$$\phi_{\delta} = \frac{1}{\pi} U\delta b\left[\sqrt{1-x^2}\,\cos^{-1}c - (x-c)\log N\right]$$

$$\phi_{\dot{\delta}} = \frac{1}{2\pi}\dot{\delta} b^2\left[\sqrt{1-c^2}\,\sqrt{1-x^2} + (x-2c)\sqrt{1-x^2}\,\cos^{-1}c\right.$$

$$\left. -(x-c)^2 \log N\right] \qquad \text{(A.4)}$$

where

$$N = \frac{1 - cx - \sqrt{1-x^2}\,\sqrt{1-c^2}}{x-c}$$

Due to the presence of inflow, the resultant air flow sensed at $x = ba$ in the plunging direction is $(\dot{h} - v)$. The velocity potential due to inflow, which can be obtained by substituting $(-v)$ for $\dot{h}$ into the velocity potential $\phi_{\dot{h}}$ in Eqs. (A.4), is given by

$$\phi_v = -vb\sqrt{1-x^2} \qquad \text{(A.5)}$$

The total velocity potential which satisfies the two-dimensional boundary condition, including the effect of variable inflow, is obtained by summing the individual contributions, since for a linear problem the superposition principle applies, i.e.

$$\phi = \phi_{\alpha} + \phi_{\dot{h}} + \phi_v + \phi_{\dot{\alpha}} + \phi_{\delta} + \phi_{\dot{\delta}} \qquad \text{(A.6)}$$

The noncirculatory lift and moments are obtained by substituting Eqs. (A.4) – (A.6) into Eqs. (A.1) – (A.3) and performing the required integrations. Before doing this however, it is convenient to interchange the integration and differentiation operations in Eqs. (A.1) – (A.3) , which yields the following equivalent expressions for the uncirculatory lift, pitching moment, and hinge moment:

$$L_{NC} = 2\rho b \frac{d}{dt}\left[\int_{-1}^{+1} \phi\, dx\right] \qquad \text{(A.7)}$$

$$M_{yNC} = -2\rho b^2 \frac{d}{dt}\left[\int_{-1}^{+1} \phi(x-c)dx\right] + 2\rho Ub\int_{-1}^{+1} \phi dx$$

$$- b(c-a)L_{NC} \tag{A.8}$$

$$M_{hNC} = -2\rho b \frac{d}{dt}\left[\int_{c}^{1} \phi(x-c)dx\right] + 2\rho Ub\int_{c}^{1} \phi dx \tag{A.9}$$

When Eqs. (A.4) – (A.6) are substituted into Eqs. (A.7) – (A.9), various integrals involving the velocity potentials in Eq. (A.6) arise, and must be evaluated. These integrals are evaluated in Ref. 52 as follows:

$$\int_{-1}^{+1} \phi_\alpha dx = \frac{b}{2} U\alpha\pi$$

$$\int_{-1}^{+1} \phi_{\dot{h}} dx = \frac{b}{2}\dot{h}\pi$$

$$\int_{-1}^{+1} \phi_{\dot{\alpha}} dx = -\dot{\alpha}b^2\frac{\pi a}{2}$$

$$\int_{-1}^{+1} \phi_\delta dx = -\frac{b}{2} U\delta T_4$$

$$\int_{-1}^{+1} \phi_{\dot{\delta}} dx = -\frac{b^2}{2}\dot{\delta}T_1$$

$$\int_{-1}^{+1} \phi_\alpha (x-c)dx = -\frac{b}{2} U\alpha c\pi$$

$$\int_{-1}^{+1} \phi_{\dot{h}} (x-c)dx = -\frac{b}{2}\dot{h}c\pi$$

$$\int_{-1}^{+1} \phi_{\dot{\alpha}} (x-c)dx = \dot{\alpha}b^2 T_{14}\pi$$

$$\int_{-1}^{+1} \phi_\delta (x-c)dx = -\frac{b}{2} U\delta T_8$$

$$\int_{-1}^{+1} \phi_{\dot{\delta}}(x-c)dx = -\frac{b^2}{2}\dot{\delta}T_7$$

$$\int_{c}^{1} \phi_{\alpha}dx = -\frac{b}{2}U\alpha T_4$$

$$\int_{c}^{1} \phi_{\dot{h}}dx = -\frac{b}{2}\dot{h}T_4$$

$$\int_{c}^{1} \phi_{\dot{\alpha}}dx = \dot{\alpha}b^2T_9$$

$$\int_{c}^{1} \phi_{\delta}dx = -\frac{b}{2\pi}U\delta T_5$$

$$\int_{c}^{1} \phi_{\dot{\delta}}dx = -\frac{b^2}{2\pi}\dot{\delta}T_2$$

$$\int_{c}^{1} \phi_{\alpha}(x-c)dx = -\frac{b}{2}U\alpha T_1$$

$$\int_{c}^{1} \phi_{\dot{h}}(x-c)dx = -\frac{b}{2}\dot{h}T_1$$

$$\int_{c}^{1} \phi_{\dot{\alpha}}(x-c)dx = \dot{\alpha}b^2T_{13}$$

$$\int_{c}^{1} \phi_{\delta}(x-c)dx = -\frac{b}{2\pi}U\delta T_2$$

$$\int_{c}^{1} \phi_{\dot{\delta}}(x-c)dx = -\frac{b^2}{2\pi}\dot{\delta}T_3 \qquad \text{(A.10)}$$

The quantities denoted by T with a numerical subscript, used in the above and subsequent expressions, represent constants involving the nondimensional airfoil dimensions a and c. These constants, which are taken from Ref. 52, are defined at the end of this Appendix.

Additional integrals, not represented in Eqs. (A.10), arise which involve the velocity potential ϕ_v, which accounts for the presence of inflow. These integrals can be evaluated

by substituting $(-v)$ for $\dot{h}$ into the integrals in Eq. (A.10) involving the velocity potential $\phi_{\dot{h}}$ due to the plunging velocity. Making the substitutions yields:

$$\int_{-1}^{+1} \phi_v dx = -\frac{b}{2} v\pi$$

$$\int_{-1}^{+1} \phi_v (x-c) dx = \frac{b}{2} vc\pi$$

$$\int_{c}^{1} \phi_v dx = \frac{b}{2} vT_4$$

$$\int_{c}^{1} \phi_v (x-c) dx = \frac{b}{2} vT_1 \qquad \text{(A.11)}$$

Using Eqs. (A.6) through (A.11), the following expressions for the noncirculatory lift, pitching moment and hinge moment are obtained:

$$L_{NC} = 2\rho b[\frac{b}{2}(\dot{U}\alpha + U\dot{\alpha})\pi + \frac{b}{2}\ddot{h}\pi - \frac{b}{2}\dot{v}\pi - \ddot{\alpha}b^2\frac{\pi a}{2}$$

$$- \frac{b}{2}(\dot{U}\delta + U\dot{\delta})T_4 - \frac{b^2}{2}\ddot{\delta}T_1] \qquad \text{(A.12)}$$

$$M_{yNC} = -2\rho b^2[-\frac{b}{2}(\dot{U}\alpha + U\dot{\alpha})c\pi - \frac{b}{2}\ddot{h}c\pi + \frac{b}{2}\dot{v}c\pi$$

$$+ \ddot{\alpha}b^2T_{14}\pi - \frac{b}{2}(\dot{U}\delta + U\dot{\delta})T_8 - \frac{b^2}{2}\ddot{\delta}T_7]$$

$$+ 2\rho Ub[\frac{b}{2}U\alpha\pi + \frac{b}{2}\dot{h}\pi - \frac{b}{2}v\pi - \dot{\alpha}b^2\frac{\pi a}{2} - \frac{b}{2}U\delta T_4$$

$$- \frac{b^2}{2}\dot{\delta}T_1] - b(c-a)L_{NC} \qquad \text{(A.13)}$$

$$M_{hNC} = -2\rho b^2[-\frac{b}{2}(\dot{U}\alpha + U\dot{\alpha})T_1 - \frac{b}{2}\ddot{h}T_1 + \frac{b}{2}\dot{v}T_1$$

$$+ \ddot{\alpha}b^2T_{13} - \frac{b}{2\pi}(\dot{U}\delta + U\dot{\delta})T_2 - \frac{b^2}{2\pi}\ddot{\delta}T_3] \qquad \text{(A.14)}$$

Note that in the above expressions, the time derivatives of the free stream velocity has not been set to zero, as was done in Ref. 52.

Collecting like terms, Eqs. (A.12) – (A.14) become

$$L_{NC} = \frac{1}{2}\rho(2\pi)b^2[\dot{U}\alpha + U\dot{\alpha} + \ddot{h} - \dot{v} - \ddot{\alpha}(ba) - 2(\dot{U}\delta + U\dot{\delta})\frac{T_4}{2\pi} - 2b\ddot{\delta}\frac{T_1}{2\pi}] \tag{A.15}$$

$$M_{yNC} = \frac{1}{2}\rho(2\pi)b^2\{U^2\alpha - (\frac{1}{8} + a^2)b^2\ddot{\alpha} - 2\frac{T_4}{2\pi}U^2\delta + \frac{1}{2\pi}[T_8 - T_1 + (c-a)T_4](2b)U\dot{\delta} + 2\frac{1}{2\pi}[T_7 + (c-a)T_1]b^2\ddot{\delta} + (ba)(\ddot{h} - \dot{v}) + U(\dot{h} - v) + (ba)\dot{U}\alpha + \frac{1}{2\pi}[T_8 + (c-a)T_4](2b)\dot{U}\delta\} \tag{A.16}$$

$$M_{hNC} = -\rho b^2[U^2\alpha T_4 - (2T_9 + T_1)bU\dot{\alpha} + 2T_{13}b^2\ddot{\alpha} + 2U^2\delta\frac{T_5}{2\pi} - 2b^2\ddot{\delta}\frac{T_3}{2\pi} + T_4U(\dot{h} - v) - bT_1\dot{U}\alpha - bT_1(\ddot{h} - \dot{v}) - 2b\frac{T_2}{2\pi}\dot{U}\delta] \tag{A.17}$$

In the expression for the noncirculatory pitching moment, the relation

$$T_{14} = \frac{1}{16} + \frac{1}{2}ac$$

taken from Eqs. (A.31), has been used to simplify the expression.

A.2.2 *Circulatory Lift and Moment*

From Ref. 52 the circulatory lift (positive up), pitching moment (clockwise positive), and control flap hinge moment, respectively, for the whole wing-aileron system[52] are

$$L_C = 2\pi\rho UbQC(k) \tag{A.18}$$

$$M_{yC} = 2\pi\rho UbQ[(ba + \frac{b}{2})C(k) - \frac{b}{2}] \tag{A.19}$$

$$M_{hC} = -\rho Ub^2Q[T_{12}C(k) - T_4] \tag{A.20}$$

where C(k) is Theodorsen's lift deficiency function[52] which depends on the reduced flutter frequency $k = \omega b/U$.

The parameter Q in Eqs. (A.18) – (A.20) is defined in Ref. 52 as

$$Q = U\alpha + \dot{h} + (\frac{b}{2} - ba)\dot{\alpha} + \frac{T_{10}}{\pi}U\delta + b\frac{T_{11}}{2\pi}\dot{\delta} \tag{A.21}$$

This quantity appears in the expression for the total circulation about the wing-aileron system calculated by enforcing the Kutta condition at the trailing edge. Superimposing the effect of inflow, the parameter Q becomes

$$Q = U\alpha + (\dot{h} - v) + (\frac{b}{2} - ba)\dot{\alpha} + \frac{T_{10}}{\pi}U\delta + b\frac{T_{11}}{2\pi}\dot{\delta} \tag{A.22}$$

The substitution Eq. (A.22) into Eqs. (A.18) – (A.20) yields expressions for the circulatory lift, pitching moment and hinge moment, respectively, which include the effects of time-dependent free stream velocity and variable inflow.

A.3 CHANGE OF NOTATION

In modifying Theodorsen's unsteady aerodynamic theory, the original airfoil notation used in Ref. 52 was adopted for convenience. However, for the rotary-wing application it is necessary to modify this notation. The relationship between the notation of Ref. 52 and the notation used in this study is given below:

$$b = \frac{1}{2}(c_b + c_{cs})$$

$$ba = X_A - \frac{1}{4}(c_b + 2c_{cs})$$

$$bc = \frac{1}{2}(c_b - c_{cs}) \tag{A.23}$$

The second of Eqs. (A.23) implies the assumption that the aerodynamic center of the blade cross-section is located at a distance of 1/4 of the blade chord from the leading edge.

For rotary-wing applications, the pitch angle $\alpha(t)$ is frequently[38,45,50,53] interpreted as the total pitch angle of the blade

$$\alpha = \theta_G + \phi \tag{A.24}$$

The same interpretation is made in this study.

The modified aerodynamic loads derived in this Appendix are expressed below in terms of the parameters of this study by using Eqs. (A.23) and (A.24), and substituting them into Eqs. (A.15) – (A.22). Furthermore, the free stream velocity U is replaced by U_T, and the quantity $(v - \dot{h})$ is replaced by U_P, where U_T and U_P represent, respectively, the the components of the total air velocity sensed by the blade approximately parallel and normal to the hub plane. Finally, the flat plate lift curve slope of 2π is replaced by the incompressible lift curve slope a_o and ρ_A is used to denote the air density.

Introducing these substitutions, the final expressions for the noncirculatory and circulatory lift, pitching moment and hinge moment used in this study are

$$L_{NC} = \frac{1}{8}\rho_A a_o (c_b + c_{cs})^2 \{\dot{U}_T(\theta_G + \phi) + U_T(\dot{\theta}_G + \dot{\phi})$$

$$- [X_A - \frac{1}{4}(c_b + 2c_{cs})](\ddot{\theta}_G + \ddot{\phi}) - \dot{U}_P$$

$$- 2(\dot{U}_T\delta + U_T\dot{\delta})\frac{T_4}{a_o} - (c_b + c_{cs})\ddot{\delta}\frac{T_1}{a_o}\} \tag{A.25}$$

$$M_{yNC} = \frac{1}{8}\rho_A a_o (c_b + c_{cs})^2 \{U_T^2(\theta_G + \phi) - U_T U_P$$

$$- \frac{1}{32}(c_b + c_{cs})^2(\ddot{\theta}_G + \ddot{\phi}) - [X_A - \frac{1}{4}(c_b + 2c_{cs})]^2(\ddot{\theta}_G + \ddot{\phi})$$

$$+ [X_A - \frac{1}{4}(c_b + 2c_{cs})][\dot{U}_T(\theta_G + \phi) - \dot{U}_P]$$

$$- 2\frac{T_4}{a_o}U_T^2\delta - \frac{T_1}{a_o}(c_b + c_{cs})U_T\dot{\delta}$$

$$+ [\frac{T_8}{a_o}(c_b + c_{cs}) + (\frac{3}{2}c_b - 2X_A)\frac{T_4}{a_o}](\dot{U}_T\delta + U_T\dot{\delta})$$

$$+ \frac{1}{2}(c_b + c_{cs})[\frac{T_7}{a_o}(c_b + c_{cs}) + (\frac{3}{2}c_b - 2X_A)\frac{T_1}{a_o}]\ddot{\delta}\} \qquad \text{(A.26)}$$

$$M_{hNC} = -\frac{1}{4}\rho_A(c_b + c_{cs})^2\{U_T^2T_4(\theta_G + \phi) + \frac{1}{2}T_{13}(c_b + c_{cs})^2(\ddot{\theta}_G + \ddot{\phi})$$

$$- \frac{1}{2}(2T_9 + T_1)(c_b + c_{cs})U_T(\dot{\theta}_G + \dot{\phi})$$

$$+ \frac{1}{2}(c_b + c_{cs})T_1[\dot{U}_P - U_T(\theta_G + \phi)] - U_TU_PT_4$$

$$+ 2U_T^2\frac{T_5}{a_o}\delta - \frac{1}{2}(c_b + c_{cs})^2\ddot{\delta}\frac{T_3}{a_o} - (c_b + c_{cs})\frac{T_2}{a_o}\dot{U}_T\delta\} \qquad \text{(A.27)}$$

$$L_C = \frac{1}{2}\rho_A a_o(c_b + c_{cs})U_T\{U_T(\theta_G + \phi) - U_P$$

$$+ [\frac{1}{2}(c_b + 3c_{cs}) - X_A](\dot{\theta}_G + \dot{\phi})$$

$$+ 2\frac{T_{10}}{a_o}U_T\delta + \frac{1}{4}(2c_b + 3c_{cs})\frac{T_{11}}{a_o}\dot{\delta}\}C(k) \qquad \text{(A.28)}$$

$$M_{yC} = \frac{1}{2}\rho_A a_o(c_b + c_{cs})U_T\{U_T(\theta_G + \phi) - U_P$$

$$+ [\frac{1}{2}(c_b + 3c_{cs}) - X_A](\dot{\theta}_G + \dot{\phi}) + 2\frac{T_{10}}{a_o}U_T\delta$$

$$+ \frac{1}{4}(2c_b + 3c_{cs})\frac{T_{11}}{a_o}\dot{\delta}\}[(X_A - \frac{1}{4}c_{cs})C(k) - \frac{1}{4}(c_b + c_{cs})] \qquad \text{(A.29)}$$

$$M_{hC} = -\frac{1}{4}\rho_A(c_b + c_{cs})^2 U_T\{U_T(\theta_G + \phi) - U_P$$

$$+ [\frac{1}{2}(c_b + 3c_{cs}) - X_A](\dot{\theta}_G + \dot{\phi})$$

$$+ 2\frac{T_{10}}{a_o}U_T\delta + \frac{1}{4}(2c_b + 3c_{cs})\frac{T_{11}}{a_o}\dot{\delta}\}[T_{12}C(k) - T_4] \qquad (A.30)$$

A.4 DEFINITION OF COEFFICIENTS USED BY THEODORSEN

The various parameters denoted by T with a numerical subscript appearing in the expressions for the aerodynamic loads represent constants which arise in the integration of the velocity potentials along the airfoil chord. These constants are defined by Theodorsen[52] as follows:

$$T_1 = -\frac{1}{3}\sqrt{1-c^2}\,(2+c^2) + c\cos^{-1}c$$

$$T_2 = T_6 = c(1-c^2) - \sqrt{1-c^2}\,(1+c^2)\cos^{-1}c + c(\cos^{-1}c)^2$$

$$T_3 = -(\frac{1}{8} + c^2)(\cos^{-1}c)^2 + \frac{1}{4}c\sqrt{1-c^2}\,\cos^{-1}c(7+2c^2)$$

$$-\frac{1}{8}(1-c^2)(5c^2+4)$$

$$T_4 = -\cos^{-1}c + c\sqrt{1-c^2}$$

$$T_5 = -(1-c^2) - (\cos^{-1}c)^2 + 2c\sqrt{1-c^2}\,\cos^{-1}c$$

$$T_7 = -(\frac{1}{8} + c^2)\cos^{-1}c + \frac{1}{8}c\sqrt{1-c^2}\,(7+2c^2)$$

$$T_8 = -\frac{1}{3}\sqrt{1-c^2}\,(2c^2+1) + c\cos^{-1}c$$

$$T_9 = \frac{1}{2}[\frac{1}{3}(\sqrt{1-c^2})^3 + aT_4]$$

$$T_{10} = \sqrt{1-c^2} + \cos^{-1}c$$

$$T_{11} = \cos^{-1}c(1-2c) + \sqrt{1-c^2}\,(2-c)$$

$$T_{12} = \sqrt{1-c^2}\,(2+c) - \cos^{-1}c(2c+1)$$

$$T_{13} = \frac{1}{2}[-T_7 - (c-a)T_1]$$

$$T_{14} = \frac{1}{16} + \frac{1}{2}ac \qquad \text{(A.31)}$$

where a and c are the nondimensional airfoil parameters used by Theodorsen which have already been defined. From Eqs. (A.23) these can be defined in terms of the airfoil characteristics used in this study:

$$c = \frac{bc}{b} = \frac{c_b - c_{cs}}{c_b + c_{cs}}$$

$$a = \frac{ba}{b} = \frac{2X_A}{(c_b + c_{cs})} - \frac{c_b + 2c_{cs}}{2(c_b + c_{cs})}$$

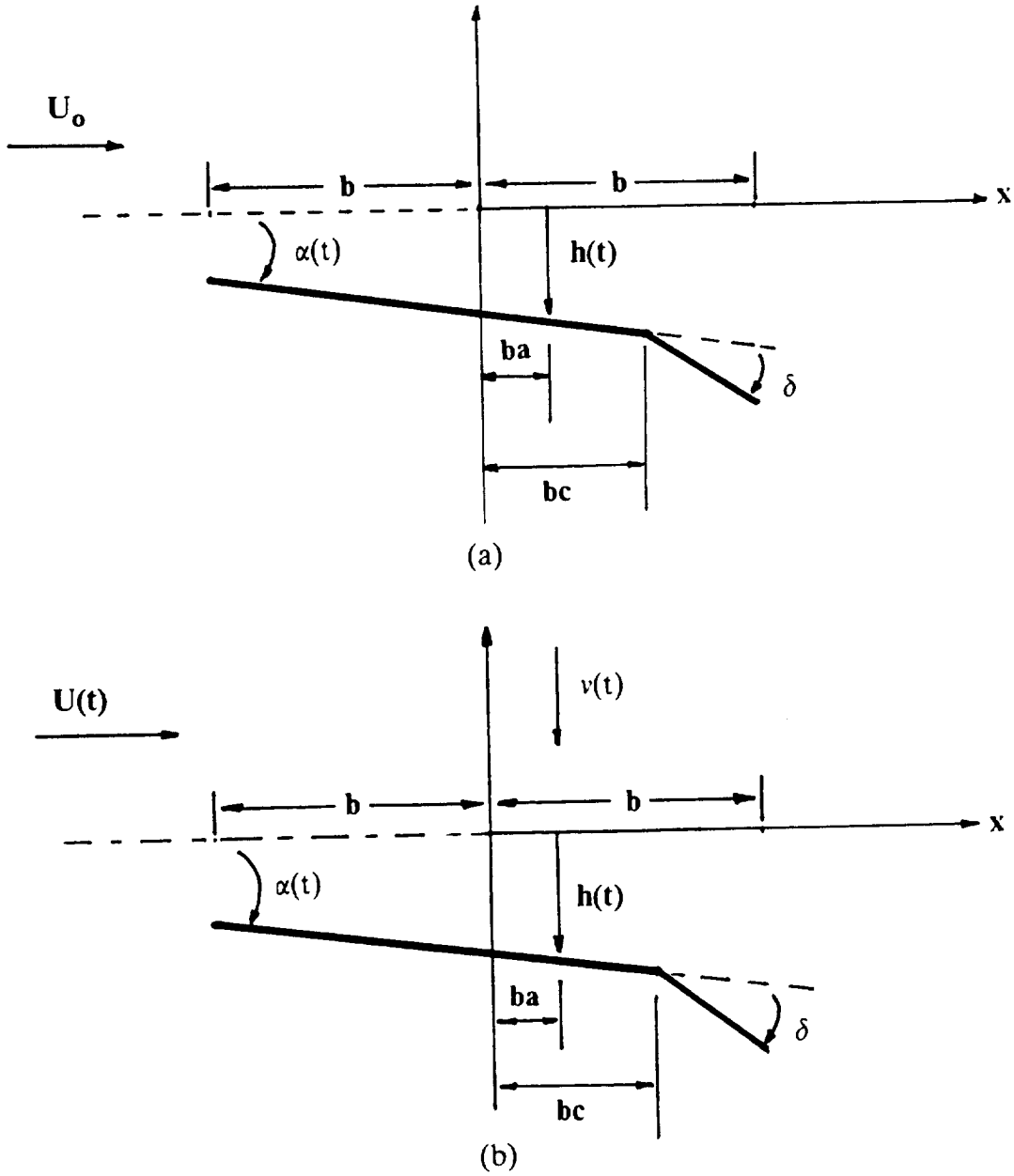

Figure A.1: (a) Airfoil-aileron combination undergoing plunging and pitching motions in a uniform stream. (b) Airfoil-flap combination with time varying free stream and inflow.

Appendix B

EXPLICIT FORMULATION USING A SYMBOLIC MANIPULATION PROGRAM

The main obstacle encountered in the explicit formulation of the equations of of motion is the rapid proliferation of the number of terms in the explicit expressions as each succeeding mathematical operation required in the derivation is performed. Keeping track of each of these terms can be tedious and time-consuming, even when an ordering scheme, which necessarily accompanies explicit formulations, is employed to neglect the higher order terms. Fortunately, substantial increases in computer power during the last decade, as represented by high computational speeds and the availability of large core memory at low cost, have enabled the relegation of the tedious algebraic tasks to the computer. Many symbolic manipulation programs exist which can be used to derive the equations of motion of the blade in explicit form. These equations can then be converted into FORTRAN code for inclusion into a computer analysis code. Since the algebraic tasks are relegated to a computer, it is fairly easy to retain as many terms as desired. In addition, the equations can easily be rederived by the computer to reflect any changes in the aeroelastic model.

Symbolic manipulation programs enlist an arsenal of functions and subroutines which, when invoked by the appropriate command, perform specific mathematical operations on indicated symbolic expressions to yield the desired result. The user generally has the option of entering the commands interactively or in a batch format. For lengthy derivations it is preferable to save the specific sequence of commands into a file and execute them in batch format. This facilitates the review of the specific sequence of commands for correctness both before and after execution and allows the user to make minor changes in the derivation, if desired.

B.1 ORDERING SCHEME

Explicit formulations require the employment of an ordering scheme to neglect the higher order terms, even when the tedious algebraic tasks are relegated to a computer. Unless a systematic approach is employed neglect higher order terms, the length of the expressions can become too large, requiring vast amounts of computer time and memory to perform the required symbolic manipulations, and may ultimately lead to a system crash, if all available memory is exhausted. Thus the ordering scheme is convenient for reducing the size of the expressions. By judiciously assigning appropriate orders of magnitude to the various terms encountered in the expressions, all terms which can be considered negligible are eliminated, thus saving valuable computer time and memory.

The ordering scheme used in this study is described in Chapter 2. The basis of the ordering scheme is a small dimensionless parameter ε which represents typical blade slopes due to elastic deformation. It is known for helicopter blades that ε is in the range $0.1 < \varepsilon < 0.2$. The ordering scheme used in this study is based on the assumption that terms of the order of $O(\varepsilon^2)$ are neglected in comparison with unity.

Orders of magnitude can only be assigned to nondimensional quantities. The dimensional parameters R, M_b and Ω , which denote the rotor radius, blade mass, and rotor speed, respectively, are used to express all dimensional parameters appearing in the equations in nondimensional form. Orders of magnitude can then assigned by selecting, based on experience, a typical value for the particular parameter under consideration.

Caution must be exercised when implementing an ordering scheme so as to avoid neglecting potentially important terms. This is best accomplished by careful insight into the problem when establishing a cut-off level for the ordering scheme at each stage of the derivation. Here the cut-off level designates the order of magnitude at which all terms of higher order are neglected. Until the final stages of the derivation, the primary motivating factor in establishing the cut-off level is the desire to keep the expressions to a manageable size while retaining as many terms as is practical; it is only in the final stages that the ordering scheme should be strictly enforced. If the ordering scheme is strictly enforced throughout the entire derivation then important terms may be erroneously neglected. This

is due to the fact that the relative orders of magnitude of the various terms can change when certain mathematical operations, such as integration or differentiation, are performed, resulting in the loss of important terms at critical stages of the derivation if the ordering scheme is enforced too strictly. Therefore it is important to relax the implementation of the ordering scheme until the final stages of the the derivation.

B.2 SYMBOLIC MANIPULATION METHODOLOGY

The major steps in the formulation of a set of explicit equations of motion using a symbolic manipulation program are listed briefly below. These steps are expanded upon later for the particular symbolic manipulation program MACSYMA, which has been used extensively in this study.

(1) Definitions: All functional dependences and orders of magnitude of the various parameters must be defined. In addition, all user defined functions and expressions which would be convenient to have at hand must be defined. Finally the starting cut-off level for the ordering scheme is established.

(2) Algebraic manipulations and mathematical operations: Predefined quantities and expressions are combined and manipulated using the appropriate commands and user defined functions to develop the desired result.

(3) Expansion and conversion to FORTRAN code: The explicit expressions are expanded into a sum of product terms involving the various parameters of the problem. At this stage the ordering scheme is strictly enforced. The expressions are then converted to FORTRAN code in preparation for incorporation into the analysis code.

B.3 SYMBOLIC MANIPULATION USING MACSYMA

The general-purpose computer algebra system MACSYMA is used throughout this study to develop explicit expressions for the equations of motion of an isolated rotor blade. The program MACSYMA (version 420) is installed on a Symbolics 3650 dedicated LISP machine running Genera 7.0. The Symbolics machine is networked via Ethernet to a Sun 3/280 computer on which all of the numerical computations are performed.

A detailed description of the syntax and usage of the various MACSYMA commands used to develop the explicit equations of motion are beyond the scope of this study, and can be found in Ref. 59. However, a brief description of the usage of the various MACSYMA commands used are given when appropriate. In this study, the sequence of MACSYMA commands used to derive the expressions are saved in a file and executed in batch format. Batch files are executed using the MACSYMA command **BATCH(***"filename.mac"***)** where *filename.mac* represents the name of the batch file containing the MACSYMA commands. All MACSYMA commands will be written in **BOLD** capitals, and the arguments will be written in lower case *italic*.

The basic steps required in the formulation of explicit equations using symbolic manipulation are discussed below.

B.3.1 *Definitions*

Before proceeding with the derivation of the equation of motion, the following definitions must be made:

(1) All functional dependencies of the various parameters used in the study must be defined using the **DEPENDS(***funlist, varlist***)** command, where the variables in *funlist* are declared to depend on *varlist*. If the functional dependence of a variable is not established beforehand, then derivatives of the variable using the **DIFF(***exp, v, n***)** command, which evaluates the derivative of *exp* with respect to *v* *n* times, will be equated to zero.

(2) All orders of magnitude of the parameters used in the study must be defined using the **RATWEIGHT(***var, w***)** command, which assigns a weight of *w* to *var*. The value of *w* re-

presents the value of the exponent of ε for the given parameter according to the ordering scheme.

(3) All user defined functions must be defined using the := operator, i.e.

FunctionName(args) := *body;*

The user defined function used in this study is the **CROSS(*u, v*)** command which crosses the vector *u* with the vector *v*. The **CROSS(*u, v*)** command is created as follows

```
CROSS(U,V) := MATRIX([U[2].V[3] - U[3].V[2]],
                     [U[3].V[1] - U[1].V[3]],
                     [U[1].V[2] - U[2].V[1]]);
```

(4) All transformation matrices between the various coordinate systems must be defined. These are defined using the **MATRIX(*row1,...,rowN*)** command, which defines a rectangular matrix with the indicated rows. Since the transformation matrices represent orthonormal transformations, the inverse transformations can be obtained using the **TRANSPOSE(*matrix*)** command.

It is important to note that vectors are defined using the **MATRIX(*row1,...,rowN*)** command by defining each row as having only one element.

(5) Any quantities and expressions which would be convenient to have at hand should be defined.

(6) Finally an initial cut-off level to the ordering scheme must be established using the **RATWTLVL:***value* command. This causes a product term to be set equal to zero if its weight exceeds *value*.

B.3.2 *Algebraic Manipulations and Mathematical Operations*

Once all of the functional dependencies, orders of magnitude, user defined functions, and convenient quantities and expressions have been defined, the expressions may be manipulated using the various MACSYMA commands and operations available to the user. The most important of these are listed below.

Addition and subtraction are accomplished using the + and - signs, respectively, and scalar multiplication and division are accomplished using the * and / symbols, respectively. Matrix multiplication and vector inner products are performed by placing a period between the two terms.

Substitutions are performed using either the **SUBST(***a, b, c***)** command or the **RATSUBST(***a, b, c***)** command, where *a* is substituted for all occurrences of *b* in expression *c*. The main difference between the two commands is that the **RATSUBST(***a, b, c***)** command invokes the ordering scheme while the **SUBST(***a, b, c***)** command performs a purely syntactic substitution.

The function **RATCOEF(***exp, var, n***)** can be used to obtain the coefficient of the expression *var**n* in the expression *exp*. This command is useful when it is desired to determine whether there are any occurrences of *exp**n* in a given expression. If there are no occurrences then the command returns a result of zero.

A given expression can be rationally expanded and simplified using the **RATEXPAND(***exp***)** command. This command, and also the **RATSUBST(***a, b, c***)** and the **RATCOEF(***exp, var, n***)** command, invoke the ordering scheme whereby all product terms in the expression whose net weight is higher than the value set by the **RATWTLVL:***value* command are set to zero.

B.3.3 *Expansion and Conversion to FORTRAN Code*

Once the explicit expressions have been derived they must be put into their final form and then converted to FORTRAN expressions. The steps for doing this are listed below.

(1) First the final level of the ordering scheme must be established using the **RATWTLVL:***value* command.

(2) Next the expressions are rationally expanded and simplified using the **RATEXPAND(***exp***)** command. This command also invokes the ordering scheme by neglecting all higher order terms according to the level established by the **RATWTLVL:***value* command.

(3) Next all variable names which are not legal FORTRAN variable names are replaced syntactically with legal ones using the **SUBST(***a, b, c***)** command.

(4) The expressions are then converted into FORTRAN assignment statements using the **FORTRAN(***exp***)** command.

(5) Finally, the expressions are saved into a file using the **WRITEFILE(***"filename.for"***)** command.

The FORTRAN expressions are then transferred to the Sun 3/280 via Ethernet and incorporated into the FORTRAN computer code.

Appendix C

EXPLICIT EXPRESSIONS FOR THE ROOT LOADS ACTING ON THE OFFSET-HINGED SPRING RESTRAINED BLADE MODEL

Explicit expressions for the force and moment at the blade root are developed in this appendix for the offset-hinged spring restrained blade model. In addition, an explicit expression for the total moment about the control surface hinge, required to calculate the power required to drive the control surface to implement control, is also derived.

General explicit expressions for the distributed loads acting on the blade and control surface have been developed in Chapter 3 in terms of the three displacement quantities u, v and w and the rotational quantity ϕ. Explicit expressions for the distributed loads acting on the blade and control surface for the offset-hinged spring restrained blade model are obtained by substituting Eqs. (4.3) and (4.4) into these general expressions. Once this has been done the loads at the blade root are obtained by integrating the distributed loads along the span of the blade and control surface. The substitutions and integrations are performed symbolically using the symbolic manipulation program MACSYMA, as described in Appendix B.

Before performing the integrations along the span it is convenient to decompose the total geometric pitch angle into an x-dependent component and a time dependent component as follows:

$$\theta_G = \theta_{pt}(x) + \theta_{pc}(t)$$

Basic trigonometric relations allow us to write:

$$\cos(\theta_G + \phi) = \cos\theta_{pt}\cos(\theta_{pc} + \phi) - \sin\theta_{pt}\sin(\theta_{pc} + \phi) \tag{C.1a}$$

$$\sin(\theta_G + \phi) = \sin\theta_{pt}\cos(\theta_{pc} + \phi) + \cos\theta_{pt}\sin(\theta_{pc} + \phi) \tag{C.1b}$$

$$\cos(\theta_G + \phi + \delta) = \cos\theta_{pt}\cos(\theta_{pc} + \phi + \delta) - \sin\theta_{pt}\sin(\theta_{pc} + \phi + \delta) \tag{C.1c}$$

$$\sin(\theta_G + \phi + \delta) = \sin\theta_{pt}\cos(\theta_{pc} + \phi + \delta) + \cos\theta_{pt}\sin(\theta_{pc} + \phi + \delta) \qquad \text{(C.1d)}$$

These expansions are used in the integration of the distributed loads along the span of the blade and the control flap.

C.1 INERTIAL ROOT LOADS

The inertial loads at the blade root are obtained by integrating the distributed inertial loads developed in Chapter 3 along the span of the blade once they have been expressed entirely in terms of the blade degrees of freedom. The inertial root loads are formulated in the "2" system, in which the distributed inertial loads have been developed.

C.1.1 *Blade Inertial Loads*

For the offset-hinged spring restrained blade model the differential force at the blade root due to the inertial loads acting on the blade is given by

$$d\vec{F}_{Ib} = \vec{p}_{Ib}\,dx$$

where $\vec{p}_{Ib}$ represents the distributed inertial force acting on the blade, which can be expressed in the "2" system as

$$\vec{p}_{Ib} = p_{Ibx2}\,\hat{e}_{x2} + p_{Iby2}\,\hat{e}_{y2} + p_{Ibz2}\,\hat{e}_{z2}$$

The x_2, y_2 and z_2 components of $\vec{p}_{Ib}$ for the spring restrained blade model are obtained from the expressions developed in Chapter 3 by substituting Eqs. (4.3) and (4.4) into Eqs. (3.20).

The total force at the blade root is obtained by integrating the differential force along the span of the blade

$$\vec{F}_{Ib} = \int_0^{L_b} \vec{p}_{Ib}\,dx \qquad \text{(C.2)}$$

which can be expressed in the "2" system as

$$\vec{F}_{Ib} = F_{Ibx2}\,\hat{e}_{x2} + F_{Iby2}\,\hat{e}_{y2} + F_{Ibz2}\,\hat{e}_{z2}$$

where

$$F_{Ibx2} = \int_0^{L_b} p_{Ibx2}\,dx$$

$$= M_b\Omega^2(x_b + e) + 2M_b x_b\Omega\dot{\zeta} + M_b x_b\beta_p(\ddot{\beta} - \beta\Omega^2)$$

$$+ M_b x_b[(\ddot{\zeta}\zeta + \dot{\zeta}^2 + \ddot{\beta}\beta + \dot{\beta}^2) - \frac{1}{2}\Omega^2(\zeta^2 + \beta^2)]$$

$$- 2M_b[y_b\sin(\theta_{pc} + \phi) + z_b\cos(\theta_{pc} + \phi)]\Omega(\dot{\theta}_{pc} + \dot{\phi}) \qquad \text{(C.3a)}$$

$$F_{Iby2} = \int_0^{L_b} p_{Iby2}\,dx$$

$$= 2M_b x_b\Omega\dot{\beta}\beta_p + M_b x_b(\zeta\Omega^2 - \ddot{\zeta}) + 2M_b x_b\Omega(\dot{\zeta}\zeta + \dot{\beta}\beta)$$

$$+ M_b[y_b\cos(\theta_{pc} + \phi) - z_b\sin(\theta_{pc} + \phi)][\Omega(\Omega + 2\dot{\zeta})$$

$$+ (\dot{\theta}_{pc} + \dot{\phi})^2 + 2\Omega(\dot{\theta}_{pc} + \dot{\phi})(\beta + \beta_p)]$$

$$+ M_b[y_b\sin(\theta_{pc} + \phi) + z_b\cos(\theta_{pc} + \phi)][(\ddot{\theta}_{pc} + \ddot{\phi})$$

$$+ 2\Omega\dot{\beta} - 2\Omega(\dot{\theta}_{pc} + \dot{\phi})\zeta] \qquad \text{(C.3b)}$$

$$F_{Ibz2} = \int_0^{L_b} p_{Ibz2}\,dx$$

$$= M_b x_b(\ddot{\zeta}\zeta + \dot{\zeta}^2 + \ddot{\beta}\beta + \dot{\beta}^2)\beta_p - M_b x_b\ddot{\beta}$$

$$+ M_b[y_b\cos(\theta_{pc} + \phi) - z_b\sin(\theta_{pc} + \phi)][\ddot{\zeta}(\beta + \beta_p)$$

$$+ 2\dot{\beta}\dot{\zeta} + \ddot{\beta}\zeta - (\ddot{\theta}_{pc} + \ddot{\phi})]$$

$$+ M_b[y_b \sin(\theta_{pc} + \phi) + z_b \cos(\theta_{pc} + \phi)][(\dot{\theta}_{pc} + \dot{\phi})^2$$

$$- (\ddot{\theta}_{pc} + \ddot{\phi})(\beta + \beta_p)\zeta] \tag{C.3c}$$

In the above integrations over the blade span the following integrals involving products of x-dependent quantities have been substituted directly into the expressions:

$$\int_0^{L_b} m_b \, dx = M_b \tag{C.4a}$$

$$\int_0^{L_b} m_b \, x \, dx = M_b x_b \tag{C.4b}$$

$$\int_0^{L_b} m_b X_{Ib} \cos\theta_{pt} \, dx = M_b y_b \tag{C.4c}$$

$$\int_0^{L_b} m_b X_{Ib} \sin\theta_{pt} \, dx = M_b z_b \tag{C.4d}$$

where M_b is the total mass of one rotor blade and the triad (x_b, y_b, z_b) represent the coordinates of the blade center of mass from the blade root.

For the offset-hinged spring restrained blade model the differential moment about the blade root due to the inertial loads acting on the blade can be expressed as

$$d\vec{M}_{Ib} = (\vec{q}_{Ib} + x\hat{e}_{x4} \times \vec{p}_{Ib})\, dx$$

where $\vec{q}_{Ib}$ represents the distributed inertial moment acting on the spring restrained blade, which can be expressed in the "2" system as

$$\vec{q}_{Ib} = q_{Ibx2}\hat{e}_{x2} + q_{Iby2}\hat{e}_{y2} + q_{Ibz2}\hat{e}_{z2}$$

The x_2, y_2 and z_2 components of $\vec{q}_{Ib}$ for the spring restrained blade are obtained from the general expressions developed in Chapter 3 by substituting Eqs. (4.3) and (4.4) into Eqs. (3.23).

The total moment about the blade root is obtained by integrating the differential root moment along the span of the blade

$$\vec{M}_{lb} = \int_0^{L_b} (\vec{q}_{lb} + x\hat{e}_{x4} \times \vec{p}_{lb})\, dx \tag{C.5}$$

which can be expressed in the "2" system as

$$\vec{M}_{lb} = M_{lbx2}\,\hat{e}_{x2} + M_{lby2}\,\hat{e}_{y2} + M_{lbz2}\,\hat{e}_{z2}$$

where

$$M_{lbx2} = \int_0^{L_b} q_{lbx2}\, dx + \zeta \int_0^{L_b} x\, p_{lbz2}\, dx - (\beta + \beta_p) \int_0^{L_b} x\, p_{lby2}\, dx \tag{C.6a}$$

$$M_{lby2} = \int_0^{L_b} q_{lby2}\, dx - \int_0^{L_b} x\, p_{lbz2}\, dx + (\beta + \beta_p) \int_0^{L_b} x\, p_{lbx2}\, dx \tag{C.6b}$$

$$M_{lbz2} = \int_0^{L_b} q_{lbz2}\, dx + \int_0^{L_b} x\, p_{lby2}\, dx - \zeta \int_0^{L_b} x\, p_{lbx2}\, dx \tag{C.6c}$$

Before performing the above integrations it is convenient to define the following integrals:

$$\int_0^{L_b} m_b\, x^2\, dx = I_b \tag{C.7a}$$

$$\int_0^{L_b} m_b\, x\, X_{lb} \cos\theta_{pt}\, dx = I_{yb} \tag{C.7b}$$

$$\int_0^{L_b} m_b\, x\, X_{lb} \sin\theta_{pt}\, dx = I_{zb} \tag{C.7c}$$

$$\int_0^{L_b} (I_{MB2} + I_{MB3})\, dx = J_b \tag{C.7d}$$

$$\int_0^{L_b} (I_{MB2} - I_{MB3}) \cos\theta_{pt} \sin\theta_{pt}\, dx = I_{mbr23} \tag{C.7e}$$

$$\int_0^{L_b} (I_{MB2} \cos^2\theta_{pt} + I_{MB3} \sin^2\theta_{pt})\, dx = I_{mbr2} \tag{C.7f}$$

$$\int_0^{L_b} (I_{MB2} \sin^2\theta_{pt} + I_{MB3} \cos^2\theta_{pt})\, dx = I_{mbr3} \qquad \text{(C.7g)}$$

Using the previous integral definitions along with Eqs. (C.1) , allows us to evaluate the following integrals over the blade span:

$$\int_0^{L_b} [I_{MB2} \sin^2(\theta_G + \phi) + I_{MB3} \cos^2(\theta_G + \phi)]\, dx$$

$$= I_{mbr2} \sin^2(\theta_{pc} + \phi) + I_{mbr3} \cos^2(\theta_{pc} + \phi) + I_{mbr23} \sin 2(\theta_{pc} + \phi)$$

$$\int_0^{L_b} (I_{MB2} - I_{MB3}) \cos(\theta_G + \phi) \sin(\theta_G + \phi)\, dx$$

$$= I_{mbr23} \cos 2(\theta_{pc} + \phi) + (I_{mbr2} - I_{mbr3}) \cos(\theta_{pc} + \phi) \sin(\theta_{pc} + \phi)$$

$$\int_0^{L_b} [I_{MB2} \cos^2(\theta_G + \phi) + I_{MB3} \sin^2(\theta_G + \phi)]\, dx$$

$$= I_{mbr2} \cos^2(\theta_{pc} + \phi) + I_{mbr3} \sin^2(\theta_{pc} + \phi) - I_{mbr23} \sin 2(\theta_{pc} + \phi)$$

Making use of the above expressions, the following integrals appearing in Eqs. (C.6) can be evaluated as:

$$\int_0^{L_b} q_{Ibx2}\, dx = [I_{yb} \cos(\theta_{pc} + \phi) - I_{zb} \sin(\theta_{pc} + \phi)][(\zeta\Omega^2 - \ddot{\zeta})(\beta + \beta_p)\zeta$$

$$- \ddot{\beta} + (\ddot{\zeta}\zeta + \dot{\zeta}^2 + \ddot{\beta}\beta + \dot{\beta}^2)\beta_p]$$

$$+ [I_{yb} \sin(\theta_{pc} + \phi) + I_{zb} \cos(\theta_{pc} + \phi)][(\ddot{\zeta} - \zeta\Omega^2)$$

$$- 2\Omega(\dot{\zeta}\zeta + \dot{\beta}\beta_p + \dot{\beta}\beta)]$$

$$- J_b(\ddot{\theta}_{pc} + \ddot{\phi})$$

$$+ [(I_{mbr2} - I_{mbr3}) \cos(\theta_{pc} + \phi) \sin(\theta_{pc} + \phi)$$

$$+ I_{mbr23} \cos 2(\theta_{pc} + \phi)]\Omega[(\Omega + 2\dot{\zeta}) + 2(\dot{\theta}_{pc} + \dot{\phi})(\beta + \beta_p)]$$

$$+ 2[I_{mbr2} \cos^2(\theta_{pc} + \phi) + I_{mbr3} \sin^2(\theta_{pc} + \phi)$$

$$- I_{mbr23} \sin 2(\theta_{pc} + \phi)]\Omega[(\dot{\theta}_{pc} + \dot{\phi})\zeta - \dot{\beta}]$$

$$+ [I_{mbr2} \sin^2(\theta_{pc} + \phi) + I_{mbr3} \cos^2(\theta_{pc} + \phi)$$

$$+ I_{mbr23} \sin 2(\theta_{pc} + \phi)][2\dot{\zeta}\dot{\beta} + \zeta\ddot{\beta} + (\beta + \beta_p)(\Omega^2\zeta + \ddot{\zeta})] \tag{C.8}$$

$$\int_0^{L_b} q_{lby2}\, dx = M_b\Omega^2 e[y_b \sin(\theta_{pc} + \phi) + z_b \cos(\theta_{pc} + \phi)]$$

$$- [I_{yb} \cos(\theta_{pc} + \phi) - I_{zb} \sin(\theta_{pc} + \phi)][\Omega^2(\beta + \beta_p) + \ddot{\beta}]\zeta$$

$$+ [I_{yb} \sin(\theta_{pc} + \phi) + I_{zb} \cos(\theta_{pc} + \phi)][\Omega(\Omega + 2\dot{\zeta})$$

$$- (\Omega^2\beta_p + \ddot{\beta})\beta + (\ddot{\zeta}\zeta + \dot{\zeta}^2 + \ddot{\beta}\beta + \dot{\beta}^2) - \frac{1}{2}\Omega^2(\zeta^2 + \beta^2)]$$

$$- J_b(\ddot{\theta}_{pc} + \ddot{\phi})\zeta$$

$$+ [(I_{mbr2} - I_{mbr3}) \cos(\theta_{pc} + \phi) \sin(\theta_{pc} + \phi)$$

$$+ I_{mbr23} \cos 2(\theta_{pc} + \phi)][(\zeta\Omega^2 - \ddot{\zeta}) - 2(\dot{\theta}_{pc} + \dot{\phi})\dot{\beta}]$$

$$+ [I_{mbr2} \cos^2(\theta_{pc} + \phi) + I_{mbr3} \sin^2(\theta_{pc} + \phi)$$

$$- I_{mbr23} \sin 2(\theta_{pc} + \phi)[\ddot{\beta} - \Omega^2(\beta + \beta_p) - 2(\dot{\theta}_{pc} + \dot{\phi})(\Omega + \dot{\zeta})] \tag{C.9}$$

$$\int_0^{L_b} q_{lbz2}\, dx = - M_b\Omega^2 e[y_b \cos(\theta_{pc} + \phi) - z_b \sin(\theta_{pc} + \phi)]$$

$$+ [I_{yb} \cos(\theta_{pc} + \phi) - I_{zb} \sin(\theta_{pc} + \phi)][- \Omega(\Omega + 2\dot{\zeta}) + (\ddot{\zeta} - \zeta\Omega^2)\zeta$$

$$+ (\beta\Omega^2 - \ddot{\beta})\beta_p + \frac{1}{2}\Omega^2(\zeta^2 + \beta^2) - (\ddot{\zeta}\zeta + \dot{\zeta}^2 + \ddot{\beta}\beta + \dot{\beta}^2)]$$

$$+ [I_{yb}\sin(\theta_{pc} + \phi) + I_{zb}\cos(\theta_{pc} + \phi)](\ddot{\zeta} - \zeta\Omega^2)(\beta + \beta_p)$$

$$- J_b(\ddot{\theta}_{pc} + \ddot{\phi})(\beta + \beta_p)$$

$$+ [(I_{mbr2} - I_{mbr3})\cos(\theta_{pc} + \phi)\sin(\theta_{pc} + \phi)$$

$$+ I_{mbr23}\cos 2(\theta_{pc} + \phi)][\ddot{\beta} - 2(\dot{\theta}_{pc} + \dot{\phi})(\Omega + \dot{\zeta})]$$

$$- [I_{mbr2}\sin^2(\theta_{pc} + \phi) + I_{mbr3}\cos^2(\theta_{pc} + \phi)$$

$$+ I_{mbr23}\sin 2(\theta_{pc} + \phi)][\ddot{\zeta} + 2(\dot{\theta}_{pc} + \dot{\phi})\dot{\beta}] \qquad \text{(C.10)}$$

$$\int_0^{L_b} x\, p_{lbx2}\, dx = M_b x_b \Omega^2 e + I_b\Omega(\Omega + 2\dot{\zeta}) + I_b\beta_p(\ddot{\beta} - \beta\Omega^2)$$

$$+ I_b[(\ddot{\zeta}\zeta + \dot{\zeta}^2 + \ddot{\beta}\beta + \dot{\beta}^2) - \frac{1}{2}\Omega^2(\zeta^2 + \beta^2)]$$

$$- 2[I_{yb}\sin(\theta_{pc} + \phi) + I_{zb}\cos(\theta_{pc} + \phi)]\Omega(\dot{\theta}_{pc} + \dot{\phi}) \qquad \text{(C.11)}$$

$$\int_0^{L_b} x\, p_{lby2}\, dx = I_b(\zeta\Omega^2 - \ddot{\zeta}) + 2I_b\Omega(\dot{\zeta}\zeta + \dot{\beta}\beta + \dot{\beta}\beta_p)$$

$$+ [I_{yb}\cos(\theta_{pc} + \phi) - I_{zb}\sin(\theta_{pc} + \phi)][\Omega(\Omega + 2\dot{\zeta})$$

$$+ (\dot{\theta}_{pc} + \dot{\phi})^2 + \Omega(\dot{\theta}_{pc} + \dot{\phi})(\beta + \beta_p)]$$

$$+ [I_{yb}\sin(\theta_{pc} + \phi) + I_{zb}\cos(\theta_{pc} + \phi)][(\ddot{\theta}_{pc} + \ddot{\phi})$$

$$+ 2\Omega\dot{\beta} - 2\Omega(\dot{\theta}_{pc} + \dot{\phi})\zeta] \qquad \text{(C.12)}$$

$$\int_0^{L_b} x\, p_{lbz2}\, dx = I_b(\ddot{\zeta}\zeta + \dot{\zeta}^2 + \ddot{\beta}\beta + \dot{\beta}^2)\beta_p - I_b\ddot{\beta}$$

$$+ [I_{yb}\cos(\theta_{pc}+\phi) - I_{zb}\sin(\theta_{pc}+\phi)][\ddot{\zeta}(\beta+\beta_p) - (\ddot{\theta}_{pc}+\ddot{\phi})]$$

$$+ [I_{yb}\sin(\theta_{pc}+\phi) + I_{zb}\cos(\theta_{pc}+\phi)][(\dot{\theta}_{pc}+\dot{\phi})^2$$

$$- (\ddot{\theta}_{pc}+\ddot{\phi})(\beta+\beta_p)\zeta] \qquad (C.13)$$

The integral definitions represented by Eqs. (C.4) and (C.7) have been used in evaluating the previous integrals.

Substituting Eqs. (C.8) – (C.13) into Eqs. (C.6) yields the components of the moment about the the blade root in the "2" system due to the inertial loads acting on the blade:

$$M_{Ibx2} = - I_b\ddot{\beta}\zeta - I_b(\zeta\Omega^2 - \ddot{\zeta})(\beta+\beta_p) + I_b(\ddot{\zeta}\zeta + \dot{\zeta}^2 + \ddot{\beta}\beta + \dot{\beta}^2)$$

$$- 2I_b\Omega(\dot{\zeta}\zeta + \dot{\beta}\beta + \dot{\beta}\beta_p)(\beta+\beta_p)$$

$$+ [I_{yb}\cos(\theta_{pc}+\phi) - I_{zb}\sin(\theta_{pc}+\phi)][-\ddot{\beta} - (\ddot{\theta}_{pc}+\ddot{\phi})\zeta$$

$$- \Omega(\Omega+2\dot{\zeta})(\beta+\beta_p) - (\dot{\theta}_{pc}+\dot{\phi})^2(\beta+\beta_p)]$$

$$+ [I_{yb}\sin(\theta_{pc}+\phi) + I_{zb}\cos(\theta_{pc}+\phi)][(\ddot{\zeta} - \zeta\Omega^2) - 2\Omega(\dot{\zeta}\zeta + \dot{\beta}\beta_p + \dot{\beta}\beta)$$

$$+ (\dot{\theta}_{pc}+\dot{\phi})^2\zeta - (\beta+\beta_p)(\ddot{\theta}_{pc}+\ddot{\phi}) - 2\Omega(\beta+\beta_p)\dot{\beta}$$

$$+ 2\Omega(\dot{\theta}_{pc}+\dot{\phi})(\beta+\beta_p)\zeta]$$

$$- J_b(\ddot{\theta}_{pc}+\ddot{\phi})$$

$$+ [(I_{mbr2} - I_{mbr3})\cos(\theta_{pc}+\phi)\sin(\theta_{pc}+\phi)$$

$$+ I_{mbr23}\cos 2(\theta_{pc}+\phi)]\Omega[(\Omega+2\dot{\zeta}) + 2(\dot{\theta}_{pc}+\dot{\phi})(\beta+\beta_p)]$$

$$+ 2[I_{mbr2}\cos^2(\theta_{pc}+\phi) + I_{mbr3}\sin^2(\theta_{pc}+\phi)$$

$$- I_{mbr23} \sin 2(\theta_{pc} + \phi)]\Omega[(\dot{\theta}_{pc} + \dot{\phi})\zeta - \dot{\beta}]$$

$$+ [I_{mbr2} \sin^2(\theta_{pc} + \phi) + I_{mbr3} \cos^2(\theta_{pc} + \phi)$$

$$+ I_{mbr23} \sin 2(\theta_{pc} + \phi)][2\dot{\zeta}\dot{\beta} + \zeta\ddot{\beta} + (\beta + \beta_p)(\Omega^2\zeta + \ddot{\zeta})] \qquad \text{(C.14a)}$$

$$M_{lby2} = M_b x_b \Omega^2 e(\beta + \beta_p) + M_b \Omega^2 e[y_b \sin(\theta_{pc} + \phi) + z_b \cos(\theta_{pc} + \phi)]$$

$$+ I_b\ddot{\beta} + I_b\Omega(\Omega + 2\dot{\zeta})(\beta + \beta_p) - I_b(\ddot{\zeta}\zeta + \dot{\zeta}^2 + \ddot{\beta}\beta + \dot{\beta}^2) - \frac{1}{2} I_b(\zeta^2 + \beta^2)(\beta + \beta_p)$$

$$+ I_b(\ddot{\beta} - \Omega^2\beta)(\beta + \beta_p)\beta_p + I_b(\ddot{\zeta}\zeta + \dot{\zeta}^2 + \ddot{\beta}\beta + \dot{\beta}^2)(\beta + \beta_p)$$

$$- [I_{yb} \cos(\theta_{pc} + \phi) - I_{zb} \sin(\theta_{pc} + \phi)][\Omega^2(\beta + \beta_p)\zeta + \ddot{\beta}\zeta$$

$$- (\ddot{\theta}_{pc} + \ddot{\phi}) + (\beta + \beta_p)\ddot{\zeta}]$$

$$+ [I_{yb} \sin(\theta_{pc} + \phi) + I_{zb} \cos(\theta_{pc} + \phi)][\Omega(\Omega + 2\dot{\zeta}) - (\dot{\theta}_{pc} + \dot{\phi})^2$$

$$- 2\Omega(\dot{\theta}_{pc} + \dot{\phi})(\beta + \beta_p) + (\ddot{\theta}_{pc} + \ddot{\phi})(\beta + \beta_p)\zeta]$$

$$- J_b(\ddot{\theta}_{pc} + \ddot{\phi})\zeta$$

$$+ [(I_{mbr2} - I_{mbr3}) \cos(\theta_{pc} + \phi) \sin(\theta_{pc} + \phi)$$

$$+ I_{mbr23} \cos 2(\theta_{pc} + \phi)][(\zeta\Omega^2 - \ddot{\zeta}) - 2(\dot{\theta}_{pc} + \dot{\phi})\dot{\beta}]$$

$$+ [I_{mbr2} \cos^2(\theta_{pc} + \phi) + I_{mbr3} \sin^2(\theta_{pc} + \phi)$$

$$- I_{mbr23} \sin 2(\theta_{pc} + \phi)][\ddot{\beta} - \Omega^2(\beta + \beta_p) - 2(\dot{\theta}_{pc} + \dot{\phi})(\Omega + \dot{\zeta})] \qquad \text{(C.14b)}$$

$$M_{lbz2} = - M_b x_b \Omega^2 e\zeta - M_b \Omega^2 e[y_b \cos(\theta_{pc} + \phi) - z_b \sin(\theta_{pc} + \phi)]$$

$$- I_b\ddot{\zeta} + 2I_b\Omega(\beta + \beta_p)\dot{\beta} - I_b(\ddot{\beta} - \Omega^2\beta)\beta_p\zeta - I_b\zeta(\ddot{\zeta}\zeta + \dot{\zeta}^2 + \ddot{\beta}\beta + \dot{\beta}^2)$$

$$+ \frac{1}{2} I_b \Omega^2 \zeta (\zeta^2 + \beta^2)$$

$$+ [I_{yb} \cos(\theta_{pc} + \phi) - I_{zb} \sin(\theta_{pc} + \phi)][(\ddot{\zeta} - \zeta\Omega^2)\zeta$$

$$+ (\dot{\theta}_{pc} + \dot{\phi})^2 + \Omega(\dot{\theta}_{pc} + \dot{\phi})(\beta + \beta_p)]$$

$$+ [I_{yb} \sin(\theta_{pc} + \phi) + I_{zb} \cos(\theta_{pc} + \phi)][(\ddot{\zeta} - \zeta\Omega^2)(\beta + \beta_p)$$

$$+ (\ddot{\theta}_{pc} + \ddot{\phi}) + 2\Omega\dot{\beta}]$$

$$- J_b(\ddot{\theta}_{pc} + \ddot{\phi})(\beta + \beta_p)$$

$$+ [(I_{mbr2} - I_{mbr3}) \cos(\theta_{pc} + \phi) \sin(\theta_{pc} + \phi)$$

$$+ I_{mbr23} \cos 2(\theta_{pc} + \phi)][\ddot{\beta} - 2(\dot{\theta}_{pc} + \dot{\phi})(\Omega + \dot{\zeta})]$$

$$- [I_{mbr2} \sin^2(\theta_{pc} + \phi) + I_{mbr3} \cos^2(\theta_{pc} + \phi)$$

$$+ I_{mbr23} \sin 2(\theta_{pc} + \phi)][\ddot{\zeta} + 2(\dot{\theta}_{pc} + \dot{\phi})\dot{\beta}] \qquad \text{(C.14c)}$$

C.1.2 *Control Flap Inertial Loads*

For the offset-hinged spring restrained blade model the differential force at the blade root due to the inertial loads acting on the control surface can be expressed as

$$d\vec{F}_{Ic} = \vec{p}_{Ic}\, dx$$

where $\vec{p}_{Ic}$ represents the distributed inertial force acting on the control surface, which can be expressed in the "2" system as

$$\vec{p}_{Ic} = p_{Icx2}\, \hat{e}_{x2} + p_{Icy2}\, \hat{e}_{y2} + p_{Icz2}\, \hat{e}_{z2}$$

The x_2, y_2 and z_2 components of $\vec{p}_{Ic}$ for the spring restrained blade model are obtained from the general expressions developed in Chapter 3 by substituting Eqs. (4.3) and (4.4) into Eqs. (3.43).

The total force at the blade root is obtained by integrating the differential force along the span of the control surface, i.e.

$$\vec{F}_{Ic} = \int_{x_{cs}}^{x_{cs}+L_{cs}} \vec{p}_{Ic}\, dx \tag{C.15}$$

which can be expressed in the "2" system as

$$\vec{F}_{Ic} = F_{Icx2}\,\hat{e}_{x2} + F_{Icy2}\,\hat{e}_{y2} + F_{Icz2}\,\hat{e}_{z2}$$

where

$$F_{Icx2} = \int_{x_{cs}}^{x_{cs}+L_{cs}} p_{Icx2}\, dx$$

$$= M_c\Omega^2(x_c + e) + 2M_c x_c\Omega\dot{\zeta}$$

$$+ 2M_c\Omega[y_c \sin(\theta_{pc} + \phi + \delta) + z_c \cos(\theta_{pc} + \phi + \delta)]\Omega(\dot{\theta}_{pc} + \dot{\phi} + \dot{\delta})$$

$$+ 2M_c\Omega[y_h \sin(\theta_{pc} + \phi) + z_h \cos(\theta_{pc} + \phi)]\Omega(\dot{\theta}_{pc} + \dot{\phi}) \tag{C.16a}$$

$$F_{Icy2} = \int_{x_{cs}}^{x_{cs}+L_{cs}} p_{Icy2}\, dx$$

$$= 2M_c x_c\Omega\dot{\beta}\beta_p + M_c x_c(\zeta\Omega^2 - \ddot{\zeta}) + 2M_c x_c\Omega(\dot{\zeta}\zeta + \dot{\beta}\beta)$$

$$- M_c[y_c \cos(\theta_{pc} + \phi + \delta) - z_c \sin(\theta_{pc} + \phi + \delta)][\Omega(\Omega + 2\dot{\zeta})$$

$$+ (\dot{\theta}_{pc} + \dot{\phi} + \dot{\delta})^2 + 2\Omega(\dot{\theta}_{pc} + \dot{\phi} + \dot{\delta})(\beta + \beta_p)]$$

$$- M_c[y_c \sin(\theta_{pc} + \phi + \delta) + z_c \cos(\theta_{pc} + \phi + \delta)][2\Omega\dot{\beta}$$

$$+ (\ddot{\theta}_{pc} + \ddot{\phi} + \ddot{\delta}) - 2\Omega(\dot{\theta}_{pc} + \dot{\phi} + \dot{\delta})\zeta]$$

$$- M_c[y_h \cos(\theta_{pc} + \phi) - z_h \sin(\theta_{pc} + \phi)][\Omega(\Omega + 2\dot{\zeta})$$

$$+ (\dot{\theta}_{pc} + \dot{\phi})^2 + 2\Omega(\dot{\theta}_{pc} + \dot{\phi})(\beta + \beta_p)]$$

$$- M_c[y_h \sin(\theta_{pc} + \phi) + z_h \cos(\theta_{pc} + \phi)][2\Omega\dot{\beta}$$

$$+ (\ddot{\theta}_{pc} + \ddot{\phi}) - 2\Omega(\dot{\theta}_{pc} + \dot{\phi})\zeta] \qquad \text{(C.16b)}$$

$$F_{lcz2} = \int_{x_{cs}}^{x_{cs} + L_{cs}} p_{lcz2}\, dx$$

$$= - M_c x_c \ddot{\beta}$$

$$+ M_c[y_c \cos(\theta_{pc} + \phi + \delta) - z_c \sin(\theta_{pc} + \phi + \delta)][- \ddot{\beta}\zeta$$

$$- (\beta + \beta_p)\ddot{\zeta} - 2\dot{\beta}\dot{\zeta} + (\ddot{\theta}_{pc} + \ddot{\phi} + \ddot{\delta})]$$

$$- M_c[y_c \sin(\theta_{pc} + \phi + \delta) + z_c \cos(\theta_{pc} + \phi + \delta)][(\dot{\theta}_{pc} + \dot{\phi} + \dot{\delta})^2$$

$$- (\ddot{\theta}_{pc} + \ddot{\phi} + \ddot{\delta})(\beta + \beta_p)\zeta]$$

$$+ M_c[y_h \cos(\theta_{pc} + \phi) - z_h \sin(\theta_{pc} + \phi)][- \ddot{\beta}\zeta$$

$$- (\beta + \beta_p)\ddot{\zeta} - 2\dot{\beta}\dot{\zeta} + (\ddot{\theta}_{pc} + \ddot{\phi})]$$

$$- M_c[y_h \sin(\theta_{pc} + \phi) + z_h \cos(\theta_{pc} + \phi)][(\dot{\theta}_{pc} + \dot{\phi})^2$$

$$- (\ddot{\theta}_{pc} + \ddot{\phi})(\beta + \beta_p)\zeta] \qquad \text{(C.16c)}$$

The following integral definitions have been used in evaluating the previous expressions:

$$\int_{x_{cs}}^{x_{cs}+L_{cs}} m_c \, dx = M_c \tag{C.17a}$$

$$\int_{x_{cs}}^{x_{cs}+L_{cs}} m_c x \, dx = M_c x_c \tag{C.17b}$$

$$\int_{x_{cs}}^{x_{cs}+L_{cs}} m_c X_{Ic} \cos\theta_{pt} \, dx = M_c y_c \tag{C.17c}$$

$$\int_{x_{cs}}^{x_{cs}+L_{cs}} m_c X_{Ic} \sin\theta_{pt} \, dx = M_c z_c \tag{C.17d}$$

$$\int_{x_{cs}}^{x_{cs}+L_{cs}} m_c X_H \cos\theta_{pt} \, dx = M_c y_h \tag{C.17e}$$

$$\int_{x_{cs}}^{x_{cs}+L_{cs}} m_c X_H \sin\theta_{pt} \, dx = M_c z_h \tag{C.17f}$$

where M_c represents the mass of one control surface.

For the offset-hinged spring restrained blade model the differential moment about the blade root due to the inertial loads acting on the control surface can be expressed as

$$d\vec{M}_{Ic} = [\vec{q}_{Ih} + (x\,\hat{e}_{x4} + \bar{y}_H\,\hat{e}_{y5} + \bar{z}_H\,\hat{e}_{z5}) \times \vec{p}_{Ic}]\,dx$$

where $\vec{q}_{Ih}$ represents the distributed inertial moment about the control surface hinge, which can be expressed in the "2" system as

$$\vec{q}_{Ih} = q_{Ihx2}\,\hat{e}_{x2} + q_{Ihy2}\,\hat{e}_{y2} + q_{Ihz2}\,\hat{e}_{z2}$$

The x_2, y_2 and z_2 components of $\vec{q}_{Ih}$ for the spring restrained blade model are obtained from the general expressions developed in Chapter 3 by substituting Eqs. (4.3) and (4.4) into Eqs. (3.46).

The total moment about the blade root is obtained by integrating the differential moment along the span of the control surface, i.e.

$$\vec{M}_{Ic} = \int_{x_{cs}}^{x_{cs}+L_{cs}} [\vec{q}_{Ih} + (x\,\hat{e}_{x4} + \bar{y}_H\,\hat{e}_{y5} + \bar{z}_H\,\hat{e}_{z5}) \times \vec{p}_{Ic}]\,dx \tag{C.18}$$

which can be expressed in the "2" system as

$$\vec{M}_{Ic} = \vec{M}_{Icx2}\,\hat{e}_{x2} + M_{Icy2}\,\hat{e}_{y2} + M_{Icz2}\,\hat{e}_{z2}$$

where

$$M_{Icx2} = \int_{x_{cs}}^{x_{cs}+L_{cs}} q_{Ihx2}\,dx$$

$$+ \int_{x_{cs}}^{x_{cs}+L_{cs}} X_H \sin(\theta_G + \phi)\, p_{Icy2}\,dx$$

$$- \int_{x_{cs}}^{x_{cs}+L_{cs}} X_H \cos(\theta_G + \phi)\, p_{Icz2}\,dx$$

$$+ \zeta \int_{x_{cs}}^{x_{cs}+L_{cs}} x\, p_{Icz2}\,dx - (\beta + \beta_p) \int_{x_{cs}}^{x_{cs}+L_{cs}} x\, p_{Icy2}\,dx \tag{C.19a}$$

$$M_{Icy2} = \int_{x_{cs}}^{x_{cs}+L_{cs}} q_{Ihy2}\,dx - \int_{x_{cs}}^{x_{cs}+L_{cs}} X_H \sin(\theta_G + \phi)\, p_{Icx2}\,dx$$

$$- \zeta \int_{x_{cs}}^{x_{cs}+L_{cs}} X_H \cos(\theta_G + \phi)\, p_{Icz2}\,dx$$

$$- (\beta + \beta_p) \int_{x_{cs}}^{x_{cs}+L_{cs}} X_H \sin(\theta_G + \phi)\, p_{Icz2}\,dx$$

$$- \int_{x_{cs}}^{x_{cs}+L_{cs}} x\, p_{Icz2}\,dx + (\beta + \beta_p) \int_{x_{cs}}^{x_{cs}+L_{cs}} x\, p_{Icx2}\,dx \tag{C.19b}$$

$$M_{Icz2} = \int_{x_{cs}}^{x_{cs}+L_{cs}} q_{Ihz2}\,dx + \int_{x_{cs}}^{x_{cs}+L_{cs}} X_H \cos(\theta_G + \phi)\, p_{Icx2}\,dx$$

$$+ \zeta \int_{x_{cs}}^{x_{cs}+L_{cs}} X_H \cos(\theta_G + \phi)\, p_{Icy2}\,dx$$

$$+ (\beta + \beta_p)\int_{x_{cs}}^{x_{cs}+L_{cs}} X_H \sin(\theta_G + \phi)\, p_{Icy2}\, dx$$

$$+ \int_{x_{cs}}^{x_{cs}+L_{cs}} x\, p_{Icy2}\, dx - \zeta \int_{x_{cs}}^{x_{cs}+L_{cs}} x\, p_{Icx2}\, dx \qquad \text{(C.19c)}$$

Before performing the above integrations it is convenient to define the following integrals:

$$\int_{x_{cs}}^{x_{cs}+L_{cs}} m_c x^2\, dx = I_c \qquad \text{(C.20a)}$$

$$\int_{x_{cs}}^{x_{cs}+L_{cs}} m_c X_{Ic} x \cos\theta_{pt}\, dx = I_{yc} \qquad \text{(C.20b)}$$

$$\int_{x_{cs}}^{x_{cs}+L_{cs}} m_c X_{Ic} x \sin\theta_{pt}\, dx = I_{zc} \qquad \text{(C.20c)}$$

$$\int_{x_{cs}}^{x_{cs}+L_{cs}} m_c X_H x \cos\theta_{pt}\, dx = I_{yh} \qquad \text{(C.20d)}$$

$$\int_{x_{cs}}^{x_{cs}+L_{cs}} m_c X_H x \sin\theta_{pt}\, dx = I_{zh} \qquad \text{(C.20e)}$$

$$\int_{x_{cs}}^{x_{cs}+L_{cs}} m_c X_H^2\, dx = J_h \qquad \text{(C.20f)}$$

$$\int_{x_{cs}}^{x_{cs}+L_{cs}} (I_{MC2} + I_{MC3})\, dx = J_c \qquad \text{(C.20g)}$$

$$\int_{x_{cs}}^{x_{cs}+L_{cs}} (I_{MC2} - I_{MC3}) \cos\theta_{pt} \sin\theta_{pt}\, dx = I_{mcr23} \qquad \text{(C.20h)}$$

$$\int_{x_{cs}}^{x_{cs}+L_{cs}} (I_{MC2} \cos^2\theta_{pt} + I_{MC3} \sin^2\theta_{pt})\, dx = I_{mcr2} \qquad \text{(C.20i)}$$

$$\int_{x_{cs}}^{x_{cs}+L_{cs}} (I_{MC2} \sin^2\theta_{pt} + I_{MC3} \cos^2\theta_{pt})\, dx = I_{mcr3} \qquad \text{(C.20j)}$$

$$\int_{x_{cs}}^{x_{cs}+L_{cs}} m_c X_H^2 \cos^2\theta_{pt}\, dx = J_{yh} \tag{C.20k}$$

$$\int_{x_{cs}}^{x_{cs}+L_{cs}} m_c X_H^2 \sin^2\theta_{pt}\, dx = J_{zh} \tag{C.20l}$$

$$\int_{x_{cs}}^{x_{cs}+L_{cs}} m_c X_H^2 \sin\theta_{pt} \cos\theta_{pt}\, dx = J_{yzh} \tag{C.20m}$$

$$\int_{x_{cs}}^{x_{cs}+L_{cs}} m_c X_H X_{Ic}\, dx = J_{hc} \tag{C.20n}$$

$$\int_{x_{cs}}^{x_{cs}+L_{cs}} m_c X_H X_{Ic} \cos^2\theta_{pt}\, dx = J_{yhc} \tag{C.20o}$$

$$\int_{x_{cs}}^{x_{cs}+L_{cs}} m_c X_H X_{Ic} \sin^2\theta_{pt}\, dx = J_{zhc} \tag{C.20p}$$

$$\int_{x_{cs}}^{x_{cs}+L_{cs}} m_c X_H X_{Ic} \cos\theta_{pt} \sin\theta_{pt}\, dx = J_{yzhc} \tag{C.20q}$$

Using the above integral definitions along with Eqs. (C.1) , the following integrals can be evaluated:

$$\int_{x_{cs}}^{x_{cs}+L_{cs}} [I_{MC2} \sin^2(\theta_G + \phi + \delta) + I_{MC3} \cos^2(\theta_G + \phi + \delta)]\, dx$$

$$= I_{mcr2} \sin^2(\theta_{pc} + \phi + \delta) + I_{mcr3} \cos^2(\theta_{pc} + \phi + \delta) + I_{mcr23} \sin 2(\theta_{pc} + \phi + \delta)$$

$$\int_{x_{cs}}^{x_{cs}+L_{cs}} (I_{MC2} - I_{MC3}) \cos(\theta_G + \phi + \delta) \sin(\theta_G + \phi + \delta)\, dx$$

$$= I_{mcr23} \cos 2(\theta_{pc} + \phi + \delta) + (I_{mcr2} - I_{mcr3}) \cos(\theta_{pc} + \phi + \delta) \sin(\theta_{pc} + \phi + \delta)$$

$$\int_{x_{cs}}^{x_{cs}+L_{cs}} [I_{MC2} \cos^2(\theta_G + \phi + \delta) + I_{MC3} \sin^2(\theta_G + \phi + \delta)]$$

$$= I_{mcr2} \cos^2(\theta_{pc} + \phi + \delta) + I_{mcr3} \sin^2(\theta_{pc} + \phi + \delta) - I_{mcr23} \sin 2(\theta_{pc} + \phi + \delta)$$

$$\int_{x_{cs}}^{x_{cs}+L_{cs}} m_c X_H X_{lc} \cos(\theta_G + \phi)\cos(\theta_G + \phi + \delta)\,dx$$

$$= J_{yhc}\cos(\theta_{pc} + \phi)\cos(\theta_{pc} + \phi + \delta) + J_{zhc}\sin(\theta_{pc} + \phi)\sin(\theta_{pc} + \phi + \delta)$$

$$- J_{yzhc}\sin(2\theta_{pc} + 2\phi + \delta)$$

$$\int_{x_{cs}}^{x_{cs}+L_{cs}} m_c X_H X_{lc} \cos(\theta_G + \phi)\sin(\theta_G + \phi + \delta)\,dx$$

$$= J_{yhc}\cos(\theta_{pc} + \phi)\sin(\theta_{pc} + \phi + \delta) - J_{zhc}\sin(\theta_{pc} + \phi)\cos(\theta_{pc} + \phi + \delta)$$

$$+ J_{yzhc}\cos(2\theta_{pc} + 2\phi + \delta)$$

$$\int_{x_{cs}}^{x_{cs}+L_{cs}} m_c X_H X_{lc} \sin(\theta_G + \phi)\sin(\theta_G + \phi + \delta)\,dx$$

$$= J_{yhc}\sin(\theta_{pc} + \phi)\sin(\theta_{pc} + \phi + \delta) + J_{zhc}\cos(\theta_{pc} + \phi)\cos(\theta_{pc} + \phi + \delta)$$

$$+ J_{yzhc}\sin(2\theta_{pc} + 2\phi + \delta)$$

$$\int_{x_{cs}}^{x_{cs}+L_{cs}} m_c X_H X_{lc} \sin(\theta_G + \phi)\cos(\theta_G + \phi + \delta)\,dx$$

$$= J_{yhc}\sin(\theta_{pc} + \phi)\cos(\theta_{pc} + \phi + \delta) - J_{zhc}\cos(\theta_{pc} + \phi)\sin(\theta_{pc} + \phi + \delta)$$

$$+ J_{yzhc}\cos(2\theta_{pc} + 2\phi + \delta)$$

$$\int_{x_{cs}}^{x_{cs}+L_{cs}} m_c X_H^2 \cos^2(\theta_G + \phi)\,dx$$

$$= J_{yh}\cos^2(\theta_{pc} + \phi) + J_{zh}\sin^2(\theta_{pc} + \phi) - J_{yzh}\sin 2(\theta_{pc} + \phi)$$

$$\int_{x_{cs}}^{x_{cs}+L_{cs}} m_c X_H^2 \sin^2(\theta_G + \phi)\,dx$$

$$= J_{zh}\cos^2(\theta_{pc} + \phi) + J_{yh}\sin^2(\theta_{pc} + \phi) + J_{yzh}\sin 2(\theta_{pc} + \phi)$$

$$\int_{x_{cs}}^{x_{cs}+L_{cs}} m_c X_H^2 \cos(\theta_G + \phi)\sin(\theta_G + \phi)\,dx$$

$$= J_{yzh}\cos 2(\theta_{pc} + \phi) + (J_{yh} - J_{zh})\cos(\theta_{pc} + \phi)\sin(\theta_{pc} + \phi)$$

Using the above integrals, the following integrals appearing in Eqs. (C.19) can be evaluated.

$$\int_{x_{cs}}^{x_{cs}+L_{cs}} q_{Ihx2}\,dx = M_{Ihx2}$$

$$= -[J_{yhc}\cos(\theta_{pc} + \phi)\sin(\theta_{pc} + \phi + \delta) + J_{yzhc}\cos(2\theta_{pc} + 2\phi + \delta)$$

$$- J_{zhc}\sin(\theta_{pc} + \phi)\cos(\theta_{pc} + \phi + \delta)]\Omega(\Omega + 2\dot{\zeta})$$

$$- J_{hc}[(\ddot{\theta}_{pc} + \ddot{\phi})\cos\delta + (\dot{\theta}_{pc} + \dot{\phi})^2\sin\delta]$$

$$+ [I_{yc}\cos(\theta_{pt} + \phi + \delta) - I_{zc}\sin(\theta_{pt} + \phi + \delta)]\ddot{\beta}$$

$$- [I_{yc}\sin(\theta_{pc} + \phi + \delta) + I_{zc}\cos(\theta_{pc} + \phi + \delta)][(\ddot{\zeta} - \zeta\Omega^2)$$

$$- 2\Omega(\dot{\zeta}\zeta + \dot{\beta}\beta_p + \dot{\beta}\beta)]$$

$$- J_c(\ddot{\theta}_{pc} + \ddot{\phi} + \ddot{\delta})$$

$$+ [(I_{mcr2} - I_{mcr3})\cos(\theta_{pc} + \phi + \delta)\sin(\theta_{pc} + \phi + \delta)$$

$$+ I_{mcr23}\cos 2(\theta_{pc} + \phi + \delta)]\Omega[(\Omega + 2\dot{\zeta}) + 2(\dot{\theta}_{pc} + \dot{\phi} + \dot{\delta})(\beta + \beta_p)]$$

$$+ 2[I_{mcr2}\cos^2(\theta_{pc} + \phi + \delta) + I_{mcr3}\sin^2(\theta_{pc} + \phi + \delta)$$

$$- I_{mcr23}\sin 2(\theta_{pc} + \phi + \delta)]\Omega[(\dot{\theta}_{pc} + \dot{\phi} + \dot{\delta})\zeta - \dot{\beta}]$$

$$+ [I_{mcr2}\sin^2(\theta_{pc} + \phi + \delta) + I_{mcr3}\cos^2(\theta_{pc} + \phi + \delta)$$

$$+ I_{mcr23} \sin 2(\theta_{pc} + \phi + \delta)][2\dot{\zeta}\dot{\beta} + \zeta\ddot{\beta} + (\beta + \beta_p)(\Omega^2\zeta + \ddot{\zeta})] \tag{C.21}$$

$$\int_{x_{cs}}^{x_{cs} + L_{cs}} q_{ihy2}\, dx = M_{iy2}$$

$$= -2[J_{yhc} \sin(\theta_{pc} + \phi) \sin(\theta_{pc} + \phi + \delta) + J_{yzhc} \sin(2\theta_{pc} + 2\phi + \delta)$$

$$+ J_{zhc} \cos(\theta_{pc} + \phi) \cos(\theta_{pc} + \phi + \delta)]\Omega(\dot{\theta}_{pc} + \dot{\phi})$$

$$- M_c\Omega^2 e[y_c \sin(\theta_{pc} + \phi + \delta) + z_c \cos(\theta_{pc} + \phi + \delta)]$$

$$+ [I_{yc} \cos(\theta_{pc} + \phi + \delta) - I_{zc} \sin(\theta_{pc} + \phi + \delta)][\Omega^2(\beta + \beta_p) + \ddot{\beta}]\zeta$$

$$- [I_{yc} \sin(\theta_{pc} + \phi + \delta) + I_{zc} \cos(\theta_{pc} + \phi + \delta)]\Omega(\Omega + 2\dot{\zeta})$$

$$- J_c(\ddot{\theta}_{pc} + \ddot{\phi} + \ddot{\delta})\zeta$$

$$+ [(I_{mcr2} - I_{mcr3}) \cos(\theta_{pc} + \phi + \delta) \sin(\theta_{pc} + \phi + \delta)$$

$$+ I_{mcr23} \cos 2(\theta_{pc} + \phi + \delta)][(\zeta\Omega^2 - \ddot{\zeta}) - 2(\dot{\theta}_{pc} + \dot{\phi} + \dot{\delta})\dot{\beta}]$$

$$+ [I_{mcr2} \cos^2(\theta_{pc} + \phi + \delta) + I_{mcr3} \sin^2(\theta_{pc} + \phi + \delta)$$

$$- I_{mcr23} \sin 2(\theta_{pc} + \phi + \delta)][\ddot{\beta} - \Omega^2(\beta + \beta_p)$$

$$- 2(\dot{\theta}_{pc} + \dot{\phi} + \dot{\delta})(\Omega + \dot{\zeta})] \tag{C.22}$$

$$\int_{x_{cs}}^{x_{cs} + L_{cs}} q_{ihz2}\, dx = M_{ihz2}$$

$$= 2[J_{yhc} \sin(\theta_{pc} + \phi) \cos(\theta_{pc} + \phi + \delta) + J_{yzhc} \cos(2\theta_{pc} + 2\phi + \delta)$$

$$- J_{zhc} \cos(\theta_{pc} + \phi) \sin(\theta_{pc} + \phi + \delta)]\Omega(\dot{\theta}_{pc} + \dot{\phi})$$

$$+ M_c\Omega^2 e[y_c \cos(\theta_{pc} + \phi + \delta) - z_c \sin(\theta_{pc} + \phi + \delta)]$$

$$+ [I_{yc}\cos(\theta_{pc}+\phi+\delta) - I_{zc}\sin(\theta_{pc}+\phi+\delta)]\Omega(\Omega+2\dot{\zeta})$$

$$- [I_{yc}\sin(\theta_{pc}+\phi+\delta) + I_{zc}\cos(\theta_{pc}+\phi+\delta)](\ddot{\zeta} - \zeta\Omega^2)(\beta+\beta_p)$$

$$- J_c(\ddot{\theta}_{pc}+\ddot{\phi}+\ddot{\delta})(\beta+\beta_p)$$

$$+ [(I_{mcr2} - I_{mcr3})\cos(\theta_{pc}+\phi+\delta)\sin(\theta_{pc}+\phi+\delta)$$

$$+ I_{mcr23}\cos 2(\theta_{pc}+\phi+\delta)][\ddot{\beta} - 2(\dot{\theta}_{pc}+\dot{\phi}+\dot{\delta})(\Omega+\dot{\zeta})]$$

$$- [I_{mcr2}\sin^2(\theta_{pc}+\phi+\delta) + I_{mrc3}\cos^2(\theta_{pc}+\phi+\delta)$$

$$+ I_{mcr23}\sin 2(\theta_{pc}+\phi+\delta)][\ddot{\zeta} + 2(\dot{\theta}_{pc}+\dot{\phi}+\dot{\delta})\dot{\beta}] \qquad \text{(C.23)}$$

$$\int_{x_{cs}}^{x_{cs}+L_{cs}} X_H \sin(\theta_G+\phi)\, p_{Icy2}\, dx$$

$$= [I_{yh}\sin(\theta_{pc}+\phi) + I_{zh}\cos(\theta_{pc}+\phi)][2\Omega\dot{\beta}\beta_p + (\zeta\Omega^2 - \ddot{\zeta})]$$

$$- [J_{yhc}\sin(\theta_{pc}+\phi)\cos(\theta_{pc}+\phi+\delta) - J_{zhc}\cos(\theta_{pc}+\phi)\sin(\theta_{pc}+\phi+\delta)$$

$$+ J_{yzhc}\cos(2\theta_{pc}+2\phi+\delta)](\dot{\theta}_{pc}+\dot{\phi}+\dot{\delta})^2$$

$$- [J_{yhc}\sin(\theta_{pc}+\phi)\sin(\theta_{pc}+\phi+\delta) + J_{zhc}\cos(\theta_{pc}+\phi)\cos(\theta_{pc}+\phi+\delta)$$

$$+ J_{yzhc}\sin(2\theta_{pc}+2\phi+\delta)](\ddot{\theta}_{pc}+\ddot{\phi}+\ddot{\delta})$$

$$- [J_{yzh}\cos 2(\theta_{pc}+\phi) + \frac{1}{2}(J_{yh} - J_{zh})\sin 2(\theta_{pc}+\phi)][(\dot{\theta}_{pc}+\dot{\phi})^2$$

$$+ \Omega(\Omega+2\dot{\zeta}) + 2\Omega(\dot{\theta}_{pc}+\dot{\phi})(\beta+\beta_p)]$$

$$+ [J_{zh}\cos^2(\theta_{pc}+\phi) + J_{yh}\sin^2(\theta_{pc}+\phi)$$

$$+ J_{yzh}\sin 2(\theta_{pc}+\phi)][(\ddot{\theta}_{pc}+\ddot{\phi}) + 2\Omega\dot{\beta} - 2\Omega(\dot{\theta}_{pc}+\dot{\phi})\dot{\zeta}] \qquad \text{(C.24)}$$

$$\int_{x_{cs}}^{x_{cs}+L_{cs}} X_H \cos(\theta_G+\phi)\, p_{lcz2}\, dx = -[I_{yh}\cos(\theta_{pc}+\phi) - I_{zh}\sin(\theta_{pc}+\phi)]\ddot{\beta}$$

$$+ [J_{yhc}\cos(\theta_{pc}+\phi)\cos(\theta_{pc}+\phi+\delta) + J_{zhc}\sin(\theta_{pc}+\phi)\sin(\theta_{pc}+\phi+\delta)$$

$$- J_{yzhc}\sin(2\theta_{pc}+2\phi+\delta)](\ddot{\theta}_{pc}+\ddot{\phi}+\ddot{\delta})$$

$$- [J_{yhc}\cos(\theta_{pc}+\phi)\sin(\theta_{pc}+\phi+\delta) - J_{zhc}\sin(\theta_{pc}+\phi)\cos(\theta_{pc}+\phi+\delta)$$

$$+ J_{yzhc}\cos(2\theta_{pc}+2\phi+\delta)](\dot{\theta}_{pc}+\dot{\phi}+\dot{\delta})^2$$

$$+ [J_{yh}\cos^2(\theta_{pc}+\phi) + J_{zh}\sin^2(\theta_{pc}+\phi)$$

$$- J_{yzh}\sin 2(\theta_{pc}+\phi)][(\ddot{\theta}_{pc}+\ddot{\phi}) - (\beta+\beta_p)\ddot{\zeta} - 2\dot{\beta}\dot{\zeta} - \ddot{\beta}\zeta]$$

$$- [(J_{yh}-J_{zh})\cos(\theta_{pc}+\phi)\sin(\theta_{pc}+\phi)$$

$$+ J_{yzh}\cos 2(\theta_{pc}+\phi)][(\dot{\theta}_{pc}+\dot{\phi})^2 - (\ddot{\theta}_{pc}+\ddot{\phi})(\beta+\beta_p)\zeta] \quad \text{(C.25)}$$

$$\int_{x_{cs}}^{x_{cs}+L_{cs}} X_H \sin(\theta_G+\phi)\, p_{lcz2}\, dx = -[I_{yh}\sin(\theta_{pc}+\phi) + I_{zh}\cos(\theta_{pc}+\phi)]\ddot{\beta}$$

$$+ [J_{yhc}\sin(\theta_{pc}+\phi)\cos(\theta_{pc}+\phi+\delta) - J_{zhc}\cos(\theta_{pc}+\phi)\sin(\theta_{pc}+\phi+\delta)$$

$$+ J_{yzhc}\cos(2\theta_{pc}+2\phi+\delta)](\ddot{\theta}_{pc}+\ddot{\phi}+\ddot{\delta})$$

$$- [J_{yhc}\sin(\theta_{pc}+\phi)\sin(\theta_{pc}+\phi+\delta) + J_{zhc}\cos(\theta_{pc}+\phi)\cos(\theta_{pc}+\phi+\delta)$$

$$+ J_{yzhc}\sin(2\theta_{pc}+2\phi+\delta)](\dot{\theta}_{pc}+\dot{\phi}+\dot{\delta})^2$$

$$+ [(J_{yh}-J_{zh})\cos(\theta_{pc}+\phi)\sin(\theta_{pc}+\phi)$$

$$+ J_{yzh}\cos 2(\theta_{pc}+\phi)][(\ddot{\theta}_{pc}+\ddot{\phi}) - (\beta+\beta_p)\ddot{\zeta} - 2\dot{\beta}\dot{\zeta} - \ddot{\beta}\zeta]$$

$$- [J_{zh}\cos^2(\theta_{pc}+\phi) + J_{yh}\sin^2(\theta_{pc}+\phi)$$

$$+ J_{yzh} \sin 2(\theta_{pc} + \phi)][(\dot{\theta}_{pc} + \dot{\phi})^2 - (\ddot{\theta}_{pc} + \ddot{\phi})(\beta + \beta_p)\zeta] \tag{C.26}$$

$$\int_{x_{cs}}^{x_{cs} + L_{cs}} X_H \cos(\theta_G + \phi)\, p_{lcy2}\, dx$$

$$= [I_{yh} \cos(\theta_{pc} + \phi) - I_{zh} \sin(\theta_{pc} + \phi)][2\Omega\dot{\beta}\beta_p + (\zeta\Omega^2 - \ddot{\zeta})]$$

$$- [J_{yhc} \cos(\theta_{pc} + \phi) \cos(\theta_{pc} + \phi + \delta) + J_{zhc} \sin(\theta_{pc} + \phi) \sin(\theta_{pc} + \phi + \delta)$$

$$- J_{yzhc} \sin(2\theta_{pc} + 2\phi + \delta)](\dot{\theta}_{pc} + \dot{\phi} + \dot{\delta})^2$$

$$- [J_{yhc} \cos(\theta_{pc} + \phi) \sin(\theta_{pc} + \phi + \delta) - J_{zhc} \sin(\theta_{pc} + \phi) \cos(\theta_{pc} + \phi + \delta)$$

$$+ J_{yzhc} \cos(2\theta_{pc} + 2\phi + \delta)](\ddot{\theta}_{pc} + \ddot{\phi} + \ddot{\delta})$$

$$- [J_{yh} \cos^2(\theta_{pc} + \phi) + J_{zh} \sin^2(\theta_{pc} + \phi)$$

$$- J_{yzh} \sin 2(\theta_{pc} + \phi)][(\dot{\theta}_{pc} + \dot{\phi})^2 + \Omega(\Omega + 2\dot{\zeta}) + 2\Omega(\dot{\theta}_{pc} + \dot{\phi})(\beta + \beta_p)]$$

$$- [(J_{yh} - J_{zh}) \cos(\theta_{pc} + \phi) \sin(\theta_{pc} + \phi)$$

$$+ J_{yzh} \cos 2(\theta_{pc} + \phi)][(\ddot{\theta}_{pc} + \ddot{\phi}) + 2\Omega\dot{\beta} - 2\Omega(\dot{\theta}_{pc} + \dot{\phi})\zeta] \tag{C.27}$$

$$\int_{x_{cs}}^{x_{cs} + L_{cs}} X_H \sin(\theta_G + \phi)\, p_{lcx2}\, dx = M_c[y_h \sin(\theta_{pc} + \phi) + z_h \cos(\theta_{pc} + \phi)]\Omega^2 e$$

$$+ [I_{yh} \sin(\theta_{pc} + \phi) + I_{zh} \cos(\theta_{pc} + \phi)]\Omega(\Omega + 2\dot{\zeta})$$

$$+ 2[J_{yhc} \sin(\theta_{pc} + \phi) \sin(\theta_{pc} + \phi + \delta) + J_{zhc} \cos(\theta_{pc} + \phi) \cos(\theta_{pc} + \phi + \delta)$$

$$+ J_{yzhc} \sin(2\theta_{pc} + 2\phi + \delta)]\Omega(\dot{\theta}_{pc} + \dot{\phi} + \dot{\delta})$$

$$+ 2[J_{zh} \cos^2(\theta_{pc} + \phi) + J_{yh} \sin^2(\theta_{pc} + \phi)$$

$$+ J_{yzh} \sin 2(\theta_{pc} + \phi)]\Omega(\dot{\theta}_{pc} + \dot{\phi}) \tag{C.28}$$

$$\int_{x_{cs}}^{x_{cs}+L_{cs}} X_H \cos(\theta_G+\phi)\, p_{lcx2}\, dx = M_c[y_h \cos(\theta_{pc}+\phi) - z_h \sin(\theta_{pc}+\phi)]\Omega^2 e$$

$$+ [I_{yh}\cos(\theta_{pc}+\phi) - I_{zh}\sin(\theta_{pc}+\phi)]\Omega(\Omega+2\dot{\zeta})$$

$$+ 2[J_{yhc}\cos(\theta_{pc}+\phi)\sin(\theta_{pc}+\phi+\delta) - J_{zhc}\sin(\theta_{pc}+\phi)\cos(\theta_{pc}+\phi+\delta)$$

$$+ J_{yzhc}\cos(2\theta_{pc}+2\phi+\delta)]\Omega(\dot{\theta}_{pc}+\dot{\phi}+\dot{\delta})$$

$$+ 2[(J_{yh}-J_{zh})\cos(\theta_{pc}+\phi)\sin(\theta_{pc}+\phi)$$

$$+ J_{yzh}\cos 2(\theta_{pc}+\phi)]\Omega(\dot{\theta}_{pc}+\dot{\phi}) \qquad \text{(C.29)}$$

$$\int_{x_{cs}}^{x_{cs}+L_{cs}} x\, p_{lcx2}\, dx = M_c x_c \Omega^2 e + I_c\Omega(\Omega+2\dot{\zeta})$$

$$+ 2[I_{yc}\sin(\theta_{pc}+\phi+\delta) + I_{zc}\cos(\theta_{pc}+\phi+\delta)]\Omega(\dot{\theta}_{pc}+\dot{\phi}+\dot{\delta})$$

$$+ 2[I_{yh}\sin(\theta_{pc}+\phi) + I_{zh}\cos(\theta_{pc}+\phi)]\Omega(\dot{\theta}_{pc}+\dot{\phi}) \qquad \text{(C.30)}$$

$$\int_{x_{cs}}^{x_{cs}+L_{cs}} x\, p_{lcy2}\, dx = I_c(\zeta\Omega^2 - \ddot{\zeta}) + 2I_c\Omega(\dot{\zeta}\zeta + \dot{\beta}\beta + \dot{\beta}\beta_p)$$

$$- [I_{yc}\cos(\theta_{pc}+\phi+\delta) - I_{zc}\sin(\theta_{pc}+\phi+\delta)][\Omega(\Omega+2\dot{\zeta})$$

$$+ (\dot{\theta}_{pc}+\dot{\phi}+\dot{\delta})^2 + \Omega(\dot{\theta}_{pc}+\dot{\phi}+\dot{\delta})(\beta+\beta_p)]$$

$$- [I_{yc}\sin(\theta_{pc}+\phi+\delta) + I_{zc}\cos(\theta_{pc}+\phi+\delta)][(\ddot{\theta}_{pc}+\ddot{\phi}+\ddot{\delta})$$

$$+ 2\Omega\dot{\beta} - 2\Omega(\dot{\theta}_{pc}+\dot{\phi}+\dot{\delta})\zeta]$$

$$- [I_{yh}\cos(\theta_{pc}+\phi) - I_{zh}\sin(\theta_{pc}+\phi)][\Omega(\Omega+2\dot{\zeta})$$

$$+ (\dot{\theta}_{pc}+\dot{\phi})^2 + \Omega(\dot{\theta}_{pc}+\dot{\phi})(\beta+\beta_p)]$$

$$- [I_{yh} \sin(\theta_{pc} + \phi) + I_{zh} \cos(\theta_{pc} + \phi)][(\ddot{\theta}_{pc} + \ddot{\phi})$$

$$+ 2\Omega\dot{\beta} - 2\Omega(\dot{\theta}_{pc} + \dot{\phi})\zeta] \tag{C.31}$$

$$\int_{x_{cs}}^{x_{cs} + L_{cs}} x\, p_{Icz2}\, dx = - I_c\ddot{\beta}$$

$$- [I_{yc} \cos(\theta_{pc} + \phi + \delta) - I_{zc} \sin(\theta_{pc} + \phi + \delta)][\ddot{\zeta}(\beta + \beta_p) - (\ddot{\theta}_{pc} + \ddot{\phi} + \ddot{\delta})]$$

$$- [I_{yc} \sin(\theta_{pc} + \phi + \delta) + I_{zc} \cos(\theta_{pc} + \phi + \delta)][(\dot{\theta}_{pc} + \dot{\phi} + \dot{\delta})^2$$

$$- (\ddot{\theta}_{pc} + \ddot{\phi} + \ddot{\delta})(\beta + \beta_p)\zeta]$$

$$- [I_{yh} \cos(\theta_{pc} + \phi) - I_{zh} \sin(\theta_{pc} + \phi)][\ddot{\zeta}(\beta + \beta_p) - (\ddot{\theta}_{pc} + \ddot{\phi})]$$

$$- [I_{yh} \sin(\theta_{pc} + \phi) + I_{zh} \cos(\theta_{pc} + \phi)][(\dot{\theta}_{pc} + \dot{\phi})^2$$

$$- (\ddot{\theta}_{pc} + \ddot{\phi})(\beta + \beta_p)\zeta] \tag{C.32}$$

Explicit expressions for the x_2, y_2 and z_2 components of $\vec{M}_{Ic}$ are obtained by substituting Eqs. (C.21) – (C.32) into Eqs. (C.19).

C.2 GRAVITATIONAL ROOT LOADS

The blade gravitational loads at the blade root are obtained by integrating the distributed gravitational loads along the span of the blade. The gravitational root loads are developed in the "2" system in which system the distributed gravity loads were developed in Chapter 3. The gravitational root moment is then transformed to the "3" system in which the equations of motion are formulated.

C.2.1 *Blade Gravity Loads*

For the offset-hinged spring restrained blade model the differential force at the blade root due to the gravitational loads acting on the blade can be expressed as

$$d\vec{F}_{Gb} = \vec{p}_{Gb}\, dx$$

where $\vec{p}_{Gb}$ represents the distributed gravitational force acting on the blade, which can be expressed in the "2" system as

$$\vec{p}_{Gb} = p_{Gbx2}\,\hat{e}_{x2} + p_{Gby2}\,\hat{e}_{y2} + p_{Gbz2}\,\hat{e}_{z2}$$

The x_2, y_2 and z_2 components of $\vec{p}_{Gb}$ for the spring restrained blade model are obtained by substituting Eqs. (4.3) and (4.4) into Eqs. (3.55).

The total force at the blade root is obtained by integrating the differential force along the span of the blade, i.e.

$$\vec{F}_{Gb} = \int_0^{L_b} \vec{p}_{Gb}\, dx \tag{C.33}$$

which can be expressed in the "2" system as

$$\vec{F}_{Gb} = F_{Gbx2}\,\hat{e}_{x2} + F_{Gby2}\,\hat{e}_{y2} + F_{Gbz2}\,\hat{e}_{z2}$$

where

$$F_{Gbx2} = \int_0^{L_b} p_{Gbx2}\, dx = -M_b g \sin\alpha_R \cos\psi \tag{C.34a}$$

$$F_{Gby2} = \int_0^{L_b} p_{Gby2}\, dx = M_b g \sin\alpha_R \sin\psi \tag{C.34b}$$

$$F_{Gbz2} = \int_0^{L_b} p_{Gbz2}\, dx = -M_b g \cos\alpha_R \tag{C.34c}$$

where the integrals defined by Eqs. (C.4) have been used to evaluate the above expressions.

For the offset-hinged spring restrained blade model the differential moment about the blade root due to the gravitational loads acting on the blade can be expressed as

$$d\vec{M}_{Gb} = (\vec{q}_{Gb} + x\,\hat{e}_{x4} \times \vec{p}_{Gb})\,dx$$

where $\vec{q}_{Gb}$ represents the distributed gravitational moment acting on the blade, which can be expressed in the "2" system as

$$\vec{q}_{Gb} = q_{Gbx2}\,\hat{e}_{x2} + q_{Gby2}\,\hat{e}_{y2} + q_{Gbz2}\,\hat{e}_{z2}$$

The x_2, y_2 and z_2 components of $\vec{q}_{Gb}$ for the spring restrained blade model are obtained by substituting Eqs. (4.3) and (4.4) into Eqs. (3.57).

The total moment about the blade root is obtained by integrating the differential moment along the span of the blade, i.e.

$$\vec{M}_{Gb} = \int_0^{L_b} (\vec{q}_{Gb} + x\,\hat{e}_{x4} \times \vec{p}_{Gb})\,dx \tag{C.35}$$

which can be expressed in the "2" system as

$$\vec{M}_{Gb} = M_{Gbx2}\,\hat{e}_{x2} + M_{Gby2}\,\hat{e}_{y2} + M_{Gbz2}\,\hat{e}_{z2}$$

where

$$M_{Gbx2} = \int_0^{L_b} q_{Gbx2}\,dx + \zeta\int_0^{L_b} x\,p_{Gbz2}\,dx - (\beta + \beta_p)\int_0^{L_b} x\,p_{Gby2}\,dx \tag{C.36a}$$

$$M_{Gby2} = \int_0^{L_b} q_{Gby2}\,dx - \int_0^{L_b} x\,p_{Gbz2}\,dx + (\beta + \beta_p)\int_0^{L_b} x\,p_{Gbx2}\,dx \tag{C.36b}$$

$$M_{Gbz2} = \int_0^{L_b} q_{Gbz2}\,dx + \int_0^{L_b} x\,p_{Gby2}\,dx - \zeta\int_0^{L_b} x\,p_{Gbx2}\,dx \tag{C.36c}$$

The various integrals appearing in Eqs. (C.36) can be evaluated as follows.

$$\int_0^{L_b} q_{Gbx2}\,dx = -\,M_b g[y_b \cos(\theta_{pc} + \phi) - z_b \sin(\theta_{pc} + \phi)][\cos\alpha_R$$

$$- (\beta + \beta_p)\zeta \sin \alpha_R \sin \psi]$$

$$- M_b g[y_b \sin(\theta_{pc} + \phi) + z_b \cos(\theta_{pc} + \phi)] \sin \alpha_R \sin \psi \tag{C.37}$$

$$\int_0^{L_b} q_{Gby2}\, dx = - M_b g[y_b \cos(\theta_{pc} + \phi) - z_b \sin(\theta_{pc} + \phi)][\cos \alpha_R$$

$$- (\beta + \beta_p) \sin \alpha_R \cos \psi]\zeta$$

$$- M_b g[y_b \sin(\theta_{pc} + \phi) + z_b \cos(\theta_{pc} + \phi)][(\beta + \beta_p) \cos \alpha_R$$

$$+ \sin \alpha_R \cos \psi] \tag{C.38}$$

$$\int_0^{L_b} q_{Gbz2}\, dx = - M_b g[y_b \sin(\theta_{pc} + \phi) + z_b \cos(\theta_{pc} + \phi)] \sin \alpha_R \sin \psi$$

$$- M_b g[y_b \cos(\theta_{pc} + \phi) - z_b \sin(\theta_{pc} + \phi)] \sin \alpha_R(\zeta \sin \psi - \cos \psi) \tag{C.39}$$

$$\int_0^{L_b} x p_{Gbx2}\, dx = - M_b g x_b \sin \alpha_R \cos \psi \tag{C.40}$$

$$\int_0^{L_b} x p_{Gby2}\, dx = M_b g x_b \sin \alpha_R \sin \psi \tag{C.41}$$

$$\int_0^{L_b} x p_{Gbz2}\, dx = - M_b g x_b \cos \alpha_R \tag{C.42}$$

where the integral definitions represented by Eqs. (C.4) have been used to evaluate the previous expressions.

Substituting Eqs. (C.37) – (C.42) into Eqs. (C.36) yields:

$$M_{Gbx2} = - M_b g[y_b \cos(\theta_{pc} + \phi) - z_b \sin(\theta_{pc} + \phi)][\cos \alpha_R$$

$$- (\beta + \beta_p)\zeta \sin \alpha_R \sin \psi]$$

$$- M_b g[y_b \sin(\theta_{pc} + \phi) + z_b \cos(\theta_{pc} + \phi)] \sin \alpha_R \sin \psi$$

$$- M_b g x_b \zeta \cos \alpha_R - M_b g x_b(\beta + \beta_p) \sin \alpha_R \sin \psi \tag{C.43a}$$

$$M_{Gby2} = -M_b g[y_b \cos(\theta_{pc} + \phi) - z_b \sin(\theta_{pc} + \phi)][\cos \alpha_R$$

$$-(\beta + \beta_p) \sin \alpha_R \cos \psi]\zeta$$

$$- M_b g[y_b \sin(\theta_{pc} + \phi) + z_b \cos(\theta_{pc} + \phi)][(\beta + \beta_p) \cos \alpha_R$$

$$+ \sin \alpha_R \cos \psi]$$

$$+ M_b g x_b \cos \alpha_R - M_b g x_b (\beta + \beta_p) \sin \alpha_R \cos \psi \qquad \text{(C.43b)}$$

$$M_{Gbz2} = -M_b g[y_b \cos(\theta_{pc} + \phi) - z_b \sin(\theta_{pc} + \phi)] \sin \alpha_R(\zeta \sin \psi - \cos \psi)$$

$$- M_b g[y_b \sin(\theta_{pc} + \phi) + z_b \cos(\theta_{pc} + \phi)] \sin \alpha_R \sin \psi$$

$$+ M_b g x_b \sin \alpha_R \sin \psi + M_b g x_b \zeta \sin \alpha_R \cos \psi \qquad \text{(C.43c)}$$

C.2.2 *Control Flap Gravity Loads*

For the offset-hinged spring restrained blade model the differential force at the blade root due to the gravitiational loads acting on the control surface can be expressed as

$$d\vec{F}_{Gc} = \vec{p}_{Gc}\, dx$$

where $\vec{p}_{Gc}$ represents the distributed gravitational force acting on the control surface, which can be expressed in the "2" system as

$$\vec{p}_{Gc} = p_{Gcx2}\, \hat{e}_{x2} + p_{Gcy2}\, \hat{e}_{y2} + p_{Gcz2}\, \hat{e}_{z2}$$

The x_2, y_2 and z_2 components of $\vec{p}_{Gc}$ for the spring restrained blade model are obtained by substituting Eqs. (4.3) and (4.4) into Eqs (3.61).

The total force at the blade root is obtained by integrating the differential force along the span of the control surface, i.e.

$$\vec{F}_{Gc} = \int_{x_{cs}}^{x_{cs} + L_{cs}} \vec{p}_{Gc}\, dx \qquad \text{(C.44)}$$

which can be expressed in the "2" system as

$$\vec{F}_{Gc} = F_{Gcx2}\,\hat{e}_{x2} + F_{Gcy2}\,\hat{e}_{y2} + F_{Gcz2}\,\hat{e}_{z2}$$

where

$$F_{Gcx2} = \int_{x_{cs}}^{x_{cs}+L_{cs}} p_{Gcx2}\,dx = -M_c g \sin\alpha_R \cos\psi \tag{C.45a}$$

$$F_{Gcy2} = \int_{x_{cs}}^{x_{cs}+L_{cs}} p_{Gcy2}\,dx = M_c g \sin\alpha_R \sin\psi \tag{C.45b}$$

$$F_{Gcz2} = \int_{x_{cs}}^{x_{cs}+L_{cs}} p_{Gcz2}\,dx = -M_c g \cos\alpha_R \tag{C.45c}$$

where the integrals defined by Eqs. (C.17) have been used to evaluate the integrals.

For the offset-hinged spring restrained blade model the differential moment about the blade root due to the gravitational loads acting on the control surface can be expressed as:

$$d\vec{M}_{Gc} = [\vec{q}_{Gh} + (x\,\hat{e}_{x4} + \bar{y}_H\,\hat{e}_{y5} + \bar{z}_H\,\hat{e}_{z5}) \times \vec{p}_{Gc}]\,dx$$

where $\vec{q}_{Gh}$ represents the distributed gravitational moment about the control surface hinge, which can be expressed in the "2" system as

$$\vec{q}_{Gh} = q_{Ghx2}\,\hat{e}_{x2} + q_{Ghy2}\,\hat{e}_{y2} + q_{Ghz2}\,\hat{e}_{z2}$$

The x_2, y_2 and z_2 components of $\vec{q}_{Gh}$ for the spring restrained blade model are obtained by substituting Eqs. (4.3) and (4.4) into Eqs. (3.63).

The total moment about the blade root is obtained by integrating the differential moment along the span of the control surface

$$\vec{M}_{Gc} = \int_{x_{cs}}^{x_{cs}+L_{cs}} [\vec{q}_{Gh} + (x\hat{e}_{x4} + \bar{y}_H\,\hat{e}_{y5} + \bar{z}_H\,\hat{e}_{z5}) \times \vec{p}_{Gc}]\,dx \tag{C.46}$$

which can be expressed in the "2" system as

$$M_{Gc} = M_{Gcx2}\,\hat{e}_{x2} + M_{Gcy2}\,\hat{e}_{y2} + M_{Gcz2}\,\hat{e}_{z2}$$

where

$$M_{Gcx2} = \int_{x_{cs}}^{x_{cs}+L_{cs}} q_{Ghx2}\,dx$$

$$- \int_{x_{cs}}^{x_{cs}+L_{cs}} X_H \cos(\theta_G + \phi)[(\beta + \beta_p)\zeta p_{Gcy2} + p_{Gcz2}]\,dx$$

$$+ \int_{x_{cs}}^{x_{cs}+L_{cs}} X_H \sin(\theta_G + \phi)\, p_{Gcy2}\,dx$$

$$+ \zeta \int_{x_{cs}}^{x_{cs}+L_{cs}} x\, p_{Gcz2}\,dx - (\beta + \beta_p)\int_{x_{cs}}^{x_{cs}+L_{cs}} x\, p_{Gcy2}\,dx \qquad \text{(C.47a)}$$

$$M_{Gcy2} = \int_{x_{cs}}^{x_{cs}+L_{cs}} q_{Ghy2}\,dx$$

$$+ \int_{x_{cs}}^{x_{cs}+L_{cs}} X_H \cos(\theta_G + \phi)[(\beta + \beta_p)p_{Gcx2} - p_{Gcz2}]\zeta\,dx$$

$$- \int_{x_{cs}}^{x_{cs}+L_{cs}} X_H \sin(\theta_G + \phi)[(\beta + \beta_p)p_{Gcz2} + p_{Gcx2}]\,dx$$

$$- \int_{x_{cs}}^{x_{cs}+L_{cs}} x\, p_{Gcz2}\,dx + (\beta + \beta_p)\int_{x_{cs}}^{x_{cs}+L_{cs}} x\, p_{Gcx2}\,dx \qquad \text{(C.47b)}$$

$$M_{Gcz2} = \int_{x_{cs}}^{x_{cs}+L_{cs}} q_{Ghz2}\,dx$$

$$+ \int_{x_{cs}}^{x_{cs}+L_{cs}} X_H \cos(\theta_G + \phi)(\zeta p_{Gcy2} + p_{Gcx2})\,dx$$

$$+ (\beta + \beta_p)\int_{x_{cs}}^{x_{cs}+L_{cs}} X_H \sin(\theta_G + \phi)p_{Gcy2}\,dx$$

$$+ \int_{x_{cs}}^{x_{cs}+L_{cs}} x\, p_{Gcy2}\,dx - \zeta \int_{x_{cs}}^{x_{cs}+L_{cs}} x\, p_{Gcx2}\,dx \qquad \text{(C.47c)}$$

The various integrals appearing in Eqs. (C.47) can be evaluated as follows:

$$\int_{x_{cs}}^{x_{cs}+L_{cs}} q_{Ghx2}\,dx = M_{Ghx2}$$

$$= M_c g[y_c \cos(\theta_{pc}+\phi+\delta) - z_c \sin(\theta_{pc}+\phi+\delta)][\cos\alpha_R$$

$$-(\beta+\beta_p)\zeta \sin\alpha_R \sin\psi]$$

$$+ M_c g[y_c \sin(\theta_{pc}+\phi+\delta) + z_c \cos(\theta_{pc}+\phi+\delta)] \sin\alpha_R \sin\psi \qquad (C.48)$$

$$\int_{x_{cs}}^{x_{cs}+L_{cs}} q_{Ghy2}\,dx = M_{Ghy2}$$

$$= M_c g[y_c \cos(\theta_{pc}+\phi+\delta) - z_c \sin(\theta_{pc}+\phi+\delta)][\cos\alpha_R$$

$$-(\beta+\beta_p)\sin\alpha_R \cos\psi]\zeta$$

$$+ M_c g[y_c \sin(\theta_{pc}+\phi+\delta) + z_c \cos(\theta_{pc}+\phi+\delta)][(\beta+\beta_p)\cos\alpha_R$$

$$+\sin\alpha_R \cos\psi] \qquad (C.49)$$

$$\int_{x_{cs}}^{x_{cs}+L_{cs}} q_{Ghz2}\,dx = M_{Ghrz2}$$

$$= M_c g[y_c \cos(\theta_{pc}+\phi+\delta) - z_c \sin(\theta_{pc}+\phi+\delta)] \sin\alpha_R(\zeta \sin\psi - \cos\psi)$$

$$+ M_c g[y_c \sin(\theta_{pc}+\phi+\delta) + z_c \cos(\theta_{pc}+\phi+\delta)] \sin\alpha_R \sin\psi \qquad (C.50)$$

$$\int_{x_{cs}}^{x_{cs}+L_{cs}} X_H \cos(\theta_G+\phi)\, p_{Gcx2}\,dx$$

$$= -M_c g[y_h \cos(\theta_{pc}+\phi) - z_h \sin(\theta_{pc}+\phi)] \sin\alpha_R \cos\psi \qquad (C.51)$$

$$\int_{x_{cs}}^{x_{cs}+L_{cs}} X_H \sin(\theta_G+\phi)\, p_{Gcx2}\,dx$$

$$= -M_c g[y_h \sin(\theta_{pc}+\phi) + z_h \cos(\theta_{pc}+\phi)] \sin\alpha_R \cos\psi \qquad (C.52)$$

$$\int_{x_{cs}}^{x_{cs}+L_{cs}} X_H \cos(\theta_G+\phi)\, p_{Gcy2}\,dx$$

$$= M_c g[y_h \cos(\theta_{pc} + \phi) - z_h \sin(\theta_{pc} + \phi)] \sin \alpha_R \sin \psi \tag{C.53}$$

$$\int_{x_{cs}}^{x_{cs} + L_{cs}} X_H \sin(\theta_G + \phi)\, p_{Gcy2}\, dx$$

$$= M_c g[y_h \sin(\theta_{pc} + \phi) + z_h \cos(\theta_{pc} + \phi)] \sin \alpha_R \sin \psi \tag{C.54}$$

$$\int_{x_{cs}}^{x_{cs} + L_{cs}} X_H \cos(\theta_G + \phi)\, p_{Gcz2}\, dx$$

$$= - M_c g[y_h \cos(\theta_{pc} + \phi) - z_h \sin(\theta_{pc} + \phi)] \cos \alpha_R \tag{C.55}$$

$$\int_{x_{cs}}^{x_{cs} + L_{cs}} X_H \sin(\theta_G + \phi)\, p_{Gcz2}\, dx$$

$$= - M_c g[y_h \sin(\theta_{pc} + \phi) + z_h \cos(\theta_{pc} + \phi)] \cos \alpha_R \tag{C.56}$$

$$\int_{x_{cs}}^{x_{cs} + L_{cs}} x\, p_{Gcx2}\, dx = - M_c g x_c \sin \alpha_R \sin \psi \tag{C.57}$$

$$\int_{x_{cs}}^{x_{cs} + L_{cs}} x\, p_{Gcy2}\, dx = M_c g x_c \sin \alpha_R \sin \psi \tag{C.58}$$

$$\int_{x_{cs}}^{x_{cs} + L_{cs}} x\, p_{Gcz2}\, dx = - M_c g x_c \cos \alpha_R \tag{C.59}$$

The integral definitions represented by Eqs. (C.17) have been used to evaluate the above integrals.

Substituting Eqs. (C.48) – (C.59) into Eqs. (C.47) yields:

$$\begin{aligned} M_{Gcx2} = {} & M_c g[y_c \cos(\theta_{pc} + \phi + \delta) - z_c \sin(\theta_{pc} + \phi + \delta)][\cos \alpha_R \\ & - (\beta + \beta_p)\zeta \sin \alpha_R \sin \psi] \\ & + M_c g[y_c \sin(\theta_{pc} + \phi + \delta) + z_c \cos(\theta_{pc} + \phi + \delta)] \sin \alpha_R \sin \psi \\ & + M_c g[y_h \cos(\theta_{pc} + \phi) - z_h \sin(\theta_{pc} + \phi)][-\cos \alpha_R \\ & + (\beta + \beta_p)\zeta \sin \alpha_R \sin \psi] \end{aligned}$$

$$+ M_c g[y_h \sin(\theta_{pc} + \phi) + z_h \cos(\theta_{pc} + \phi)] \sin \alpha_R \sin \psi$$

$$- M_c g x_c \zeta \cos \alpha_R - M_c g x_c (\beta + \beta_p) \sin \alpha_R \sin \psi \qquad \text{(C.60a)}$$

$$M_{Gcy2} = M_c g[y_c \cos(\theta_{pc} + \phi + \delta) - z_c \sin(\theta_{pc} + \phi + \delta)][\cos \alpha_R$$

$$- (\beta + \beta_p) \sin \alpha_R \cos \psi]\zeta$$

$$+ M_c g[y_c \sin(\theta_{pc} + \phi + \delta) + z_c \cos(\theta_{pc} + \phi + \delta)][(\beta + \beta_p) \cos \alpha_R$$

$$+ \sin \alpha_R \cos \psi]$$

$$- M_c g[y_h \cos(\theta_{pc} + \phi) - z_h(\theta_{pc} + \phi)][-\cos \alpha_R$$

$$+ (\beta + \beta_p) \sin \alpha_R \cos \psi]\zeta$$

$$- M_c g[y_h \sin(\theta_{pc} + \phi) + z_h \cos(\theta_{pc} + \phi)][-(\beta + \beta_p) \cos \alpha_R$$

$$- \sin \alpha_R \cos \psi]$$

$$+ M_c g x_c \cos \alpha_R - M_c g x_c (\beta + \beta_p) \sin \alpha_R \cos \psi \qquad \text{(C.60b)}$$

$$M_{Gcz2} = M_c g[y_c \sin(\theta_{pc} + \phi + \delta) + z_c \cos(\theta_{pc} + \phi + \delta)] \sin \alpha_R \sin \psi$$

$$+ M_c g[y_c \cos(\theta_{pc} + \phi + \delta) - z_c \sin(\theta_{pc} + \phi + \delta)] \sin \alpha_R(\zeta \sin \psi - \cos \psi)$$

$$+ M_c g[y_h \cos(\theta_{pc} + \phi) - z_h \sin(\theta_{pc} + \phi)][\zeta \sin \alpha_R \sin \psi$$

$$- \sin \alpha_R \cos \psi]$$

$$+ M_c g[y_h \sin(\theta_{pc} + \phi) + z_h \cos(\theta_{pc} + \phi)](\beta + \beta_p) \sin \alpha_R \sin \psi$$

$$+ M_c g x_c \sin \alpha_R \sin \psi + M_c g x_c \zeta \sin \alpha_R \cos \psi \qquad \text{(C.60c)}$$

C-5

C.3 AERODYNAMIC ROOT LOADS

The total aerodynamic force and moment at the blade root are determined by integrating the distributed aerodynamic loads developed in Chapter 3 along the span of the blade. The integrations are performed directly in the "5" system in which the distributed aerodynamic loads have been formulated. After obtaining the root loads, the aerodynamic moment about the blade root is transformed to the "3" system, in which the equations of motion are formulated.

C.3.1 *Blade Aerodynamic Loads*

For the offset-hinged spring restrained blade model the differential force at the blade root due to the aerodynamic loads acting on the blade is given by

$$d\vec{F}_{Ab} = \vec{p}_{Ab}\, dx$$

where $\vec{p}_{Ab}$ represents the distributed aerodynamic force acting on the blade, which can be expressed in the "5" system as

$$\vec{p}_{Ab} = p_{Aby5}\hat{e}_{y5} + p_{Abz5}\hat{e}_{z5}$$

The y_5 and z_5 components of $\vec{p}_{Ab}$ for the spring restrained blade model are obtained from the expressions developed in Chapter 3 by substituting Eqs. (4.3) and (4.4) into Eqs. (3.109).

The total force at the blade root is obtained by integrating the differential force along the span of the blade, i.e.

$$\vec{F}_{Ab} = \int_0^{L_b} \vec{p}_{Ab}\, dx \qquad \text{(C.61)}$$

which can be expressed in the "5" system as

$$\vec{F}_{Ab} = F_{Aby5}\hat{e}_{y5} + F_{Abz5}\hat{e}_{z5}$$

Before integrating the aerodynamic loads along the span of the blade it is convenient to define two sets of aerodynamic coefficients. The first set is associated with the integration of the aerodynamic lift and moment along the span of the blade; the second set is associated with the integration of the aerodynamic drag. In the integration of the aerodynamic loads along the span of the blade a plethora of integrals involving the products of various powers of x and the pretwist distribution of the blade $\theta_{pt}(x)$ arise. A scheme for consistently keeping track of the numerous integrals used in this derivation has been devised. The following scheme is used to define a set of coefficients associated with the integration of the aerodynamic lift and moment along the span of the blade:

$$A_{nm} = \rho_A a_o c_b \int_0^{L_b} R_{LM}\, x^n\, \theta_{pt}^m(x)\, dx \tag{C.62}$$

where R_{LM} represents the reverse flow parameter defined in Chapter 3 which is associated with the integration of the aerodynamic lift and moment along the span of the blade.

Similarly, the following scheme is used to define a set of coefficients associated with the integration of the aerodynamic drag along the blade span:

$$B_n = \rho_A a_o c_b \int_0^{L_b} R_D\, x^n\, dx \tag{C.63}$$

where R_D represents the reverse flow parameter defined in Chapter 3 associated with the integration of the aerodynamic drag along the span of the blade.

Using the scheme represented by Eq. (C.62) the following set of aerodynamic coefficients which arise in the integration of the aerodynamic lift and moment along the span of the blade are defined as follows:

$$A_{00} = \rho_A a_o c_b \int_0^{L_b} R_{LM}\, dx \tag{C.64a}$$

$$A_{01} = \rho_A a_o c_b \int_0^{L_b} R_{LM}\, \theta_{pt}(x)\, dx \tag{C.64b}$$

$$A_{02} = \rho_A a_o c_b \int_0^{L_b} R_{LM}\, \theta_{pt}^2(x)\, dx \tag{C.64c}$$

$$A_{10} = \rho_A a_o c_b \int_0^{L_b} R_{LM} \, x \, dx \tag{C.64d}$$

$$A_{11} = \rho_A a_o c_b \int_0^{L_b} R_{LM} \, x \, \theta_{pt}(x) \, dx \tag{C.64e}$$

$$A_{12} = \rho_A a_o c_b \int_0^{L_b} R_{LM} \, x \, \theta_{pt}^2(x) \, dx \tag{C.64f}$$

$$A_{20} = \rho_A a_o c_b \int_0^{L_b} R_{LM} \, x^2 \, dx \tag{C.64g}$$

$$A_{21} = \rho_A a_o c_b \int_0^{L_b} R_{LM} \, x^2 \, \theta_{pt}(x) \, dx \tag{C.64h}$$

$$A_{22} = \rho_A a_o c_b \int_0^{L_b} R_{LM} \, x^2 \, \theta_{pt}^2(x) \, dx \tag{C.64i}$$

$$A_{30} = \rho_A a_o c_b \int_0^{L_b} R_{LM} \, x^3 \, dx \tag{C.64j}$$

$$A_{31} = \rho_A a_o c_b \int_0^{L_b} R_{LM} \, x^3 \, \theta_{pt}(x) \, dx \tag{C.64k}$$

Similarly, using the scheme represented by Eqs. (C.63) the following set of aerodynamic coefficients associated with the integration of the aerodynamic drag along the span of the blade are defined as follows:

$$B_0 = \rho_A a_o c_b \int_0^{L_b} R_D \, dx \tag{C.65a}$$

$$B_1 = \rho_A a_o c_b \int_0^{L_b} R_D \, x \, dx \tag{C.65b}$$

$$B_2 = \rho_A a_o c_b \int_0^{L_b} R_D \, x^2 \, dx \tag{C.65c}$$

$$B_3 = \rho_A a_o c_b \int_0^{L_b} R_D \, x^3 \, dx \tag{C.65d}$$

Performing the integration for each component in Eq. (C.61) yields

$$F_{Aby5} = \int_0^{L_b} p_{Aby5}\, dx$$

$$= A_{00}\{[\frac{1}{8}c_b(X_A - \frac{1}{4}c_b)(\ddot{\theta}_{pc} + \ddot{\phi})(\theta_{pc} + \phi) + \frac{1}{2}(\lambda\Omega R)(X_A - \frac{1}{2}c_b)(\dot{\theta}_{pc} + \dot{\phi})$$

$$- \frac{1}{8}c_b\Omega e(\theta_{pc} + \phi)(\dot{\theta}_{pc} + \dot{\phi}) - \frac{1}{2}(\lambda\Omega R)\Omega e(\theta_{pc} + \phi) + \frac{1}{2}(\lambda\Omega R)^2]$$

$$+ [-\frac{1}{8}c_b(\theta_{pc} + \phi)^2\zeta - \frac{1}{8}c_b(\dot{\theta}_{pc} + \dot{\phi})(\theta_{pc} + \phi)\zeta - \frac{1}{2}(\lambda\Omega R)(\theta_{pc} + \phi)\zeta$$

$$+ \frac{1}{2}(X_A - \frac{1}{2}c_b)(\dot{\theta}_{pc} + \dot{\phi})(\beta + \beta_p) - \frac{1}{8}c_b\Omega(\theta_{pc} + \phi)^2$$

$$- \frac{1}{2}\Omega e(\theta_{pc} + \phi)(\beta + \beta_p) + \frac{1}{8}c_b(\theta_{pc} + \phi)\dot{\beta}$$

$$+ (\lambda\Omega R)(\beta + \beta_p)](\mu\Omega R)\cos\psi$$

$$+ [\frac{1}{8}c_b\Omega(\theta_{pc} + \phi)^2\zeta - \frac{1}{8}c_b(\dot{\theta}_{pc} + \dot{\phi})(\theta_{pc} + \phi) - \frac{1}{2}(\lambda\Omega R)(\theta_{pc} + \phi)$$

$$- \frac{1}{8}\Omega c_b(\theta_{pc} + \phi)(\beta + \beta_p)](\mu\Omega R)\sin\psi$$

$$- \frac{1}{2}(\theta_{pc} + \phi)(\beta + \beta_p)(\mu\Omega R)^2\cos\psi\sin\psi$$

$$+ [-\frac{1}{2}(\theta_{pc} + \phi)(\beta + \beta_p)\zeta + \frac{1}{2}(\beta + \beta_p)^2](\mu\Omega R)^2\cos^2\psi\}$$

$$+ A_{01}\{[\frac{1}{8}c_b(X_A - \frac{1}{4}c_b)(\ddot{\theta}_{pc} + \ddot{\phi}) - \frac{1}{8}c_b\Omega e(\dot{\theta}_{pc} + \dot{\phi}) - \frac{1}{2}(\lambda\Omega R)\Omega e]$$

$$+ [-\frac{1}{4}c_b(\theta_{pc} + \phi)\dot{\zeta} - \frac{1}{8}c_b(\dot{\theta}_{pc} + \dot{\phi})\zeta - \frac{1}{2}(\lambda\Omega R)\zeta - \frac{1}{4}c_b\Omega(\theta_{pc} + \phi)$$

$$- \frac{1}{2}\Omega e(\beta + \beta_p) + \frac{1}{8}c_b\dot{\beta}](\mu\Omega R)\cos\psi$$

$$+ [\frac{1}{4}c_b\Omega(\theta_{pc} + \phi)\zeta - \frac{1}{8}c_b(\dot{\theta}_{pc} + \dot{\phi}) - \frac{1}{2}(\lambda\Omega R)$$

$$- \frac{1}{8}c_b\Omega(\beta + \beta_p)](\mu\Omega R)\sin\psi$$

$$- \frac{1}{2}(\beta + \beta_p)(\mu\Omega R)^2\cos\psi\sin\psi - \frac{1}{2}(\beta + \beta_p)\zeta(\mu\Omega R)^2\cos^2\psi\}$$

$$+ A_{02}[- \frac{1}{8}c_b(\Omega + \dot{\zeta})(\mu\Omega R)\cos\psi + \frac{1}{8}c_b\Omega\zeta(\mu\Omega R)\sin\psi]$$

$$+ A_{10}\{[- \frac{1}{8}c_b(\theta_{pc} + \phi)^2\ddot{\zeta} - \frac{1}{8}c_b(\dot{\theta}_{pc} + \dot{\phi})\dot{\zeta}(\theta_{pc} + \phi) - \frac{1}{2}(\lambda\Omega R)(\theta_{pc} + \phi)\dot{\zeta}$$

$$+ \frac{1}{8}c_b\Omega(\theta_{pc} + \phi)\dot{\zeta}(\beta + \beta_p) - \frac{1}{4}(\lambda\Omega R)\Omega(\theta_{pc} + \phi)\zeta^2$$

$$- \frac{1}{2}\Omega^2 e(\theta_{pc} + \phi)(\beta + \beta_p)\zeta + \frac{1}{8}c_b\Omega(\theta_{pc} + \phi)\dot{\beta}\zeta$$

$$+ (\lambda\Omega R)\Omega(\beta + \beta_p)\zeta + \frac{1}{2}(X_A - \frac{1}{2}c_b)(\dot{\theta}_{pc} + \dot{\phi})\dot{\beta}$$

$$- \frac{1}{8}c_b\Omega(\dot{\theta}_{pc} + \dot{\phi})(\theta_{pc} + \phi) + \frac{1}{2}(\lambda\Omega R)\Omega(\theta_{pc} + \phi)\beta\beta_p$$

$$+ \frac{1}{4}(\lambda\Omega R)\Omega(\theta_{pc} + \phi)\beta^2 - \frac{1}{2}(\lambda\Omega R)\Omega(\theta_{pc} + \phi)$$

$$- \frac{1}{2}\Omega e(\theta_{pc} + \phi)\dot{\beta} + \frac{1}{8}c_b(\theta_{pc} + \phi)\ddot{\beta} + (\lambda\Omega R)\dot{\beta}]$$

$$+ [- \frac{1}{2}(\theta_{pc} + \phi)\dot{\zeta}(\beta + \beta_p) - \frac{3}{4}\Omega(\theta_{pc} + \phi)(\beta + \beta_p)\zeta^2 - \frac{1}{2}(\theta_{pc} + \phi)\dot{\beta}\zeta$$

$$+ \Omega(\beta + \beta_p)^2\zeta + \frac{1}{2}\Omega(\theta_{pc} + \phi)\beta(\beta + \beta_p)\beta_p$$

$$+ \frac{1}{4}\Omega(\theta_{pc} + \phi)\beta^2(\beta + \beta_p) - \frac{1}{2}\Omega(\theta_{pc} + \phi)(\beta + \beta_p)$$

$$+ \dot{\beta}(\beta + \beta_p)](\mu\Omega R)\cos\psi$$

$$+ [- \frac{1}{2}\Omega(\theta_{pc} + \phi)(\beta + \beta_p)\zeta - \frac{1}{2}(\theta_{pc} + \phi)\dot{\beta}](\mu\Omega R)\sin\psi\}$$

$$+ A_{11}\{[-\frac{1}{4}c_b(\theta_{pc}+\phi)\ddot{\zeta}-\frac{1}{4}c_b\Omega(\theta_{pc}+\phi)\zeta\dot{\zeta}-\frac{1}{8}c_b(\dot{\theta}_{pc}+\dot{\phi})\dot{\zeta}$$

$$-\frac{1}{2}(\lambda\Omega R)\dot{\zeta}+\frac{1}{8}c_b\Omega\dot{\zeta}(\beta+\beta_p)-\frac{1}{16}c_b\Omega(\dot{\theta}_{pc}+\dot{\phi})\zeta^2$$

$$-\frac{1}{4}(\lambda\Omega R)\Omega\zeta^2-\frac{1}{2}\Omega^2 e(\beta+\beta_p)\zeta+\frac{1}{8}c_b\Omega\dot{\beta}\zeta$$

$$+\frac{1}{8}c_b\Omega(\dot{\theta}_{pc}+\dot{\phi})\beta\beta_p+\frac{1}{16}c_b\Omega(\dot{\theta}_{pc}+\dot{\phi})\beta^2$$

$$-\frac{1}{8}c_b\Omega(\dot{\theta}_{pc}+\dot{\phi})+\frac{1}{4}c_b\Omega(\theta_{pc}+\phi)(\beta+\beta_p)\dot{\beta}-\frac{1}{2}\Omega e\dot{\beta}$$

$$+\frac{1}{2}(\lambda\Omega R)\Omega\beta\beta_p+\frac{1}{4}(\lambda\Omega R)\Omega\beta^2-\frac{1}{2}(\lambda\Omega R)\Omega+\frac{1}{8}c_b\ddot{\beta}]$$

$$+[-\frac{1}{2}(\beta+\beta_p)\ddot{\zeta}-\frac{3}{4}\Omega(\beta+\beta_p)\zeta^2-\frac{1}{2}\dot{\beta}\zeta$$

$$-\frac{1}{2}\Omega(\beta+\beta_p)](\mu\Omega R)\cos\psi$$

$$+[-\frac{1}{2}\Omega(\beta+\beta_p)\zeta-\frac{1}{2}\dot{\beta}](\mu\Omega R)\sin\psi\}$$

$$+ A_{12}[-\frac{1}{8}c_b\ddot{\zeta}-\frac{1}{8}c_b\Omega\zeta\dot{\zeta}+\frac{1}{8}c_b\Omega(\beta+\beta_p)\dot{\beta}]$$

$$+ A_{20}[-\frac{1}{2}(\theta_{pc}+\phi)\dot{\beta}\dot{\zeta}-\frac{1}{2}\Omega^2(\theta_{pc}+\phi)(\beta+\beta_p)\zeta+\Omega\dot{\beta}(\beta+\beta_p)\zeta$$

$$-\frac{1}{2}\Omega(\theta_{pc}+\phi)\dot{\beta}+\frac{1}{2}\dot{\beta}^2]$$

$$+ A_{21}[-\frac{1}{2}(\Omega+\dot{\zeta})\dot{\beta}-\frac{1}{2}\Omega^2(\beta+\beta_p)\zeta]$$

$$+ B_0(\frac{C_{do}}{a_o})\{[-\frac{1}{2}(\lambda\Omega R)^2-\frac{1}{2}\Omega^2 e^2]$$

$$+[-(\lambda\Omega R)(\beta+\beta_p)-e\Omega\zeta](\mu\Omega R)\cos\psi-e\Omega(\mu\Omega R)\sin\psi$$

$$+ [-\frac{1}{2}\zeta^2 - \frac{1}{2}(\beta + \beta_p)^2](\mu\Omega R)^2 \cos^2\psi - \frac{1}{2}(\mu\Omega R)^2 \sin^2\psi$$

$$- \zeta(\mu\Omega R)^2 \cos\psi \sin\psi \}$$

$$+ B_1(\frac{C_{do}}{a_o})\{[- \Omega e(\Omega + \dot{\zeta}) - (\lambda\Omega R)\dot{\beta}]$$

$$+ [- (\Omega + \dot{\zeta})\zeta - \dot{\beta}(\beta + \beta_p)](\mu\Omega R)\cos\psi$$

$$+ [- (\Omega + \dot{\zeta}) - \frac{1}{2}\Omega\zeta^2 + \Omega\beta\beta_p + \frac{1}{2}\Omega\beta^2](\mu\Omega R)\sin\psi \}$$

$$+ B_2(\frac{C_{do}}{a_o})[- \frac{1}{2}(\Omega + \dot{\zeta})^2 - \frac{1}{2}\Omega^2\zeta^2 + \beta\beta_p\Omega^2 + \frac{1}{2}\Omega^2\beta^2 - \frac{1}{2}\dot{\beta}^2] \qquad \text{(C.66a)}$$

$$F_{Abz5} = \int_0^{L_b} p_{Abz5}\, dx$$

$$= A_{00}\{[- \frac{1}{8}c_b(X_A - \frac{1}{4}c_b)(\ddot{\theta}_{pc} + \ddot{\phi}) - \frac{1}{2}\Omega e(X_A - \frac{1}{2}c_b)(\dot{\theta}_{pc} + \dot{\phi})$$

$$+ \frac{1}{8}c_b\Omega e(\dot{\theta}_{pc} + \dot{\phi}) + \frac{1}{2}\Omega^2 e^2(\theta_{pc} + \phi) - \frac{1}{2}(\lambda\Omega R)\Omega e]$$

$$+ [\frac{1}{8}c_b(\Omega + \dot{\zeta})(\theta_{pc} + \phi) - \frac{1}{2}X_A(\dot{\theta}_{pc} + \dot{\phi})\zeta + \frac{3}{8}c_b(\dot{\theta}_{pc} + \dot{\phi})\zeta$$

$$+ \Omega e(\theta_{pc} + \phi)\zeta - \frac{1}{2}(\lambda\Omega R)\zeta - \frac{1}{2}\Omega e(\beta + \beta_p) - \frac{1}{8}c_b\dot{\beta}](\mu\Omega R)\cos\psi$$

$$+ [- \frac{1}{8}c_b\Omega(\theta_{pc} + \phi)\zeta - \frac{1}{2}X_A(\dot{\theta}_{pc} + \dot{\phi}) + \frac{3}{8}c_b(\dot{\theta}_{pc} + \dot{\phi})$$

$$+ \Omega e(\theta_{pc} + \phi) - \frac{1}{2}(\lambda\Omega R) + \frac{1}{8}c_b\Omega(\beta + \beta_p)](\mu\Omega R)\sin\psi$$

$$+ [\frac{1}{2}(\theta_{pc} + \phi)\zeta^2 - \frac{1}{2}(\beta + \beta_p)\zeta](\mu\Omega R)^2 \cos^2\psi$$

$$+ \frac{1}{2}(\theta_{pc} + \phi)(\mu\Omega R)^2 \sin^2\psi$$

$$+ [(\theta_{pc} + \phi)\zeta - \frac{1}{2}(\beta + \beta_p)](\mu\Omega R)^2 \cos\psi \sin\psi\}$$

$$+ A_{01}\{\frac{1}{2}\Omega^2 e^2 + [\frac{1}{8}c_b(\Omega + \dot{\zeta}) + \Omega e\zeta](\mu\Omega R)\cos\psi$$

$$+ (-\frac{1}{8}c_b\Omega\zeta + \Omega e)(\mu\Omega R)\sin\psi$$

$$+ \frac{1}{2}\zeta^2(\mu\Omega R)^2\cos^2\psi + \frac{1}{2}(\mu\Omega R)^2\sin^2\psi + \zeta(\mu\Omega R)^2\cos\psi\sin\psi\}$$

$$+ A_{10}\{[\frac{1}{8}c_b(\theta_{pc} + \phi)\ddot{\zeta} - \frac{1}{2}X_A(\dot{\theta}_{pc} + \dot{\phi})\dot{\zeta} + \frac{3}{8}c_b(\dot{\theta}_{pc} + \dot{\phi})\dot{\zeta} + \Omega e(\theta_{pc} + \phi)\ddot{\zeta}$$

$$- \frac{1}{2}(\lambda\Omega R)\ddot{\zeta} - \frac{1}{8}c_b\Omega(\beta + \beta_p)\zeta - \frac{1}{4}(\lambda\Omega R)\Omega\zeta^2 - \frac{1}{2}\Omega^2 e(\beta + \beta_p)\zeta$$

$$- \frac{1}{8}c_b\Omega\dot{\beta}\zeta - \frac{1}{2}\Omega X_A(\dot{\theta}_{pc} + \dot{\phi}) + \frac{3}{8}c_b\Omega(\dot{\theta}_{pc} + \dot{\phi})$$

$$+ \Omega^2 e(\theta_{pc} + \phi) + \frac{1}{2}(\lambda\Omega R)\Omega\beta\beta_p + \frac{1}{4}(\lambda\Omega R)\Omega\beta^2$$

$$- \frac{1}{2}(\lambda\Omega R)\Omega - \frac{1}{2}\Omega e\dot{\beta} - \frac{1}{8}c_b\ddot{\beta}]$$

$$+ [(\Omega + \dot{\zeta})(\theta_{pc} + \phi)\zeta - \frac{1}{2}(\Omega + \dot{\zeta})(\beta + \beta_p) - \frac{1}{2}\dot{\beta}\zeta](\mu\Omega R)\cos\psi$$

$$+ [(\Omega + \dot{\zeta})(\theta_{pc} + \phi) + \frac{1}{2}\Omega(\theta_{pc} + \phi)\zeta^2 - \frac{1}{2}\Omega(\beta + \beta_p)\zeta$$

$$- \Omega(\theta_{pc} + \phi)\beta\beta_p - \frac{1}{2}\Omega\beta^2(\theta_{pc} + \phi) - \frac{1}{2}\dot{\beta}](\mu\Omega R)\sin\psi\}$$

$$+ A_{11}\{(\frac{1}{8}c_b\ddot{\zeta} + \Omega e\dot{\zeta} + \Omega^2 e) + \zeta(\Omega + \dot{\zeta})(\mu\Omega R)\cos\psi$$

$$+ [(\Omega + \dot{\zeta}) + \frac{1}{2}\Omega\zeta^2 - \Omega\beta\beta_p - \frac{1}{2}\Omega\beta^2](\mu\Omega R)\sin\psi\}$$

$$+ A_{20}[\frac{1}{2}(\Omega + \dot{\zeta})^2(\theta_{pc} + \phi) - \frac{1}{2}\dot{\beta}\dot{\zeta} + \frac{1}{2}\Omega^2(\theta_{pc} + \phi)\zeta^2 - \frac{1}{2}\Omega^2(\beta + \beta_p)\zeta$$

$$- \Omega^2\beta\beta_p(\theta_{pc} + \phi) - \frac{1}{2}\Omega^2\beta^2(\theta_{pc} + \phi) - \frac{1}{2}\Omega\dot{\beta}]$$

$$+ A_{21}[\frac{1}{2}(\Omega + \dot{\zeta})^2 + \frac{1}{2}\Omega^2\zeta^2 - \Omega^2\beta\beta_p - \frac{1}{2}\Omega^2\beta^2]$$

$$+ B_0(\frac{C_{do}}{a_o})[- \frac{1}{2}(\lambda\Omega R)(\mu\Omega R)\sin\psi - \frac{1}{2}(\beta + \beta_p)(\mu\Omega R)^2\cos\psi\sin\psi]$$

$$+ B_1(\frac{C_{do}}{a_o})[- \frac{1}{2}(\lambda\Omega R)\Omega - \frac{1}{2}\Omega(\beta + \beta_p)(\mu\Omega R)\cos\psi - \frac{1}{2}\dot{\beta}(\mu\Omega R)\sin\psi]$$

$$- B_2(\frac{C_{do}}{a_o})\frac{1}{2}\Omega\dot{\beta} \qquad \text{(C.66b)}$$

where the aerodynamic coefficients defined by Eqs. (C.64) and (C.65) have been used to evaluate the above expressions.

For the offset-hinged spring restrained blade model the differential moment about the blade root due to the aerodynamic loads acting on the blade can be expressed as

$$d\vec{M}_{Ab} = (\vec{q}_{Ab} + x\hat{e}_{x4} \times \vec{p}_{Ab})\,dx$$

where $\vec{q}_{Ab}$ represents the distributed aerodynamic moment acting on the blade, which can be expressed in the "5" system as

$$\vec{q}_{Ab} = q_{Abx5}\hat{e}_{x5}$$

The x_5 component of $\vec{q}_{Ab}$ for the spring restrained blade model is obtained from the expression developed in Chapter 3 by substituting Eqs. (4.3) and (4.4) into Eq. (3.110).

The total moment about the blade root is obtained by integrating the differential moment along the span of the blade, i.e.

$$M_{Ab} = \int_0^{L_b} (\vec{q}_{Ab} + x\hat{e}_{x4} \times \vec{p}_{Ab})\,dx \qquad \text{(C.67)}$$

which can be expressed in the "5" system as

$$\vec{M}_{Ab} = M_{Abx5}\hat{e}_{x5} + M_{Aby5}\hat{e}_{y5} + M_{Abz5}\hat{e}_{z5}$$

where

$$M_{Abx5} = \int_0^{L_b} q_{Abx5}\, dx$$

$$= A_{00}\{[-\frac{1}{2}(\lambda\Omega R)\Omega e X_A - \frac{1}{256}c_b^3(\ddot{\theta}_{pc} + \ddot{\phi})]$$

$$+ [-\frac{1}{2}(\lambda\Omega R)X_A\zeta + \frac{1}{8}c_b\Omega(X_A - \frac{1}{4}c_b)(\theta_{pc} + \phi)$$

$$- \frac{1}{2}\Omega e X_A(\beta + \beta_p) - \frac{1}{8}c_b(X_A - \frac{1}{4}c_b)\dot{\beta}](\mu\Omega R)\cos\psi$$

$$+ [-\frac{1}{2}(X_A - \frac{1}{2}c_b)(X_A - \frac{1}{4}c_b)(\dot{\theta}_{pc} + \dot{\phi}) + \Omega e X_A(\theta_{pc} + \phi)$$

$$- \frac{1}{2}(\lambda\Omega R)X_A + \frac{1}{8}c_b\Omega(X_A - \frac{1}{4}c_b)(\beta + \beta_p)$$

$$+ c_b\Omega e(\frac{C_{mo}}{a_o})](\mu\Omega R)\sin\psi$$

$$- \frac{1}{2}X_A(\beta + \beta_p)\zeta(\mu\Omega R)^2\cos^2\psi$$

$$+ [\frac{1}{2}X_A(\theta_{pc} + \phi) + \frac{1}{2}c_b(\frac{C_{mo}}{a_o})](\mu\Omega R)^2\sin^2\psi$$

$$+ [X_A(\theta_{pc} + \phi)\zeta + c_b(\frac{C_{mo}}{a_o})\zeta - \frac{1}{2}X_A(\beta + \beta_p)](\mu\Omega R)^2\cos\psi\sin\psi\}$$

$$+ A_{01}[\frac{1}{8}c_b\Omega(X_A - \frac{1}{4}c_b)(\mu\Omega R)\cos\psi + \Omega e X_A(\mu\Omega R)\sin\psi$$

$$+ \frac{1}{2}X_A(\mu\Omega R)^2\sin^2\psi + X_A\zeta(\mu\Omega R)^2\cos\psi\sin\psi]$$

$$+ A_{10}\{[-\frac{1}{2}(\lambda\Omega R)X_A\dot{\zeta} - \frac{1}{2}\Omega(X_A - \frac{1}{2}c_b)(X_A - \frac{1}{4}c_b)(\dot{\theta}_{pc} + \dot{\phi})$$

$$+ \Omega^2 e X_A(\theta_{pc} + \phi) - \frac{1}{2}(\lambda\Omega R)\Omega X_A - \frac{1}{2}\Omega e X_A\dot{\beta}$$

$$- \frac{1}{8}c_b(X_A - \frac{1}{4}c_b)\ddot{\beta} + c_b\Omega^2 e(\frac{C_{mo}}{a_o})]$$

$$+ [- \frac{1}{2}X_A(\beta + \beta_p)\dot{\zeta} + \Omega X_A(\theta_{pc} + \phi)\zeta - \frac{1}{2}X_A\dot{\beta}\zeta$$

$$+ c_b\Omega(\frac{C_{mo}}{a_o})\zeta - \frac{1}{2}\Omega X_A(\beta + \beta_p)](\mu\Omega R)\cos\psi$$

$$+ [X_A(\Omega + \dot{\zeta})(\theta_{pc} + \phi) + c_b(\frac{C_{mo}}{a_o})\dot{\zeta} - \frac{1}{2}\Omega X_A(\beta + \beta_p)\zeta$$

$$- \frac{1}{2}X_A\dot{\beta} + c_b\Omega(\frac{C_{mo}}{a_o})](\mu\Omega R)\sin\psi\}$$

$$+ A_{11}[\Omega^2 e X_A + \Omega X_A\zeta(\mu\Omega R)\cos\psi + X_A(\Omega + \dot{\zeta})(\mu\Omega R)\sin\psi]$$

$$+ A_{20}[\frac{1}{2}X_A\Omega(\Omega + 2\dot{\zeta})(\theta_{pc} + \phi) - \frac{1}{2}X_A\dot{\beta}\dot{\zeta} + \frac{1}{2}c_b\Omega(\Omega + 2\dot{\zeta})(\frac{C_{mo}}{a_o})$$

$$- \frac{1}{2}\Omega^2 X_A(\beta + \beta_p)\zeta - \frac{1}{2}\Omega X_A\dot{\beta} + \frac{1}{2}c_b\Omega^2(\frac{C_{mo}}{a_o})]$$

$$+ A_{21}\frac{1}{2}X_A\Omega(\Omega + 2\dot{\zeta}) \qquad \text{(C.68a)}$$

$$M_{Aby5} = -\int_0^{L_b} x\, p_{Abz5}\, dx$$

$$= A_{10}\{[\frac{1}{8}c_b(X_A - \frac{1}{4}c_b)(\ddot{\theta}_{pc} + \ddot{\phi}) + \frac{1}{2}\Omega e(X_A - \frac{1}{2}c_b)(\dot{\theta}_{pc} + \dot{\phi})$$

$$- \frac{1}{8}c_b\Omega e(\dot{\theta}_{pc} + \dot{\phi}) - \frac{1}{2}\Omega^2 e^2(\theta_{pc} + \phi) + \frac{1}{2}(\lambda\Omega R)\Omega e]$$

$$+ [- \frac{1}{8}c_b(\Omega + \dot{\zeta})(\theta_{pc} + \phi) + \frac{1}{2}X_A(\dot{\theta}_{pc} + \dot{\phi})\zeta - \frac{3}{8}c_b(\dot{\theta}_{pc} + \dot{\phi})\zeta$$

$$- \Omega e(\theta_{pc} + \phi)\zeta + \frac{1}{2}(\lambda\Omega R)\zeta + \frac{1}{2}\Omega e(\beta + \beta_p) + \frac{1}{8}c_b\dot{\beta}](\mu\Omega R)\cos\psi$$

$$+ [\frac{1}{8}c_b\Omega(\theta_{pc} + \phi)\zeta + \frac{1}{2}X_A(\dot{\theta}_{pc} + \dot{\phi}) - \frac{3}{8}c_b(\dot{\theta}_{pc} + \dot{\phi})$$

$$- \Omega e(\theta_{pc} + \phi) + \frac{1}{2}(\lambda\Omega R) - \frac{1}{8}c_b\Omega(\beta + \beta_p)](\mu\Omega R)\sin\psi$$

$$+ [- \frac{1}{2}(\theta_{pc} + \phi)\zeta^2 + \frac{1}{2}(\beta + \beta_p)\zeta](\mu\Omega R)^2\cos^2\psi$$

$$- \frac{1}{2}(\theta_{pc} + \phi)(\mu\Omega R)^2\sin^2\psi$$

$$+ [- (\theta_{pc} + \phi)\zeta + \frac{1}{2}(\beta + \beta_p)](\mu\Omega R)^2\cos\psi\sin\psi\}$$

$$+ A_{11}\{ - \frac{1}{2}\Omega^2e^2 - [\frac{1}{8}c_b(\Omega + \dot{\zeta}) + \Omega e\zeta](\mu\Omega R)\cos\psi$$

$$+ (\frac{1}{8}c_b\Omega\zeta - \Omega e)(\mu\Omega R)\sin\psi$$

$$- \frac{1}{2}\zeta^2(\mu\Omega R)^2\cos^2\psi - \frac{1}{2}(\mu\Omega R)^2\sin^2\psi - \zeta(\mu\Omega R)^2\cos\psi\sin\psi\}$$

$$+ A_{20}\{[- \frac{1}{8}c_b(\theta_{pc} + \phi)\ddot{\zeta} + \frac{1}{2}X_A(\dot{\theta}_{pc} + \dot{\phi})\dot{\zeta} - \frac{3}{8}c_b(\dot{\theta}_{pc} + \dot{\phi})\dot{\zeta} - \Omega e(\theta_{pc} + \phi)\dot{\zeta}$$

$$+ \frac{1}{2}(\lambda\Omega R)\dot{\zeta} + \frac{1}{8}c_b\Omega(\beta + \beta_p)\zeta + \frac{1}{4}(\lambda\Omega R)\Omega\zeta^2 + \frac{1}{2}\Omega^2e(\beta + \beta_p)\zeta$$

$$+ \frac{1}{8}c_b\Omega\dot{\beta}\zeta + \frac{1}{2}\Omega X_A(\dot{\theta}_{pc} + \dot{\phi}) - \frac{3}{8}c_b\Omega(\dot{\theta}_{pc} + \dot{\phi})$$

$$- \Omega^2e(\theta_{pc} + \phi) - \frac{1}{2}(\lambda\Omega R)\Omega\beta\beta_p - \frac{1}{4}(\lambda\Omega R)\Omega\beta^2$$

$$+ \frac{1}{2}(\lambda\Omega R)\Omega + \frac{1}{2}\Omega e\dot{\beta} + \frac{1}{8}c_b\ddot{\beta}]$$

$$+ [- (\Omega + \dot{\zeta})(\theta_{pc} + \phi)\zeta + \frac{1}{2}(\Omega + \dot{\zeta})(\beta + \beta_p) + \frac{1}{2}\dot{\beta}\zeta](\mu\Omega R)\cos\psi$$

$$+ [- (\Omega + \dot{\zeta})(\theta_{pc} + \phi) - \frac{1}{2}\Omega(\theta_{pc} + \phi)\zeta^2 + \frac{1}{2}\Omega(\beta + \beta_p)\zeta$$

$$+ \Omega(\theta_{pc} + \phi)\beta\beta_p + \frac{1}{2}\Omega\beta^2(\theta_{pc} + \phi) + \frac{1}{2}\dot{\beta}](\mu\Omega R)\sin\psi\}$$

$$+ A_{21}\{(- \frac{1}{8}c_b\ddot{\zeta} - \Omega e\dot{\zeta} - \Omega^2e) - \zeta(\Omega + \dot{\zeta})(\mu\Omega R)\cos\psi$$

$$+ [-(\Omega + \dot{\zeta}) - \frac{1}{2}\Omega\zeta^2 + \Omega\beta\beta_p + \frac{1}{2}\Omega\beta^2](\mu\Omega R)\sin\psi\}$$

$$+ A_{30}[-\frac{1}{2}(\Omega + \dot{\zeta})^2(\theta_{pc} + \phi) + \frac{1}{2}\dot{\beta}\dot{\zeta} - \frac{1}{2}\Omega^2(\theta_{pc} + \phi)\zeta^2 + \frac{1}{2}\Omega^2(\beta + \beta_p)\zeta$$

$$+ \Omega^2\beta\beta_p(\theta_{pc} + \phi) + \frac{1}{2}\Omega^2\beta^2(\theta_{pc} + \phi) + \frac{1}{2}\Omega\dot{\beta}]$$

$$+ A_{31}[-\frac{1}{2}(\Omega + \dot{\zeta})^2 - \frac{1}{2}\Omega^2\zeta^2 + \Omega^2\beta\beta_p + \frac{1}{2}\Omega^2\beta^2]$$

$$+ B_1(\frac{C_{do}}{a_o})[\frac{1}{2}(\lambda\Omega R)(\mu\Omega R)\sin\psi + \frac{1}{2}(\beta + \beta_p)(\mu\Omega R)^2\cos\psi\sin\psi]$$

$$+ B_2(\frac{C_{do}}{a_o})[\frac{1}{2}(\lambda\Omega R)\Omega + \frac{1}{2}\Omega(\beta + \beta_p)(\mu\Omega R)\cos\psi + \frac{1}{2}\dot{\beta}(\mu\Omega R)\sin\psi]$$

$$+ B_3(\frac{C_{do}}{a_o})\frac{1}{2}\Omega\dot{\beta} \qquad \text{(C.68b)}$$

$$M_{Abz5} = \int_0^{L_b} x\, p_{Aby5}\, dx$$

$$= A_{10}\{[\frac{1}{8}c_b(X_A - \frac{1}{4}c_b)(\ddot{\theta}_{pc} + \ddot{\phi})(\theta_{pc} + \phi)$$

$$+ \frac{1}{2}(\lambda\Omega R)(X_A - \frac{1}{2}c_b)(\dot{\theta}_{pc} + \dot{\phi}) - \frac{1}{8}c_b\Omega e(\theta_{pc} + \phi)(\dot{\theta}_{pc} + \dot{\phi})$$

$$- \frac{1}{2}(\lambda\Omega R)\Omega e(\theta_{pc} + \phi) + \frac{1}{2}(\lambda\Omega R)^2]$$

$$+ [-\frac{1}{8}c_b(\theta_{pc} + \phi)^2\dot{\zeta} - \frac{1}{8}c_b(\dot{\theta}_{pc} + \dot{\phi})(\theta_{pc} + \phi)\zeta - \frac{1}{2}(\lambda\Omega R)(\theta_{pc} + \phi)\zeta$$

$$+ \frac{1}{2}(X_A - \frac{1}{2}c_b)(\dot{\theta}_{pc} + \dot{\phi})(\beta + \beta_p) - \frac{1}{8}c_b\Omega(\theta_{pc} + \phi)^2$$

$$- \frac{1}{2}\Omega e(\theta_{pc} + \phi)(\beta + \beta_p) + \frac{1}{8}c_b(\theta_{pc} + \phi)\dot{\beta}$$

$$+ (\lambda\Omega R)(\beta + \beta_p)](\mu\Omega R)\cos\psi$$

$$+ [\frac{1}{8}c_b\Omega(\theta_{pc}+\phi)^2\zeta - \frac{1}{8}c_b(\dot{\theta}_{pc}+\dot{\phi})(\theta_{pc}+\phi) - \frac{1}{2}(\lambda\Omega R)(\theta_{pc}+\phi)$$

$$- \frac{1}{8}\Omega c_b(\theta_{pc}+\phi)(\beta+\beta_p)](\mu\Omega R)\sin\psi$$

$$- \frac{1}{2}(\theta_{pc}+\phi)(\beta+\beta_p)(\mu\Omega R)^2\cos\psi\sin\psi$$

$$+ [-\frac{1}{2}(\theta_{pc}+\phi)(\beta+\beta_p)\zeta + \frac{1}{2}(\beta+\beta_p)^2](\mu\Omega R)^2\cos^2\psi\}$$

$$+ A_{11}\{[\frac{1}{8}c_b(X_A - \frac{1}{4}c_b)(\ddot{\theta}_{pc}+\ddot{\phi}) - \frac{1}{8}c_b\Omega e(\dot{\theta}_{pc}+\dot{\phi}) - \frac{1}{2}(\lambda\Omega R)\Omega e]$$

$$+ [-\frac{1}{4}c_b(\theta_{pc}+\phi)\dot{\zeta} - \frac{1}{8}c_b(\dot{\theta}_{pc}+\dot{\phi})\zeta - \frac{1}{2}(\lambda\Omega R)\zeta - \frac{1}{4}c_b\Omega(\theta_{pc}+\phi)$$

$$- \frac{1}{2}\Omega e(\beta+\beta_p) + \frac{1}{8}c_b\dot{\beta}](\mu\Omega R)\cos\psi$$

$$+ [\frac{1}{4}c_b\Omega(\theta_{pc}+\phi)\zeta - \frac{1}{8}c_b(\dot{\theta}_{pc}+\dot{\phi}) - \frac{1}{2}(\lambda\Omega R)$$

$$- \frac{1}{8}c_b\Omega(\beta+\beta_p)](\mu\Omega R)\sin\psi$$

$$- \frac{1}{2}(\beta+\beta_p)(\mu\Omega R)^2\cos\psi\sin\psi - \frac{1}{2}(\beta+\beta_p)\zeta(\mu\Omega R)^2\cos^2\psi\}$$

$$+ A_{12}[-\frac{1}{8}c_b(\Omega+\dot{\zeta})(\mu\Omega R)\cos\psi + \frac{1}{8}c_b\Omega\zeta(\mu\Omega R)\sin\psi]$$

$$+ A_{20}\{[-\frac{1}{8}c_b(\theta_{pc}+\phi)^2\ddot{\zeta} - \frac{1}{8}c_b(\dot{\theta}_{pc}+\dot{\phi})\dot{\zeta}(\theta_{pc}+\phi) - \frac{1}{2}(\lambda\Omega R)(\theta_{pc}+\phi)\dot{\zeta}$$

$$+ \frac{1}{8}c_b\Omega(\theta_{pc}+\phi)\dot{\zeta}(\beta+\beta_p) - \frac{1}{4}(\lambda\Omega R)\Omega(\theta_{pc}+\phi)\zeta^2$$

$$- \frac{1}{2}\Omega^2 e(\theta_{pc}+\phi)(\beta+\beta_p)\zeta + \frac{1}{8}c_b\Omega(\theta_{pc}+\phi)\dot{\beta}\zeta$$

$$+ (\lambda\Omega R)\Omega(\beta+\beta_p)\zeta + \frac{1}{2}(X_A - \frac{1}{2}c_b)(\dot{\theta}_{pc}+\dot{\phi})\dot{\beta}$$

$$-\frac{1}{8}c_b\Omega(\dot{\theta}_{pc}+\dot{\phi})(\theta_{pc}+\phi)+\frac{1}{2}(\lambda\Omega R)\Omega(\theta_{pc}+\phi)\beta\beta_p$$

$$+\frac{1}{4}(\lambda\Omega R)\Omega(\theta_{pc}+\phi)\beta^2-\frac{1}{2}(\lambda\Omega R)\Omega(\theta_{pc}+\phi)$$

$$-\frac{1}{2}\Omega e(\theta_{pc}+\phi)\dot{\beta}+\frac{1}{8}c_b(\theta_{pc}+\phi)\ddot{\beta}+(\lambda\Omega R)\dot{\beta}]$$

$$+[-\frac{1}{2}(\theta_{pc}+\phi)\dot{\zeta}(\beta+\beta_p)-\frac{3}{4}\Omega(\theta_{pc}+\phi)(\beta+\beta_p)\zeta^2-\frac{1}{2}(\theta_{pc}+\phi)\dot{\beta}\zeta$$

$$+\Omega(\beta+\beta_p)^2\zeta+\frac{1}{2}\Omega(\theta_{pc}+\phi)\beta(\beta+\beta_p)\beta_p$$

$$+\frac{1}{4}\Omega(\theta_{pc}+\phi)\beta^2(\beta+\beta_p)-\frac{1}{2}\Omega(\theta_{pc}+\phi)(\beta+\beta_p)$$

$$+\dot{\beta}(\beta+\beta_p)](\mu\Omega R)\cos\psi$$

$$+[-\frac{1}{2}\Omega(\theta_{pc}+\phi)(\beta+\beta_p)\zeta-\frac{1}{2}(\theta_{pc}+\phi)\dot{\beta}](\mu\Omega R)\sin\psi\}$$

$$+A_{21}\{[-\frac{1}{4}c_b(\theta_{pc}+\phi)\ddot{\zeta}-\frac{1}{4}c_b\Omega(\theta_{pc}+\phi)\zeta\dot{\zeta}-\frac{1}{8}c_b(\dot{\theta}_{pc}+\dot{\phi})\dot{\zeta}$$

$$-\frac{1}{2}(\lambda\Omega R)\ddot{\zeta}+\frac{1}{8}c_b\Omega\dot{\zeta}(\beta+\beta_p)-\frac{1}{16}c_b\Omega(\dot{\theta}_{pc}+\dot{\phi})\zeta^2$$

$$-\frac{1}{4}(\lambda\Omega R)\Omega\zeta^2-\frac{1}{2}\Omega^2e(\beta+\beta_p)\zeta+\frac{1}{8}c_b\Omega\beta\zeta$$

$$+\frac{1}{8}c_b\Omega(\dot{\theta}_{pc}+\dot{\phi})\beta\beta_p+\frac{1}{16}c_b\Omega(\dot{\theta}_{pc}+\dot{\phi})\beta^2$$

$$-\frac{1}{8}c_b\Omega(\dot{\theta}_{pc}+\dot{\phi})+\frac{1}{4}c_b\Omega(\theta_{pc}+\phi)(\beta+\beta_p)\dot{\beta}-\frac{1}{2}\Omega e\dot{\beta}$$

$$+\frac{1}{2}(\lambda\Omega R)\Omega\beta\beta_p+\frac{1}{4}(\lambda\Omega R)\Omega\beta^2-\frac{1}{2}(\lambda\Omega R)\Omega+\frac{1}{8}c_b\ddot{\beta}]$$

$$+[-\frac{1}{2}(\beta+\beta_p)\ddot{\zeta}-\frac{3}{4}\Omega(\beta+\beta_p)\zeta^2-\frac{1}{2}\dot{\beta}\zeta$$

$$- \frac{1}{2}\Omega(\beta + \beta_p)](\mu\Omega R)\cos\psi$$

$$+ [- \frac{1}{2}\Omega(\beta + \beta_p)\zeta - \frac{1}{2}\dot{\beta}](\mu\Omega R)\sin\psi\}$$

$$+ A_{22}[- \frac{1}{8}c_b\ddot{\zeta} - \frac{1}{8}c_b\Omega\zeta\dot{\zeta} + \frac{1}{8}c_b\Omega(\beta + \beta_p)\dot{\beta}]$$

$$+ A_{30}[- \frac{1}{2}(\theta_{pc} + \phi)\dot{\beta}\dot{\zeta} - \frac{1}{2}\Omega^2(\theta_{pc} + \phi)(\beta + \beta_p)\zeta + \Omega\dot{\beta}(\beta + \beta_p)\zeta$$

$$- \frac{1}{2}\Omega(\theta_{pc} + \phi)\dot{\beta} + \frac{1}{2}\dot{\beta}^2]$$

$$+ A_{31}[- \frac{1}{2}(\Omega + \dot{\zeta})\dot{\beta} - \frac{1}{2}\Omega^2(\beta + \beta_p)\zeta]$$

$$+ B_1(\frac{C_{do}}{a_o})\{[- \frac{1}{2}(\lambda\Omega R)^2 - \frac{1}{2}\Omega^2 e^2]$$

$$+ [- (\lambda\Omega R)(\beta + \beta_p) - e\Omega\zeta](\mu\Omega R)\cos\psi - e\Omega(\mu\Omega R)\sin\psi$$

$$+ [- \frac{1}{2}\zeta^2 - \frac{1}{2}(\beta + \beta_p)^2](\mu\Omega R)^2\cos^2\psi - \frac{1}{2}(\mu\Omega R)^2\sin^2\psi$$

$$- \zeta(\mu\Omega R)^2\cos\psi\ \sin\psi\}$$

$$+ B_2(\frac{C_{do}}{a_o})\{[- \Omega e(\Omega + \dot{\zeta}) - (\lambda\Omega R)\dot{\beta}]$$

$$+ [- (\Omega + \dot{\zeta})\zeta - \dot{\beta}(\beta + \beta_p)](\mu\Omega R)\cos\psi$$

$$+ [- (\Omega + \dot{\zeta}) - \frac{1}{2}\Omega\zeta^2 + \Omega\beta\beta_p + \frac{1}{2}\Omega\beta^2](\mu\Omega R)\sin\psi\}$$

$$+ B_3(\frac{C_{do}}{a_o})[- \frac{1}{2}(\Omega + \dot{\zeta})^2 - \frac{1}{2}\Omega^2\zeta^2 + \beta\beta_p\Omega^2 + \frac{1}{2}\Omega^2\beta^2 - \frac{1}{2}\dot{\beta}^2] \qquad \text{(C.68c)}$$

where the aerodynamic coefficients given by Eqs. (C.64) and (C.65) have been used in the above expression.

C.3.2 *Control Flap Aerodynamic Loads*

For the offset-hinged spring restrained blade model the differential force at the blade root due to the additional aerodynamic loads produced by the control surface is given by

$$d\vec{F}_{Ac} = \vec{p}_{Ac}\, dx$$

where $\vec{p}_{Ac}$ represents the contribution to the total distributed aerodynamic force acting on the blade from the control surface, which can be expressed in the "5" system as

$$\vec{p}_{Ac} = p_{Acy5}\hat{e}_{y5} + p_{Acz5}\hat{e}_{z5}$$

The y_5 and z_5 components of $\vec{p}_{Ac}$ for the spring restrained blade model are obtained from the expressions developed in Chapter 3 by substituting Eqs. (4.3) and (4.4) into Eqs. (3.119).

The total force at the blade root can be obtained by integrating the differential force along the span of the control surface, i.e.

$$\vec{F}_{Ac} = \int_{x_{cs}}^{x_{cs}+L_{cs}} \vec{p}_{Ac}\, dx \qquad \text{(C.70)}$$

which can be expressed in the "5" system as

$$\vec{F}_{Ac} = F_{Acy5}\hat{e}_{y5} + F_{Acz5}\hat{e}_{z5}$$

Before integrating the distributed aerodynamic loads along the span of the control surface it is convenient to define two sets of aerodynamic coefficients. The first set is associated with the integration of the aerodynamic lift and moment; the second is associated with the integration of the aerodynamic drag. In the integration of the aerodynamic loads along the span of the control surface a plethora of integrals consisting of products of various powers of x and the pretwist distribution $\theta_{pt}(x)$ arise. A scheme for consistently tracking the numerous integrals associated with the derivation has been devised. The following scheme is used to assign coefficients to the various integrals which arise in the integration of the additional aerodynamic lift and moment due to the control surface:

$$C_{nm} = \rho_A a_o C_f \int_{x_{cs}}^{x_{cs}+L_{cs}} x^n \theta_{pt}^m(x)\, dx \tag{C.71}$$

where C_f represents the aerodynamic correction factor defined in Chapter 3 associated with the additional aerodynamic lift and moment due to the presence of an aerodynamic surface predicted using two-dimensional quasi-steady aerodynamics.

Similarly, the following scheme is used to assign symbols to the various integrals associated with the integration of the additional aerodynamic drag acting on the blade due to the presence of the control surface:

$$D_n = \rho_A a_o \int_{x_{cs}}^{x_{cs}+L_{cs}} x^n\, dx \tag{C.72}$$

The aerodynamic coefficients defined by Eqs. (C.71) and (C.72) are substituted directly into Eqs. (C.75) in order to obtain explicit expressions for the force at the blade root due to the aerodynamic loads acting on the control surface.

Using the scheme defined by Eq. (C.71) the following set of aerodynamic coefficients which arise in the integration of the aerodynamic lift and moment along the span of the control surface are defined as follows:

$$C_{00} = \rho_A a_o C_f \int_{x_{cs}}^{x_{cs}+L_{cs}} dx \tag{C.73a}$$

$$C_{01} = \rho_A a_o C_f \int_{x_{cs}}^{x_{cs}+L_{cs}} \theta_{pt}(x)\, dx \tag{C.73b}$$

$$C_{02} = \rho_A a_o C_f \int_{x_{cs}}^{x_{cs}+L_{cs}} \theta_{pt}^2(x)\, dx \tag{C.73c}$$

$$C_{10} = \rho_A a_o C_f \int_{x_{cs}}^{x_{cs}+L_{cs}} x\, dx \tag{C.73d}$$

$$C_{11} = \rho_A a_o C_f \int_{x_{cs}}^{x_{cs}+L_{cs}} x\, \theta_{pt}(x)\, dx \tag{C.73e}$$

$$C_{12} = \rho_A a_o C_f \int_{x_{cs}}^{x_{cs}+L_{cs}} x\,\theta_{pt}^2(x)\,dx \tag{C.73f}$$

$$C_{20} = \rho_A a_o C_f \int_{x_{cs}}^{x_{cs}+L_{cs}} x^2\,dx \tag{C.73g}$$

$$C_{21} = \rho_A a_o C_f \int_{x_{cs}}^{x_{cs}+L_{cs}} x^2\,\theta_{pt}(x)\,dx \tag{C.73h}$$

$$C_{22} = \rho_A a_o C_f \int_{x_{cs}}^{x_{cs}+L_{cs}} x^2\,\theta_{pt}^2(x)\,dx \tag{C.73i}$$

$$C_{30} = \rho_A a_o C_f \int_{x_{cs}}^{x_{cs}+L_{cs}} x^3\,dx \tag{C.73j}$$

$$C_{31} = \rho_A a_o C_f \int_{x_{cs}}^{x_{cs}+L_{cs}} x^3\,\theta_{pt}(x)\,dx \tag{C.73k}$$

Similarly, the following set of aerodynamic coefficients which arise in the integration of the aerodynamic drag along the span of the control surface are defined as follows:

$$D_0 = \rho_A a_o \int_{x_{cs}}^{x_{cs}+L_{cs}} dx \tag{C.74a}$$

$$D_1 = \rho_A a_o \int_{x_{cs}}^{x_{cs}+L_{cs}} x\,dx \tag{C.74b}$$

$$D_2 = \rho_A a_o \int_{x_{cs}}^{x_{cs}+L_{cs}} x^2\,dx \tag{C.74c}$$

$$D_3 = \rho_A a_o \int_{x_{cs}}^{x_{cs}+L_{cs}} x^3\,dx \tag{C.74d}$$

Performing the integration of each component in Eqs. (C.70) yields

$$F_{Acy5} = \int_{x_{cs}}^{x_{cs}+L_{cs}} p_{Acy5}\,dx$$

$$= C_{00}\{[-\frac{1}{8}(\lambda\Omega R)c_b(2c_b+3c_{cs})(\frac{T_{11}}{a_o})\dot{\delta}-(\lambda\Omega R)c_b\Omega e(\frac{T_{10}}{a_o})\delta$$

$$+\frac{1}{2}(\lambda\Omega R)^2c_{cs}]$$

$$+[-(\lambda\Omega R)c_b\zeta(\frac{T_{10}}{a_o})\delta-\frac{1}{4}c_bc_{cs}\Omega(\theta_{pc}+\phi)^2$$

$$+\frac{1}{4}c_b(c_b+2c_{cs})\Omega(\theta_{pc}+\phi)(\frac{T_4}{a_o})\delta-c_b\Omega e(\beta+\beta_p)(\frac{T_{10}}{a_o})\delta$$

$$-\frac{1}{8}c_b(2c_b+3c_{cs})(\beta+\beta_p)(\frac{T_{11}}{a_o})\dot{\delta}+(\lambda\Omega R)c_{cs}(\beta+\beta_p)](\mu\Omega R)\cos\psi$$

$$+[-\frac{1}{4}c_bc_{cs}(\theta_{pc}+\phi)(\dot{\theta}_{pc}+\dot{\phi})+\frac{1}{4}c_b(c_b+2c_{cs})(\theta_{pc}+\phi)(\frac{T_4}{a_o})\dot{\delta}$$

$$-\frac{1}{2}(\lambda\Omega R)c_{cs}(\theta_{pc}+\phi)-(\lambda\Omega R)(c_b+c_{cs})(\frac{T_{10}}{a_o})\delta](\mu\Omega R)\sin\psi$$

$$+[-c_b(\beta+\beta_p)\zeta(\frac{T_{10}}{a_o})\delta+\frac{1}{2}c_{cs}(\beta+\beta_p)^2](\mu\Omega R)^2\cos^2\psi$$

$$+[-\frac{1}{2}c_{cs}(\theta_{pc}+\phi)(\beta+\beta_p)$$

$$-(c_b+c_{cs})(\beta+\beta_p)(\frac{T_{10}}{a_o})\delta](\mu\Omega R)^2\cos\psi\sin\psi\}$$

$$+C_{01}\{[-\frac{1}{2}c_bc_{cs}\Omega(\theta_{pc}+\phi)+\frac{1}{4}c_b(c_b+2c_{cs})\Omega(\frac{T_4}{a_o})\delta](\mu\Omega R)\cos\psi$$

$$+[-\frac{1}{4}c_bc_{cs}(\dot{\theta}_{pc}+\dot{\phi})+\frac{1}{4}c_b(c_b+2c_{cs})(\frac{T_4}{a_o})\dot{\delta}$$

$$-\frac{1}{2}(\lambda\Omega R)c_{cs}](\mu\Omega R)\sin\psi$$

$$-\frac{1}{2}c_{cs}(\beta+\beta_p)(\mu\Omega R)^2\cos\psi\sin\psi\}$$

$$-C_{02}\frac{1}{4}c_bc_{cs}\Omega(\mu\Omega R)\cos\psi$$

$$+ C_{10}\{[-(\lambda\Omega R)c_b\dot{\zeta}(\frac{T_{10}}{a_o})\delta - \frac{1}{4}c_b c_{cs}\Omega(\theta_{pc}+\phi)(\dot{\theta}_{pc}+\dot{\phi})$$

$$+ \frac{1}{4}c_b(c_b+2c_{cs})\Omega(\theta_{pc}+\phi)(\frac{T_4}{a_o})\dot{\delta} - \frac{1}{2}(\lambda\Omega R)c_{cs}\Omega(\theta_{pc}+\phi)$$

$$- \frac{1}{8}c_b(2c_b+3c_{cs})\dot{\beta}(\frac{T_{11}}{a_o})\dot{\delta} - (\lambda\Omega R)(c_b+c_{cs})\Omega(\frac{T_{10}}{a_o})\delta$$

$$- c_b\Omega e\dot{\beta}(\frac{T_{10}}{a_o})\delta + (\lambda\Omega R)c_{cs}\dot{\beta}]$$

$$+ [-c_b(\beta+\beta_p)\dot{\zeta}(\frac{T_{10}}{a_o})\delta - c_b\dot{\beta}\zeta(\frac{T_{10}}{a_o})\delta - \frac{1}{2}c_{cs}\Omega(\theta_{pc}+\phi)(\beta+\beta_p)$$

$$- (c_b+c_{cs})\Omega(\beta+\beta_p)(\frac{T_{10}}{a_o})\delta + c_{cs}\dot{\beta}(\beta+\beta_p)](\mu\Omega R)\cos\psi$$

$$+ [-c_b\Omega(\beta+\beta_p)\zeta(\frac{T_{10}}{a_o})\delta - \frac{1}{2}c_{cs}(\theta_{pc}+\phi)\dot{\beta}$$

$$- (c_b+c_{cs})\dot{\beta}(\frac{T_{10}}{a_o})\delta](\mu\Omega R)\sin\psi\}$$

$$+ C_{11}\{[-\frac{1}{4}c_b c_{cs}\Omega(\dot{\theta}_{pc}+\dot{\phi}) + \frac{1}{4}c_b(c_b+2c_{cs})\Omega(\frac{T_4}{a_o})\dot{\delta} - \frac{1}{2}(\lambda\Omega R)c_{cs}\Omega]$$

$$- \frac{1}{2}c_{cs}\Omega(\beta+\beta_p)(\mu\Omega R)\cos\psi - \frac{1}{2}c_{cs}\dot{\beta}(\mu\Omega R)\sin\psi\}$$

$$+ C_{20}[-c_b\dot{\beta}\zeta(\frac{T_{10}}{a_o})\delta - c_b\Omega^2(\beta+\beta_p)\zeta(\frac{T_{10}}{a_o})\delta - \frac{1}{2}c_{cs}\Omega(\theta_{pc}+\phi)\dot{\beta}$$

$$- (c_b+c_{cs})\Omega\dot{\beta}(\frac{T_{10}}{a_o})\delta + \frac{1}{2}c_{cs}\dot{\beta}^2]$$

$$- C_{21}\frac{1}{2}c_{cs}\Omega\dot{\beta}$$

$$- \frac{1}{2}D_0 c_{cs}\frac{C_{do}}{a_o}(\mu\Omega R)^2\sin^2\psi$$

$$- D_1 c_{cs}\Omega\frac{C_{do}}{a_o}(\mu\Omega R)\sin\psi$$

$$- \frac{1}{2} D_2 c_{cs} \Omega^2 \frac{C_{do}}{a_o} \qquad \text{(C.75a)}$$

$$F_{Acz5} = \int_{x_{cs}}^{x_{cs} + L_{cs}} p_{Acz5}\, dx$$

$$= C_{00}\{ - \frac{1}{4} c_b^2 \Omega (\frac{T_4}{a_o}) \delta (\mu \Omega R) \cos \psi$$

$$+ [- \frac{1}{4} c_b^2 (\frac{T_4}{a_o}) \dot{\delta} + \frac{1}{8} c_b (2c_b + 3c_{cs}) (\frac{T_{11}}{a_o}) \dot{\delta}$$

$$+ 2c_b \Omega e (\frac{T_{10}}{a_o}) \delta - \frac{1}{2} (\lambda \Omega R) c_{cs}] (\mu \Omega R) \sin \psi$$

$$+ [\frac{1}{2} c_{cs} (\theta_{pc} + \phi) + (c_b + c_{cs}) (\frac{T_{10}}{a_o}) \delta] (\mu \Omega R)^2 \sin^2 \psi$$

$$+ [2c_b \zeta (\frac{T_{10}}{a_o}) \delta - \frac{1}{2} c_{cs} (\beta + \beta_p)] (\mu \Omega R)^2 \cos \psi \sin \psi \}$$

$$+ C_{01} \frac{1}{2} c_{cs} (\mu \Omega R)^2 \sin^2 \psi$$

$$+ C_{10}\{[- \frac{1}{4} c_b^2 \Omega (\frac{T_4}{a_o}) \dot{\delta} + \frac{1}{8} c_b (2c_b + 3c_{cs}) \Omega (\frac{T_{11}}{a_o}) \dot{\delta}$$

$$+ 2c_b \Omega^2 e (\frac{T_{10}}{a_o}) \delta - \frac{1}{2} (\lambda \Omega R) c_{cs} \Omega]$$

$$+ [2c_b \Omega \zeta (\frac{T_{10}}{a_o}) \delta - \frac{1}{2} c_{cs} \Omega (\beta + \beta_p)] (\mu \Omega R) \cos \psi$$

$$+ [2c_b \dot{\zeta} (\frac{T_{10}}{a_o}) \delta + c_{cs} \Omega (\theta_{pc} + \phi) + 2(c_b + c_{cs}) \Omega (\frac{T_{10}}{a_o}) \delta$$

$$- \frac{1}{2} c_{cs} \dot{\beta}] (\mu \Omega R) \sin \psi \}$$

$$+ C_{11} c_{cs} \Omega (\mu \Omega R) \sin \psi$$

$$+ C_{20}[2c_b \Omega \dot{\zeta} (\frac{T_{10}}{a_o}) \delta + \frac{1}{2} c_{cs} \Omega^2 (\theta_{pc} + \phi) + (c_b + c_{cs}) \Omega^2 (\frac{T_{10}}{a_o}) \delta - \frac{1}{2} c_{cs} \Omega \dot{\beta}]$$

$$+ C_{21}\frac{1}{2}c_{cs}\Omega^2 \qquad \text{(C.75b)}$$

where the aerodynamic coefficients defined by Eqs. (C.73) and (C.74) have been used in evaluating the above expressions.

For the offset-hinged spring restrained blade model the differential moment about the blade root due to the additional aerodynamic loads acting on the blade due to the presence of the control surface can be expressed as

$$d\vec{M}_{Ac} = (\vec{q}_{Ac} + x\hat{e}_{x4} \times \vec{p}_{Ac})\,dx$$

where $\vec{q}_{Ac}$ represents the contribution to the total distributed aerodynamic moment acting on the blade from the control surface, which can be expressed in the "5" system as

$$\vec{q}_{Ac} = q_{Acx5}\hat{e}_{x5}$$

The x_5 component of $\vec{q}_{Ac}$ is obtained from the general expressions developed in Chapter 3 by substituting Eqs. (4.3) and (4.4) into Eq. (3.120).

The total moment about the blade root is obtained by integrating the differential moment along the span of the control surface

$$\vec{M}_{Ac} = \int_{x_{cs}}^{x_{cs}+L_{cs}} (\vec{q}_{Ac} + x\hat{e}_{x4} \times \vec{p}_{Ac})\,dx \qquad \text{(C.76)}$$

which can be expressed in the "5" system as

$$\vec{M}_{Ac} = M_{Acx5}\hat{e}_{x5} + M_{Acy5}\hat{e}_{y5} + M_{Acz5}\hat{e}_{z5}$$

where

$$M_{Acx5} = \int_{x_{cs}}^{x_{cs}+L_{cs}} q_{Acx5}\,dx$$

$$= C_{00}\{\frac{1}{8}c_b^2\Omega e\frac{T_{18}}{a_o}\dot{\delta} + \frac{1}{16}c_b^2(c_b + c_{cs})\frac{T_{17}}{a_o}\ddot{\delta}$$

$$+ \frac{T_{18}}{a_o}[\frac{1}{8}c_b^2\zeta\dot{\delta} + \frac{1}{8}c_b^2\zeta\dot{\delta} + \frac{1}{8}(c_b + c_{cs})^2\Omega\delta](\mu\Omega R)\cos\psi$$

$$+\frac{T_{18}}{a_o}[-\frac{1}{8}c_b^2\Omega\zeta\delta+\frac{1}{8}(c_b+c_{cs})^2\dot{\delta}](\mu\Omega R)\sin\psi$$

$$+[-\frac{1}{2}c_b^2\Omega e(\frac{T_4}{a_o})\delta-\frac{1}{8}c_b^2(c_b+c_{cs})(\frac{T_1}{a_o})\dot{\delta}](\mu\Omega R)\sin\psi$$

$$+[\frac{1}{2}c_{cs}(X_A-\frac{1}{4}c_b)(\theta_{pc}+\phi)+(c_b+c_{cs})(X_A-\frac{1}{4}c_b)(\frac{T_{10}}{a_o})\delta$$

$$-\frac{1}{8}c_{cs}^2(\theta_{pc}+\phi)-\frac{1}{4}(c_b+c_{cs})^2(\frac{T_4}{a_o})\delta$$

$$-\frac{1}{2}c_{cs}(c_b+c_{cs})(\frac{T_{10}}{a_o})\delta](\mu\Omega R)^2\sin^2\psi$$

$$-\frac{1}{2}c_b^2\zeta(\frac{T_4}{a_o})\delta(\mu\Omega R)^2\cos\psi\sin\psi\}$$

$$+C_{01}[\frac{1}{2}c_{cs}(X_A-\frac{1}{4}c_b)-\frac{1}{8}c_{cs}^2](\mu\Omega R)^2\sin^2\psi$$

$$+C_{10}\{\frac{T_{18}}{a_o}[\frac{1}{8}c_b^2\ddot{\zeta}\delta+\frac{1}{8}c_b^2\dot{\zeta}\dot{\delta}+\frac{1}{8}(c_b+c_{cs})^2\Omega\dot{\delta}]$$

$$+[-\frac{1}{2}c_b^2\Omega^2e(\frac{T_4}{a_o})\delta-\frac{1}{8}c_b^2(c_b+c_{cs})\Omega(\frac{T_1}{a_o})\dot{\delta}]$$

$$-\frac{1}{2}c_b^2\Omega\zeta(\frac{T_4}{a_o})\delta(\mu\Omega R)\cos\psi$$

$$+[-\frac{1}{2}c_b^2\dot{\zeta}(\frac{T_4}{a_o})\delta+c_{cs}(X_A-\frac{1}{4}c_b)\Omega(\theta_{pc}+\phi)$$

$$+2(c_b+c_{cs})(X_A-\frac{1}{4}c_b)\Omega(\frac{T_{10}}{a_o})\delta-\frac{1}{4}c_{cs}^2\Omega(\theta_{pc}+\phi)$$

$$-\frac{1}{2}(c_b+c_{cs})^2\Omega(\frac{T_4}{a_o})\delta-c_{cs}(c_b+c_{cs})\Omega(\frac{T_{10}}{a_o})\delta](\mu\Omega R)\sin\psi$$

$$+C_{11}[c_{cs}(X_A-\frac{1}{4}c_b)\Omega-\frac{1}{4}c_{cs}^2\Omega](\mu\Omega R)\sin\psi$$

$$+C_{20}[-\frac{1}{2}c_b^2\Omega\zeta(\frac{T_4}{a_o})\delta+\frac{1}{2}c_{cs}(X_A-\frac{1}{4}c_b)\Omega^2(\theta_{pc}+\phi)$$

$$+ (c_b + c_{cs})(X_A - \frac{1}{4}c_b)\Omega^2(\frac{T_{10}}{a_o})\delta - \frac{1}{8}c_{cs}^2\Omega^2(\theta_{pc} + \phi)$$

$$- \frac{1}{4}(c_b + c_{cs})^2\Omega^2(\frac{T_4}{a_o})\delta - \frac{1}{2}c_{cs}(c_b + c_{cs})\Omega^2(\frac{T_{10}}{a_o})\delta]$$

$$+ C_{21}[\frac{1}{2}c_{cs}(X_A - \frac{1}{4}c_b)\Omega^2 - \frac{1}{8}c_{cs}^2\Omega^2] \qquad \text{(C.77a)}$$

$$M_{Acy5} = -\int_{x_{cs}}^{x_{cs} + L_{cs}} x\, p_{Acz5}\, dx$$

$$= C_{10}\{\frac{1}{4}c_b^2\Omega(\frac{T_4}{a_o})\delta(\mu\Omega R)\cos\psi$$

$$+ [\frac{1}{4}c_b^2(\frac{T_4}{a_o})\dot{\delta} - \frac{1}{8}c_b(2c_b + 3c_{cs})(\frac{T_{11}}{a_o})\delta - 2c_b\Omega e(\frac{T_{10}}{a_o})\delta$$

$$+ \frac{1}{2}(\lambda\Omega R)c_{cs}](\mu\Omega R)\sin\psi$$

$$+ [-\frac{1}{2}c_{cs}(\theta_{pc} + \phi) - (c_b + c_{cs})(\frac{T_{10}}{a_o})\delta](\mu\Omega R)^2\sin^2\psi$$

$$+ [-2c_b\zeta(\frac{T_{10}}{a_o})\delta + \frac{1}{2}c_{cs}(\beta + \beta_p)](\mu\Omega R)^2\cos\psi\sin\psi\}$$

$$- C_{11}\frac{1}{2}c_{cs}(\mu\Omega R)^2\sin^2\psi$$

$$+ C_{20}\{[\frac{1}{4}c_b^2\Omega(\frac{T_4}{a_o})\dot{\delta} - \frac{1}{8}c_b(2c_b + 3c_{cs})\Omega(\frac{T_{11}}{a_o})\dot{\delta}$$

$$- 2c_b\Omega^2e(\frac{T_{10}}{a_o})\delta + \frac{1}{2}(\lambda\Omega R)c_{cs}\Omega]$$

$$+ [-2c_b\Omega\zeta(\frac{T_{10}}{a_o})\delta + \frac{1}{2}c_{cs}\Omega(\beta + \beta_p)](\mu\Omega R)\cos\psi$$

$$+ [-2c_b\dot{\zeta}(\frac{T_{10}}{a_o})\delta - c_{cs}\Omega(\theta_{pc} + \phi) - 2(c_b + c_{cs})\Omega(\frac{T_{10}}{a_o})\delta$$

$$+ \frac{1}{2}c_{cs}\dot{\beta}](\mu\Omega R)\sin\psi\}$$

$$- C_{21} c_{cs} \Omega (\mu \Omega R) \sin \psi$$

$$+ C_{30} [- 2 c_b \Omega \dot{\zeta} (\frac{T_{10}}{a_o}) \delta - \frac{1}{2} c_{cs} \Omega^2 (\theta_{pc} + \phi) - (c_b + c_{cs}) \Omega^2 (\frac{T_{10}}{a_o}) \delta + \frac{1}{2} c_{cs} \Omega \dot{\beta}]$$

$$- C_{31} \frac{1}{2} c_{cs} \Omega^2 \qquad \text{(C.77b)}$$

$$M_{Acz5} = \int_{x_{cs}}^{x_{cs} + L_{cs}} x \, p_{Acy5} \, dx$$

$$= C_{10} \{ [- \frac{1}{8} (\lambda \Omega R) c_b (2 c_b + 3 c_{cs}) (\frac{T_{11}}{a_o}) \dot{\delta} - (\lambda \Omega R) c_b \Omega e (\frac{T_{10}}{a_o}) \delta$$

$$+ \frac{1}{2} (\lambda \Omega R)^2 c_{cs}]$$

$$+ [- (\lambda \Omega R) c_b \zeta (\frac{T_{10}}{a_o}) \delta - \frac{1}{4} c_b c_{cs} \Omega (\theta_{pc} + \phi)^2$$

$$+ \frac{1}{4} c_b (c_b + 2 c_{cs}) \Omega (\theta_{pc} + \phi) (\frac{T_4}{a_o}) \delta - c_b \Omega e (\beta + \beta_p) (\frac{T_{10}}{a_o}) \delta$$

$$- \frac{1}{8} c_b (2 c_b + 3 c_{cs}) (\beta + \beta_p) (\frac{T_{11}}{a_o}) \dot{\delta} + (\lambda \Omega R) c_{cs} (\beta + \beta_p)] (\mu \Omega R) \cos \psi$$

$$+ [- \frac{1}{4} c_b c_{cs} (\theta_{pc} + \phi) (\dot{\theta}_{pc} + \dot{\phi}) + \frac{1}{4} c_b (c_b + 2 c_{cs}) (\theta_{pc} + \phi) (\frac{T_4}{a_o}) \dot{\delta}$$

$$- \frac{1}{2} (\lambda \Omega R) c_{cs} (\theta_{pc} + \phi) - (\lambda \Omega R) (c_b + c_{cs}) (\frac{T_{10}}{a_o}) \delta] (\mu \Omega R) \sin \psi$$

$$+ [- c_b (\beta + \beta_p) \zeta (\frac{T_{10}}{a_o}) \delta + \frac{1}{2} c_{cs} (\beta + \beta_p)^2] (\mu \Omega R)^2 \cos^2 \psi$$

$$+ [- \frac{1}{2} c_{cs} (\theta_{pc} + \phi) (\beta + \beta_p)$$

$$- (c_b + c_{cs}) (\beta + \beta_p) (\frac{T_{10}}{a_o}) \delta] (\mu \Omega R)^2 \cos \psi \sin \psi \}$$

$$+ C_{11} \{ [- \frac{1}{2} c_b c_{cs} \Omega (\theta_{pc} + \phi) + \frac{1}{4} c_b (c_b + 2 c_{cs}) \Omega (\frac{T_4}{a_o}) \delta] (\mu \Omega R) \cos \psi$$

$$+ [- \frac{1}{4} c_b c_{cs} (\dot{\theta}_{pc} + \dot{\phi}) + \frac{1}{4} c_b (c_b + 2c_{cs}) (\frac{T_4}{a_o}) \dot{\delta}$$

$$- \frac{1}{2} (\lambda \Omega R) c_{cs}] (\mu \Omega R) \sin \psi$$

$$- \frac{1}{2} c_{cs} (\beta + \beta_p) (\mu \Omega R)^2 \cos \psi \sin \psi \}$$

$$- C_{12} \frac{1}{4} c_b c_{cs} \Omega (\mu \Omega R) \cos \psi$$

$$+ C_{20} \{ [- (\lambda \Omega R) c_b \dot{\zeta} (\frac{T_{10}}{a_o}) \delta - \frac{1}{4} c_b c_{cs} \Omega (\theta_{pc} + \phi) (\dot{\theta}_{pc} + \dot{\phi})$$

$$+ \frac{1}{4} c_b (c_b + 2c_{cs}) \Omega (\theta_{pc} + \phi) (\frac{T_4}{a_o}) \dot{\delta} - \frac{1}{2} (\lambda \Omega R) c_{cs} \Omega (\theta_{pc} + \phi)$$

$$- \frac{1}{8} c_b (2c_b + 3c_{cs}) \dot{\beta} (\frac{T_{11}}{a_o}) \dot{\delta} - (\lambda \Omega R) (c_b + c_{cs}) \Omega (\frac{T_{10}}{a_o}) \delta$$

$$- c_b \Omega e \dot{\beta} (\frac{T_{10}}{a_o}) \delta + (\lambda \Omega R) c_{cs} \dot{\beta}]$$

$$+ [- c_b (\beta + \beta_p) \dot{\zeta} (\frac{T_{10}}{a_o}) \delta - c_b \dot{\beta} \zeta (\frac{T_{10}}{a_o}) \delta - \frac{1}{2} c_{cs} \Omega (\theta_{pc} + \phi) (\beta + \beta_p)$$

$$- (c_b + c_{cs}) \Omega (\beta + \beta_p) (\frac{T_{10}}{a_o}) \delta + c_{cs} \dot{\beta} (\beta + \beta_p)] (\mu \Omega R) \cos \psi$$

$$+ [- c_b \Omega (\beta + \beta_p) \zeta (\frac{T_{10}}{a_o}) \delta - \frac{1}{2} c_{cs} (\theta_{pc} + \phi) \dot{\beta}$$

$$- (c_b + c_{cs}) \dot{\beta} (\frac{T_{10}}{a_o}) \delta] (\mu \Omega R) \sin \psi \}$$

$$+ C_{21} \{ [- \frac{1}{4} c_b c_{cs} \Omega (\dot{\theta}_{pc} + \dot{\phi}) + \frac{1}{4} c_b (c_b + 2c_{cs}) \Omega (\frac{T_4}{a_o}) \dot{\delta} - \frac{1}{2} (\lambda \Omega R) c_{cs} \Omega]$$

$$- \frac{1}{2} c_{cs} \Omega (\beta + \beta_p) (\mu \Omega R) \cos \psi - \frac{1}{2} c_{cs} \dot{\beta} (\mu \Omega R) \sin \psi \}$$

$$+ C_{30} [- c_b \dot{\beta} \zeta (\frac{T_{10}}{a_o}) \delta - c_b \Omega^2 (\beta + \beta_p) \zeta (\frac{T_{10}}{a_o}) \delta - \frac{1}{2} c_{cs} \Omega (\theta_{pc} + \phi) \dot{\beta}$$

$$- (c_b + c_{cs})\Omega\dot{\beta}\left(\frac{T_{10}}{a_o}\right)\delta + \frac{1}{2}c_{cs}\dot{\beta}^2]$$

$$- C_{31}\frac{1}{2}c_{cs}\Omega\dot{\beta}$$

$$- \frac{1}{2}D_1 c_{cs}\frac{C_{do}}{a_o}(\mu\Omega R)^2 \sin^2\psi$$

$$- D_2 c_{cs}\Omega\frac{C_{do}}{a_o}(\mu\Omega R)\sin\psi$$

$$- \frac{1}{2}D_3 c_{cs}\Omega^2\frac{C_{do}}{a_o} \tag{C.77c}$$

where the aerodynamic coefficients defined in Eqs. (C.73) and (C.74) have been used in the above expressions.

The total aerodynamic moment about the control surface hinge is obtained by integrating the distributed aerodynamic hinge moment

$$M_{A\delta} = \int_{x_{cs}}^{x_{cs} + L_{cs}} \vec{q}_{Ahx5}\, dx \tag{C.78}$$

which yields:

$$M_{A\delta} = \frac{C_{00}}{a_o}(c_b + c_{cs})^2\{[\frac{1}{8}(c_b + c_{cs})\Omega(\theta_{pc} + \phi)T_1$$

$$+ \frac{1}{4}(c_b + c_{cs})\Omega\frac{T_2}{a_o}\delta](\mu\Omega R)\cos\psi$$

$$+ [\frac{1}{8}(c_b + c_{cs})(\dot{\theta}_{pc} + \dot{\phi})(2T_9 + T_1) - \frac{1}{2}\Omega e(\theta_{pc} + \phi)T_{12} - \Omega e\frac{T_{15}}{a_o}\delta$$

$$- \frac{1}{16}(2c_b + 3c_{cs})\frac{T_{16}}{a_o}\dot{\delta} + \frac{1}{4}(\lambda\Omega R)T_{12}](\mu\Omega R)\sin\psi$$

$$+ [-\frac{1}{4}(\theta_{pc} + \phi)T_{12} - \frac{1}{2}\frac{T_{15}}{a_o}\delta](\mu\Omega R)^2\sin^2\psi$$

$$+ [-\frac{1}{2}(\theta_{pc} + \phi)\zeta T_{12} - \zeta\frac{T_{15}}{a_o}\delta + \frac{1}{4}(\beta + \beta_p)T_{12}](\mu\Omega R)^2\cos\psi\sin\psi\}$$

$$+ \frac{C_{01}}{a_o}(c_b + c_{cs})^2[\frac{1}{8}(c_b + c_{cs})\Omega T_1(\mu\Omega R)\cos\psi - \frac{1}{2}\Omega e T_{12}(\mu\Omega R)\sin\psi$$

$$- \frac{1}{4}T_{12}(\mu\Omega R)^2\sin^2\psi - \frac{1}{2}\zeta T_{12}(\mu\Omega R)^2\cos\psi\sin\psi]$$

$$+ \frac{C_{10}}{a_o}(c_b + c_{cs})^2\{[\frac{1}{8}(c_b + c_{cs})\Omega(\dot{\theta}_{pc} + \dot{\phi})(2T_9 + T_1) - \frac{1}{2}\Omega^2 e(\theta_{pc} + \phi)T_{12}$$

$$- \Omega^2 e\frac{T_{15}}{a_o}\delta - \frac{1}{16}(2c_b + 3c_{cs})\Omega\frac{T_{16}}{a_o}\dot{\delta} + \frac{1}{4}(\lambda\Omega R)\Omega T_{12}]$$

$$+ [-\frac{1}{2}\Omega(\theta_{pc} + \phi)\zeta T_{12} - \Omega\zeta\frac{T_{15}}{a_o}\delta + \frac{1}{4}\Omega(\beta + \beta_p)T_{12}](\mu\Omega R)\cos\psi$$

$$+ [-\frac{1}{2}(\theta_{pc} + \phi)(\Omega + \dot{\zeta})T_{12}$$

$$- (\Omega + \dot{\zeta})\frac{T_{15}}{a_o}\delta + \frac{1}{4}\dot{\beta}T_{12}](\mu\Omega R)\sin\psi\}$$

$$+ \frac{C_{11}}{a_o}(c_b + c_{cs})^2[-\frac{1}{2}\Omega^2 e T_{12} - \frac{1}{2}\Omega\zeta T_{12}(\mu\Omega R)\cos\psi$$

$$- \frac{1}{2}(\Omega + \dot{\zeta})T_{12}(\mu\Omega R)\sin\psi]$$

$$+ \frac{C_{20}}{a_o}(c_b + c_{cs})^2[-\frac{1}{4}\Omega(\Omega + 2\dot{\zeta})(\theta_{pc} + \phi)T_{12} - \frac{1}{2}\Omega(\Omega + 2\dot{\zeta})\frac{T_{15}}{a_o}\delta$$

$$+ \frac{1}{4}\Omega\dot{\beta}T_{12}]$$

$$- \frac{1}{4}\frac{C_{21}}{a_o}(c_b + c_{cs})^2\Omega(\Omega + 2\dot{\zeta})T_{12} \qquad \text{(C.79)}$$

where the aerodynamic coefficients defined by Eqs. (C.73) and (C.74) have been used to evaluate the above expression.

C.4 TOTAL ROOT LOADS

The resultant force and moment at the blade root is obtained by summing the contributions from the inertial, gravitational and aerodynamic loads acting on the blade and the control flap

$$\vec{F}_R = \vec{F}_{Ib} + \vec{F}_{Ic} + \vec{F}_{Gb} + \vec{F}_{Gc} + \vec{F}_{Ab} + \vec{F}_{Ac} \tag{C.80}$$

Similarly, the total moment about the blade root is given by

$$\vec{M}_R = \vec{M}_{Ib} + \vec{M}_{Ic} + \vec{M}_{Gb} + \vec{M}_{Gc} + \vec{M}_{Ab} + \vec{M}_{Ac} \tag{C.81}$$

Since the equations of motion are formulated in this study in the "3" system, it is necessary to express $\vec{M}_R$ in the "3" system, i.e.

$$\vec{M}_R = M_{Rx3}\hat{e}_{x3} + M_{Ry3}\hat{e}_{y3} + M_{Rz3}\hat{e}_{z3} \tag{C.82}$$

The inertial and gravitational root loads have been formulated in the "2" system and the aerodynamic root loads have been formulated in the "5" system. Before the components of the total root moment in the "3" system can be determined it is necessary to transform the inertial, gravitational and aerodynamic root moments to the "3" system. This is accomplished using the coordinate transformations defined in Chapter 2.

After transforming the various components to the "3" system, the following expressions are obtained:

$$\begin{aligned} M_{Rx3} = {} & M_{Ibx2} + M_{Icx2} + M_{Gbx2} + M_{Gcx2} + M_{Abx5} + M_{Acx5} \\ & + \beta_p(M_{Ibz2} + M_{Icz2}) + \beta_p(M_{Gbz2} + M_{Gcz2}) \\ & - \zeta(M_{Aby5} + M_{Acy5}) - \beta(M_{Abz5} + M_{Acz5}) \end{aligned} \tag{C.83a}$$

$$\begin{aligned} M_{Ry3} = {} & M_{Iby3} + M_{Icy3} + M_{Gby3} + M_{Gcy3} + M_{Aby3} + M_{Acy3} \\ & + \zeta(M_{Abx5} + M_{Acx5}) \end{aligned} \tag{C.83b}$$

$$M_{Rz3} = + M_{Ibz2} + M_{Icz2} + M_{Gbz2} + M_{Gcz2} + M_{Abz5} + M_{Acz5}$$

$$- \beta_p(M_{Ibx2} + M_{Icx2}) - \beta_p(M_{Gbx2} + M_{Gcx2})$$

$$+ \beta(M_{Abx5} + M_{Acx5}) - \beta\zeta(M_{Aby5} + M_{Acy5}) \qquad \text{(C.83c)}$$

C.5 HINGE MOMENT

The total moment about the control surface hinge axis, which is oriented parallel to the elastic axis of the blade, is required later in this study in order to calculate the power required to drive the control surface. The total hinge moment about the hinge axis is obtained by summing the contributions of the inertial, gravitational and aerodynamic loads. The hinge moment is assumed to act about an axis parallel to the x_4 axis. The total hinge moment is given by

$$M_\delta = M_{I\delta} + M_{G\delta} + M_{A\delta} \qquad \text{(C.84)}$$

where

$$M_{I\delta} = M_{Ihrx2} + \zeta M_{Ihry2} + (\beta + \beta_b)M_{Ihrz2} \qquad \text{(C.85)}$$

$$M_{G\delta} = M_{Ghx2} + \zeta M_{Ghy2} + (\beta + \beta_p)M_{Ghz2} \qquad \text{(C.86)}$$

REPORT DOCUMENTATION PAGE

Form Approved
OMB No. 0704-0188

1. AGENCY USE ONLY *(Leave blank)*	2. REPORT DATE	3. REPORT TYPE AND DATES COVERED
	June 1994	Contractor Report

4. TITLE AND SUBTITLE

Vibration Reduction in Helicopter Rotors Using an Actively Controlled Partial Span Trailing Edge Flap Located on the Blade

5. FUNDING NUMBERS

NAG2-477
NGT-50444

6. AUTHOR(S)

T. A. Millott and P. P. Friedmann

7. PERFORMING ORGANIZATION NAME(S) AND ADDRESS(ES)

University of California
Mechanical, Aerospace and Nuclear Engineering Department
Los Angeles, CA 90024

8. PERFORMING ORGANIZATION REPORT NUMBER

A-94096

9. SPONSORING/MONITORING AGENCY NAME(S) AND ADDRESS(ES)

National Aeronautics and Space Administration
Washington, DC 20546-0001

10. SPONSORING/MONITORING AGENCY REPORT NUMBER

NASA CR-4611

11. SUPPLEMENTARY NOTES

Technical Monitor: Steve Jacklin, NASA Ames Research Center, MS T-042, Moffett Field, CA 94035-1000
(415) 604-4567

12a. DISTRIBUTION/AVAILABILITY STATEMENT

Unclassified — Unlimited
Subject Category 39

12b. DISTRIBUTION CODE

13. ABSTRACT ***(Maximum 200 words)***

This report describes an analytical study of vibration reduction in a four-bladed helicopter rotor using an actively controlled, partial span, trailing edge flap located on the blade. The vibration reduction produced by the actively controlled flap (ACF) is compared with that obtained using individual blade control (IBC), in which the entire blade is oscillated in pitch. For both cases a deterministic feedback controller is implemented to reduce the 4/rev hub loads. For all cases considered, the ACF produced vibration reduction comparable with that obtained using IBC, but consumed only 10–30% of the power required to implement IBC. A careful parametric study is conducted to determine the influence of blade torsional stiffness, spanwise location of the control flap, and hinge moment correction on the vibration reduction characteristics of the ACF. The results clearly demonstrate the feasibility of this new approach to vibration reduction. It should be emphasized that the ACF, used together with a conventional swashplate, is completely decoupled from the primary flight control system and thus it has no influence on the airworthiness of the helicopter. This attribute is potentially a significant advantage when compared to IBC.

14. SUBJECT TERMS	15. NUMBER OF PAGES
Rotary wing aeroservoelasticity, Active control of vibrations	420
	16. PRICE CODE: A18

17. SECURITY CLASSIFICATION OF REPORT	18. SECURITY CLASSIFICATION OF THIS PAGE	19. SECURITY CLASSIFICATION OF ABSTRACT	20. LIMITATION OF ABSTRACT
Unclassified	Unclassified		

NSN 7540-01-280-5500

Standard Form 298 (Rev. 2-89)
Prescribed by ANSI Std. Z39-18
298-102

GPO 586-071/19213